Amir Nobahar

Innovative combination of chemical and biological strategies for the recovery of metals from metal-bearing wastewaters and leachates

Doctoral studies in Biological Sciences

Branch of Biochemistry and Biotechnology

Algarve University

Faculty of Science and Technology

CCMAR

2023

Amir Nobahar

Innovative combination of chemical and biological strategies for the recovery of metals from metal-bearing wastewaters and leachates

Doctoral studies in Biological Sciences

Branch of Biochemistry and Biotechnology

Supervised by Prof. Maria Clara Costa

Co-supervised by Dr. Jorge Carlier

Algarve University

Faculty of Science and Technology

CCMAR

2023

Innovative combination of chemical and biological strategies for the recovery of metals from metal-bearing wastewaters and leachates

Declaration of authorship of work

I declare to be the author of this work, which is original and unpublished. Authors and works consulted are properly cited in the text and are included in the reference list.

_____

Amir Nobahar

Acknowledgements

First and foremost I am extremely grateful to my supervisors, Professor Dr. Maria Clara Costa and Dr. Jorge Carlier for their invaluable advice, continuous support, and patience during my PhD study. Their immense knowledge and plentiful experiences have encouraged me in all the time of my academic research and daily life.

I would like to thank Prof. João Lourenço, Dr. Vera Almeida Gomes, Dr. Graça Miguel and Dr. Isabel Marín-Beltrán for their technical supports and valuable advices. I would like to express my gratitude to Prof. Dr. Adelino Canario for his supports and encouragements throughout my studies. Thanks to Centro de Ciências do Mar (CCMAR) and all its members that have made my study and life in the Portugal a wonderful time. Additionally, I am thankful to Prof. Ana Paula Paiva and Dr. Carlos Nogueira for providing the necessary samples during my studies. I am glad to have met and worked with Tânia, Alemu, Ines, Alba, Luiz, Joana, Eduardo, Fatima, Mook, Brigida, Joao, and … and thank for a cherished time spent together in the lab, and in social settings.

My family and loved ones have been my backbone throughout the PhD. A special thank you to my parents and sisters. Without their tremendous understanding and encouragement in the past few years, it would be impossible for me to complete my study. Thank you Gisou for being so special to me, for the love we share making us together in the good and bad moments, for your support, patience and great help. Additionally, I would like to thank my friends: Nemat, Samyar, Aydin, Ata and Navid; they are exceptional, and they make my life a lot more easy and pleasant. My acknowledgements would not be complete without saying a heartfelt thank you to all the people in Portugal. Special thanks to Soeiro family, Joao, Marilia, Antonio and Maria for being an inspiration and for giving me my first taste of the real Portugal.

‘It always seems impossible until it is done’ – Nelson Mandela

List of Publications

This thesis is based on the following original articles:

In Periodic Scientific Journals

1. Nobahar, A., Carlier, J.D. and Costa, M.C. (2023) 'Recovery of catalytic metals from leaching solutions of spent automotive catalytic converters using plant extracts', *Clean Technologies and Environmental Policy* [Preprint]. doi:10.1007/s10098-023-02523-1.
2. **Nobahar, Amir**; Bejiga Melka, Alemu; Marín-Beltrán, Isabel; Neves, Luiz; Costa, Maria Clara; Carlier, Jorge Dias. "Zinc recovery from an extreme copper-free acid mine drainage: studying the prior separation of iron by solvent extraction using AliCy and/or alkalinization". Journal of Sustainable metallurgy (2022): https://doi.org/10.1007/s40831-022-00588-8
3. **Nobahar, Amir**; Bejiga Melka, Alemu; Pusta, Alexandra; Lourenço, João Paulo; Carlier, Jorge Daniel Dias; Costa, Maria Clara. "A new application of SX to extreme AMD producing copper solutions suitable for electrochemical and biological recovery processes". Mine Water and the Environment (2022): https://doi.org/10.1007/s10230-022-00858-7
4. **Nobahar, Amir**; Carlier, Jorge Dias; Miguel, Maria Graça; Costa, Maria Clara. "A review of plant metabolites with metal interaction capacity: a green approach for industrial applications". BioMetals (2021): http://dx.doi.org/10.1007/s10534-021-00315-y

In Periodic Scientific Journals (Under Revision)

1. **Nobahar, Amir**; Carlier, Jorge Dias., Lorenco, Costa, Maria Clara. "Separation and recovery of gold from synthetic gold unimetallic solution and printed circuit board leachate by plant extracts as gold nano and micro particles". Journal of chemical technology and biotechnology (2022, under revision).
2. **Nobahar, Amir**; Fitasab, Eduardo Trindade; Costa, Maria Clara; Carlier, Jorge Dias. "Enrichment of acidophilic sulfate-reducing bacteria, their application in metal attenuation of acid mine drainage and studies of procaryotic communities on the tested conditions" Applied Microbiology and Biotechnology. (2022, under revision).

Abstract

This dissertation applied pioneering approaches that benefits the potential of both solvent extraction (SX) and bio-recovery strategies based on the use of bacterial communities and plant extracts as metal separation and recovery technique. In this regard, metal recovery from an extreme acid mine drainage (AMD) was initially performed for Cu SX with Acorga M5640 that was then stripped with 2M sulfuric acid, allowing to rise the Cu concentration to over 46 g/l, which was then recovered as CuS nanoparticles through the addition of biogenic sulfide. Thereafter, the rafiinate from the mentioned SX process, was subjected to Zn recovery studies. In these studies, Fe^{3+} was found to be nuisance in Zn recovery and was separated from the solution by SX with AliCy followed by alkalinization of its aqueous raffinate to pH 3.25 or 3.50. Thereafter, Zn was recovered as ZnS nanoparticles through precipitation by biogenic sulfide at pH=3.5. In addition, AMD remediation studies were investigated by applying acidophilic SRB consortium that was obtained from the enrichment of sediments of an inactive Cu mine at pH 4.00 with methanol as carbon source. The metal removal from AMD by the mentioned consortium revealed promising results when a 20% (v/v) supplement of Postgate B base (except lactate) was added to AMD. Metataxonomic analysis showed the presence of *Desulfosporosinus* genus in all enrichment and AMD remediation studies, with highest relative abundances in cultures enriched with methanol at pH 4.00 and in AMD remediation tests with lowest Postgate base supplements. Another part of this study investigated the potential of plant extracts in PGMs and precious metals recovery from different leachates. These studies revealed the high potential of red raspberry (*Rubus Idaeus* L.) leaves hydroalcoholic extract in Pd precipitation (>60%) from spent autocatalytic converters leachates as nanoparticles and also in Au precipitation (~96%,) from printed circuit boards leachates as microparticle clusters of Au nanoparticles. Contribution of functional groups of the phytochemicals present in the extracts were studied in the Pd and Au ions' bio-reduction and bio-stabilization.

Keywords: acid mine drainage, metal leachate, metal bio-recovery, solvent extraction, sulfate-reducing bacteria, nanoparticles green synthesis

Resumo

A acumulação de metais no meio ambiente tem diversos efeitos negativos que se tendem a agravar com a sua crescente procura e utilização. Assim, a recuperação de metais a partir de fontes secundárias, nomeadamente de resíduos sólidos e de águas residuais, usando tecnologias ambientalmente e economicamente sustentáveis é da maior prioridade. Nesse contexto, explorou-se nesta tese a combinação pioneira de processos químicos de extração líquido-líquido, também conhecidos por extração por solventes (SX), e de estratégias de biorrecuperação baseadas na utilização de comunidades bacterianas e extratos de plantas, tendo em vista a recuperação de metais de fontes secundárias.

O capítulo 2 da presente tese aborda a recuperação de cobre de uma Água Ácida da Mina (AMD) de São Domingos com uma concentração extrema por combinação de um processo de SX para separação deste metal, seguido da sua recuperação da fase aquosa com Bactérias Redutoras de Sulfato (SRB). O estudo, efetuado com diferentes extratantes e fases orgânicas, mostrou que o extratante Acorga M5640 (30% (v/v) em diluente Shell GTL + 2,5 % (v/v) octanol) foi o mais eficiente e seletivo, permitindo a separação de ~96% do cobre em apenas uma etapa. Quanto ao agente de reextração, o ácido sulfúrico 2 M foi o selecionado, permitindo, através de ciclos sucessivos de extração e reextração, atingir uma concentração de cobre de ~46 g/L na fase aquosa purificada, o que é suficiente para a recuperação do metal por via eletrolítica. A recuperação biológica do cobre dessa solução foi a alternativa estudada. Para o efeito adicionou-se o sobrenadante de uma cultura de SRB, de modo a obter diferentes razões molares de S e Cu. Uma razão superior a 1,75 resultou na precipitação de mais de 95% de cobre na forma de nanopartículas de covelite (CuS). A recuperação subsequente do zinco da AMD sem cobre, contendo ~53g/L de Fe e ~2g/L de Zn é o objeto do capítulo 3 desta tese. A presença de ferro em grande concentração e a necessidade de separação de ambos os metais com vista à posterior recuperação do zinco constituíram um desafio, que resultou na testagem de diversas metodologias, como por exemplo adição de agentes alcalinos e SX usando nomeadamente um líquido iónico (AliCy, diluído em querosene), preparado no laboratório, bem como a combinação de ambas as técnicas. A estratégia que se revelou mais eficaz consistiu na combinação de um ciclo de SX com Alicy para remoção do ferro, seguida de ajuste do pH da solução aquosa para pH 3,25 ou 3,5, de modo a remover o ferro restante. A maior parte do Fe^{3+}, ~92%, foi separado por SX, sendo o remanescente

separado por precipitação, com uma perda de zinco de ~12% e ~17% em cada uma das duas etapas. A maior recuperação de zinco da solução aquosa (~83%) foi conseguida a partir da solução de pH=3,5 através da adição de sulfureto gerado biologicamente por SRB, tendo-se obtido nanopartículas de Wurzite e Esfalerite (ZnS) com tamanho compreendido entre 2 a 22 nm, aglomeradas em estruturas maiores. Este trabalho mostrou pela primeira vez o potencial do líquido iónico Alicy para a separação de Fe^{3+} de soluções ácidas multimetálicas, o que é importante tendo em conta que este metal é um interferente significativo em diversos processos de recuperação metálica.

No capítulo 4 estudou-se a atividade de SRB enriquecidas a partir de sedimentos da área mineira de São Domingos afetados por AMD a diferentes valores de pH (de 2 a 6) e na presença de diferentes fontes de carbono e eletrões (metanol, glicerol e etanol), tendo em vista a possibilidade de desenvolver processos de biorremediação e/ou de biorrecuperação de metais diretamente a partir de AMD sem necessidade prévia de neutralização. Foi possível obter redução do ião sulfato a pH=4 na presença de metanol (>99%), sendo esse consórcio de SBR e essa fonte de C selecionada para testes de remoção de metais a partir da AMD, usando diferentes razões volume/volume de AMD e meio de crescimento Postgate B modificado sem lactato e com pH inicial de 4,5. Os resultados mais promissores foram obtidos com uma razão de 80% de AMD e 20% de meio Postgate B modificado, tendo-se obtido uma remoção de mais de 99% dos metais após 28 dias de ensaio. A análise metataxonómica da evolução da população nos estudos de enriquecimento revelou a presença do género *Desulfosporosinus* em todas as amostras enriquecidas, com maior abundância relativa em amostras enriquecidas em metanol a pH=4. A análise metataxonómica nos ensaios de biorremoção de metais revelou igualmente a presença do género *Desulfosporosinus* em todas as condições testadas, com a maior abundância relativa nas amostras com 100% de AMD. O aumento da razão de meio Postgate B modificado favoreceu e aumentou a abundância relativa de outras SRB acidófilas, principalmente da família *Clostridiaceae.*

No capítulo 5, estudou-se o potencial de extratos hidroalcoólicos de *Cistus ladanifer* L., *Erica andevalensis* e *Rubus idaeus* L. para a recuperação de PGMs a partir de soluções sintéticas unimetálicas e multimetálicas, mimetizando nomeadamente lixiviados de catalisadores automóveis (ACCs). Os ensaios com soluções unimetálicas mostraram que o extrato de *R. idaeus* consegue separar cerca de 70% de Pd e menos de 40% dos outros metais testados (Al, Ce, Fe e Pt). A aplicação de extratos de plantas a dois lixiviados de

ACCs mostrou que o extrato de *R. idaeus* conduz a elevada remoção (>60%) de Pd e Pt com precipitação de menos de 20% dos outros metais presentes na solução. A análise por espetroscopia molecular de UV-Vis é consistente com a biorredução dos iões Pd^{2+} a nanopartículas de Pd^{0} e a análise por FTIR revelou a possível contribuição dos grupos funcionais dos fitoquímicos presentes no extrato para a biorredução e estabilização das nanopartículas obtidas. A análise de STEM-EDX sugere que as nanopartículas de Pd^{0} apresentam elevada pureza e por HRSTEM foi possível verificar que o tamanho das partículas se situa entre 2.5 a 17 nm com um tamanho médio Feret de 6.1 nm, tendo igualmente confirmado a sua estrutura cristalina, com distâncias interplanares de ~0.22 nm.

No capítulo 6 investigou-se o potencial das mesmas plantas utilizadas no capítulo 5 na separação de metais preciosos a partir de soluções unimetálicas sintéticas e a partir de um lixiviado de Placas de Circuito Impresso (PCBs). Os resultados com as soluções multimetálicas revelaram que os extratos de *R. idaeus* e *E. andevalensis* permitiram a separação de mais de 95% do Au^{3+} inicialmente presente na solução. A aplicação dos extratos de plantas à solução real da lixiviação dos PCBs permitiu uma remoção de 96%, 95% e 90% do ouro com os extratos de *R. idaeus*, *C. ladanifer* e *E. andevalensis*, respetivamente. Da redução de Au^{3+} com o extrato de *R. idaeus* resultou a obtenção de nanoparticulas de Au^{0}, tal como sugerido pelos resultados de espetroscopia molecular de UV-Vis. A análise por FTIR parece confirmar o envolvimento de metabolitos secundários na biorreducão e estabilização das nanopartículas. A análise das partículas por XRD confirmou tratar-se de Au^{0} e a análise por STEM-EDS confirmou a presença de micro agregados de Au (~0.8 μm) de elevada pureza em forma de flor, ou com morfologia cúbica aparente. A análise por HRSTEM mostrou a dimensão das partículas individuais (~20 nm) que compõem os agregados.

Palavras-chave:
Água ácida de mina, lixiviados metálicos, biorremediação/biorrecuperação metálica, extração por solventes, bactérias redutoras de sulfato, síntese verde de nanopartículas

List of Contents

List of Figures

List of Tables

List of annexes

Supplemantary figures

Supplemantary tables

List of Abbreviations

ACC - automotive catalytic converter

AMD - acid mine drainage

AMP - adenosine monophosphate

APS - adenosine phosphosulfate

aSRB - acidophilic sulfate-reducing bacteria

ASV - amplicon sequence variant

ATP - adenosine triphosphate

DSR - dissimilatory sulfate reduction

ECs: electronic components

EDS - energy-dispersive X-ray system

EDX - energy-dispersive X-ray system

Eh - redox potential

FFT - Fast Fourier Transform

FTIR - Fourier Transform Infrared spectroscopy

GCMS - gas chromatography-mass spectrometry

HAADF - high-angle annular dark-field imaging

HRSTEM - high-resolution scanning transmission microscopy

ICP-MS - inductively coupled plasma mass spectrometry

IL - ionic liquids

ITS - Internal transcribed spacer

LLE - liquid-liquid extraction

LOD - limits of detection

MWW - municipal wastewater

NCBI - national center for biotechnology information

NI - Not Indicated

NPs - nanoparticles

OTU - Operational taxonomic unit

PB-m - Postgate B macronutrients base

PCB - printed circuit boards

PCR - Polymerase Chain Reaction

PE - plant extract

PGM - platinum group metals

PM - precious metals

REE - rare earth elements

rRNA - ribosomal ribonucleic acid

SAED: Selected Area Electron Diffraction

SBRs - sequence batch reactors

SEM - scanning electron microscopy

SPR: Surface Plasmon Resonance

SR - sulfate reduction

SRB - sulfate-reducing bacteria

STEM - scanning transmission electron microscopy

SX - solvent extraction

TBP - tributyl phosphate

TEM - transmission electron microscopy

UV - ultraviolet

VP-SEM-EDX: variable pressure scanning electron microscope coupled with energy dispersive x-ray spectrometry

WEEE: waste electrical and electronic equipments

WWTP - wastewater treatment plant

XRD - X-ray powder diffraction

CHAPTER 1

General Introduction

1.1. Secondary sources of metals in the modern era

Human activities and vast global industrialization have been led to the generation of large quantities of metal solid and liquid wastes. Introduction of these wastes to the environment is a global concern, since, unlike organic contaminants, metals are not biodegradable and tend to accumulate in the environment and living organisms, causing serious environmental and health problems (Raskin et al. 1994; Macaskie et al. 2010; Sharma et al. 2021). Faced with more and more stringent regulations, heavy metals are nowadays priority pollutants and are becoming one of the most serious environmental problems (Raffa et al. 2021). This situation is accompanied by the primary resource scarcity of some metals, and, in the near future, is estimated to be one of the most important issues confronting human society (Watari et al. 2021). High living standards along with population growth, that is expected to pass the 10 billion until the end of the century (UNDESA 2015), will be pushing the demand for minerals and metals resources. Different studies have predicted the depletion of some primary metal sources in the near future and the necessity of a transition toward circular economy through metal recycling from secondary sources (Sverdrup and Ragnarsdottir 2016; Schipper et al. 2018; Watari et al. 2021; Hunt et al. 2021). Some examples of important secondary sources of metals studied in this work are mining wastes and acid mine drainage, spent autocatalytic converters and printed circuit boards that are described in more details in the following sections.

1.1.1. Acid mine drainage

Acid mine drainage (AMD) is a persistent and conceivably dangerous form of pollution caused by extensive sulfide mining activities, as evidenced by different studies (Akcil and Koldas 2006; Egiebor and Oni 2007; Costa et al. 2008; Pozo-Antonio et al. 2014; Nordstrom et al. 2015; Fischer et al. 2022; Montes-Atenas 2022). Main minerals responsible for AMD generation are pyrite (FeS_2), pyrrhotite ($Fe_{1-x}S$, where $0 < x < 0.2$), arsenopyrite (FeAsS) (Park et al. 2019), enargite (Cu3AsS4), galena (PbS), and sphalerite (ZnS) (Dold 2008). In the mining operations of copper and gold ores, the none economic part of the treated material is 99% and 99.9% respectively, that are classified as wastes and are deposited in tailing impoundments and natural depressions such as lagoons and lakes (Dold 2008). Even though metals concentrations in these materials are not economically attractive for extraction, they still contain different sulfide minerals in high

concentrations compared to Earth's crust. These minerals are stable in anoxic and dry conditions, while through mining activities, tailings rich in metal sulfides are generated and exposed to the environment (Skousen et al. 2019). In contact with air and water they are no longer stable and undergo oxidation, which results in sulfuric acid formation and liberation of different heavy metals (Dold 2008; Naidu et al. 2019). Pyrite oxidation reaction in the presence of water and oxygen is described in equations 1 and 2. Pyrite goes into dual oxidation stages; initially ferrous iron and sulfuric acid is generated (Eq. 1.1) and then by the oxidation of ferrous iron, ferric iron is produced (Eq. 1.2) (Tomiyama et al. 2019; Igarashi et al. 2020).

$$FeS_2 + 3.5O_2 + H_2O \rightarrow Fe^{2+} + 2SO_4^{2-} + 2H^+ \qquad \text{Eq. 1.1}$$

$$Fe^{2+} + 0.25O_2 + H^+ \leftrightarrow Fe^{3+} + 0.5\ H_2O \qquad \text{Eq. 1.2}$$

The generated ferric iron will further oxidize the pyrite and increases the oxidation reaction process (Eq. 1.2) (Tabelin et al. 2017; Igarashi et al. 2020). As presented in equations 1.1 and 1.3, up to 18 moles of acidity can be produced through oxidation of 1 mole of iron sulfide (Igarashi et al. 2020).

$$FeS_2 + 14Fe^{3+} + 8H_2O \rightarrow 15Fe^{2+} + 16H^+ + 2SO_4^{2-} \qquad \text{Eq. 1.3}$$

Since natural pyrite is usually incorporated with various heavy metals and metalloids, the generated AMD can contain high concentrations of toxic elements including Se and As, and also heavy metals like Pb, Cu, Zn, Ni etc. (Casiot et al. 2005; Park et al. 2019; Tabelin et al. 2019). It is also known that the pyrite oxidation can be accelerated by some chemolithotrophic Fe-oxidizing microorganisms by a factor of 10^6 (Singer and Stumm 1970; Johnson 2003). Table 1.1 represents the concentration of sulfate and different metals in AMD originating from different mining areas around the world. Mining processes, host rocks and climate conditions are among the major factors that influence the nature of generated AMD, which can then be classified by Ficklin diagrams to interpret variations in AMD chemistry between different deposit types (Ficklin et al. 1992; Plumlee et al. 1999).

Table 1.1. Concentration of sulfate and different metals in AMD originating from different mining areas around the world

Location	Mine type	Concentration (mg/l)								References
		SO_4^{2-}	Al	Ca	Cu	Fe	Mg	Mn	Zn	
South Korea	Coal	1950	10	1070	NI	186	272	13	NI	(Seo et al. 2017)
South Africa	Coal	NI	245	498	NI	2135	428	30	6.9	(Kefeni et al. 2017a)
Brazil	Coal	6300	NI	232	NI	2822	199	50	25	(Buzzi et al. 2013)
Czech Republic	Coal	1375	19.9	296.6	NI	53.3	130.1	6.2	0.4	(Heviánková et al. 2014)
Portugal	Cu	3100	NI	163	49	497	NI	75	107	(Costa and Duarte 2005)
China	Cu	NI	63.4	NI	14.7	331.2	67	66.3	80.4	(Chen et al. 2014b)
Chile	Cu	4671	382.6	185.9	531.2	1.1	NI	72	44.7	(Pino et al. 2020)
Brazil	Au	18.2	445	347	95.7	467	NI	2575	82	(Amaral et al. 2018)
Russia	Au	27000	520	630	32	8600	420	18	140	(Bortnikova et al. 2020)
South Africa	Au	NI	224.5	498.6	0.2	2135	428.3	30.2	6.9	(Kefeni et al. 2015)
Spain	Pyrite	2122	163	81.6	11.7	153	199	21.9	51.2	(Nieto et al. 2007)
Spain	Pyrite	11700	251	441	165	744	1104	467	976	(Ayora et al. 2016)
Spain	Pyrite	NI	251	154	82	1141	127	115	78	(López et al. 2021)
China	Pyrite	6883	117	NI	NI	3150	NI	27.7	4.9	(Chen et al. 2015b)
China	Pyrite	7931	1878	NI	NI	3580	NI	145.7	80.9	(Chen et al. 2015b)
Australia	Ag	3499	472	547	5.8	564	590	58	145	(Pozo et al. 2017)
Australia	Cu–Au–Ag	17430	1233	534	77.2	16.7	2265	161.4	48.9	(Kaur et al. 2018)
Finland	Cu–Zn	NI	260	500	35.3	443	771	29.3	410	(Tolonen et al. 2014)
China	Pb–Zn	6690	53	NI	4.4	1240	NI	13.7	144.4	(Chen et al. 2015b)
China	Polymetallic	6966	168	NI	60.4	520	NI	116.7	80.1	(Chen et al. 2015b)

NI: Not Indicated

The release of AMD to the environment not only causes biotic impairments through direct toxicity, disturbance of nutrient cycles, habitats' modifications due to precipitation of metals etc., but also results in poor water quality, unsuitable for human and animal use, irrigation and industrial purposes (Figure 1.1) (Skousen et al. 2017; Rooyen and Staden 2020). The vast negative effects of AMD has been shown by Costa et al. (2008, 2009), Casiot et al. (2009) and Gray and Delaney (2008) in Europe, David (2003) and Yang et al. (2007) in Asia, Soucek et al. (2000) and Cherry et al. (2001) in United States, Grout and Levings (2001) and Sracek et al. (2004) in Canada, Winterbourn (2000) in New Zeland and Lei et al. (2010) and Edraki et al. (2005) in Australia.

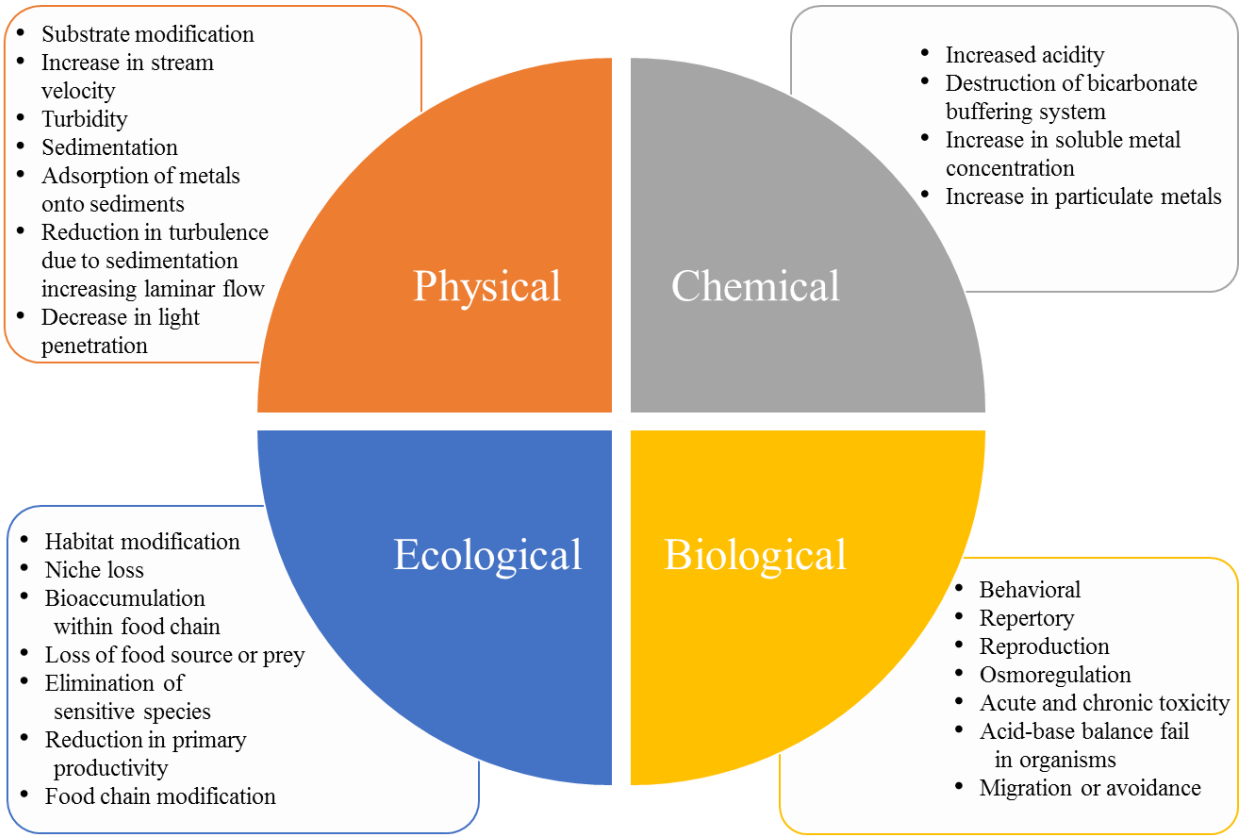

Figure 1.1. Physicochemical, biological and ecological effects of acid mine drainage on the environment (Adapted from Ighalo et al. (2022)).

Therefore, due to the urgent necessity of metal recycling from AMD and also the toxic effects of AMD to the environment, effective AMD remediation methods has gained more attention in the past decades (Gupta and Sar 2020; Gupta et al. 2020).

1.1.1.1. AMD originating from São Domingos mining area

São Domingos is one of the most representative abandoned mining districts in the Portuguese sector of the Iberian Pyrite Belt (Figure 1.2). The mining activities in São Domingos dates back to pre-Roman times and it was active until 1966 (Pérez-López et al. 2008). The AMD from this region is generated by the oxidation of different metal sulfide compounds and flows through several reddish-yellow diverting channels and dams, reaching to the Guadiana river, main water stream in the region (Figure 1.2 and Figure 1.3-A) (Álvarez-Valero et al. 2008). The intense mining activity in this mine has resulted in the presence of various mining related wastes and significantly large volumes of AMD in the open pit (Figure 1.3-B) (Pérez-López et al. 2008). The pollution originating from the mine as a result of continuous leaching of the residues is still important. In addition, a part of AMD generated in the Achada do Gamo zone remains in an impoundment in the area where low-grade copper ores were roasted in piles and washed with acidic water to extract the copper that was later precipitated onto iron sheets in a cementation tank. The impoundment is surrounded by slag remaining from the roasted pyrite ore piles, roasted iron oxide (hematite-rich) ore, and leached materials in seasonally flooded areas (Álvarez-Valero et al. 2008). The AMD generated in this impoundment has a very dark color, seems highly dense and extremely contaminated, likely due to successive cycles of accumulation in winters and evaporation in summers (Figure 1.3-C). Other impoundment in the area with a relatively constant AMD influent and effluent has considerably lower concentration of different metals and sulfate (Figure 1.3-D). Previous studies have reported the high acidity (≈ pH 2) of the AMD generating in São Domingos mining area with approximate concentration of sulfate (1000–5000 mg/L), Al (100–500 mg/L), Fe (50–500 mg/L), Zn (20–150 mg/L), Cu (20–100 mg/L), and Mn (5–20 mg/L) (Costa and Duarte 2005; Costa et al. 2008).

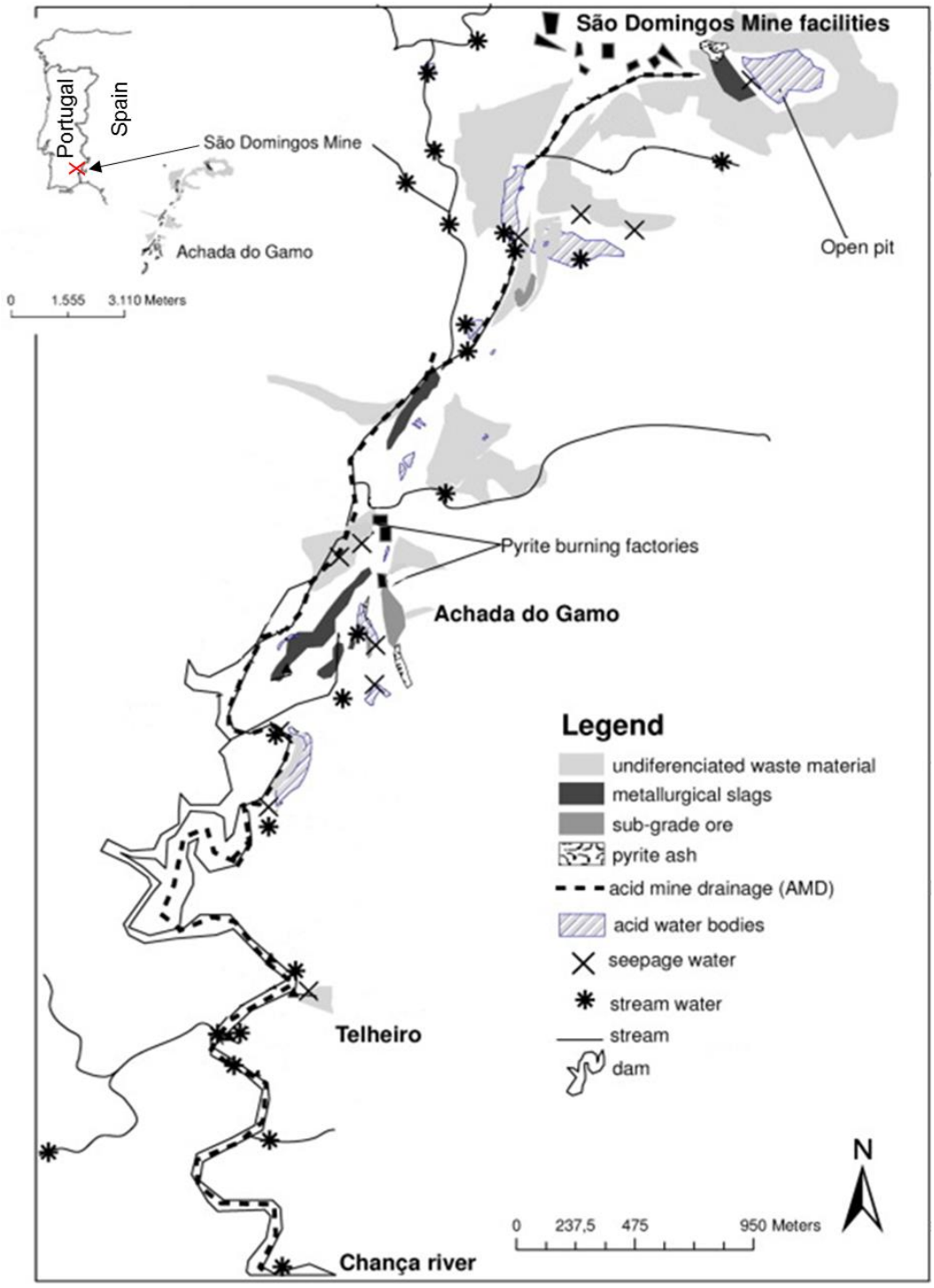

Figure 1.2. São Domingos mining area with the location of different sites. Adapted from Abreu et al. (2008).

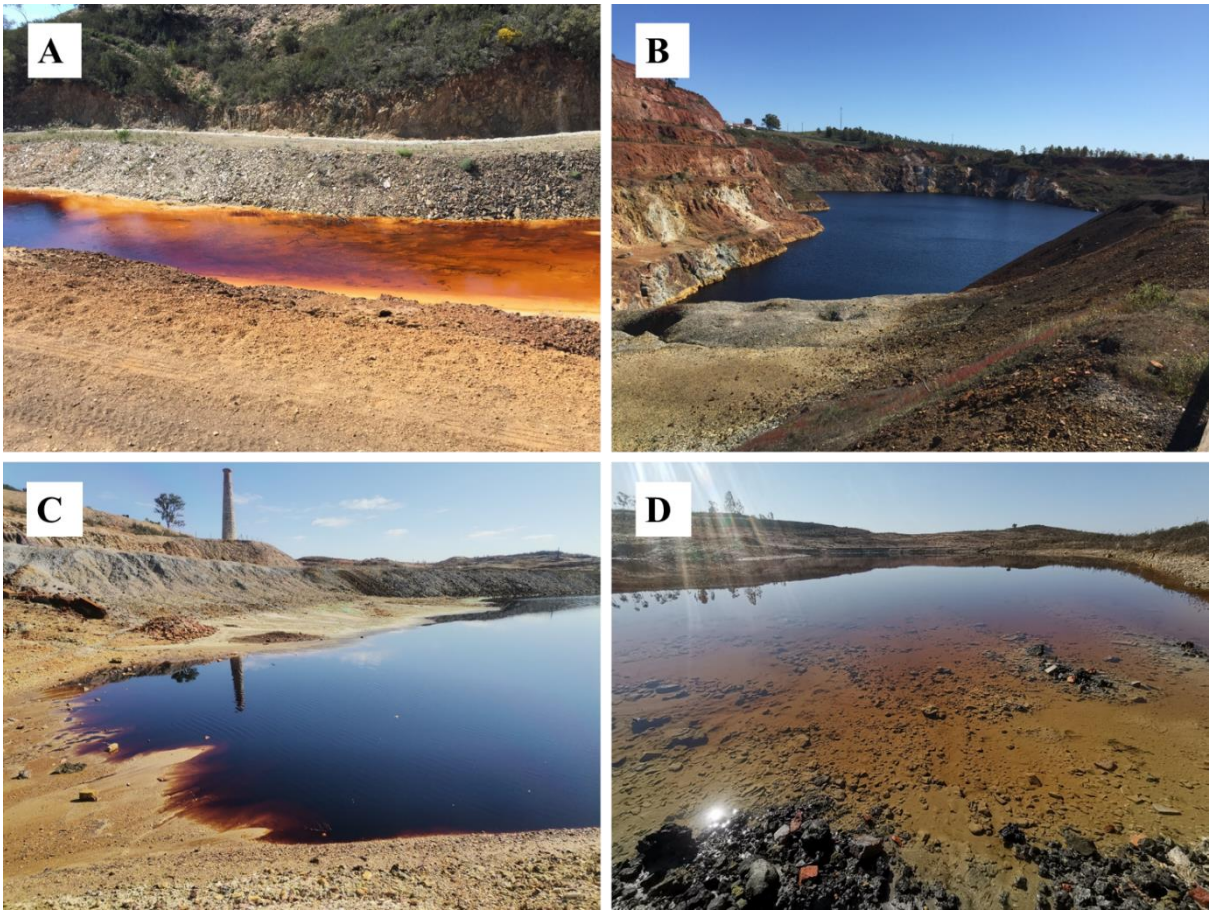

Figure 1.3. São Domingos mining area: A) metal and sulfate bearing diverting channels, B) AMD in open pit C) impoundment with extremely contaminated AMD D) impoundment with normal AMD.

The climate of the Southern West of the Iberian Peninsula favors the generation of AMD in the São Domingos mining area and the treatment of the AMD generated is still an issue. By now, the development of treatment processes of the AMD originating from São Domingos mining area has been an ongoing process by several multidisciplinary research teams and only short-term solutions have been described (Ferreira et al. 2021) due to the elevated acidity and concentration of metals (mainly as Fe), which rapidly saturate the treatment systems (Álvarez-Valero et al. 2008; Ferreira et al. 2021). Empresa de Desenvolvimento Mineiro, S.A. (EDM: the responsible company of the environmental passive recovery of degraded mining areas in Portugal) is currently invenstigating

for the solutions of the environmental problems and for the mining heritage preservation and valorization of the São Domingos mining area (GPGMS 2010). The main and final objective of the company is the volume reduction of AMD generating in the site up to 84% and channel construction on the Western banks and Eastern valley slopes in order to collect and deviate clean and non-contaminated surface waters (EDM 2019).

1.1.2. Automotive catalytic converters (ACCs)

Platinum Group Metals (PGMs), include Platinum (Pt), Palladium (Pd), Iridium (Ir), Ruthenium (Ru), Rh (Rhodium) and Osmium (Os), are nowadays extensively used in high technology applications because of their distinctive properties such as catalytic activity, high electrical conductivity and resistance to oxidation and corrosion (Yakoumis et al. 2021).

Since the mid-1970, due to strict environmental regulations, all the petrol engine cars are obligated to be equipped with catalytic converters for the conversion of dangerous gases such as carbon monoxide, nitrogen oxides etc. to convert them in other gases with less toxicity (Fornalczyk and Saternus 2011; Saguru et al. 2018). Catalytic conversion is mainly carried out by the Pd, Pt and Rh present on the honeycomb in a short time and by now, alternative methods for this process with more economical viability and high catalytic efficiencies have not been found (Morcali 2020). Every year, a considerable part of the global extraction of PGMs is applied in ACC production, comprising 44% of Pt, 72% of Pd and 80% Rh (Fornalczyk and Saternus 2011; Hughes et al. 2021). Thus, used ACCs that are replaced or from automobiles that reach the end of their life become a secondary source of these metals (Figure 1.4). PGMs grades in the ores range from 3 to 8 g/t (Kyriakakis, 2005), while, the monoliths of ACCs contains PGMs in a range of 1000-3000 g/t (Karim and Ting 2021). Table 1.2 summarizes the total content of PGMs in the ACCs reported by different studies.

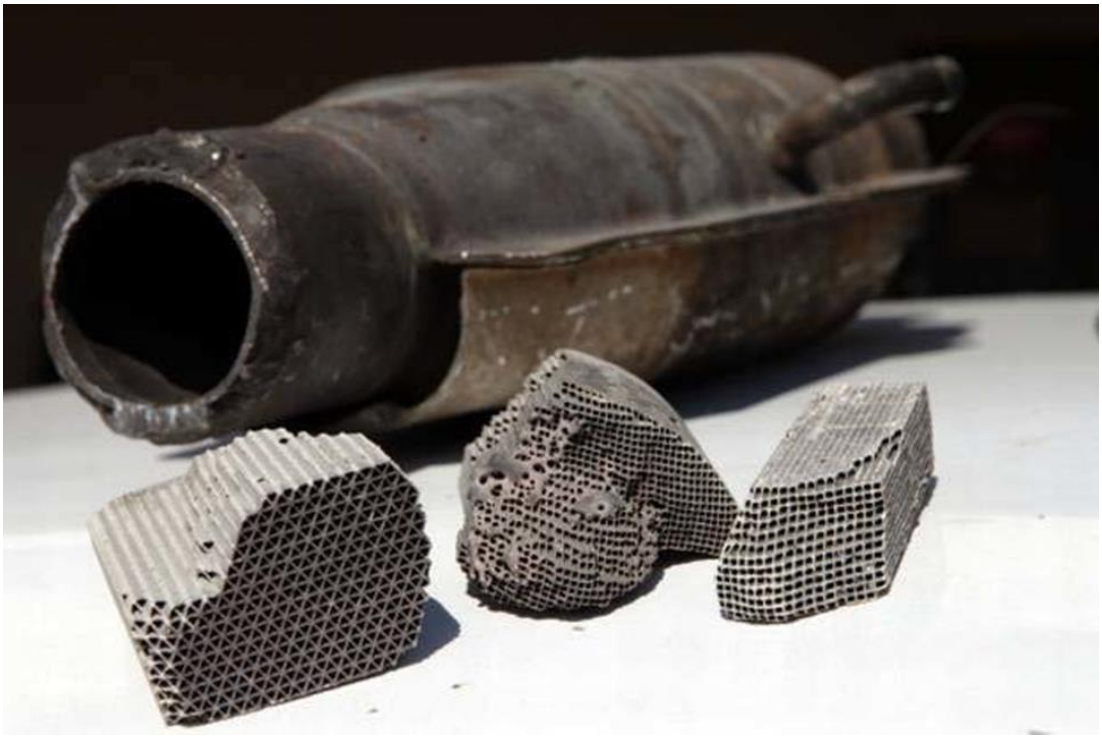

Figure 1.4. Used ACC and honeycomb cores (Varun Kumar et al. 2015).

In addition, the rapidly increasing of PGMs industrial applications in commercial scale has been caused a serious depletion in the primary sources of these metals (Moleko-Boyce et al. 2022). Therefore, to meet the future demand of the PGMs, recycling these metals is critical from both financial and environmental standpoints. Different studies recently revealed the increasing inclination in PGMs recovery from spent ACCs (Morcali 2020; Yakoumis et al. 2021; Manjunath et al. 2021; Ilyas and Kim 2022; Paiva et al. 2022).

Table 1.2. Typical PGM content in ACCs based on information reported by different studies.

Reference	Total PGMs content (mg/kg)	Content of PGMs species (mg/kg) in the ACCs		
		Pt	Pd	Rh
(Harjanto et al. 2006)	12000	3790	5820	2390
(Upadhyay et al. 2013)	3160	1800	1200	160
(Kim et al. 2000)	2830	2300	530	NI
(Chen et al. 2015a)	1940	NI	1698	242
(Kim et al. 2016)	1430	1280	NI	150
(Chen et al. 2014a)	1160	370	630	160
(Willner et al. 2015)	840	840	NI	NI
(Nogueira et al. 2014)	572	NI	441	131
(Kirichenko et al. 2014)	540	110	360	70
(Fornalczyk et al. 2016)	400	400	NI	NI
(Kirichenko et al. 2014)	385	380	3.8	1.1
(Kirichenko et al. 2014)	230	130	76	24

NI: Not Indicated

1.1.3. Printed circuit boards (PCBs)

Vast technological developments and innovations in the last decades has led to generation of high amounts of waste electrical and electronic equipments (WEEE). Based on the reports by United Nations, in 1992, about 14 Mt of WEEE was generated, which in 2002 was increased to 24 Mt, reached to about 54 Mt in 2019 (Baldé et al. 2017; Forti et al. 2020) and is predicted to surpass 74 Mt in 2023 (Forti et al. 2020).

Electronic industries consume significantly high amounts of metals and more specifically precious metals (PMs). Printed circuit boards (PCBs) are the main component of WEEE and consist on

about 3% of their total weight (Cayumil et al. 2016). PCBs contain a variety of more than 60 different elements (Hadi et al. 2013; Yang et al. 2019) and metal content of PCBs is reported to include almost 30 wt%. Metallic section of PCBs include base metals (Cu and Zn), heavy metals (Pb, Cd and Ni) and precious metals (Au, Pd and Ag) (Chen et al. 2015c; Cayumil et al. 2016) along with high amounts of non-metal content like epoxy resins, fiber glass etc. In the PCBs, Au is used due to its excellent conductivity and stability (important as protective layer in the contacts), while Pd is applied in contacts and multilayer ceramic capacitors and Ag is applied in solder and contacts. In terms of Au content, PCBs are divided as low (100 g/t), medium (100- 400 g/t) and high Au content (>400 g/t) (Kellner 2008; Estrada-Ruiz et al. 2016). In Table 1.3, some typical metallic concentrations in PCBs are presented based on the literature.

Table 1.3. Metal composition (%) of PCBs reported in the literature

Metals	**Reported metal percentage by different authors**							
	(Palanisamy and Kandasamy 2020)	(Shuey et al. 2005)	(Zhao et al. 2004)	(Chatterjee 2008)	(Ghosh et al. 2015)	(Flandinet et al. 2012)	(Szałatkiewicz 2014)	(Bizzo et al. 2014)
Ag	0.028	NI	0.33	0.223	0.134	0.045	0.0079	NI
Al	7	2	4.7	4.78	1	NI	NI	NI
Au	0.011	0.1	0.008	0.725	0.035	0.025	0.0068	NI
Cr	NI	NI	NI	NI	NI	0.356	NI	NI
Cu	24	20	26.8	6.5	13	14.6	28.7	24.2
Fe	12	8	5.3	0.11	5	4.79	0.6	0.18
Mg	NI	NI	NI	NI	NI	NI	NI	0.12
Ni	2	2	1.5	0.95	0.1	1.65	NI	0.61
Pb	3	2	NI	4.19	0.3	2.96	1.3	NI
Pd	NI	NI	NI	0.025	0.021	0.022	0.003	NI
Sb	NI	4	0.06	NI	NI	NI	NI	NI
Sn	NI	4	1	NI	NI	5.62	3.8	NI
Zn	0.4	1	0.45	2.17	NI	NI	NI	NI

NI: Not Indicated

Metal content of PCBs is higher than natural ores and therefore, metal recovery from these resources is highly advantageous. As instance, national standards for Cu smelting in China has reported that the exploitation of 1 ton of Cu from natural Cu ores requires 1400-1700 kg of coal to maintain the energy. Obviously, metal recovery from PCBs can decrease significantly the energy requirement and processing costs in metallurgical industry (Duan et al. 2015; Zeng et al. 2015).

1.2. Metal recovery from secondary resources

Development of environmentally friendly and economically viable metal recycling routes aiming the efficient metal separation and recovery from secondary resources is vital to achieve sustainable management of resources and to diminish the environmental threats (Wang and Ren 2014). Metal recovery from different resources can be performed through pyrometallurgical, bio-hydrometallurgical and hydrometallurgical processes.

Pyrometallurgical processes are general methods for metal recovery from metal containing resources through thermal treatment for the physical and chemical transformation of the material for metals separation and recovery. Smelting, roasting, converting and refining are different methods of pyrometallurgy. Due to thermal processing steps, these methods require high energy resources and generate polluting emissions (Havlik et al. 2010). Bio-hydrometallurgical methods employ generally microorganisms for the solubilization of the metals. The bio-leaching process is usually conducted by iron- and sulfur- oxidizing microorganisms (Brierley 2008). Metal recovery through bio-hydrometallurgical methods are low cost procedures that require low energy and are highly environmental friendly, while the main disadvantage of the bio-hydrometallurgical methods is the very slow reaction kinetics of the process (Brierley 2008; Lederer and Pollmann 2022). On the other hand, hydrometallurgical metal recovery processes are those that chemical reactions are performed in aqueous or organic solutions with three main steps of leaching, purification and metal recovery (Gunarathne et al. 2022). In the hydrometallurgical processes, leaching is the initial step to extract metals e.g. from secondary resources with different reagents, such as hydrochloric acid, nitric acid, sulfuric acid, H_2O_2, thiourea, potassium iso-cyanate, potassium iodide and iodine, ferric chloride, aqua-regia, cyanides, thiosulphate etc. (Krishnan et al. 2021). In the purification step, the target metal is separated and purified by subjecting the solution to purification processes like

solvent extraction (SX), precipitation, cementation, ion exchange, distillation and filtration (Liu et al. 2013b). In the final step, the target metal can be recovered through different processes such as precipitation, gaseous reduction, electrolysis, etc. (Krishnan et al. 2021).

Hydrometallurgical metal recovery processes have many advantages over pyrometallurgical methods. The main advantages of hydrometallurgical processes are their suitability to both high and low-grade ores, and the fact that they are more environmentally and economically viable, with possibility of performing the operations in wide scale, less energy requirement, less pollution generation (specially air pollution), diverse reagent options and easier leaching methods (Binnemans et al. 2013; Yoon et al. 2014; Suja et al. 2014; Swain and Mishra 2019; Jeon et al. 2020; Krishnan et al. 2021; Gunarathne et al. 2022).

Currently for the metal recovery processes, hydrometallurgical methods are favored over pyrometallurgical methods and are developing every day. Sections 1.2.1., 1.2.2. and 1.2.3. are dedicated to detailed description of some hydrometallurgical processes involving solvent extraction, acidophilic/acid-tolerant sulfate reducing bacteria and plants aiming metal recovery.

1.2.1. Solvent extraction

Solvent extraction (SX), also known as liquid-liquid extraction is a powerful chemical technique of separation that allows recovery of metal ions from both diluted and concentrated aqueous solutions (Andersson and Reinhardt 1983). SX has been widely used on industrial scale for metal recovery from aqueous leaching solutions in the hydrometallurgical treatment of ores and secondary materials (Hedrich et al. 2018). In the hydrometallurgical industry, the SX processes use organic phases consisting of extractants diluted in solvents to specifically separate target metal ions from impure multimetallic leaching solutions, which are then stripped from the organic phase to aqueous pure solutions from which the metals can be finally recovered (Davis-Belmar et al. 2012; Ruiz et al. 2019). After extraction, the target metal is stripped from the metal-loaded organic phase by an aqueous solution, which results in a concentrated solution of the metal of interest (Figure 1.5) (Mansur et al. 2008). The achieved solution, can then be used for further refining process like electrolysis or electrowinning, crystallization, evaporation, precipitation, etc. (Dreisinger 2009).

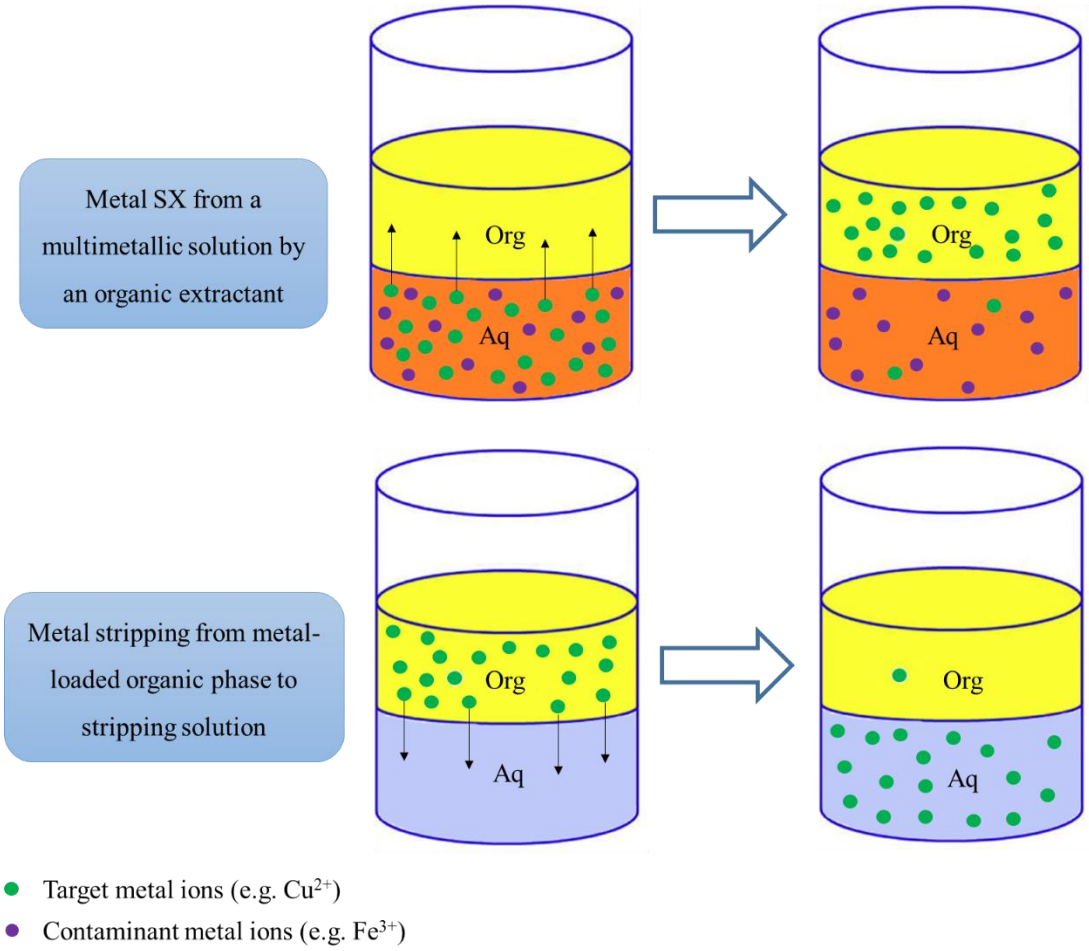

Figure 1.5. An example of SX process from a solution with Cu^{2+} as target metal and Fe^{3+} as contaminant metal.

There are many advantages in metals SX over other methods including the high separation and recovery of metals from the wastewaters/leachate with low target metal concentration, technological availability and technical solutions, high selectivity and mass transport with low reaction time (de los Ríos et al. 2010). The main negative points of SX can be pointed as the environmental hazards of the organic solvent (flammable kerosene is the most commonly used organic solvent), formation of the undesirable third phase and lack of universal technique for different metals and different matrices (Regel-Rosocka and Alguacil 2013; Lei et al. 2022).

SX process is a widely explored method of separation of metals including Cu, Zn, Fe, Cr, Co, Ni, platinum group metals (PGMs) and rare earth elements (REEs) (Mansur et al. 2008). In the next sections, SX processes and reagents developed for Cu and Zn in sulfate matrices are described in more details.

1.2.1.1. Copper solvent extraction

In Cu hydrometallurgy, hydroxyoxime extractants have been commercially used for Cu SX, mainly from sulfate solutions (Jergensen 1999; Sepúlveda et al. 2022). Chloride anions in the solution has negative effect on the Cu extraction by hydroxyoxime extractants (Shakibania et al. 2020) and solutions containing sulfate anion are favorable for Cu extraction by this type of extractants. In addition, it is known that hydroxyoxime extractants are highly selective in Cu^{2+} extraction over Fe^{3+} in low pH values (Younas et al. 2015; Ruiz et al. 2020; Nozari and Azizi 2020), however, there are reports indicating Cu^{2+} and Fe^{3+} co-extraction with some hydroxyoxime type Cu extractants (Simpson et al. 1996).

In copper extraction, an organic solvent containing a reagent as extractant with the ability of selective Cu extraction into the organic phase is subjected to a Cu bearing multimetallic leachate, that is followed by a stripping step in which the extracted Cu is transfered from the organic phase and is loaded into an acidic aqueous solution. The extraction mechanism of hydroxyoxime type extractants from the multimetallic leaching solution by the organic extractant is based on the exchange reactions of Cu cations with ionizable hydrogen atoms present on the extractant molecules, through a reversible reaction (Eq. 1.4), which results in Cu-chelate complex formation (Kordosky 1992; Alguacil and Alonso 2002; Szymanowski and Kyuchoukov 2002; Agarwal et al. 2012):

$$Cu^{2+} + 2HR \leftrightarrow CuR_2 + 2H^+ \qquad \text{Eq. 1.4}$$

where HR is the extractant and CuR_2 is the chelate complex. The equilibrium constant of this reaction is described by Ruiz et al. (2021) as in equation 1.5:

$$K = \frac{(\overline{CuR_2})(H^+)^2}{(Cu^{2+})(\overline{HR})^2} = \frac{[\overline{CuR_2}][H^+]^2}{[Cu^{2+}][\overline{HR}]^2} \times \frac{\gamma\overline{CuR_2} \times \gamma H^{+2}}{\gamma Cu^{2+} \times \gamma \overline{HR}^2} \qquad \text{Eq. 1.5}$$

In equation 1.5, round brackets are indications of the activity of reagents and products, while square brackets are related to the concentrations (molar) and γ represents the activity coefficient.

As presented in equation 1.4, through extraction reaction, formation of 1 mole of Cu chelate with the organic extractant, results in the release of 2 moles of hydrogen ions into the aqueous solution and therefore, results in a decrease in pH of the solution. Subsequently, in the stripping reaction (reversed reaction of Eq. 1.4), Cu ions are transferred into the highly acidic stripping solution and through this reaction, for each mole of Cu released to the solution, 2 moles of hydrogen are transferred into the organic extractant (Ruiz et al. 2020). After the stripping step, the organic extractant gets ready for another round of extraction. Hence, in both extraction and stripping steps, the most important variable affecting the Cu extraction at equilibrium is the acidity of the aqueous solution (Ruiz et al. 2020).

Since 1968, hydroxyoxime extractants have been widely used for Cu recovery in commercial scale (Kordosky 1992). Currently, two hydroxyoxime type extractants including ketoxime (2-hydroxy-5-nonylacetophenone oxime) and aldoxime (the 5-nonylsalicylaldoxime) are the most commonly Cu extractants used in industrial scale (Aksamitowski and Wieszczycka 2020; Nozari and Azizi 2020). Ketoxime type extractants are considered weak Cu extractants, however, demonstrate high Cu extraction efficiencies in leachates with low Cu content and pH values higher than 2 (Hein 2010). Cu stripping from these extractants is easy and requires low concentrations of acid in the stripping solution (Ruiz et al. 2021). On the other side, aldoxime type extractants are considered very strong Cu extractants that are more efficient specially in the leachates with high Cu concentrations and pH values below 1 (Aksamitowski and Wieszczycka 2020). Cu stripping from the Cu loaded aldoxime extractants is more difficult and requires strong sulfuric acid solutions for successful Cu stripping and, for this reason, pure form of these types of extractants are rarely used in industries (Ruiz et al. 2019). However, these types of extractants are the main component of commercially applied Cu extractants in combination with ketoxime or with an equilibrium modifier in different ratios to avoid the high strength of extractant. There are different commercially available mixtures of aldoxime-ketoxime Cu extractants. The most widely used extractants include LIX 984N and LIX 973N with 1:1 and 7:3 ratios of aldoxime to ketoxime. In addition, M series of Acorga extractants include a weak extractant that is referred to as Acorga

M5910, moderate strength extractant like TXIB-modified aldoxime and more strong extractant as M5640 (Ruiz et al. 2020, 2021).

In the industrial scale, Cu SX is normally operated continuously in series of countercurrent extraction and stripping series steps. A mechanical stirring mixer forms a dispersion of organic extractant and aqueous phase, which results in rapid extraction of Cu due to large interfacial contact produced by dispersion. Thereafter, two phases are separated in a settler by gravity and will be ready for the stripping, or the next stage of countercurrent extraction (Ruiz et al. 2020).

1.2.1.2. Zinc solvent extraction

Zn is one of the important endangered metals which is a crucial element for different industrial sectors and any form of life on Earth (Tolchin 2014; Reichl and Schatz 2020). Nowadays, about 30% of world's Zn production arises from the Zn recovery from secondary resources (Wang et al. 2021). Different hydrometallurgical processes for the Zn recovery from secondary resources have been described and among those, SX plays an important role in Zn separation and recovery from these sources.

Commercial Zn extractants from sulfate media are usually from organophosphorus (dialkylphosphorus acids) family and their thio-substituted analogues. These group of extractants reject anion species like fluoride and chlorides, which is determinant in Zn recovery from some secondary resources and complex ores (Deep and de Carvalho 2008). Zn complex formation and recovery with this group of extractants takes place through a pH dependent reaction (Eq. 1.6) (Cole and Sole 2003):

$$Zn^{2+}_{(aq)} + mHA_{(org)} \leftrightarrow \ ZnA_2.(m-2)HA_{(org)} + \ 2H^{+}_{(aq)} \qquad \text{Eq. 1.6}$$

In this equation, HA is the hydrogen containing extractant (acidic extractant) and *m* can be 2 and 4. In this reaction, for every mole of extracted Zn, 2 moles of H is released to the solution.

It is known that based on the extraction conditions, different metal species along with Zn can be extracted to the organophosphorus extractants (Cortina et al. 1995; Principe and Demopoulos 2004; Flett 2005; Regel-Rosocka and Wisniewski 2011). However, as instance, CYANEX 272 and D2EHPA are known for their high Zn selectivity in the presence of Ni and Co, with an easy

stripping with low concentrations of sulfuric acid (Mansur et al. 2008; Gharabaghi et al. 2013; Tanong et al. 2017; Liu et al. 2021). Different commercially used Zn extractants such as phosphoric-acid extractant (like D2EHPA (di(2-ethylhexyl)phosphoric acid)), phosphonic acid extractant (Ionquest 801), phosphinic acid extractants (CYANEX 272y and CYANEX 301y) lose their selectivity toward Zn in the presence of Fe^{3+} (Cole and Sole 2003; Principe and Demopoulos 2004; Mansur et al. 2008; Deep and de Carvalho 2008; de los Ríos et al. 2010; Long et al. 2010). Fe^{3+} is known as the most nuisance metal in Zn recovery processes, since in Zn extraction with organophosphorus extractants, Fe^{3+} is highly extracted with the formation of more stable complexes than Zn (Sinha et al. 2014). While the extracted Fe can be stripped from the CYANEX 272 and Ionquest 801 by sulfuric acid, D2EHPA will get poisoned with Fe and its stripping with sulfuric acid is not possible, while a treatment stage of Fe contaminated D2EHPA with high concentrations of HCl will be necessary (Cole and Sole 2003). D2EHPA is known for its good Zn extraction efficiency in high acidities with no pH adjustment requirements (Lupi and Pilone 2020; Noah et al. 2022). In addition, it is known that D2EHPA has high stripping efficiencies by the normal spent zinc electrolyte, while by increasing the D2EHPA concentration in the organic solvent, the extraction curves can be shifted to lower pH values (Cole and Sole 2003; Noah et al. 2022). An advantage of D2EHPA is that Fe will not be stripped from the organic phase by sulfuric acid stripping solution, which is beneficial when the concentration of Fe is very low and co-extracted traces of Fe will not contaminate the electrolyte (Cole and Sole 2003). At normal pH values of leaching solution, Cu, Ni, CO and Cd cannot be extracted by D2EHPA, while Sn, Tl, Bi and In are co-extracted (Drzazga et al. 2021). Tributyl phosphate (TBP) is another commercialized extractant with effective selectivity toward Zn over Fe^{3+} from leachates (Mansur et al. 2008). The main drawback of this extractant is the high extractant concentration requirement (80-100%) in the organic phase and the high Fe co-extraction in the leachates with very high initial Fe content (Mansur et al. 2008).

1.2.2. Sulfate reducing bacteria

Sulfate reducing bacteria (SRB) are a group of diverse anaerobic microbes, existing in different natural ecosystems and engineered environments. SRB utilize inorganic sulfate as terminal electron acceptor through dissimilatory sulfate reduction process (also referred as sulfate

respiration) for their metabolism and growth, resulting in sulfide production (LeGall and Fauque 1988; Fauque et al. 1988; Rabus et al. 2006; Muyzer and Stams 2008; Barton and Fauque 2022a). Most of the known SRB are classified into 60 genera and in at least three phyla within the domain Bacteria (*Desulfobacterota*, *Nitrospirota*, and *Firmicutes*) and two classes of the domain Archaea (*Archaeoglobi* and *Thermoproteia*) (Itoh et al. 1998; Castro et al. 2000; Mori et al. 2003; Rabus et al. 2006; Ollivier et al. 2007; Muyzer and Stams 2008; Waite et al. 2020).

1.2.2.1. Dissimilatory sulfate reduction

In dissimilatory sulfate reduction (DSR) by SRB, sulfate (SO_4^{2-}) initially is reduced into sulfite (SO_3^{2-}), which is finally converted to sulfide (S^{2-}). In the first step, $SO_4^{2-}$is activated by ATP sulfurylase enzyme, in which, the mentioned enzyme catalyzes the SO_4^{2-} binding to the ATP molecule and formation of APS (adenosine phosphosulfate) (Qian et al. 2019). Then, the SO_4^{2-} present in the APS molecule, gets reduced by APS reductase and results in SO_3^{2-} production, two electron consumption and the release of AMP (adenosine monophosphate) (Figure 1.6-a) (Qian et al. 2019).

In the second step, as presented in Figure 1.6-b, two mechanisms are described for the SO_3^{2-} conversion into S^{2-}. Based on one of the proposed mechanisms by Peck and LeGall (1982), SO_3^{2-} goes to a reduction step into HS^- by bisulfite reductase enzyme. The other pathway, referred as the trithionate pathway described by Fitz and Cypionka (1989), suggests the involvement of different enzymes including thiosulfate reductase, trithionate reductase and sulfite reductase with intermediates in the last stage like trithionate and thiosulfate. Based on this mechanism, SO_3^{2-} reduction occurs by dissimilatory sulfite reductase (DsrAB) to DsrC trisulfide (Santos et al. 2015; Anantharaman et al. 2018). Thereafter, the reduction of DsrC trisulfide is performed by DsrMKJOP complex to sulfide and DsrCr, in which DsrCr acts as physiological partner for DsrAB in the SO_3^{2-} reduction (Venceslau et al. 2014). Despite the pathway's unanswered questions, current research provides resounding evidences of DsrC and DsrAB as essential proteins in the metabolism of SRB dissimilating SO_3^{2-} to S^{2-} (Qian et al. 2019).

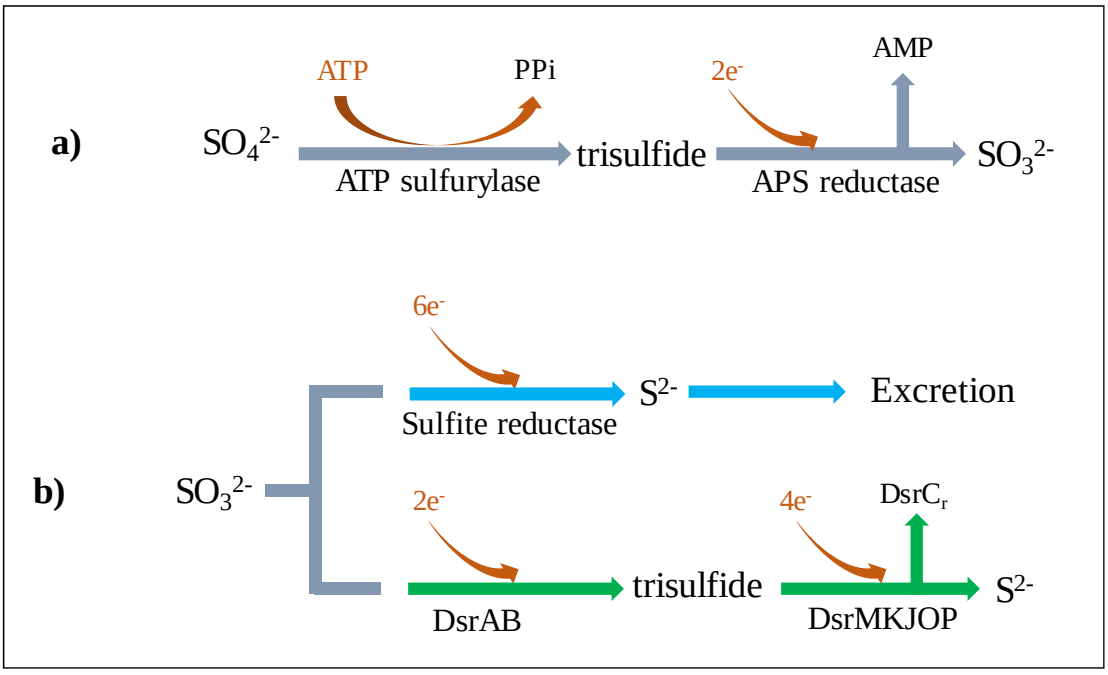

Figure 1.6. Dissimilatory sulfate reduction process to sulfide: a) sulfate activation and sulfite production and b) suggested pathways for sulfite reduction (Qian et al. 2019).

The generated sulfide reacts with the metal ions present in solution resulting in the formation of highly insoluble metal sulfides (Eq. 1.7). Through this reaction, HS^- is hydrolyzed into H^+ and S^{2-}, which will further lower the pace of pH enhancement by microbial metabolism (Sánchez-Andrea et al. 2014).

$$HS^- + Me^{2+} \rightarrow MeS \downarrow + H^+ \qquad \text{Eq. 1.7}$$

Through this reaction, different metals are effectively separated from the solution and the wastes are converted into useful products. The main advantage of application of this method in metal and sulfate bearing wastewater treatment is its high efficiency, low maintenance costs and the easy separation of the generated solids (metal sulfides) from the treated water.

1.2.2.2. SRB activity range

There are several important factors that need to be taken into consideration regarding the SRB activity including a) susceptibility to the alteration of pH, temperature, hydraulic oscillation and

substrate loading, b) high levels of sulfide during the SRB activity may have toxic effects on the SRB growth during the process and afterwards, additional oxidization process will be needed for the sulfide conversion into elemental sulfur, c) concentration of microbial groups in the reactor and the creation of symbiotic relation between them, such as SRB consortia with methanogenics, d) the duration for full mineralization of organic materials is substantially greater than for aerobic processes because of the multistage biodegradation process (Rambabu et al. 2020).

SRB usually prefer neutral pH values (6 to 8) for their optimal growth (Dworkin and Falkow 2006). They can withstand temperatures between -5 and 75 °C and can quickly adapt to temperature fluctuations (Cocos et al. 2002). However, most of the SRB are mesophiles and have an optimum temperature range of 28 to 30 °C and temperature is known to have significant effect on the metabolic rates of the bacteria (Hao et al. 2003; Virpiranta et al. 2019). In addition, mixed SRB cultures are known to be more resilient to extreme environments compared to their pure counterparts (Alexandrino et al. 2011; Carlier et al. 2020; Barton and Fauque 2022b). SRB can utilize a variety of carbon and energy sources as electron donors such as H_2, acetate, lactate, formate, ethanol, methanol, malate, butyrate, glycerol, acetaldehyde, succinate, methylated compounds, saturated hydrocarbons and amino acids (Rambabu et al. 2020). In the SRB bioreactor operations, normally AMD remediation are based on the utilization of salts mixtures and inexpensive organic materials that can be locally available like sludge, sawdust, sugarcane waste, hay, yeast extract, wine waste, manures etc. (Martins et al. 2009, 2011; Ballester et al. 2017; Hurtado et al. 2018; Carlier et al. 2019, 2020). To remove the most metal and sulfate from these mixes, optimization of these organic sources for effective microbial growth is highly crucial to maximize the removal of metal and sulfate from AMD (Kefeni et al. 2017b).

1.2.2.3. Sulfidogenic bioreactors in AMD remediation

Sulfidogenic bioreactors in AMD remediation have different advantages over other technologies including possibility of metal recovery through pH controlled differential metal precipitation (Boonstra et al. 1999), significant reduction of metals and sulfate concentrations in the effluent (Feng et al. 2000), generation of negligible potentially dangerous material, high performance and predictability (Ighalo et al. 2022). Through several years, different types of sulfidogenic bioreactors have been designed and studied for the efficient sulfate reduction and

separation/removal of metals in passive and active modes. The main privileges of active sulfidogenic bioreactors over passive methods are possibility of selective heavy metals separation and recovery, lower sulfate concentration in the effluent and predictable performance (Isosaari and Sillanpää 2017; Gopi Kiran et al. 2017), while costs of construction and operation in active mode is significantly higher than passive treatment operations (Rambabu et al. 2020).

Active reactors are normally performed in batch, semi-continuous and continuous flow modes and the continuous mode is the most commonly used mode of this type of reactors (Rambabu et al. 2020). In the active sulfidogenic reactors, SRB culture rich in sulfide is mixed with raw AMD and a part of metals are initially precipitated. Thereafter, during the SRB activity, sulfate present in the AMD is reduced to sulfide and the remaining of the metals are precipitated. In the cases where AMD does not have enough sulfate for optimum performance of the SRB system, excessive source of chemical sulfate is added to the reactor for the optimum sulfate reduction. In the processes called as Thiopaq, a separate microbial population is employed in which, sulfur oxidizing bacteria (SOB) do the conversion of the excessive sulfide into elemental sulfur (Bekmezci et al. 2011). The beneficiation from the sulfidogenic reactors in AMD remediation is gaining more attention and, depending on the main purposes, AMD remediation or AMD remediation and metal recovery, different operational designs are purposed, in which, one-stage and two-stage reactors are the most widely applied methods.

1.2.2.3.1. One-stage processes

When the purpose of the reactor is AMD remediation (but not metal recovery), so called one-stage reactor or all-in-one is more favorable, where the sulfate reduction and the precipitation of metal sulfides occur in a single stage approach (Rambabu et al. 2020) (Figure 1.7). In these reactors, pH of the AMD is initially increased by lime or other alkaline components to creat optimal pH for the neutrophilic SRB growth (pH 6 to 8). AMD chemical alkalinization has substantial operating costs, in which management of generated sludge would further increases the overall costs (Ňancucheo et al. 2017). After the neutralization step, AMD is transferred to the bioreactor (along with the substrate) and then more alkalinity is generated due to sulfide production by SRB, which enhances precipitation of metals (Martins et al. 2010). The excessive amount of sulfide can be transferred into another reactor where oxidation of sulfide occurs into elemental sulfur (Bekmezci et al. 2011).

One-stage AMD remediation processes are relatively inexpensive, however, streams with high acidity or with high concentrations of metals and sulfate, are less likely to be properly treated with their use (Rambabu et al. 2020).

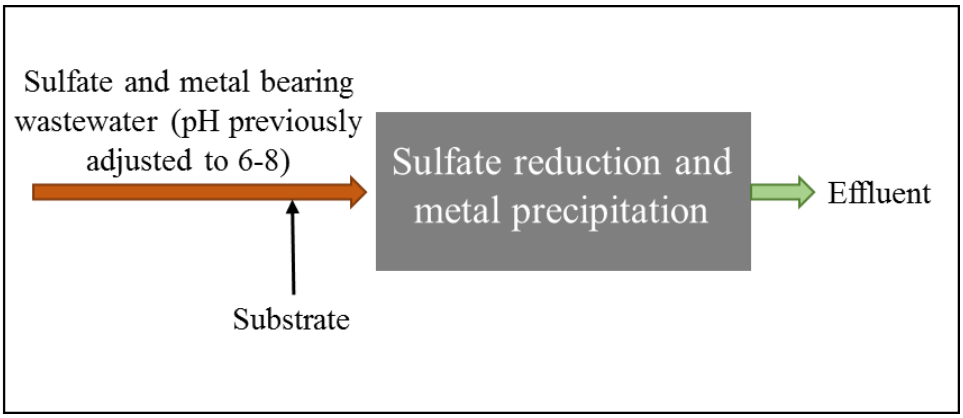

Figure 1.7. One-stage SRB bioreactor configurations in active treatment of AMD.

1.2.2.3.2. Two-stage reactors (Precipitation of metals prior to sulfate reduction)

In the cases where metal recovery is also a purpose, usually two-stage reactors are applied for differential metallic sulfide precipitation operations, where in the initial reactor, SRB reduce the sulfate and result in sulfide production, while in the second reactor, the produced sulfide from the first reactor meets the raw AMD in controlled conditions (mainly pH) (Martins et al. 2010; Rambabu et al. 2020). In the second reactor, metal sulfides are separated based on the solubility of each/group of metal sulfides (Figure 1.8) (Lewis 2010); as instance, Cu can be recovered from AMD at pH values below 2 as CuS by addition of the the previously prepared (produced in the first bioreactor) sulfide rich effluent (Figure 1.9-a) and/or by injecting the sulfide gas (Figure 1.9-b) to the second bioreactor. Thereafter, by increasing the pH to 4 and sulfide addition, Zn can be recovered as ZnS. Finally, the pH of the AMD can be adjusted to suitable pH values for the SRB consortium growth and the sulfate of the AMD will be transformed by SRB to sulfide, which would precipitate and separate the remaining metals such as Fe and Mn from the solution as sulfides or hydroxides at pH values about 7 (based on the pH dependence of metal sulfide solubilities(Lewis 2010)) (Vitor et al. 2015; Rambabu et al. 2020).

Figure 1.8.

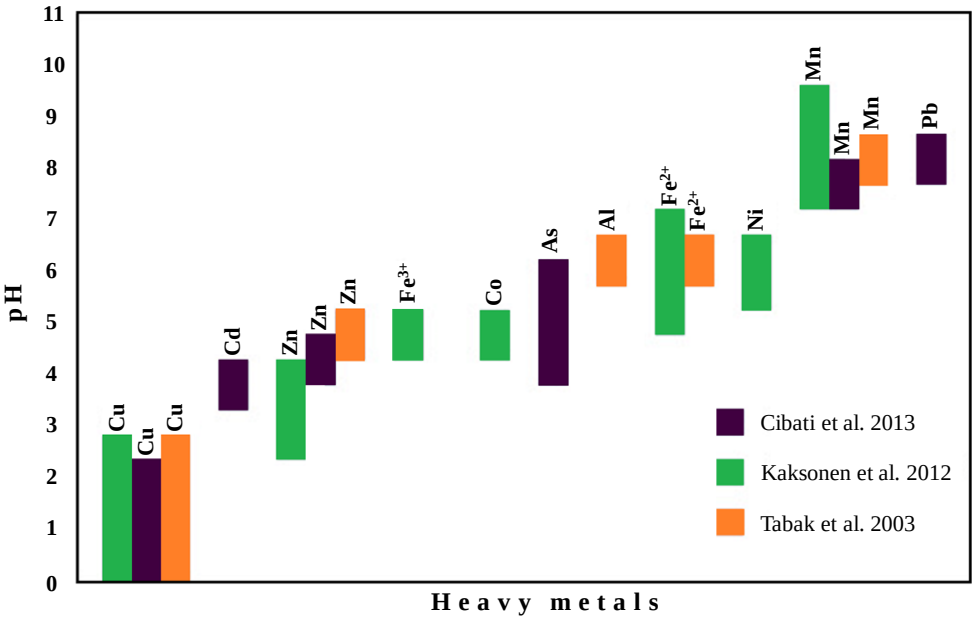

Suggested pH ranges for the selective metal sulfide precipitation from AMD (Tabak et al. 2003; Kaksonen and Sahinkaya 2012; Cibati et al. 2013).

Finally, the generated sulfide-rich effluent can be used for a new cycle of metal recovery from AMD. Another method for metal recovery from AMD by SRB reactors is conducted by performing bioreactor operations at pH values between 4 to 4.5, where Cu, Zn and Ni can be separated differentially and can then be recovered, while Fe will stay in the solution (Tabak et al. 2003; Veeken et al. 2003; Ňancucheo and Johnson 2012). In both cases, the pH values of the influent and the bioreactor is highly important in the effectiveness of the metal recovery process, due to its effect on the differential metal sulfide precipitation and also on the size and quality of the formed metal sulfide particles (Sánchez-Andrea et al. 2014).

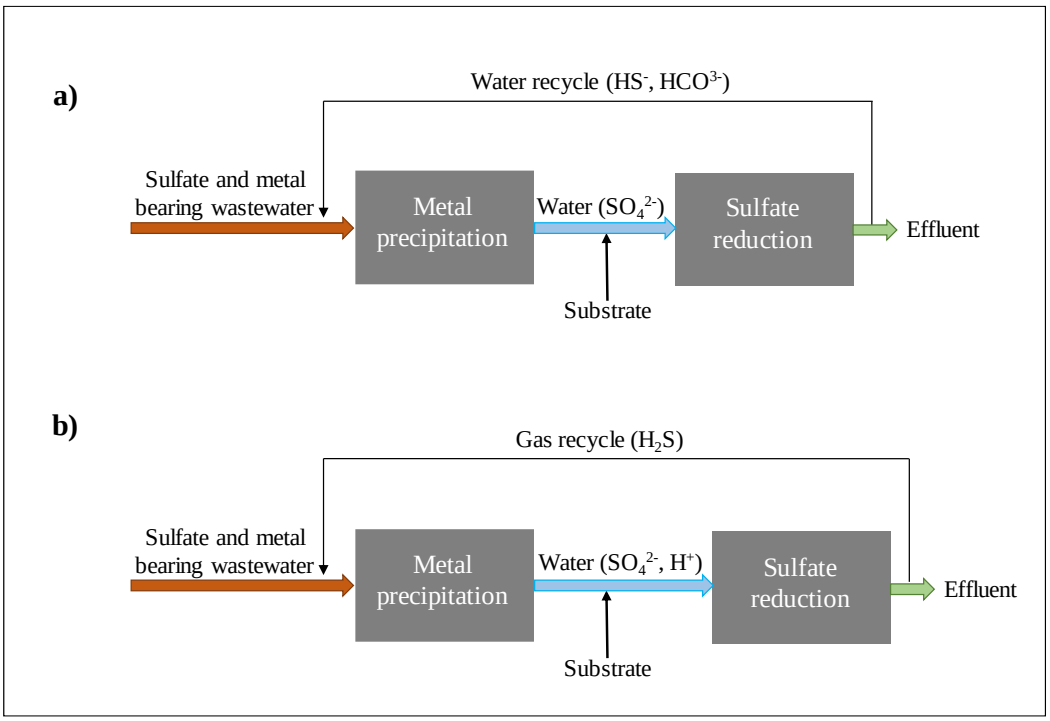

Figure 1.9. Two-stage SRB bioreactor configurations in active treatment of AMD with sulfide injection to raw AMD by the a) sulfide rich effluent and b) sulfide gas recycled from the effluent.

The operational design is also known to have direct effect on the size and settling properties of the metal sulfide particles. As instance, in the two-stage reactors, sulfide injection as gas or sulfide rich bioreactor effluent from the first reactor will suddenly increase the sulfide concentration in the raw AMD, which will result in small metal sulfide particle formation, while, in one-stage reactors, the produced sulfide by SRB, increase gradually and homogeneously, which will result in more growth of the metal sulfide crystals which will result in bigger particles and easier separation operations (Sánchez-Andrea et al. 2014). One-stage reactors are sometimes more attractive than the other design due to other the less operational costs, simple process design and avoiding the necessity of sulfide transportation and its corrosive effects.

1.2.2.4. Acidophilic/acid tolerant SRB

SRB usually prefer neutral pH values (6 to 8) for their optimal growth (Dworkin and Falkow 2006) and pH values lower than 6, significantly inhibits the microbial sulfate reduction (Dvorak et al. 1992). For this reason, the pH of the influent of the bioreactor is previously neutralized to decrease the negative effect of low pH to the SRB activity. The pH neutralization of the influent is usually incorporated by chemical alkalinization, mainly using limestone or other chemical alkaline agents such as calcium carbonate, sodium carbonate and sodium hydroxide (Estrada Rendon et al. 1999; Klein et al. 2013).

However, different studies have revealed the existence of different acidophilic/acid tolerant SRB (Tuttle et al. 1969; Hard et al. 1997; Küsel et al. 2001; Kimura et al. 2006; Church et al. 2007; Koschorreck 2008; Senko et al. 2009; Alazard et al. 2010; Sánchez-Andrea et al. 2013), with sulfate reduction potential in highly acidic AMD waters without pH control requirements. This possibility lowers the bioreactor operation costs by avoiding the neutralization step. In addition, since methanogens are more sensitive than SRBs to low pH, bioreactor operations in low pH will result in a better outcompete of SRB with methanogenic bacteria (Janssen et al. 1999; Bijmans 2008). Therefore, as a result of lower growth of methanogenic bacteria, the competition on the substrate (electron donor) is reduced and the overall growth of the SRB will be more efficient. The competition of different microbial groups on the substrate have been extensively reported in the literature (Stams et al. 2005; van Houten et al. 2006). Furthermore, the generated sulfide in low pH values is mostly in gaseous phase, that facilitates the the sulfide separation from the effluent and its application in metal precipitation (Tabak et al. 2003; Veeken et al. 2003) and/or posterior oxidation to elemental sulfur (Janssen et al. 1999).

Most of the bioreactors that are operated by acidophilic/acid tolerant SRB (aSRB), do not require pH control and due to the SRB activity and alkalinity generation, the pH of the AMD increases with the bacterial activity (Kaksonen et al. 2004; Hiibel et al. 2008, 2011; Sánchez-Andrea et al. 2012). For the metal recovery operations, highly pure metal sulfide production is vital which depends on the pH, concentrations of different metals and sulfide in the reactor (Tabak et al. 2003; Huisman et al. 2006) and many studies achieved a successful selective metal recovery through controlled pH (Bijmans 2008, 2009; Bijmans et al. 2009b, a, 2010; Ňancucheo and Johnson 2012).

1.2.2.5. Main factors influencing sulfate reduction at low pH

H^+ concentration

The H^+ concentration in a logarithmic scale results in the pH value of a solution and therefore, H^+ concentration in a solution with pH 3 is 10,000 times higher than another solution with pH 7. Low pH values will result in H^+ diffusion gradient to the cell membrane and as the pH lowers (higher H^+ concentration), more H^+ diffusion will occur and the microbial cell will need to pump H^+ to the out of the cell more actively to breakeven the H^+ diffusion force (Sánchez-Andrea et al. 2014). Therefore, in the low pH values, microbes are required to spend more energy to maintain neutral internal pH and will have lower energy for the microbial growth. However, studies reveal that sulfate reduction in lower pH values results in higher Gibbs free energy than in that of higher pH values (Bijmans 2009) and when this additional energy counterbalances the extra energy required for H^+ pumping to the out of the cell, the growth and development of aSRBs will occur. Moreover, some other mechanisms for aSRB have been reported such as ATP production by utilizing H^+ motive force, expulsion of vesicles containing H^+, etc. (Sánchez-Andrea et al. 2014).

Organic acids

It is known that organic acids have negative roles in SRB growth at low pH and their inhibitory effect is dependent on their dissociation constants in different acidities. Lactic acid for example has a pKa of 3.08 ($Ka=8.3\times10^{-4}$) and therefore, 50% of the lactate at pH 3 will be in the form of undissociated lactic acid, which can diffuse into the bacterial cells. Inside the cells (normally with higher pH), the undissociated acids get dissociated and release H^+ which will reduce the internal pH of the microbial cell and therefore, the cell will need to invest more energy to pump even more H^+ to the outside of the cell. Sánchez-Andrea et al. (2014) describe this point as the main reasons of failure in aSRB isolation with lactate as carbon source in different studies. Other non-ionic electron donors such as ethanol, methanol, glycerol, sugars and H_2 are more suitable electron donors for sulfate reduction in acidic conditions (Johnson et al. 2009; Alazard et al. 2010; Meier et al. 2012; Sánchez-Andrea et al. 2013).

In addition, some SRB oxidize organic substrates completely to CO_2 (Sánchez-Andrea et al. 2013), which are referred as complete oxidizers while some others, oxidize the organic substrate to acetate

and CO_2, which are called incomplete oxidizers. At pH values below 4.75, acetic acid is the main form of the acetate, which has high toxic effects on the most of the microbes including SRBs (Wichlacz et al. 1986; Alexander et al. 1987; Kishimoto et al. 1991). Most of the known SRB are incomplete oxidizers and in axenic cultures, acetate accumulation can have inhibitory effect on SRB, while in mixed cultures, other types of anaerobic bacteria can metabolize the released acetate by SRB and avoid its growth inhibition.

Sulfide concentration

Inhibitory effect of the sulfide on the SRB growth and activity is highly depended on the sulfide species including H_2S, HS^- and S^{2-} (Icgen and Harrison 2006). Figure 1.10 illustrates sulfide speciation across the pH range. Undissociated form of sulfide (H_2S) has inhibitory effect on the SRB growth (Colleran et al. 1995; Moosa and Harrison 2006) since this form of sulfide can diffuse into the bacterial cells (Ghose and Wiken 1955). In the neutral pH, the pKa of H_2S is 7 and therefore, through the SRB activity, similar quantities of HS^- and H_2S is produced, while almost 99% of the product is in the form of H_2S in acidic conditions (e.g. pH 5), meaning the higher inhibitory effect on the SRB growth. The diffused H_2S into the bacterial cell can react with different metal ions present in the cytoplasm and disturb the normal microbial metabolism (Madigan et al. 2000), thus may affecting the bacterial performance aiming bioremediation processes.

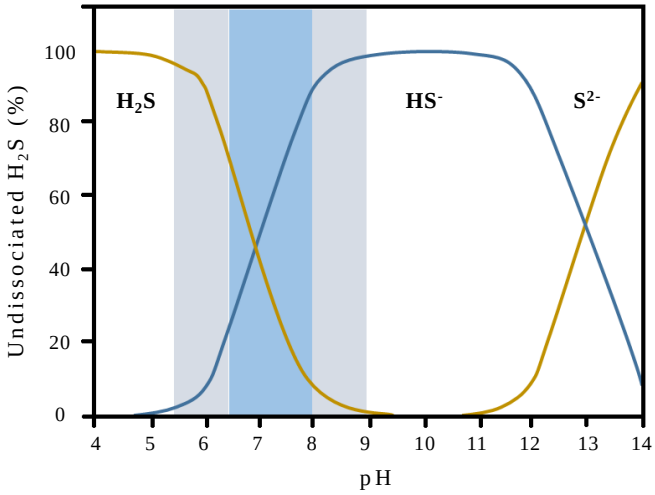

Figure 1.10. Sulfide speciation as a function of pH at 25 °C. Optimum ranges of SRB are shown in gray and blue areas (adapted from (Kaksonen and Puhakka 2007)).

A modified version of the next section was published as:

Nobahar, Amir; Carlier, Jorge Dias; Miguel, Maria Graça; Costa, Maria Clara. "A review of plant metabolites with metal interaction capacity: a green approach for industrial applications". BioMetals (2021): http://dx.doi.org/10.1007/s10534-021-00315-y

1.2.3. Plant metabolites with metal interaction capacity: a green approach for industrial applications

Plants are valuable resources for all living organisms existing on our planet and have evolved to survive in soils containing very low available metals (Morales et al. 2018), while others have lived in habitats with high heavy metal contents. As a result, they have developed strategies for metal uptake (micronutrients) and delivery from roots to different parts of the plant (González-Guerrero et al. 2016) benefiting from different active phytochemicals. They have also developed mechanisms to overcome the toxicity of heavy metals in their growing bed, which include exclusion, inactivation and organic ligands exudation (Choppala et al. 2014). These renewable resources provide raw materials and phytochemicals, notably secondary metabolites like alkaloids, flavonoids, tannins, phenolic acids, saponins, steroids, *etc*., with many different mechanisms of interaction with metals that can be used for different industrial purposes.

Plant active compounds, depending on their nature, contain polar functional groups, such as carboxyl, phenolic, hydroxyl, sulfo and amino groups that are capable of interacting with metal ions through different mechanisms such as complex/chelate formation (Mejáre and Bülow 2001; Clemens 2001; Ma et al. 2016), reduction (Sharma et al. 1998; Ma et al. 2016; Ishak et al. 2019), ion exchange (Gurung et al. 2013; Anjum et al. 2015; Li et al. 2017), sorption (Pietrobelli et al. 2009; Akpomie et al. 2015), electrostatic attraction (Yermiyahu and Kinraide 2005), covalent binding (Anjum et al. 2015), van der Waals attraction (Pietrobelli et al. 2009) and precipitation (Pietrobelli et al. 2009; Ma et al. 2016).

1.2.3.1. Plant metabolites with metal interaction potential

1.2.3.1.1. Organic acids

Organic acids are organic compounds possessing the carboxyl group (R-COOH) which has acidic characteristics usually associated to their ability to donate protons to water molecules (Brønsted-Lowry theory), in what is called dissociation reactions. Different organic acids such as citric, oxalic, malic, malonic, aconitic and tartaric acids, possess at least one carboxyl group, that after losing their proton may act as oxygen-electron donor ligands (Anjum et al. 2015), thus reacting with metals and forming complexes and chelates. Organic acids possess varying negative charges (due to dissociation of the carboxylic groups depending on the medium pH) responsible for complex formation with many different metal ions in the solutions.

It has been argued that organic acids complexation with metals plays a vital role in transporting the heavy metals from roots to shoots (Rascio and Navari-Izzo 2011). For instance, citrate has a strong metal ion chelation capacity, especially for Fe^{2+} (Clemens 2001), Al^{3+} (Ownby and Popham 1990), Ni^{2+} (Ferrero et al. 2020) and Zn^{2+} (Godbold et al. 1984). Also, there are works reporting that citrate has a high affinity for other metals like Zn, Ni, Cd, and Co (Anjum et al. 2015).

1.2.3.1.2. Amino acids

Amino acids are a type of organic acids that contain amine and carboxyl groups coupled with particular side chains for each amino acid (Nelson and Cox 2005). Amino acids and their derivatives are compounds with metal interaction capabilities, cheap and soluble in aqueous media. These features, make them an essential part in elevating plant tolerance through metal stress.

There are studies suggesting that these compounds may form five membered chelates with different metals through their amine and carboxylate groups (*N, O*-chelation) (Laurie 1995). They may also have other metal binding sites on the side chain of their molecules, making them able to interact with a variety of metals. Groups such as the imidazole ring (a planar 5-membered ring with the general formula of 1,3-C_3N_2) of histidine, the phenol ring of tyrosine, the β- and γ-carboxylate groups in glutamate and aspartate, the thiol group (R-SH) of cysteine and the thioether moiety (R-S-R) of methionine are often the important metal binding sites in amino acids (Laurie 1995).

The non-proteinogenous amino acid nicotianamine is a vital component of plant metal assimilation and homeostasis as it is a capable metal chelator; it has a key role in uptake, phloem transport and cytoplasmic distribution (Agnihotri and Seth 2019). Literature provides evidence regarding the accumulation of nicotianamine in plants upon exposure to different metals specially Zn, Cu, Fe, Ni and Cd (Irtelli et al. 2009; Mehes-Smith et al. 2013; Chen et al. 2018). The presence of six functional groups gives nicotianamine its octahedral coordination and potential for the chelation of different metals (Figure 1.11) (Rellán-Álvarez et al. 2008).

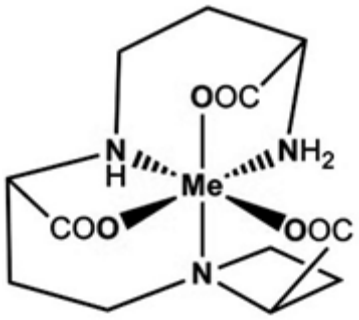

Figure 1.11. Structure of nicotamine-metal complex (Kutrowska and Szelag 2014).

1.2.3.1.3. Proteins

Proteins are large natural molecules composed of one or more chains of amino acids in a specific order. They interact with different metal ions and therefore, these interactions play an important role in biological systems. Plant waste (such as soybean, corn *etc.*) and waste from agricultural industries are often composed of protein-rich biomass, a part of which has been used as a source of peptides and amino acids. For example, calmodulin that can be found in plants like *Arabidopsis thaliana, Oryza sativa, Nicotiana tabacum, Medicago truncatula, Glycine max, etc.* (Ranty et al. 2006) is a calcium-binding protein (with two domains, each domain contains two Ca^{2+} binding sites) which is present in both apo- and holo-form in plant cells (Chin and Means 2000).

Moreover, among protein-based metal chelators, metallothioneins are an important class. Metallothioneins possess a thiol group (–SH group) being S- an electron donor ligand. They have low mass and are Cystein-rich metal-binding proteins (Cysteine (*Cys*) is a semi essential proteinogenic amino acid with a thiol side) that are distributed in prokaryotic and eukaryotic organisms and according to the arrangement of *Cys* residues are classified as Class I and II

(Cobbett and Goldsbrough 2002). All the plant metallothioneins are in Class II and typically contain two *Cys*-rich metal binding domains in carboxy- and amino- terminal regions (Cobbett and Goldsbrough 2002). Covalent binding of metal atoms involves sulfhydryl cysteine residues. The C-terminal part (the α-domain) can bind to the four divalent metal ions, while the N-terminal part of the peptide is designated as β-domain and has three binding sites for divalent metal ions (Ruttkay-Nedecky et al. 2013).

1.2.3.1.4. Alkaloids

Alkaloids are low molecular weight compounds and are generally alkaline due to the presence of a nitrogen atom in their heterocyclic ring. Indeed, the properties of alkaloids are highly affected by the precise position of N atom. The low distribution of these compounds in the living organisms is due to their negatively charged nitrogen (Pelletier 1996). Alkaloids are divided into more than 20 classes like piperidine, pyridine, pyrrolidine, tropane *etc*. (Yang and Stöckigt 2010; Debnath et al. 2018).

There are reports indicating that many alkaloids can form complexes with different metals which is the case of xanthine-based alkaloids (like caffeine) (Umaley and Aswar 2015), pyridine group alkaloids like nicotine (Fazary et al. 2017), cinchona (quinoline group) (Boratyński et al. 2019), sparteine (quinolizidine group) (Jasiewicz 2009), quinoline derivatives (DiMauro et al. 2003) and isoquinoline derivatives (like berberine) (Khan et al. 2019; Neag et al. 2018) *etc.*

1.2.3.1.5. Phenols

Phenolic compounds are mainly distinguished by the hexagonal aromatic ring bonded directly to at least one (phenol) or more (polyphenol) hydroxyl groups (-OH) and other substituents, such as methoxyl or carboxyl groups, which are responsible for the polar character of these compounds and allow their dissolution in water (Michalak 2006). They are separated into numerous diverse groups and are characterized by the number of comprised carbon atoms bonded to the main phenolic structure such as phenolic acids, flavonoids, stilbenes, coumarins, hydrolysable tannins, monolignols, lignans and lignins (Cheynier et al. 2013). Phenolic compounds are one of the most

important group of secondary metabolites synthesized by plants. They comprise 0.5- 5% of plants' dry weight (Swanson 2003) and are present in different plants and their wastes.

Phenols' functional groups provide significant capacity in scavenging free radicals, as well as hydrogen atoms or electrons donation, which is determinant for their metal ions chelating capability (Kaurinovic and Vastag 2019). However, Kulbat (2016) showed that these valuable properties of phenols can also be due to the presence of nucleophilic aromatic rings in conjunction with the occurrence of definite functional groups such as carboxyl, hydroxyl and carbonyl groups, making them able to bind to different metals (Liu et al. 2018).

1.2.3.1.6. Flavonoids

Flavonoids are derivatives of simple phenols with a general chemical structure based on 15-carbon skeleton (Figure 1.12) consisting of two phenyl rings (A and B) and a heterocyclic ring (C) (Scotti et al. 2011). In plants, the synthesis of flavonoids is reported to increase under microbial infection, injury, decrease in temperature and deficiency of nutrients (Michalak 2006). This class of phenolic compounds are extensively distributed in all plants and exist mainly in higher concentrations in photosynthesizing cells. Importantly, some flavonoids protect plants from heavy metal stress as they are proficient metal (such as Cu, Zn, Fe) chelators, avoiding creation of hydroxyl radicals through Fenton's reaction (Williams et al. 2004).

Flavonol group molecules have three main sites that can be potentially coordinated with transition metal ions including the 3-hydroxyl and the 4-carbonyl groups in the C ring, the 5-hydroxyl group of the A ring and the 4-carbonyl group in the C ring and the 3′- and 4′-hydroxyl groups of the B ring (Figure 1.12) (Rice-Evans 2004; Williams et al. 2004; Samsonowicz and Regulska 2017). Pietta (2000) suggested that the binding sites for metals in the flavonoid molecules are the 4-oxo and 5-hydroxyl groups between the A and C rings and the catechol moiety in the ring B, the 3-hydroxyl and 4-oxo groups in the heterocyclic ring C (Figure 1.12). The importance of the catechol moiety in the B ring for the Cu^{2+} chelate formation has been reported by Brown et al. (1998) as the major contributory site of copper chelation (Brown et al. 1998). Quercetin is a well-recognized compound for chelate formation and stabilization of iron ions. Due to considerably high antioxidant activity and complex formation with Cd(II) and low toxicity, sulfonic water soluble

derivatives of quercetin and morin are reported as potential candidates for detoxification of cadmium (Chlebda et al. 2010).

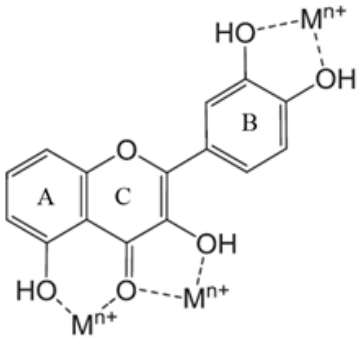

Figure 1.12. Typical metal (M) chelation sites in flavonols (Pietta 2000).

1.2.3.1.7. Tannins

Tannins are a class of phenol-containing macromolecules that are synthesized by higher plants and accumulated in their tissues (Shirmohammadli et al. 2018). They are categorized as water soluble phenolics compounds with a molar mass in the range of 300 and 3000 Da with some common features that enables the classification of these types of compounds in two main groups: hydrolysable tannins and condensed tannins (Khanbabaee and van Ree 2001). Hydrolysable tannins include gallotannines and ellagitannines that are respectively comprised of gallic acid or hexahydroxydiphenic acid esters linked to a sugar moiety, while more complicated ones can be formed by oxidative transformations that can yield macrocyclic ellagitannins (Okuda et al. 2000). Condensed tannins (nonhydrolyzable), also called procyanidins are polymers containing three ring flavanols linked with carbon-carbon bonds. Monomer units of condensed tannins are identified by the number of hydroxyl groups on the B-ring: procyanidins have a di-hydroxy B-ring, but prodelphinidins have a tri-hydroxy B-ring (Kraus et al. 2003). These monomer units might have a stereochemistry of both *cis* and *trans* C2–C3 (Schofield et al. 2001).

Tannins are cheap and widespread natural polyphenoles and are well known for their biological activities including their potential to serve as antioxidants, protein precipitants and metal chelators. Following cellulose, hemicellulose and lignin, they have the highest abundancy in plant biomass (Arbenz and Avérous 2015). Studies suggest that high tannin content can help plants to overcome the toxicity of high levels of metals in soils (Michalak 2006). Frequent catechol and galloyl

groups, allow tannins to form stable chelates with some transitional metallic ions like iron among other metals (Lee et al. 2017).

1.2.3.1.8. Saponins

Saponins are natural glycosides of steroids, or triterpenoids (sapogenins) and a carbohydrate moiety by ester or ether linkages with foaming characteristics. They are a class of non-ionic biosurfactants found in more than 500 kinds of plants with high surface activity, biodegradability, eco-friendly and low toxicity (Tang et al. 2017). They are included in a large group of protective molecules named '*phytoprotectants'* or '*phytoanticipins'* (Francis et al. 2002) and can make up to 30% of the plant's dry mass (Fenwick et al. 1991). Saponins are divided in eleven main classes including dammaranes, cycloartanes, tirucallanes, oleananes, lupanes, taraxasteranes, ursanes, lanostanes, hopanes, cucurbitanes and steroids. Because of the existence of a lipophilic aglycone (sapogenin) and hydrophilic sugar chain, saponins have amphiphilic properties resulting in foam formation (with liquid-gas phases), dispersion abilities (with liquid-solid phases) and emulsifier effect (with liquid-liquid phases) (Kregiel et al. 2017), and thus have been used as a detergent (Vincken et al. 2007).

Saponins are also reported as important agents for heavy metal removal from aqueous wastes aiming for the remediation of contaminated sites due to their ability to form chemical complexes with metals (Abed el Aziz et al. 2017). In fact, different studies describe saponins as naturally occurring chelating agents that can be used for the elimination of contaminants caused by several heavy metals including Cd, Pb, As, Cr, Cu and Zn from contaminated waters and soils (Kiliç et al. 2011). It is reported that saponins can remove and retain heavy metals from their original solutions by complex formation with their carboxyl group (Gao et al. 2012a). Saponins are very suitable compounds for remediation of very low concentrations of heavy metals due to the presence of hydroxyl and carbonyl groups in their structure (Figure 1.13) (Chen et al. 2008). During the heavy metal (like Pb, Cr, Cu, Ni, Zn) removal through different procedures such as sequential sludge washing, Huang and Liu (2013) described saponins' capability in complex formation with the mentioned heavy metals.

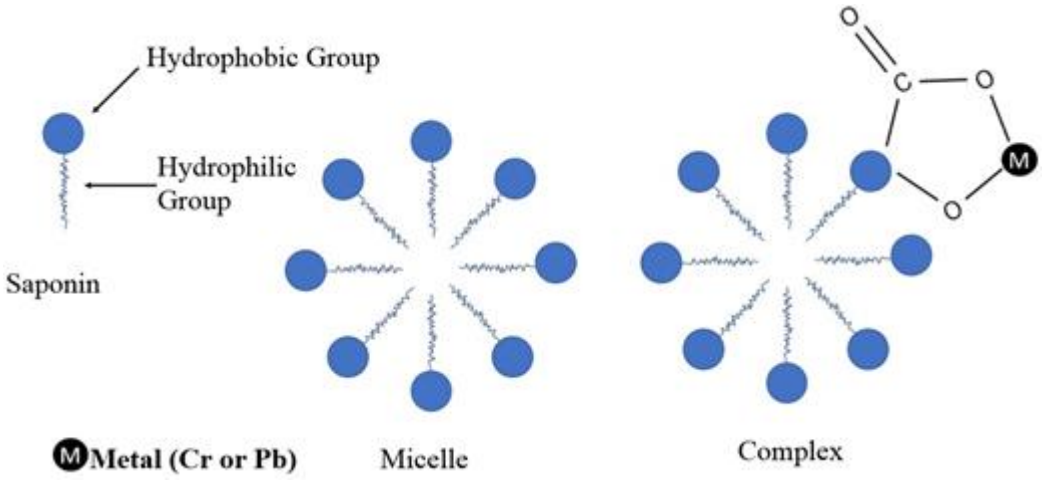

Figure 1.13. Reaction mechanism of metal ions with hydroxyl and carbonyl groups of saponins (Tang et al. 2017).

1.2.3.1.9. Polysaccharides

It is well known that polysaccharides are chain carbohydrate molecules originating from plants and therefore are abundant, renewable and biodegradable resources with the capacity to be interacted by chemical and physical mechanisms to an extensive number of molecules (Ciesielski et al. 2003). During the last few decades many studies were focused on the synthesis of cost-efficient biosorbents from the biomass of different resources (Won et al. 2014). Between different materials, plant polysaccharides (like cellulose) were found to be very suitable candidates for the adsorption of various metal ions (Gurung et al. 2014).

In their polymeric chain, polysaccharides possess several functional groups (carboxyl, hydroxyl and amino), which gives them their high and selective metal adsorption capacities (O'Connell et al. 2008; Liu et al. 2013a). Biosorption is a combination of different mechanisms including complexation, ion exchange, electrostatic attraction, adsorption, Van der Waals attraction and covalent binding (Montazer-Rahmati et al. 2011; Witek-Krowiak 2012).

Polysaccharides such as starch (Yuryev et al. 2002) and their derivatives (cyclodextrin) (Del Valle 2004) are effective natural metal adsorbent polymers. However, natural forms of polysaccharides have inadequate chemical resistance and structural strength, making them unsuitable for a direct application as biosorbents. Therefore, these natural compounds need some chemical modifications

by cross-linking and surface grafting to be more efficient biopolymeric adsorbents. For example, there are works suggesting that modifications could be applied to starch in order to make it a good adsorbent for heavy metals and dyes by the introduction of active groups like carboxylate, xanthate, amine, phosphate, acrylate and many other groups that have chelating abilities (Kweon et al. 2001).

1.2.3.2. Applications of the plant-based compounds with metal interaction ability

Strict environmental regulations applied to contaminants discharged from industrial operations are being introduced in most of the developed and developing countries (Abdel-Aty et al. 2013). Commonly used methods of metal recovery/removal from solutions and soils are frequently not economically viable and there is a lack of efficiency in metal recovery or removal especially when the concentration of metals in wastewaters is low (Hammaini et al. 2003). Beside this, the chemical compounds being used in the metal industries and then released into the environment in wastewaters could be harmful to both ecosystems and human. Thus, in recent years, more attention has been paid to biological methods for the treatment of heavy metal bearing effluents aiming to reduce their concentrations in the environment to acceptable levels. For this reason, utilization of plant-based compounds can represent a promising alternative that deserve to be explored.

1.2.3.2.1. Metal insolubilization

Chemical precipitation of metals is one of the most widely used methodologies applied for metal/heavy metal removal from different metal contaminated effluents. However, conventional methods like chemical precipitation that are being used for the treatment of wastewaters polluted with metals have some limitations (Aziz et al. 2008; Ayangbenro and Babalola 2017; Kanamarlapudi et al. 2018), such as the high costs of the reagents involved.

Plant compounds such as phenols, saponins, alkaloids *etc.* extracted from plants have potential to precipitate metals depending on their nature and this ability usually relies on complex/chelate formation and the reduction of metals by these compounds. As an example, these compounds could be utilized to precipitate or separate different metals from metal bearing solutions. For instance, McDonald et al. (1996) reports the successful precipitation of zinc and copper using tannins and

low molecular weight phenols extracted from plants. Gatew and Mersha (2015) used *Moringa stenopetala* seed powder extract to remove chromium from tannery wastewater which results in 99.86% of chromium removal. In addition, Agwaramgbo et al. (2012) described the successful lead (Pb) precipitation from an aqueous solution by aqueous extracts of some plants. In another work, Lathan et al. (2013) used some plant extracts rich in polyphenols to remove lead from a solution (with initial concentration of 1280 mg/l) and reported that spinach, tea and instant coffee extracts efficiently precipitated more than 90% of the lead in the solution. These results proved the metal bio-reduction methods assisted by plant extracts rich in phenols/polyphenols is very effective to remove and recover metals from wastewater.

Moreover, some researchers suggested that saponins could be applied as natural chelating agents to solve the problems caused by different heavy metals like Cd, Cr, Zn, Cu, As and Pb from wastewater and soil (Kiliç et al. 2011; Gonzalez-Valdez et al. 2013).

1.2.3.2.2. Synthesis of metal nanoparticles

In parallel with growing consciousness of the necessity of green chemistry and sustainability, environmentally friendly methods for biosynthesis of nanoparticles are gaining more attention. One of the methods to synthesize nanoparticles is the green synthesis technique which is ecological friendly, simple, cheap and very fast (Mittal et al. 2013). Biosynthesis of nanoparticles by plant extracts is a way to reduce the use of hazardous chemicals compounds, avoiding the environmental pollution and therefore the biological routes for synthesis of nanomaterials are getting more popular. Nanoparticles synthesized using plants are reported to be highly stable and more variable in shape and dimensions (Iravani 2011). It is shown by many research studies that plants containing high amounts of active metabolites including phenols, flavonoids, saponins, steroids, alkaloids that can act as reducing, capping or stabilizing agents, have substantial capabilities to reduce and maintain metals into their respective nanoparticles (Ajitha et al. 2016; Mystrioti et al. 2016; Sigamoney et al. 2016; Martínez-Cabanas et al. 2016; Devatha et al. 2016; Siddiqi and Husen 2017). Utilizing plant extracts as reducing, capping and stabilizing agents obviates the need to use different chemical reagents for all those purposes (El-Seedi et al. 2019).

Capping agents are biological or chemical components (Figure 1.14) that naturally restrict the reaction and the particle growth in the nanoparticles synthesis; the reduced metals form

nanostructures like nanoparticles or nanocrystals, which frequently needs to be capped appropriately to be stable, biocompatible and functional against aggregation in different biological systems (Vadlapudi 2015). Capping agents follow different mechanisms such as steric and depletion stabilization, electrostatic, hydration and van der Waals forces (Kim et al. 2004). Usually, the H-donating ability of polyphenols are associated to the metal ion reduction capacity. Due to the redox reaction that leads to the reduction of metal ions, the OH group in the reduced form of polyphenols is converted into a carbonyl group (C=O), that electrostatically stabilizes the metal nanoparticles (Figure 1.14) (El-Seedi et al. 2019). The main functional groups present in different plant compounds such as carbonyl, hydroxyl, methoxide and amino are known to bind to metal ions through electrostatic interactions and reduce them (Küünal et al. 2018). Hydroxyl groups and other substituents, such as methoxyl or carboxyl groups in the phenolic compounds are key groups for the metal chelation potential of those plant-based compounds.

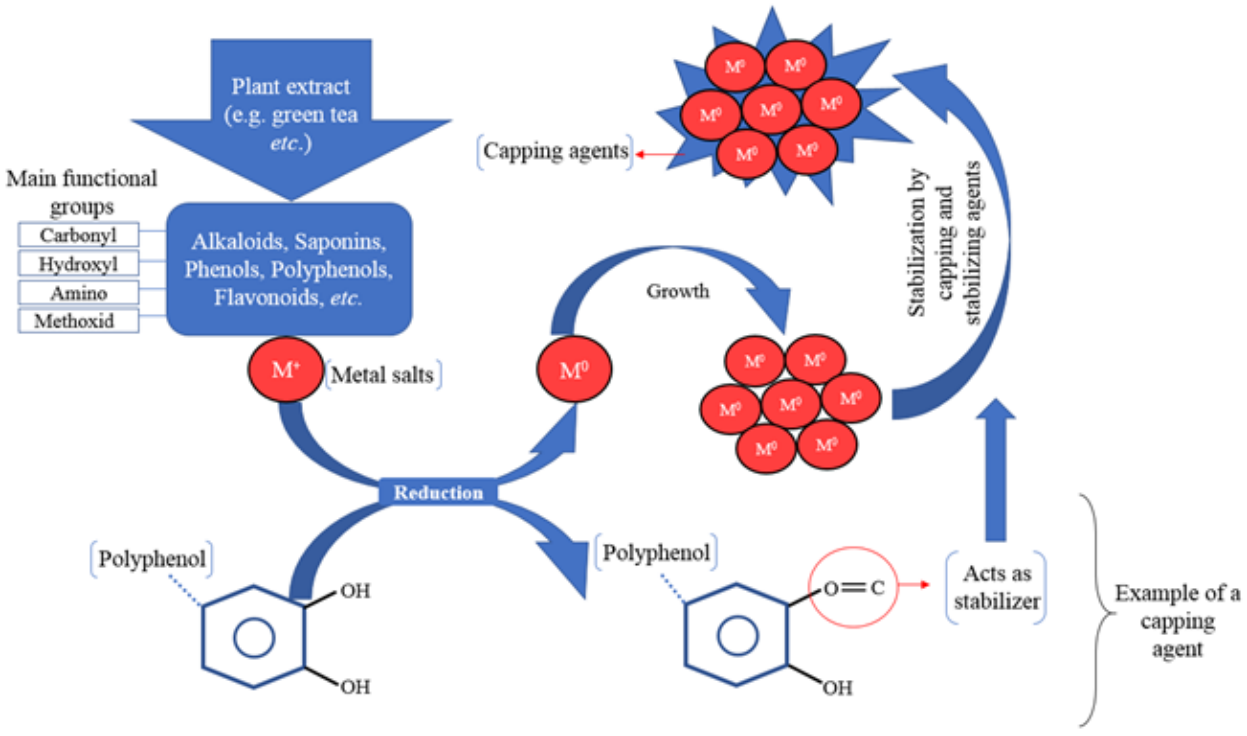

Figure 1.14. Suggested mechanism for metal reduction and metallic nanoparticle synthesis.

There are many reports regarding different metallic nanoparticle synthesis using plant compounds; for instance, *Ambrosia maritima, Callicarpa maingayi* and *Coleus aromaticus* extracts were used for the synthesis of metallic Ag nanoparticles (Shameli et al. 2012; Vanaja and Annadurai 2013; El-Seedi et al. 2016). Polyphenols extracted from the leaf of *Tabebuia berteroi* (Vellaichamy and Periakaruppan 2016) and flavonoids, tannins and phenolics extracted from *Withania coagulans* are shown as responsible compounds for the reduction of lead and iron ions into their metallic nanoparticles, so along with graphene oxide the respective nanocomposite is formed (Atarod et al. 2016). The flower extract of *Anthemis xylopoda* (Nasrollahzadeh and Sajadi 2015), leaf extract of *Ziziphus ziziphus* (Aljabali et al. 2018), extract of *Garcinia mangostana* fruit peels (Xin Lee et al. 2016) and many others were reported for Au(III) reduction into Au^0 nanoparticles. Also, Nasrollahzadeh and Sajadi (2015) used the quercetin (flavonol) rich leaf extract of *Ginkgo biloba* to reduce Cu(II) to Cu(0) nanoparticles in a two-step process, without requiring any additional agents for capping or stabilizing the particles. In another work, Pd/CuO nanoparticles were effectively synthesized by seed extracts of *Theobroma cocoa*, which contains phenolic antioxidants (Nasrollahzadeh et al. 2015).

The separation and recovery of metals from secondary wastes and resources as nanoparticles is an attractive subject for further investigations, due to benefiting extensively availabile, low cost and environmentally friendly plant material in stimulation of the circular economy, saving the primary resources with environmental viability.

1.3. **Thesis objectives, organization, and connection between charpters**

The present thesis is focused on the recovery of endangered (copper and zinc) and valuable metals (gold, platinum and palladium) from different secondary resources including:

i. Acid mine drainage (AMD) generated in São Domingos mining area were used for Cu and Zn recovery experiments. Metal recovery strategies were performed from two different AMD samples; a) AMD generated in open pit containing normal concentrations of sulfate and metals and b) from an impoundment with extremely contaminated AMD.
ii. Printed circuit boards (PCBs) were initially subjected to the leaching of base and valuable metals and thereafter, Au recovery experiments from the pregnant leaching solutions were performed.

iii. The leaching solutions of two different auto catalytic converters (ACCs) were used as a) a spent ACC from a Seat Ibiza 1995 with 23 years of use, and b) a spent ACC from a Honda Civic 1998, with 20 years of use. The leachates were provided by Professor Ana Paula Paiva from Faculdade de Ciências - Universidade de Lisboa (FCUL). Experiments targeting PGMs recovery from these leachates were performed.

Metal recovery strategies from the mentioned secondary sources were performed through a combination of innovative, environmentally and economically sustainable chemical and biological techniques mainly as:

i. Solvent extraction (SX) technique was applied employing commercial extractants including Acorga M5640, LIX 54, LIX 622, LIX 622 N, and LIX 864 for selective separation of Cu, D2EHPA and Cyanex 272 for selective Zn extraction and the synergistic mixtures of Aliquat 336 and Cyanex 272 for selective Fe extraction from extremely contaminated AMD.
ii. The potential of the bioactive compounds present in ethanolic extracts of *Rubus idaeus* L., *Cistus ladanifer* L. and *Erica andevalensis* was investigated for the recovery of the PGMs from two ACC leaching solutions and also for gold recovery from the PCBs leaching solution.
iii. The presence of acidophilic sulfate reducing bacteria (SRB) in sediments from the confluence region of AMD and municipal wastewater treatment plant effluents located in São domingos mining area, Alentejo, Portugal was investigated. Thereafter, the bioremediation potential of the obtained acidophilic/acid tolerant SRB consortium was assessed by introduction of the enriched consortium to the AMD sample at pH 4.5 (to avoid or minimize the AMD neutralization step).

1.4. **References**

Abdel -Aty AM, Ammar NS, Abdel Ghafar HH, Ali RK (2013) Biosorption of cadmium and lead from aqueous solution by fresh water alga Anabaena sphaerica biomass. J Adv Res 4:367–374. https://doi.org/10.1016/j.jare.2012.07.004

Abed el Aziz M, Ashour A, Madbouly H, et al (2017) Investigations on Green Preparation of Heavy Metal Saponin Complexes. J Water Environ Nanotechnol 2:. https://doi.org/10.22090/jwent.2017.02.005

Abreu MM, Tavares MT, Batista MJ (2008) Potential use of Erica andevalensis and Erica australis in phytoremediation of sulphide mine environments: São Domingos, Portugal. J Geochem Explor 96:210–222. https://doi.org/10.1016/j.gexplo.2007.04.007

Agarwal S, Reis MTA, Ismael MRC, et al (2012) Modeling of the Extraction Equilibrium of Copper from Sulfate Solutions with Acorga M5640. Solvent Extr Ion Exch 30:536–551. https://doi.org/10.1080/07366299.2012.670603

Agnihotri A, Seth CS (2019) Transgenic Brassicaceae. In: Transgenic Plant Technology for Remediation of Toxic Metals and Metalloids. Elsevier, pp 239–255
Agwaramgbo L, Thomas C, GrayS C, et al (2012) An Evaluation of Edible Plant Extracts for the Phytoremediation of Lead Contaminated Water. J Environ Prot 03:722–730. https://doi.org/10.4236/jep.2012.38086
Ajitha B, Ashok Kumar Reddy Y, Rajesh KM, Sreedhara Reddy P (2016) Sesbania grandiflora leaf extract assisted green synthesis of silver nanoparticles: Antimicrobial activity. Mater Today Proc 3:1977–1984. https://doi.org/10.1016/j.matpr.2016.04.099
Akcil A, Koldas S (2006) Acid Mine Drainage (AMD): causes, treatment and case studies. J Clean Prod 14:1139–1145. https://doi.org/10.1016/j.jclepro.2004.09.006
Akpomie KG, Dawodu FA, Adebowale KO (2015) Mechanism on the sorption of heavy metals from binary-solution by a low cost montmorillonite and its desorption potential. Alex Eng J 54:757–767. https://doi.org/10.1016/j.aej.2015.03.025
Aksamitowski P, Wieszczycka K (2020) Copper(II) Chelating Agents. In: Ochowiak M, Woziwodzki S, Mitkowski PT, Doligalski M (eds) Practical Aspects of Chemical Engineering. Springer International Publishing, Cham, pp 17–26
Alazard D, Joseph M, Battaglia-Brunet F, et al (2010) Desulfosporosinus acidiphilus sp. nov.: a moderately acidophilic sulfate-reducing bacterium isolated from acid mining drainage sediments: New taxa: Firmicutes (Class Clostridia, Order Clostridiales, Family Peptococcaceae). Extremophiles 14:305–312. https://doi.org/10.1007/s00792-010-0309-4
Alexander B, Leach S, Ingledew WJ (1987) The Relationship between Chemiosmotic Parameters and Sensitivity to Anions and Organic Acids in the Acidophile Thiobacillus Ferrooxidans. Microbiology 133:1171–1179. https://doi.org/10.1099/00221287-133-5-1171
Alexandrino M, Macías F, Costa R, et al (2011) A bacterial consortium isolated from an Icelandic fumarole displays exceptionally high levels of sulfate reduction and metals resistance. J Hazard Mater 187:362–370. https://doi.org/10.1016/j.jhazmat.2011.01.035
Alguacil FJ, Alonso M (2002) Recovery of Cu(II) from diluted aqueous solutions by non-dispersive solvent extraction. Revista de Metalurgia 263–269
Aljabali A, Akkam Y, Al Zoubi M, et al (2018) Synthesis of Gold Nanoparticles Using Leaf Extract of Ziziphus zizyphus and their Antimicrobial Activity. Nanomaterials 8:174. https://doi.org/10.3390/nano8030174
Álvarez-Valero AM, Pérez-López R, Matos J, et al (2008) Potential environmental impact at São Domingos mining district (Iberian Pyrite Belt, SW Iberian Peninsula): evidence from a chemical and mineralogical characterization. Environ Geol 55:1797–1809. https://doi.org/10.1007/s00254-007-1131-x
Amaral MCS, Grossi LB, Ramos RL, et al (2018) Integrated UF–NF–RO route for gold mining effluent treatment: From bench-scale to pilot-scale. Desalination 440:111–121. https://doi.org/10.1016/j.desal.2018.02.030
Anantharaman K, Hausmann B, Jungbluth SP, et al (2018) Expanded diversity of microbial groups that shape the dissimilatory sulfur cycle. ISME J 12:1715–1728. https://doi.org/10.1038/s41396-018-0078-0
Andersson SO, Reinhardt H (1983) Recovery of metals from liquid effluents, 1st edn. John Wiley & Sons
Anjum NA, Hasanuzzaman M, Hossain MA, et al (2015) Jacks of metal/metalloid chelation trade in plants; an overview. Front Plant Sci 6:. https://doi.org/10.3389/fpls.2015.00192

Arbenz A, Avérous L (2015) Chemical modification of tannins to elaborate aromatic biobased macromolecular architectures. Green Chem 17:2626–2646. https://doi.org/10.1039/C5GC00282F

Atarod M, Nasrollahzadeh M, Mohammad Sajadi S (2016) Green synthesis of Pd/RGO/Fe 3 O 4 nanocomposite using Withania coagulans leaf extract and its application as magnetically separable and reusable catalyst for the reduction of 4-nitrophenol. J Colloid Interface Sci 465:249–258. https://doi.org/10.1016/j.jcis.2015.11.060

Ayangbenro A, Babalola O (2017) A New Strategy for Heavy Metal Polluted Environments: A Review of Microbial Biosorbents. Int J Environ Res Public Health 14:94. https://doi.org/10.3390/ijerph14010094

Ayora C, Macías F, Torres E, et al (2016) Recovery of Rare Earth Elements and Yttrium from Passive-Remediation Systems of Acid Mine Drainage. Environ Sci Technol 50:8255–8262. https://doi.org/10.1021/acs.est.6b02084

Aziz HA, Adlan MohdN, Ariffin KS (2008) Heavy metals (Cd, Pb, Zn, Ni, Cu and Cr(III)) removal from water in Malaysia: Post treatment by high quality limestone. Bioresour Technol 99:1578–1583. https://doi.org/10.1016/j.biortech.2007.04.007

Baldé CP, Forti V, Gray V, et al (2017) The Global E-waste Monitor – 2017, United Nations University (UNU). International Telecommunication Union (ITU) & International Solid Waste Association (ISWA), Bonn/Geneva/Vienna

Ballester A, Castro L, Costa MC, et al (2017) Design of remediation pilot plants for the treatment of industrial metal-bearing effluents (BIOMETAL DEMO project): Lab tests. Hydrometallurgy 168:103–115. https://doi.org/10.1016/j.hydromet.2016.10.010

Barton LL, Fauque GD (2022a) Sulfate-Reducing Prokaryotes: Changing Paradigms. In: Sulfate-Reducing Bacteria and Archaea. Springer International Publishing, Cham, pp 1–55

Barton LL, Fauque GD (2022b) Ecology of Dissimilatory Sulfate Reducers: Life in Extreme Conditions and Activities of SRB. In: Sulfate-Reducing Bacteria and Archaea. Springer International Publishing, Cham, pp 463–527

Bekmezci OK, Ucar D, Kaksonen AH, Sahinkaya E (2011) Sulfidogenic biotreatment of synthetic acid mine drainage and sulfide oxidation in anaerobic baffled reactor. J Hazard Mater 189:670–676. https://doi.org/10.1016/j.jhazmat.2011.01.087

Bijmans MFM (2008) Effect of Sulfide Removal on Sulfate Reduction at pH 5 in a Hydrogen Fed Gas-Lift Bioreactor. J Microbiol Biotechnol 1809–1818. https://doi.org/10.4014/jmb.0800.109

Bijmans MFM (2009) Sulfate Reduction at pH 5 in a High-Rate Membrane Bioreactor: Reactor Performance and Microbial Community Analyses. J Microbiol Biotechnol. https://doi.org/10.4014/jmb.0809.502

Bijmans MFM, de Vries E, Yang C-H, et al (2010) Sulfate reduction at pH 4.0 for treatment of process and wastewaters. Biotechnol Prog NA-NA. https://doi.org/10.1002/btpr.400

Bijmans MFM, van Helvoort P-J, Buisman CJN, Lens PNL (2009a) Effect of the sulfide concentration on zinc bio-precipitation in a single stage sulfidogenic bioreactor at pH 5.5. Sep Purif Technol 69:243–248. https://doi.org/10.1016/j.seppur.2009.07.023

Bijmans MFM, van Helvoort P-J, Dar SA, et al (2009b) Selective recovery of nickel over iron from a nickel–iron solution using microbial sulfate reduction in a gas-lift bioreactor. Water Res 43:853–861. https://doi.org/10.1016/j.watres.2008.11.023

Binnemans K, Jones PT, Blanpain B, et al (2013) Recycling of rare earths: a critical review. J Clean Prod 51:1–22. https://doi.org/10.1016/j.jclepro.2012.12.037

Bizzo W, Figueiredo R, de Andrade V (2014) Characterization of Printed Circuit Boards for Metal and Energy Recovery after Milling and Mechanical Separation. Materials 7:4555–4566. https://doi.org/10.3390/ma7064555

Boonstra J, van Lier R, Janssen G, et al (1999) Biological treatment of acid mine drainage. In: Process Metallurgy. Elsevier, pp 559–567

Boratyński PJ, Zielińska-Błajet M, Skarżewski J (2019) Cinchona Alkaloids—Derivatives and Applications. In: The Alkaloids: Chemistry and Biology. Elsevier, pp 29–145

Bortnikova S, Gaskova O, Yurkevich N, et al (2020) Chemical Treatment of Highly Toxic Acid Mine Drainage at A Gold Mining Site in Southwestern Siberia, Russia. Minerals 10:867. https://doi.org/10.3390/min10100867

Brierley CL (2008) How will biomining be applied in future? Trans Nonferrous Met Soc China 18:1302–1310. https://doi.org/10.1016/S1003-6326(09)60002-9

Brown EJ, Khodr H, Hider CR, Rice-Evans CA (1998) Structural dependence of flavonoid interactions with Cu2+ ions: implications for their antioxidant properties. Biochem J 330:1173–1178. https://doi.org/10.1042/bj3301173

Buzzi DC, Viegas LS, Rodrigues MAS, et al (2013) Water recovery from acid mine drainage by electrodialysis. Miner Eng 40:82–89. https://doi.org/10.1016/j.mineng.2012.08.005

Carlier JD, Alexandre LM, Luís AT, Costa MC (2019) Potential of industrial by-products and wastes from the Iberian Peninsula as carbon sources for sulphate-reducing bacteria. Int J Environ Sci Technol 16:4719–4738. https://doi.org/10.1007/s13762-018-02197-z

Carlier JD, Luís AT, Alexandre LM, Costa MC (2020) Feasibility of Co-Treating Olive Mill Wastewater and Acid Mine Drainage. Mine Water Environ 39:859–880. https://doi.org/10.1007/s10230-020-00719-1

Casiot C, Egal M, Elbaz-Poulichet F, et al (2009) Hydrological and geochemical control of metals and arsenic in a Mediterranean river contaminated by acid mine drainage (the Amous River, France); preliminary assessment of impacts on fish (Leuciscus cephalus). Appl Geochem 24:787–799. https://doi.org/10.1016/j.apgeochem.2009.01.006

Casiot C, Lebrun S, Morin G, et al (2005) Sorption and redox processes controlling arsenic fate and transport in a stream impacted by acid mine drainage. Sci Total Environ 347:122–130. https://doi.org/10.1016/j.scitotenv.2004.12.039

Castro HF, Williams NH, Ogram A (2000) Phylogeny of sulfate-reducing bacteria1. FEMS Microbiol Ecol 31:1–9. https://doi.org/10.1111/j.1574-6941.2000.tb00665.x

Cayumil R, Khanna R, Rajarao R, et al (2016) Concentration of precious metals during their recovery from electronic waste. Waste Manag 57:121–130. https://doi.org/10.1016/j.wasman.2015.12.004

Chatterjee P (2008) Health costs of recycling. BMJ 337:a296–a296. https://doi.org/10.1136/bmj.a296

Chen A, Wang S, Zhang L, Peng J (2015a) Optimization of the microwave roasting extraction of palladium and rhodium from spent automobile catalysts using response surface analysis. Int J Miner Process 143:18–24. https://doi.org/10.1016/j.minpro.2015.08.007

Chen L, Hu M, Huang L, et al (2015b) Comparative metagenomic and metatranscriptomic analyses of microbial communities in acid mine drainage. ISME J 9:1579–1592. https://doi.org/10.1038/ismej.2014.245

Chen M, Huang J, Ogunseitan OA, et al (2015c) Comparative study on copper leaching from waste printed circuit boards by typical ionic liquid acids. Waste Manag 41:142–147. https://doi.org/10.1016/j.wasman.2015.03.037

Chen S, Sahito ZA, Zhang M, et al (2018) Identification and Characterization of Four Nicotianamine Synthase Genes in *Sedum alfredii* Hance. J Biobased Mater Bioenergy 12:551–559. https://doi.org/10.1166/jbmb.2018.1803

Chen S, Shen S, Cheng Y, et al (2014a) Effect of O2, H2 and CO pretreatments on leaching Rh from spent auto-catalysts with acidic sodium chlorate solution. Hydrometallurgy 144–145:69–76. https://doi.org/10.1016/j.hydromet.2014.01.018

Chen T, Yan B, Lei C, Xiao X (2014b) Pollution control and metal resource recovery for acid mine drainage. Hydrometallurgy 147–148:112–119. https://doi.org/10.1016/j.hydromet.2014.04.024

Chen W-J, Hsiao L-C, Chen KK-Y (2008) Metal desorption from copper(II)/nickel(II)-spiked kaolin as a soil component using plant-derived saponin biosurfactant. Process Biochem 43:488–498. https://doi.org/10.1016/j.procbio.2007.11.017

Cherry DS, Currie RJ, Soucek DJ, et al (2001) An integrative assessment of a watershed impacted by abandoned mined land discharges. Environ Pollut 111:377–388. https://doi.org/10.1016/S0269-7491(00)00093-2

Cheynier V, Comte G, Davies KM, et al (2013) Plant phenolics: Recent advances on their biosynthesis, genetics, and ecophysiology. Plant Physiol Biochem 72:1–20. https://doi.org/10.1016/j.plaphy.2013.05.009

Chin D, Means AR (2000) Calmodulin: a prototypical calcium sensor. Trends Cell Biol 10:322–328. https://doi.org/10.1016/S0962-8924(00)01800-6

Chlebda E, Magdalan J, Merwid-Ląd A, et al (2010) Influence of water-soluble flavonoids, quercetin-5′-sulfonic acid sodium salt and morin-5′-sulfonic acid sodium salt, on antioxidant parameters in the subacute cadmium intoxication mouse model. Exp Toxicol Pathol 62:105–108. https://doi.org/10.1016/j.etp.2009.02.118

Choppala G, Saifullah, Bolan N, et al (2014) Cellular Mechanisms in Higher Plants Governing Tolerance to Cadmium Toxicity. Crit Rev Plant Sci 33:374–391. https://doi.org/10.1080/07352689.2014.903747

Church CD, Wilkin RT, Alpers CN, et al (2007) Microbial sulfate reduction and metal attenuation in pH 4 acid mine water. Geochem Trans 8:10. https://doi.org/10.1186/1467-4866-8-10

Cibati A, Cheng KY, Morris C, et al (2013) Selective precipitation of metals from synthetic spent refinery catalyst leach liquor with biogenic H2S produced in a lactate-fed anaerobic baffled reactor. Hydrometallurgy 139:154–161. https://doi.org/10.1016/j.hydromet.2013.01.022

Ciesielski W, Lii C, Yen M-T, Tomasik P (2003) Interactions of starch with salts of metals from the transition groups. Carbohydr Polym 51:47–56. https://doi.org/10.1016/S0144-8617(02)00108-X

Clemens S (2001) Molecular mechanisms of plant metal tolerance and homeostasis. Planta 212:475–486. https://doi.org/10.1007/s004250000458

Cobbett C, Goldsbrough P (2002) P HYTOCHELATINS AND M ETALLOTHIONEINS : Roles in Heavy Metal Detoxification and Homeostasis. Annu Rev Plant Biol 53:159–182. https://doi.org/10.1146/annurev.arplant.53.100301.135154

Cocos IA, Zagury GJ, Clément B, Samson R (2002) Multiple factor design for reactive mixture selection for use in reactive walls in mine drainage treatment. Water Res 36:167–177. https://doi.org/10.1016/S0043-1354(01)00238-X

Cole PM, Sole KC (2003) Zinc solvent extraction in the process industries. Miner Process Extr Metall Rev 24:91–137. https://doi.org/10.1080/08827500306897

Colleran E, Finnegan S, Lens P (1995) Anaerobic treatment of sulphate-containing waste streams. Antonie Van Leeuwenhoek 67:29–46. https://doi.org/10.1007/BF00872194

Cortina JL, Miralles N, Sastre AM, Aguilar M (1995) Solid-liquid extraction studies of Zn(II), Cu(II) and Cd(II) from chloride media with impregnated resins containing mixtures of organophosphorus compounds immobilized on to Amberlite XAD2. Hydrometallurgy 37:301–322. https://doi.org/10.1016/0304-386X(94)00029-3

Costa MC, Duarte JC (2005) Bioremediation of Acid Mine Drainage Using Acidic Soil and Organic Wastes for Promoting Sulphate-Reducing Bacteria Activity on a Column Reactor. Water Air Soil Pollut 165:325–345. https://doi.org/10.1007/s11270-005-6914-7

Costa MC, Martins M, Jesus C, Duarte JC (2008) Treatment of Acid Mine Drainage by Sulphate-reducing Bacteria Using Low Cost Matrices. Water Air Soil Pollut 189:149–162. https://doi.org/10.1007/s11270-007-9563-1

Costa MC, Santos ES, Barros RJ, et al (2009) Wine wastes as carbon source for biological treatment of acid mine drainage. Chemosphere 75:831–836. https://doi.org/10.1016/j.chemosphere.2008.12.062

David CPC (2003) establishing the impact of acid mine drainage through metal bioaccumulation and taxa richness of benthic insects in a tropical asian stream (the philippines). Environ Toxicol Chem 22:2952. https://doi.org/10.1897/02-529

Davis-Belmar CS, Gallardo I, Demergasso C, Rautenbach G (2012) Effect of organic extractant LIX 84IC, pH and temperature changes on bioleaching microorganisms during SX treatment. Hydrometallurgy 129–130:135–139. https://doi.org/10.1016/j.hydromet.2012.09.004

de los Ríos AP, Hernández-Fernández FJ, Lozano LJ, et al (2010) Removal of Metal Ions from Aqueous Solutions by Extraction with Ionic Liquids. J Chem Eng Data 55:605–608. https://doi.org/10.1021/je9005008

Debnath B, Singh WS, Das M, et al (2018) Role of plant alkaloids on human health: A review of biological activities. Mater Today Chem 9:56–72. https://doi.org/10.1016/j.mtchem.2018.05.001

Deep A, de Carvalho JMR (2008) Review on the Recent Developments in the Solvent Extraction of Zinc. Solvent Extr Ion Exch 26:375–404. https://doi.org/10.1080/07366290802179267

Del Valle EMM (2004) Cyclodextrins and their uses: a review. Process Biochem 39:1033–1046. https://doi.org/10.1016/S0032-9592(03)00258-9

Devatha CP, Thalla AK, Katte SY (2016) Green synthesis of iron nanoparticles using different leaf extracts for treatment of domestic waste water. J Clean Prod 139:1425–1435. https://doi.org/10.1016/j.jclepro.2016.09.019

DiMauro EF, Mamai A, Kozlowski MC (2003) Synthesis, Characterization, and Metal Complexes of a Salen Ligand Containing a Quinoline Base. Organometallics 22:850–855. https://doi.org/10.1021/om0205795

Dold B (2008) Sustainability in metal mining: from exploration, over processing to mine waste management. Rev Environ Sci Biotechnol 7:275–285. https://doi.org/10.1007/s11157-008-9142-y

Dreisinger D (2009) Keynote address: Hydrometallurgical process development for complex ores and concentrates. J South Afr Inst Min Metall 109:253–271

Drzazga M, Palmowski A, Benke G, et al (2021) Recovery of germanium and indium from leaching solution of germanium dross using solvent extraction with TOA, TBP and D2EHPA. Hydrometallurgy 202:105605. https://doi.org/10.1016/j.hydromet.2021.105605

Duan H, Wang J, Huang Q (2015) Encouraging the environmentally sound management of C&D waste in China: An integrative review and research agenda. Renew Sustain Energy Rev 43:611–620. https://doi.org/10.1016/j.rser.2014.11.069

Dvorak DH, Hedin RS, Edenborn HM, McIntire PE (1992) Treatment of metal-contaminated water using bacterial sulfate reduction: Results from pilot-scale reactors. Biotechnol Bioeng 40:609–616. https://doi.org/10.1002/bit.260400508

Dworkin M, Falkow S (eds) (2006) The prokaryotes: a handbook on the biology of bacteria, 3rd ed. Springer, New York ; [London]

EDM (2019) Empresa de Desemvolvimento Mineiro, SA., Evironmental Remediation of the São Domingos Mine

Edraki M, Golding SD, Baublys KA, Lawrence MG (2005) Hydrochemistry, mineralogy and sulfur isotope geochemistry of acid mine drainage at the Mt. Morgan mine environment, Queensland, Australia. Appl Geochem 20:789–805. https://doi.org/10.1016/j.apgeochem.2004.11.004

Egiebor NO, Oni B (2007) Acid rock drainage formation and treatment: a review. Asia-Pac J Chem Eng 2:47–62. https://doi.org/10.1002/apj.57

El-Seedi HR, El-Shabasy RM, Khalifa SAM, et al (2019) Metal nanoparticles fabricated by green chemistry using natural extracts: biosynthesis, mechanisms, and applications. RSC Adv 9:24539–24559. https://doi.org/10.1039/C9RA02225B

El-Seedi HR, Zahran M, Khalifa SAM, El-Kemary M (2016) Spectral characterisation of the silver nanoparticles biosynthesised using Ambrosia maritima plant. Micro Nano Lett 11:311–314. https://doi.org/10.1049/mnl.2015.0572

Estrada Rendon CM, Amara G, Leonard P, et al (1999) Acid Mine Drainage (AMD) treatment by sulphate reducing bacteria. In: Process Metallurgy. Elsevier, pp 577–585

Estrada-Ruiz RH, Flores-Campos R, Gámez-Altamirano HA, Velarde-Sánchez EJ (2016) Separation of the metallic and non-metallic fraction from printed circuit boards employing green technology. J Hazard Mater 311:91–99. https://doi.org/10.1016/j.jhazmat.2016.02.061

Fauque G, Peck HD, Moura JJG, et al (1988) The three classes of hydrogenases from sulfate-reducing bacteria of the genus *Desulfovibrio*. FEMS Microbiol Lett 54:299–344. https://doi.org/10.1111/j.1574-6968.1988.tb02748.x

Fazary AE, Ju Y-H, Fawy KF, et al (2017) Nicotine – Metal ion interactions in solutions: Potentiometric, cyclic voltammetry investigations and quantum chemical calculations. J Chem Thermodyn 112:283–292. https://doi.org/10.1016/j.jct.2017.05.024

Feng D, Aldrich C, Tan H (2000) Treatment of acid mine water by use of heavy metal precipitation and ion exchange. Miner Eng 13:623–642. https://doi.org/10.1016/S0892-6875(00)00045-5

Fenwick GR, Price KR, Tsukamoto C, Okubo K (1991) Saponins. In: Toxic Substances in Crop Plants. Elsevier, pp 285–327

Ferreira RA, Pereira MF, Magalhães JP, et al (2021) Assessing local acid mine drainage impacts on natural regeneration-revegetation of São Domingos mine (Portugal) using a mineralogical, biochemical and textural approach. Sci Total Environ 755:142825. https://doi.org/10.1016/j.scitotenv.2020.142825

Ferrero AL, Walsh PR, Rajakaruna N (2020) The ecophysiology, genetics, adaptive significance, and biotechnology of nickel hyperaccumulation in plants. In: Physiological and Biotechnological Aspects of Extremophiles. Elsevier, pp 327–347

Ficklin WH, Plumlee GS, Smith KS, McHugh JB (1992) Geochemical classification of mine drainages and natural drainages in mineralized areas. Balkema, Rotterdam

Fischer S, Jarsjö J, Rosqvist G, Mörth C-M (2022) Catchment-scale microbial sulfate reduction (MSR) of acid mine drainage (AMD) revealed by sulfur isotopes. Environ Pollut 292:118478. https://doi.org/10.1016/j.envpol.2021.118478

Fitz RM, Cypionka H (1989) A study on electron transport-driven proton translocation in Desulfovibrio desulfuricans. Microbiol Arch 152:369–376. https://doi.org/10.1007/BF00425175

Flandinet L, Tedjar F, Ghetta V, Fouletier J (2012) Metals recovering from waste printed circuit boards (WPCBs) using molten salts. J Hazard Mater 213–214:485–490. https://doi.org/10.1016/j.jhazmat.2012.02.037

Flett DS (2005) Solvent extraction in hydrometallurgy: the role of organophosphorus extractants. J Organomet Chem 690:2426–2438. https://doi.org/10.1016/j.jorganchem.2004.11.037

Fornalczyk A, Kraszewski M, Willner J, et al (2016) Dissolution of Metal Supported Spent Auto Catalysts in Acids. Arch Metall Mater 61:233–236. https://doi.org/10.1515/amm-2016-0043

Fornalczyk A, Saternus M (2011) Catalytic converters as a source of platinum. Metalurgija 261–264

Forti V, Balde C, Kuehr R, Bel G (2020) The Global E-waste Monitor 2020: Quantities, flows and the circular economy potential. United Nations University/United Nations Institute for Training and Research, International Telecommunication Union, and International Solid Waste Association, Bonn, Geneva and Rotterdam

Francis G, Kerem Z, Makkar HPS, Becker K (2002) The biological action of saponins in animal systems: a review. Br J Nutr 88:587–605. https://doi.org/10.1079/BJN2002725

Gao L, Kano N, Sato Y, et al (2012) Behavior and Distribution of Heavy Metals Including Rare Earth Elements, Thorium, and Uranium in Sludge from Industry Water Treatment Plant and Recovery Method of Metals by Biosurfactants Application. Bioinorg Chem Appl 2012:1–11. https://doi.org/10.1155/2012/173819

Gatew S, Mersha W (2015) Tannery wastes water treatment using *Moringa Stenopetala* seed extract. Glob J Environ Sci 12:29. https://doi.org/10.4314/gjes.v12i1.4

Gharabaghi M, Irannajad M, Azadmehr AR (2013) Separation of nickel and zinc ions in a synthetic acidic solution by solvent extraction using D2EHPA and Cyanex 272. Physicochem Probl Miner Process. https://doi.org/10.5277/PPMP130121

Ghose TK, Wiken T (1955) Inhibition of Bacterial Sulphate-Reduction in Presence of Short Chain Fatty Acids. Physiol Plant 8:116–135. https://doi.org/10.1111/j.1399-3054.1955.tb08965.x

Ghosh B, Ghosh MK, Parhi P, et al (2015) Waste Printed Circuit Boards recycling: an extensive assessment of current status. J Clean Prod 94:5–19. https://doi.org/10.1016/j.jclepro.2015.02.024

Godbold DL, Horst WJ, Collins JC, et al (1984) Accumulation of zinc and Organic Acids in Roots of Zinc Tolerant and Non-tolerant Ecotypes of Deschampsia caespitosa. J Plant Physiol 116:59–69. https://doi.org/10.1016/S0176-1617(84)80084-X

González-Guerrero M, Escudero V, Saéz Á, Tejada-Jiménez M (2016) Transition Metal Transport in Plants and Associated Endosymbionts: Arbuscular Mycorrhizal Fungi and Rhizobia. Front Plant Sci 7:. https://doi.org/10.3389/fpls.2016.01088

Gonzalez-Valdez LS, Almaraz-Abarca N, Proal-Nájera JB, et al (2013) SURFACTANT PROPERTIES OF THE SAPONINS OF AgaveDurangensis, APPLICATIONON ARSENIC REMOVAL. Int J Eng App Sci 4:

Gopi Kiran M, Pakshirajan K, Das G (2017) An overview of sulfidogenic biological reactors for the simultaneous treatment of sulfate and heavy metal rich wastewater. Chem Eng Sci 158:606–620. https://doi.org/10.1016/j.ces.2016.11.002

GPGMS (2010) Guide of the Portuguese Geological and Mines Sites

Gray NF, Delaney E (2008) Comparison of benthic macroinvertebrate indices for the assessment of the impact of acid mine drainage on an Irish river below an abandoned Cu–S mine. Environ Pollut 155:31–40. https://doi.org/10.1016/j.envpol.2007.11.002

Grout JA, Levings CD (2001) Effects of acid mine drainage from an abandoned copper mine, Britannia Mines, Howe Sound, British Columbia, Canada, on transplanted blue mussels (Mytilus edulis). Mar Environ Res 51:265–288. https://doi.org/10.1016/S0141-1136(00)00104-5

Gunarathne V, Rajapaksha AU, Vithanage M, et al (2022) Hydrometallurgical processes for heavy metals recovery from industrial sludges. Crit Rev Environ Sci Technol 52:1022–1062. https://doi.org/10.1080/10643389.2020.1847949

Gupta A, Sar P (2020) Characterization and application of an anaerobic, iron and sulfate reducing bacterial culture in enhanced bioremediation of acid mine drainage impacted soil. J Environ Sci Health Part A 55:464–482. https://doi.org/10.1080/10934529.2019.1709362

Gupta V, Courtemanche J, Gunn J, Mykytczuk N (2020) Shallow floating treatment wetland capable of sulfate reduction in acid mine drainage impacted waters in a northern climate. J Environ Manage 263:110351. https://doi.org/10.1016/j.jenvman.2020.110351

Gurung M, Adhikari BB, Gao X, et al (2014) Sustainability in the Metallurgical Industry: Chemically Modified Cellulose for Selective Biosorption of Gold from Mixtures of Base Metals in Chloride Media. Ind Eng Chem Res 53:8565–8576. https://doi.org/10.1021/ie403203g

Gurung M, Adhikari BB, Morisada S, et al (2013) N-aminoguanidine modified persimmon tannin: A new sustainable material for selective adsorption, preconcentration and recovery of precious metals from acidic chloride solution. Bioresour Technol 129:108–117. https://doi.org/10.1016/j.biortech.2012.11.012

Hadi P, Gao P, Barford JP, McKay G (2013) Novel application of the nonmetallic fraction of the recycled printed circuit boards as a toxic heavy metal adsorbent. J Hazard Mater 252–253:166–170. https://doi.org/10.1016/j.jhazmat.2013.02.037

Hammaini A, González F, Ballester A, et al (2003) Simultaneous uptake of metals by activated sludge. Miner Eng 16:723–729. https://doi.org/10.1016/S0892-6875(03)00166-3

Hao OJ, Mara D, Horan N (2003) Sulphate-Reducing Bacteria. Academic Press, London, pp 459–469

Hard BC, Friedrich S, Babel W (1997) Bioremediation of acid mine water using facultatively methylotrophic metal-tolerant sulfate-reducing bacteria. Microbiol Res 152:65–73. https://doi.org/10.1016/S0944-5013(97)80025-0

Harjanto S, Cao Y, Shibayama A, et al (2006) Leaching of Pt, Pd and Rh from Automotive Catalyst Residue in Various Chloride Based Solutions. Mater Trans 47:129–135. https://doi.org/10.2320/matertrans.47.129

Havlik T, Orac D, Petranikova M, et al (2010) Leaching of copper and tin from used printed circuit boards after thermal treatment. J Hazard Mater 183:866–873. https://doi.org/10.1016/j.jhazmat.2010.07.107

Hedrich S, Kermer R, Aubel T, et al (2018) Implementation of biological and chemical techniques to recover metals from copper-rich leach solutions. Hydrometallurgy 179:274–281. https://doi.org/10.1016/j.hydromet.2018.06.012

Hein H (2010) Selecting between weak and strong extractants on acid solutions in copper SX. In: Proceedings of Copper 2010. Hamburg, Germany, pp 1925–1939

Heviánková S, Bestová I, Kyncl M (2014) The application of wood ash as a reagent in acid mine drainage treatment. Miner Eng 56:109–111. https://doi.org/10.1016/j.mineng.2013.10.032

Hiibel SR, Pereyra LP, Breazeal MVR, et al (2011) Effect of Organic Substrate on the Microbial Community Structure in Pilot-Scale Sulfate-Reducing Biochemical Reactors Treating Mine Drainage. Environ Eng Sci 28:563–572. https://doi.org/10.1089/ees.2010.0237

Hiibel SR, Pereyra LP, Inman LY, et al (2008) Microbial community analysis of two field-scale sulfate-reducing bioreactors treating mine drainage. Environ Microbiol 10:2087–2097. https://doi.org/10.1111/j.1462-2920.2008.01630.x

Huang W, Liu Z (2013) Biosorption of Cd(II)/Pb(II) from aqueous solution by biosurfactant-producing bacteria: Isotherm kinetic characteristic and mechanism studies. Colloids Surf B Biointerfaces 105:113–119. https://doi.org/10.1016/j.colsurfb.2012.12.040

Hughes AE, Haque N, Northey SA, Giddey S (2021) Platinum Group Metals: A Review of Resources, Production and Usage with a Focus on Catalysts. Resources 10:93. https://doi.org/10.3390/resources10090093

Huisman JL, Schouten G, Schultz C (2006) Biologically produced sulphide for purification of process streams, effluent treatment and recovery of metals in the metal and mining industry. Hydrometallurgy 83:106–113. https://doi.org/10.1016/j.hydromet.2006.03.017

Hunt C, Romero J, Jara J, Lagos G (2021) Copper demand forecasts and predictions of future scarcity. Resour Policy 73:102123. https://doi.org/10.1016/j.resourpol.2021.102123

Hurtado C, Viedma P, Cotoras D (2018) Design of a bioprocess for metal and sulfate removal from acid mine drainage. Hydrometallurgy 180:72–77. https://doi.org/10.1016/j.hydromet.2018.07.006

Icgen B, Harrison S (2006) Exposure to sulfide causes populations shifts in sulfate-reducing consortia. Res Microbiol 157:784–791. https://doi.org/10.1016/j.resmic.2006.04.004

Igarashi T, Herrera PS, Uchiyama H, et al (2020) The two-step neutralization ferrite-formation process for sustainable acid mine drainage treatment: Removal of copper, zinc and arsenic, and the influence of coexisting ions on ferritization. Sci Total Environ 715:136877. https://doi.org/10.1016/j.scitotenv.2020.136877

Ighalo JO, Kurniawan SB, Iwuozor KO, et al (2022) A review of treatment technologies for the mitigation of the toxic environmental effects of acid mine drainage (AMD). Process Saf Environ Prot 157:37–58. https://doi.org/10.1016/j.psep.2021.11.008

Ilyas S, Kim H (2022) Recovery of Platinum-Group Metals from an Unconventional Source of Catalytic Converter Using Pressure Cyanide Leaching and Ionic Liquid Extraction. JOM 74:1020–1026. https://doi.org/10.1007/s11837-021-05119-6

Iravani S (2011) Green synthesis of metal nanoparticles using plants. Green Chem 13:2638. https://doi.org/10.1039/c1gc15386b

Irtelli B, Petrucci WA, Navari-Izzo F (2009) Nicotianamine and histidine/proline are, respectively, the most important copper chelators in xylem sap of Brassica carinata under conditions of copper deficiency and excess. J Exp Bot 60:269–277. https://doi.org/10.1093/jxb/ern286

Ishak NAI, Kamarudin SK, Timmiati SN (2019) Green synthesis of metal and metal oxide nanoparticles via plant extracts: an overview. Mater Res Express 6:112004. https://doi.org/10.1088/2053-1591/ab4458

Isosaari P, Sillanpää M (2017) Use of Sulfate-Reducing and Bioelectrochemical Reactors for Metal Recovery from Mine Water. Sep Purif Rev 46:1–20. https://doi.org/10.1080/15422119.2016.1156548

Itoh T, Suzuki K -i., Nakase T (1998) Thermocladium modestius gen. nov., sp. nov., a new genus of rod-shaped, extremely thermophilic crenarchaeote. Int J Syst Bacteriol 48:879–887. https://doi.org/10.1099/00207713-48-3-879

Janssen AJH, Lettinga G, de Keizer A (1999) Removal of hydrogen sulphide from wastewater and waste gases by biological conversion to elemental sulphur. Colloids Surf Physicochem Eng Asp 151:389–397. https://doi.org/10.1016/S0927-7757(98)00507-X

Jasiewicz B (2009) Sparteine and α-Isosparteine Complexes with Zn(II) and Cu(II): Structure and Spectroscopic Properties. Mini-Rev Org Chem 6:275–282. https://doi.org/10.2174/157019309789371622

Jeon S, Tabelin CB, Park I, et al (2020) Ammonium thiosulfate extraction of gold from printed circuit boards (PCBs) of end-of-life mobile phones and its recovery from pregnant leach solution by cementation. Hydrometallurgy 191:105214. https://doi.org/10.1016/j.hydromet.2019.105214

Jergensen GV (ed) (1999) Copper leaching, solvent extraction, and electrowinning technology. Society for Mining, Metallurgy, and Exploration, Littleton, CO

Johnson DB (2003) Chemical and Microbiological Characteristics of Mineral Spoils and Drainage Waters at Abandoned Coal and Metal Mines. Water Air Soil Pollut Focus 3:47–66. https://doi.org/10.1023/A:1022107520836

Johnson DB, Jameson E, Rowe OF, et al (2009) Sulfidogenesis at Low pH by Acidophilic Bacteria and its Potential for the Selective Recovery of Transition Metals from Mine Waters. Adv Mater Res 71–73:693–696. https://doi.org/10.4028/www.scientific.net/AMR.71-73.693

Kaksonen AH, Plumb JJ, Franzmann PD, Puhakka JA (2004) Simple organic electron donors support diverse sulfate-reducing communities in fluidized-bed reactors treating acidic metal- and sulfate-containing wastewater. FEMS Microbiol Ecol 47:279–289. https://doi.org/10.1016/S0168-6496(03)00284-8

Kaksonen AH, Puhakka JA (2007) Sulfate Reduction Based Bioprocesses for the Treatment of Acid Mine Drainage and the Recovery of Metals. Eng Life Sci 7:541–564. https://doi.org/10.1002/elsc.200720216

Kaksonen AH, Sahinkaya E (2012) Review of sulfate reduction based bioprocesses for acid mine drainage treatment and metals recovery. pp 207–2014

Kanamarlapudi SLRK, Chintalpudi VK, Muddada S (2018) Application of Biosorption for Removal of Heavy Metals from Wastewater. In: Derco J, Vrana B (eds) Biosorption. InTech

Karim S, Ting Y-P (2021) Recycling pathways for platinum group metals from spent automotive catalyst: A review on conventional approaches and bio-processes. Resour Conserv Recycl 170:105588. https://doi.org/10.1016/j.resconrec.2021.105588

Kaur G, Couperthwaite SJ, Hatton-Jones BW, Millar GJ (2018) Alternative neutralisation materials for acid mine drainage treatment. J Water Process Eng 22:46–58. https://doi.org/10.1016/j.jwpe.2018.01.004

Kaurinovic B, Vastag D (2019) Flavonoids and Phenolic Acids as Potential Natural Antioxidants. In: Shalaby E (ed) Antioxidants. IntechOpen

Kefeni KK, Mamba BB, Msagati TAM (2017a) Magnetite and cobalt ferrite nanoparticles used as seeds for acid mine drainage treatment. J Hazard Mater 333:308–318. https://doi.org/10.1016/j.jhazmat.2017.03.054

Kefeni KK, Msagati TAM, Mamba BB (2017b) Acid mine drainage: Prevention, treatment options, and resource recovery: A review. J Clean Prod 151:475–493. https://doi.org/10.1016/j.jclepro.2017.03.082

Kefeni KK, Msagati TM, Mamba BB (2015) Synthesis and characterization of magnetic nanoparticles and study their removal capacity of metals from acid mine drainage. Chem Eng J 276:222–231. https://doi.org/10.1016/j.cej.2015.04.066

Kellner R (2008) Integrated Approach to e-Waste Recycling. In: Hester RE, Harrison RM (eds) Issues in Environmental Science and Technology. Royal Society of Chemistry, Cambridge, pp 111–160

Khan T-M, Gul NS, Lu X, et al (2019) Rhodium(III) complexes with isoquinoline derivatives as potential anticancer agents: *in vitro* and *in vivo* activity studies. Dalton Trans 48:11469–11479. https://doi.org/10.1039/C9DT01951K

Khanbabaee K, van Ree T (2001) Tannins: Classification and Definition. Nat Prod Rep 18:641–649. https://doi.org/10.1039/b101061l

Kiliç E, Font J, Puig R, et al (2011) Chromium recovery from tannery sludge with saponin and oxidative remediation. J Hazard Mater 185:456–462. https://doi.org/10.1016/j.jhazmat.2010.09.054

Kim C-H, Woo SI, Jeon SH (2000) Recovery of Platinum-Group Metals from Recycled Automotive Catalytic Converters by Carbochlorination. Ind Eng Chem Res 39:1185–1192. https://doi.org/10.1021/ie9905355

Kim KD, Han DN, Kim HT (2004) Optimization of experimental conditions based on the Taguchi robust design for the formation of nano-sized silver particles by chemical reduction method. Chem Eng J 104:55–61. https://doi.org/10.1016/j.cej.2004.08.003

Kim M, Park S, Lee J, Choubey PK (2016) A novel zero emission concept for electrogenerated chlorine leaching and its application to extraction of platinum group metals from spent automotive catalyst. Hydrometallurgy 159:19–27. https://doi.org/10.1016/j.hydromet.2015.10.030

Kimura S, Hallberg KB, Johnson DB (2006) Sulfidogenesis in Low pH (3.8–4.2) Media by a Mixed Population of Acidophilic Bacteria. Biodegradation 17:57–65. https://doi.org/10.1007/s10532-005-3050-4

Kirichenko AS, Seregin AN, Volkov AI (2014) Developing a Technology for Recycling Automotive Exhaust-Gas Catalysts. Metallurgist 58:250–255. https://doi.org/10.1007/s11015-014-9897-z

Kishimoto N, Kosako Y, Tano T (1991) Acidobacterium capsulatum gen. nov., sp. nov.: An acidophilic chemoorganotrophic bacterium containing menaquinone from acidic mineral environment. Curr Microbiol 22:1–7. https://doi.org/10.1007/BF02106205

Klein R, Tischler JS, Mühling M, Schlömann M (2013) Bioremediation of Mine Water. In: Schippers A, Glombitza F, Sand W (eds) Geobiotechnology I. Springer Berlin Heidelberg, Berlin, Heidelberg, pp 109–172

Kordosky GA (1992) Copper solvent extraction: The state of the art. JOM 44:40–45. https://doi.org/10.1007/BF03223049

Koschorreck M (2008) Microbial sulphate reduction at a low pH: Microbial sulphate reduction at low pH. FEMS Microbiol Ecol 64:329–342. https://doi.org/10.1111/j.1574-6941.2008.00482.x

Kraus TEC, Dahlgren RA, Zasoski RJ (2003) Tannins in nutrient dynamics of forest ecosystems - a review. Plant Soil 256:41–66. https://doi.org/10.1023/A:1026206511084

Kregiel D, Berlowska J, Witonska I, et al (2017) Saponin-Based, Biological-Active Surfactants from Plants. In: Najjar R (ed) Application and Characterization of Surfactants. InTech

Krishnan S, Zulkapli NS, Kamyab H, et al (2021) Current technologies for recovery of metals from industrial wastes: An overview. Environ Technol Innov 22:101525. https://doi.org/10.1016/j.eti.2021.101525

Kulbat K (2016) The role of phenolic compounds in plant resistance. 80:97–108

Küsel K, Roth U, Trinkwalter T, Peiffer S (2001) Effect of pH on the anaerobic microbial cycling of sulfur in mining-impacted freshwater lake sediments. Environ Exp Bot 46:213–223. https://doi.org/10.1016/S0098-8472(01)00103-4

Kutrowska A, Szelag M (2014) Low-molecular weight organic acids and peptides involved in the long-distance transport of trace metals. Acta Physiol Plant 36:1957–1968. https://doi.org/10.1007/s11738-014-1576-y

Küünal S, Rauwel P, Rauwel E (2018) Plant extract mediated synthesis of nanoparticles. In: Emerging Applications of Nanoparticles and Architecture Nanostructures. Elsevier, pp 411–446

Kweon D-K, Choi J-K, Kim E-K, Lim S-T (2001) Adsorption of divalent metal ions by succinylated and oxidized corn starches. Carbohydr Polym 46:171–177. https://doi.org/10.1016/S0144-8617(00)00300-3

Lathan N, Edwards S, Thomas C, Agwaramgbo L (2013) Comparative Study of Lead Removal by Extracts of Spinach, Coffee, and Tea. J Environ Prot 04:250–257. https://doi.org/10.4236/jep.2013.43029

Laurie S (1995) Handbook of metal-ligand interactions in biological fluids. Bioinorganic chemistry. Marcel Dekker, New York

Lederer FL, Pollmann K (2022) Recycling Technologies – Biohydrometallurgy. In: Holuszko ME, Kumar A, Espinosa DCR (eds) Electronic Waste, 1st edn. Wiley, pp 189–212

Lee YA, Lee J, Kim DW, et al (2017) Mussel-inspired surface functionalization of porous carbon nanosheets using polydopamine and Fe^{3+} /tannic acid layers for high-performance electrochemical capacitors. J Mater Chem A 5:25368–25377. https://doi.org/10.1039/C7TA08010G

LeGall J, Fauque G (1988) Dissimilatory reduction of sulfur compounds. Wiley N Y 587–639

Lei L, Song C, Xie X, et al (2010) Acid mine drainage and heavy metal contamination in groundwater of metal sulfide mine at arid territory (BS mine, Western Australia). Trans Nonferrous Met Soc China 20:1488–1493. https://doi.org/10.1016/S1003-6326(09)60326-5

Lei S, Sun W, Yang Y (2022) Solvent extraction for recycling of spent lithium-ion batteries. J Hazard Mater 424:127654. https://doi.org/10.1016/j.jhazmat.2021.127654

Lewis AE (2010) Review of metal sulphide precipitation. Hydrometallurgy 104:222–234. https://doi.org/10.1016/j.hydromet.2010.06.010
Li H, Dong X, da Silva EB, et al (2017) Mechanisms of metal sorption by biochars: Biochar characteristics and modifications. Chemosphere 178:466–478. https://doi.org/10.1016/j.chemosphere.2017.03.072
Liu B, Wang D, Yu G, Meng X (2013a) Adsorption of heavy metal ions, dyes and proteins by chitosan composites and derivatives — A review. J Ocean Univ China 12:500–508. https://doi.org/10.1007/s11802-013-2113-0
Liu J, Wen S, Chen Y, et al (2013b) Process Optimization and Reaction Mechanism of Removing Copper From an Fe-Rich Pyrite Cinder Using Chlorination Roasting. J Iron Steel Res Int 20:20–26. https://doi.org/10.1016/S1006-706X(13)60136-3
Liu W, Zhang J, Xu Z, et al (2021) Study on the Extraction and Separation of Zinc, Cobalt, and Nickel Using Ionquest 801, Cyanex 272, and Their Mixtures. Metals 11:401. https://doi.org/10.3390/met11030401
Liu Y-S, Chang Y-C, Chen H-H (2018) Silver nanoparticle biosynthesis by using phenolic acids in rice husk extract as reducing agents and dispersants. J Food Drug Anal 26:649–656. https://doi.org/10.1016/j.jfda.2017.07.005
Long H, Chai L, Qin W, Tang S (2010) Solvent extraction of zinc from zinc sulfate solution. J Cent South Univ Technol 17:760–764. https://doi.org/10.1007/s11771-010-0553-x
López J, Reig M, Vecino X, Cortina JL (2021) Arsenic impact on the valorisation schemes of acidic mine waters of the Iberian Pyrite Belt: Integration of selective precipitation and spiral-wound nanofiltration processes. J Hazard Mater 403:123886. https://doi.org/10.1016/j.jhazmat.2020.123886
Lupi C, Pilone D (2020) Effectiveness of saponified D2EHPA in Zn(II) selective extraction from concentrated sulphuric solutions. Miner Eng 150:106278. https://doi.org/10.1016/j.mineng.2020.106278
Ma Y, Oliveira RS, Freitas H, Zhang C (2016) Biochemical and Molecular Mechanisms of Plant-Microbe-Metal Interactions: Relevance for Phytoremediation. Front Plant Sci 7:. https://doi.org/10.3389/fpls.2016.00918
Macaskie LE, Mikheenko IP, Yong P, et al (2010) Today's wastes, tomorrow's materials for environmental protection. Hydrometallurgy 104:483–487. https://doi.org/10.1016/j.hydromet.2010.01.018
Madigan MT, Martinko JM, Parker J, Brock J (2000) Biology of Microorganisms (9th ed), Prentice Hall, Upper Saddler River, NJ (2000). 9
Manjunath N, Rajashekhar CR, Venkatesh J, et al (2021) Forensic Studies on Spent Catalytic Converters to Examine the Effect of Diesel and B100 Pongamia Biodiesel on Emissions. Sustainability 13:10729. https://doi.org/10.3390/su131910729
Mansur MB, Rocha SDF, Magalhães FS, Benedetto J dos S (2008) Selective extraction of zinc(II) over iron(II) from spent hydrochloric acid pickling effluents by liquid–liquid extraction. J Hazard Mater 150:669–678. https://doi.org/10.1016/j.jhazmat.2007.05.019
Martínez-Cabanas M, López-García M, Barriada JL, et al (2016) Green synthesis of iron oxide nanoparticles. Development of magnetic hybrid materials for efficient As(V) removal. Chem Eng J 301:83–91. https://doi.org/10.1016/j.cej.2016.04.149
Martins M, Faleiro ML, Barros RJ, et al (2009) Biological sulphate reduction using food industry wastes as carbon sources. Biodegradation 20:559–567. https://doi.org/10.1007/s10532-008-9245-8

Martins M, Faleiro ML, Silva G, et al (2011) Dynamics of bacterial community in up-flow anaerobic packed bed system for acid mine drainage treatment using wine wastes as carbon source. Int Biodeterior Biodegrad 65:78–84. https://doi.org/10.1016/j.ibiod.2010.09.005

Martins M, Santos ES, Pires C, et al (2010) Production of irrigation water from bioremediation of acid mine drainage: comparing the performance of two representative systems. J Clean Prod 18:248–253. https://doi.org/10.1016/j.jclepro.2009.10.013

McDonald M, Mila I, Scalbert A (1996) Precipitation of Metal Ions by Plant Polyphenols: Optimal Conditions and Origin of Precipitation. J Agric Food Chem 44:599–606. https://doi.org/10.1021/jf950459q

Mehes-Smith M, Nkongolo K, Cholew E (2013) Coping Mechanisms of Plants to Metal Contaminated Soil. In: Silvern S (ed) Environmental Change and Sustainability. InTech

Meier J, Piva A, Fortin D (2012) Enrichment of sulfate-reducing bacteria and resulting mineral formation in media mimicking pore water metal ion concentrations and pH conditions of acidic pit lakes. FEMS Microbiol Ecol 79:69–84. https://doi.org/10.1111/j.1574-6941.2011.01199.x

Mejáre M, Bülow L (2001) Metal-binding proteins and peptides in bioremediation and phytoremediation of heavy metals. Trends Biotechnol 19:67–73. https://doi.org/10.1016/S0167-7799(00)01534-1

Michalak A (2006) Phenolic Compounds and Their Antioxidant Activity in Plants Growing under Heavy Metal Stress. Pol J Environ Stud 15:523–530

Mittal AK, Chisti Y, Banerjee UC (2013) Synthesis of metallic nanoparticles using plant extracts. Biotechnol Adv 31:346–356. https://doi.org/10.1016/j.biotechadv.2013.01.003

Moleko-Boyce P, Makelane H, Ngayeka MZ, Tshentu ZR (2022) Recovery of Platinum Group Metals from Leach Solutions of Spent Catalytic Converters Using Custom-Made Resins. Minerals 12:361. https://doi.org/10.3390/min12030361

Montazer-Rahmati MM, Rabbani P, Abdolali A, Keshtkar AR (2011) Kinetics and equilibrium studies on biosorption of cadmium, lead, and nickel ions from aqueous solutions by intact and chemically modified brown algae. J Hazard Mater 185:401–407. https://doi.org/10.1016/j.jhazmat.2010.09.047

Montes-Atenas G (2022) Fundamentals and Practical Aspects of Acid Mine Drainage Treatment: An Overview from Mine Closure Perspective. In: Wastewater Treatment [Working Title]. IntechOpen

Moosa S, Harrison STL (2006) Product inhibition by sulphide species on biological sulphate reduction for the treatment of acid mine drainage. Hydrometallurgy 83:214–222. https://doi.org/10.1016/j.hydromet.2006.03.026

Morales F, Pavlovič A, Abadía A, Abadía J (2018) Photosynthesis in Poor Nutrient Soils, in Compacted Soils, and under Drought. In: Adams III WW, Terashima I (eds) The Leaf: A Platform for Performing Photosynthesis. Springer International Publishing, Cham, pp 371–399

Morcali MH (2020) A new approach to recover platinum-group metals from spent catalytic converters via iron matte. Resour Conserv Recycl 159:104891. https://doi.org/10.1016/j.resconrec.2020.104891

Mori K, Kim H, Kakegawa T, Hanada S (2003) A novel lineage of sulfate-reducing microorganisms: Thermodesulfobiaceae fam. nov., Thermodesulfobium narugense , gen. nov., sp. nov., a new thermophilic isolate from a hot spring. Extremophiles 7:283–290. https://doi.org/10.1007/s00792-003-0320-0

Muyzer G, Stams AJM (2008) The ecology and biotechnology of sulphate-reducing bacteria. Nat Rev Microbiol 6:441–454. https://doi.org/10.1038/nrmicro1892

Mystrioti C, Xanthopoulou TD, Tsakiridis P, et al (2016) Comparative evaluation of five plant extracts and juices for nanoiron synthesis and application for hexavalent chromium reduction. Sci Total Environ 539:105–113. https://doi.org/10.1016/j.scitotenv.2015.08.091

Naidu G, Ryu S, Thiruvenkatachari R, et al (2019) A critical review on remediation, reuse, and resource recovery from acid mine drainage. Environ Pollut 247:1110–1124. https://doi.org/10.1016/j.envpol.2019.01.085

Ňancucheo I, Bitencourt JAP, Sahoo PK, et al (2017) Recent Developments for Remediating Acidic Mine Waters Using Sulfidogenic Bacteria. BioMed Res Int 2017:1–17. https://doi.org/10.1155/2017/7256582

Ňancucheo I, Johnson DB (2012) Selective removal of transition metals from acidic mine waters by novel consortia of acidophilic sulfidogenic bacteria: Acidophilic sulfidogenic bioreactors. Microb Biotechnol 5:34–44. https://doi.org/10.1111/j.1751-7915.2011.00285.x

Nasrollahzadeh M, Mohammad Sajadi S (2015) Green synthesis of copper nanoparticles using Ginkgo biloba L. leaf extract and their catalytic activity for the Huisgen [3+2] cycloaddition of azides and alkynes at room temperature. J Colloid Interface Sci 457:141–147. https://doi.org/10.1016/j.jcis.2015.07.004

Nasrollahzadeh M, Sajadi SM (2015) Preparation of Au nanoparticles by Anthemis xylopoda flowers aqueous extract and their application for alkyne/aldehyde/amine A ^{3} -type coupling reactions. RSC Adv 5:46240–46246. https://doi.org/10.1039/C5RA08927A

Nasrollahzadeh M, Sajadi SM, Rostami-Vartooni A, Bagherzadeh M (2015) Green synthesis of Pd/CuO nanoparticles by Theobroma cacao L. seeds extract and their catalytic performance for the reduction of 4-nitrophenol and phosphine-free Heck coupling reaction under aerobic conditions. J Colloid Interface Sci 448:106–113. https://doi.org/10.1016/j.jcis.2015.02.009

Neag MA, Mocan A, Echeverría J, et al (2018) Berberine: Botanical Occurrence, Traditional Uses, Extraction Methods, and Relevance in Cardiovascular, Metabolic, Hepatic, and Renal Disorders. Front Pharmacol 9:557. https://doi.org/10.3389/fphar.2018.00557

Nelson DL, Cox MM (2005) Lehninger principles of biochemistry, 4th ed. W.H. Freeman, New York

Nieto JM, Sarmiento AM, Olías M, et al (2007) Acid mine drainage pollution in the Tinto and Odiel rivers (Iberian Pyrite Belt, SW Spain) and bioavailability of the transported metals to the Huelva Estuary. Environ Int 33:445–455. https://doi.org/10.1016/j.envint.2006.11.010

Noah NFM, Othman N, Kahar INS, Suliman SS (2022) Potential use of synergist D2EHPA/Cyanex 302 in kerosene system for reactive extraction: Zinc recovery and organic phase regeneration. Chem Eng Process - Process Intensif 176:108976. https://doi.org/10.1016/j.cep.2022.108976

Nogueira CA, Paiva AP, Oliveira PC, et al (2014) Oxidative leaching process with cupric ion in hydrochloric acid media for recovery of Pd and Rh from spent catalytic converters. J Hazard Mater 278:82–90. https://doi.org/10.1016/j.jhazmat.2014.05.099

Nordstrom DK, Blowes DW, Ptacek CJ (2015) Hydrogeochemistry and microbiology of mine drainage: An update. Appl Geochem 57:3–16. https://doi.org/10.1016/j.apgeochem.2015.02.008

Nozari I, Azizi A (2020) An Investigation into the Extraction Behavior of Copper from Sulfate Leach Liquor Using Acorga M5640 Extractant: Mechanism, Equilibrium, and Thermodynamics. Min Metall Explor 37:1673–1680. https://doi.org/10.1007/s42461-020-00280-z

O'Connell DW, Birkinshaw C, O'Dwyer TF (2008) Heavy metal adsorbents prepared from the modification of cellulose: A review. Bioresour Technol 99:6709–6724. https://doi.org/10.1016/j.biortech.2008.01.036

Okuda T, Yoshida T, Hatano T (2000) Correlation of oxidative transformations of hydrolyzable tannins and plant evolution. Phytochemistry 55:513–529. https://doi.org/10.1016/S0031-9422(00)00232-6

Ollivier B, Cayol JL, Fauque G (2007) Sulphate-reducing bacteria from oil fields environments and deep-sea hydrothermal vents. Camb Univ Press Camb 305–328

Ownby JD, Popham HR (1990) Citrate Reverses the Inhibition of Wheat Root Growth Caused by Aluminum. J Plant Physiol 135:588–591. https://doi.org/10.1016/S0176-1617(11)80641-3

Paiva AP, Piedras FV, Rodrigues PG, Nogueira CA (2022) Hydrometallurgical recovery of platinum-group metals from spent auto-catalysts – Focus on leaching and solvent extraction. Sep Purif Technol 286:120474. https://doi.org/10.1016/j.seppur.2022.120474

Palanisamy MM, Kandasamy K (2020) Comparative studies on bentonite clay and peanut shell carbon recovering heavy metals from printed circuit boards. J Ceram Process Res 21:75–85. https://doi.org/10.36410/JCPR.2020.21.1.75

Park I, Tabelin CB, Jeon S, et al (2019) A review of recent strategies for acid mine drainage prevention and mine tailings recycling. Chemosphere 219:588–606. https://doi.org/10.1016/j.chemosphere.2018.11.053

Peck M, LeGall J (1982) Biochemistry of dissimilatory sulphate reduction. Philos Trans R Soc Lond B Biol Sci 298:443–466. https://doi.org/10.1098/rstb.1982.0091

Pelletier SW (ed) (1996) Alkaloids: chemical and biological perspectives. Vol. 11: ... Wiley, New York

Pérez-López R, Álvarez-Valero AM, Nieto JM, et al (2008) Use of sequential extraction procedure for assessing the environmental impact at regional scale of the São Domingos Mine (Iberian Pyrite Belt). Appl Geochem 23:3452–3463. https://doi.org/10.1016/j.apgeochem.2008.08.005

Pietrobelli JMT de A, Módenes AN, Fagundes-Klen MR, Espinoza-Quiñones FR (2009) Cadmium, Copper and Zinc Biosorption Study by Non-Living Egeria densa Biomass. Water Air Soil Pollut 202:385–392. https://doi.org/10.1007/s11270-009-9987-x

Pietta P-G (2000) Flavonoids as Antioxidants. J Nat Prod 63:1035–1042. https://doi.org/10.1021/np9904509

Pino L, Beltran E, Schwarz A, et al (2020) Optimization of nanofiltration for treatment of acid mine drainage and copper recovery by solvent extraction. Hydrometallurgy 195:105361. https://doi.org/10.1016/j.hydromet.2020.105361

Plumlee GS, Smith KS, Montour MR, et al (1999) Geologic controls on the composition of natural waters and mine waters draining diverse mineral-deposit types. In: The environmental geochemistry of mineral deposits, Part B: case studies and research topics. Society of Economic Geologists, Littleton., pp 373–432

Pozo G, Pongy S, Keller J, et al (2017) A novel bioelectrochemical system for chemical-free permanent treatment of acid mine drainage. Water Res 126:411–420. https://doi.org/10.1016/j.watres.2017.09.058

Pozo-Antonio S, Puente-Luna I, Lagüela-López S, Veiga-Ríos M (2014) Techniques to correct and prevent acid mine drainage: A review. DYNA 81:73. https://doi.org/10.15446/dyna.v81n186.38436

Principe F, Demopoulos GP (2004) Comparative study of iron(III) separation from zinc sulphate–sulphuric acid solutions using the organophosphorus extractants, OPAP and D2EHPA: Part I: Extraction. Hydrometallurgy 74:93–102. https://doi.org/10.1016/j.hydromet.2004.01.004

Qian Z, Tianwei H, Mackey HR, et al (2019) Recent advances in dissimilatory sulfate reduction: From metabolic study to application. Water Res 150:162–181. https://doi.org/10.1016/j.watres.2018.11.018

Rabus R, Hansen TA, Widdel F (2006) Dissimilatory Sulfate- and Sulfur-Reducing Prokaryotes. In: Dworkin M, Falkow S, Rosenberg E, et al. (eds) The Prokaryotes. Springer New York, New York, NY, pp 659–768

Raffa CM, Chiampo F, Shanthakumar S (2021) Remediation of Metal/Metalloid-Polluted Soils: A Short Review. Appl Sci 11:4134. https://doi.org/10.3390/app11094134

Rambabu K, Banat F, Pham QM, et al (2020) Biological remediation of acid mine drainage: Review of past trends and current outlook. Environ Sci Ecotechnology 2:100024. https://doi.org/10.1016/j.ese.2020.100024

Ranty B, Aldon D, Galaud J-P (2006) Plant Calmodulins and Calmodulin-Related Proteins: Multifaceted Relays to Decode Calcium Signals. Plant Signal Behav 1:96–104. https://doi.org/10.4161/psb.1.3.2998

Rascio N, Navari-Izzo F (2011) Heavy metal hyperaccumulating plants: How and why do they do it? And what makes them so interesting? Plant Sci 180:169–181. https://doi.org/10.1016/j.plantsci.2010.08.016

Raskin I, Kumar PN, Dushenkov S, Salt DE (1994) Bioconcentration of heavy metals by plants. Curr Opin Biotechnol 5:285–290. https://doi.org/10.1016/0958-1669(94)90030-2

Regel-Rosocka M, Alguacil FJ (2013) Recent trends in metals extraction. Rev Metal 49:292–316. https://doi.org/10.3989/revmetalm.1344

Regel-Rosocka M, Wisniewski M (2011) Selective removal of zinc(II) from spent pickling solutions in the presence of iron ions with phosphonium ionic liquid Cyphos IL 101. Hydrometallurgy 110:85–90. https://doi.org/10.1016/j.hydromet.2011.08.012

Reichl C, Schatz M (2020) World Mining Data. Vienna

Rellán-Álvarez R, Abadía J, Álvarez-Fernández A (2008) Formation of metal-nicotianamine complexes as affected by pH, ligand exchange with citrate and metal exchange. A study by electrospray ionization time-of-flight mass spectrometry. Rapid Commun Mass Spectrom 22:1553–1562. https://doi.org/10.1002/rcm.3523

Rice-Evans C (2004) Flavonoids and isoflavones: absorption, metabolism, and bioactivity. Free Radic Biol Med 36:827–828. https://doi.org/10.1016/j.freeradbiomed.2003.12.012

Rooyen M, Staden PJ (2020) Deriving Value from Acid Mine Drainage. In: Fosso-Kankeu E, Wolkersdorfer C, Burgess J (eds) Recovery of Byproducts from Acid Mine Drainage Treatment, 1st edn. Wiley, pp 235–261

Ruiz MC, González I, Rodriguez V, Padilla R (2019) Solvent Extraction of Copper from Sulfate–Chloride Solutions Using LIX 84-IC and LIX 860-IC. Miner Process Extr Metall Rev 1–8. https://doi.org/10.1080/08827508.2019.1647839

Ruiz MC, González I, Rodriguez V, Padilla R (2021) Solvent Extraction of Copper from Sulfate–Chloride Solutions Using LIX 84-IC and LIX 860-IC. Miner Process Extr Metall Rev 42:1–8. https://doi.org/10.1080/08827508.2019.1647839

Ruiz MC, Risso J, Seguel J, Padilla R (2020) Solvent extraction of copper from sulfate-chloride solutions using mixed and modified hydroxyoxime extractants. Miner Eng 146:106109. https://doi.org/10.1016/j.mineng.2019.106109

Ruttkay-Nedecky B, Nejdl L, Gumulec J, et al (2013) The Role of Metallothionein in Oxidative Stress. Int J Mol Sci 14:6044–6066. https://doi.org/10.3390/ijms14036044

Saguru C, Ndlovu S, Moropeng D (2018) A review of recent studies into hydrometallurgical methods for recovering PGMs from used catalytic converters. Hydrometallurgy 182:44–56. https://doi.org/10.1016/j.hydromet.2018.10.012

Samsonowicz M, Regulska E (2017) Spectroscopic study of molecular structure, antioxidant activity and biological effects of metal hydroxyflavonol complexes. Spectrochim Acta A Mol Biomol Spectrosc 173:757–771. https://doi.org/10.1016/j.saa.2016.10.031

Sánchez-Andrea I, Sanz JL, Bijmans MFM, Stams AJM (2014) Sulfate reduction at low pH to remediate acid mine drainage. J Hazard Mater 269:98–109. https://doi.org/10.1016/j.jhazmat.2013.12.032

Sánchez-Andrea I, Stams AJM, Amils R, Sanz JL (2013) Enrichment and isolation of acidophilic sulfate-reducing bacteria from Tinto River sediments: Acidophilic SRB from Tinto River. Environ Microbiol Rep n/a-n/a. https://doi.org/10.1111/1758-2229.12066

Sánchez-Andrea I, Triana D, Sanz JL (2012) Bioremediation of acid mine drainage coupled with domestic wastewater treatment. Water Sci Technol 66:2425–2431. https://doi.org/10.2166/wst.2012.477

Santos AA, Venceslau SS, Grein F, et al (2015) A protein trisulfide couples dissimilatory sulfate reduction to energy conservation. Science 350:1541–1545. https://doi.org/10.1126/science.aad3558

Schipper BW, Lin H-C, Meloni MA, et al (2018) Estimating global copper demand until 2100 with regression and stock dynamics. Resour Conserv Recycl 132:28–36. https://doi.org/10.1016/j.resconrec.2018.01.004

Schofield P, Mbugua DM, Pell AN (2001) Analysis of condensed tannins: a review. Anim Feed Sci Technol 91:21–40. https://doi.org/10.1016/S0377-8401(01)00228-0

Scotti L, Fernandes MB, Muramatsu E, et al (2011) 13C NMR spectral data and molecular descriptors to predict the antioxidant activity of flavonoids. Braz J Pharm Sci 47:241–249. https://doi.org/10.1590/S1984-82502011000200005

Senko JM, Zhang G, McDonough JT, et al (2009) Metal Reduction at Low pH by a *Desulfosporosinus* species: Implications for the Biological Treatment of Acidic Mine Drainage. Geomicrobiol J 26:71–82. https://doi.org/10.1080/01490450802660193

Seo EY, Cheong YW, Yim GJ, et al (2017) Recovery of Fe, Al and Mn in acid coal mine drainage by sequential selective precipitation with control of pH. CATENA 148:11–16. https://doi.org/10.1016/j.catena.2016.07.022

Sepúlveda R, Toro N, Hernández P, et al (2022) Solvent Extraction of Metal Ions from Synthetic Copper Leaching Solution Using R4NCy. Metals 12:1053. https://doi.org/10.3390/met12061053

Shakibania S, Mahmoudi A, Mokmeli M, Rashchi F (2020) The effect of chloride ions on copper solvent extraction from sulfate-chloride medium using LIX 984N. Miner Eng 156:106498. https://doi.org/10.1016/j.mineng.2020.106498

Shameli K, Bin Ahmad M, Jaffar Al-Mulla EA, et al (2012) Green Biosynthesis of Silver Nanoparticles Using Callicarpa maingayi Stem Bark Extraction. Molecules 17:8506–8517. https://doi.org/10.3390/molecules17078506

Sharma P, Kumar S, Pandey A (2021) Bioremediated techniques for remediation of metal pollutants using metagenomics approaches: A review. J Environ Chem Eng 9:105684. https://doi.org/10.1016/j.jece.2021.105684

Sharma SS, Schat H, Vooijs R (1998) In vitro alleviation of heavy metal-induced enzyme inhibition by proline. Phytochemistry 49:1531–1535. https://doi.org/10.1016/S0031-9422(98)00282-9

Shirmohammadli Y, Efhamisisi D, Pizzi A (2018) Tannins as a sustainable raw material for green chemistry: A review. Ind Crops Prod 126:316–332. https://doi.org/10.1016/j.indcrop.2018.10.034

Shuey SA, Vildal EE, Taylor PR (2005) Pyrometallurgical processing of electronic waste. march st. Louis, MO, pp 67–70

Siddiqi KS, Husen A (2017) Recent advances in plant-mediated engineered gold nanoparticles and their application in biological system. J Trace Elem Med Biol 40:10–23. https://doi.org/10.1016/j.jtemb.2016.11.012

Sigamoney M, Shaik S, Govender P, et al (2016) African leafy vegetables as bio-factories for silver nanoparticles: A case study on Amaranthus dubius C Mart. Ex Thell. South Afr J Bot 103:230–240. https://doi.org/10.1016/j.sajb.2015.08.022

Simpson J, Navarro P, Alguacil FJ (1996) Iron(III) extraction by LIX 860 and its influence on copper(II) extraction from sulphuric solutions. Hydrometallurgy 42:13–20

Singer PC, Stumm W (1970) Acidic Mine Drainage: The Rate-Determining Step. Science 167:1121–1123. https://doi.org/10.1126/science.167.3921.1121

Sinha MK, Sahu SK, Meshram P, Pandey BD (2014) Solvent extraction and separation of zinc and iron from spent pickle liquor. Hydrometallurgy 147–148:103–111. https://doi.org/10.1016/j.hydromet.2014.05.006

Skousen J, Zipper CE, Rose A, et al (2017) Review of Passive Systems for Acid Mine Drainage Treatment. Mine Water Environ 36:133–153. https://doi.org/10.1007/s10230-016-0417-1

Skousen JG, Ziemkiewicz PF, McDonald LM (2019) Acid mine drainage formation, control and treatment: Approaches and strategies. Extr Ind Soc 6:241–249. https://doi.org/10.1016/j.exis.2018.09.008

Soucek DJ, Cherry DS, Currie RJ, et al (2000) Laboratory to field validation in an integrative assessment of an acid mine drainage-impacted watershed. Environ Toxicol Chem 19:1036–1043. https://doi.org/10.1002/etc.5620190433

Sracek O, Choquette M, Gélinas P, et al (2004) Geochemical characterization of acid mine drainage from a waste rock pile, Mine Doyon, Québec, Canada. J Contam Hydrol 69:45–71. https://doi.org/10.1016/S0169-7722(03)00150-5

Stams AJM, Plugge CM, de Bok FAM, et al (2005) Metabolic interactions in methanogenic and sulfate-reducing bioreactors. Water Sci Technol 52:13–20. https://doi.org/10.2166/wst.2005.0493

Suja E, Nancharaiah YV, Venugopalan VP (2014) Biogenic nanopalladium production by self-immobilized granular biomass: Application for contaminant remediation. Water Res 65:395–401. https://doi.org/10.1016/j.watres.2014.08.005

Sverdrup HU, Ragnarsdottir KV (2016) A system dynamics model for platinum group metal supply, market price, depletion of extractable amounts, ore grade, recycling and stocks-in-

use. Resour Conserv Recycl 114:130–152. https://doi.org/10.1016/j.resconrec.2016.07.011
Swain N, Mishra S (2019) A review on the recovery and separation of rare earths and transition metals from secondary resources. J Clean Prod 220:884–898. https://doi.org/10.1016/j.jclepro.2019.02.094
Swanson (2003) Tannins and Polyphenols. Encycl Food Sci Nut 5729–5733
Szałatkiewicz J (2014) Metals content in printed circuit board waste. Polish J Environm Studies 23:2365–2369
Szymanowski J, Kyuchoukov G (2002) Extraction of Copper(II) from Chloride Systems with Individual and Mixed Extractants. Can Metall Q 41:399–408. https://doi.org/10.1179/cmq.2002.41.4.399
Tabak HH, Scharp R, Burckle J, et al (2003) Advances in biotreatment of acid mine drainage and biorecovery of metals: 1.Metal precipitation for recovery and recycle. Biodegradation 14:423–436. https://doi.org/10.1023/A:1027332902740
Tabelin CB, Corpuz RD, Igarashi T, et al (2019) Hematite-catalysed scorodite formation as a novel arsenic immobilisation strategy under ambient conditions. Chemosphere 233:946–953. https://doi.org/10.1016/j.chemosphere.2019.06.020
Tabelin CB, Veerawattananun S, Ito M, et al (2017) Pyrite oxidation in the presence of hematite and alumina: I. Batch leaching experiments and kinetic modeling calculations. Sci Total Environ 580:687–698. https://doi.org/10.1016/j.scitotenv.2016.12.015
Tang J, He J, Liu T, Xin X (2017) Removal of heavy metals with sequential sludge washing techniques using saponin: optimization conditions, kinetics, removal effectiveness, binding intensity, mobility and mechanism. RSC Adv 7:33385–33401. https://doi.org/10.1039/C7RA04284A
Tanong K, Tran L-H, Mercier G, Blais J-F (2017) Recovery of Zn (II), Mn (II), Cd (II) and Ni (II) from the unsorted spent batteries using solvent extraction, electrodeposition and precipitation methods. J Clean Prod 148:233–244. https://doi.org/10.1016/j.jclepro.2017.01.158
Tolchin AC (2014) 2012 Minerals Yearbook-Zinc
Tolonen E-T, Sarpola A, Hu T, et al (2014) Acid mine drainage treatment using by-products from quicklime manufacturing as neutralization chemicals. Chemosphere 117:419–424. https://doi.org/10.1016/j.chemosphere.2014.07.090
Tomiyama S, Igarashi T, Tabelin CB, et al (2019) Acid mine drainage sources and hydrogeochemistry at the Yatani mine, Yamagata, Japan: A geochemical and isotopic study. J Contam Hydrol 225:103502. https://doi.org/10.1016/j.jconhyd.2019.103502
Tuttle JH, Dugan PR, Macmillan CB, Randles CI (1969) Microbial Dissimilatory Sulfur Cycle in Acid Mine Water. J Bacteriol 97:594–602. https://doi.org/10.1128/jb.97.2.594-602.1969
Umaley K, Aswar A (2015) Molecular Interaction Study of Caffeine with Metal Ions in Aqueous Solution through Internal Pressure. IJCPS 4:244–250
UNDESA UN Department of Economic and Social Affairs (2015) Population Division World Population Prospects: The 2015 Revision
Upadhyay AK, Lee J, Kim E, et al (2013) Leaching of platinum group metals (PGMs) from spent automotive catalyst using electro-generated chlorine in HCl solution: Leaching of platinum group metals from spent automotive catalyst. J Chem Technol Biotechnol n/a-n/a. https://doi.org/10.1002/jctb.4057
Vadlapudi V (2015) Novel Capping Agents for Nanomaterials. Eur J App Sci 7:297–301

van Houten BHGW, Roest K, Tzeneva VA, et al (2006) Occurrence of methanogenesis during start-up of a full-scale synthesis gas-fed reactor treating sulfate and metal-rich wastewater. Water Res 40:553–560. https://doi.org/10.1016/j.watres.2005.12.004

Vanaja M, Annadurai G (2013) Coleus aromaticus leaf extract mediated synthesis of silver nanoparticles and its bactericidal activity. Appl Nanosci 3:217–223. https://doi.org/10.1007/s13204-012-0121-9

Varun Kumar T, Balaji S, Mohan K, Hari Gautham K (2015) Performance of magnetic fuel induction technology to reduce the exhaust emission. ARPN Journal of Engineering and Applied Sciences 10:

Veeken AHM, Akoto L, Hulshoff Pol LW, Weijma J (2003) Control of the sulfide (S2−) concentration for optimal zinc removal by sulfide precipitation in a continuously stirred tank reactor. Water Res 37:3709–3717. https://doi.org/10.1016/S0043-1354(03)00262-8

Vellaichamy B, Periakaruppan P (2016) Silver nanoparticle-embedded RGO-nanosponge for superior catalytic activity towards 4-nitrophenol reduction. RSC Adv 6:88837–88845. https://doi.org/10.1039/C6RA19834A

Venceslau S, Stockdreher Y, Dahl C, Pereira I (2014) Bacterial heterodisulfide" DsrC is a key protein in dissimilatory sulfur metabolism. Biochim Biophys Acta Bioenerg 1837:1148–1164. https://doi.org/10.1016/j.bbabio.2014.03.007

Vincken J-P, Heng L, de Groot A, Gruppen H (2007) Saponins, classification and occurrence in the plant kingdom. Phytochemistry 68:275–297. https://doi.org/10.1016/j.phytochem.2006.10.008

Virpiranta H, Taskila S, Leiviskä T, et al (2019) Development of a process for microbial sulfate reduction in cold mining waters – Cold acclimation of bacterial consortia from an Arctic mining district. Environ Pollut 252:281–288. https://doi.org/10.1016/j.envpol.2019.05.087

Vitor G, Palma TC, Vieira B, et al (2015) Start-up, adjustment and long-term performance of a two-stage bioremediation process, treating real acid mine drainage, coupled with biosynthesis of ZnS nanoparticles and ZnS/TiO2 nanocomposites. Miner Eng 75:85–93. https://doi.org/10.1016/j.mineng.2014.12.003

Waite DW, Chuvochina M, Pelikan C, et al (2020) Proposal to reclassify the proteobacterial classes Deltaproteobacteria and Oligoflexia, and the phylum Thermodesulfobacteria into four phyla reflecting major functional capabilities. Int J Syst Evol Microbiol 70:5972–6016. https://doi.org/10.1099/ijsem.0.004213

Wang H, Ren ZJ (2014) Bioelectrochemical metal recovery from wastewater: A review. Water Res 66:219–232. https://doi.org/10.1016/j.watres.2014.08.013

Wang J, Zhang Y, Cui K, et al (2021) Pyrometallurgical recovery of zinc and valuable metals from electric arc furnace dust – A review. J Clean Prod 298:126788. https://doi.org/10.1016/j.jclepro.2021.126788

Watari T, Nansai K, Nakajima K (2021) Major metals demand, supply, and environmental impacts to 2100: A critical review. Resour Conserv Recycl 164:105107. https://doi.org/10.1016/j.resconrec.2020.105107

Wichlacz PL, Unz RF, Langworthy TA (1986) Acidiphilium angustum sp. nov., Acidiphilium facilis sp. nov., and Acidiphilium rubrum sp. nov.: Acidophilic Heterotrophic Bacteria Isolated from Acidic Coal Mine Drainage. Int J Syst Bacteriol 36:197–201. https://doi.org/10.1099/00207713-36-2-197

Williams RJ, Spencer JPE, Rice-Evans C (2004) Flavonoids: antioxidants or signalling molecules? Free Radic Biol Med 36:838–849. https://doi.org/10.1016/j.freeradbiomed.2004.01.001

Willner J, Kaduková J, Fornalczyk A, et al (2015) Possibilities Of Metals Extracton From Spent Metallic Automotive Catalytic Converters By Using Biometallurgical Method. Arch Metall Mater 60:1877–1880. https://doi.org/10.1515/amm-2015-0320

Winterbourn M (2000) Aluminium and iron burdens of aquatic biota in New Zealand streams contaminated by acid mine drainage: effects of trophic level. Sci Total Environ 254:45–54. https://doi.org/10.1016/S0048-9697(00)00437-X

Witek-Krowiak A (2012) Analysis of temperature-dependent biosorption of Cu2+ ions on sunflower hulls: Kinetics, equilibrium and mechanism of the process. Chem Eng J 192:13–20. https://doi.org/10.1016/j.cej.2012.03.075

Won SW, Kotte P, Wei W, et al (2014) Biosorbents for recovery of precious metals. Bioresour Technol 160:203–212. https://doi.org/10.1016/j.biortech.2014.01.121

Xin Lee K, Shameli K, Miyake M, et al (2016) Green Synthesis of Gold Nanoparticles Using Aqueous Extract of *Garcinia mangostana* Fruit Peels. J Nanomater 2016:1–7. https://doi.org/10.1155/2016/8489094

Yakoumis I, Panou M, Moschovi AM, Panias D (2021) Recovery of platinum group metals from spent automotive catalysts: A review. Clean Eng Technol 3:100112. https://doi.org/10.1016/j.clet.2021.100112

Yang J, Wang H, Zhang G, et al (2019) Recycling organics from non-metallic fraction of waste printed circuit boards by a novel conical surface triboelectric separator. Resour Conserv Recycl 146:264–269. https://doi.org/10.1016/j.resconrec.2019.03.008

Yang JE, Kim HJ, Ok Y-S, et al (2007) Treatment of abandoned coal mine discharged waters using lime wastes. Geosci J 11:111–114. https://doi.org/10.1007/BF02913923

Yang L, Stöckigt J (2010) Trends for diverse production strategies of plant medicinal alkaloids. Nat Prod Rep 27:1469. https://doi.org/10.1039/c005378c

Yermiyahu U, Kinraide TB (2005) Binding and electrostatic attraction of trace elements to plant root surfaces. In: Biogeochemistry of Trace Elements in the Rhizosphere. Elsevier, pp 365–389

Yoon H-S, Kim C-J, Chung KW, et al (2014) Leaching kinetics of neodymium in sulfuric acid of rare earth elements (REE) slag concentrated by pyrometallurgy from magnetite ore. Korean J Chem Eng 31:1766–1772. https://doi.org/10.1007/s11814-014-0078-3

Younas M, Druon-Bocquet S, Romero J, Sanchez J (2015) Experimental and Theoretical Investigation of Distribution Equilibria and Kinetics of Copper(II) Extraction with LIX 84 I and TFA. Sep Sci Technol 50:1523–1531. https://doi.org/10.1080/01496395.2014.978943

Yuryev VP, Cesàro A, Bergthaller WJ (eds) (2002) Starch and starch containing origins: structure, properties, and new technologies. Nova Science Publishers, New York

Zeng X, Li J, Liu L (2015) Solving spent lithium-ion battery problems in China: Opportunities and challenges. Renew Sustain Energy Rev 52:1759–1767. https://doi.org/10.1016/j.rser.2015.08.014

Zhao Y, Wen X, Li B, Tao D (2004) Recovery of copper from waste printed circuit boards. Min Metall Explor 21:99–102. https://doi.org/10.1007/BF03403310

CHAPTER 2

A New Application of Solvent Extraction to Separate Copper from Extreme Acid Mine Drainage Producing Solutions for Electrochemical and Biological Recovery Processes

A New Application of Solvent Extraction to Separate Copper from Extreme Acid Mine Drainage Producing Solutions for Electrochemical and Biological Recovery Processes A modified version of this chapter was published as:

A modified version of this chapter was published as:

Nobahar, Amir; Bejiga Melka, Alemu; Pusta, Alexandra; Lourenço, João Paulo; Carlier, Jorge Daniel Dias; Costa, Maria Clara (2022) A new application of SX to extreme AMD producing copper solutions suitable for electrochemical and biological recovery processes". Mine Water and the Environment: https://doi.org/10.1007/s10230-022-00858-7

Nobahar, Amir; Bejiga Melka, Alemu; Carlier, Jorge Daniel Dias; Costa, Maria Clara (2021) Solvent Extraction to Recover Copper from Extreme Acid Mine Drainage. In Proceedings of the 14th IMWA Congress – "Mine Water Management for Future Generations", 12–15 July, Cymru, Wales. Stanley P, Wolkersdorfer C, Wolkersdorfer K (Editors). pp 406-411

Abstract

Over the last decade, AMD waters have gained more attention as a potential source of metals due to the emerging need to recover or recycle metals from secondary resources. Metals recovery supports sustainability and the development of a circular economy with benefits for resource conservation and the environment. In this study, five extractants (Acorga M5640, LIX 54, LIX 622, LIX 622N, and LIX 864) diluted (15% (v/v)) in Shell GTL with 2.5% (v/v) octanol were compared and evaluated for Cu recovery from an extreme AMD sample (5.3 ± 0.3 g/L Cu) collected at the inactive São Domingos Mine in the Iberian Pyrite Belt of Portugal. Of the five extractants, Acorga M5640 showed the best selective efficiency. Further tests showed that 30% (v/v) of this extractant was able to selectively extract ≈ 96.0% of the Cu from the AMD in one extraction step and all of the remaining Cu (to below detection) in three steps. Among the different stripping agents tested, 2M sulfuric acid was the most efficient, with ≈ 99% of the Cu stripped, and the recyclability of the organic phase was confirmed in five successive cycles of extraction

and stripping. Furthermore, contact time tests revealed that the extraction kinetics allows the transfer of ≈97% of the Cu in 15 min, and aqueous to organic phase ratios tests demonstrated a maximum loading capacity of ≈16 g/L Cu in the organic phase. Raising the concentration of Cu in the stripping solution (2M sulfuric acid) to ≈46 g/L through successive striping steps showed the potential to recover elemental Cu using traditional electrowinning. Finally, a biological approach for Cu recovery from the stripping solution was evaluated by adding the supernatant of a sulfate-reducing bacteria culture to make different molar ratios of biogenic sulfide to copper; ratios over 1.75 resulted in precipitation of more than 95% of the Cu as covellite nanoparticles.

Keywords: Copper recovery; AMD remediation; liquid-liquid extraction; metal bio-recovery

Graphical abstract

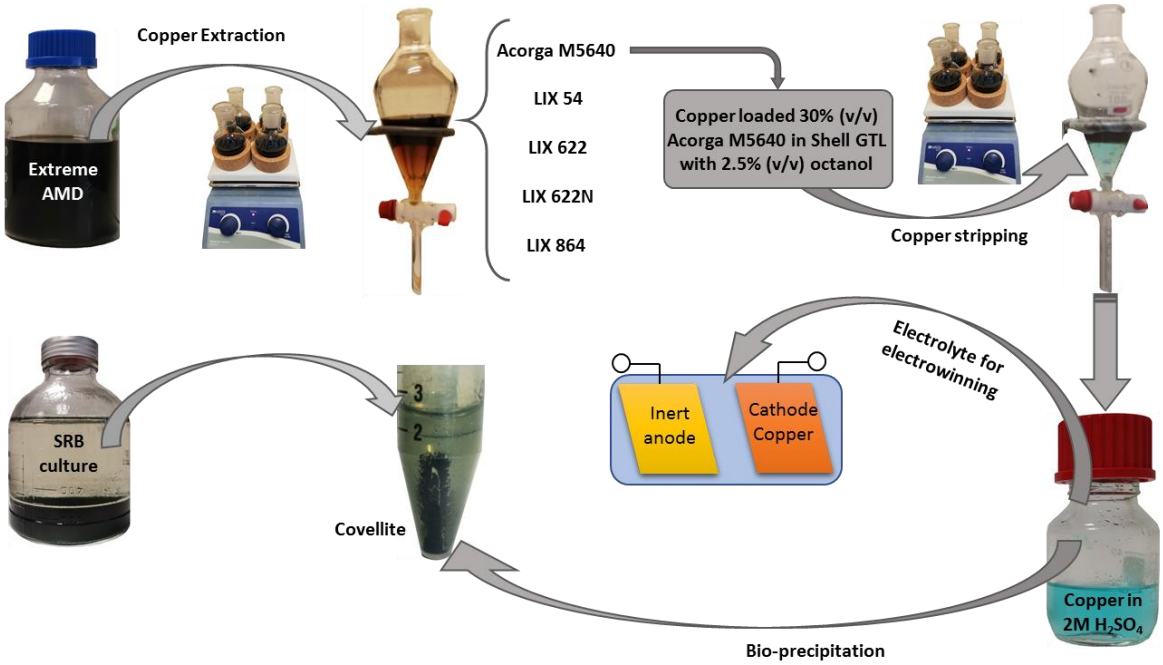

2.1. **Introduction**

Acid mine drainage (AMD) is formed by the oxidation of sulfide-rich ores exposed to the atmosphere by mining (Kefeni et al. 2017). Conventional pH control with cost-effective neutralizing reagents has been the most widely used approach for AMD treatment (Kalin et al.

2006; Taylor et al. 2005), but lime neutralization produces large amounts of precipitated metals and sludge that require further management and appropriate disposal. AMD is being increasingly considered a secondary source of metals with the goal of establishing effective methods to recover metals from AMD, increasing the circular economy, and contributing to environmental protection and resource conservation (e.g. (Macías et al. 2017; Wang and Ren 2014)).

Portugal has more than 100 inactive mine sites (Morais et al. 2008), and São Domingos is one of the most representative mining districts in the Portuguese sector of the Iberian Pyrite Belt. The intensive mining activity has caused environmental deterioration of the area (Álvarez-Valero et al. 2008; Batista 2000; Matos et al. 2006). The massive ore body of the São Domingos Mine consists of 45 to 48% total sulfur, primarily in the form of pyrite (FeS_2), chalcopyrite ($CuFeS_2$), sphalerite (ZnS), galena (PbS), and blended [(Zn, Fe)S] minerals that are usually found in association with pyrite (Oliveira and Oliveira 1996). Currently, no measures are in place to remediate the local environment affected by the inactive mine, and local watercourses and surrounding soils are heavily contaminated with various metals. Considering the size of the São Domingos area (≈50 km^2) affected by historical mining and the volume and type of wastewaters, an environmentally friendly and economically viable AMD treatment and recovery method is needed to reduce the associated environmental problems, recover metals, and increase the availability of water for irrigation.

Most metal supplied to the global economy is obtained through mining of finite sources that are rapidly decreasing due to economic expansion, higher living standards, and modern industrialisation (Arndt et al. 2017; Segura-Salazar and Tavares 2018). Copper (Cu) is one of the important metals present in high concentrations in the São Domingos AMD, and its recovery could generate additional economic activity and value due to its high demand. Since 2011, the recycling rate of Cu has been continuously decreasing (from 36% in 2011 to 29% in 2016), while refined secondary production is relatively stable over the same period (ICSG 2018). According to available data, 20,474,372 metric tons of Cu are produced per year (based on 2018 data) (Reichl and Schatz 2020), and, according to the International Copper Study Group (2019), global Cu consumption will continuously increase due to population growth, product innovation, and economic development. In a recent study using different scenarios with regression and stock dynamics methods, Schipper et al. (2018) estimated the Cu demand for the year 2100 to be in the

range of 3 to 21 times the current Cu demand. Indeed, estimates of the short-term supply risk criticality indicate that in the next two to three decades, different industrial sectors will struggle to maintain their demand for several metals (Elshkaki et al. 2016; European Commission 2014; Frenzel et al. 2015). As a result, to meet future Cu demand, a combination of primary raw materials coming from mines plus recycled and recovered materials from secondary sources is required, preferably taking advantage of eco-friendly and sustainable technological improvements and more efficient process designs. Until now, metal recycling rates from secondary sources are still very low, and significant potential exists for improving metals recovery from such sources (Schäfer and Schmidt 2019).

In this context, solvent extraction (SX) is a powerful technique that allows the recovery of metal ions from both diluted and concentrated solutions (Andersson and Reinhardt 1983). SX is a well-demonstrated and widely used technique at the industrial scale for separation and recovery of metals from aqueous solutions in the hydrometallurgical treatment of ores and other secondary materials (Hedrich et al. 2018). In the hydrometallurgical industry, SX processes make use of organic phases consisting of extractants diluted in solvents to specifically target metal ions (e.g. Cu^{2+}) from impure multi-metallic leaching solutions; the metals are then stripped from the organic phase into pure aqueous solutions from which the metals can be recovered (Davis-Belmar et al. 2012; Ruiz et al. 2019). Nevertheless, such processes are often challenged by the inability to separate valuable metals from low-concentration, metal-bearing solutions (Nordstrom et al. 2017; Matinde 2018). For example, Cu recovery by SX from waters with Cu concentrations below 1 g/L is not considered economically viable (Sole and Hardwick 2016).

The most widely used commercial Cu extractants, recognised for their selectivity, are hydroxy oxime-type organic acids, such as Acorga and LIX extractants (Ruiz et al. 2020; Vander Linden 1998). The equilibrium reaction of cupric ion (Cu^{2+}) with these extractants has attracted interest, and several models have been proposed (e.g. Alguacil et al. 2004). In the case of Acorda M5640, Agarwal et al. (2010, 2012) reported that the extractant optimises the metallurgical performance relative to ketoxime-based extractants while protecting against nitration and oxidative degradation. These characteristics reduce the extractant consumption and improve operational reliability, as it ensures a final high-quality extractant that can be reused in the extraction circuit (Alguacil et al.

2004). In the extraction reaction, Cu^{2+}complexes with the extractant and releases a hydrogen ion, according to the reversible mechanism (Flett et al. 1973) presented in equation. 2.1:

$$Cu^{2+} + 2HE \rightleftarrows CuE_2 + 2H^{+} \qquad \text{(Eq. 2.1)}$$

where E is the extractant and CuE_2 is the Cu-chelate complex.

In this reaction, the acidity of the aqueous phases in the extraction and stripping stages controls the loading and stripping of Cu to and from the organic phase (Hoh and Wang 2007).

In recent years, technologies that recover value from metal-bearing wastewaters have gained attention as a way to reduce the negative impact of mine water treatment processes. Moreover, combining chemical and biological extraction technologies to remove and recover metals can improve the adaptability to changes in feed flow and the ease of operation, which are essential characteristics in the treatment process. The use of sulfate-reducing bacteria (SRB) is a good option for metal recovery from mine-impacted waters (Kaksonen and Puhakka 2007; Villa-Gomez et al. 2011). Biogenic sulfide is advantageous because it allows the formation of insoluble metal sulfides, even at low metal concentrations and low pH values (Lewis 2010).

The need to develop alternative processes for metal recovery from secondary sources stimulated the present research. The application of an SX process like those used in the hydrometallurgical industry for extraction of Cu from pregnant solutions was tested and optimised to separate this metal from extreme AMD waters, using a mine water sample collected at the São Domingos Mine as a model. In addition, a process was tested to recover Cu from the resulting purified solution using biogenically produced sulfide to precipitate covellite nanoparticles.

2.2. **Materials and methods**

2.2.1. Extreme AMD

Mina de São Domingos, a village in southeastern Portugal, has a mine that was exploited during the Roman and Islamic occupations of the Iberian Peninsula that was the largest mine operating in Europe between 1857 and 1966. The primary ore body was a massive pyrite deposit, and Cu and sulfur (S) were the main elements extracted (Tavares et al. 2008).

Since mining activity ceased in the 1960s, the vast mining area, from the open-pit to the ruins of the Achada do Gamo factories where the ore was processed and the large waste piles were deposited, has produced a significant environmental footprint. Here the most prominent concern is AMD with high concentrations of sulfate (SO_4^{2-}) and metals, mainly aluminium (Al), iron (Fe), Cu, zinc (Zn), and manganese (Mn) (Álvarez-Valero et al. 2008; Pereira et al. 2004).

Most of the AMD flows through several reddish-yellow diversion channels and dams until merging in a unique stream that joins the Mosteirão stream, which enters the Reservoir of Chança River, a major tributary of the Guadiana River. However, some AMD generated in the Achada do Gamo zone remains in two impoundments: one of about 8700 m^2 (Figure 2.1-area 2) and another of about 2400 m^2 (Figure 2.1-area 3). These impoundments are in the area where low-grade Cu ores were roasted in piles and washed with acidic water to extract the Cu that was later precipitated onto iron sheets in a cementation tank. The impoundments are surrounded by slag remaining from the roasted pyrite ore piles (sulfur factory tailings), roasted iron oxide (hematite-rich) ore, and leached materials in seasonally flooded areas (Álvarez-Valero et al. 2008). The AMD in the larger impoundment has a very dark colour, is very dense and extremely contaminated, likely due to successive cycles of accumulation in winters and evaporation in summers, and was the source of the AMD sample used in our work (Figure 2.1-area 2). The sample was collected on 25 October 2018 and immediately transported (≈90 min transport time) to the laboratory for characterisation and Cu recovery tests.

Figure 2.1. Aerial view of the the São Domingos mining area and a closer view of the sampled zone obtained from Google Maps: coordinates: 37°40'06.7"N 7°29'28.5"W. 1) Open pit mine; 2) Sampled impoundment with extreme acid mine drainage (AMD); 3) Another AMD impoundment; A) Roasted pyrite ore slag; B) Modern slag.

2.2.2. Solvent Extraction

The extraction procedures and the experiments performed to select the extractant and optimise and characterise the extraction conditions are described in Melka (2019). The initial metal concentrations (Fe, Al, Cu, Zn, and Mn) in the raw AMD, $[M_{aq}]_i$, and their final concentrations in the aqueous phase after solvent extraction, $[M_{aq}]_f$, were measured. The metal concentrations in the final organic phase, $[M_{org}]_f$, were calculated by mass balance, and their removal efficiencies were determined by: Removal % = $100 \times [M_{org}]_f / [M_{aq}]_i$. The extraction distribution ratios (D) of the target metal ions were calculated as $D = [M_{org}]_f / [M_{aq}]_f$.

2.2.3. Recovery Through Bioprecipitation

2.2.3.1. Precipitation with biogenic sulfide

The addition of the sulfide-rich liquid phase from an SRB culture was tested as a method to precipitate Cu sulfide (covellite) from the loaded stripping solution (2M H_2SO_4) obtained after SX with the selected organic phase. Three stripping solutions from successive extractions and stripping steps were mixed to produce enough Cu solution for the tests.

The SRB consortium used in our work was enriched using Postgate B medium (Postgate 1984) inoculated with sludge from a wastewater treatment plant located in southern Portugal and incubated at room temperature (25 ± 3 °C) under anaerobic conditions (for SRB enrichment details see Carlier et al. 2019). The SRB consortium is maintained in the laboratory through successive cultures in Postgate B medium inoculated with 1 to 10% (v/v) of previous cultures. A fresh culture was prepared and used when all sulfate in the medium had been reduced to sulfide. Sulfate reduction was monitored by analysing the sulfate and sulfide concentrations in the culture medium every three days.

To find the optimal sulfide to Cu ratio (S:Cu) that would maximize Cu precipitation, a fixed volume of stripping solution was mixed with different volumes of bacterial culture media to test different S:Cu ratios above the stoichiometric value of 1:1 for CuS (covelite). The mixtures were maintained in closed Falcon tubes for 24 h at room temperature (25 ± 3 °C), and the volumes were then adjusted to a constant volume with distilled water to facilitate centrifugation and calculations. Afterwards, the mixtures were centrifuged at 2500×g for 20 min at room temperature, and the supernatants were collected and used for Cu determination and mass balance calculations of Cu precipitation efficiencies.

After removing the supernatant, the precipitates were covered with 45 ml of a 50% (v/v) ethanol in water solution and sonicated for 15 minutes. The samples were then centrifuged for 15 min at 2500×g for 10 min at room temperature, and the supernatant was discarded. Afterwards, they were washed overnight with 96% ethanol in an orbital shaker and centrifuged at 2500×g for 60 min at room temperature, and the supernatant was removed. Finally, the precipitates were dried under vacuum overnight.

2.2.4. Analytical Methods

A pH/E meter GLP 21 (Crison) with a glass pH electrode (VWR, SJ 223) was used to measure pH. A Pt electrode coupled with a reference-saturated calomel electrode (CRISON, 52 61) was used to measure redox, which was converted to Eh using a conversion factor of 241 mV. A UV-visible spectrophotometer DR2800 (Hach-Lange) was used to measure sulfate and sulfide concentrations using the sulfaVer4 (Method 8051, Hach-Lange) and the methylene blue (Method 8131, Hach-Lange) methods, respectively. The samples collected for metals determination were acidified with concentrated nitric acid (5%). Flame atomic absorption spectroscopy (FAAS) with a novAA 350 system (Analytik Jena) was used to measure the concentrations of Fe, Zn, Cu, Mn, and chromium (Cr), and microwave plasma atomic emission spectrometry with a 4200 MP-AES (Agilent) was used to measure the concentrations of Al, arsenic (As), and cobalt (Co). In both methods, calibration curves were built using standards prepared from the following stock solutions in 0.5 M HNO_3: $Fe(NO_3)_3$, $Zn(NO_3)_2$, $Cu(NO_3)_2$, and $NaNO_3$ (Merck Certipur, Germany); $Mn(NO_3)_2$, $Al(NO_3)_3$, $As(NO_3)_3$, and $Co(NO_3)_2$ (Panreac AA, Spain); and $Cr(NO_3)_3$ (BDH Laboratory Supplies, England). The concentrations of lead (Pb), nickel (Ni), selenium (Se), cadmium (Cd), magnesium (Mg), sodium (Na), and calcium (Ca) were determined by inductively coupled plasma mass spectrometry (ICP-MS) at an external accredited laboratory (Hidrolab, Spain). Ferrous iron (Fe^{2+}) concentrations were determined with a UV-visible spectrophotometer DR2800 (Hach-Lange) using the 1,10-Phenanthroline (Method 8146, Hach-Lange) procedure at 510 nm, and ferric iron (Fe^{3+}) concentrations were calculated by difference with total iron determined by FAAS.

The precipitates collected and washed in the recovery experiments were analysed by x-ray diffraction (XRD), by a variable pressure scanning electron microscope coupled with energy dispersive x-ray spectrometry (VP-SEM-EDX), and by transmission electron microscopy (TEM). XRD analysis was performed using a PANalytical X'Pert Pro powder diffractometer, operating at 45 kV and 30 mA, with Cu Kα radiation filtered by Ni. The XRD patterns were recorded using an X'Celerator detector, with a step size (2θ) of 0.03° and a time per step of 400 s. Peak analysis and crystalline phase identification were conducted using High-Score Plus software with the ICDD PDF-2 database. The crystal size of each sample was estimated using the Scherrer equation, $CS = \frac{K.\lambda}{\beta.\cos\theta}$, considering a form factor of 0,94. VP-SEM-EDX analysis was carried out using a Hitachi™

S3700N SEM coupled to a Bruker™ XFlash 5010 SDD EDS Detector®. The samples were analysed at low vacuum (40 Pa) with an accelerating 5- and 20-kV voltage.

For the TEM analysis, precipitates were resuspended in ethanol and sonicated for 30 min to pulverise the samples. Then, 5 µl of each sample were applied to 400 mesh Cu grids with thin carbon support (01844-F, Carbon Film only on 400 mesh, Cu, Tedpella), and the grids were dried and stored in a desiccator until imaging. Samples in the grids were imaged with a JEOL JEM-2100 electron microscope, operating a LaB6 electron gun at 200 kV, and images were acquired with a "OneView" 4k x 4k CCD camera.

To analyze the purity of covellite, 64.47 mg of precipitates (weighted using a Sartorius MSA36S-000-DH Micro Balance) were dissolved in 2.5 mL of aqua regia using a temperature ramp from 50 to 107 °C for 6 h, followed by a period of 16 h at 107 °C. At the end, 4 mL of concentrated nitric acid was added, and the final volume (6.2 mL) was noted for calculations. Finally, a 1:3 dilution in dionized water (Milli-Q® purification system) was used for elemental analysis.

2.3. **Results and discussion**

2.3.1. Extreme AMD

The AMD sample collected at the São Domingos inactive mine from the impoundment near the old sulfur factories of Achada do Gamo was analyzed at CCMAR's laboratories for pH, sulfate, Fe, Al, Cu, Zn, Mn, As, and Co). In addition, several other metals (Cr, Pb, Ni, Se, Cd, Mg, Na, Ca) were determined by an external accredited laboratory. The AMD composition is presented in Table 2.1.

Table 2.1. Initial characterization of the extreme AMD sample from Mina de São Domingos (impoundment next to the sulphur factory ruins at Achada do Gamo) collected on 25 October 2018 [mg/L, and standard units for pH].

Parameter	Value	Standard Deviation
pH	1.19	-
SO_4^{2-}*	142,000	15,100

Fe*	63,200	6,074
Fe^{3+}	55,500	6,630
Fe^{2+}	7,770	551
Al*	6,470	148
Cu*	5,250	313
Zn*	1,960	449
Mn*	131	2
As*	21.40	0.09
Co*	6.46	0.03
Pb **	5.280	-
Ni **	3.040	-
Se **	1.990	-
Cd **	1.890	-
Cr*	1.16	0.07
Mg **	0.260	-
Na **	0.251	-
Ca **	0.138	-

* Averages and standard deviations of five determinations using independent dilutions at CCMAR

** Analysis at the accredited laboratory Hidrolab (see analytical methods).

The acidity and the pollutant concentrations in the AMD sample used in our work were much higher than those in samples collected from the flowing AMD streams, which usually have pH values between 2 to 3 and have the following approximate pollutant concentration ranges: sulfate (1000 to 5000 mg/L), Al (100 to 500 mg/L), Fe (50 to 500 mg/L), Zn (20 to 150 mg/L), Cu (20 to 100 mg/L), and Mn (5 to 20 mg/L) (e.g. Costa and Duarte 2005; Costa et al. 2008). The AMD sampled can be classified as *High-acid* and *Extreme-Metal* using the Ficklin diagram, where the sum of the concentrations of Zn, Cu, Pb, Cd, Co, and Ni (rather than more common metals such as Fe, Al, and Mn) is plotted against pH (Ficklin et al. 1992; GARD Guide, Chapter 2).

2.3.2. Solvent Extraction

2.3.2.1. Extractant selection

Among the five tested extractants, Acorga M5640 and LIX 622 more specifically extracted Cu, while LIX 864, LIX 54, and LIX 622N co-extracted iron and zinc, iron, and aluminium, and iron, respectively (Supplemental Figure S- 2.1). The extraction distribution ratios are presented in Table 2.2. Of the 5,250 ± 313 mg/L initial Cu concentration, 85 ± 4% was extracted from the aqueous phase to the organic phase containing Acorga M5640, and 37 ± 1% was extracted to the organic phase with LIX 622. LIX 54 preferentially extracted Fe over Cu from this AMD sample: just 2 ± 1% of Cu was extracted, but 20 ± 1% of Fe was co-extracted.

Table 2.2. Extraction distribution ratios (D) of primary metals in the extreme AMD sample, with 15% (v/v) of each extractant diluted in Shell GTL + 2.5% (v/v) octanol, using an A/O = 1/1 and a contact time of 30 minutes at room temperature (25 ± 3 ºC).

Extractants	Metal	Distribution ratio (D)*
ACORGA M5640	Fe	-
	Al	-
	Cu	5.16
	Zn	-
	Mn	-
Lix622	Fe	-
	Al	-
	Cu	0.59
	Zn	-
	Mn	-
Lix864	Fe	0.26
	Al	-
	Cu	4.38
	Zn	0.005
	Mn	-
Lix54	Fe	0.24
	Al	0.01
	Cu	0.02
	Zn	-
	Mn	-
Lix622N	Fe	0.11

Al	-
Cu	5.77
Zn	-
Mn	-

* $D = [M_{org}]_f / [M_{aq}]_f$
- metal not detected in extractant
A/O aqueous/organic volume ratio

The higher efficiency of Acorga M5640 to specifically extract Cu from such extreme AMD confirms previous results obtained using model and leaching multi-metallic solutions. For example, Ochromowicz and Chmielewski (2013) showed that Acorga M5640 is a superior extractant for Cu compared to LIX 984N and LIX 612N-LV for multi-metallic sulfuric acid leachates. Wang et al. (2019b) successfully extracted over 90% of Cu from multi-metallic sulfuric acid leachates of printed circuit boards (from electrical and electronic equipment) using Acorga M5640, and Tanaydin and Demirkiran (2020) found that Cu can be extracted from perchloric acid leachates of malachite ore using Acorga M5640.

2.3.2.2. Extraction optimisation and characterisation

Based on the results obtained in the extractants' screening, Acorga M5640 was selected for the subsequent experiments to optimise and characterise the extraction of Cu from the extreme AMD sample collected at the São Domingos Mine.

For the optimisation, different concentrations of Acorga M5640 in the organic phase were tested to find the best ratio of the extractant active compound to Cu ions. The Cu extraction percentage increased as the Acorga M5640 concentration increased in the organic phase, and the maximum efficiency of 96.0 ± 3% (which corresponds to 5,040 ± 158 mg/L Cu extracted) was achieved with 30% (v/v) Acorga M5640 (Figure 2.2). This corresponds to 0.57 mol/L of the extractant's active compound (5-nonyl-2-hydroxy-benzaldoxime) to 0.0694 mol/L of Cu extracted, making an ≈ 8:1 ratio of active compound to Cu ions. Considering the complexity of the chemical matrix in the AMD sample, this can be considered a good ratio. It is just four times higher than the theoretical ratio of 2:1 in the equation expressing the extraction reaction of Cu with Acorga M5640 in sulfuric systems (see Eq. 1). On the other hand, the 8:1 ratio estimated in our work is three times lower

than the 24:1 ratio reported by Agarwal et al. (2010) when using 20% (v/v) Acorga M5640 (0.38 M active compound) diluted in ShellSol D70 (also a kerosene-like diluent); the 24:1 ratio result held for both the initial aqueous solutions these authors tested (1 g/L Cu^{2+} and a more complex solution of 1 g/L Cu^{2+}, 40 g/L Zn(II), and 15 g/L Fe(III) at pH 1.4).

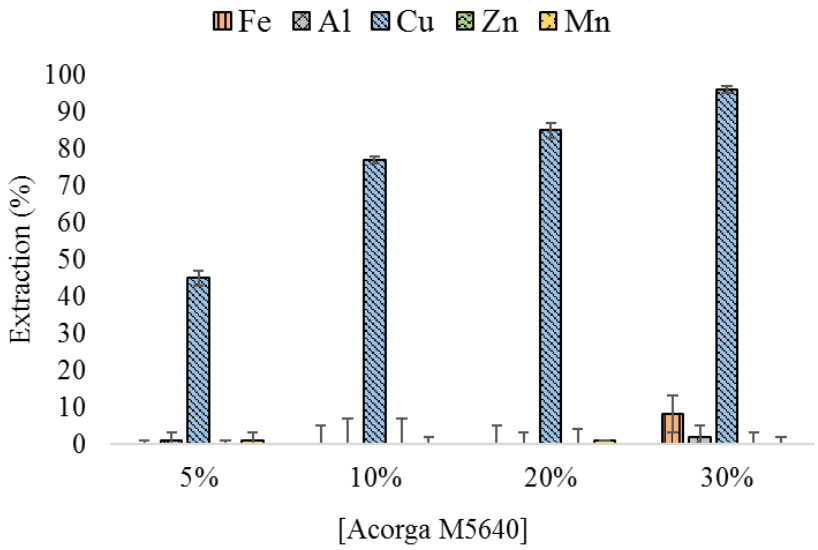

Figure 2.2. Extraction efficiencies from the extreme AMD with Acorga M5640 at concentrations of 5, 10, 20 and 30 % (v/v) diluted in Shell GTL + 2.5 % (v/v) octanol, using an A/O = 1/1 and a 60-minutes contact time at room temperature (25 ± 3ºC). Results are averages of triplicates, and the error bars are standard deviations.

In the test with 30% Acorga M5640, the extraction of iron reached 8 ± 5%, which reveals a high co-extraction of iron since its concentration in the initial extreme AMD sample is about 12 times higher than the concentration of Cu. This corresponds to a final concentration in the organic phase of 5,060 ± 3,160 mg/L iron, similar to the Cu concentration achieved. Nevertheless, it is possible to separate these two metals in the stripping process (see below). The iron extraction (albeit in a small percentage) raised the question of some loss of specificity for Cu under these extraction conditions, leading to additional analysis of another concentrated contaminant: arsenic. The results (0 ± 1 % arsenic removal) indicate that this metalloid is not efficiently extracted. Thus, 30% Acorga M5640 was chosen as the optimal percentage, and additional parameters were studied

using this extractant concentration, including contact time (kinetics), Cu loading capacity in the organic phase, efficiency of stripping agents, and organic phase recyclability.

Finally, the raffinate water resulting from the extraction of Cu under these conditions has the potential to undergo further recovery because it still contains high concentrations of sulfate (133 g/L), metals, and metalloids (primarily Fe: 58,200 mg/L, Al: 6,340 mg/L, Zn: 1,960 mg/L, Mn: 131 mg/L and As: 21 mg/L). Indeed, zinc is another important metal with growing demand, for which the recovery from secondary sources will need to have a major role in the next 50 years (Sverdrup et al. 2019). Thus, the recovery of zinc from industrial wastes has beem a focus of research for decades (e.g. Jha et al. 2001). Moreover, sulfuric acid could potentially be recovered and contribute to the economic feasibility of an integrated recovery process from extreme AMD samples. For example, Nleya et al. (2016) have reviewed techniques used to recover sulfuric acid from various wastewater solutions and studied the sustainability assessment of the recovery and utilisation of acid from AMD. In any case, the raffinate from the Cu extraction process under study in our work cannot be released to the environment without prior treatment.

2.3.2.3. Contact Time (Kinetics)

The extraction of Cu from the extreme AMD using 30% (v/v) Acorga M5640 with an aqueous:organic (A/O) volume ratio of 1:1 required 5 min to transfer 92% of the Cu to the organic phase; after 15 min, the maximum Cu transfer (≈97%) was achieved (Figure 2.3). Wang et al. (2019b) found that only 1 min was needed with $CuSO_4$ and chloride leaching solutions (with ≈ 6 g/L Cu at pH 1.1) to achieve over 90% Cu extraction with 16% (v/v) Acorga M5640 in kerosene. One significant difference that could have accounted for the longer time to achieve the extraction equilibrium in our work is the extremely high concentrations of other metals in our AMD sample. Nevertheless, our results are fairly consistent with the 85% Cu recovery from sulfuric acid feed solutions of 10 g/L Cu at pH 0.75 reported by Ochromowicz and Chmielewski (2013), who used 30% (v/v) Acorga 5640 diluted in a kerosene-type diluent Escaid® 100, with a contact time of 5 min at 25°C and an A/O ratio of 0.75:1. In addition, Wang et al. (2019b) did not add alcohol to the diluent, and in our work, 2.5% (v/v) octanol was added. Adding alcohol to the solvent used to dilute Acorga M5640 may affect the extraction of Cu. Agarwal et al. (2010) reported that adding 5% isotridecanol to the organic phase with 10% Acorga M5640 slightly

impeded the rate of recovery by changing the equilibrium to 96% extraction in 1 min instead of the 99% achieved without the addition of alcohol or with the addition of 2.5% isotridecanol.

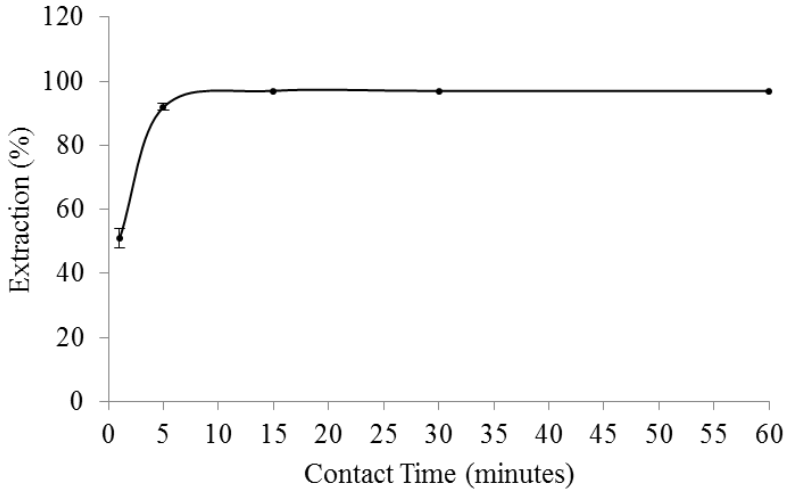

Figure 2.3. Copper extraction efficiency from the extreme AMD with 30% v/v ACORGA M5640 in Shell GTL + 2.5 % (v/v) octanol, using an A/O = 1/1 and different contact times (1, 5, 15, 30 and 60 minutes) at room temperature (25 ± 3ºC). Results are averages of duplicates, and the error bars are mean deviations.

2.3.2.4. Loading Capacity of Cu in the Organic Phase

The loading capacity of Cu extracted from the extreme AMD to 30% (v/v) Acorga M5640 in Shell GTL with 2.5 % (v/v) octanol was determined by raising the aqueous/organic (A/O) volume ratio (Figure 2.4). The results revealed good extraction performance, with a maximum loading capacity of 16.2 g/L of Cu in the organic phase. Afterwards, three consecutive cycles of extraction without the stripping step were carried out, always using the same organic phase but new extreme AMD in each cycle, to evaluate the potential to build up the Cu concentration in the organic phase through successive extractions and the capacity of accumulating concentrations of Cu up to ≈ 16 g/L (Supplemental Table S- 2.1).

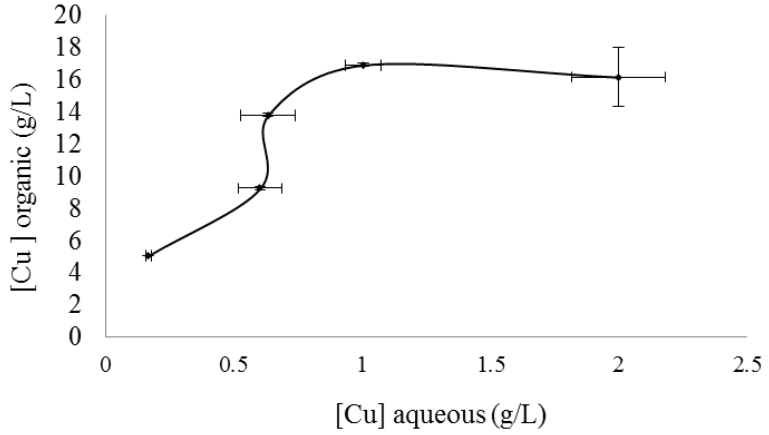

Figure 2.4. Equilibrium isotherm for the extraction of copper from the extreme AMD, using different A/O volume ratios (1/1, 2/1, 3/1, 4/1, and 5/1, graph points from left to right) using 30% (v/v) Acorga M5640 in Shell GTL + 2.5 % (v/v) octanol and a contact time of 60 minutes at room temperature (25 ± 3ºC). Results are averages of duplicates, and the error bars are mean deviations.

Agarwal et al. (2012) studied the extraction equilibrium of Cu from sulfate media with Acorga M5640 in ShellSol D70 (kerosene-like solvent). They proposed a model considering the non-ideality of the extractant (due to the dimerisation of the active compound) to predict the distribution ratio and the Cu loading isotherms. In that work, they reported maximum loading capacities of 11 g/L Cu in 20% (v/v) Acorga M5640 in ShellSol D70, using extraction isotherms built either with simulated values or experimental results. Subsequently, Vasilyev et al. (2017) studied the extraction equilibrium of Cu in the organic phase over a wide range of Acorga M5640 extractant (5–25 vol%) in kerosene and using various Cu concentrations (1–45 g/L) in the aqueous phase, and confirmed that the extraction is highly correlated with the total concentration of the extractant in the organic phase. Moreover, the phase equilibrium model they developed and validated also accounts for the non-ideality of the organic phase: the extraction of Cu from the aqueous phase increased nonlinearly with an increase of extractant concentration in the organic phase for values above ≈14% (v/v) Acorga M5640, with a less pronounced increase in Cu extraction at higher values. In addition to the limitations due to the high viscosity and high operational costs of concentrated Acorga M5640, these authors also pointed to chemical limitations. However, according to Vasilyev et al. (2017) neither the dimerisation of the unreacted extractant molecules

nor the solvation of the Cu-extractant complexes was sufficient to explain the organic phase non-ideality.

In our work, Acorga M5640 was also diluted in a kerosene-like solvent (Shell GTL), but 2.5% (v/v) octanol was added for two reasons: (1) according to Agarwal et al. (2010), although the presence of 2.5% (v/v) isotridecanol in the solvent does not increase the Cu transference, it favours the rejection of iron; (2) according to Ferreira et al. (2010), adding 2.5% (v/v) isotridecanol to the solvent improved the stripping efficiency. Ferreira et al. (2010) reported a loading capacity of 5.2 g/L Cu in 10% (v/v) Acorga M5640 in ShellSol D70 with 2.5% isotridecanol when using leaching solutions with pH values of ≈1 as aqueous phases. Agarwal et al. (2010) have determined maximum loading capacities of 4.8, 5.2, and 5.5 g/L Cu for organic phases with 10% (v/v) Acorga M5640 in kerosene-like solvent (ShellSol D70) with 5% isotridecanol, with 2.5% isotridecanol, and without any alcohol, respectively. These authors also reported 10 and 11 g/L Cu loading capacities for systems with 20% (v/v) Acorga M5640 in solvents with 5% isotridecanol and without added alcohol, respectively. This allows us to roughly estimate a loading capacity of 10.5 g/L Cu for an organic phase with 20% (v/v) Acorga M5640 in a solvent with 2.5% alcohol.

By plotting these reported loading capacities for systems with Acorga M5640 in solvents with 2.5% alcohol and the loading capacity of Cu achieved in our work against the respective percentages of extractant, a linear correlation was obtained ($y = 0.55x - 0.3667$) with high confidence ($R^2 = 0.9996$). This suggests a linear phase equilibrium model for systems using 10% to 30% (v/v) Acorga M5640 in kerosene-like solvents with 2.5% (v/v) alcohol. Our results also suggest the ideality of such type of organic phase, contrasting with the non-linear models reported by Agarwal et al. (2012) and Vasilyev et al. (2017) for this extractant when diluted in such solvents without any alcohol. Nevertheless, the objective of our work was not to develop and validate a phase equilibrium model but rather to evaluate the feasibility of Cu recovery from complex wastewaters such as the extreme AMD.

2.3.2.5. Stripping Agents

Different stripping agents were tested for the re-extraction of Cu from the loaded organic phases, which consisted of 30% (v/v) Acorga M5640 in Shell GTL with 2.5% (v/v) octanol. First, tests using three different acidic solutions at 0.1M revealed stripping efficiencies in the following order:

sulfuric acid > nitric acid > hydrochloric acid, although all had efficiencies below 30% (Figure 2.5-a). Then, a further experiment with the two best acidic solutions at higher molarities achieved the highest Cu stripping efficiency of sulfuric acid (Figure 2.5-b). In that experiment, sulfuric acid concentrations of 1M and 2M produced Cu stripping percentages of 95% and 99%, yielding Cu concentrations in the stripping solutions of 4,790 and 4,990 mg/L, respectively. Moreover, the stripping percentages of iron were low (1.3% to 1.8%) in the four tests, which in this case is particularly important due to the above-mentioned high co-extraction of this metal. The sulfuric acid concentrations of 1M and 2M stripped 1.5% and 1.6% of the iron in the organic phase, generating concentrations of this metal in the stripping solutions of 76 and 81 mg/L, respectively.

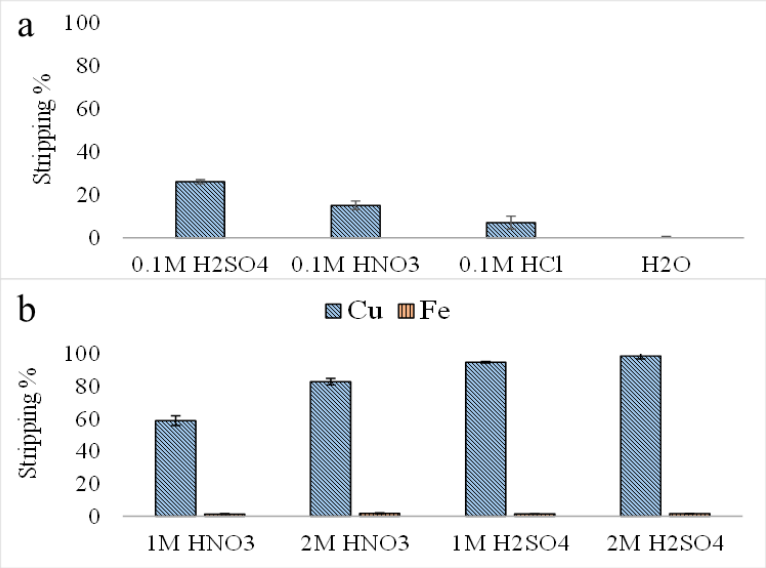

Figure 2.5. Copper and iron stripping from loaded 30% (v/v) Acorga M5640 in Shell GTL + 2.5% (v/v) octanol, with an A/O = 1/1 and contact time of 60 minutes at 25 ± 3°C, (a) with sulfuric acid, nitric acid, and hydrochloric acid at 0.1M and with a control of distilled water, (b) with nitric acid and sulfuric acid at 1M and 2M. Results are averages of duplicates, and the error bars are mean deviations.

Other works have shown that sulfuric acid is highly efficient for stripping Cu from organic phases with Acorga M5640 (e.g. Ferreira et al. 2010; Vasilyev et al. 2017; Wang et al. 2019b). Moreover, according to experimental data reported by Alguacil et al. (2004), in addition to a higher stripping efficiency, sulfuric acid has a less degradative effect on Acorga M5640 than nitric acid. Therefore,

2M sulfuric acid was selected as the optimal stripping solution for the process and was used in the subsequently reported experiments.

2.3.2.6. Organic Phase Recyclability

In practical applications, the stability and recyclability of extractants are required factors for the economic and environmental sustainability of the extraction process. Supplemental Figure S- 2.2 shows the effect of reusing the organic phase (30% (v/v) Acorga M5640 in Shell GTL with 2.5% (v/v) octanol) in successive cycles of extraction and stripping. After five extraction cycles, the Cu extraction efficiency remained unchanged. In the first cycle, the Cu extraction efficiency was 96 ± 1%, and in the fifth cycle, it was 96.0 ± 0.5%.

Deep et al. (2010) reported insignificant changes (<0.5%) in five successive cycles of extraction and stripping to recover Cu from a sulfuric acid leaching liquor of a mined zinc concentrate (from the Neves-Corvo Mine, Portugal), using 25% (v/v) Acorga M5640 in ESCAID 110 plus 12.5% (v/v) isodecanol as the organic phase, and using a synthetic spent cell electrolyte (25 g/L Cu in 180 g L/H_2SO_4) as the stripping solution. However, after the stripping step, the authors washed the organic phase with water before its reuse in subsequent extraction cycles; in our experiments, the organic phase was directly reused without a washing step. Wang et al. (2019b) also reused the organic phase (16% (v/v) Acorga M5640 in kerosene) directly, without washing after stripping, in successive cycles of extraction and stripping (with 2.5 M sulfuric acid) when testing the recovery of Cu from a sulfuric acid leaching liquor of printed circuit boards from electronic equipment waste. They reported a 5% decrease over the first five cycles, followed by stabilising extraction efficacy in seven subsequent additional cycles.

In our work, despite the co-extraction of iron and its accumulation in the organic phase (since it is barely stripped with 2M sulfuric acid), the stable Cu extraction efficiency in the successive extraction cycles (Figure S- 2.2) indicates that iron is not effectively competing with Cu for the extractant's active compound. While Cu ions form complexes with the active compound (5-nonyl-2-hydroxy-benzaldoxime) of Acorga M5640, steric hindrance prevents the formation of iron complexes (Deep et al. 2010). Thus, the slight decrease in the extraction efficiency observed by Wang et al. (2019b) in five successive cycles may have been caused by the relatively low Cu

stripping efficiency (90%) reported by those authors, compared with that achieved in our work (99%).

Another important characteristic for the successive utilisation of the organic phase is the immiscibility of both organic and aqueous phases. In the system under study, the phases separated clearly and quickly once the stirring stopped. Moreover, an experiment consisting of two extractions performed in 100 mL cylinders (with strong magnetic stirring for 60 min to achieve adequate contact between phases) revealed that the volumes (50 mL each) did not change (for an error of 0.5% due to the visual analysis of volumes using cylinder markings). Therefore, major losses of extractant and organic solvent in large- scale operations are not expected.

2.3.2.7. Complete Cu Extraction

Another important aspect is extracting all Cu from the extreme AMD to avoid putative Cu contamination in subsequent processes that aim to recover other metals. The experiments of consecutive extraction cycles using new organic phases and the same aqueous phase revealed that three cycles are required to extract Cu from the extreme AMD to a concentration below the FAAS detection limit in the aqueous phase (Figure S- 2.3).

2.3.2.8. Electrolyte Production for Cu Electrowinning

The hydrometallurgical processes for Cu recovery generally involve three steps: leaching, solvent extraction, and electrowinning. In Cu electrowinning, the Cu^{2+} dissolved in the H_2SO_4 (electrolyte solution) is reduced on cathode surfaces to pure metallic Cu when direct current is applied between anodes and cathodes. The spent electrolyte solution, which will still have a relatively high concentration of Cu (≈25 to ≈35 g/L Cu), is returned to the solvent extraction step as a stripping solution to recover Cu^{2+} from the loaded organic phase (Aksamitowski et al. 2018; Alguacil and Regel-Rosocka 2018; Schlesinger et al. 2011). Thus, when developing a hydrometallurgical process involving solvent extraction and electrowinning, it is essential that Cu concentrations in the initial stripping solution exceed those found in the spent electrolyte solutions. With that aim, four consecutive cycles of extraction and stripping were carried out, always using the same stripping solution (2M H_2SO_4) but with new organic phases loaded with Cu (Table 2.3). The results

show that it is possible to achieve ≈35 g/L Cu in the stripping solution, maintaining striping efficiencies above 95%, and that it is feasible to reach ≈46 g/L Cu even if the stripping efficiency drops to ≈77%. This means that with this process, it is viable to extract Cu from this extreme mine water and transfer it to electrolyte-like solutions with Cu concentrations suitable for the electrowinning process.

Table 2.3. Copper concentrations in the initial organic phase (30% Acorga M5640 in Shell GTL + 2.5% (v/v) octanol) and final stripping solution (2M H_2SO_4) in four consecutive cycles of extraction and stripping. The same stripping solution was used with new organic phases loaded with copper. Conditions were an A/O ratio of 1/1 and a contact time of 60 minutes at room temperature (25 ± 3oC). Results are averages of 3 replicates ± standard deviations.

Cycle	[Copper] in initial organic phase (g/L)	[Copper] in final stripping solution (g/L)	Copper stripping efficiency (%)
1	5.56 ± 0.07	5.3 ± 0.5	95.3
2	16.11 ± 0.03	21 ± 3	97.5
3	13.8 ± 0.1	34.5 ± 0.9	97.8
4	15 ± 2	46 ± 3	76.7

2.3.3. Cu Recovery with Biogenic Sulfide

The recovery of Cu from a loaded stripping solution (2M H_2SO_4 with 8,360 ± 124 mg/L Cu) obtained in the SX process under study was attempted using sulfide generated by SRB. The SRB culture inoculated for that purpose evolved as expected (Figure S- 2.4) and was used 28 days after inoculation, when most of the sulfate (>90%) had been reduced to sulfide (the concentration of sulfide was 377 ± 9 mg/L). The results achieved by mixing a fixed volume of stripping solution with different volumes of the supernatant from a bacterial culture indicate that an S:Cu ratio of 1.75 is needed to ensure complete Cu precipitation (>95%), and higher ratios are unnecessary (Figure S- 2.5).

The XRD pattern generated with the precipitates produced (after washing) revealed prominent peaks corresponding to covellite (CuS), along with a few small peaks that did not match any crystalline phase pattern in the database (Figure 2.6). The estimated crystal size of the covellite phase was 15 nm. Mapping of the precipitates using SEM-EDX revealed the presence of Cu and sulfur in the particles, as expected for covellite (CuS), and traces of carbon around them indicating low contamination of precipitates with organic compounds. Moreover, point analysis of one of the particles showed an approximate Cu:S ratio of approximately 18:21, which is close to the expected 1:1 molar ratio for covellite (Figure 2.7).

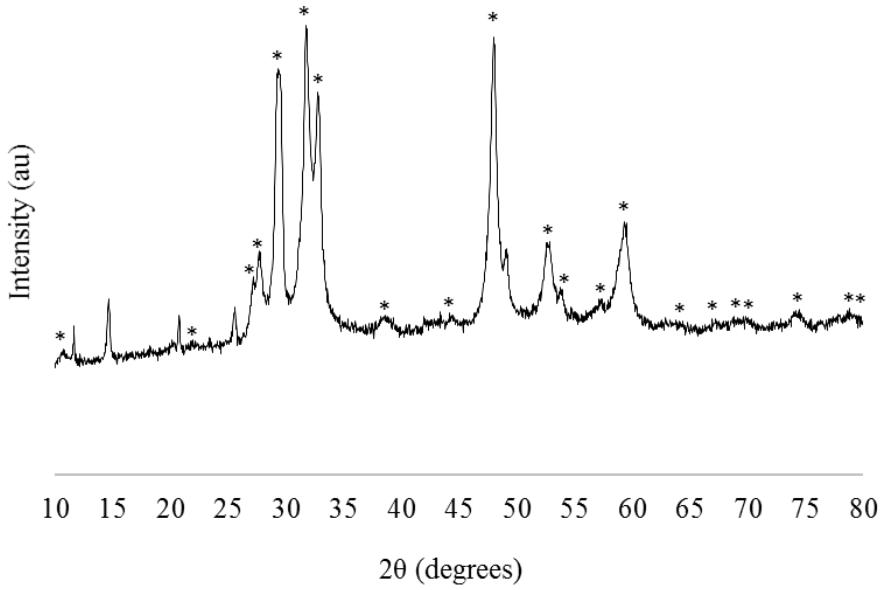

Figure 2.6. XRD pattern of precipitates obtained by adding the supernatant from a biogenic sulfide-rich (377 ± 9 mg/L S^{2-}) SRB culture medium to a 2M H_2SO_4 stripping solution loaded with copper (8356 ± 124 mg/L copper) from the solvent extraction process to recover copper from the extreme AMD. The "*" symbol refers to the peaks for covellite (ICDD PDF2 database, reference code 01-078-0877).

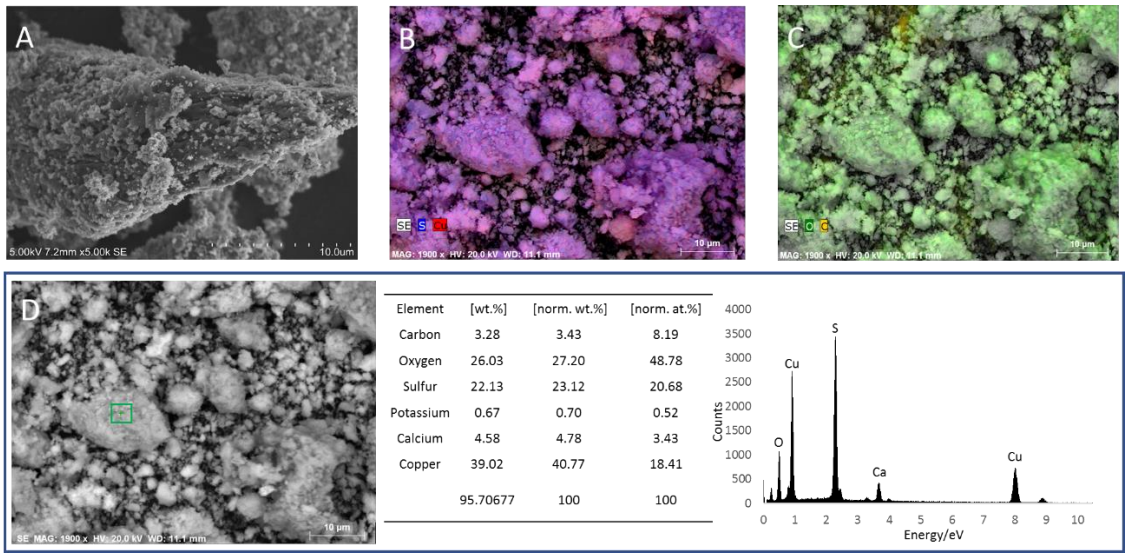

Figure 2.7. SEM-EDX mapping of precipitates obtained by adding the supernatant from a biogenic sulfide-rich (377 ± 9 mg/L S^{2-}) SRB culture medium to a 2M H_2SO_4 stripping solution loaded with copper (8,360 ± 124 mg/L copper). A) SEM image of the particles. SEM-EDX mapping of B) sulfur and copper, C) carbon and oxygen. D) point analysis of covellite.

The samples prepared for TEM analysis showed *a priori* evidence of incomplete dispersion of crystalline particles (aggregates were visible by eye). Still, the samples were suitable for TEM imaging and the results allowed us to identify two types of particles:

- Nanoparticles with a wide range of sizes and shapes, caused by the agglomeration of different numbers of smaller unique nanoparticles, for which it is possible (in some cases) to recognise hexagonal shapes and internal crystalline structures (Figure 2.8). Automatic measurements of 4,820 particles in the 12 TEM images, using the ParticleSizer v1.0.9 plugin (Wanger and Eglinger 2021) on the Fiji – ImageJ software (Schindelin et al. 2012), revealed a particle Feret size range from 3 to 87 nm with a mean of 12 ± 9 nm and sizes fitting a normal distribution (for a 1% probability (α=0.01) in a Kolmogorov-Smirnov test).

- Micro-sized structures of needle-like and radiating forms containing multiple small nanoparticles (Figure 2.9). Manual measurements of 10 particles, using the Fiji – ImageJ software (Schindelin et al. 2012), revealed a particle Feret size range from 2 to 5.5 µm with a mean of 4 ± 1 µm (the size distribution of these large agglomerates was not studied).

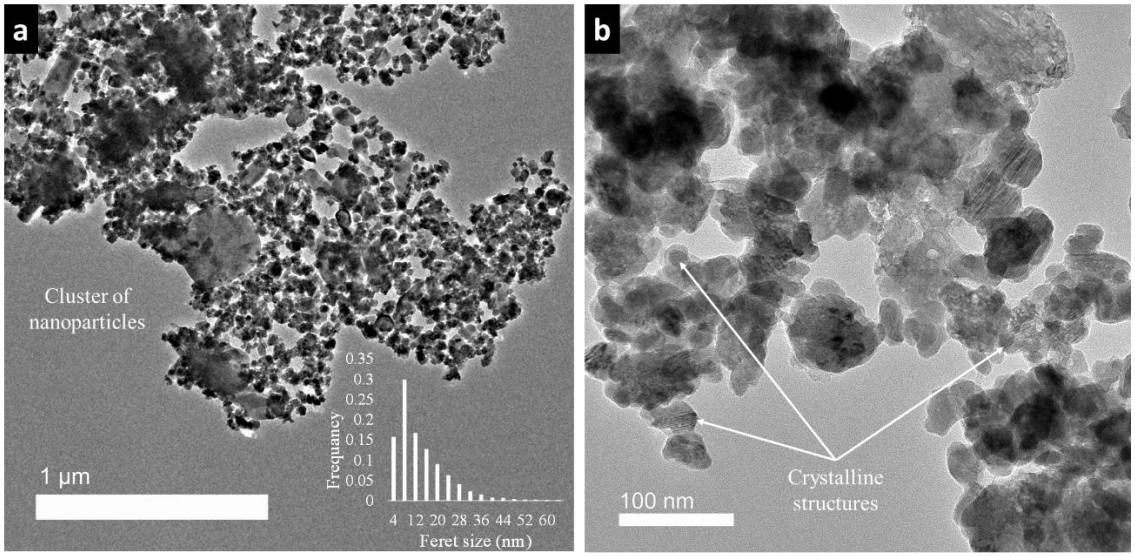

Figure 2.8. TEM images of precipitates obtained by adding the supernatant from a biogenic sulfide-rich (377 ± 9 mg/L S^{2-}) SRB culture medium to a 2M H_2SO_4 stripping solution loaded with copper (8,360 ± 124 mg/L copper), showing (a) a cluster of nanoparticles of multiple sizes together with the distribution of sizes for 4,820 particles measured in 12 TEM images and (b) nanoparticles with visible hexagonal-like shapes and internal crystalline structures.

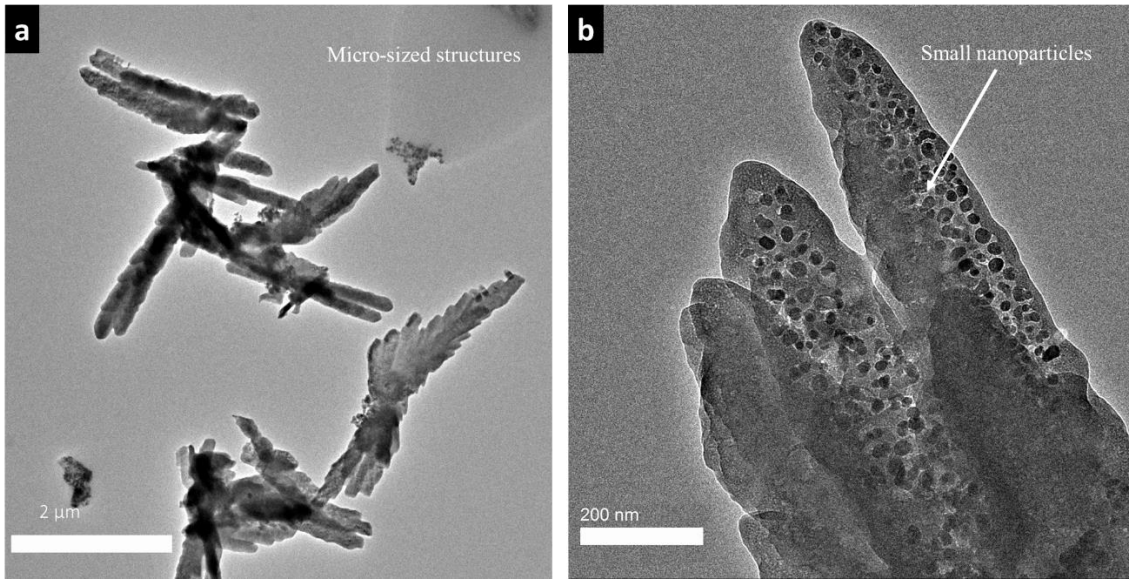

Figure 2.9. TEM images of precipitates obtained by adding the supernatant from a biogenic sulfide-rich (377 ± 9 mg/L S^{2-}) SRB culture medium to a 2M H_2SO_4 stripping solution loaded with copper (8,360 ± 124 mg/L copper), showing (a) a group of micro-sized particles of needle-like and radiating forms and (b) a detail of one structures with visible nanoparticles.

These results reveal that adding biogenic sulfide to the Cu stripping solution can produce covellite nanoparticles aggregated in larger structures that may be larger than 10 µm. Larger aggregates can be an advantage in a production process because it is easier to collect larger aggregates than nanoparticles. Sonication can be used to pulverise large aggregates into nanoparticles.

In a previous work in which a SRB growth medium containing biogenic sulfide was directly added to a much less concentrated (100 mg/L Cu) artificial Cu sulfate solution, precipitation of Cu (>95%) as covellite particles was also achieved using an S:Cu ratio of 2:1 (Costa et al. 2013). These results, in combination with our own, suggest that it is possible to produce covellite (nano)particles from sulfuric acid stripping solutions containing a wide range of Cu concentrations. Therefore, the solvent extraction process described herein can be applied to AMD waters of different Cu concentration levels and can be followed by a covellite precipitation process by adding biogenic sulfide-rich media to the loaded stripping solution.

It is known that Cu^{2+} ions can react with sulfide and form covellite (CuS) precipitates at low pH values (e.g. Sampaio et al. 2009), and the production of covellite with biogenic sulfide directly added to AMD samples has been reported previously (e.g. Silva et al. 2019). However, to our knowledge, this is the first report about the addition of biogenic sulfide to a purified Cu solution obtained by SX from an AMD sample, which has the great advantage of reducing the risk of co-precipitation of other metal sulfide particles.

Due to their unique optical, electrical, and catalytic properties (Yadav et al. 2019), chalcogenide semiconductor covellite nanoparticles are promising new materials for a wide range of applications, including optoelectronic devices (Coughlan et al. 2017), solar cells (van der Stam et al. 2016), lithium-ion batteries (Jiang et al. 2019), nanoscale switches (Sakamoto et al. 2003), sensors (Coughlan et al. 2017), photodegradation of pollutants (Wang et al. 2009), photocatalysis (van der Stam et al. 2016), and biomedicine (Goel et al. 2014; Yadav et al. 2019). However, the purity of covellite must be considered for each specific application. In our work, analysis of the

covellite revealed 97.3% purity for a covellite weight calculated based on the Cu concentration in the dissolved precipitates, and the sum of constituents other than Cu (Table S- 2.2). Moreover, the relatively high unidentified "other" constituents (1.5%) may be related to anions that could have binded to the metal cations (mainly calcium and iron) and formed precipitates. Therefore, further purification steps may be performed depending on the desired application.

2.4. **Conclusions**

This work attempts to contribute in two ways to raising the interest in implementing metal recovery from AMD-affected areas. Such an approach will treat highly contaminated mine waters, decreasing the environmental impact of AMD and simultaneously increase the circular economy of metals.

The reported results confirm the potential utility of using a SX process with 30% (v/v) Acorga M5640 in kerosene-like solvents with 2.5% octanol to extract over 95% of the Cu present in highly acidic, metal-rich AMD, generating 2M sulfuric acid solutions with Cu concentrations greater than 45 g/L that are suitable as electrolytes for the well-established Cu electrowinning process that often accompanies the acid-leaching of oxide Cu ores.

Our work also demonstrates the feasibility of combining SX systems with biological processes that add biogenic sulfide at S:Cu ratios of ≈ 2:1 to recover the extracted Cu as covellite nanoparticles. The covellite produced can be used in a variety of renewable energy, biomedical, and other applications.

2.5. **References**

Agarwal S, Ferreira AE, Santos SMC, Reis MTA, Ismael MRC, Correia MJN, Carvalho JMR (2010) Separation and recovery of copper from zinc leach liquor by solvent extraction using Acorga M5640. Int J Miner Process 97(1–4):85–91. https://doi.org/10.1016/j.minpro.2010.08.009

Agarwal S, Reis MTA, Ismael MRC, Correia MJN, Carvalho JMR (2012) Modeling of the Extraction Equilibrium of Copper from Sulfate Solutions with Acorga M5640. Solvent Extr Ion Exch 30(5):536–551. https://doi.org/10.1080/07366299.2012.670603

Aksamitowski P, Wieszczycka K, Wojciechowska I (2018) Selective copper extraction from sulfate media with N,N-dihexyl-N′-hydroxypyridine-carboximidamides as extractants. Sep Purif Technol 201:186–192. https://doi.org/10.1016/j.seppur.2018.02.051

Alguacil FJ, Alonso M, López-Delgado A, Navarro P (2004) Modelling copper (II) liquid-liquid extraction: the system Acorga M5640-Exxsol D100-CuSO4-H2SO4. J Chem Res (s) 2004(3):196–197. https://doi.org/10.3184/0308234041640591

Álvarez-Valero AM, Pérez-López R, Matos J, Capitán MA, Nieto JM, Sáez R, Delgado J, Caraballo M (2008) Potential environmental impact at São Domingos mining district (Iberian Pyrite Belt, SW Iberian Peninsula): evidence from a chemical and mineralogical characterization. Environ Geol 55(8):1797–1809. https://doi.org/10.1007/s00254-007-1131-x

Andersson SO, Reinhardt H (1983) Recovery of metals from liquid effluents, 1st edn. John Wiley & Sons

Arndt NT, Fontboté L, Hedenquist JW, Kesler SE, Thompson JFH, Wood DG (2017) Future Global Mineral Resources. Geochem Persp 1–171. https://doi.org/10.7185/geochempersp.6.1

Batista M (2000) Environmental State in the Portuguese Test Site S. Domingos Mine: Past and Present. Instituto Geológico e Mineiro-Ministério da Economia Available from http://www.cemsd.pt/node/2439

Carlier JD, Alexandre LM, Luís AT, Costa MC (2019) Potential of industrial by-products and wastes from the Iberian Peninsula as carbon sources for sulphate-reducing bacteria. Int J Environ Sci Technol 16(8):4719–4738. https://doi.org/10.1007/s13762-018-02197-z

Costa MC, Duarte JC (2005) Bioremediation of Acid Mine Drainage Using Acidic Soil and Organic Wastes for Promoting Sulphate-Reducing Bacteria Activity on a Column Reactor. Water Air Soil Pollut 165(1–4):325–345. https://doi.org/10.1007/s11270-005-6914-7

Costa MC, Martins M, Jesus C, Duarte JC (2008) Treatment of Acid Mine Drainage by Sulphate-reducing Bacteria Using Low Cost Matrices. Water Air Soil Pollut 189(1–4):149–162. https://doi.org/10.1007/s11270-007-9563-1

Coughlan C, Ibáñez M, Dobrozhan O, Singh A, Cabot A, Ryan KM (2017) Compound Copper Chalcogenide Nanocrystals. Chem Rev 117(9):5865–6109. https://doi.org/10.1021/acs.chemrev.6b00376

da Costa JP, Girão AV, Lourenço JP, Monteiro OC, Trindade T, Costa MC (2013) Green synthesis of covellite nanocrystals using biologically generated sulfide: Potential for bioremediation systems. J Environ Manage 128:226–232. https://doi.org/10.1016/j.jenvman.2013.05.034

Davis-Belmar CS, Gallardo I, Demergasso C, Rautenbach G (2012) Effect of organic extractant LIX 84IC, pH and temperature changes on bioleaching microorganisms during SX treatment. Hydrometallurgy 129–130:135–139. https://doi.org/10.1016/j.hydromet.2012.09.004

Deep A, Kumar P, Carvalho JMR (2010) Recovery of copper from zinc leaching liquor using ACORGA M5640. Sep Purif Technol 76(1):21–25. https://doi.org/10.1016/j.seppur.2010.09.015

Elshkaki A, Graedel TE, Ciacci L, Reck BK (2016) Copper demand, supply, and associated energy use to 2050. Glob Environ Change 39:305–315. https://doi.org/10.1016/j.gloenvcha.2016.06.006

European Commission (2014) Report on Critical Raw Materials for the EU

Ferreira AE, Agarwal S, Machado RM, Gameiro MLF, Santos SMC, Reis MTA, Ismael MRC, Correia MJN, Carvalho JMR (2010) Extraction of copper from acidic leach solution with Acorga M5640 using a pulsed sieve plate column. Hydrometallurgy 104(1):66–75. https://doi.org/10.1016/j.hydromet.2010.04.013

Ficklin WH, Plumlee GS, Smith KS, McHugh JB (1992) Geochemical classification of mine drainages and natural drainages in mineralized areas. Balkema, Rotterdam, pp 381–384
Flett DS, Okuhara DN, Spink DR (1973) Solvent extraction of copper by hydroxy oximes. J Inorg Nucl 35(7):2471–2487. https://doi.org/10.1016/0022-1902(73)80315-X
Frenzel M, Tolosana-Delgado R, Gutzmer J (2015) Assessing the supply potential of high-tech metals – A general method. Resour Policy 46:45–58. https://doi.org/10.1016/j.resourpol.2015.08.002
GARD Guide (Global Acid Rock Drainage Guide) (Chapter 2) The Acid Rock Drainage Process
Goel S, Chen F, Cai W (2014) Synthesis and Biomedical Applications of Copper Sulfide Nanoparticles: From Sensors to Theranostics. Small 10(4):631–645. https://doi.org/10.1002/smll.201301174
Hedrich S, Kermer R, Aubel T, Martin M, Schippers A, Johnson DB, Janneck E (2018) Implementation of biological and chemical techniques to recover metals from copper-rich leach solutions. Hydrometallurgy 179:274–281. https://doi.org/10.1016/j.hydromet.2018.06.012
Hoh Y-C, Wang W-K (2007) Fundamental aspects of lead extraction and stripping by a liquid ion exchange reagent. J Chem Technol Biotechnol 31(1):345–350. https://doi.org/10.1002/jctb.503310147
ICSG (2018) The World Copper Factbook. Tech Rep. International Copper Study Group
International Copper Study Group (2019) The World Copper Fact Book
Jha MK, Kumar V, Singh RJ (2001) Review of hydrometallurgical recovery of zinc from industrial wastes. Resour Conserv Recycl 33(1):1–22. https://doi.org/10.1016/S0921-3449(00)00095-1
Jiang K, Chen Z, Meng X (2019) CuS and Cu_2S as Cathode Materials for Lithium Batteries: A Review. ChemElectroChem 6(11):2825–2840. https://doi.org/10.1002/celc.201900066
Jose Alguacil F, Regel-Rosocka M (2018) Hydrometallurgical treatment of hazardous copper Cottrell dusts to recover copper. Physicochem Probl Miner Process ISSN 2084-4735. https://doi.org/10.5277/PPMP1880
Kaksonen AH, Puhakka JA (2007) Sulfate Reduction Based Bioprocesses for the Treatment of Acid Mine Drainage and the Recovery of Metals. Eng Life Sci 7(6):541–564. https://doi.org/10.1002/elsc.200720216
Kalin M, Fyson A, Wheeler WN (2006) The chemistry of conventional and alternative treatment systems for the neutralization of acid mine drainage. Sci Total Environ 366(2–3):395–408. https://doi.org/10.1016/j.scitotenv.2005.11.015
Kefeni KK, Msagati TAM, Mamba BB (2017) Acid mine drainage: Prevention, treatment options, and resource recovery: A review. J Clean Prod 151:475–493. https://doi.org/10.1016/j.jclepro.2017.03.082
Lewis AE (2010) Review of metal sulphide precipitation. Hydrometallurgy 104(2):222–234. https://doi.org/10.1016/j.hydromet.2010.06.010
Macías F, Pérez-López R, Caraballo MA, Cánovas CR, Nieto JM (2017) Management strategies and valorization for waste sludge from active treatment of extremely metal-polluted acid mine drainage: A contribution for sustainable mining. J Clean Prod 141:1057–1066. https://doi.org/10.1016/j.jclepro.2016.09.181
Matinde E (2018) Mining and metallurgical wastes: a review of recycling and re-use practices. J S Afr Inst Min Metall 118(8). https://doi.org/10.17159/2411-9717/2018/v118n8a5

Matos JX, Pereira Z, Oliveira V, Oliveira JT (2006) The geological setting of the São Domingos pyrite orebody, Iberian Pyrite Belt. Proceedings of the VII National Geology Congress. Universidade de Évora, Estremoz, Portugal. 283-286

Morais C, Rosado L, Mirão J, Pinto AP, Nogueira P, Candeias AE (2008) Impact of acid mine drainage from Tinoca Mine on the Abrilongo dam (southeast Portugal). Mineral Mag 72(1):467–472. https://doi.org/10.1180/minmag.2008.072.1.467

Nleya Y, Simate GS, Ndlovu S (2016) Sustainability assessment of the recovery and utilisation of acid from acid mine drainage. J Clean Prod 113:17–27. https://doi.org/10.1016/j.jclepro.2015.11.005

Nordstrom DK, Bowell RJ, Campbell KM, Alpers CN (2017) Challenges in Recovering Resources from Acid Mine Drainage. Conference publication. 13th International Mine Water Association Congress - Mine Water Circular Economy. Lappeenranta, Finland. 1138-1146. http://pubs.er.usgs.gov/publication/70190131

Ochromowicz K, Chmielewski T (2013) Solvent extraction of copper(II) from concentrated leach liquors. Physicochem Probl Miner Process. ISSN 2084-4735. https://doi.org/10.5277/PPMP130132

Oliveira JT, Oliveira V (1996) Síntese da Geologia da faixa piritosa, em Portugal, e das principais minerações assoaciadas. Castro Verde, Castro Verde, Portugal [Portuguese]

Pereira R, Ribeiro R, Gonçalves F (2004) Plan for an Integrated Human and Environmental Risk Assessment in the S. Domingos Mine Area (Portugal). Hum Ecol Risk Assess 10(3):543–578. https://doi.org/10.1080/10807030490452197

Postgate JR (1984) The Sulphate-Reducing Bacteria. Cambridge Univ Press

Reichl C, Schatz M (2020) World mining data

Ruiz MC, González I, Rodriguez V, Padilla R (2019) Solvent Extraction of Copper from Sulfate–Chloride Solutions Using LIX 84-IC and LIX 860-IC. Miner Process Extr Metall. 1–8. https://doi.org/10.1080/08827508.2019.1647839

Ruiz MC, Risso J, Seguel J, Padilla R (2020) Solvent extraction of copper from sulfate-chloride solutions using mixed and modified hydroxyoxime extractants. Miner Eng. 146:106109. https://doi.org/10.1016/j.mineng.2019.106109

Sakamoto T, Sunamura H, Kawaura H, Hasegawa T, Nakayama T, Aono M (2003) Nanometer-scale switches using copper sulfide. Appl Phys Lett 82(18):3032–3034. https://doi.org/10.1063/1.1572964

Sampaio RMM, Timmers RA, Xu Y, Keesman KJ, Lens PNL (2009) Selective precipitation of Cu from Zn in a pS controlled continuously stirred tank reactor. J Hazard Mater 165(1–3):256–265. https://doi.org/10.1016/j.jhazmat.2008.09.117

Schäfer P, Schmidt M (2019) Discrete-Point Analysis of the Energy Demand of Primary versus Secondary Metal Production. Environ Sci Technol :acs.est.9b05101. https://doi.org/10.1021/acs.est.9b05101

Schindelin J, Arganda-Carreras I, Frise E, Kaynig V, Longair M, Pietzsch T, Preibisch S, Rueden C, Saalfeld S, Schmid B, Tinevez J-Y, White DJ, Hartenstein V, Eliceiri K, Tomancak P, Cardona A (2012) Fiji: an open-source platform for biological-image analysis. Nat Methods 9(7):676–682. https://doi.org/10.1038/nmeth.2019

Schipper BW, Lin H-C, Meloni MA, Wansleeben K, Heijungs R, van der Voet E (2018) Estimating global copper demand until 2100 with regression and stock dynamics. Resour Conserv Recycl 132:28–36. https://doi.org/10.1016/j.resconrec.2018.01.004

Schlesinger ME, King MJ, Sole KC, Davenport WG (2011) Electrowinning. In: Extractive Metallurgy of Copper. Elsevier, pp 349–372
Segura-Salazar J, Tavares L (2018) Sustainability in the Minerals Industry: Seeking a Consensus on Its Meaning. Sustainability 10(5):1429. https://doi.org/10.3390/su10051429
Silva PMP, Lucheta AR, Bitencourt JAP, Carmo ALV do, Cuevas IPÑ, Siqueira JO, Oliveira GC de, Alves JO (2019) Covellite (CuS) Production from a Real Acid Mine Drainage Treated with Biogenic H2S. Metals 9(2):206. https://doi.org/10.3390/met9020206
Sole KC, Hardwick E (2016) Recovery of copper from Chilean mine waste waters. Technische Universität Bergakademie Freiberg: Leipzig, Germany.
Sverdrup HU, Olafsdottir AH, Ragnarsdottir KV (2019) On the long-term sustainability of copper, zinc and lead supply, using a system dynamics model. Resour Conserv Recycl. X 4:100007. https://doi.org/10.1016/j.rcrx.2019.100007
Tanaydın MK, Demirkıran N (2020) Kinetic models for the extraction of copper by Acorga M5640 after leaching of malachite ore in perchloric acid solutions and the stripping of copper from loaded organic phase. Braz J Chem Eng 37(2):399–414. https://doi.org/10.1007/s43153-020-00032-y
Tavares MT, Sousa AJ, Abreu MM (2008) Ordinary kriging and indicator kriging in the cartography of trace elements contamination in São Domingos mining site (Alentejo, Portugal). J Geochem Explor. 98(1–2):43–56. https://doi.org/10.1016/j.gexplo.2007.10.002
Taylor J, Pape S, Murphy N (2005) A summary of passive and active treatment technologies for acid and metalliferous drainage (AMD). Fremantle, Australia
Vander Linden J (1998) Selective recuperation of copper by supported liquid membrane (SLM) extraction. J Membrane Sci 139(1):125–135. https://doi.org/10.1016/S0376-7388(97)00252-4
van der Stam W, Berends AC, de Mello Donega C (2016) Prospects of Colloidal Copper Chalcogenide Nanocrystals. ChemPhysChem 17(5):559–581. https://doi.org/10.1002/cphc.201500976
Vasilyev F, Virolainen S, Sainio T (2017) Modeling the phase equilibrium in liquid–liquid extraction of copper over a wide range of copper and hydroxyoxime extractant concentrations. Chem Eng Sci 171:88–99. https://doi.org/10.1016/j.ces.2017.05.003
Villa-Gomez D, Ababneh H, Papirio S, Rousseau DPL, Lens PNL (2011) Effect of sulfide concentration on the location of the metal precipitates in inversed fluidized bed reactors. J Hazard Mater :S0304389411005486. https://doi.org/10.1016/j.jhazmat.2011.05.002
Wang H, Ren ZJ (2014) Bioelectrochemical metal recovery from wastewater: A review. Water Res 66:219–232. https://doi.org/10.1016/j.watres.2014.08.013
Wang L, Li Q, Sun X, Wang L (2019) Separation and recovery of copper from waste printed circuit boards leach solution using solvent extraction with Acorga M5640 as extractant. Sep Sci Technol 54(8):1302–1311. https://doi.org/10.1080/01496395.2018.1539106
Wang X, Fang Z, Lin X (2009) Copper sulfide nanotubes: facile, large-scale synthesis, and application in photodegradation. J Nanopart Res 11(3):731–736. https://doi.org/10.1007/s11051-008-9480-2
Wanger T, Eglinger J (2021) particlesizer: v1.0.9. ImageJ plugin to derive number based size distributions based on recorded TEM images
Yadav S, Shrivas K, Bajpai PK (2019) Role of precursors in controlling the size, shape and morphology in the synthesis of copper sulfide nanoparticles and their application for

fluorescence detection. J Alloys Compd 772:579–592. https://doi.org/10.1016/j.jallcom.2018.08.132

2.6. **Annexes**

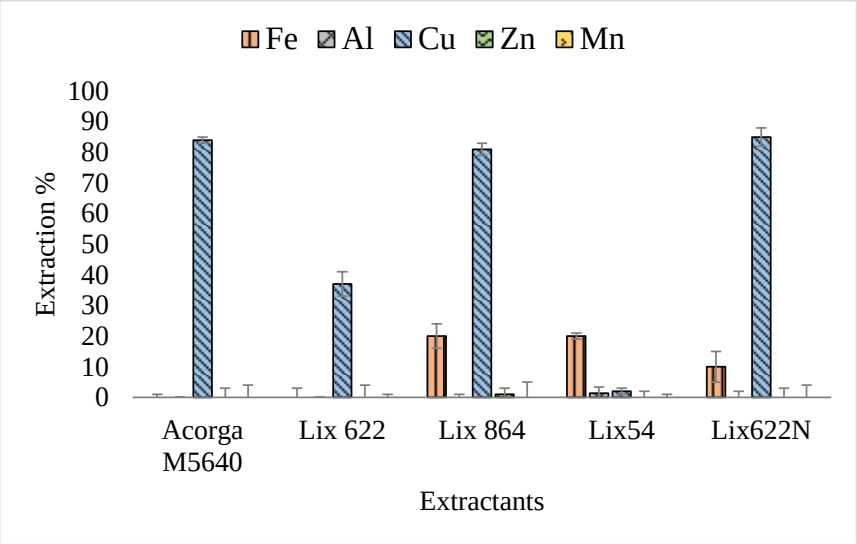

Figure S- 2.1. Screening of extractants for copper separation from the extreme AMD, with 15% (v/v) of each extractant diluted in Shell GTL + 2.5% (v/v) octanol, using an A/O = 1/1 and a contact time of 30 minutes at room temperature (25 ± 3 ºC). Results are averages of duplicates, and the error bars are mean deviations.

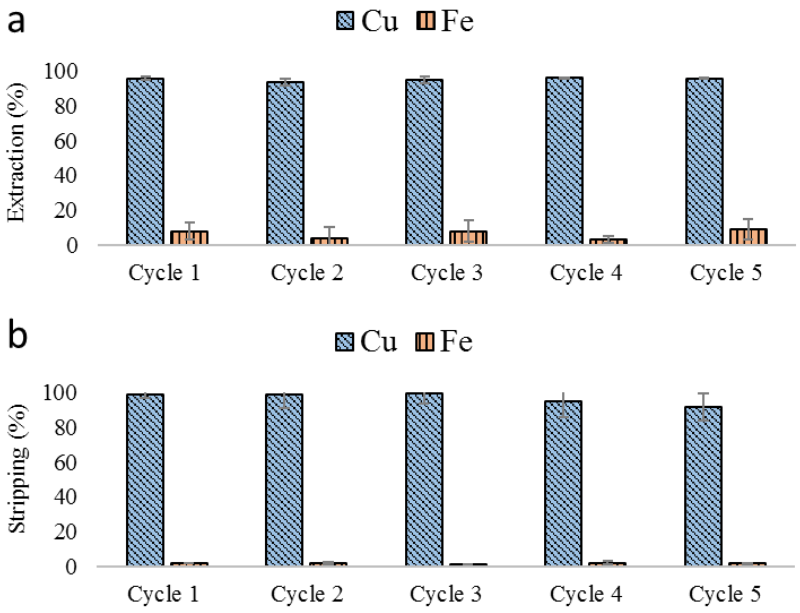

Figure S- 2.2. (a) Extraction and (b) stripping of copper and iron in five successive cycles of extraction and stripping, using the extreme AMD and the same organic phase (30% (v/v) Acorga M5640 in Shell GTL + 2.5% (v/v) octanol) but with new stripping solutions (2M H_2SO_4), with an A/O = 1/1, and a contact time of 60 minutes at room temperature 25 ± 3ºC. Results are averages of triplicates, and the error bars are standard deviations.

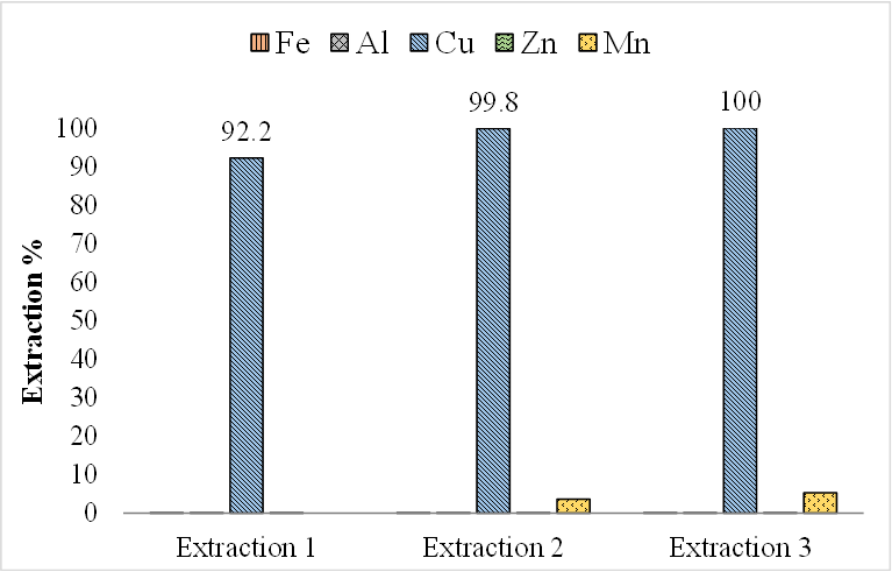

Figure S- 2.3. Cumulative extraction efficiencies in three successive new extractions from the same extreme AMD with 30% v/v ACORGA M5640 in Shell GTL + 2.5 % (v/v) octanol, using an A/O = 1/1 and a contact time of 60 minutes at room temperature 25 ± 3ºC.

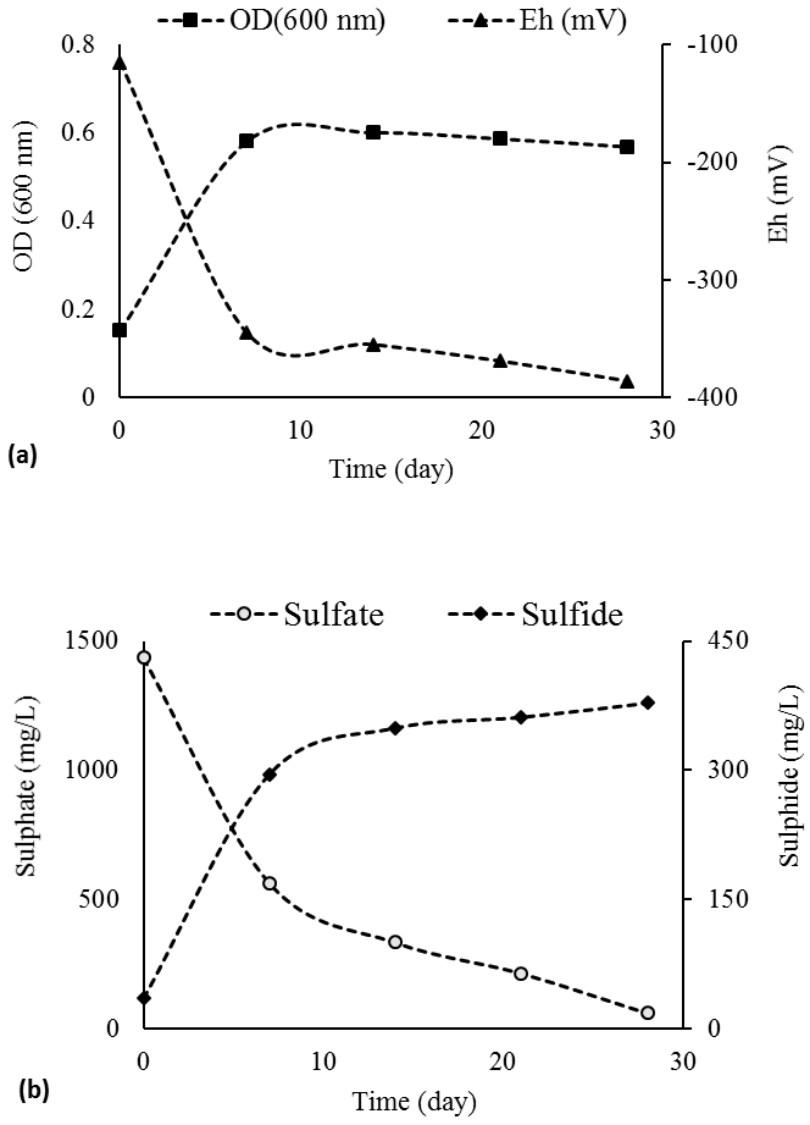

Figure S- 2.4. Evolution of growth parameters of SRB in Postage B medium measured during incubation after inoculation with a previously SRB enriched culture; (a) optical density (OD at 600 nm) and redox potential (Eh) and (b) sulfate and sulfide concentrations.

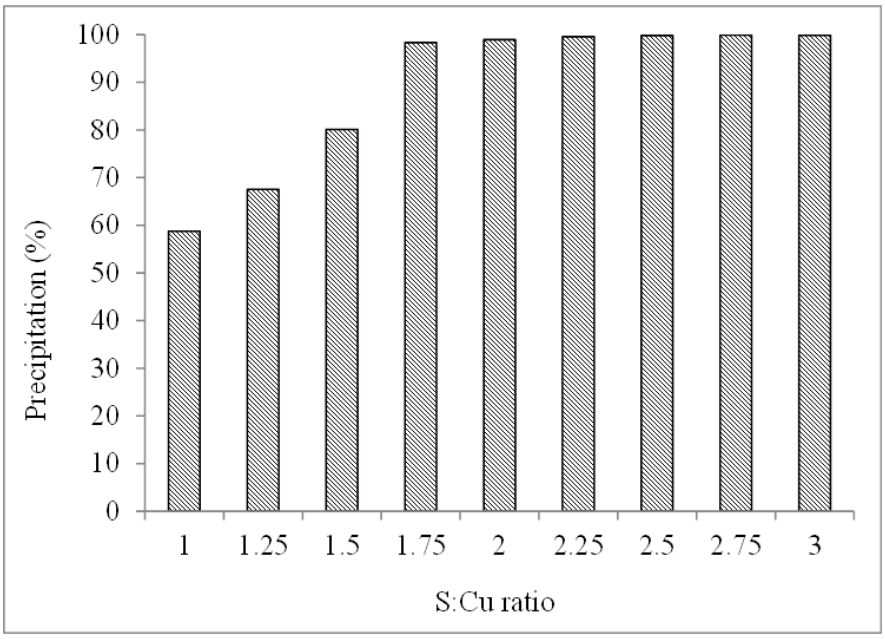

Figure S- 2.5. Efficiency of copper precipitation in a 2M H_2SO_4 stripping solution loaded with copper (8356 ± 124 mg/L copper) from the solvent extraction process tested to recover copper from the extreme AMD, after addition of a sulfide rich (377 ± 9 mg/L S^{2-}) SRB culture medium to make different S:Cu ratios.

Table S- 2.1. Copper concentrations at equilibrium in three consecutive cycles of extraction without stripping, using the same organic phase (30% Acorga M5640 in Shell GTL with 2.5% octanol) but new AMD in each cycle, with an A/O = 1/1 and 60 minutes contact time at room temperature (25 ± 3ºC). Results are averages of triplicates ± standard deviations.

Cycle	[Copper] in final organic phase (g/L)	[Copper] in final aqueous phase (g/L)
1	5.06 ± 0.02	0.17 ± 0.01
2	11.5 ± 0.02	0.345 ± 0.007
3	16.1 ± 0.007	0.64 ± 0.03

Table S- 2.2. Concentrations and percentages of elements other than copper in the digested (10.4 g/L) covellite particles produced by addition of biogenic sulfide to the SX stripping solution.

Contaminants	Concentration (mg/L)	%
Ca	51.3	0.493
Fe	43.1	0.414
Al	11.1	0.107
Na	11.0	0.106
Mg	2.01	0.019
As	1.83	0.018
Zn	1.68	0.016
Pb	0.39	0.004
Se	0.2	0.002
Mn	0.15	0.001
Co	0.09	0.001
Cd	0.09	0.001
Cr	0.09	0.001
Ni	0.06	0.001
others	154	1.477
Sum	277	2.661

CHAPTER 3

Zinc recovery from an extreme copper-free acid mine drainage: studying the prior separation of ferric iron by solvent extraction using AliCy and/or alkalinization

Zinc recovery from an extreme copper-free acid mine drainage: studying the prior separation of ferric iron by solvent extraction using AliCy and/or alkalinization

A modified version of this chapter was published as:

Nobahar, Amir; Bejiga Melka, Alemu; Marín-Beltrán, Isabel; Neves, Luiz; Costa, Maria Clara; Carlier, Jorge Dias. "Zinc recovery from an extreme copper-free acid mine drainage: studying the prior separation of iron by solvent extraction using AliCy and/or alkalinization". Journal of Sustainable metallurgy (2022): https://doi.org/10.1007/s40831-022-00588-8

Abstract

Zn recovery attempts from a copper-free extreme Acid Mine Drainage with ~53g/L Fe and ~2g/L Zn revealed Fe co-extraction in solvent extraction with 0.9M D2EHPA or a mixture of 0.72M D2EHPA and 0.18M Cyanex 272, and simultaneous precipitation of Fe during zinc sulfide recovery through biogenic sulfide addition. Therefore, alkalinization, solvent extraction with the self-prepared ionic liquid AliCy diluted in kerosene, and combinations of both these methods were studied for the separation of ferric iron (Fe^{3+}) from such water, prior to Zn recovery. The most efficient strategy tested was a solvent extraction cycle with AliCy followed by alkalinization of its aqueous raffinate to pH 3.25 or 3.5. As a result of this approach, ~92% of Fe^{3+} is separated by SX and the remaining is removed by precipitation, with just ~12% or ~17% Zn losses, respectively. Afterwards, the highest Zn recovery from water resulting from such combination of process was achieved by precipitation through addition of biogenic sulfide at pH=3.5. The obtained precipitates are nanoparticles of Wurzite and Sphalerite (ZnS) of sizes between 2 to 22 nm agglomerated into larger structures. This work shows for the first time the potential of AliCy to separate Fe^{3+} from acidic multimetallic solutions, a known contaminant of several metal recovery processes.

Keywords

Acid mine drainage; ionic liquid; iron solvent extraction; metal bio-recovery; zinc sulfide

Graphical abstract

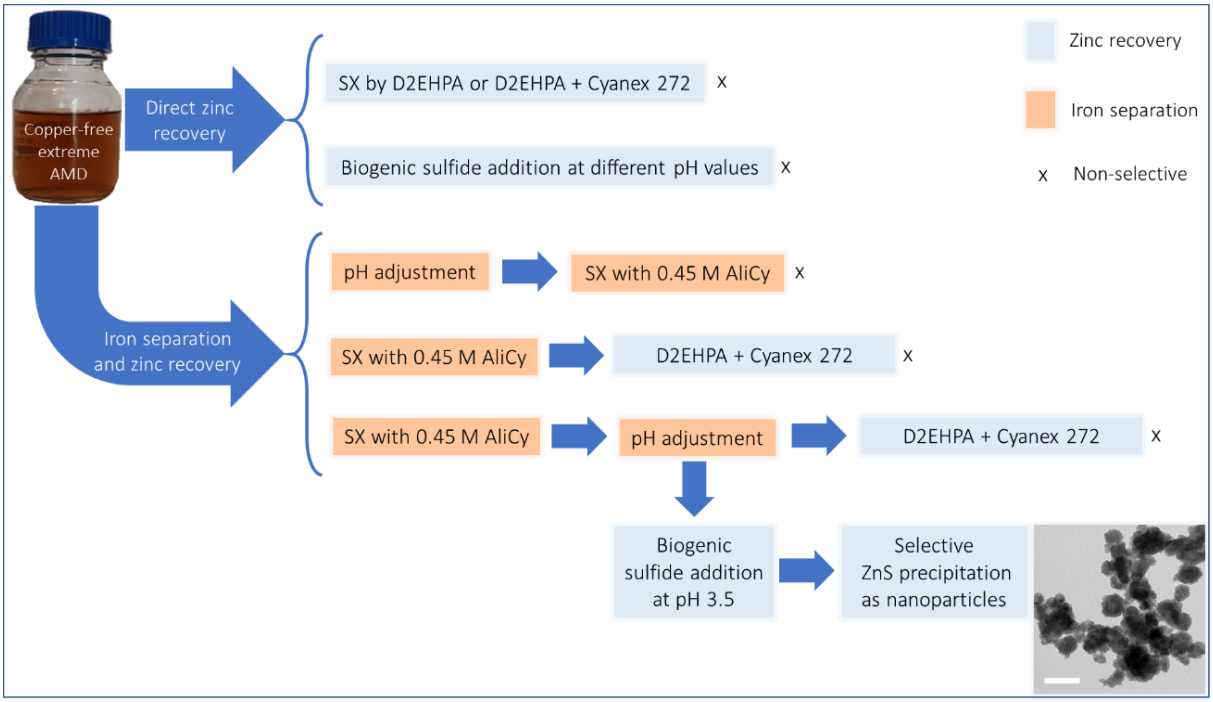

3.1. Introduction

As a result of rapid industrialization and increasing demand for metals, there are major concerns regarding the future availability of metals that are found on the endangered list of elements due to their low abundance and difficulty to obtain. Zn, one of the important endangered metals, is a crucial element for different industrial sectors and any form of life on Earth (Graedel et al. 2005; Tolchin 2014). According to world annual data of mining per capita, 12 643 000 metric tons of Zn are totally produced per year (data of 2018 year) (Reichl and Schatz 2020), and approximately 30% of global Zn production arises from recycling (Schneeberger et al. 2012). Demand for Zn by the end of this century is expected to increase continuously up to 130% (Watari et al. 2021). Besides, Sverdrup et al., (2019) believe that after 2052, the amount of Zn in use will be larger than in ore deposits and thereafter, it will be supplied mostly from Zn recovery from secondary sources and less from mining.

One of the possible secondary sources of metals is water affected by Acid Mine Drainage (AMD), an extended environmental problem characterized by high acidity and elevated concentrations of SO_4^{2-} and different metals such as Fe, Zn and Cu (Naidu et al. 2019). Mining activities are often associated with the production of large volumes of AMD (Johnson and Hallberg 2005) which causes severe environmental impacts, particularly on soil, water resources and aquatic organisms (Shim et al. 2015; Galhardi and Bonotto 2016). In South West Spain and South of Portugal mining activity has been deeply intense due to the polymetallic massive sulfide deposits of the Iberian Pyrite Belt, and the total affected area by mining activity is estimated as 5000 ha (Martínez et al. 2019). Recently Moreno-González et al. (2020) have reported very high concentrations (up to 408 g/L of SO_4^{2-}, 194 g/L of Fe, 11 g/L of Zn, 2.2 g/L of As) and very low pH in waters in the Iberian Pyrite Belt area.

The need for sustainable approaches of AMD treatment has led to focus on water reuse and resource recovery. However, despite the available remediation approaches, AMD treatment associated to metal recovery remains a challenge. Although many researchers have discussed the metal precipitation from AMD (Johnson and Hallberg 2005; RoyChowdhury et al. 2015), only a few number have focused on the metal recovery (Kefeni et al. 2017; Cánovas et al. 2020). Naidu et al. (2019) reviewed methods that are currently being used for treatment and metal recovery from AMD via chemical, electrochemical and biological methods. Recent research has been focused on searching for suitable combinations of physical, chemical and biological methods for the selective recovery of metals from AMD (Naidu et al. 2019; Nanusha et al. 2019; Luptáková et al. 2020; Wang et al. 2021). Yet, efficient recycling methods are still required that can address both the environmental and economic perspectives.

Among the various processes, solvent extraction (SX) has got a wider application among other techniques, as it shows high metal selectivity and extraction efficiency from aqueous leaching solutions in the hydrometallurgical treatment of ores and secondary materials (Hedrich et al. 2018). The SX process is focused on the removal of specific constituents by transferring them from the aqueous phase to an immiscible non-aqueous phase. It is an extensively used method for the recovery and purification of metals because of being simple, selective and cost-efficient with less reaction time and favorable reaction conditions (Coll et al. 2012). Among the reagents used in Zn SX, organophosphorus acid based extractants play a significant role. Various kinds of extractants are used for Zn SX processes such as; Di-(2-ethylhexyl) phosphoric acid (D2EHPA), tributyl

phosphate (TBP), Bis-(2,4,4-trimethylpentyl) phosphinic acid (Cyanex 272) and the synergistic mixture of D2EPHA and Cyanex 272 (Deep and de Carvalho 2008). These organophosphorus extractants primarily behave as cation exchangers (Eq. 3.1) and the extraction of Zn(II) is pH dependent (Mansur et al. 2008; Deep and de Carvalho 2008).

$$Zn^{2+}_{(aq)} + mHA_{(org)} \rightarrow ZnA_2HA_{(m-2)(org)} + 2H^+ \qquad \text{Eq. 3.1}$$

where HA is the extractant molecule, and *m* can vary from 2 to 4.

Fe is frequently present in AMD as ferrous (Fe^{2+}) and ferric iron (Fe^{3+}), and is generally considered as an impurity (and trouble) in the hydrometallurgical processing of Zn (Jha et al. 2001; Sinha et al. 2014). Both Zn^{2+} and Fe^{3+} are extracted by organophosphorus extractants such as D2EHPA, Octylphenyl acid phosphate (OPAP), and Mono-(2-ethylhexyl) phosphoric acid (M2EHPA) (Principe and Demopoulos 2004; Azizitorghabeh et al. 2015). Thus, several chemical precipitation strategies have been applied in Zn industries for a previous removal of dissolved Fe^{3+}, such as jarosite (Dutrizac and Jambor 2000; Pappu et al. 2006), goethite (Davey and Scott 1976; Pradel et al. 1993), hematite (Ismael and Carvalho 2003) and paragoethite (ferrihydrite and schwertmannite) (Jambor and Dutrizac 1998; Loan et al. 2002; Loan et al. 2006; Claassen and Sandenbergh 2006) processes. However, these processes have economical disadvantages, due to their high operational costs. Thus, experiments on Fe^{3+} extraction from synthetic and real metallic SO_4^{2-} solutions by SX have been performed using different extractants, such as trioctylmethylammonium chloride (Aliquat 336) (Tait 1992), bis 2,4,4-trimethylpentyphosphinic acid (Cyanex 272) (Biswas et al. 2007), Cyanex 923 (Stefánsson 2007), octylphenyl acid phosphate (Principe and Demopoulos 2004) and methyl isobutyl ketone (Sunda and Huntsman 2003). Plus, a recent focus has been towards producing Fe marketable products from waste liquors by applying SX (Agrawal and Sahu 2010; Mishra et al. 2010). Interestingly, when the self-prepared ionic liquid trioctylmethylammonium/2,4,4-trimethylpentyl phosphinate synthesized from the two extractants Aliquat 336 and Cyanex 272 (called AliCy when first tested for boron extraction by Fortuny et al. (2012)) was investigated by Devi (2016) for Cu extraction from a synthetic multi-metallic sulfuric acid solution revealed an extraction rate of metal ions in the order of Fe>Zn>Cu>Cd>Co>Ni. Yet, to our knowledge the so-called ionic liquid AliCy was never explored for the separation of Fe prior to the recovery of other metals.

The efficacy of selective metal recovery by these methods from liquid waste streams largely depends on the matrix composition and chemical speciation of the targeted metal in the waste

(Zhuang et al. 2015) as each metal has unique features and physical-chemical properties that generate specific mechanisms of action (Luch 2012; Magalhães et al. 2015). For example, Fe in the ferrous oxidation state (Fe^{2+}) is soluble across a broad pH range from highly acidic to mildly alkaline (< pH 7~8), whereas Fe^{3+} is soluble only in acid solutions (< pH 3~4) (Monhemius 2017). Indeed, there have been investigations on selective precipitation of metals at controlled pH values. For instance, Rao et al. (1996) studied a precipitation process to remove Fe in the form of Fe^{3+} hydroxide ($Fe(OH)_3$) at pH 3.5 by adding lime and hydrogen peroxide followed by the recovery of Zn as zinc sulfide (ZnS) through injection of Na_2S. Nevertheless, these type of techniques require oxidizing and neutralizing agents (Mauchauffée et al. 2008; Jameson et al. 2010; Park et al. 2013; Park et al. 2015), which make them not cost-attractive.

Another promising approach, potentially less costly, is based on the use of sulfate-reducing bacteria (SRB), which use SO_4^{2-} as terminal electron acceptor in their anaerobic metabolism of the organic matter, reducing it to sulfide. Thus, the bacterially produced hydrogen sulfide can react with some metal ions to form insoluble metal sulfides. The use of biogenic sulfide released by SRB has been proven to efficiently precipitate zinc sulfides from unimetallic synthetic Zn solutions(Pinto da Costa et al. 2012; Vitor et al. 2015). Moreover, it is known that the solubility of metal sulfides varies for each metal differently with pH changes (Lewis 2010), and that precipitation of metal ions with hydrogen sulfide is largely dependent on the sulfide speciation, which in turn is pH-dependent, as given in equations 3.2 and 3.3 (Zvimba et al. 2011).

$$M^{2+} + HS^- \rightarrow MS + H^+ \qquad \text{Eq. 3.2}$$

$$H^+ + OH^- \rightarrow H_2O \qquad \text{Eq. 3.3}$$

Indeed, different reports indicate promising results regarding the selective separation of different metals using hydrogen sulfide generated by SRB at appropriate and controlled pH values (Foucher et al. 2001; Tabak et al. 2003; Veeken et al. 2003; Ucar et al. 2011; Ňancucheo and Johnson 2012; Steudel 2020). For instance, Foucher et al. (2001) performed selective recovery of Cu and Zn at pH 2.8 and 3.5, respectively, using SRB, and removal of Ni and Fe with sulfide at pH 6.

This study is the second part of a work performed aiming to contribute to enhance the recovery of metals from AMD. The first part revealed that SX with 30% (v/v) Acorga M5640 in kerosene with 2.5% octanol can extract over 95% of the Cu present in highly acidic and metal-rich AMD, and that 2M sulfuric acid solutions can re-extract Cu form such organic phase producing solutions with

concentrations of this metal above 45 g/L, thus useful for electrochemical or biological recovery processes (Nobahar et al. 2022). Now, the present study is focused on the recovery of Zn from the aqueous raffinate (henceforward referred as copper-free AMD) obtained from that Cu SX process with Acorga M5640. Zn recovery was tested by SX and by biogenic sulfide precipitation directly from such copper-free AMD as well as after the removal of Fe^{3+}. Different approaches were tested for Fe^{3+} removal: pH adjustment, SX with the self-prepared ionic liquid AliCy and combining both these methods. Furthermore, since (to our knowledge) this is the first time AliCy was tested to extract Fe^{3+} from such type of water, several experiments and analysis were performed to optimize and characterize this SX process.

3.2. Materials and methods

3.2.1. Copper-free AMD

In a previous work Cu was extracted from an extremely concentrated AMD collected at the São Domingos Mine, Portugal, through SX using Acorga M5640 diluted in a kerosene-like diluent (Shell GTL) with 2.5% (v/v) octanol as the extractant (Nobahar et al. 2022). The so-called copper-free AMD used in this work is the aqueous phase resulting from that SX process and was initially characterized for its pH and main metals (Table 3.1).

Table 3.1. Characterization of copper-free AMD obtained from an extreme AMD collected at the São Domingos mine after three cycles of SX with 30% (v/v) Acorga M5640 in Shell GTL + 2.5 % (v/v) octanol with an aqueous to organic phase volumes ratio (A/O) of 1 and a contact time of 60 minutes.

Parameter	Average	Standard Deviation	Units
pH	1.45	0.03	Standard unit (s.u.)
Eh	497	18	mV
[Fe]	52570	3729	mg/L
[Fe^{3+}]	46132	4186	
[Fe^{2+}]	6439	457	
[Al]	7298	634	
[Zn]	1824	242	
[Mn]	156	11	

3.2.2. Workflow

Aiming the removal of Fe^{3+} before Zn recovery, alkalinization tests to precipitate this ion and SX experiments to optimize and characterize its separation using AliCy in kerosene as extractant were carried out. In what concerns Zn, its direct recovery from the copper-free AMD was tested through SX using D2EHPA and D2EHPA plus Cyanex 272 on one side, and by biogenic sulfide addition on another side. Moreover, the recovery of Zn from the waters resulting from the Fe^{3+} separation processes was also tested by SX using D2EHPA plus Cyanex 272 and by biogenic sulfide addition. Table 3.2 summarizes the type of processes studied for Fe^{3+} removal and/or Zn recovery. Finally, the zinc sulfide precipitates obtained without Fe contamination were characterized.

Table 3.2. Procedures tested aiming Zn recovery from the copper-free AMD, organized by specific objectives.

Objective	Source	Process(es)
Ferric iron removal	copper-free AMD	Alkalinization
		SX with AliCy (optimization and characterization)
		Alkalinization + SX with AliCy
		SX with AliCy + Alkalinization
Zinc recovery	copper-free AMD	SX with D2EHPA
		SX with D2EHPA and Cyanex 272 – pH 1.5
		ZnS precipitation with biogenic sulfide
	Water obtained after ferric iron removal from copper-free AMD	SX with AliCy + SX with D2EHPA and Cyanex 272
		SX with AliCy + alkalinization + SX with D2EHPA and Cyanex 272
		SX with AliCy + alkalinization + ZnS precipitation with biogenic sulfide

3.2.3. Fe^{3+} removal from copper-free AMD

3.2.3.1. Alkalinization

It is known that Fe^{3+} can be removed from solution through alkalinization. The metal speciation-pH plots generated with the Medusa-Hydra software (Puigdomenech 2015) for simplified SO_4^{2-} matrixes show that Fe^{3+} begins to hydrolyze and form solid (oxy)hydroxides at low acidities (pH

> ~2), while Zn^{2+} hydrolyses and precipitates as hydroxide solids at higher acidities (pH > ~6) (Figure S- 3.1 andFigure S- 3.2). Seeking for an optimum pH, causing the highest precipitation of Fe^{3+} with the less Zn losses, the copper-free AMD was alkalinized to different pH values (2.0, 2.5, 2.75, 3.0, 3.25, 3.5, 4.0) by addition of sodium hydroxide solutions (5 M or 1 M or 0.5 M) and samples centrifuged (2800 g for 5 minutes at room temperature) for solids removal and subsequent metal analysis.

3.2.3.2. SX with AliCy (optimization and characterization)

The tested AliCy was prepared as described by Fortuny et al. (2012) with minimal modifications: equimolar concentrations (varying depending on the test) of Aliquat 336 and Cyanex 272 diluted in kerosene were mixed with an equal volume of 0.5 M sodium bicarbonate ($NaHCO_3$) aqueous solution for 10 minutes with vigorous magnetic stirring, in an open flask to allow the release of the CO_2 formed. Then, the aqueous phase was discarded using a decantation funnel and the organic phase mixed again with 0.5 M aqueous sodium bicarbonate solution as described before. It is recommended that to dilute the viscous Aliquat 336 in kerosene the mixture is heated in a water bath at 65ºC.

Devi (2016) reported that the extraction of Cu using AliCy reached a maximum value just after 5 minutes at 30 ± 1 ºC. In this work the Fe^{3+} SX experiments with AliCy were performed at room temperature (25 ± 3 ºC) and the contact time between the aqueous and the organic phases was always 60 minutes to guarantee maximum extractions. Larger volumes (10 to 70 mL total of both phases) were mixed in 100 mL round bottom flasks using magnetic stirrers, while smaller volumes (2 to 10 mL total) were mixed in centrifuge tubes shaken in the horizontal position. In both cases, the rotation speeds were in the range of 250 to 600 rpm to ensure the maximum mass transfer.

Several SX tests were carried out aiming to find optimal conditions for the extraction of Fe^{3+} from the copper-free AMD without co-extracting Zn. First, different AliCy concentrations in kerosene and different aqueous to organic phase volume (A/O) ratios were tested and one combination of these parameters was selected for further tests using copper-free AMD at different pH values. The pH values tested were the natural pH of copper-free AMD (pH 1.5) plus two acidified (pH 0.5 and 1.0) and two alkalinized (pH 2.0 and 2.5), because this is the range where the complexes having Fe^{3+} can be more abundant and where different complexes of Zn^{2+} can be present according to the Eh-pH diagrams generated with the Medusa-Hydra software [65] mimicking the Fe^{3+} (~1 M) or

the Zn (~0.03 M) plus the SO_4^{2-} concentrations (~1.5 M) in the copper-free AMD, assuming the average temperature (25ºC) of the laboratory where the SX tests were performed (Figure S- 3.3 andFigure S- 3.4). Then, using selected combinations of these parameters (AliCy concentration, A/O ratio and pH of copper-free AMD), a second extraction cycle was tested using newly prepared organic phase with the aqueous phase raffinate obtained from the first extraction cycle.

On the other hand, the re-extraction (stripping) of Fe from the loaded organic phase was first tested with different agents (just H_2O and 2 M sulfuric acid (H_2SO_4), 2 M nitric acid (HNO_3), 2 M hydrochloric acid (HCl), 2 M oxalic acid ($C_2H_2O_4$) and 2 M ammonium sulfate ($(NH_4)_2SO_4$) aqueous solutions), and then the selected agent (sulfuric acid) was tested at different concentrations. The molarities of sulfuric acid tested were 0.25 M, 0.5 M, 1.0 M, and 2.0 M because in this range different types of complexes having Fe^{3+} can be more abundant, according to the Eh-pH diagrams generated with the Medusa-Hydra software [65] for the approximate concentration of Fe in the extractant organic phase (~0.3 M), assuming complete stripping and a temperature of 25ºC (Figure S- 3.5).

Afterwards, to assess the organic phase's reusability, SX tests were carried out using non-regenerated and regenerated organic phases resulting from the stripping step after extraction. The organic phase regeneration was performed by mixing it two times with equal volumes of 0.5 M sodium bicarbonate aqueous solution during 10 minutes with vigorous magnetic stirring, as described above in AliCy preparation. Finally, 4 cycles of extraction and stripping were performed using a successively regenerated organic phase as the extractant and 2 M sulfuric acid solutions for stripping.

Finally, aiming to shed light on the Fe extraction mechanism, Fourier Transform Infrared Spectroscopy (FTIR) analysis of kerosene, AliCy in kerosene and Fe loaded AliCy in kerosene were performed.

3.2.3.3. Alkalinization + SX with AliCy

The copper-free AMD obtained after alkalinization to pH 2.75 and solids removal by centrifugation (2800 g for 5 minutes at room temperature) was re-acidified to its original pH (1.5) and subjected to SX with 0.45 M AliCy in kerosene aiming to extract the remaining Fe^{3+} in solution.

3.2.3.4. SX with AliCy + alkalinization

With the same objective, the aqueous phase raffinate obtained after Fe extraction from the raw copper-free AMD (pH=1.5) by SX with 0.45 M AliCy in kerosene was alkalinized to different pH values (2.0, 2.5, 2.75, 3.0, 3.25, 3.5 and 4.0) using sodium hydroxide solutions.

3.2.4. Zn recovery from copper-free AMD

3.2.4.1. SX with D2EHPA and with D2EHPA and Cyanex 272

Di-(2-ethylhexyl) phosphoric acid (D2EHPA) is a known Zn extractant from different types of metals-containing waters. Moreover, it has been proven that synergistic extractions with D2EHPA and other extractants can improve the extraction and separation of Zn from different matrixes, such as chloride pickle liquors (Azizitorghabeh et al. 2017) or SO_4^{2-} leach solutions (Asadi et al. 2018). This second work reports that SX with a mixture of 80% D2EHPA and 20% Cyanex 272 performed at 25°C, pH 3, an A/O ratio of 1, and a contact time of 25 min, showed the best synergistic effect to improve Zn extraction from a SO_4^{2-} leach liquor, while TBP acted more as a phase modifier. Moreover, in that work it is reported that the extraction of Zn in the pH range from 1.5 to 3.0 varied just between ~30% to ~40% if using D2EHPA or just between ~30% and 35% if using Cyanex 272. Therefore, since the AMD generated at the São Domingo's mining area is also a SO_4^{2-}-based matrix, in this work the SX experiments to test the extraction of Zn from the copper-free AMD were carried out with its natural acidity (pH ~1.5) and under conditions similar to those reported by (Asadi et al. 2018): with an A/O ratio of 1, a contact time of 30 minutes and at room temperature (25 ± 3 ºC). Total volumes of 50 mL for both phases were mixed in 100 mL round bottom flasks using magnetic stirrers with rotations in the range of 500 to 600 rpm.

Two experiments were performed: on one side 0.9 M D2EHPA in kerosene with 3% TBP was tested and on another side a mixture of 0.72 M D2EHPA and 0.18M Cyanex 272 in kerosene with 3% TBP was tested.

3.2.4.2. ZnS precipitation with biogenic sulfide

A SRB culture, previously enriched from sediments of a wastewater treatment plant (WWTP) anaerobic lagoon and maintained by successive subculturing in Postgate B growth medium (Postgate 1984), was used as source of sulfide. The sulfide rich medium (after SRB growth) was

added to copper-free AMD at different pH values aiming to find optimal conditions to selectively precipitate zinc sulfide. For that, the pH of both the copper-free AMD (pH = 1.5) and of the sulfide rich medium (pH = 6.5) were adjusted to the different tested values (pH = 1.0, 1.5, 2.0, 2.5 and 2.75) until becoming stable for 24 hours. 1 M sulfuric acid was used to decrease the pH and 5 M, 1 M and 0.5 M sodium hydroxide solutions were used to increase the pH. The SRB culture, before being acidified to the tested pH values, was centrifuged at 2800 g for 5 minutes at room temperature and the pellet discarded to eliminate bacterial cells and other solids. The copper-free AMD samples, in this case after the alkalinization, were also centrifuged at 2800 g for 5 minutes at room temperature and the pellet discarded to eliminate metal precipitates formed.

The volumes of copper-free AMD and SRB culture to be mixed were calculated based on the concentrations before centrifugations and pH adjustments. Thus, the target ratio of sulfide to zinc molarity (S/Zn) was 50 times the 1:1 stoichiometric value of ZnS to assure enough quantity of sulfide (because it is highly volatile). Nevertheless, the real tested S/Zn ratios were calculated based on concentrations measured just before mixing the sulfide rich medium and the copper-free AMD supernatants of tested pH values. Finally, the metals precipitation efficiency was calculated using the concentration of metals in solutions before mixing, and 72 hours after mixture and collection of precipitates by centrifugation (2800 g for 20 min at room temperature).

3.2.5. Zn recovery after Fe^{3+} removal

3.2.5.1. SX with AliCy + SX with D2EHPA and Cyanex 272

Seeking the selective extraction of Zn from the raffinate obtained after Fe^{3+} removal from the raw copper-free AMD by SX with 0.45 M AliCy, a subsequent SX experiment was performed using the synergistic mixture of 0.72 M D2EHPA and 0.18 M Cyanex 272 in kerosene with 3% (v/v) TBP as organic phase (under the conditions described above in section "*SX with D2EHPA and with D2EHPA and Cyanex 272"*).

3.2.5.2. SX with AliCy + alkalinization + SX with D2EHPA and Cyanex 272

Aiming to improve the selective extraction of Zn, another SX experiment was performed, this time using a synergistic mixture of 1.44 M D2EHPA and 0.36 M Cyanex 272 in kerosene with 3% (v/v) TBP as organic phase, and the following aqueous phase: the AliCy SX's raffinate alkalinized to

pH 3.25, after solids removal (by centrifugation at 2800 g for 5 minutes at room temperature) and reacidification to pH 2.0. This reacidification step was because the Zn selectivity by various extractants, including D2EHPA and Cyanex 272, decays at pH > 2.5 (Owusu 1998; Gharabaghi et al. 2013; Jha et al. 2014). The SX conditions were once again as described above in section "*SX with D2EHPA and with D2EHPA and Cyanex 272"*.

3.2.5.3. SX with AliCy + alkalinization + ZnS precipitation with biogenic sulfide

The selective recovery of Zn from the raffinate obtained after Fe^{3+} SX from the raw copper-free AMD with 0.45 M AliCy in kerosene was also attempted by addition of biogenic sulfide rich media (after SRB growth) at controlled pH values: 2.0, 2.5, 2.75, 3.0, 3.25 and 3.5.

3.2.6. Analytical methods

In each SX experiment, the concentration of each main metal (M) in the original AMD (Fe, Al, Cu, Zn, Mn) was determined in the initial aqueous phase of copper-free AMD - $[M_{aq}]_i$ - and in the final aqueous phase after SX - $[M_{aq}]_f$, while the concentrations of these metals in the final organic phase - $[M_{org}]_f$ - were calculated by mass balance. The removal efficiency of each metal was then calculated by dividing $[M_{org}]_f$ by $[M_{aq}]_i$ and multiplying the result by 100. The distribution ratio was also calculated as $D = [M_{org}]_f / [M_{aq}]_f$.

The pH was measured using a pH/E Meter GLP 21 (Crison) with a glass pH electrode (VWR, SJ 223). The SO_4^{2-} concentration was determined with a UV-visible spectrometer DR2800 (Hach-Lange) using the sulfaVer4 (Method 8051, Hach-Lange) procedure at 450 nm. The concentrations of Fe, Zn, and Mn were determined through flame atomic absorption spectroscopy with a novAA 350 system (Analytik Jena), and the concentration of Al was measured by microwave plasma atomic emission spectrometry with a 4200 MP-AES (Agilent). Calibration curves were built using standards prepared from metals stock solutions of 1000 mg/L metal in 0.5 M nitric acid: Fe and Zn (Merck Certipur, Germany), Mn and Al (Panreac AA, Spain). Several samples' dilutions were prepared in 1% (v/v) nitric acid (0.224 M), and the lowest dilutions fitting in the linear calibration curves were chosen. Fe^{2+} concentration was analyzed with a UV-visible spectrometer DR2800 (Hach-Lange) using the 1,10-Phenanthroline (Method 8146, Hach-Lange) procedure at 510 nm

and Fe^{3+} concentration was calculated by mass balance with total Fe determined by atomic absorption.

FTIR measurements were performed using a Nicolet iN10MX micro-FTIR (Thermo Scientific, USA) equipped with a MCT detector cooled with liquid nitrogen. Analyses were conducted in reflection mode, by spreading a drop of the sample onto a reflectance holder. Spectra were collected in the middle infrared region (from 2000 to 675 cm^{-1}) recording 16 scans at 4 cm^{-1} spectral resolution. Three measurements were performed for each sample to assure the robustness of the analysis.

The characterization of zinc sulfide precipitates, after they were washed in 96% (v/v) ethanol overnight under orbital shaking, centrifuged (2800 g for 60 min at room temperature) for liquid removal and dried under vacuum, was done by analysis of (i) X-ray diffraction (XRD), (ii) Variable pressure scanning electron microscope coupled with energy dispersive X-ray spectrometry (VP-SEM-EDX) and (iii) Transmission Electron Microscopy (TEM). XRD analysis was performed using a microdifractometer Bruker™ D8 Discover®, operating at 40 KV and 40 mA, with Cu Kα radiation. The XRD patterns were acquired using a LYNXEYE detector, with a step size (2θ) of 0.03° and a step time of 1920 s. The identification of crystalline phases was performed with the DIFFRAC.SUITE EVA® software using the Powder Diffraction File (PDF-2) X-ray patterns database of the International Centre for Diffraction Data. VP-SEM-EDX analysis were carried out using a Hitachi™ S3700N SEM coupled to a Bruker™ XFlash 5010 SDD EDS Detector®. The samples were mounted on adhesive carbon tape and analyzed at low vacuum (40 Pa) and with an accelerating voltage of 5 and 20 kV. For TEM analysis the precipitates were re-suspended in ethanol and sonicated during 30 minutes for pulverization. Then, 5 µl of samples were applied to 400 mesh copper grids with thin carbon support (01844-F, Carbon Film only on 400 mesh, Copper, Tedpella). The grids allowed to dry and then stored the samples in a desiccator until imaging. Samples were imaged with a JEOL JEM-2100 electron microscope, operating a LaB6 electron gun at 200 kV and images were acquired with a "OneView" 4k x 4k CCD camera.

3.3. **Results**

3.3.1. Fe^{3+} removal from copper-free AMD

3.3.1.1. Alkalinization

Aiming to prevent Fe contamination in Zn recovery processes, different processes to remove Fe^{3+} from the copper-free AMD were tested. The first test was to raise the pH seeking for an optimum value to precipitate Fe^{3+} but not Zn. As expected, the precipitation of Fe increased as the pH raised; however, Zn started also to precipitate (Figure 3.1). Removals of Fe reached 85% to 90% for pH values from 3.0 to 4.0. However, the loss of Zn by simultaneous precipitation was considerably high (10% to 30%). Nevertheless, at pH 2.75 the removal of Fe was ~71% and the loss of Zn was just ~4%.

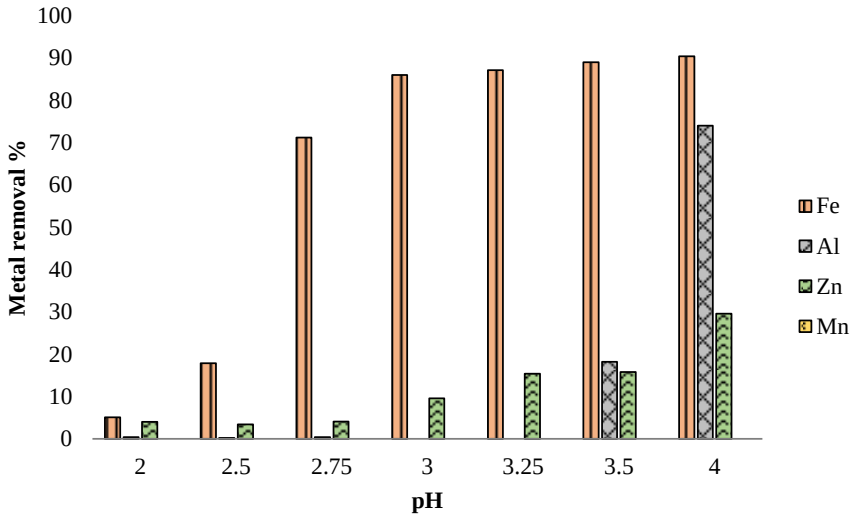

Figure 3.1. Metals removal by pH adjustment through addition of NaOH to the copper-free AMD.

3.3.1.2. SX with AliCy

The experiments performed aiming to optimize and characterize AliCy's SX are summarized on Figure 3.2.

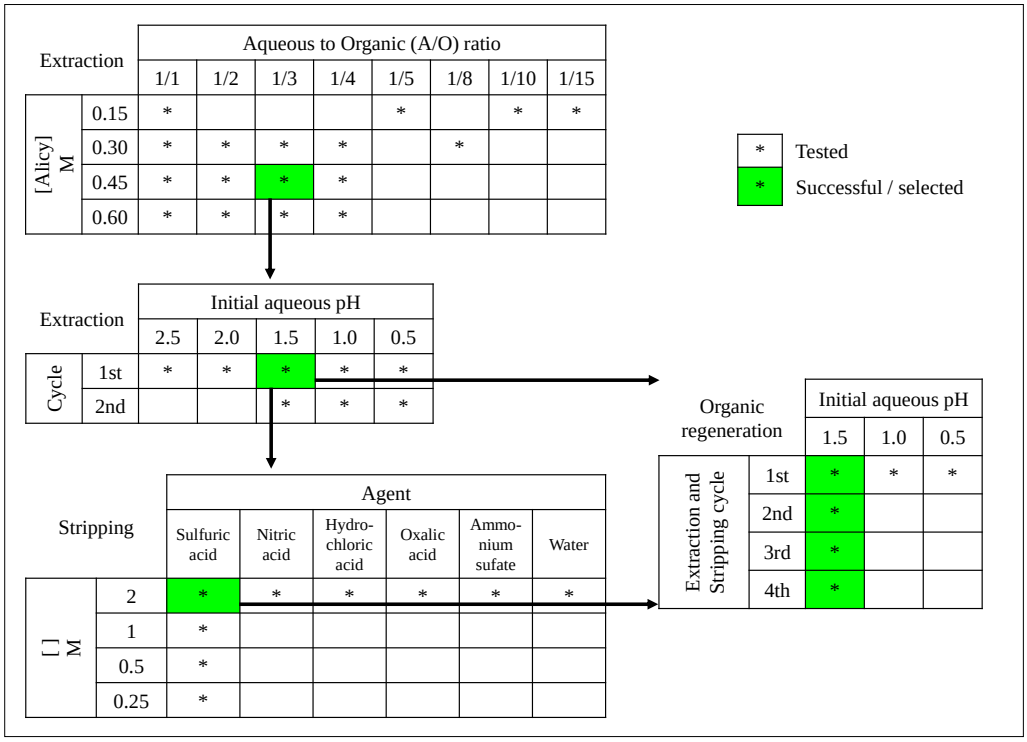

Figure 3.2. Experimental flowsheet for AliCy's SX optimization and characterization.

The maximum Fe loading capacity achieved in the organic phase was ~ 26.6 g/L in 0.6M AliCy for an A/O ratio of 1/1, and a close value of ~25.1 g/L was obtained in 0.45M AliCy also for an A/O ratios of 1/1. In both these cases the Fe extraction from the copper-free AMD was below 60%. Despite that, greater Fe extractions, in the range of 80% to 90%, were achieved with all the four AliCy concentrations tested, but at different A/O ratios: 1/10 for 0.15M; 1/4 for 0.3M; 1/3 for 0.45M and 1/2 for 0.6M (Figure S- 3.6 toFigure S- 3.9). When lower A/O ratios than these were tested, the Fe extraction was similar or just slightly higher, but Zn co-extraction increased to values (~25% to 80%) that are unreasonable if the goal is the subsequent recovery of this metal. Based on these results, the additional experiments to characterize Fe SX from the copper-free AMD were performed using 0.45 M AliCy in kerosene as extractant at a A/O ratio of 1/3.

The SX tests with copper-free AMD at different acidic values revealed high co-extractions of all tested metals (Fe, Al, Zn and Mn) for pH 2.5 and pH 2.0, but similar selective Fe extraction patterns

were achieved for the natural pH of the solution of 1.5 and for the acidified pH of 1.0 (~81% for Fe and ≤ 5% for other metals), while a lower selective Fe extraction percentage (~60%) was observed for the most acidified pH of 0.5 (Figure S- 3.10). This suggests that the AliCy's organic phase extracted Fe^{3+} in the form of $FeSO_4^+$, because according to the Eh-pH diagram obtained by theoretical simulation (Figure S- 3.3) this Fe compound is present in solutions with pH from ~0.6 to ~1.5 but not when the pH is outside this interval.

Afterwards, the attempts of second SX cycles to further remove Fe from the obtained aqueous raffinates (of the Fe selective first SXs) revealed unexpected results: in the three cases (which started with copper-free AMD at pHs 0.5, 1.0 and 1.5) there was a dramatic loss of Fe extraction efficiency, both in extraction percentage and in Fe selectivity (Figure S- 3.11). A possible explanation for this phenomenon is the lower concentration of Fe^{3+} ions to compete with the other metal ions for the extractant in the second SX cycle (Table 3.3). Indeed, AliCy is also able to extract other metals than Fe; for instance, extraction rates from a multimetallic sulfuric acid solution were reported in the order of Fe>Zn>Cu>Cd>Co>Ni (Devi 2016). Looking to the Eh-pH diagram plotted for Zn, and considering the fact that the pH values of raffinates tested for the second SX cycle were above 1.0, it seems that after most of Fe^{3+} was removed the Zn was extracted in the form of $Zn(SO_4)_2^{2-}$ (Figure S- 3.4 andFigure S- 3.11).

The extraction percentages and D values obtained for the metals studied in this SX process clearly indicate high efficiency for Fe^{3+} extraction (Table 3.3). SO_4^{2-} was also analyzed in this SX conditions, and the observed high co-extraction of this ion suggests it has a role in the Fe^{3+} extraction mechanism. Since the study of Fe speciation revealed that most of this metal in the initial copper-free AMD was in the ferric ion state (~46 g/L Fe^{3+}) and that ~92% of it was extracted, an additional SX test performed performed with 0.45 M AliCy in kerosene and a synthetic ferric sulfate ($Fe_2(SO_4)_3$) solution. This test revealed ~97% extraction of the initial 55 g/L Fe^{3+}.

Table 3.3. Extraction efficiency of 0.45 M AliCy in kerosene applied to copper-free AMD, using with an A/O of 1/3 and a contact time of 60 minutes. Results are averages and standard deviations of three independent SX experiments.

Extractants	Metals and SO_4^{2-}	[Initial] $_{\text{copper-free AMD}}$ (g/L)	Extraction %	Distribution ratios D

	Fe	53 ± 4	84 ± 1	5.3 ± 0.6
	Fe^{3+}	46 ± 4	92 ± 3	13 ± 5
	Fe^{2+}	6.4 ± 0.5	28 ± 10*	0.4 ± 0.2
0.45M AliCy	Al	7.3 ± 0.6	4 ± 3	0.05 ± 0.03
	Zn	1.8 ± 0.2	3 ± 5	0.04 ± 0.06
	Mn	0.156 ± 0.001	4 ± 4	0.04 ± 0.04
	SO_4^{2-}	142 ± 15	80 ± 1	3.93 ± 0.03

* Fe^{2+} is not extracted by organophosphorus extractants (Regel-Rosocka and Wisniewski 2011), therefore this ~28% was probably the result of Fe^{2+} oxidation to Fe^{3+} which was then extracted (concentrations of Fe^{2+} and Fe^{3+} determined as described in methods).

In what concerns the Fe re-extraction (stripping), a first experiment using A/O ratios of 1/1 showed that 2 M sulfuric acid was the most effective agent among several tested (Figure S- 3.12). Then, Fe stripping from a loaded organic phase of 0.45M AliCy was tested using sulphuric acid at different molarities and 2M showed the highest efficiency (Figure S- 3.13). In addition, a further test of Fe stripping using 2 M sulfuric acid and loaded organic phases of 0.3M, 0.45M and 0.6M AliCy in kerosene, still at A/O ratios of 1/1, revealed efficiencies of ~95%, ~91% and ~86%, respectively.

Regarding the reusability of AliCy in kerosene as extractant for the removal of Fe from copper-free AMD, a SX test using such organic phase directly after stripping with 2 M sulfuric acid revealed poor efficiency for Fe extraction (metals removal = 80% for Mn, 35% for Fe, 10% for Al and 6% for Zn). Yet, SX tests using a regenerated organic phase revealed good Fe extraction efficiencies, both for selectivity and percentage (Figure S- 3.14). In fact, four cycles of extraction and stripping from raw copper-free AMD were successfully performed using a successively regenerated organic phase of 0.45 M AliCy in kerosene as extractant and new 2 M sulfuric acid solution for stripping in each cycle (Figure S- 3.15 andFigure S- 3.16).

The fact that AliCy was prepared with sodium bicarbonate solution and that it was necessary to be regenerated with this solution after Fe^{3+} extraction suggests that an ion exchange mechanism could occur, in which the Na somehow bound to the extractant would be replaced by Fe^{3+} or a complex with this ion. The measurement of 0.085 ± 0.027 g/L Na and 2.52 ± 0.1 g/L Na in the copper-free AMD before and after Fe^{3+} extraction (with 0.45 M AliCy using A/O = 1/3), respectively, gives

strength to this idea. However, the extracted Fe to incremented Na molarities ratio of ~7 indicates that the extraction mechanism may not be a simple direct substitution.

Aiming to shed light on the extraction mechanism, FTIR spectra were obtained for Kerosene and for AliCy diluted in kerosene before and after Fe^{3+} SX extraction (Figure 3.3). Analyzing both the FTIR spectra of kerosene and of AliCy diluted in kerosene allowed to identify the main peaks expected in the analyzed range of wavenumbers for the respective chemical functional groups. Then, when Fe^{3+} is loaded, after extraction either from the synthetic iron sulfate solution or from the copper-free AMD, the following changes are visible in the FTIR spectra: (i) the peak at ~1147 cm^{-1} (attributed to the P=O group) switches to two peaks in its proximity (at ~1128 and ~1168 cm^{-1}), (ii) the peak at ~1048 cm^{-1} (attributed to C–N linkages) moves to ~1059 cm^{-1} and (iii) the peak at ~812 cm^{-1} (attributed to NC_3 antisymmetric vibrations) moves to ~821 cm-1. In the discussion section there is a detailed explanation about the identification of these functional groups with supporting references.

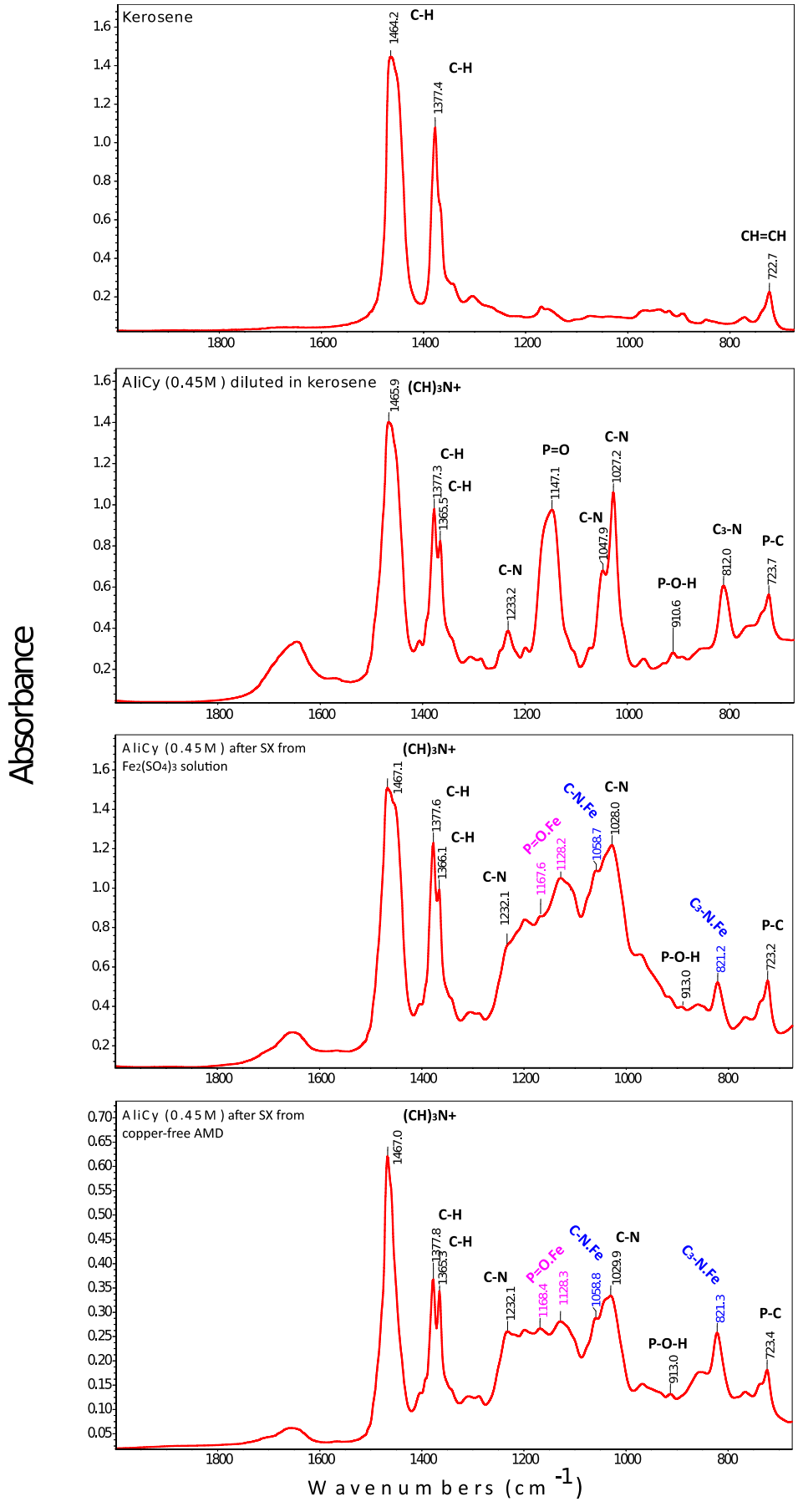
Kerosene
C-H
1464.2
C-H
1377.4
CH=CH
722.7
AliCy (0.45M) diluted in kerosene
(CH)3N+
1465.9
C-H
1377.3
C-H
1365.5
C-N
1233.2
P=O
1147.1
C-N
1047.9
C-N
1027.2
P-O-H
910.6
C3-N
812.0
P-C
723.7
AliCy (0.45M) after SX from Fe2(SO4)3 solution
(CH)3N+
1467.1
C-H
1377.6
C-H
1366.1
C-N
1232.1
P=O.Fe
1167.6
C-N.Fe
1128.2
C-N
1058.7
1028.0
P-O-H
913.0
C3-N.Fe
821.2
P-C
723.2
AliCy (0.45M) after SX from copper-free AMD
(CH)3N+
1467.0
C-H
1377.8
C-H
1365.3
C-N
1232.1
P=O.Fe
1168.4
C-N.Fe
1128.3
C-N
1058.8
1029.9
P-O-H
913.0
C3-N.Fe
821.3
P-C
723.4
Absorbance
Wavenumbers (cm-1)

Figure 3.3. FTIR spectra of: Kerosene, 0.45 M AliCy diluted in kerosene and 0.45 M AliCy in kerosene loaded either with Fe^{3+} from iron sulfate solution, or from copper-free AMD. The peaks of characteristic vibrational groups are identified, and respective changes due to putative interactions with the Fe^{3+} ion are shown in pink and blue colors.

3.3.1.3. Alkalinization + SX with AliCy

Despite the promising results of removing Fe^{3+} from copper-free AMD by SX with AliCy in kerosene and the possibility of reusing this organic phase, it was not possible to completely remove total Fe, nor all the Fe^{3+}, by this approach. Therefore, further experiments combining this process and alkalinization were performed seeking to remove the most as possible Fe (especially Fe^{3+}) with minimum losses of Zn.

The first combination of processes tested was a SX using 0.45M AliCy in kerosene with the following aqueous phase: the copper-free AMD alkalinized to pH 2.75, after solids removal by centrifugation and a final reacidification back to pH 1.5 (Table 3.4). This approach led to similar results of those obtained in the second cycle of extraction with AliCy (Figure S- 3.11): a decay in Fe extraction and a rise in the extraction of other metals. The fact that alkalinization at such pH (2.75) removes essentially Fe^{3+} helps to support the justification proposed above for this phenomenon: less Fe^{3+} ions to compete with the other metal ions for the extractant.

Table 3.4. Extraction efficiency of 0.45 M AliCy in kerosene applied to the copper-free AMD obtained after pH adjustment to 2.75, solids removal and reacidification back to pH 1.5, with an A/O of 1/3 and a contact time of 60 minutes. Results are the average and the mean absolute deviation of 2 replicates.

Extractants	**Metals**	**[Initial]$_{\text{copper-free AMD after pH adjusted to 2.75 and then back to pH 1.5}}$ (g/L)**	**Extraction %**	**Distribution ratios D**
0.45M AliCy	Fe	6.17 ± 0.4	61 ± 6	1.6 ± 0.4
	Al	3.0 ± 0.3	75 ± 1	3.0 ± 0.2
	Zn	0.71 ± 0.2	97.0 ± 0.3	32 ± 3
	Mn	0.06 ± 0.02	13 ± 2	0.15 ± 0.03

3.3.1.4. SX with AliCy + Alkalinization

The strategy reverse to the one described above was performed by raising the pH of the aqueous phase coming out of SX from raw copper-free AMD with 0.45 M AliCy in kerosene. The best combination of higher Fe removal and less Zn loss due to simultaneous precipitation was achieved with pH values 3.0, 3.25 and 3.5 (Figure 3.4).

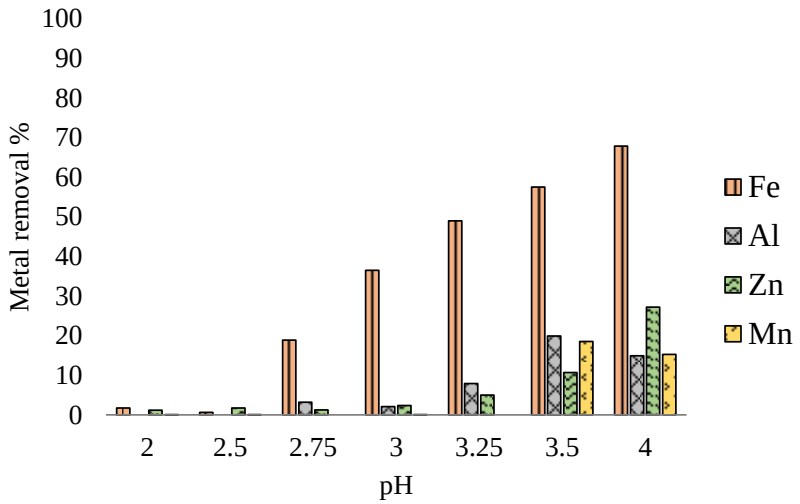

Figure 3.4. Metals removal by pH adjustment through addition of NaOH to the raffinate obtained from one SX cycle on copper-free AMD with 0.45 M AliCy in kerosene (at A/O of 1/3).

3.3.2. Zn recovery from copper-free AMD

3.3.2.1. SX with D2EHPA and with D2EHPA and Cyanex 272

The tests to extract Zn directly from the copper-free AMD using 0.9 M D2EHPA or a mixture of 0.72 M D2EHPA and 0.18 M Cyanex 272 revealed low efficiency, both in Zn extraction percentage and in selectivity (Table 3.5). While the yield of Zn recovery would be increased with higher concentrations of extractant or lower A/O ratios, the observed co-extraction of Fe^{3+} is a known problem in the hydrometallurgical industry that is not so easy to solve. Thus, performing a direct Zn SX process to such water would be possible just if Fe^{3+} can be efficiently separated in a prior step.

Table 3.5. Extraction efficiency from the copper-free AMD, using 0.9 M D2EHPA in kerosene with 3% (v/v) TBP and using a mixture of 0.72 M D2EHPA plus 0.18 M Cyanex 272 in kerosene with 3% (v/v) TBP, with an A/O ratio of 1 and a contact time of 30 minutes. Results are given as the average and the mean absolute deviation of 2 replicates.

Extractants	Metals	[Initial] $_{\text{copper-free AMD}}$ (g/L)	Extraction %	Distribution ratios D
0.9 M D2HEPA	Fe	53 ± 4	40 ± 1	0.67 ± 0.04
	Al	7.3 ± 0.6	5.0 ± 0.4	0.053 ± 0.005
	Zn	1.8 ± 0.2	45 ± 6	0.8 ± 0.2
	Mn	0.156 ± 0.001	4 ± 2	0.04 ± 0.02
0.72 M D2EHPA 0.18 M Cyanex 272	Fe	53 ± 4	33 ± 11	0.5 ± 0.3
	Al	7.3 ± 0.6	2 ± 1	0.016 ± 0.004
	Zn	1.8 ± 0.2	57 ± 7	1.4 ± 0.4
	Mn	0.156 ± 0.001	0.0 ± 0.5	0.000 ± 0.004

3.3.2.2. ZnS precipitation with biogenic sulfide

A SRB culture with good SO_4^{2-} reduction activity was used when more than 90% of the initial SO_4^{2-} had been reduced and the concentration of sulfide was 342 ± 7 mg/L. The sulfide to zinc ratios (S/Zn) calculated based on sulfide measurements just before mixing the sulfide rich medium and the copper-free AMD supernatants of tested pH values were in the range of 20 to 50. These ratios are much higher than the stoichiometric value for ZnS precipitates, thus assuring sulfide was not a limiting factor.

For pH values of 2.5 and lower there was no significant metals precipitation, while for pH 2.75 most (~0.685 g/L or ~96%) of the Zn initially in solution (~0.713 g/L) precipitated (Figure 3.5). However, simultaneous precipitation of Fe (~0.62 g/L) occurred and though the percentage was just ~10% of the initial Fe concentration in the copper-free AMD alkalinized to pH 2.75 (~6.2 g/L Fe), it still corresponds to a relatively high Fe contamination of recovered Zn. (These concentrations of Zn and Fe seem lower than expected due to a dilution factor of 2.452 caused by volume raise during pH adjustment.) If zinc sulfide was obtained with relatively small amounts of Fe, this direct addition of sulfide to such water could be applied to produce feeding materials for Zn smelters. However, the observed level of contamination hampers this approach.

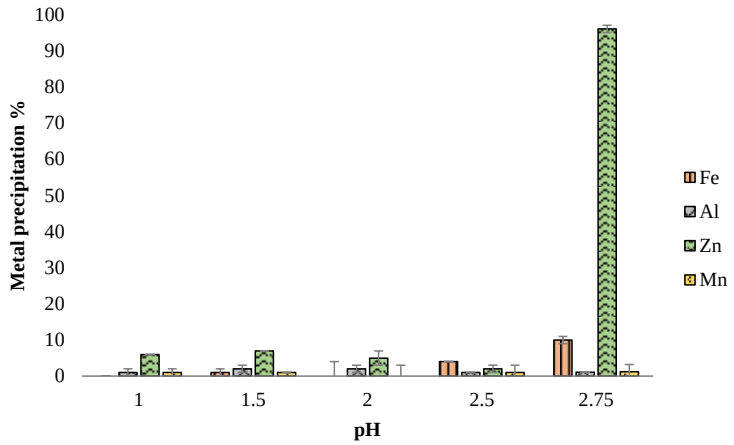

Figure 3.5. Metals precipitation 72 hours after adding sulfide rich supernatant of a SRB culture to copper-free AMD at controlled pH values and making S/Zn ratios above 20. Results are given as the average and the mean absolute deviation of 2 replicates.

The results obtained with both Zn recovery approaches tested directly on the extreme copper-free AMD have shown the importance of removing Fe^{3+} prior to applying Zn hydrometallurgical processes on such water.

3.3.3. Zn recovery after Fe^{3+} removal

3.3.3.1. SX with AliCy + SX with D2EHPA and Cyanex 272

The SX with the synergistic mixture of 0.72 M D2EHPA and 0.18 M Cyanex 272 in kerosene with 3% (v/v) TBP applied to the aqueous phase coming out of the SX from copper-free AMD using 0.45 M AliCy in kerosene revealed extraction percentages of Zn (~51%) and Fe (~23%) (Table 3.6) in the same range of those achieved in the SX using the same extractant system applied directly to the copper-free AMD (~57% and ~33%, respectively) (Table 3.5). Hence, the quantity of Fe co-extracted with Zn was much lower because of its lower initial concentration. Even so, the extracted Fe (~1.9 g/L) is still higher than the extracted Zn (~0.9 g/L).

Table 3.6. Extraction efficiency from the raffinate obtained from one SX cycle on copper-free AMD with 0.45 M AliCy in kerosene (with A/O = 1/3), using a mixture of 0.72 M D2EHPA plus

0.18 M Cyanex 272 in kerosene with 3% (v/v) TBP, with an A/O ratio of 1/1 and a contact time of 30 minutes. Results are the average and the mean absolute deviation of 2 replicates.

Extractants	Metals	[Initial] copper-free AMD out of SX with AliCy (g/L)	Extraction %	Distribution ratios D
0.72M D2EHPA 0.18M Cyanex 272	Fe	8.4 ± 0.9	22.60 ± 0.03	0.292 ± 0.001
	Al	7.0 ± 0.2	7 ± 2	0.08 ± 0.02
	Zn	1.7 ± 0.1	51 ± 1	1.06 ± 0.04
	Mn	0.150 ± 0.004	2.6 ± 0.9	0.03 ± 0.01

3.3.3.2. SX with AliCy + alkalinization + SX with D2EHPA plus Cyanex 272

The SX with higher molarities of extractants D2EHPA (1.44 M) and Cyanex 272 (0.32 M) in kerosene with 3% (v/v) TBP applied now to the raffinate from SX with 0.45 M AliCy and copper-free AMD alkalinized to pH 3.25 and then (after solids removal by centrifugation) reacidified to pH 2.0, allowed to improve the extraction efficiency of Zn (Table 3.7), comparing with the SX with 0.72 M D2EHPA and 0.18 M Cyanex 272 from the raffinate obtained after SX with AliCy and copper-free AMD without any further pH adjustment (Table 3.6). However, the co-extracted Fe (~0.5 g/L) was still high in relation to the extracted Zn (~0.9 g/L).

Table 3.7. Extraction efficiency from the raffinate obtained from one SX cycle on copper-free AMD with 0.45 M AliCy in kerosene (during 60 minutes with A/O = 1/3) alkalized to pH 3.25 (solids removed) and reacidified to pH 2.0, using a mixture of 1.44 M D2EHPA plus 0.32 M Cyanex 272 in kerosene with 3% (v/v) TBP (during 30 minutes with A/O = 1/1). Results are the average and the mean absolute deviation of 2 replicates.

Extractants	Metals	[Initial] copper-free AMD out of SX with AliCy, alkalized to pH 3.25 (solids removed) and reacidified to pH 2.0 (g/L)	Extraction %	Distribution ratios D
1.44M D2EHPA 0.32M Cyanex 272	Fe	2.8 ± 0.9	18 ± 3	0.22 ± 0.04
	Al	4.3 ± 0.2	12 ± 3	0.14 ± 0.04
	Zn	1.1 ± 0.1	88.0 ± 0.6	7.4 ± 0.1
	Mn	0.099 ± 0.004	23 ± 1	0.31 ± 0.01

3.3.3.3. SX with AliCy + alkalinization + ZnS precipitation with biogenic sulfide

Finally, the addition of biogenic sulfide rich media (after SRB growth) to the aqueous phase coming out of the SX with 0.45M AliCy and copper-free AMD, at controlled pH, was proven to be a successful strategy to recover Zn. The precipitation was specific for Zn at all tested pH values, with total precipitation achieved by mixing acidified (to pH 3.5) biogenic sulfide rich medium with the alkalinized (to pH of 3.5) aqueous phase coming from the SX with 0.45M AliCy in kerosene and copper-free AMD (Figure 3.6).

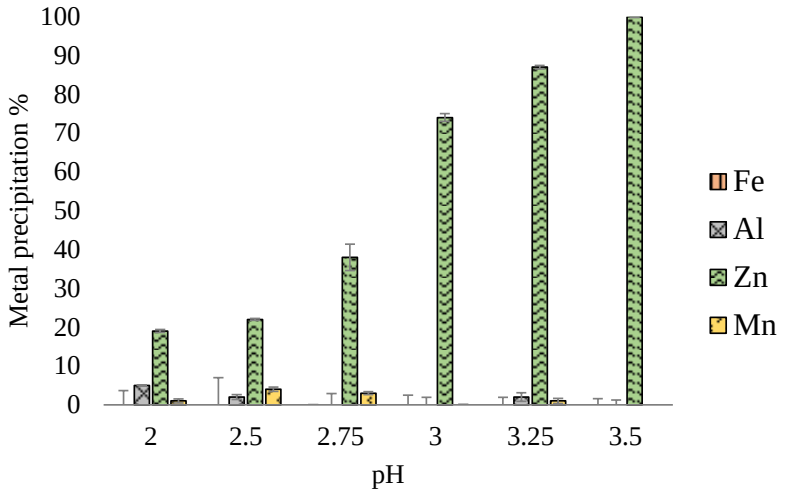

Figure 3.6. Metals precipitation 72 hours after adding sulfide rich supernatant of a SRB culture to the raffinate obtained from one SX cycle on copper-free AMD with 0.45 M AliCy in kerosene (at A/O of 1/3) at controlled pH values, making S/Zn ratios above 20. Results are shown as the average of 2 replicates and the error bars are mean absolute deviations.

3.3.4. Characterization of zinc sulfide precipitates

The precipitates obtained by mixing biogenic sulfide rich medium with the alkalinized raffinate from the SX with 0.45M AliCy in kerosene and copper-free AMD at a controlled pH of 3.5 had the expected white color of zinc sulfide.

The X-ray diffraction pattern of these particles revealed main peaks corresponding to zinc sulfide (ZnS) in its two types of crystalline structures, wurtzite and sphalerite (Figure 3.7). However, the

small size of these peaks and their location in bulging areas of the diffractogram indicates that a portion of the ZnS was amorphous and the crystallization was still occurring.

The SEM imaging revealed particles of about 50 µm and the SEM-EDX mapping of these particles revealed, apart from the oxygen always present and the carbon from the tape used to mount the precipitates, the main presence of Zn and S in a ratio of normalized relative concentrations of 1 (Figure 3.8), which is exactly the expected ratio for ZnS. Besides, the mapping analysis revealed some small roundish spots of Ca incrusted in the particles and a point analysis on one of these spots revealed considerable Ca normalized relative concentration (4.53%) and more S (11.36 %) than Zn (2.27%). These values allow to suggest these spots are composed of gypsum ($CaSO_4 \cdot 2H_2O$) or its anhydrous form, anhydrite ($CaSO_4$).

In what concerns the TEM analysis, although the precipitates were sonicated for 30 minutes for this analysis, aggregates were visible and a broad range of particles sizes was observed indicating incomplete dispersion of particles (Figure 3.9). A total of 3648 particles were automatically measured in four TEM images, using the ParticleSizer v1.0.9 plugin (Wanger and Eglinger 2021) on the Fiji – ImageJ software (Schindelin et al. 2012), with default values on Settings Manager´s parameters except for the "Irregular watershed convexity threshold", which was changed to 1.0 to allow a better identification of particles in the aggregates. Yet, by using this value, several image spots which are just noise background were detected as very small particles. To eliminate this error caused by such automatic measurements and enumerations, the real smallest size of particles in the images was visually identified and measured as 12 nm. Then, the particles having smaller sizes than that were eliminated from the list before statistical analysis of particle sizes. This approach revealed particles having a Feret size average of 70 ± 60 nm, varying from 12 to 727 nm and fitting a normal distribution (for a 1‰ probability (α=0.001) in a Kolmogorov-Smirnov test). Interestingly, in the TEM images with higher magnifications it is possible to visualize that these particles are composed of smaller particles (Figure 3.9). The automatic measurements of 1217 of such smaller nanoparticles within three larger particles (~70 nm) reveled a range of sizes from 2 to 22 nm with an average size of 4.2 ± 2.8 nm following a normal distribution (α=0.001).

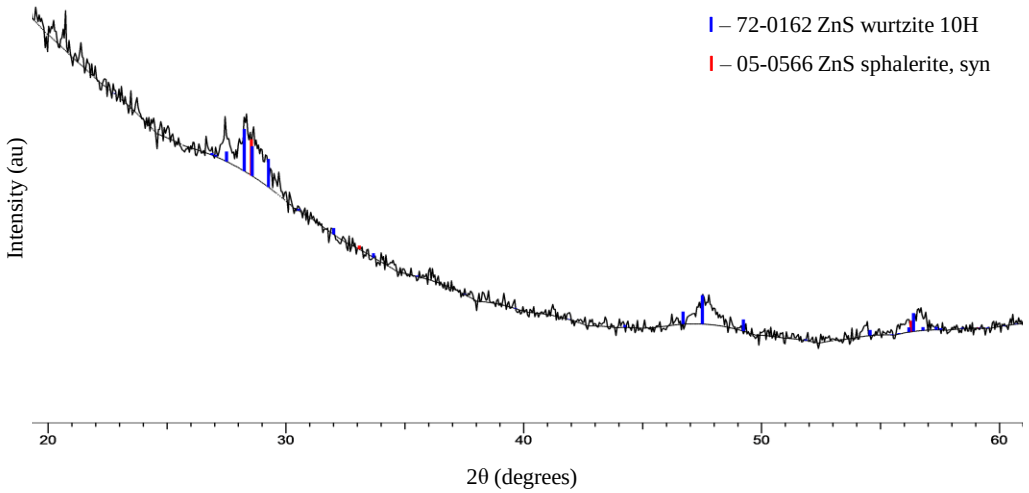

Figure 3.7. X-ray patterns of precipitates obtained by adding a sulfide rich SRB culture supernatant to the raffinate obtained from one SX cycle on copper-free AMD with 0.45 M AliCy in kerosene (with A/O = 1/3), at a controlled pH of 3.5. The red and the blue bars show the position of the standard peaks.

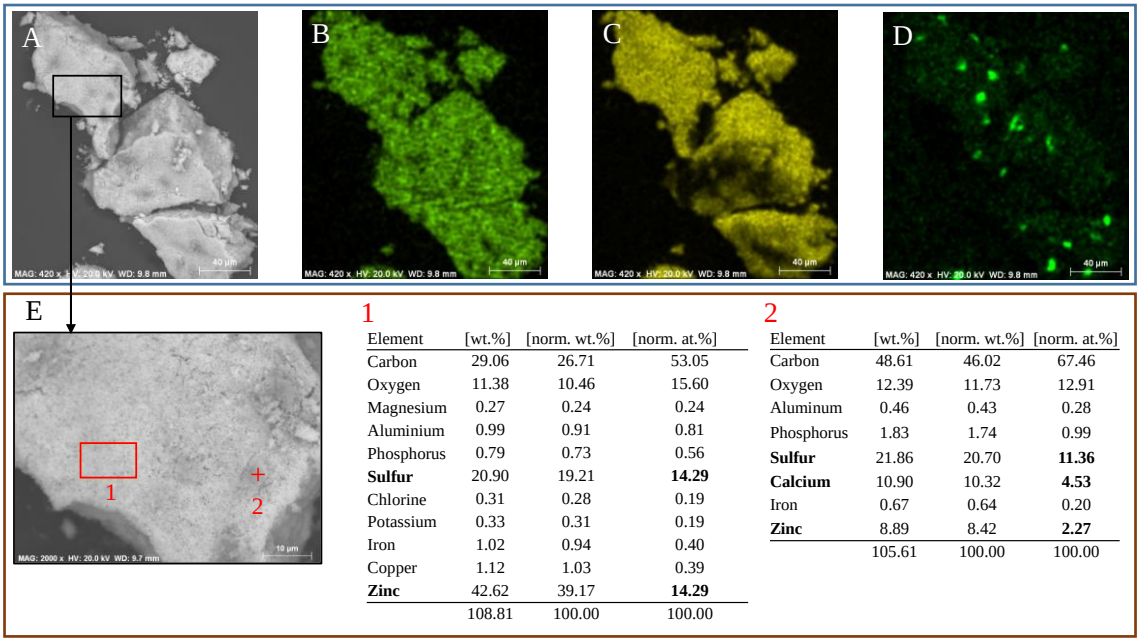

1

Element	[wt.%]	[norm. wt.%]	[norm. at.%]
Carbon	29.06	26.71	53.05
Oxygen	11.38	10.46	15.60
Magnesium	0.27	0.24	0.24
Aluminium	0.99	0.91	0.81
Phosphorus	0.79	0.73	0.56
Sulfur	20.90	19.21	**14.29**
Chlorine	0.31	0.28	0.19
Potassium	0.33	0.31	0.19
Iron	1.02	0.94	0.40
Copper	1.12	1.03	0.39
Zinc	42.62	39.17	**14.29**
	108.81	100.00	100.00

2

Element	[wt.%]	[norm. wt.%]	[norm. at.%]
Carbon	48.61	46.02	67.46
Oxygen	12.39	11.73	12.91
Aluminum	0.46	0.43	0.28
Phosphorus	1.83	1.74	0.99
Sulfur	21.86	20.70	**11.36**
Calcium	10.90	10.32	**4.53**
Iron	0.67	0.64	0.20
Zinc	8.89	8.42	**2.27**
	105.61	100.00	100.00

Figure 3.8. SEM-EDX mapping of precipitates obtained by adding a sulfide rich SRB culture supernatant to the raffinate obtained from one SX cycle on copper-free AMD with 0.45 M AliCy

in kerosene (with A/O = 1/3), at a controlled pH of 3.5. A) SEM image of the particles. B) Zn, C) S and D) Ca SEM-EDX mapping. E) sites of SEM-EDX analysis on one particle: 1- area on the main material composing the particle, E2- point on one of the of roundish spots of a different material. [wt.%] = weight %; [norm. wt.%] = normalized weight %; [norm. at.%] = normalized atoms %.

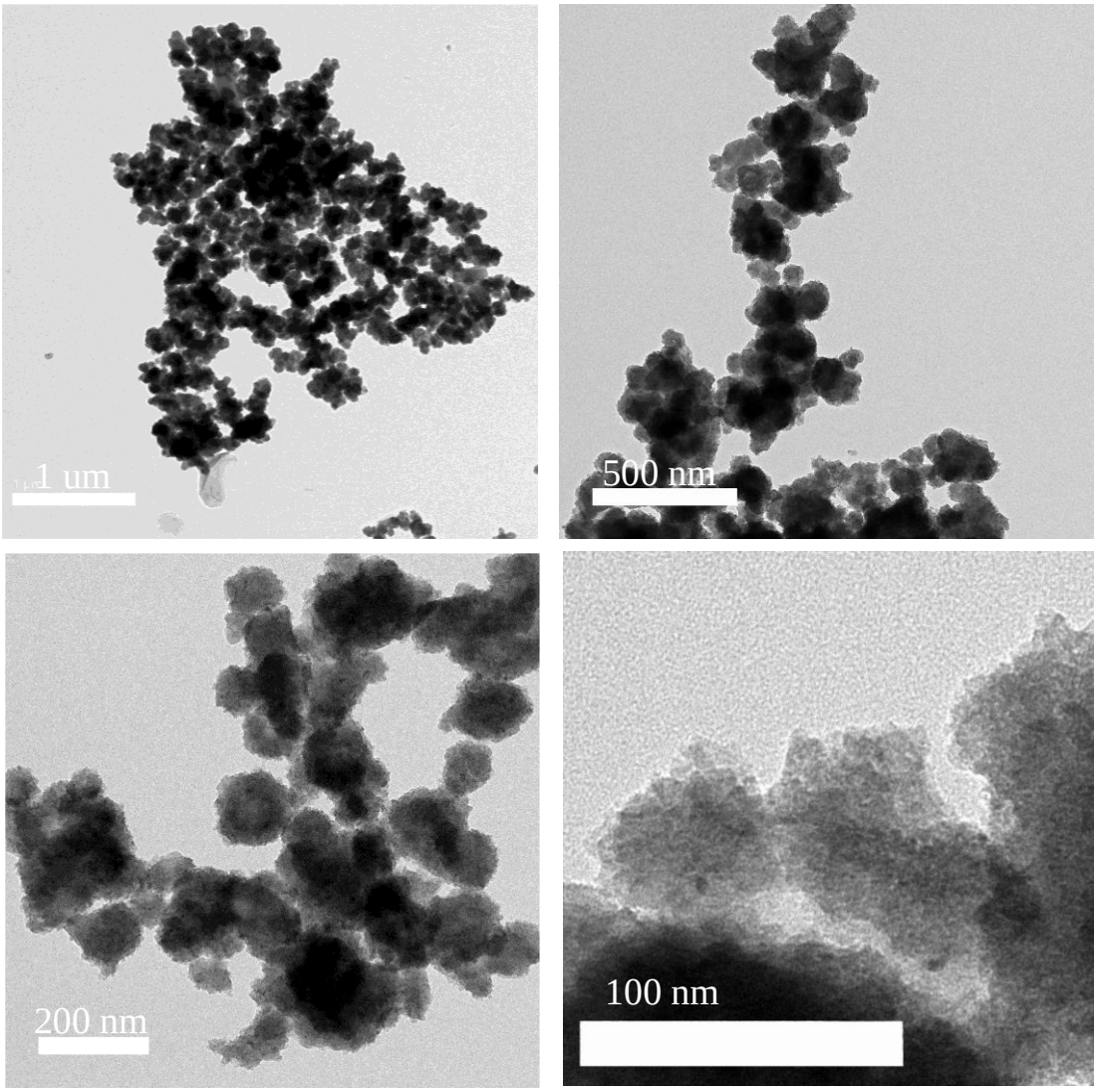

Figure 3.9. TEM images at different magnifications of precipitates obtained by adding a sulfide rich SRB culture supernatant to the raffinate obtained from one SX cycle on copper-free AMD with 0.45 M AliCy in kerosene (with A/O = 1/3), at a controlled pH of 3.5, showing clusters of

particles of multiple sizes with nanoparticles comprising them visible in the most amplified image (right bottom corner).

3.4. **Discussion**

This work aimed to study (i) the removal of Fe^{3+} from copper-free AMD (the raffinate obtained after Cu extraction with Acorga M5640 from an extreme AMD), (ii) the recovery of Zn directly from the extreme copper-free AMD and (iii) the recovery of Zn from the water obtained after Fe^{3+} removal through SX using AliCy and/or alkalinization. Table 3.8 summarizes the best results obtained in the several tested processes (described in detail in the results section), regarding the major issues observed: Zn recovery *vs* Fe contamination and Zn loss *vs* Fe removal.

Table 3.8. Summary of main results for Zn recoveries or losses and Fe contaminations or removals in the several processes and combinations of processes tested. The results are presented as percentages to the initial concentrations in the copper-free AMD.

Objective	**Process(es)**	**Zinc recovery (rec.)** **Iron contamination (cont.)**	**Zinc loss** **Iron removal (rem.)**
Ferric iron removal from copper-free AMD	Alkalinization to pH values from 2.75 to 3.5		4 to 16 % Zn loss 71 to 89 % Fe rem.
	SX with 0.45M AliCy in kerosene		7 ± 5 % Zn loss 84 ± 1 % Fe rem.
	Alkalinization to pH 2.75 + SX with 0.45M AliCy		97.1 ± 0.3 % Zn loss 89 ± 6 % Fe rem.
	SX with 0.45M AliCy + Alkalinization to pH 3.0 to 3.5		9 to 17 % Zn loss 90 to 94 % Fe rem.
Zinc recovery from copper-free AMD	SX with 0.9M D2EHPA	45 ± 6 % Zn rec. 40 ± 1 % Fe cont.	
	SX with 0.72M D2EHPA and 0.18M Cyanex 272	57 ± 7 % Zn rec. 33 ± 11 % Fe cont.	
	ZnS precipitation using biogenic sulfide (at pH 2.75)	92 ± 1 % Zn rec. 3 ± 1 % Fe cont.	
Zinc recovery from water obtained after ferric iron removal from copper-free AMD	SX with 0.45M AliCy + SX with 0.72M D2EHPA and 0.18M Cyanex 272	47 ± 6 % Zn rec. 4 ± 1 % Fe cont.	
	SX with 0.45M AliCy + alkalinization to pH 3.25 + SX with 1.44M D2EHPA and 0.32M Cyanex 272	78 ± 6 % Zn rec. 2 ± 4 % Fe cont.	
	SX with 0.45M AliCy + Alkalinization to pH 3.5 + ZnS precipitation using biogenic sulfide	83 ± 5 % Zn rec. Not detected Fe cont.	

The alkalinization of copper-free AMD to pH 2.75 allowed to remove ~71% of the total Fe with a loss of Zn of just ~4%. However, since the initial Fe concentration is extremely high (~53 g/L) the remaining Fe in solution was still high.

The use of AliCy for Fe^{3+} removal was tested with different concentrations, different A/O ratios, and with the extreme copper-free AMD adjusted to different acidities. The results showed that AliCy concentrations as low as 0.15 M and as high as 0.6 M can be used with A/O ratios of 1/10 and 1/2, respectively, in such type of extreme AMD waters with pH values ranging from 1 to 1.5, to selectively extract about 84% of total Fe (~90% of Fe^{3+}). Such Fe extraction patterns from the extreme copper-free AMD with AliCy generates plots for the log(D) *vs.* log[AliCy] (where D is the distribution ratio) with slopes of 1.09 ± 0.02, which indicates a ratio of one mole of extractant involved with one mole of Fe atoms in the extracted complex. On the other hand, a high percentage of SO_4^{2-} co-extraction was observed, making a 1.24 ratio of SO_4^{2-} to Fe^{3+} moles extracted. This is not surprising since it is known that the ratio of metal cations to coordinated anions extracted with ionic liquids does not necessarily match their ratio in the aqueous phase (Jensen et al. 2002; Gaillard et al. 2012), and that metal cations or charged complexes of metal cations with anions can be transferred to the ionic liquids along with uncoordinated anions present in the aqueous phase (Janssen et al. 2013; Janssen et al. 2015). Indeed, it is not the first time that the co-extraction of Fe and SO_4^{2-} by an organophosphorus extractant is reported. Carson et al. (2020) recently reported results suggesting that SO_4^{2-} is co-extracted in a 1:2 molar ratio with Fe by Cyanex 272 and proposed that the extracted species is likely to be a polynuclear ferric iron sulfate complex.

When AliCy was first tested by Fortuny et al. (Fortuny et al. 2012) for boron extraction, the authors calculated a slope of 1.37 for the plot of log(D) *vs.* log[AliCy], and based on that they proposed that one molecule of extractant is involved in the extracted complex of boron with the extraction equilibrium represented as:

$$\text{AliCy (org)} + H^+ \text{ (aq)} + B^{3+} \text{ (aq)} + 4(OH^-) \text{ (aq)} \rightarrow \text{Ali } B(OH)_4 \cdot \text{H Cy. (org)} \qquad \text{Eq. 3.4}$$

In another work by Devi (Devi 2016), when AliCy (named A336/Cy272 by this author) was tested for Cu extraction, the plot of log(D) *vs.* log[AliCy] resulted in a slope of 2.06 and it was proposed that two molecules of extractant are involved in the extracted complex, in which the metal ion bonds with both the *Ali* and the *Cy* parts of AliCy with the following extraction reaction:

$$2\text{AliCy (org)} + Cu^{2+} \text{ (aq)} + (SO_4)^{2-} \text{ (aq)} \rightarrow \text{Cu } SO_4 \cdot 2\text{AliCy (org)} \qquad \text{Eq. 3.5}$$

In the current work, considering the Fe to extractant complex ratio of 1 and the SO_4^{2-} to Fe ratio of 1.24 estimated for the extraction of Fe by AliCy, and considering that comparing the extraction trends at different pH values with the iron species in the Eh-pH diagram suggests that $FeSO_4^+$ is the extracted form, leads to the possibility of proposing two hypotheses of equilibrium reactions:

$$AliCy\ (org) + Fe^{3+}\ (aq) + SO_4^{2-}\ (aq) \rightarrow AliCy \cdot FeSO_4^+\ (org) \qquad \text{Eq. 3.6}$$

and/or

$$2AliCy\ (org) + 2FeSO_4^+\ (aq) + SO_4^{2-}\ (aq) \rightarrow 2AliCy \cdot 2(FeSO_4)SO_4\ (org) \qquad \text{Eq. 3.7}$$

The analysis of FTIR spectra before and after Fe extraction by AliCy suggests the involvement of both the phosphate and the amine groups (each belonging to one of the two active compounds). The FTIR spectra of kerosene has the three main peaks expected in the analyzed range of wavenumbers for this type of solvent (paraffins): one at ~723 cm^{-1}, characteristic of CH=CH (cis) bonds (Gebregziabher 2018), another corresponding to the symmetrical bending vibration $\delta_s CH_3$ at ~1377 cm^{-1}, and a third corresponding to the scissoring band $\delta_s CH_2$ at ~1464 cm^{-1} (Silverstein and Webster 1997) (Figure 3.3). The first and the last become overlapped with the peaks of AliCy spectrum for the P-C bond at 723-724 cm^{-1} and for $(CH_3)N^+$ at 1465-1467 cm^{-1}, respectively, while the second is visible in the spectra of AliCy diluted in kerosene (as described below). Regarding the FTIR spectra obtained for AliCy diluted in kerosene (Figure 3.3), it has the expected peaks for the present groups, according to previous reports: P-C at 723-724 cm^{-1}, P-O-H at 910-913 cm^{-1}, P=O at 1147-1150 cm^{-1}, C-N at 1232-1233 cm^{-1}, C-H at 1364-1366 and ~1377 cm^{-1}, and $(CH_3)N^+$ at 1465-1467 cm^{-1} (Le et al. 2019; Nguyen et al. 2020). In addition to these, another three peaks are clearly visible in the spectra obtained for AliCy in kerosene shown in Figure 3.3: at 811-812 cm^{-1}, 1027-1028 cm^{-1} and ~1048 cm^{-1}. In fact similar peaks were also visible in the spectra obtained by Le et al. (2019), but they were not assigned to any group by those authors. The peak at 811-812 cm^{-1} should correspond to the NC_3 antisymmetric stretching vibration from the Aliquat 336 part of AliCy, since Assenine et al. (2021) have assigned a band at 801 cm^{-1} of trioctylmethylammonium (the cation of Aliquat 336) to that particular type of vibration. The other two peaks, at 1027-1028 cm^{-1} and at ~1048 cm^{-1}, may belong to unconjugated C–N linkages also from the Aliquat 336 part of AliCy, since according to Silverstein and Webster (1997) this type of vibration on primary, secondary and tertiary aliphatic amines is observed as medium or weak bands in the region from 1250 to 1020 cm^{-1}. Finally, when the extractant (AliCy in kerosene) is loaded with Fe, either from the synthetic iron sulfate solution or from the copper-free AMD, the following changes are visible

in the FTIR spectra: (i) the peak corresponding to the P=O group (at ~1147 cm^{-1}) switches to two peaks in its proximity (at ~1128 and ~1168 cm^{-1}), (ii) the peak at ~1048 cm^{-1} moves to ~1059 cm^{-1} and (iii) the peak at ~812 cm-1 moves to ~821 cm^{-1} (Figure 3.3**)**. On one hand, the first change indicates an interaction of the Fe^{3+} with the P=O bond of the bis2,4,4-trimethylpentyphosphinic acid (Cyanex 272) part of AliCy, as previously reported for AliCy's extraction mechanisms of other cations: Devi (2016) showed by FTIR analysis of AliCy and copper-loaded AliCy that the P=O stretching vibrations (which they observed at 1248 cm^{-1}) was disturbed and two new peaks appeared (at 1233 cm^{-1} and 1217 cm^{-1}) when Cu was loaded, thus indicating strong interaction of Cu with the P=O bond; Le et al. (2019) identified changes in the FTIR spectra of AliCy before and after hydrogen extraction at the frequency corresponding to the P=O bond (1136 cm^{-1}), with its peak decreasing to almost half after the extraction. On the other hand, the second and third changes (shifts of the peaks at 811-812 and 1048 cm^{-1} to 821 cm^{-1} and 1058 cm^{-1}, respectively) can be attributed to the involvement of the amine group from the Aliquat 336 part of AliCy in the extraction of Fe^{3+} since, as explained above, both the initial peaks should correspond to the NC_3 and C-N bonds of trioctylmethylammonium.

In what concerns the re-extraction from the organic phase, among the stripping agents tested sulfuric acid was the best to re-extract this metal from AliCy in kerosene, and 2M sulfuric acid allowed a transference of ~91%. Furthermore, it was shown that after this stripping stage, the AliCy-kerosene organic phase can be successfully regenerated for further use through a liquid-liquid mixing process with sodium bicarbonate (0.5 M). In fact, this is the process initially used to prepare AliCy, suggested by Fortuny et al. (2012), thus probably some type of similar reaction occurs in its regeneration. Still, the results obtained in this work are not enough to propose definitive equations representing the reactions involved. Nevertheless, such a proof of reusability of this organic phase is very important in terms of economic and ecological viability of its use in any SX process developed to separate Fe^{3+} from multimetallic solutions. On the other hand, metal analysis of the stripping solution revealed Fe concentrations of ~12.2 g/l but relatively negligible concentrations of other metals (~0.06 g/L Al, ~0.02 g/L Zn, ~0.001 g/L Mn), and this also accounts for the desired economic viability, since pregnant solutions with Fe can have several potential commercial values (Wei et al. 2005). For instance, they can be applied for the synthesis of Fe-based catalytically active complexes (Rydel-Ciszek et al. 2020), iron oxide nanoparticles (Sangami

and Manu 2017; Fani et al. 2018), fertilizer production (Boutchuen et al. 2019; Kasivelu et al. 2020), pigment industry (de Almeida Silva et al. 2017; Galvão et al. 2018), etc.

Other studies aiming Fe^{3+} separation from sulfate matrices by SX using extractants such as TOA (trioctylamine), TBP (tributyl phosphate), TOA-TBP (Qifeng et al. 2016), primary amine N-1923 (Li et al. 2011), secondary amine (N-methylaniline) (Borai et al. 2016), Primene JMT (Rohm & Haas Company) (Chou and Chuen Cheang Lin 1986), report higher extraction efficiencies (95% to 99%). However, these works were performed with sulfate solutions without Zn. Thus, they do not clarify if the extractants are effective to separate Fe^{3+} and Zn. Besides, considering the same range of efficiency if the mentioned extractants were applied to the copper-free AMD studied in this work the remaining Fe^{3+} in solution would still be high (0.5 to 2.3 g/L of Fe^{3+}) comparing to the concentration of Zn to be recovered.

In other works exploring SX to remove Fe, but also analyzing Zn co-extraction, the results showed the need of consecutive extraction cycles to achieve extractions above 99% as well as a certain level of Zn co-extraction. For instance, Deep et al. (2007) reported an extractant solution of 30% (v/v) Cyanex 272 and 30% (v/v) TBP in ESCAID 110 for the Fe extraction from a concentrated Fe^{3+} (50 g/l) sulfuric acid medium at pH=1.2. They showed that the extractant solution can be loaded with Fe^{3+} up to a maximum of 34% of the reagent's initial molarity, and therefore suggested six stages of consecutive extraction cycles for the recovery of more than 99% of the initial Fe^{3+} (50 g/l). Moreover, they used this extractant for the Fe separation from a Zn leaching solution (Fe=43.1 g/l, Zn= 13.6 g/l, Cu= 0.31 g/l) and report about 15% co-extraction of Zn after six cycles of SX with this extractant (Deep et al. 2007). In another study, Sarangi et al. (2007) proposed a SX method for Fe separation from a sulfate/chloride leach liquor containing various metals, including 11.8 g/L Fe, 24.8 g/L Cu and 230 mg/L Zn, aiming the subsequent recovery of Cu and Zn, by using TBP as extractant, and water as stripping agent. Results of their optimization for one SX stage showed an Fe extraction of 98% by 1 M TBP along with 9% co-extraction of Zn and no co-extraction of copper, resulting in concentrations of ~236 mg/L of Fe, ~24.8 g/L of Cu and ~209 mg/L of Zn in the aqueous phase to be further used for Cu and Zn recovery (Sarangi et al. 2007). These authors solved this incomplete removal of Fe by performing a two-stage extraction process and achieved a raffinate with just 4 mg/L Fe.

In the current work with AliCy in kerosene as extractant, the second SX cycle aiming to remove the Fe^{3+} remaining after the first SX cycle resulted in lower extraction efficiencies for this metal

(< 75%) and high percentages of Zn co-extraction (> 83%). A possible explanation can be the lower concentrations of Fe^{3+} after the first SX cycle with AliCy, thus leaving more extractants' active compounds free to interact with Zn^{2+}. In fact, according to results reported by Devi in 2016, Zn in sulfuric acid matrices is the second metal most extracted with AliCy after Fe, and the extraction of Zn increases as the pH raises.

Further alkalinization tests of AliCy SX's raffinate aiming to achieve the highest and most selective Fe^{3+} removal prior to Zn recovery showed best results for pH between 3.0 and 3.5. Indeed, these results were expected, as this is a known strategy. For example Rao et al. (1996) developed a precipitation process to remove Fe from an AMD sample with 5.9 g/l Fe and 2.8 g/l Zn, as iron hydroxide at pH 3.5 through addition of lime and oxidation with H_2O_2. The alkalinization of AliCy SX's raffinate to pH 3.0, 3.25 or 3.5, resulted in ~36.5%, ~49% or ~57% of total Fe removal by precipitation and ~2.4% ~5% or ~10.7% of Zn lost by simultaneous precipitation, respectively. More specifically, since Fe^{3+} starts precipitating as $Fe(OH)_3$ at pH ~3, and ferrous iron (Fe^{2+}) only precipitates at pH ~6 (Snoeyink and Jenkins 1980), in the case of pH adjustment to 3.0 the resulting water still had ~0.44 g/L Fe^{3+} and 3.03 g/L Fe^{2+}, while at final pH values of 3.25 and 3.5 all soluble Fe was in the form of Fe^{2+} (~2.81 g/L Fe^{2+} and ~2.30 g/L Fe^{2+}, respectively). In the case of Zn, the resulting waters had 1.08 g/L, ~1.06 or ~0.98 g/L Zn, respectively for pH 3.0, pH 3.25 and pH 3.5. In what concerns the Zn recovery, this work demonstrated that the high concentration of Fe in extreme copper-free AMD (~46.1 g/L Fe^{3+} and ~6.4 g/L Fe^{2+}) is a drawback in Zn SX processes. Fe was co-extracted in considerable amounts along with Zn when 0.9 M D2EHPA or a mixture of 0.72 M D2EHPA plus 0.18 M Cyanex 272 diluted in kerosene were used (> 30% of Fe co-extracted with Zn). In fact, selective Zn SX over Fe has been a challenge difficult to solve and widely studied by many researchers, both in sulfuric and hydrochloric acid matrices (El Dessouky et al. 2008; Asadi et al. 2018). In Zn SX, despite Fe^{2+} not getting extracted with organophosphorus extractants, Fe^{3+} can be co-extracted: TBP (Radzymińska-Lenarcik et al. 2015), Cyanex 272 (Cytec 2008), Cyphos IL 101, Cyanex 921, Cyanex 923, Cyanex 302, tributyl phosphate, Alamine 336 (Regel-Rosocka and Wisniewski 2011), D2EHPA and synergistic mixtures of D2EHPA and TBP (Azizitorghabeh et al. 2017). Thus, some authors suggested methods to extract Zn through SX from effluents containing Fe and Zn by reducing Fe^{3+} to Fe^{2+}, and consequently preventing the Fe co-extraction (Radzymińska-Lenarcik et al. 2015). Moreover, for solutions where most of the Fe is in the form of Fe^{2+} some authors suggest techniques to inhibit ferrous Fe oxidation and to keep

it in the reduced form: a shaking step of SX process in the absence of air, elimination of the hydrolysis products of organic extractants during SX and addition of Fe scraps to the aqueous solution (Regel-Rosocka and Wisniewski 2011). However, in extreme AMD waters as the one used in the current work these methods would probably not be totally effective since the initial concentration of Fe^{3+} is much higher than in the waters used by those authors.

The recovery of Zn in the form of zinc sulfide was also tested by addition of biogenic sulfide rich medium directly to the copper-free AMD at growing pH values, and at pH 2.75 the precipitation of Zn reached ~96%. However, simultaneous precipitation of a high amount of Fe occurred (~0.9 g of Fe per g of Zn). This may have happened due to the fact that zinc sulfide and Fe^{3+} precipitation can occur in the same pH range (Ucar et al. 2011; Luptakova et al. 2012), and/or the much higher concentration of Fe (~30 times) compared to Zn in the copper-free AMD created conditions for Fe^{2+} and Fe^{3+} ions to compete with Zn^{2+} ions for S^{2-}, preventing an absolute selectivity for ZnS formation at pH 2.75.

On the other hand, the experiments of Zn SX from the water obtained after Fe removal from the copper-free AMD revealed that Fe contamination was still a problem. The Fe^{3+} ions in the raffinate obtained from one SX cycle with 0.45M AliCy were still in a relatively high concentration (~3.7 g/L) and, as expected, were co-extracted with Zn in a subsequent SX with a synergistic mixture of D2EHPA and Cyanex 272 (Table 3.6). Plus, even when the pH of that raffinate was first raised to 3.25 to eliminate Fe^{3+} ions as solid complexes and then reacidified to pH 2.0 for the recovery of Zn by SX with the synergistic mixture of D2EHPA and Cyanex 272, the co-extraction of Fe was still observed (Table 3.7) probably due to oxidation of Fe^{2+} into Fe^{3+} (which can then be extracted by D2EHPA and Cyanex) during the phases mixing.

Finally, contrary to the initial unsuccessful attempt to selectively recover zinc sulfide directly from the extreme copper-free AMD, the Zn recovery process performed using biogenic sulfide was successful after removing Fe^{3+} through AliCy SX followed by alkalinization to pH 3.25 or pH 3.5. Accounting with all losses and recovery percentages, the final Zn recovery by sulfide addition at pH 3.25 or at pH 3.5 corresponds to ~77% or ~83%, respectively, of the initial concentration in the raw copper-free AMD.

The zinc sulfide precipitates obtained at pH 3.5 lead to XRD peaks corresponding to crystalline structures of wurtzite and sphalerite, with a diffractogram shape suggesting some precipitates were still amorphous. This type of XRD patterns indicating ongoing crystallization were also observed

in previous studies on the characterization of zinc sulfides obtained with biogenic sulfide (Remoundaki et al. 2008).

The SEM analysis of these precipitates revealed particles mainly composed of zinc sulfide with relatively large sizes: up to about 50 µm, thus more easily collected than dispersed nanoparticles, which may be an asset if the dispersion into nanoparticles can be performed in a later step. Curiously, the SEM analysis revealed small roundish spots with Ca and sulfur, thus probably gypsum ($CaSO_4 \cdot 2H_2O$) or anhydrite ($CaSO_4$) incrustations, in the large zinc sulfide particles. The Postgate B medium (Postgate 1984), in which the SRB were grown to provide biogenic sulfide, had ~183 mg/L of Ca, while the concentration of Ca in the AMD used was ~138 mg/L. Thus, since high volume-ratios (> 10/1) of SRB culture to AliCy SX's raffinate with pH 3.5 were tested, the source of Ca in those incrustations was mainly the former. Hence, the use of sources of sulfide without Ca would probably prevent the formation of this type of Ca deposits. Indeed, Murray et al. (2017) reported the biosynthesis of zinc sulfide precipitates by adding H_2S gas from the headspace of SRB batch cultures to synthetic solutions of zinc sulfate and obtained the same type of white precipitates but without any evidence of Ca incrustations.

The TEM analysis of these zinc sulfide precipitates, after 30 min sonication, revealed structures with a Feret size average of 70 ± 60 nm, varying from 12 to 727 nm and fitting a normal distribution (α=0.001). Moreover, the TEM images with higher magnifications allowed to visualize that those structures are composed of smaller particles with sizes from 2 to 22 nm, in a normal distribution (α=0.001) with an average of 4.2 ± 2.8 nm. These results are in reasonable agreement with other studies on the biosynthesis of ZnS particles by addition of biogenic sulfide. For example, Vitor et al. (2015) reported some clustering of the particles, which ranged between about 30 and 50 nm, in the biosynthesis of ZnS by addition of a sulfide rich effluent from a SRB bioreactor to a synthetic zinc sulfate solution. Another example is the agglomerated white precipitate comprising nanoparticles of sizes estimated at 20 to 40 nm, obtained by Murray et al. (2017) by adding biogenic sulfide gas to a zinc sulfate synthetic solution. In fact, these authors also reported smaller nanoparticles visible within those of 20 to 40 nm in the TEM images and using a differential centrifugal analysis they have confirmed the presence of nanoparticles of sizes from below 10 nm to 20 nm, with a mean size of 13 nm. Moreover, they studied the optical properties of these biogenic zinc sulfide nanoparticles and concluded they were indistinguishable from zinc sulfide quantum dots (ZnS QDs) chemically prepared for industries such as optoelectronics, highlighting

the potential of converting a biogenic sulfide gas "waste" into a high value product. In fact, nano-sized ZnS particles, both in wurtzite and sphalerite forms such as those obtained in this work, may have several other potential applications. For instance, these nanoparticles can be used as photocatalysts in H_2 production (Mendoza-Damián et al. 2019), wound treatment and skin regeneration (Han et al. 2020), photocatalyst for the degradation of toxic dyes (Aziz et al. 2020), electrochemical sensors (Vinoth et al. 2020), key role in the synthesis semiconductor nanomaterial such as CdS with various applications (Granot et al. 2004; Saravanan et al. 2011; Malarkodi et al. 2014; Wu et al. 2016), synthesis of super-hard materials (Vityaz et al. 2020), etc.

As a final remark, this work shows the effectiveness of AliCy to separate Fe^{3+} from a real acidic multimetallic solution prior to Zn recovery. Thus, it opens the way for further research aiming AliCy's applications to prevent Fe contaminations in the recovery of valuable metals from other types of waters, such as PGMs recovery from automobile catalyst leach liquors (Nowottny et al. 1997; Firmansyah et al. 2019), Mn recovery from ferruginous Mn ores (Liu et al. 2019), recovery of indium of Fe rich solutions (Van Roosendael et al. 2019) etc.

3.5. **Conclusions**

The ionic liquid called AliCy, prepared from Aliquat 336 and Cyanex 272, diluted in kerosene is efficient to extract ~90% of Fe^{3+} from extreme AMD waters with pH 1.0 to 1.5.

A SX process applied to extreme AMD waters with pH 1.0 to 1.5 using AliCy in kerosene as organic phase followed by alkalinization of the obtained raffinate to pH 3.25 to 3.5, allows to remove all Fe^{3+} from the solution with low losses of Zn.

ZnS nanoparticles can be produced from extreme AMD after Cu SX and Fe^{3+} separation by AliCY's SX followed by alkalinization to pH 3.25 to 3.5.

A first outline of possible processes to recover metals of interest from acidic solutions with Fe^{3+} contamination can be proposed: (i) Fe^{3+} separation by SX using AliCy, (ii) pH alkalinization to remove remaining Fe^{3+}, (iii) recovery of target metals.

3.6. **References**

Agrawal A, Sahu KK (2010) Treatment of Chloride Waste Pickle Liquor by Solvent Extraction for the Recovery of Iron. Miner Process Extr Metall 31(3):121–134. https://doi.org/10.1080/08827501003727006

Asadi T, Azizi A, Lee J, Jahani M (2018) Solvent extraction of zinc from sulphate leaching solution of a sulphide-oxide sample using D2EHPA and Cyanex 272. J Dispers Sci Technol 39(9):1328–1334. https://doi.org/10.1080/01932691.2017.1402338

Assenine MA, Haddad B, Paolone A, Brandán SA, Goussem M, Villemin D, Boumediene M, Rahmouni M, Bresson S (2021) Synthesis, thermal properties, vibrational spectra and computational studies of Trioctylmethylammonium bis(trifluoromethylsulfonyl)imide ionic liquid. J Mol Struct 1232:130085. https://doi.org/10.1016/j.molstruc.2021.130085

Aziz A, Ali N, Khan A, Bilal M, Malik S, Ali N, Khan H (2020) Chitosan-zinc sulfide nanoparticles, characterization and their photocatalytic degradation efficiency for azo dyes. Int J Biol Macromol 153:502–512. https://doi.org/10.1016/j.ijbiomac.2020.02.310

Azizitorghabeh A, Rashchi F, Babakhani A, Noori M (2015) Synergistic extraction and separation of Fe (III) and Zn (II) using TBP and D2EHPA. Proceedings of Pb-Zn

Azizitorghabeh A, Rashchi F, Babakhani A, Noori M (2017) Synergistic extraction and separation of Fe(III) and Zn(II) using TBP and D2EHPA. Sep Sci Technol 52(3):476–486. https://doi.org/10.1080/01496395.2016.1250778

Biswas RK, Habib MA, Karmakar AK (2007) Kinetics of Solvent Extraction of Iron(III) from Sulfate Medium by Purified Cyanex 272 using a Lewis Cell. Solvent Extr Ion Exch 25(1):79–98. https://doi.org/10.1080/07366290601067838

Borai EH, Shahr El-Din AM, El Afifi EM, Aglan RF, Abo-Aly MM (2016) Subsequent separation and selective extraction of thorium (IV), iron (III), zirconium (IV) and cerium (III) from aqueous sulfate medium. SAfr.j.chem 69. https://doi.org/10.17159/0379-4350/2016/v69a18

Boutchuen A, Zimmerman D, Aich N, Masud AM, Arabshahi A, Palchoudhury S (2019) Increased Plant Growth with Hematite Nanoparticle Fertilizer Drop and Determining Nanoparticle Uptake in Plants Using Multimodal Approach. Journal of Nanomaterials 2019:1–11. https://doi.org/10.1155/2019/6890572

Cánovas CR, Nieto JM, Macías F, Basallote MD, Olías M, Pérez-López R, Ayora C (2020) Recovery of Critical Raw Materials from Acid Mine Drainage (AMD): The EIT-Funded MORECOVERY Project. In: Fosso-Kankeu E, Wolkersdorfer C, Burgess J (eds) Recovery of Byproducts from Acid Mine Drainage Treatment, 1st edn. Wiley, pp 219–233

Carson I, Love JB, Morrison CA, Tasker PA, Moser M, Fischmann AJ, Jakovljevic B, Soderstrom MD (2020) Co-extraction of Iron and Sulfate by Bis(2,4,4-trimethylpentyl)phosphinic Acid, CYANEX®272. Solvent Extr Ion Exch 38(3):328–339. https://doi.org/10.1080/07366299.2020.1720123

Chou K-S, Chuen Cheang Lin (1986) Extracting iron from aluminum sulfate solution. Hydrometallurgy 15(3):391–397. https://doi.org/10.1016/0304-386X(86)90069-1

Claassen JO, Sandenbergh RF (2006) Particle growth parameters in the precipitation of metastable iron phases from zinc-rich solutions. Hydrometallurgy 84(3–4):165–174. https://doi.org/10.1016/j.hydromet.2006.05.015

Coll MT, Fortuny A, Kedari CS, Sastre AM (2012) Studies on the extraction of Co(II) and Ni(II) from aqueous chloride solutions using Primene JMT-Cyanex272 ionic liquid extractant. Hydrometallurgy 125–126:24–28. https://doi.org/10.1016/j.hydromet.2012.05.003

Cytec (2008) Cyanex 272 Extractant. Cytec, Canada :16

Davey PT, Scott TR (1976) Removal of iron from leach liquors by the "Goethite" process. Hydrometallurgy 2(1):25–33. https://doi.org/10.1016/0304-386X(76)90011-6

de Almeida Silva R, Menezes JCS dos S, Lopes FA, Kirchheim AP, Schneider IAH (2017) Synthesis of a Goethite Pigment by Selective Precipitation of Iron from Acidic Coal Mine Drainage. Mine Water Environ 36(3):386–392. https://doi.org/10.1007/s10230-017-0448-2

Deep A, Correia PFM, de Carvalho JMR (2007) Liquid−Liquid Extraction and Separation of a Macro Concentration of Fe^{3+}. Ind Eng Chem Res 46(17):5707–5714. https://doi.org/10.1021/ie0615279

Deep A, de Carvalho JMR (2008) Review on the Recent Developments in the Solvent Extraction of Zinc. Solvent Extr Ion Exch 26(4):375–404. https://doi.org/10.1080/07366290802179267

Devi N (2016) Solvent extraction and separation of copper from base metals using bifunctional ionic liquid from sulfate medium. Trans Nonferrous Met Soc China 26(3):874–881. https://doi.org/10.1016/S1003-6326(16)64179-1

Dutrizac JE, Jambor JL (2000) Jarosites and their application in hydrometallurgy. Rev Mineral Geochem 40:405-452.

El Dessouky SI, El-Nadi YA, Ahmed IM, Saad EA, Daoud JA (2008) Solvent extraction separation of Zn(II), Fe(II), Fe(III) and Cd(II) using tributylphosphate and CYANEX 921 in kerosene from chloride medium. Chem Eng Process: Process Intensif 47(2):177–183. https://doi.org/10.1016/j.cep.2007.03.002

Fani M, Ghandehari F, Rezaee M (2018) Biosynthesis of Iron Oxide Nanoparticles by Cytoplasmic Extract of Bacteria Lactobacillus Fermentum. J Med Chem Sci 1(2)

Firmansyah ML, Kubota F, Yoshida W, Goto M (2019) Application of a Novel Phosphonium-Based Ionic Liquid to the Separation of Platinum Group Metals from Automobile Catalyst Leach Liquor. Ind Eng Chem Res 58(9):3845–3852. https://doi.org/10.1021/acs.iecr.8b05848

Fortuny A, Coll MT, Sastre AM (2012) Use of methyltrioctyl/decylammonium bis 2,4,4-(trimethylpentyl)phosphinate ionic liquid (ALiCY IL) on the boron extraction in chloride media. Sep Purif Technol 97:137–141. https://doi.org/10.1016/j.seppur.2012.02.037

Foucher S, Battaglia-Brunet F, Ignatiadis I, Morin D (2001) Treatment by sulfate-reducing bacteria of Chessy acid-mine drainage and metals recovery. Chem Eng Sci 56(4):1639–1645. https://doi.org/10.1016/S0009-2509(00)00392-4

Gaillard C, Klimchuk O, Ouadi A, Billard I, Hennig C (2012) Evidence for the formation of UO2(NO3)42− in an ionic liquid by EXAFS. Dalton Trans 41(18):5476. https://doi.org/10.1039/c2dt30205e

Galhardi JA, Bonotto DM (2016) Hydrogeochemical features of surface water and groundwater contaminated with acid mine drainage (AMD) in coal mining areas: a case study in southern Brazil. Environ Sci Pollut Res 23(18):18911–18927. https://doi.org/10.1007/s11356-016-7077-3

Galvão JLB, Andrade HD, Brigolini GJ, Peixoto RAF, Mendes JC (2018) Reuse of iron ore tailings from tailings dams as pigment for sustainable paints. J Clean Prod 200:412–422. https://doi.org/10.1016/j.jclepro.2018.07.313

Gebregziabher G (2018) Generation of Hydrocarbon Fuels from Mixed Polymer Wastes Using Decomposer Chamber. J Energy Nat Resour 7(1):18. https://doi.org/10.11648/j.jenr.20180701.13

Gharabaghi M, Irannajad M, Azadmehr AR (2013) Separation of nickel and zinc ions in a synthetic acidic solution by solvent extraction using D2EHPA and Cyanex 272. Physicochem Probl Miner Process. https://doi.org/10.5277/PPMP130121

Graedel TE, Beers D, Bertram M, Fuse K, Gordon RB, Gritsinin A, Harper EM, Kapur A, Klee RJ, Lifset R, Memon L, Spatari S (2005) The Multilevel Cycle of Anthropogenic Zinc. J Ind Ecol 9(3):67–90. https://doi.org/10.1162/1088198054821573

Granot E, Patolsky F, Willner I (2004) Electrochemical Assembly of a CdS Semiconductor Nanoparticle Monolayer on Surfaces: Structural Properties and Photoelectrochemical Applications. J Phys Chem B 108(19):5875–5881. https://doi.org/10.1021/jp038004o

Han B, Fang WH, Zhao S, Yang Z, Hoang BX (2020) Zinc sulfide nanoparticles improve skin regeneration. Nanomed: Nanotechnol Biol Med 29:102263. https://doi.org/10.1016/j.nano.2020.102263

Hedrich S, Kermer R, Aubel T, Martin M, Schippers A, Johnson DB, Janneck E (2018) Implementation of biological and chemical techniques to recover metals from copper-rich leach solutions. Hydrometallurgy 179:274–281. https://doi.org/10.1016/j.hydromet.2018.06.012

Ismael MRC, Carvalho JMR (2003) Iron recovery from sulphate leach liquors in zinc hydrometallurgy. Miner Eng 16(1):31–39. https://doi.org/10.1016/S0892-6875(02)00310-2

Jambor JL, Dutrizac JE (1998) Occurrence and Constitution of Natural and Synthetic Ferrihydrite, a Widespread Iron Oxyhydroxide. Chem Rev 98(7):2549–2586. https://doi.org/10.1021/cr970105t

Jameson E, Rowe OF, Hallberg KB, Johnson DB (2010) Sulfidogenesis and selective precipitation of metals at low pH mediated by Acidithiobacillus spp. and acidophilic sulfate-reducing bacteria. Hydrometallurgy 104(3–4):488–493. https://doi.org/10.1016/j.hydromet.2010.03.029

Janssen CHC, Macías-Ruvalcaba NA, Aguilar-Martínez M, Kobrak MN (2015) Metal extraction to ionic liquids: the relationship between structure, mechanism and application. Int Rev Phys Chem 34(4):591–622. https://doi.org/10.1080/0144235X.2015.1088217

Janssen CHC, Sánchez A, Witkamp G-J, Kobrak MN (2013) A Novel Mechanism for the Extraction of Metals from Water to Ionic Liquids. Chem Phys Chem 14(16):3806–3813. https://doi.org/10.1002/cphc.201300686

Jensen MP, Dzielawa JA, Rickert P, Dietz ML (2002) EXAFS Investigations of the Mechanism of Facilitated Ion Transfer into a Room-Temperature Ionic Liquid. J Am Chem Soc 124(36):10664–10665. https://doi.org/10.1021/ja027476y

Jha MK, Gupta D, Choubey PK, Kumar V, Jeong J, Lee J (2014) Solvent extraction of copper, zinc, cadmium and nickel from sulfate solution in mixer settler unit (MSU). Separation and Purification Technology 122:119–127. https://doi.org/10.1016/j.seppur.2013.10.045

Jha MK, Kumar V, Singh RJ (2001) Review of hydrometallurgical recovery of zinc from industrial wastes. Resour Conserv Recycl 33(1):1–22. https://doi.org/10.1016/S0921-3449(00)00095-1

Johnson DB, Hallberg KB (2005) Acid mine drainage remediation options: a review. Sci Total Environ 338(1–2):3–14. https://doi.org/10.1016/j.scitotenv.2004.09.002

Kasivelu G, Selvaraj T, Malaichamy K, Kathickeyan D, Shkolnik D, Chaturvedi S (2020) Nano-micronutrients [γ-Fe $_2$ O $_3$ (iron) and ZnO (zinc)]: green preparation, characterization, agro-morphological characteristics and crop productivity studies in two crops (rice and maize). New J Chem 44(26):11373–11383. https://doi.org/10.1039/D0NJ02634D

Kefeni KK, Msagati TAM, Mamba BB (2017) Acid mine drainage: Prevention, treatment options, and resource recovery: A review. Journal of Cleaner Production 151:475–493. https://doi.org/10.1016/j.jclepro.2017.03.082

Le MN, Son SH, Lee MS (2019) Extraction Behavior of Hydrogen Ion by an Ionic Liquid Mixture of Aliquat 336 and Cyanex 272 in Chloride Solution. Korean J Met Mater 57(3):162–169. https://doi.org/10.3365/KJMM.2019.57.3.162

Lewis AE (2010) Review of metal sulphide precipitation. Hydrometallurgy 104(2):222–234. https://doi.org/10.1016/j.hydromet.2010.06.010

Li M, He Z, Zhou L (2011) Removal of iron from industrial grade aluminum sulfate by primary amine extraction system. Hydrometallurgy 106(3–4):170–174. https://doi.org/10.1016/j.hydromet.2010.12.018

Liu B, Zhang Y, Lu M, Su Z, Li G, Jiang T (2019) Extraction and separation of manganese and iron from ferruginous manganese ores: A review. Minerals Engineering 131:286–303. https://doi.org/10.1016/j.mineng.2018.11.016

Loan M, Newman OMG, Cooper RMG, Farrow JB, Parkinson GM (2006) Defining the Paragoethite process for iron removal in zinc hydrometallurgy. Hydrometallurgy 81(2):104–129. https://doi.org/10.1016/j.hydromet.2005.11.002

Loan M, Parkinson G, Newman M, Farrow J (2002) Iron oxy-hydroxide crystallization in a hydrometallurgical residue. J Cryst Growth 235(1–4):482–488. https://doi.org/10.1016/S0022-0248(01)01791-2

Luch A (ed) (2012) Molecular, Clinical and Environmental Toxicology: Volume 3: Environmental Toxicology. Springer Basel, Basel

Luptáková A, Mačingová E, Ubaldini S, Lupták M (2020) Combination of Chemical and Biological-Chemical Methods for Elimination of Metals from Acid Mine Drainage. Inz 2(1). https://doi.org/10.29227/IM-2020-01-45

Luptakova A, Ubaldini S, Macingova E, Fornari P, Giuliano V (2012) Application of physical–chemical and biological–chemical methods for heavy metals removal from acid mine drainage. Process Biochem 47(11):1633–1639. https://doi.org/10.1016/j.procbio.2012.02.025

Magalhães PD, da Costa Marques MR, Baptista DF, Buss DF (2015) Metal bioavailability and toxicity in freshwaters. Environ Chem Lett 13(1):69–87. https://doi.org/10.1007/s10311-015-0491-9

Malarkodi C, Rajeshkumar S, Paulkumar K, Vanaja M, Gnanajobitha G, Annadurai G (2014) Biosynthesis and Antimicrobial Activity of Semiconductor Nanoparticles against Oral Pathogens. Bioinorg Chem Appl 2014:1–10. https://doi.org/10.1155/2014/347167

Mansur MB, Rocha SDF, Magalhães FS, Benedetto J dos S (2008) Selective extraction of zinc(II) over iron(II) from spent hydrochloric acid pickling effluents by liquid–liquid extraction. J Hazard Mater 150(3):669–678. https://doi.org/10.1016/j.jhazmat.2007.05.019

Martínez NM, Basallote MD, Meyer A, Cánovas CR, Macías F, Schneider P (2019) Life cycle assessment of a passive remediation system for acid mine drainage: Towards more sustainable mining activity. J Clean Prod 211:1100–1111. https://doi.org/10.1016/j.jclepro.2018.11.224

Mauchauffée S, Meux E, Schneider M (2008) Selective precipitation of cadmium from nickel cadmium sulphate solutions using sodium decanoate. Sep Purif Technol 62(2):394–400. https://doi.org/10.1016/j.seppur.2008.02.010

Mendoza-Damián G, Hernández-Gordillo A, Fernández-García MaE, Acevedo-Peña P, Tzompantzi-Morales FJ, Pérez-Hernández R (2019) Influence of ZnS wurtzite–sphalerite junctions on ZnOCore-ZnSShell-1D photocatalysts for H2 production. Int J Hydrog Energy 44(21):10528–10540. https://doi.org/10.1016/j.ijhydene.2019.02.193

Mishra RK, Rout PC, Sarangi K, Nathsarma KC (2010) A comparative study on extraction of Fe(III) from chloride leach liquor using TBP, Cyanex 921 and Cyanex 923. Hydrometallurgy 104(2):298–303. https://doi.org/10.1016/j.hydromet.2010.07.003

Monhemius AJ (2017) The iron elephant: A brief history of hydrometallurgists' struggles with element no. 26. CIMJ 8(4). https://doi.org/10.15834/cimj.2017.21

Moreno González R, Cánovas CR, Olías M, Macías F (2020) Seasonal variability of extremely metal rich acid mine drainages from the Tharsis mines (SW Spain). Environ Pollut 259:113829. https://doi.org/10.1016/j.envpol.2019.113829

Murray AJ, Roussel J, Rolley J, Woodhall F, Mikheenko IP, Johnson DB, Gomez-Bolivar J, Merroun ML, Macaskie LE (2017) Biosynthesis of zinc sulfide quantum dots using waste off-gas from a metal bioremediation process. RSC Adv 7(35):21484–21491. https://doi.org/10.1039/C6RA17236A

Naidu G, Ryu S, Thiruvenkatachari R, Choi Y, Jeong S, Vigneswaran S (2019) A critical review on remediation, reuse, and resource recovery from acid mine drainage. Environ Pollut 247:1110–1124. https://doi.org/10.1016/j.envpol.2019.01.085

Ňancucheo I, Johnson DB (2012) Selective removal of transition metals from acidic mine waters by novel consortia of acidophilic sulfidogenic bacteria: Acidophilic sulfidogenic bioreactors. Microb Biotechnol 5(1):34–44. https://doi.org/10.1111/j.1751-7915.2011.00285.x

Nanusha MY, Carlier JD, Carvalho GI, Costa MC, Paiva AP (2019) Separation and recovery of Pd and Fe as nanosized metal sulphides by combining solvent extraction with biological strategies based on the use of sulphate-reducing bacteria. Sep Purif Technol 212:747–756. https://doi.org/10.1016/j.seppur.2018.11.062

Nguyen TTN, Nguyen VNH, Liu Y, Lee MS (2020) Analysis of the interaction in the mixture of organophosphorus acids and Aliquat 336 through the measurement of dielectric constant and viscosity. J Mol Liq 315:113738. https://doi.org/10.1016/j.molliq.2020.113738

Nobahar A, Mellka AB, Pusta A, Lourenço JP, Carlier JD, Costa MC (2022) A New Application of Solvent Extraction to Separate Copper from Extreme Acid Mine Drainage Producing Solutions for Electrochemical and Biological Recovery Processes. Mine Water Environ. https://doi.org/10.1007/s10230-022-00858-7

Nowottny C, Halwachs W, Schügerl K (1997) Recovery of platinum, palladium and rhodium from industrial process leaching solutions by reactive extraction. Separation and Purification Technology 12(2):135–144. https://doi.org/10.1016/S1383-5866(97)00041-5

Owusu G (1998) Selective extractions of Zn and Cd from Zn□Cd□Co□Ni sulphate solution using di-2-ethylhexyl phosphoric acid extractant. Hydrometallurgy 47(2–3):205–215. https://doi.org/10.1016/S0304-386X(97)00044-3

Pappu A, Saxena M, Asolekar SR (2006) Jarosite characteristics and its utilisation potentials. Sci Total Environ 359(1–3):232–243. https://doi.org/10.1016/j.scitotenv.2005.04.024

Park S-M, Yoo J-C, Ji S-W, Yang J-S, Baek K (2013) Selective recovery of Cu, Zn, and Ni from acid mine drainage. Environ Geochem Health 35(6):735–743. https://doi.org/10.1007/s10653-013-9531-1

Park S-M, Yoo J-C, Ji S-W, Yang J-S, Baek K (2015) Selective recovery of dissolved Fe, Al, Cu, and Zn in acid mine drainage based on modeling to predict precipitation pH. Environ Sci Pollut Res 22(4):3013–3022. https://doi.org/10.1007/s11356-014-3536-x

Pinto da Costa J, Girão AV, Lourenço JP, Monteiro OC, Trindade T, Costa MC (2012) Synthesis of nanocrystalline ZnS using biologically generated sulfide. Hydrometallurgy 117–118:57–63. https://doi.org/10.1016/j.hydromet.2012.02.005

Postgate JR (1984) The Sulphate-Reducing Bacteria. Cambridge Univ Press

Pradel J, Castillo S, Traverse JP, Grezes-Besset R, Darcy M (1993) Ferric hydroxide oxide from the goethite process: characterization and potential use. Ind Eng Chem Res 32(9):1801–1804. https://doi.org/10.1021/ie00021a001

Principe F, Demopoulos GP (2004) Comparative study of iron(III) separation from zinc sulphate–sulphuric acid solutions using the organophosphorus extractants, OPAP and D2EHPA. Hydrometallurgy 74(1–2):93–102. https://doi.org/10.1016/j.hydromet.2004.01.004

Puigdomenech I (2015) Hydra/medusa chemical equilibrium database and plotting software (database update: 01–01–2015; Hydra: 32 bit version 18 Aug. 2009; Medusa: 32 bit version 16 Dec. 2010). KTH Royal Institute of Technology, Stockolm

Qifeng W, Xiulian R, jingjing G, Yongxing C (2016) Recovery and separation of sulfuric acid and iron from dilute acidic sulfate effluent and waste sulfuric acid by solvent extraction and stripping. Journal of Hazardous Materials 304:1–9. https://doi.org/10.1016/j.jhazmat.2015.10.049

Radzymińska-Lenarcik E, Sulewski M, Urbaniak W (2015) Recovery of Zinc from Metallurgic Waste Sludges. Pol J Environ Stud 24:1277–1282. https://doi.org/10.15244/pjoes/31230

Rao SR, Leroux M, Finch J (1996) Resource recovery from acid mine drainage. Metals removal from acidic drainage-chemical methods (part I)

Regel-Rosocka M, Wisniewski M (2011) Selective removal of zinc(II) from spent pickling solutions in the presence of iron ions with phosphonium ionic liquid Cyphos IL 101. Hydrometallurgy 110(1–4):85–90. https://doi.org/10.1016/j.hydromet.2011.08.012

Reichl C, Schatz M (2020) World mining data

Remoundaki E, Kousi P, Joulian C, Battaglia-Brunet F, Hatzikioseyian A, Tsezos M (2008) Characterization, morphology and composition of biofilm and precipitates from a sulphate-reducing fixed-bed reactor. J Hazard Mater 153(1–2):514–524. https://doi.org/10.1016/j.jhazmat.2007.08.094

RoyChowdhury A, Sarkar D, Datta R (2015) Remediation of Acid Mine Drainage-Impacted Water. Curr Pollution Rep 1(3):131–141. https://doi.org/10.1007/s40726-015-0011-3

Rydel-Ciszek K, Pacześniak T, Zaborniak I, Błoniarz P, Surmacz K, Sobkowiak A, Chmielarz P (2020) Iron-Based Catalytically Active Complexes in Preparation of Functional Materials. Processes 8(12):1683. https://doi.org/10.3390/pr8121683

Sangami S, Manu B (2017) Synthesis of Green Iron Nanoparticles using Laterite and their application as a Fenton-like catalyst for the degradation of herbicide Ametryn in water. Environ Technol Innov 8:150–163. https://doi.org/10.1016/j.eti.2017.06.003

Sarangi K, Parhi PK, Padhan E, Palai AK, Nathsarma KC, Park KH (2007) Separation of iron(III), copper(II) and zinc(II) from a mixed sulphate/chloride solution using TBP, LIX 84I and Cyanex 923. Sep Purif Technol 55(1):44–49. https://doi.org/10.1016/j.seppur.2006.10.021

Saravanan L, Pandurangan A, Jayavel R (2011) Synthesis of cobalt-doped cadmium sulphide nanocrystals and their optical and magnetic properties. J Nanopart Res 13(4):1621–1628. https://doi.org/10.1007/s11051-010-9915-4

Schindelin J, Arganda-Carreras I, Frise E, Kaynig V, Longair M, Pietzsch T, Preibisch S, Rueden C, Saalfeld S, Schmid B, Tinevez J-Y, White DJ, Hartenstein V, Eliceiri K, Tomancak P, Cardona A (2012) Fiji: an open-source platform for biological-image analysis. Nat Methods 9(7):676–682. https://doi.org/10.1038/nmeth.2019

Schneeberger G, Antrekowitsch J, Pichler C (2012) Development of a New Recycling Process for High Zinc Containing Steel Mill Dusts including a Detailed Characterization of an Electric Arc Furnace Dust. Berg Huettenmaenn Monatsh 157(1):1–6. https://doi.org/10.1007/s00501-012-0051-6

Shim MJ, Choi BY, Lee G, Hwang YH, Yang J-S, O'Loughlin EJ, Kwon MJ (2015) Water quality changes in acid mine drainage streams in Gangneung, Korea, 10 years after treatment with limestone. J Geochem Explor 159:234–242. https://doi.org/10.1016/j.gexplo.2015.09.015

Silverstein RM, Webster FX (1997) Spectrometric Identification of Organic Compounds. John Wiley and Sons, Inc

Sinha MK, Sahu SK, Meshram P, Pandey BD (2014) Solvent extraction and separation of zinc and iron from spent pickle liquor. Hydrometallurgy 147–148:103–111. https://doi.org/10.1016/j.hydromet.2014.05.006

Snoeyink VL, Jenkins D (1980) Water chemistry. Wiley, New York

Stefánsson A (2007) Iron(III) Hydrolysis and Solubility at 25 °C. Environ Sci Technol 41(17):6117–6123. https://doi.org/10.1021/es070174h

Steudel R (2020) The chemical sulfur cycle. In: Lens PNL (ed) Environmental Technologies to Treat Sulphur Pollution: Principles and Engineering, 2nd edn. IWA Publishing, pp 11–53

Sunda W, Huntsman S (2003) Effect of pH, light, and temperature on Fe–EDTA chelation and Fe hydrolysis in seawater. Mar Chem 84(1–2):35–47. https://doi.org/10.1016/S0304-4203(03)00101-4

Sverdrup HU, Olafsdottir AH, Ragnarsdottir KV (2019) On the long-term sustainability of copper, zinc and lead supply, using a system dynamics model. Resour Conserv Recycl: X 4:100007. https://doi.org/10.1016/j.rcrx.2019.100007

Tabak HH, Scharp R, Burckle J, Kawahara FK, Govind R (2003) Advances in biotreatment of acid mine drainage and biorecovery of metals: 1.Metal precipitation for recovery and recycle. Biodegradation 14(6):423–436. https://doi.org/10.1023/A:1027332902740

Tait BK (1992) THE EXTRACTION OF SOME BASE METAL IONS BY CYANEX 30L CYANEX 302 AND THEIR BINARY EXTRACTANT MIXTURES WITH ALIQUAT 336. Solvent Extr Ion Exch 10(5):799–809. https://doi.org/10.1080/07366299208918136

Tolchin AC (2014) 2012 Minerals Yearbook-Zinc

Ucar D, Bekmezci OK, Kaksonen AH, Sahinkaya E (2011) Sequential precipitation of Cu and Fe using a three-stage sulfidogenic fluidized-bed reactor system. Miner Eng 24(11):1100–1105. https://doi.org/10.1016/j.mineng.2011.02.005

Van Roosendael S, Regadío M, Roosen J, Binnemans K (2019) Selective recovery of indium from iron-rich solutions using an Aliquat 336 iodide supported ionic liquid phase (SILP). Separation and Purification Technology 212:843–853. https://doi.org/10.1016/j.seppur.2018.11.092

Veeken AHM, Akoto L, Hulshoff Pol LW, Weijma J (2003) Control of the sulfide (S2−) concentration for optimal zinc removal by sulfide precipitation in a continuously stirred tank reactor. Water Res 37(15):3709–3717. https://doi.org/10.1016/S0043-1354(03)00262-8

Vinoth S, Govindasamy M, Wang S-F, Anandaraj S (2020) Layered nanocomposite of zinc sulfide covered reduced graphene oxide and their implications for electrocatalytic applications. Ultrason Sonochem 64:105036. https://doi.org/10.1016/j.ultsonch.2020.105036

Vitor G, Palma TC, Vieira B, Lourenço JP, Barros RJ, Costa MC (2015) Start-up, adjustment and long-term performance of a two-stage bioremediation process, treating real acid mine drainage, coupled with biosynthesis of ZnS nanoparticles and ZnS/TiO2 nanocomposites. Miner Eng 75:85–93. https://doi.org/10.1016/j.mineng.2014.12.003

Vityaz PA, Senyut VT, Kheifets ML, Kolmakov AG, Klimenko SA (2020) Synthesis of Superhard Materials Based on Sphalerite Boron Nitride Using Carbon Nanoparticles as a Phase Conversion Catalyst. Adv Mater Technol (3(19)):008–017. https://doi.org/10.17277/amt.2020.03.pp.008-017

Wang S, Liu T, Xiao X, Luo S (2021) Advances in microbial remediation for heavy metal treatment: a mini review. J Leather Sci Eng 3(1):1. https://doi.org/10.1186/s42825-020-00042-z

Wanger T, Eglinger J (2021) particlesizer: v1.0.9. ImageJ plugin to derive number based size distributions based on recorded TEM images

Watari T, Nansai K, Nakajima K (2021) Major metals demand, supply, and environmental impacts to 2100: A critical review. Resour Conserv Recycl 164:105107. https://doi.org/10.1016/j.resconrec.2020.105107

Wei X, Viadero RC, Buzby KM (2005) Recovery of Iron and Aluminum from Acid Mine Drainage by Selective Precipitation. Environ Eng Sci 22(6):745–755. https://doi.org/10.1089/ees.2005.22.745

Wu Q, Huang L, Li Z, An W, Liu D, Lin J, Tian L, Wang X, Liu B, Qi W, Wu W (2016) The Potential Application of Raw Cadmium Sulfide Nanoparticles as CT Photographic Developer. Nanoscale Res Lett 11(1):232. https://doi.org/10.1186/s11671-016-1424-7

Zhuang W-Q, Fitts JP, Ajo-Franklin CM, Maes S, Alvarez-Cohen L, Hennebel T (2015) Recovery of critical metals using biometallurgy. Curr Opin Biotechnol 33:327–335. https://doi.org/10.1016/j.copbio.2015.03.019

Zvimba JN, Mulopo J, De Beer M, Bologo L, Mashego M (2011) The dissolution characteristics of calcium sulfide and utilization as a precipitation agent in acidic wastewater effluent treatment. Water Sci Technol 63(12):2860–2866. https://doi.org/10.2166/wst.2011.599

3.7. **Annexes**

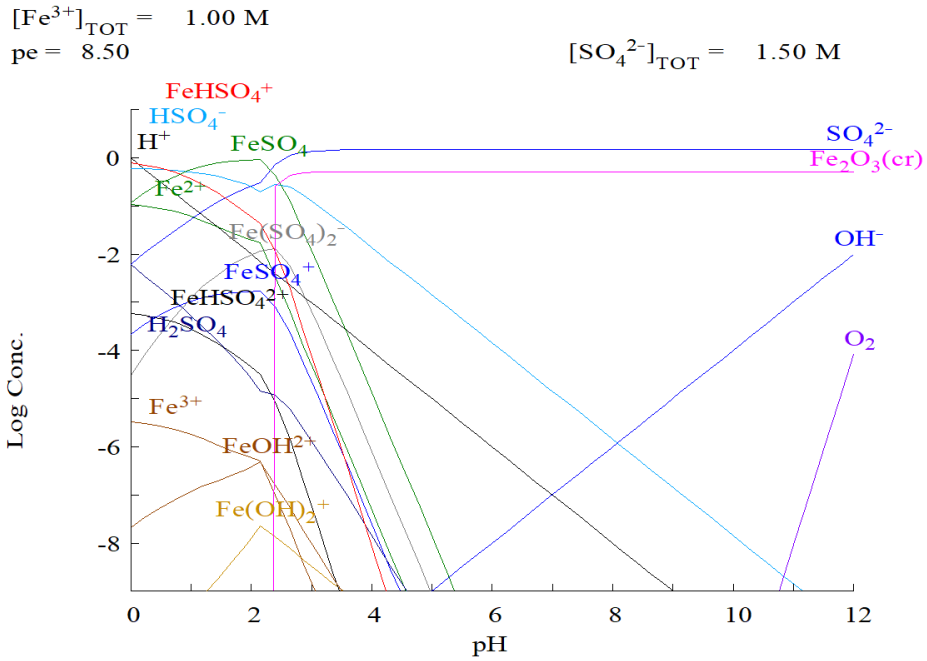

Figure S- 3.1. Balance-diagram for iron as a function of pH, built with Medusa-Hydra software (Puigdomenech, 2015) using iron and sulphate concentrations such as in the copper-free AMD. Phase type is indicated at the end of the name. *solid* - ending in (am) for amorphous, (c) or (cr) for crystalline, (s) for unknown crystallinity, examples: Fe_2O_3(cr), $Fe(OH)_3$(am). *gas* - ending in (g), example: CO_2(g). *liquid* - ending in (l), example: Hg(l). *aqueous* - any name not ending in (c), (cr), (s), (am), (g) or (l), examples of charged species: Na^+, Fe^{3+}, uncharged aqueous species: $Fe(OH)_3$.

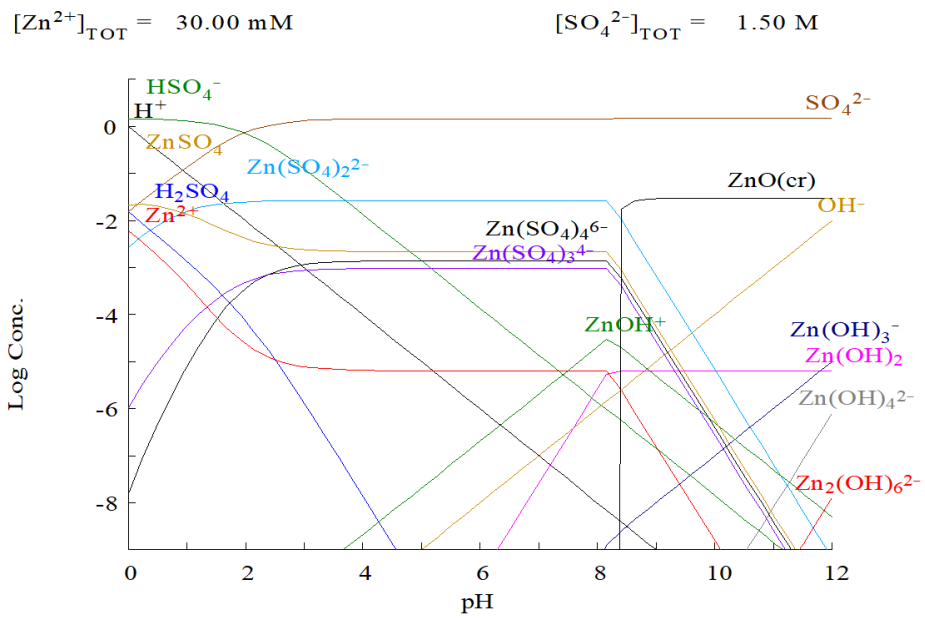

Figure S- 3.2. Balance-diagram for zinc as a function of pH, built with Medusa-Hydra software (Puigdomenech, 2015) using zinc and sulphate concentrations such as in the copper-free AMD. Phase type is indicated at the end of the name. *solid* - ending in (am) for amorphous, (c) or (cr) for crystalline, (s) for unknown crystallinity, examples: Fe_2O_3(cr), $Fe(OH)_3$(am). *gas* - ending in (g), example: CO_2(g). *liquid* - ending in (l), example: Hg(l). *aqueous* - any name not ending in (c), (cr), (s), (am), (g) or (l), examples of charged species: Na^+, Fe^{3+}, uncharged aqueous species: $Fe(OH)_3$.

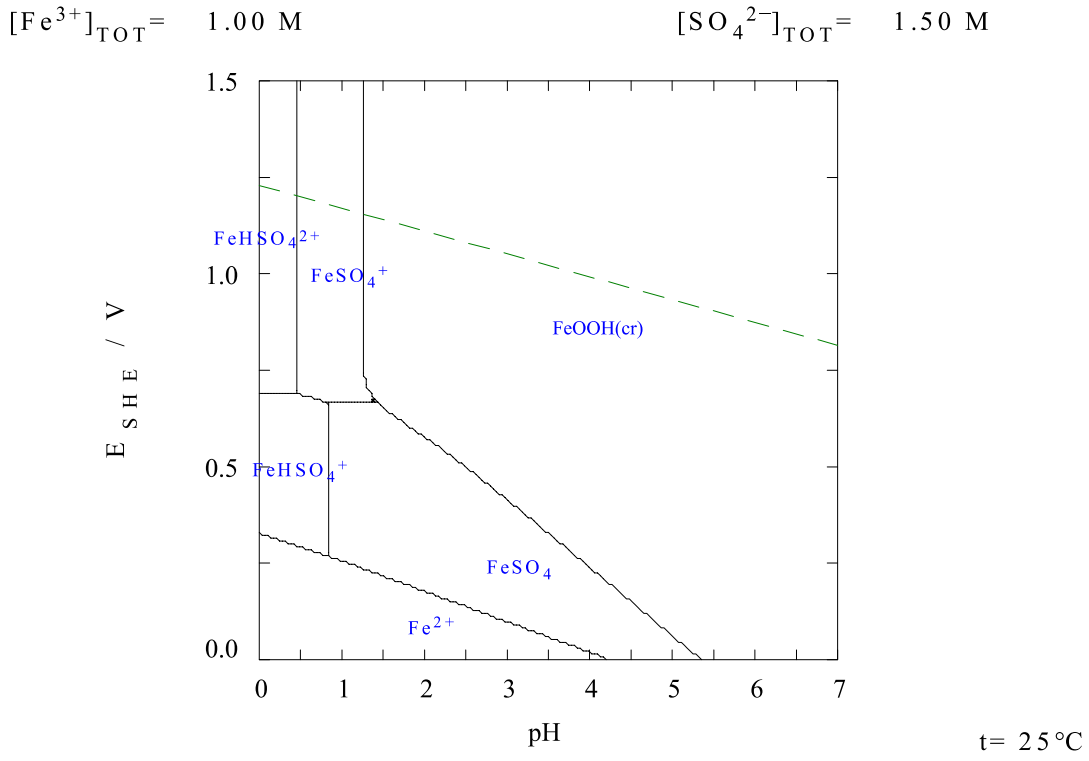

Figure S- 3.3. Eh-pH diagram for iron built with Medusa-Hydra software (Puigdomenech, 2015) using iron and sulphate concentrations such as in the copper-free AMD. The dashed green line is the upper limit of water stability (above this line water is oxidized to form oxygen gas).

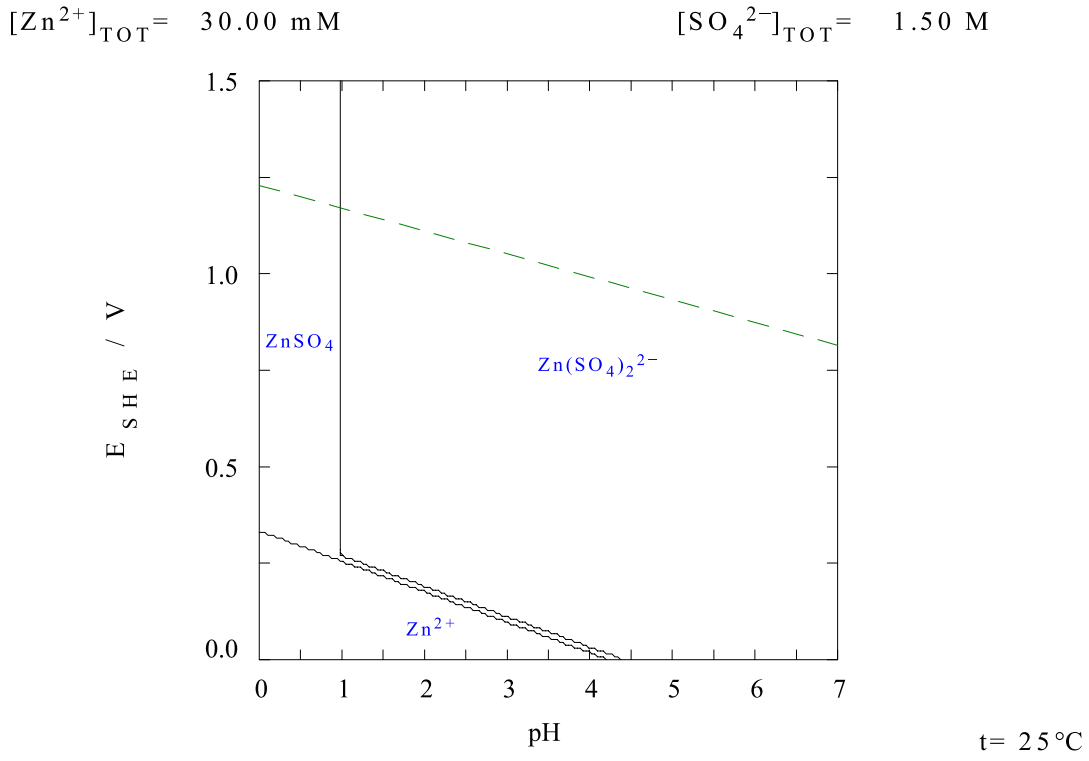

Figure S- 3.4. Eh-pH diagram for iron built with Medusa-Hydra software (Puigdomenech, 2015) using zinc and sulphate concentrations such as in the copper-free AMD. The dashed green line is the upper limit of water stability (above this line water is oxidized to form oxygen gas).

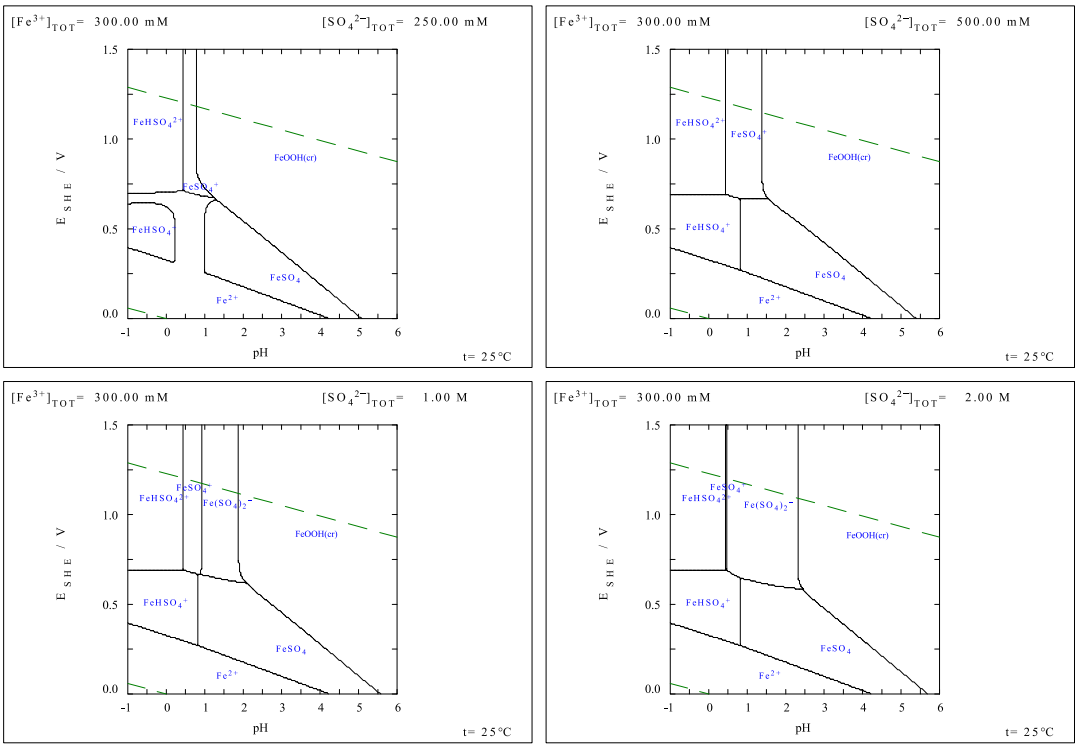

Figure S- 3.5. Eh-pH diagrams built with Medusa-Hydra software (Puigdomenech, 2015) for four different concentrations of SO_4^{2-} ions in the stripping solution and an approximate concentration of iron assuming complete stripping from a loaded organic phase (0.45 M AliCy in kerosene) after iron solvent extraction SX form the copper-free AMD at a A/O ratio of 1/3. The upper dashed green line is the upper limit of water stability (above this line water is oxidized to form oxygen gas) and the lower dashed green line is the lower limit of water stability (bellow this line water is reduced to hydrogen).

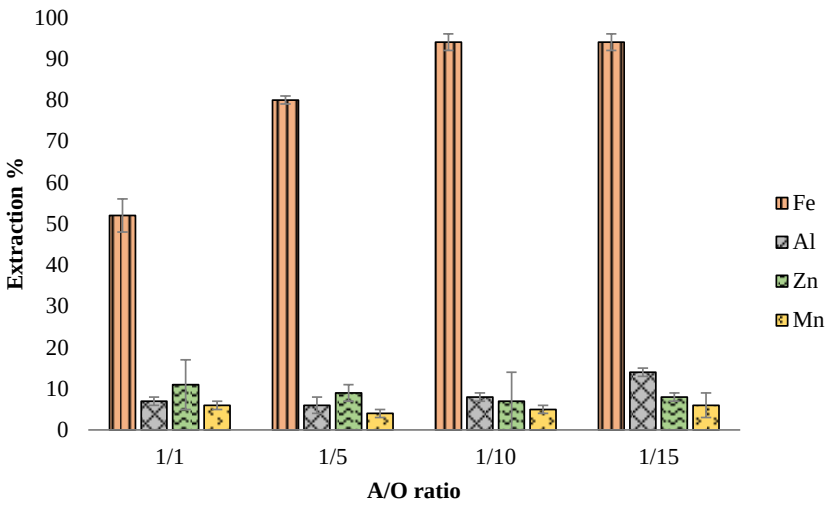

Figure S- 3.6. Extraction of main metals from the copper-free AMD, using 0.15M AliCy in kerosene with different A/O ratios and a contact time of 60 minutes. Results are averages of 2 replicates and the error bars are mean absolute deviations.

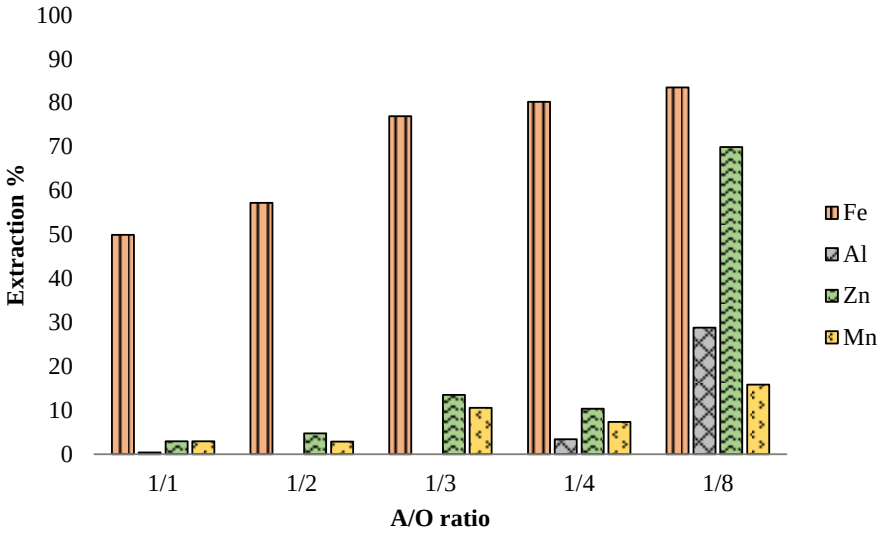

Figure S- 3.7. Extraction of main metals from the copper-free AMD, using 0.3M AliCy in kerosene with different A/O ratios and a contact time of 60 minutes.

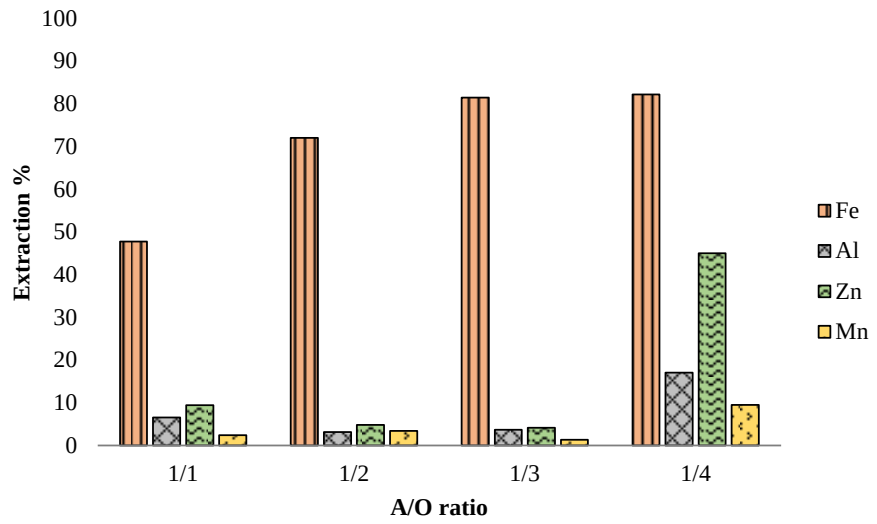

Figure S- 3.8. Extraction of main metals from the copper-free AMD, using 0.45M AliCy in kerosene with different A/O ratios and a contact time of 60 minutes.

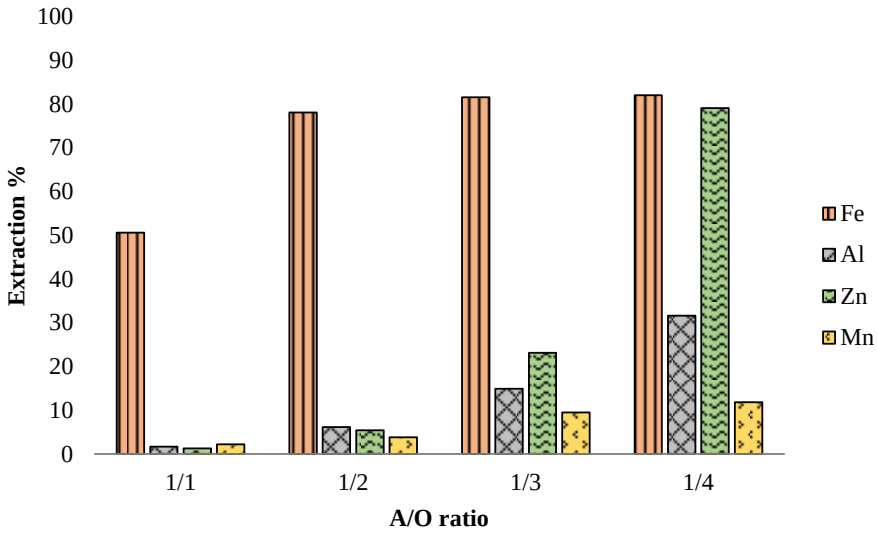

Figure S- 3.9. Extraction of main metals from the copper-free AMD, using 0.6M AliCy in kerosene with different A/O ratios and a contact time of 60 minutes.

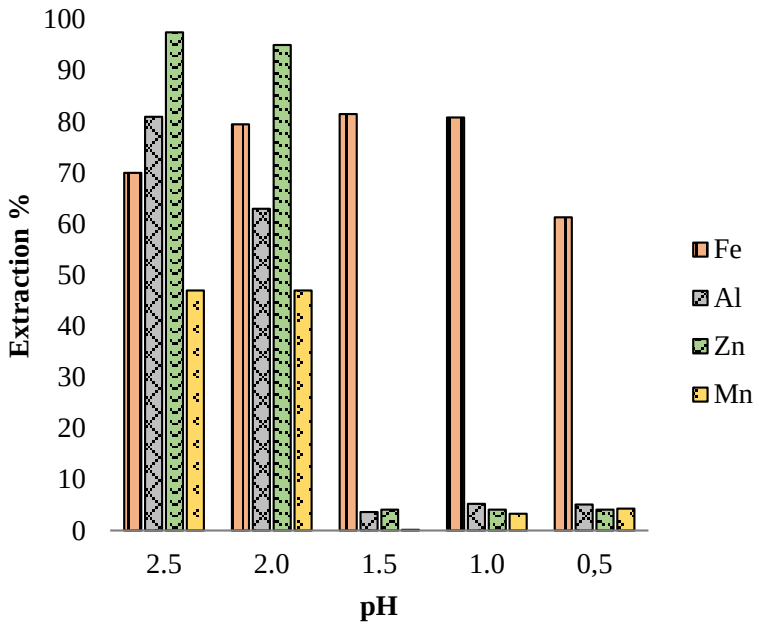

Figure S- 3.10. Extraction of main metals from the copper-free AMD at different extreme acidities, using 0.45M AliCy in kerosene with an A/O ratio of 1/3 and a contact time of 60 minutes.

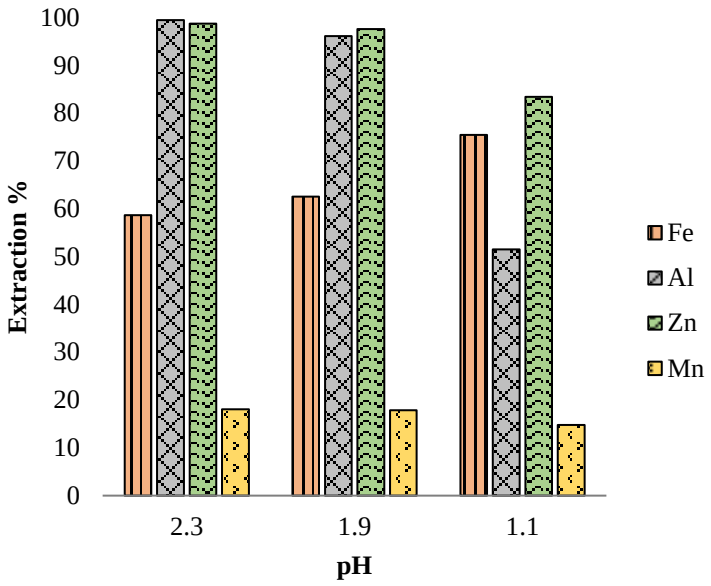

Figure S- 3.11. Extraction of main metals from the three raffinates obtained from one SX cycle on copper-free AMD at different acidities with 0.45M AliCy in kerosene (with A/O = 1/3), in a

second SX cycle using a new organic phase of 0.45M AliCy in kerosene with an A/O ratio of 1/3 and a contact time of 60 minutes.

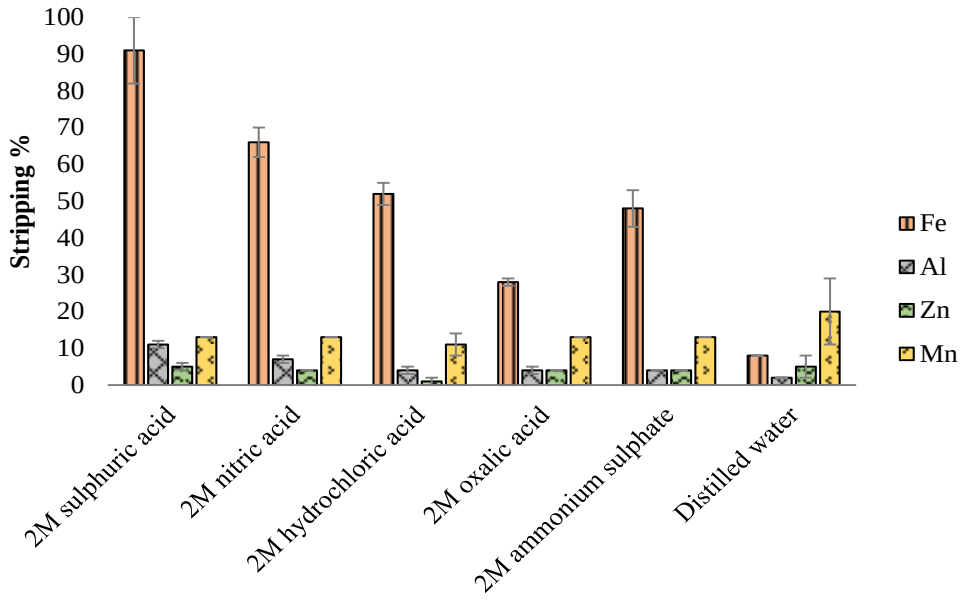

Figure S- 3.12. Stripping of main metals from the iron loaded organic phase obtained from one SX cycle on copper-free AMD with 0.15M AliCy in kerosene (with A/O = 1/10), using different agents with an A/O of 1 and contact time of 30 minutes. Results are averages of 2 replicates and the error bars are mean absolute deviations.

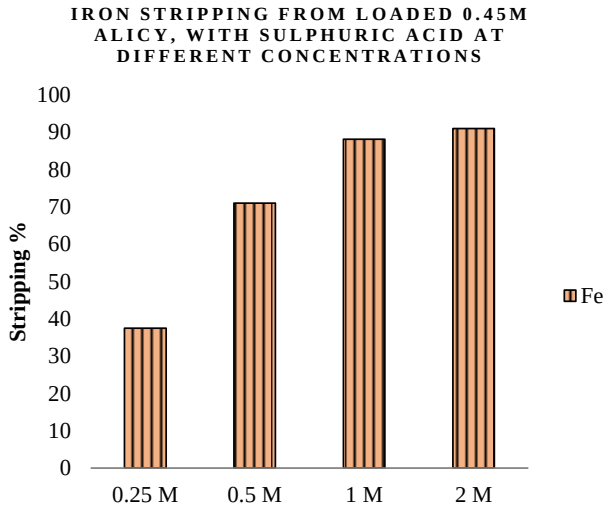

Figure S- 3.13. Iron stripping using sulphuric acid at different concentrations with an A/O of 1 and contact time of 30 minutes on the iron loaded organic phase (from SX with 0.45M AliCy in kerosene on copper-free AMD with A/O = 1/3).

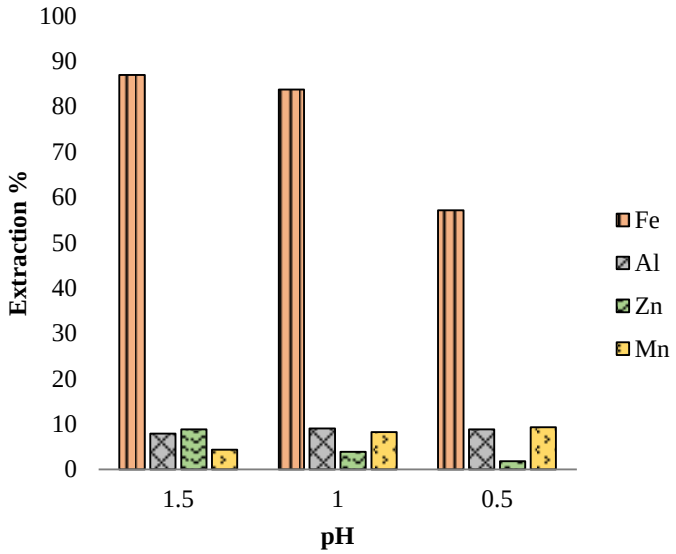

Figure S- 3.14. Extraction of main metals from the copper-free AMD at different extreme acidities, using an organic phase of 0.45M AliCy in kerosene previously used for this same purpose and then regenerated (as described in materials and methods) with an A/O ratio of 1/3 and a contact time of 60 minutes.

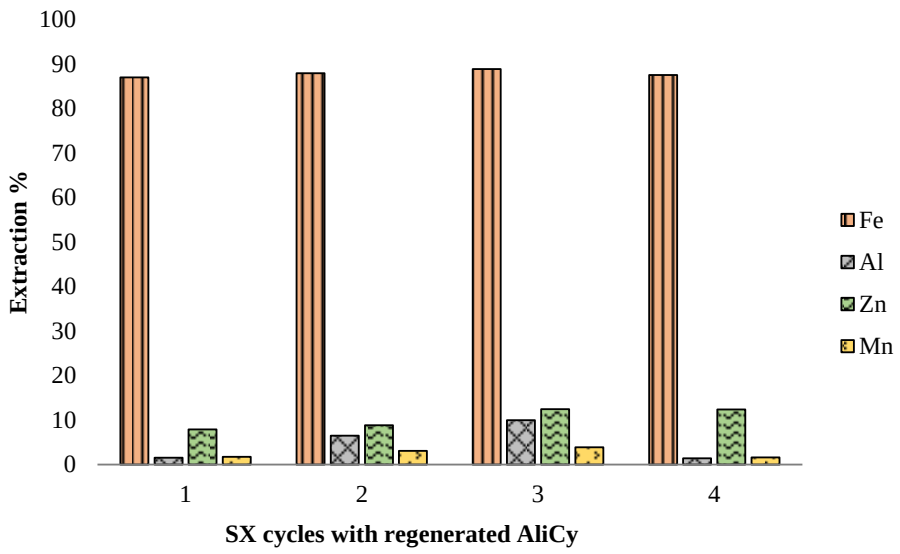

Figure S- 3.15. Four successive cycles of extraction using the same organic phase of 0.45M AliCy in kerosene, stripped with 2M sulphuric acid and regenerated as described in materials and methods after each cycle, with an A/O ratio of 1/3 and a contact time of 60 minutes.

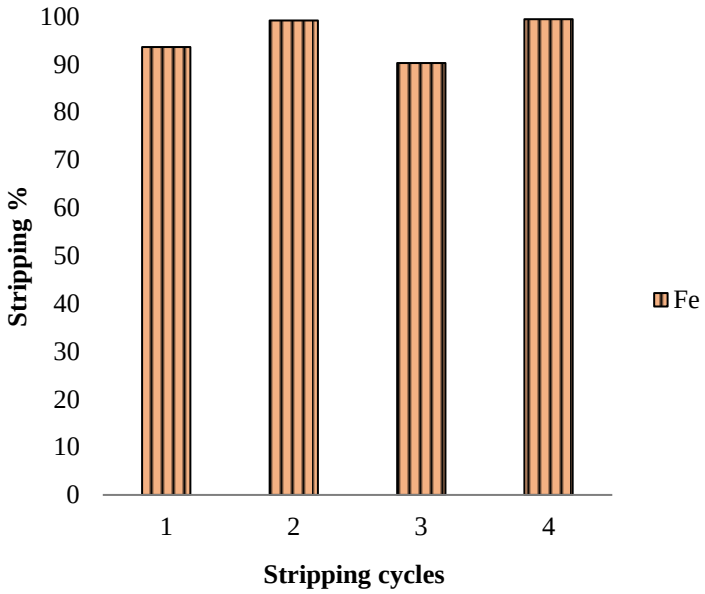

Figure S- 3.16. Four cycles of stripping using 2M sulphuric acid with an A/O of 1 and contact time of 30 minutes on the iron loaded organic phases obtained from successive SX cycles on copper-free AMD (with A/O = 1/3) with the same organic phase of 0.45M AliCy in kerosene regenerated after each cycle.

CHAPTER 4

Enrichment of acidophilic sulfate-reducing bacteria, their application in metal attenuation of acid mine drainage and studies of procaryotic communities on the tested conditions

Enrichment of acidophilic sulfate-reducing bacteria, their application in metal attenuation of acid mine drainage and studies of procaryotic communities on the tested conditions

A modified version of this chapter would be published as:

Nobahar, Amir; Fitasab, Eduardo Trindade; Costa, Maria Clara; Carlier, Jorge Dias. "Enrichment of acidophilic sulfate-reducing bacteria, their application in metal attenuation of acid mine drainage and studies of procaryotic communities on the tested conditions" Applied Microbiology and Biotechnology. (2022, under revision).

Abstract

Acid-mine drainage (AMD) is a worldwide source of environmental pollution. Bio-sulfidogenic reactors benefiting from sulfate reducing bacteria (SRB) are known as attractive technology in acidic sulfate-metal rich AMD treatment operations. Unlike neutrophilic SRB which need the protection from direct contact with low pH in sulfidogenic bioreactors, acidophilic SRB species have sulfate reduction ability in acidic conditions. In this work, AMD affected sediments recovered from an inactive copper mine were enriched in modified Postgate B media having 30 mM of methanol or glycerol or ethanol as carbon source and electron donors over a pH range of 2.00 to 6.00. At pH below 4.00 sulfate reduction activity was not observed and at pH 4.00 the most effective sulfate reduction was observed in the enrichment cultures with methanol, which were then kept by successive culturing and used as inoculum in tests of metal attenuation from AMD. The classification of colonies isolated from the enrichment cultures revealed that all SRB were *Desulfosporosinus* spp., but a fungus from *Trichoderma* genus was also present, suggesting a possible interaction favoring the growth of SRB at such pH. In the AMD bioremediation experiments, different ratios of AMD to modified Postgate B media, as a source of macronutrients, were examined at initial pH 4.50 with 30 mM methanol supplemented equally to all tests. In this study the most promising results were obtained when AMD was supplemented with 0.115% basal salts and 0.02% yeast extract (w/v) (80% AMD plus 20% Postgate B base (v/v)), with more than 99% metal separation after 28 days. Metataxonomic analysis in the enrichment studies showed the presence of *Desulfosporosinus* genus in all enrichment cultures with highest relative abundance in

cultures at pH 4.00 with methanol. Furthermore, metataxonomic analysis of the AMD remediation studies revealed the presence of *Desulfosporosinus* genus in all tested conditions with the most relative abundances in the tests with 100% AMD and 80% AMD plus 20% Postgate B, while the increase in Postgate media supplement increased the percentage of *Clostridium* members, which have been pointed as possible SRB and/or SR ameliorators.

Keywords

Acid mine drainage, metal attenuation, sulfate reducing bacteria, acidophiles, sulfate reduction

4.1. Introduction

Mining activities are among the main anthropogenic source of sulfate emission to the environment, by exposing metal sulfide minerals to the environment causing their oxidation (Brahmacharimayuma et al. 2019). As a result, acid mine drainage (AMD) waters, with high acidity and rich in sulfate and different metals are introduced to the environment with several negative impacts to the aquatic and land organisms (Ighalo et al. 2022).

AMD treatment has been widely implemented by sulfate reduction (Muyzer and Stams, 2008; Zhang et al., 2016). Sulfate reduction bioprocess by sulfate reducing bacteria (SRB) is a widely studied method applied to reduce the concentration of sulfate and different metals from AMD (Sánchez-Andrea et al. 2014a; Sun et al. 2020). SRB are a diverse group of strict anaerobic bacteria and archaea with ability of dissimilatory sulfate reduction into sulfide by oxidation of various substrates. Through the sulfate reduction bio-process, different organic materials or H_2 act as electron donors, while sulfate is electron acceptor, which results in sulfide production and energy conservation and growth of the SRB (Eq. 4.1) (Cabrera et al. 2006). As presented in Eq. 4.1, SRB consume H^+ and produce bicarbonate that rises the substrate pH (Sánchez-Andrea et al. 2014a; Zhang et al. 2016a)

$$\text{Organic material} + SO_4^{2-} \rightarrow 2CH_3COO^- + HCO_3^- + HS^- \qquad \text{Eq. 4.1}$$

The produced sulfide reacts with heavy metal ions including Cu, Zn, Fe, Ni, Pb, Cd etc. and forms very insoluble metal sulfides (Eq. 4.2), that can be then recovered and used in different industrial

operations (Foucher et al. 2001). Through this reaction, HS^- is hydrolyzed into H^+ and S^{2-} and will further lower the pace of pH enhancement by microbial metabolism (Sánchez-Andrea et al. 2014a).

$$HS^- + Me^{2+} \rightarrow MeS \downarrow + H^+ \qquad \text{Eq. 4.2}$$

A major number of the studies on SRB showed that neutral pH between 6 and 8 is required for an optimal growth (Sen and Johnson 1999; Johnson and Sánchez-Andrea 2019). For these SRB, low pH is unfavorable since more energy is expended to pump protons across the cytoplasmic membrane that results in the availability of less energy for their growth (Meier et al. 2012; Sánchez-Andrea et al. 2014a).

However, different studies have shown the existence of SRB in the extremely acidic environments (Koschorreck et al. 2003; Diaby et al. 2007; Sánchez-Andrea et al. 2011; Ňancucheo et al. 2016; Serrano and Leiva 2017) such as highly acidic mine sediments (Alazard et al. 2010; Sánchez-Andrea et al. 2015; Ňancucheo et al. 2016; Dev et al. 2021), pyritic heap bioleaching residues (Phyo et al. 2020), acidic hot spring sediments (Willis et al. 2019) etc. Furthermore, estimations through thermodynamics analyzes reveal a higher Gibbs free energy of SO_4^{2-} reduction by SRB in low pH values (Meier et al. 2012; Sánchez-Andrea et al. 2022). When this additional energy compensates the energy required to export the protons across the cytoplasmic membrane, microbial growth occurs (Meier et al. 2012). There are other mechanisms suggested for the acidophilic SRB (aSRB) growth at low pH such as ATP synthesis by utilization of the proton motive force, proton elimination by vesicles, etc. (Sánchez-Andrea et al. 2014a; Ňancucheo et al. 2017; Brahmacharimayuma et al. 2019; Qian et al. 2019). Most known aSRB are mainly belonged to the genus of *Desulfosporosinus* (Jameson et al. 2010; Sánchez-Andrea et al. 2013, 2015; Phyo et al. 2020; Dev et al. 2021), *Clostridiaceae*, *Alicyclobacillaceae* (Phyo et al. 2020), *Thermodesulfobium*, (Sánchez-Andrea et al. 2015), *Peptococcaceae*, (Santos and Johnson 2017), *Desulfitobacterium* (Sánchez-Andrea et al. 2013) and *Desulfotomaculum*, (Dev et al. 2021).

Beneficiation of the aSRB provides the possibility of AMD remediation operations without the necessity of a prior AMD neutralization step (Sheoran et al. 2010) which is assisted with additional operational costs and reagents (van Houten et al. 1994). Therefore, enrichment, selection and study of aSRB isolates/communities from different extreme environments could create innovative biotechnological advancements in AMD remediation and/or metal bio-recovery.

The present study aimed to obtain and study acidophilic SRB consortia from the sediments from the confluence region of an AMD stream and a freshwater stream receiving the municipal wastewater treatment plant effluent from the village located in the inactive copper mine of São domingos, Alentejo, Portugal and to apply it for metal attenuation from an AMD originating from the same mining area.

4.2. **Materials and methods**

4.2.1. Acidophilic SRB enrichments

4.2.1.1. Sediment collection

The sediments to be used as inoculum were collected in March 2020, from 5 sites at ~30 cm depth in the wet zone of the bank in the confluence between a water stream affected with acid mine drainage and a water stream receiving the effluent from the wastewater treatment plant of Mina de São Domingos (São domingos inactive mining area, located in the Iberian Pyrite Belt, Alentejo, Portugal) (Figure **4.1**).

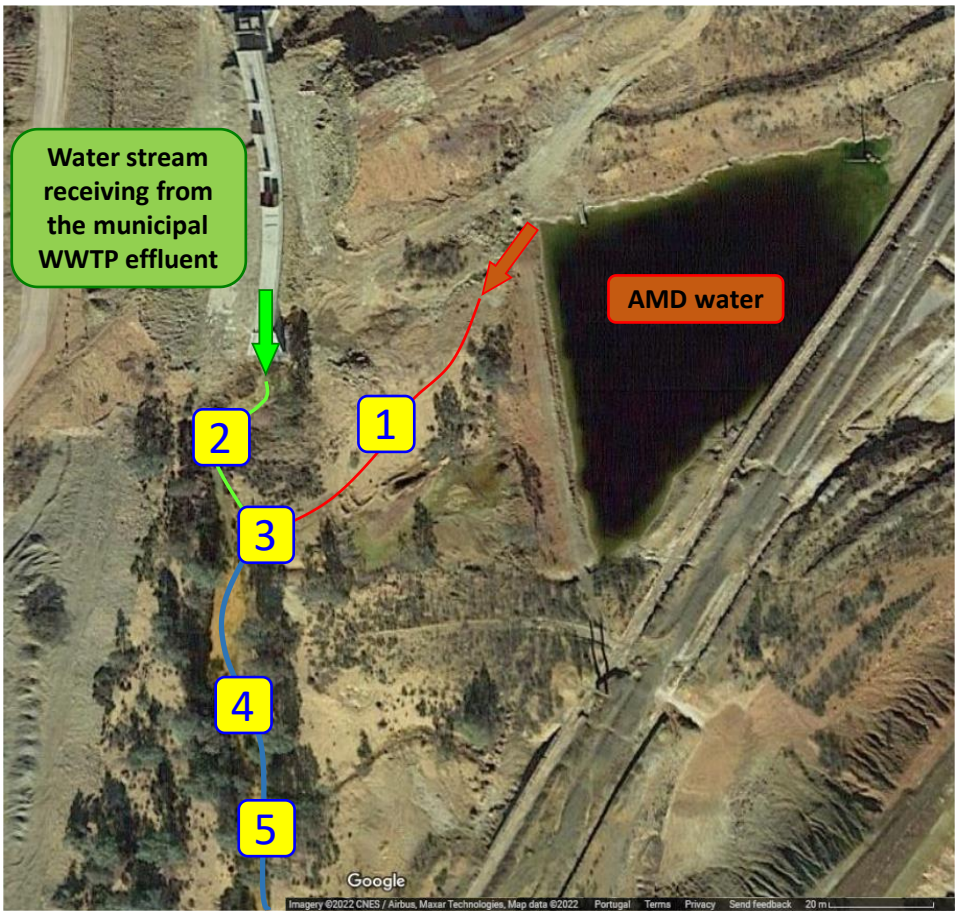

Figure 4.1. Sampling zone of the confluence of acid mine drainage stream and wastewater treatment plant.

Samples were stored at 4℃ and were immediately transferred to the lab. Measurements of pH of the sediments were performed using a 1:10 soil-to-water ratio (w/v) suspension (Thomas 1996) (Table **4.1**).

Table 4.1. pH of the sediments and water in the sampled zone.

	pH	
Site	Sediment	Water
1	3.13	2.90
2	4.04	4.86
3	5.55	3.19
4	3.96	5.01
5	3.66	2.96

4.2.1.2. Enrichment setup

Enrichment cultures were made in growth media of Postgate B base but with three different carbon sources, including glycerol, methanol, and ethanol and then were adjusted to five different pH values 2.00, 3.00, 4.00, 5.00 and 6.00, inoculated with 5% (v/v) of a mixture of the 5 sediments collected at the São Domingos mining area. The inoculum mixture for the enrichments was prepared by adding 10 g of the mixture of sediments sample to 160 mL of medium without carbon source under magnetic stirring. Pipetting to inoculate was done with cut pipette tips to avoid clogging. As controls, the Postgate B base medium with the same three carbon sources and also with the original carbon source of Postgate B, lactate, all at pH 6.00, were inoculated with a SRB consortium kept in the laboratory for several years (Carlier et al. 2019, 2020b)

4.2.1.3. Enrichment media

The liquid media base used for enrichments was adapted from Postgate B medium to grow SRB (Postgate 1984) and prepared by mixing the following reagents per liter of tap water: KH_2PO_4 (1g), NH_4HCl (1g), $FeSO_4 \cdot 7H_2O$ (0.5g), $MgSO_4 \cdot 7H_2O$ (2g), $CaSO_4 \cdot 2H_2O$ (1.25g), yeast extract (1g), ascorbic acid (0.1g) and Thioglycolic acid (75 µL). Then, 30 mM of different carbon sources/electron donners were added to each enrichment cultures as following: 1680 µL of 87% glycerol, 1140 µL of absolute ethanol and 786 µL of 99.9% methanol. Finally, the medium with each type of carbon source/electron donner was divided in six flasks and the pH of each portion adjusted using sulfuric acid to acidify and sodium hydroxide to alkalize.

4.2.1.4. Enrichment conditions and monitoring

The assays were carried out in 100-mL glass bottles with 95 mL medium and 5 mL inoculum added to each flask. The cultures were covered with 7.5 mL of liquid paraffin to prevent oxygen diffusion. Finally, the bottles were sealed with butyl rubber stoppers and aluminum crimp seals and incubated at room temperature (25±3^{o}C).

To monitor the evolution of cultures, 2-mL samples were collected from the initial media and along the experiments, through the rubber stoppers using a syringe. Sulfate and sulfide

concentrations in the liquid phase were monitored as indicators of SRB activity, while redox potential (Eh) was monitored due to its importance as a limiting factor for SRB growth. The pH, as the variable parameter of the work, was monitored to evaluate its stability and its relations with SRB activity.

4.2.2. Isolation of acidophilic SRB strains

The attempt to isolate aSRB strains was made in petri dishes with ~20 mL solid media and in 15 mL centrifuge tubes with ~14 mL solid medium. The solid medium base was like the liquid media and the carbon sources and pH values were selected according to the most promising results in the liquid media enrichment. Five plates and five tubes were prepared for each selected condition. The plates were inoculated by spreading onto the solid medium 150 µL of successive dilutions (10^{-1}, 10^{-2}, 10^{-3}, 10^{-4} and 10^{-5}) prepared from the enrichment cultures in liquid medium. The tubes, before medium solidification (kept at 60ºC in a water bath), were inoculated with 850 µL of the same successive dilutions and homogenized by tube inversion five times. Successive dilutions were made in sterile Ringer's solution, with the pH adjusted to the selected conditions.

The solid medium for strain isolation was prepared as follows: before adding the carbon source, Bacteriological Agar (15 g L) was added, kept under magnetic stirring for 5 minutes, autoclaved and left to cool down to 60°C under magnetic stirring. Then, inside a sterilized (20 min UV exposition) laminar flow chamber, the carbon source was added and after homogenization the medium was divided into the petri dishes and left to solidify before inoculation or divided into centrifuge tubes and kept at 60ºC (in water bath) until inoculation.

The solid medium in the petri dishes, after the inoculum had dried, was covered with another portion of solid medium and the plates were incubated at room temperature (25±3ºC) in a closed five-liter glass bottle with 3 candles burning inside aiming to create anaerobic conditions. In the case of isolations in 15 mL centrifuge tubes, the inoculated solid medium was covered with 1.5 mL of liquid paraffin (previously sterilized by autoclave), the tube tightly closed with the screw cap, and the incubation also carried out at room temperature (25 ± 3°C). Isolations on solid media were monitored by direct observation of the plates and tubes and looking for black colonies, a typical feature of SRB colonies in this type of media due to the formation of FeS precipitates (Postgate 1984).

4.2.2.1. Cultivation of isolates in liquid medium

Small scale cultivation of aSRB colonies isolated from the solid medium was carried out in 250 mL bottles containing modified Postgate B liquid media (Postgate 1984) at pH 4.50 and with the carbon sources that allowed SRB colonies to growth in solid media (methanol and ethanol). The pH of the cultures was adjusted with sulfuric acid. Cultures were covered with 15 mL of liquid paraffin to prevent oxygen diffusion and were sealed with butyl rubber stoppers and aluminum screw cap and incubated at room temperature (25±3ºC). Aiming to create anaerobic conditions inside the culture, the medium was purged with nitrogen gas for 5 minutes. Throughout the experiments, concentrations of sulfate and sulfide, redox potential (Eh) and also the pH of the cultures were monitored.

4.2.3. Batch reactor experiments

4.2.3.1. AMD neutralization

The AMD sample used in bioremediation experiments was collected from São Domingos mining area in the 8th of March 2020 from the lagoon nearby the sediment sampling zone (Figure **4.1**). Thereafter, it was immediately transferred to the lab and characterized (Table **4.1**). The selected seeding of aSRB for AMD treatment from the enrichment studies was the aSRB consortium obtained through enrichment studies of the sediments in the presence of methanol at pH 4.00. Therefore, the pH of the AMD was adjusted to 4.50 using sodium hydroxide and was left for one hour to settle the formed metal hydroxides. Finally, the liquid fraction was decanted and after characterization, was used in batch experiments (Table **4.2**).

Table 4.2. Concentration of the main metals and pH of the AMD collected at the São Domingos mine before and after pH adjustment to 4.50.

Metal	Before pH adjustment	After pH adjustment	
Cu	28 ± 1	25.74 ± 0.06	
Zn	45.4 ± 0.3	43.6 ± 0.4	
Fe	175 ± 13	0.24 ± 0.02	mg/L
Al	279 ± 12	12.3 ± 0.1	
Mn	19 ± 2	19.9 ± 0.2	
pH	2.60	4.50	

Experimental Setup for the Batch Tests

Batch experiments were performed to assess the capability of the selected enriched aSRB inoculum in metal separation from AMD at pH=4.50 using 30 mM methanol as carbon source. These experiments were conducted in a series of AMD to Postgate B macronutrients base ratios at pH 4.50 (hereafter, Postgate B macronutrients base is referred as PB-m) to evaluate the effect nutrient supplement by Postgate B base on SR activity and metal bio-removal and also on the structure of the consortia communities with putative roles in sulfate reduction. The ratios of AMD to PB-m (v/v) in this study were as follow: 100% AMD (no PB-m), 20% PB-m (meaning 20% PB-m plus 80% AMD and hereafter, only the PB-m ratio will be shown), 40% PB-m, 60% PB-m, 80% PB-m and 100% PB-m (no AMD). For inoculation, the consortium obtained and maintained in enrichment cultures starting at pH 4.00 with methanol as carbon source was added to the flasks at the final ratio of 1 to 10 (v/v).

4.2.3.2. Batch Tests conditions and monitoring

The assays were carried out in 200-mL glass bottles with 180 mL medium and 20 mL inoculum added to each flask. The cultures were covered with 10 mL of liquid paraffin to prevent oxygen diffusion. Finally, the bottles were sealed with butyl rubber stoppers and aluminum crimp seals and incubated at room temperature (25±3ºC).

To monitor the evolution of cultures, 2-mL samples were collected from the initial media and along the experiments, through the rubber stoppers using a syringe. Major physicochemical properties including pH, redox potential, concentration of sulfate, sulfide, Cu, Zn, Fe, Al and Mn were monitored during 34 days at intervals of 6 or 7 days.

4.2.4. Analytical methods

A pH/E Meter GLP 21 (CRISON) was used to measure redox potential with a Pt electrode coupled with a reference saturated calomel electrode (CRISON, 52 61) and pH with a glass pH electrode (VWR, SJ 223). Redox measurements were converted to Eh values using a conversion factor of 241 mV for the Pt electrode. A UV-Visible spectrometer DR2800 (Hach-Lange) was used to determine the sulfate and sulfide concentrations using the sulfaVer4 (Method 8051, Hach-Lange) and the methylene blue (Method 8131, Hach-Lange) procedures, respectively at 450 and 665 nm. Samples collected for metals analysis were initially centrifuged at 2500 g and then were acidified with concentrated nitric acid (to 5% (v/v)). Microwave plasma atomic emission spectrometry using a 4200 MP-AES (Agilent) equipment was used to measure the concentrations of Cu, Zn, Fe, Al and Mn. Calibration curves were built using standards prepared from the following stock solutions in 0.5 M HNO_3: $Cu(NO_3)_2$, $Zn(NO_3)_2$, $Fe(NO_3)_3$ (Merck Certipur, Germany); $Mn(NO_3)_2$ and $Al(NO_3)_3$ (Panreac AA, Spain).

4.2.5. Taxonomic classification of isolates

A part of the isolated colonies was picked up with a sterile spatula and divided in two. A part was fragmented and suspended in 1000 µL sterilized Ringer's solution, which was used as inoculum of new plates and centrifuge tubes with solid medium (to keep the isolates in collection) and to inoculate cultures in liquid medium. The other part was used for DNA extraction.

For DNA extraction, “DNeasy PowerSoil Pro Kit” (QUIAGEN) was used and after extraction, the concentration and quality of the extracted DNA was determined using a spectrophotometer (NanoDrop3300, Thermo Fisher Scientific). The identification and classification of the black colonies was performed using sequences from the 16S rRNA gene for prokaryotes and sequences from the 18S rRNA gene and ITS1-5.8S-ITS2 region for eukaryotes. For the amplification of the

16S rRNA gene, the universal primers 8F (also known as fD1) (5′- AGA GTT TGATCC TGG CTC AG -3 ′) (Weisburg et al. 1991) and 1492R (5′-GGT TAC CTT GTTACG ACT T-3 ′) (Lane 1991) were used, for the 18S rRNA gene the universal primers 18S-F (5′- ACC TGG TTG ATC CTG CCA GT -3′) and 18S-R (5′- TCA GCC TTG CGA CCA TAC -3′) (Sogin 1990) were used, and for the ITS1-5.8S-ITS2 region the ITS1F primer (5' CTT GGT CAT TTA GAG GAA GTA A -3′) (Gardes and Bruns 1993) and ITS4 primer (5'- TCC TCC GCT TAT TGA TAT GC -3′) (White et al. 1990) were used, all acquired from NZYTech (Lisbon, Portugal). For PCR amplifications, the following mixture was used in 0.2 mL PCR tubes: 2 µL of DNA sample (5 to 50 ng/µL), 5 µL of 10× DreamTaq buffer (including 20 mM $MgCl_2$) (ThermoFisher Scientific), 0.25 µL of DreamTaq DNA Polymerase (5 U/µL) (ThermoFisher Scientific), 1 µL dNTP solution (10 mM each), 1 µL forward primer solution (10 µM), 1 µL reverse primer solution (10 µM) and 39.75 µL sterile Milli-Q water. PCR amplification was performed in a thermal cycler (2720 Thermal Cycler, Applied Biosystems, Foster City, EUA), performing an initial denaturation step of 95°C for 10 min, 35 cycles of 95°C for 30s, 57°C for 16S rRNA and 50°C for 18S rRNA and ITS1-4 for 30s, 72°C for 90s and a final step of 7 min at 72°C. Finally, PCR products were analyzed by electrophoresis on 1% (w/v) agarose gels in 1x buffer TAE (AMRESCO, Solon, EUA), with DNA stained by the addition of 50 µL/L of GreenSafe Premium (NZYTech, Lisbon Portugal) in gel and the electrophoresis performed with 5 V per cm of gel length.

4.2.5.1. Sanger sequencing and taxonomic classification

The amplified products were sequenced by the Sanger method with the respective primers through a capillary electrophoresis sequencing system (Genetic Analyzer, Model 3130xl, Applied Biosystems, Foster City, EUA) at the Centre of Marine Sciences (CCMAR), university of Algarve, Portugal. Taxonomic classifications based on the 16S rRNA gene, the 18S rRNA gene and the ITS1-4 marker were obtained by BLAST alignment in the NCBI databases “16S ribosomal RNA sequences (Bacteria and Arcaea)”, “18S ribosomal RNA sequences (SSU) from fungi” and “Internal transcribed spacer region (ITS) from fungi”, respectively.

4.2.6. Meta-Taxonomic studies

To evaluate the transformations in the prokaryotic communities during the enrichment processes with the different carbon sources and during the AMD treatment experiments, taxonomic studies were carried using massive sequencing data of the 16S rRNA gene.

4.2.6.1. DNA extraction

The extraction and purification of DNA was performed using the DNeasy® PowerSoil® Pro Kit (QUIAGEN). For the sludge mixture used as the enrichments' inoculum, 250 mg was used as initial material. For the enriched cultures in liquid medium, 5 mL of each sample was centrifuged at 2500×g for 10 min at room temperature to collect cells and then the supernatant was discarded until the volume (pellet and remaining liquid) was 250 µL. Immediately after collection of samples, the 250 mg of sludge and each of the 250 µL samples were used for DNA extraction following the manufacturer procedures. DNA concentration and quality was evaluated using a NanoDrop spectrophotometer (NanoDrop3300, Thermo Fisher Scientific).

4.2.6.2. Next-Generation Sequencing

Library preparation and sequencing workflow were carried out at the Integrated Microbiome Resource (https://imr.bio/index.html) for full-length sequences of 16S rRNA gene amplicons. PCR amplifications were performed in duplicate using separate DNA template dilutions with the high-fidelity Phusion + polymerase and "fusion primers" (PacBio adaptors + barcodes + specific regions) in a single round of PCR. The specific regions of primers for the full-length target were the 27F (Paliy et al. 2009) = AGRGTTYGATYMTGGCTCAG and the 1492R = RGYTACCTTGTTACGACTT (Lane 1991). The amplicons of these work, together with others to make a total of 96 (including four negative PCR controls and a positive control), were visualized by electrophoretic analysis and then cleaned up and normalized in one step using the high-throughput Charm Biotech Just-a-Plate 96-well Normalization Kit. Finally, all the samples were pooled in one library which was quantified fluorometrically using the Invitrogen Qubit double-stranded DNA high-sensitivity (dsDNA HS) method, and then the library was run on a PacBio Sequel II using a new chip.

4.2.6.3. Bioinformatics Analyses

The analysis of sequences was performed through a pipeline available at the Microbiome Helper repository (Comeau et al. 2017). Namely, the standard operating procedure (SOP) PacBio CCS Amplicon SOP v1 (qiime2) (https://github.com/LangilleLab/microbiome_helper/wiki/PacBio-CCS-Amplicon-SOP-v1-(qiime2)) was used to prepare the reads and get *amplicon sequence variants* (ASVs - synonym of OTUs), and then the Amplicon SOP v2 (qiime2 2020.8) (https://github.com/LangilleLab/microbiome_helper/wiki/Amplicon-SOP-v2-(qiime2-2020.8)) was used for taxonomic classifications and diversity analysis, as summarized in the following main steps:

- Resolve orientation problems - list all sequences in the same orientation;

- Trim primers with cutadapt – to remove the primers from the reads and FILTER the reads by removing those that do not begin and end with the correct primer sequences and those that are out the size range 1300 to 1800 nt;

- Import FASTQs as QIIME 2 artifact – to import the trimmed reads into the QIIME 2 "artifact" file format (with the extension QZA);

- Summarize trimmed FASTQs - to get a report of the number of reads per sample and quality distribution across the reads;

- Denoising and pooling the reads into ASVs (syn. of OTUs) – by running the DADA2 workflow to DENOISE the reads by removing those with low quality (number of "expected errors" > 2) and trimming all to the same length (from where the quartiles of the quality score distribution per position drops below the value 25), to infer ASV's from the denoised reads as well as to REMOVE CHIMERAS BY excluding variants that result from combinations of two "parent" reads;

- Assign taxonomy to ASVs – to classify the ASVs using the Naive-Bayes approach implemented in the scikit learn Python library (https://scikit-learn.org/stable/modules/naive_bayes.html) with the SILVA full-length 16S/18S classifier database;

- Filtering resultant table – to filter out highly rare ASVs (frequency < 0.05% of the mean sample depth) and contaminant (mitochondrial and chloroplast 16S sequences), as well as to exclude any ASV that is unclassified at the phylum level;

- Generate rarefaction curves - to calculate two alpha-diversity metrics (Shannon index and Faith's phylogenetic diversity index) for all samples using growing sequencing depths and plot the respective rarefaction curves, to determine if sufficient sequencing was performed;

- Calculating diversity metrics and generating ordination plots – to calculate the beta diversity metrics Bray-Curtis Dissimilarity and Weighted UniFrac and plot respective principal coordinates analysis (PCoA) graphs to visualize relations between samples;

- Generate stacked barchart of taxa relative abundances - to plot taxonomic abundances across samples (each sample individually).

4.3. **Results and discussion**

4.3.1. Acidophilic SRB enrichments

Screening of the sulfate reduction (SR) activity by the SRB present in the collected sediment samples from São Domingos mining area was performed in modified Postgate B media (Postgate 1984) at different pH values of 2.00, 3.00, 4.00, 5.00 and 6.00, as described in materials and methods. The collected five sludge samples (Table **4.1**) were initially mixed homogenously and used as inoculum. In this type of enrichment from environmental samples, quickly (in the first hours) after inoculation, the aerobic bacteria of the inoculated community consume the available oxygen in the medium, creating optimal anoxic conditions for the growth of strictly anaerobic bacteria such as SRB. Importantly, the possible toxicity of the substrate/compound used as source of carbon and energy (electron donors) is highly suggested in sulfidogenic bioreactors performing at low pH, although alcohols, sugars, glycerol and hydrogen have been previously demonstrated as suitable electron donors (Koschorreck 2008; Bijmans et al. 2010; Ňancucheo and Johnson 2012). In this study, glycerol, methanol and ethanol were used (30 mM) separately as source of carbon and energy, being added to the prepared Postgate B media with different pH values.

Results from enrichment studies revealed no sulfate reduction activity in the cultures starting at pH 2.00 and pH 3.00, but at pH ≥ 4.00 there was SR in the presence of the three tested carbon sources (Figure **4.2**).

Highest SR activity rates were observed in the samples enriched in the presence of methanol. At pH 5.00 and 6.00, more than 99.9% of sulfate reduction was observed after 21 days of inoculation, and the most intense SR activity was from day 14 to 21 with a sharp decrease in sulfate concentration (reduction of almost 99% of the sulfate in this time range) and redox potential along with an increase in pH (Figure S- **4.2**). In the cultures starting at pH 4.00, the highest intensity of SR was observed one week later, starting at day 21 and complete SR was observed 35 days after inoculation with a rise in the pH from 4.00 to 6.86 and a decrease in redox potential from 124 mV to -310 mV (Figure **4.2**). In these tests, the final concentration of sulfide achieved was ~200 mg/L, ~100 mg/L and ~25 mg/L, in the cultures starting at pH 6.00, pH 5.00, and pH 4.00, respectively. A possible explanation for the low sulfide concentration could be the reaction of the generated sulfide with metal ions present in the sediments that were leached to the solution, originating insoluble metal sulfides. The lower the pH, the more metals could have been solubilized from the sludge. However, we did not deepen this possibility because at this stage the objective was to obtain and identify SRB populations capable of maintaining SR activity at low pH.

Regarding the enrichment cultures with glycerol as carbon source, SR activity observed at pH 6.00, 5.00 and 4.00 had similar trends as in cultures enriched with methanol, but at slightly lower rates (Figure S- **4.3**). In this regard, nearly 90% of the initial sulfate was consumed at pH 6.00, 5.00 and 4.00 after 42 days of inoculation.

The least sulfate reduction activity was observed in the cultures where ethanol was applied as carbon source. Curiously, in the cultures that started at pH 4.00, more SR activity was observed than in cultures that started with pH 5.00, and no signs of SR were detected at pH 6.00 (Figure S-**4.4**). At pH 4.00, moderate SR activity (~65% conversion of the initial sulfate) was observed after 35 days (Figure **4.2**).

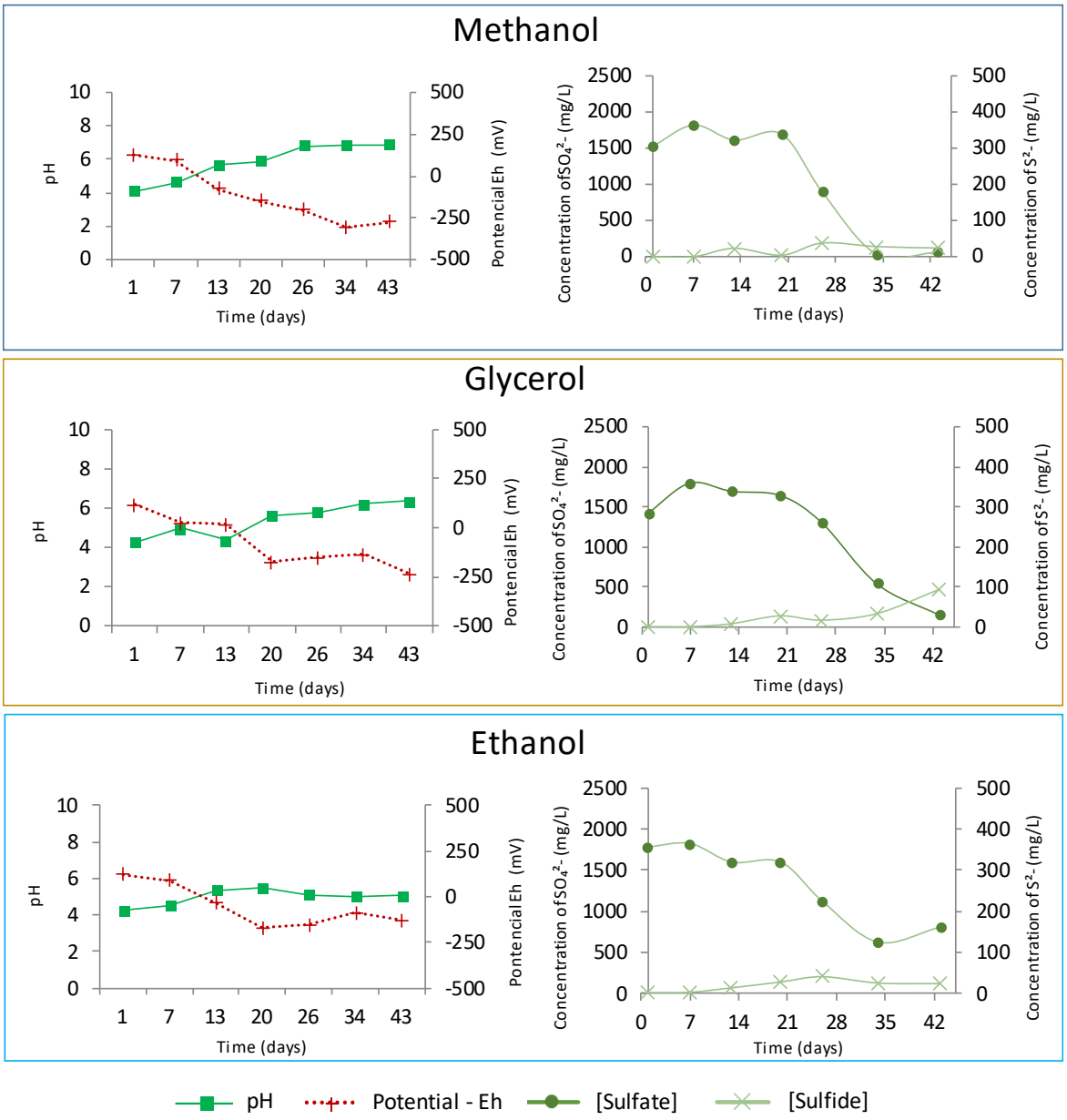

Figure 4.2. Time-course changes of pH, redox potential, sulfate reduction and sulfide generation in enrichment studies with sediments collected from São Domingos mine as inoculum, enriched in Postgate B media in the presence of three carbon sources (methanol, ethanol and glycerol) at pH 4.00 (25 ± 3℃).

4.3.2. Isolation of acidophilic SRB

The attempt to isolate aSRB strains was done at two pH values (4.00 and 4.50) with all the three tested carbon sources (glycerol, methanol and ethanol). Eleven black colonies become visible after about two weeks: just one in the petri dishes and nine in the tubes with solid medium at pH 4.00 and methanol as a carbon source plus one in a tube with solid medium at pH 4.50 and ethanol as a carbon source. The DNA from the colony isolated from petri dishes did not amplify the 16S rRNA gene but amplified the 18S rRNA gene and the ITS1-5.8S-ITS2 region, and both these amplicons' sequences allowed to classify this colony as a fungi of the *Rachicladosporium* genus. On the contrary, the colony isolated from tubes with solid medium at pH 4.50 and having ethanol as carbon source just amplified the 16S rRNA gene sequence, which was classified as being from bacteria of *Desulfosporosinus* genus. Interestingly, all the nine colonies isolated from medium at pH 4.00 with methanol as carbon source amplified the 16S rRNA gene as well as both the 18S rRNA gene and the ITS1-5.8S-ITS2 region. All the 16S amplicons revealed bands with similar and relatively high intensity in the agarose gel electrophoresis, while the 18S and the ITS1-5.8S-ITS2 amplicons revealed varying band intensities. All the 16S amplicons were sequenced and all of them were classified as belonging to *Desulfosporosinus* genus. The 18S and the ITS1-5.8S-ITS2 amplicons revealing the most intense bands (both amplified from same colony) were sequenced and the two sequences were classified as being from *Trichoderma* genus. Probably this fungus was spread along the solid medium of the tube with varying mass distribution, thus each DNA sample collected from the SRB colonies was contaminated with different amounts of DNA from the fungus. It may be possible that the presence of this fungus had a role in the fact that under these conditions more SRB colonies appeared. Indeed, the fact that the presence of a fungus was observed in the solid medium from which almost all SRB colonies were isolated (9 out of 10 colonies) raises the suspicion of some type of interaction of symbiosis or commensalism favoring the growth of SRB.

These results confirm the presence of acidophilic sulfate-reducing bacteria in the sampled area and indicate that the strategy to incubate the petri dishes was not as efficient in creating anaerobic conditions as the strategy of incubation in tubes. Another evidence from these results is that, despite the sulfate reduction activity observed in the enrichment cultures (with microbial

communities) in liquid media with the three tested carbon sources, for unknown reasons, isolated colonies in solid media have grown with methanol and ethanol but not with glycerol.

Isolated colonies were inoculated in modified liquid Postgate B medium at pH 4.50 with the same carbon source that was in the solid medium from where the colonies were picked (methanol or ethanol). Unfortunately, none of the cultures showed signs of sulfate reduction activity over the 64 days they were monitored. It can be speculated that the fungus identified in the solid medium fed on the agar and therefore was not able to proliferate in the liquid medium (in fact, no filamentous mass grew). Thus, it may be speculated that the absence of the fungus did not allow the creation of favorable conditions for the SRB; for example, by consuming all the oxygen from the medium.

4.3.3. Metal attenuation from AMD by acidophilic SRB consortium

Batch experiments were carried out to evaluate the potential of the consortium obtained through enrichment in Postgate B starting at pH 4.00 and using methanol as electron donor, in metal attenuation from AMD. In these experiments, the pH of the AMD was initially increased from 2.60 to 4.50, causing a previous precipitation of some metals mainly as hydroxides. The pH adjustment highly decreased Fe and Al concentrations in the AMD (Fe and Al concentrations dropped from ~173 to ~0.24 mg/L and from ~279 to 12 mg/L, respectively), while the concentrations of the other main metals including Cu, Zn and Mn did not undergo drastic changes (Cu, Zn and Mn were still ~25.74, ~43.6 and ~19.9 mg/L, respectively) (Table **4.2**). Besides, the pH of the prepared PB-m was also adjusted to 4.50 and thereafter, different ratios of AMD to PB-m were tested for the evaluation of the nutrient supplement necessity to the AMD to optimize SR activity of the consortium and metal removal efficiencies. It should be noted that the initial concentrations of the studied metals were not the same in all these tests. As higher as was the fraction of PB-m, the higher dilution effect of metals from AMD (Cu, Zn, Mn and Al) occurred. On the contrary, the PB-m fraction added Fe to the mixtures. The addition of inoculum, a sulfide rich aSRB enriched inoculum, to AMD and to AMD plus supplements of PB-m, caused a rapid precipitation of Cu and its concentration dropped to almost zero just after inoculation in the beginning of experiments (Figure S- **4.5**). This was expected because of the low solubility product constant of copper sulfide ($Ksp = 1.3 \times 10^{-36}$) (Zhang and Wang 2016).

On the other hand, the total Al content of the solutions in all tested conditions also dropped to almost zero after inoculation. Al does not form sulfide minerals and can precipitate by forming hydroxides in relatively acidic conditions (pH > 5.00) (Pickering 1986). In a similar study, Falagán et al. (2017) discussed that in aSRB growth culture, Al may be removed from the solution in two stages: primarily by H^+ consumption by aSRB, which is assisted in pH enhancement to pH~5.00, where Al forms hydroxysulfate precipitates, and then, SRB act as a sink for the released H^+ through the hydrolysis and precipitation of nascent Al minerals. Al removal from the solution is important due to the toxicity effect of this metal on SRB growth (Falagán et al. 2017). In our work, the quick Al removal occurred because at the time the aSRB enriched inoculum was used as inoculum it had pH ~7 (having started at pH 4, the SR activity caused a pH neutralization). Therefore, the addition of inoculum caused a slight increase of the initial pH to values between 4.73 to 4.91 in the tests with AMD and PB-m. Regarding zinc, under the tested conditions it can react with sulfide and precipitate, as the solubility product constant of zinc sulfide ($Ksp = 1.6 \times 10^{-24}$) is considerably low and it is the second insoluble sulfide product (after copper sulfide) among other metals present in the tested AMD (Zhang and Wang 2016). Therefore, Zn concentration immediately dropped after the sulfide rich inoculum addition to the flasks in all tested conditions. In the tests with less initial metals from AMD (60% and 80% PB-m plus 40% and 20% AMD, respectively) the concentration dropped immediately to almost zero. Nevertheless, in the samples with higher initial metal content, 20% PB-m plus 80% AMD and 100% AMD, zinc removal to almost zero content was achieved only after one and two weeks, respectively. The sharp initial drop of Cu and slight removal of Zn in these conditions by their reaction with sulfide caused a fast sulfide depletion; thus, just after the SR activity started to generate new sulfide, the rest of the Zn precipitated (Figure S- **4.5**).

In the case of iron, although it was almost entirely removed from the AMD when adjusted to pH 4.50, after inoculation with the sulfide-rich aSRB culture its content in the tests initially increased and then during the incubation it started to decay as SR occurred and consequently the pH raised. Since iron is part of the PB-m composition and iron sulfide (FeS) particles are produced as a consequence of SR, the explanation for this phenomenon can be the solubilization of those particles present in the inoculum (which was at pH ~7.00) when entered the acidic environment of the tested conditions (pH 4.50), since their solubility rises with the decrease in pH and has very

low solubility in higher pH values (~0.1 mg/L at pH 6.00) (based on the pH dependence of metal sulfide solubilities (Lewis 2010)).

Mn on the other hand, was among the last metals removed from the solution, which is due to the much larger solubility of MnS (Ksp = $2.5 \times 10^{-13} – 2.5 \times 10^{-10}$). Based on Hallberg and Johnson (2005), Mn^{2+} requires pH > 8 to be oxidized to Mn^{4+} and to precipitate as carbonates or hydroxides. Yoo et al. (2004b, a) studied Mn removal from AMD by SRB and reported that pH, presence of citrate, co-existence of Fe and Zn and concentration of sulfide are the most important factors in Mn removal as MnS. They report successful precipitation of MnS in the absence of Fe and Zn with excess amount of sulfide at pH 5-7. In this work, as depicted in Figure S- **4.5**, Mn was removed from all samples when pH reached more than 5 and most of the Fe and Zn were removed from the solution beside the presence of excessive amounts of sulfide, which is in agreement with the reports of Yoo et al. (2004b, a).

This study showed that adding 20% (v/v) PB-m to AMD provides enough macronutrients to promote SR activity as efficient as in the positive control with 100% PB-m. The addition of higher volumes of PB-m did not improve SR, which occurred in all these tests mainly during the second and third weeks (Table **4.3**, Figure S- **4.5**). Interestingly, in the test with 100% AMD there was also some SR activity. However, it occurred mainly just after the third week. Curiously, SR in these tests was in general less efficient than in the previous enrichment culture where 100% PB-m with the same carbon source (methanol) was used and all sulfate was consumed. It is possible that some components present in the initial sludge may play an important role in maintaining conditions favoring the activity of this SRB community.

Nevertheless, the obtained SR levels were enough to achieve efficient metals removals, as reported in other similar works. For example, Dev et al. (2021) using a bacterial consortium enriched from Arctic mine sediments in AMD remediation at pH 4.50 with glycerol as electron donor achieved 34% SR and ~99% removal of metal content (mainly Fe and Zn) after 22 days.

Metal removal in the test with minimum ratio of PB-m to AMD (20% PB-m plus 80% AMD), which contained 0.02% (w/v) yeast extract and 0.115% (w/v) of basal salts (originating from PB-m) was efficient as in the tests with other mixture ratios with high PB-m content (40%, 60% or 80% PB-m plus 60%, 40% and 20% AMD, respectively). Thus, 20% PB-m plus 80% AMD ratio was found as the most promising conditions for metals removal from the solutions due to less

costly nutrient supplement requirement. In a study by Santos and Johnson (2017), an aSRB consortium enriched from acidic metal mine sites was employed for metal removal from a synthetic AMD supplemented with 0.01% (w/v) yeast extract and 0.12% basal salts in a laboratory-scale sulfidogenic bioreactor in a continuous flow system at pH values between 4.00 and 5.00. Their results showed the adaptability of the aSRB consortium in successful sulfate reduction and removal of more than 99% of all the transition metals including Zn, Co and Ni (except Mn). Ňancucheo and Johnson (2012) also benefited from an aSRB consortium for the selective precipitation of transition metals including Cu and Zn from a synthetic AMD containing Fe, Al, 0.01% (w/v) yeast extract and 0.12% (w/v) basal salts in different pH values.

Table 4.3. Bio-removal efficiencies (%) of sulfate of the AMD and mixtures of AMD and Postgate B media by the aSRB consortium during 34 days at room temperature (25℃ ± 3).

Experimental culture	Sulfate reduction (%) after 34 days
100% PB-m	46
80% PB-m (20% AMD)	45
60% PB-m (40% AMD)	36
40% PB-m (60% AMD)	35
20% PB-m (80% AMD)	30
100% AMD	14

As shown in Figure **4.3**, in the test containing 20% PB-m plus 80% AMD, Cu was immediately removed during inoculation, while the concentration of Zn dropped from 7.64 mg/L to bellow detection, seven days after. Mn and Fe concentrations were almost constant in the solution despite sulfide generation and presence in the solution, until pH reached to 6.71 at day 20, when Fe was totally separated from the solution, while Mn was totally removed at day 28 when the pH was 6.75.

In this experiment, about 30% of the initial sulfate was reduced to sulfide and the final pH of the solution measured at day 35 was 7.12 and the redox potential reached 336 mV.

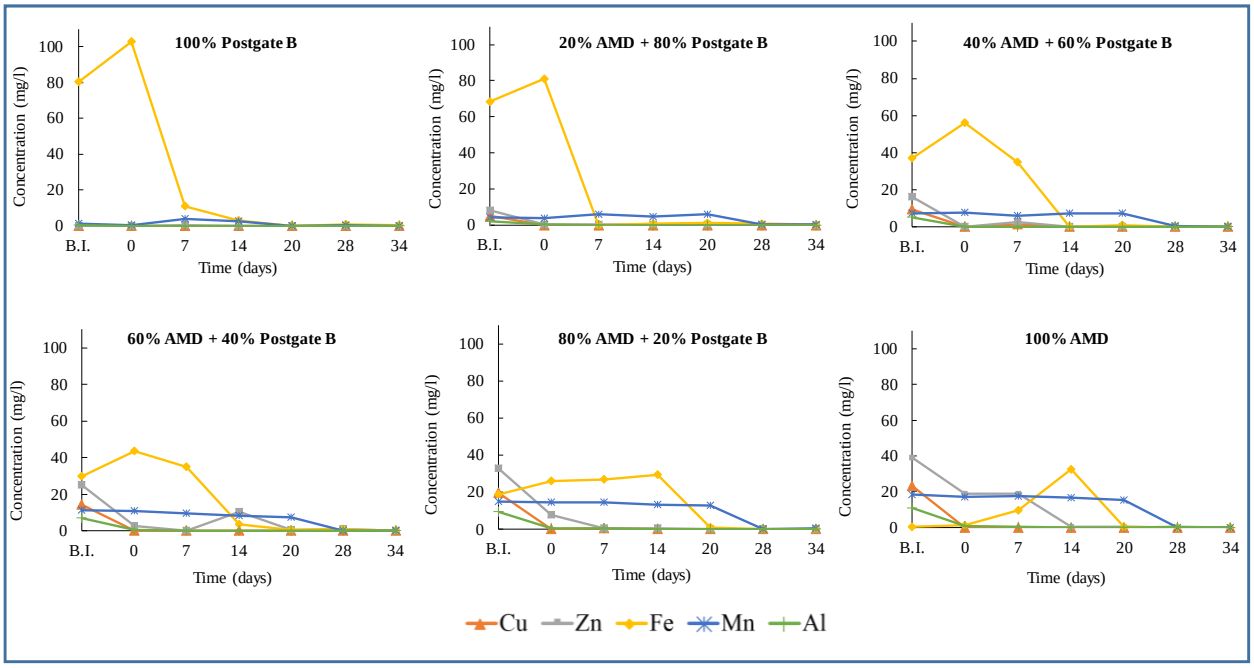

Figure 4.3. Time-course changes of main metals in the studied AMD (Cu, Zn, Fe, Al and Mn) in metal attenuation batch experiments with the selected consortium (enriched in methanol at pH 4.00) as inoculum in 100% AMD sample and in different % (v/v) ratios of PB-m plus AMD at pH 4.50 and 25 ± 3℃ (B.I.: before inoculation).

4.3.4. Metataxonomic study of enrichment cultures

4.3.4.1. Sequencing data validation and diversity analysis

After filtering and denoising the reads, the non-chimeric - total = 15477 were clustered into 525 ASVs (synonym of OTUs), which were used for taxonomic classifications. Then, in the ASVs filtering/decontamination steps, one ASV was classified as chloroplast DNA and excluded, leaving a final number of 524 ASVs and 15462 reads (Table **4.4**) and no highly rare ASVs, nor mitochondrial ASVs nor ASVs unclassified to the phylum level were discovered. Afterwards, the rarefaction curves for both the alfa-diversity indexes Faith's phylogenetic diversity and Shannon

index showed on all samples a growing trend reaching a plateau as the sequencing depth raise (Figure S- **4.6**) which indicates that the number of sequencing reads were enough to have the taxonomic diversity fully represented in all samples (even the sample with the lowest number of reads: sample E – ethanol enriched culture). These results gave confidence to continue the studies about prokaryotic communities in the enrichment cultures.

The Faith's phylogenetic diversity (faith_pd), which accounts only with the number of phylogenetic tree units within a sample, revealed much higher richness for the inoculated sludge (faith_pd ≈ 20), then for the enriched cultures with methanol, ethanol, and glycerol (faith_pd ≈ 5 - 10). Moreover, the alfa-diversity index Shannon (sh), which considers both the richness and evenness of samples, showed the prokaryotic community in the inoculated sludge among the communities of the enriched cultures; with the culture with methanol with the highest diversity (sh ≈ 6.5), followed by the enrichment culture with ethanol (sh ≈ 5.7), then the sludge (sh ≈ 5.3) and finally the culture with glycerol (sh ≈ 4.5).

Table 4.4. Number of reads obtained for each sample (E – ethanol, G – glycerol and M – methanol enrichments; S – sludge inoculum).

sample-ID	**input reads**	**correct reads (primers and size)**	**quality reads**	**non-chimeric reads**	after filtering/ decontamination
E	1571	1571	1359	1359	1359
G	5234	5234	4228	3942	3942
M	7342	7342	6135	5679	5679
S	5759	5759	4667	4497	4482
total	19906	19906	16389	15477	15462

Furthermore, for a better comparison of samples regarding their prokaryotic communities, two beta-diversity metrics were studied: 1 - Bray-Curtis Dissimilarity, which is only a measure of shared ASVs between sites or samples and 2 - the Weighted UniFrac metrics, which accounts with the number of shared ASVs, their abundancies and with their phylogenetic relations (how closely related are the ASVs).

The Bray-Curtis Dissimilarity showed that the prokaryotic communities on the enriched cultures with different carbon sources (ethanol, glycerol, and methanol) were closer to each other than to the initial community on the sludge inoculum (Table **4.5**). The Weighted UniFrac metrics revealed that the ethanol-enriched culture went through a greater change in the prokaryotic community structure initially inoculated than the cultures with methanol and glycerol. Furthermore, this index showed that the methanol culture population shared taxonomic groups and their relative abundances with the populations of both the cultures with glycerol and with ethanol, but the sets of shared taxonomic groups were different in each case (Table **4.6**).

Table 4.5. Distance matrix based on the Bray-Curtis Dissimilarity metrics (E – ethanol, G – glycerol and M – methanol enrichments; S – sludge inoculum).

	E	**G**	**M**	**S**
E	0			
G	0.872	0		
M	0.848	0.840	0	
S	0.982	0.987	0.986	0

Table 4.6. Distance matrix based on the Weighted UniFrac metrics (E – ethanol, G – glycerol and M – methanol enrichments; S – sludge inoculum).

	E	**G**	**M**	**S**
E	0			
G	0.710	0		
M	0.426	0.447	0	
S	0.809	0.664	0.669	0

4.3.4.2. Prokaryotic communities

The prokaryotic communities of the inoculated sediments and of the enrichment cultures in the presence of three different carbon sources inoculated at pH=4.00 are presented in Figure **4.4**.

The three most abundant bacterial orders in the initial sediment sample were *Burkholderiales* (48.1%), *Acidobacteriales* (12.1%) and *Acidithiobacillales* (11.9%). Moreover, the three most

abundant families in the sediments include *Gallionellaceae* (28%), *Sulfuricellaceae* (17.5%) and *Acidithiobacillaceae* (11.9%). The most dominant genera (> 5% abundance) in the sediments were identified as *Sideroxydans* (28.1%), *Sulfuriferula* (17.2%), *Acidithiobacillus* (11.9%) and *Granulicella* (7.4%). These detected taxa in the sediments are in accordance with previous reports in other sediments affected by metal polluted low pH AMD (González-Toril et al. 2010; García-Moyano et al. 2015; Zhang et al. 2019; Carlier et al. 2020a).

As expected, the structure of the prokaryotic community of the sediment was highly changed after the enrichment in Postgate B media starting at pH 4.00 and with each of the three carbon sources.

Major three bacterial orders in the enrichment cultures with methanol were *Desulfitobacteriales* (35%), *Clostridiales* (15.6%) and *Enterobacterales* (12%), while *Desulfitobacteriaceae* (35.4%), *Clostridiaceae* (14%) and *Enterobacteriaceae* (12%) were the most abundant families. The genus *Desulfosporosinus* presents the highest abundancy among the bacterial populations of the enrichment cultures with methanol as carbon source, counting about 35.4% of the whole bacterial population of the culture. In the mentioned enrichment culture, the following most dominant genera (> 5%) were *Enterobacter* (12.1%), *Clostridium_sensu_stricto*_12 (8.8%), *Microbacter* (8.8%) and *Sedimentibacter* 8.1%.

The major three bacterial orders in the enrichment cultures with ethanol were *Clostridiales* (57%), *Desulfitobacteriales* (12%) and *Lachnospirales* (7.4%) while most abundant families were *Clostridiaceae* (56.6%), *Desulfitobacteriaceae* (12.2%) and *Lachnospiraceae* (7.4%). Moreover, the most dominant genera (>5%) in the enriched samples with ethanol were *Clostridium_sensu_stricto*_10 (22.4%), *Clostridium_sensu_stricto*_12 (21.6%), *Desulfosporosinus* (12.2%), *Clostridium_sensu_stricto*_9 (7.4%), *Bacillus* (7.2%) and *Anaerocolumna* (5.8%).

The major three bacterial orders in the enrichment cultures with glycerol were *Enterobacterales* (52%), *Bacteroidales* (18.5%) and *Clostridiales* (12.7%), while most abundant families were *Enterobacteriaceae* (52%), *Paludibacteraceae* (18.5%) and *Clostridiaceae* (12.6%). In this case, *Microbacter* (18.5%), *Desulfosporosinus* (11.5%) and *Clostridium_sensu_stricto*_12 (6%) were the most dominant genera (<5%) in the enriched samples with glycerol. Nevertheless, nine ASVs assigned to *Enterobacteriaceae* family, counting for 50% of this prokaryotic population, remained with no possible taxonomic classification to genus level.

The bacteria of the *Desulfosporosinus* genus are strictly anaerobic SRB and are known to have a key role in sulfate reduction in acidic mine wastes (Mardanov et al. 2016). As mentioned before, the bacteria from this genus were present in high relative abundances in the three enrichment cultures (35.4%, 12.2% and 11.5% in the enrichments with methanol, ethanol and glycerol, respectively). SRB from *Desulfosporosinus* genus are frequently reported to be present in reactors operating at low pH and they are normally originated from acidic sediments due to their high capacity to thrive at low pH conditions (Labrenz and Banfield 2004; Church et al. 2007; Senko et al. 2009; Lee et al. 2009; Moreau et al. 2010; Hallberg 2010; Sánchez-Andrea et al. 2011, 2012). Remarkably, in some certain sites with oxidized mining waste materials, the only phylotype identified with SR capability was from *Desulfosporosinus* genus (Mardanov et al. 2016). The absence of sequences related to *Desulfosporosinus* genus in the sediments might be due to their presence as spores that hampered the DNA extraction (Labrenz and Banfield 2004), or to their rare occurrence. Indeed, it is speculated that bacteria from *Desulfosporosinus* genus in sulfide tailings form a 'rare biosphere', since their rare abundancy but active components are masked by the predominant bacterial populations (Mardanov et al. 2016). By now, some studies have enriched and isolated acidophilic SRB of *Desulfosporosinus* genus from different acidic environments such as *D. acididurans* from sediments of Rio Tinto (Sánchez-Andrea et al. 2015) and *D. acidiphilus* isolated from acid mining effluent decantation pond sediments of the mining site of Chessy-Les-Mines (Alazard et al. 2010).

In our study, 16S DNA analysis of the enrichment samples to the species level revealed the presence of *D. acididurans* (in enrichment samples with ethanol (3.8%) and glycerol (4.2%)) and *D. acidiphilus* (in enrichment samples with ethanol (1.8%), glycerol (0.3%) and methanol (0.05%)). It is reported that the pH range for *D. acididurans* growth is 3.80-7.00, with an optimum pH of 5.50 with the ability of using different electron donors including glycerol, methanol, and ethanol, resulting in CO_2 and acetate generation (Sánchez-Andrea et al. 2015). In the case of *D. acidiphilus*, it is known to have a pH range for growth from 3.60-5.50 with an optimum pH of 5.20, with SR activity in the presence of glycerol, pyruvate, lactate, H_2, fructose and glucose as electron donors (Alazard et al. 2010). In the description of this strain, it is mentioned that it is not able to use ethanol and methanol as electron donors, which might be the reason for the very low abundancy of this group of bacteria in the cultures enriched with methanol and ethanol. However, they might have been growing in these cultures by using other available electron donors (*e.g.*

released electron donors to the culture through the metabolic activity of other bacteria and/or from dead bacterial cells) (Alazard et al. 2010). Four other bacteria in *Desulfosporosinus* genus, which were not classified to the species level, were present in significantly high abundancies in the three enrichment cultures. They could be acidophilic SRB, which could reduce sulfate in acidic cultures and/or can be neutrophilic SRB that have grown after the pH rose as a result of the activity of other aSRB like *D. acididurans* and *D. acidiphilus*.

Samples enriched with methanol, contained about 12% of *Enterobacter* genus and enriched samples with glycerol, contained about 50% of *Enterobacteriaceae* order. It is known that bacteria from *Enterobacteriaceae* family have both respiratory and a fermentative types of metabolisms and most of the strains of this family can utilize citrate as sole carbon source (Frederiksen 2015). It is also known that *Enterobacter* can reduce Fe^{3+} to Fe^{2+} and have an important role in iron and organic material cycles (Liu and Wang 2016). *Clostridium* genera members were present in the three enrichment cultures with high abundancies. Members of this genera are identified as sulfate reducing (Zhang and Wang 2016; Zhang et al. 2016b; Hwang and Jho 2018), acid generating/H_2-producing bacteria (Sánchez-Andrea et al. 2014a; Vilela et al. 2019, 2021) with adaptation potential to high dissolved organic carbon and turbidity (Zhao et al. 2017). Thus, the presence of *Clostridium* genera members might have had a role in sulfate reduction and also in preventing a fast pH increase by other SRB activity in enrichment samples. Moreover, bacteria from *Microbacter* genera were observed in the enrichment samples with ethanol and methanol with high abundancies. This group of anaerobic propionigenic bacterium usually are co-exist with SRB in natural and engineered sulfidogenic environments (Lindsay et al. 2011; Sánchez-Andrea et al. 2013, 2014b). In addition, members of genus *Clostridiaceae*, *Thermodesulfovibrio* and *Desulfobulbales* family with low abundancies were found in the enrichment cultures, which may have sulfate reduction roles in the cultures. The presence of a wide range of microorganisms in the cultures' communities, increases their adaptability to different environmental conditions (Plugge et al. 2011; Ňancucheo and Johnson 2012; Ňancucheo et al. 2017), thus conferring an important plasticity in biotechnology processes based on such communities' consortia.

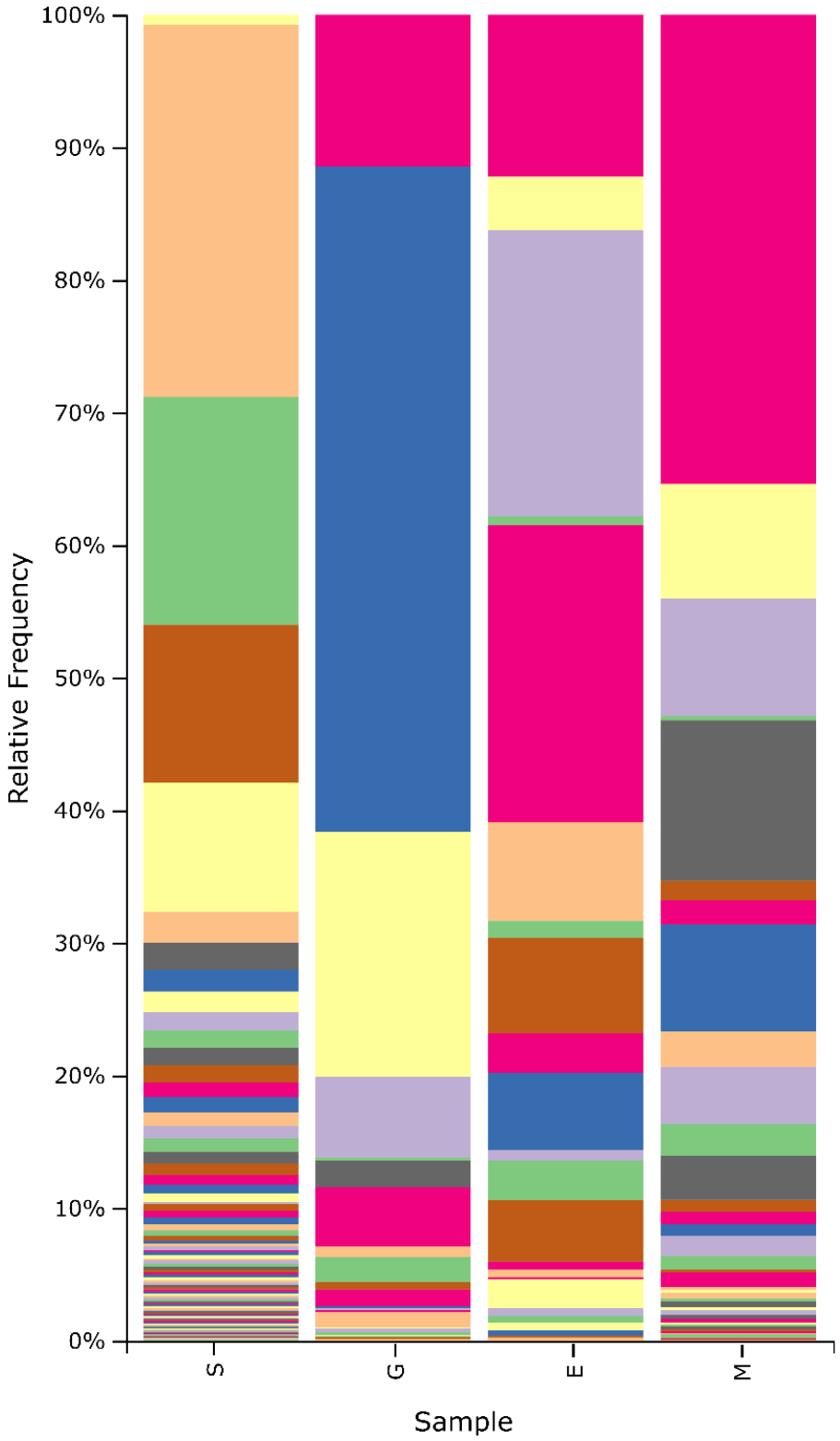
100%
90%
80%
70%
60%
50%
40%
30%
20%
10%
0%
Relative Frequency
S
G
E
M
Sample

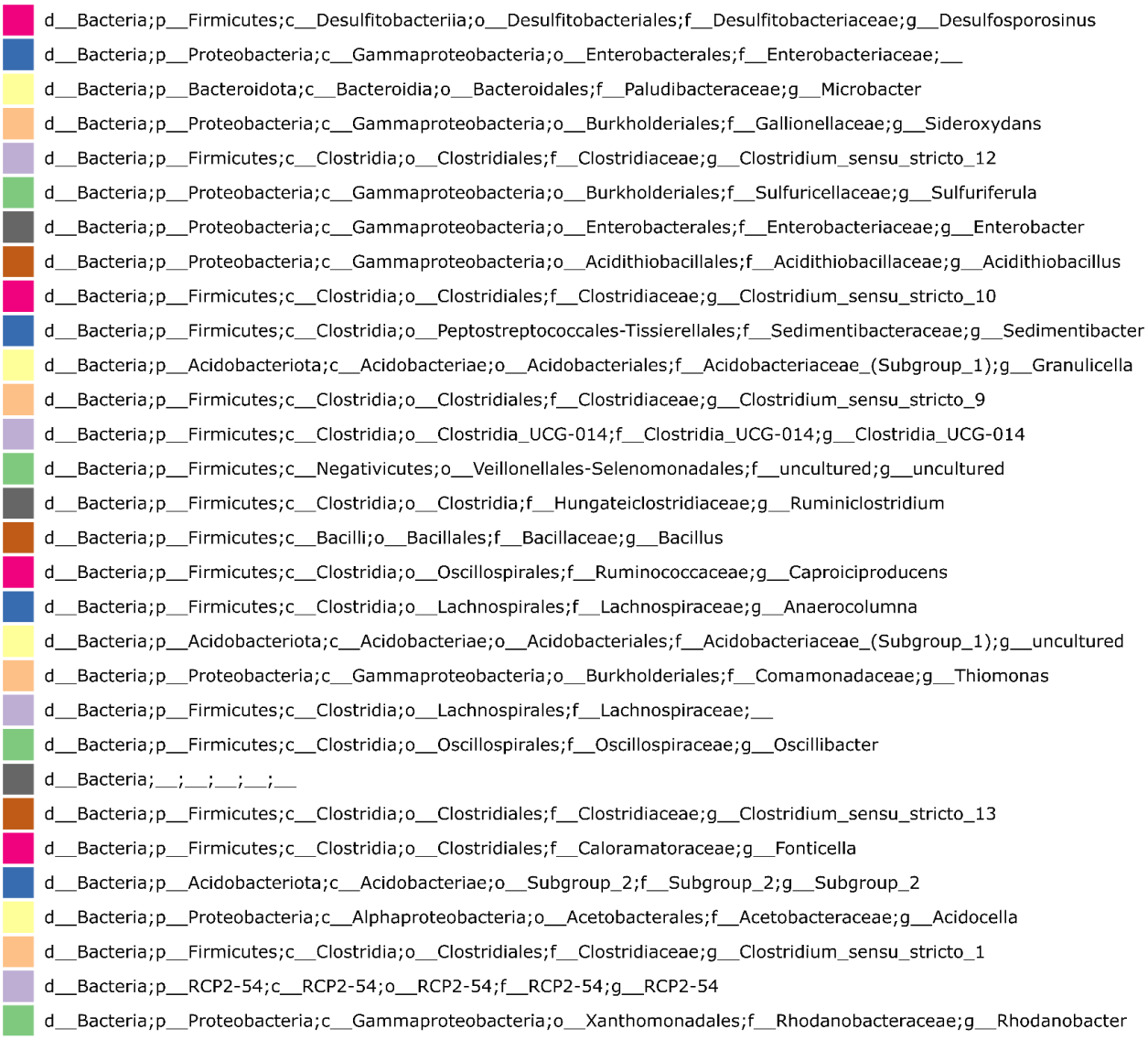

Figure 4.4. Relative abundances of the prokaryotic phylotypes at the genus level for the sediment sample (S) and enriched cultures with ethanol (E), glycerol (G) and methanol (M) at pH 4.00 and 25 ± 3℃.

4.3.5. Metataxonomic study of AMD remediation tests

4.3.5.1. Sequencing data validation and diversity analysis

After filtering and denoising the reads, the non-chimeric ones - total = 171,575 (Table S- **4.1**) were clustered into 675 ASVs, which were used for taxonomic classifications. Then, in the ASVs filtering/decontamination steps, one ASV classified as chloroplast DNA plus another as

mitochondrial DNA were excluded as well as 71 ASVs highly rare (<0.05%) or unclassified to the phylum level, leaving a final number of 602 ASVs and 171,288 reads (table S.1). Thereafter, the rarefaction curves for both the alfa-diversity indexes Shannon and the Faith's phylogenetic diversity showed a growing trend with both extracted DNA replicates (1 and 2) of all samples and reached a plateau as the sequencing depth raised (Figure S- **4.7**), which indicates that the numbers of sequencing reads were enough to have the taxonomic diversity fully represented in all cases (even the sample with the lowest number of reads: sample 100% AMD at day 14 (1764 and 1808 reads)). Moreover, both these alfa-diversity indexes showed a sharp decrease in the prokaryotic community richness after 14 days of incubation in the test with 100% AMD (where it reached the lowest values) and a subsequent slight recover of richness, while in all the other tests the trend was a decay of richness along sampled days (Table S- **4.2**).

On the other hand, prokaryotic communities in the AMD treatment batch tests were compared with Bray-Curtis Dissimilarity and the Weighted UniFrac metrics for beta-diversity. In this study, in addition to the calculation of these metrics (Table S- **4.3**, Table S- **4.4**,Table S- **4.5** and Table S- **4.6**), principal coordinates analysis (PCoA) graphs were plotted for a better visualization of relations between such high number of samples (Figure **4.5**)**.** As a general remark, both these metrics revealed samples grouped in pairs, with both DNA replicates from each sample close to each other, confirming a good representation of prokaryotic populations in both DNA samples. More in detail, the Bray-Curtis metrics (Figure **4.5**- A), which accounts just with shared ASVs, showed the enriched inoculum, and the tests just with AMD at day 14 and at day 34 all apart from each-others and separated from a major cluster of samples corresponding to AMD tests with supplements of PB-m together with controls just with PB-m. Moreover, in this major cluster, the samples from tests with just 20% PB-m plus 80% AMD are on one side, while the controls with only PB-m are on the other side. On the other hand, the Weighted UniFrac metrics (Figure **4.5**- B), which accounts also with common ancestors of ASVs and their abundances, revealed a distribution of samples with similarities to that obtained with Bray-Curtis metrics but with the samples from tests with just 20% PB-m at day 34 closer to the enriched inoculum and the samples of the major cluster without evidence of distribution related to the percentage of PB-m supplement.

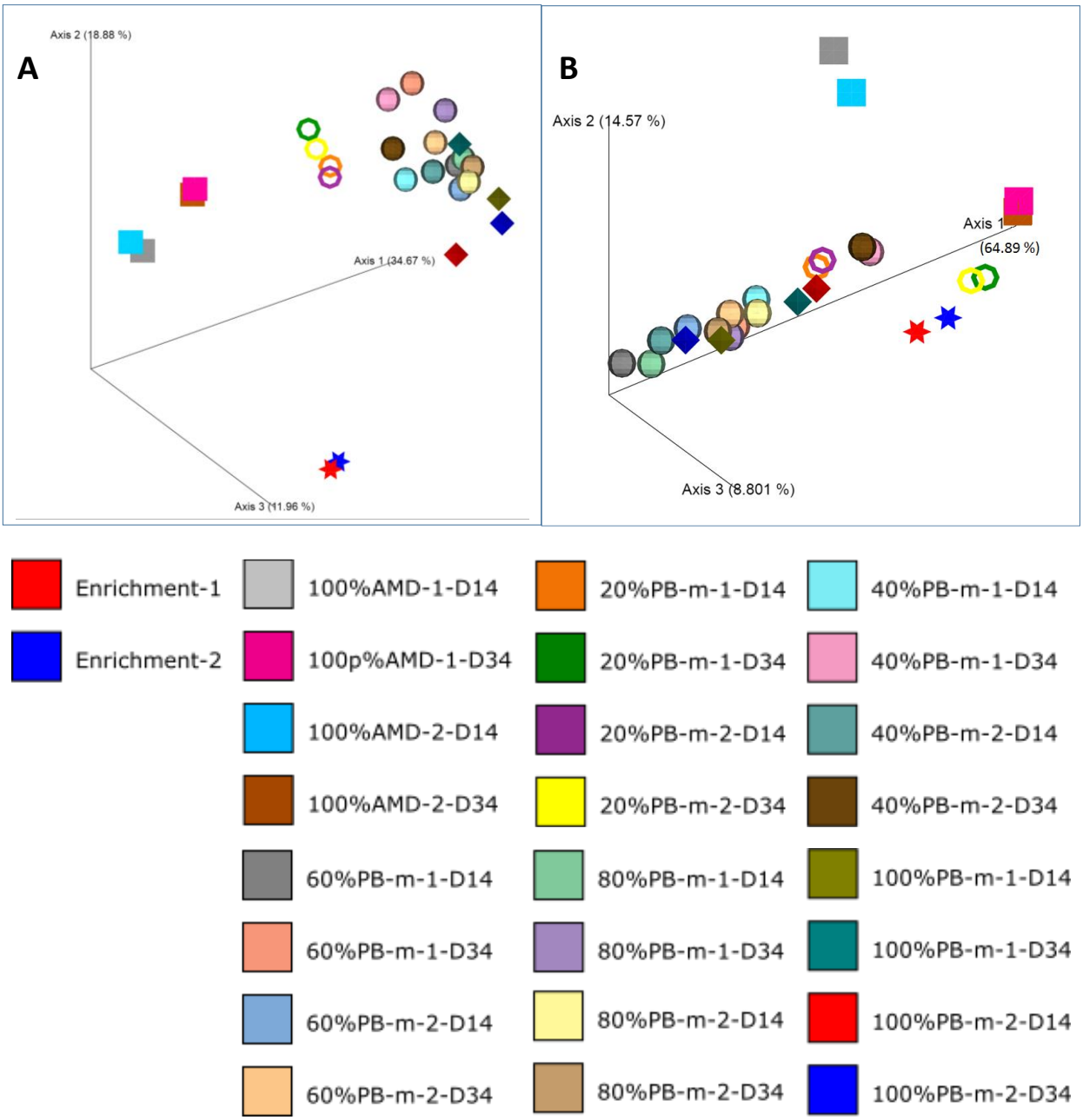

Figure 4.5. Figures with the PCoA plots of the samples from AMD treatment studies A) Bray-Curtis B) Weighted Unifrac (stars: enriched inoculum, squares: 100% AMD, rings: 20% PB-m, diamonds: 100% PB-m, Spherical: other samples).

4.3.5.2. Prokaryotic communities

The prokaryotic community of the enriched culture used as inoculum and the evolution of the prokaryotic communities in the tested conditions (control just with PB-m and different ratios of PB-m to AMD at pH 4.50 and methanol as carbon source) is depicted in Figure **4.6**. In this study, the two most abundant families observed in each sample were always *Desulfitobacteriaceae* and *Clostridiaceae*, with the sum of their abundancies between 43% and 86% and the balance between these two populations was highly affected by the AMD content in the tested conditions. At day 14, the tests with higher AMD content (100% AMD and 20% PB-m plus 80% AMD) had higher relative abundancies of bacteria from *Desulfitobacteriaceae* family and the tests with lower AMD content had higher relative abundancies of bacteria related to *Clostridiaceae* family. At day 34, this trend was even more evident and the *Desulfitobacteriaceae* family became dominant also in the test with 40% PB-m plus 60% AMD.

The increasing abundancy of the bacteria from *Clostridiaceae* family by the decrease in the AMD content continuously from 100% AMD to 100% PB-m tests (Figure **4.6**) could be explained by the possible toxicity of the metals present in the AMD for this family and/or better nutrient conditions (through PB-m supplements), which seemed to favor the growth of *Clostridiaceae*, mainly from *Clostridium_sensu_stricto*_1, *Clostridium_sensu_stricto*_12 and *Clostridium_sensu_stricto*_10 genera.

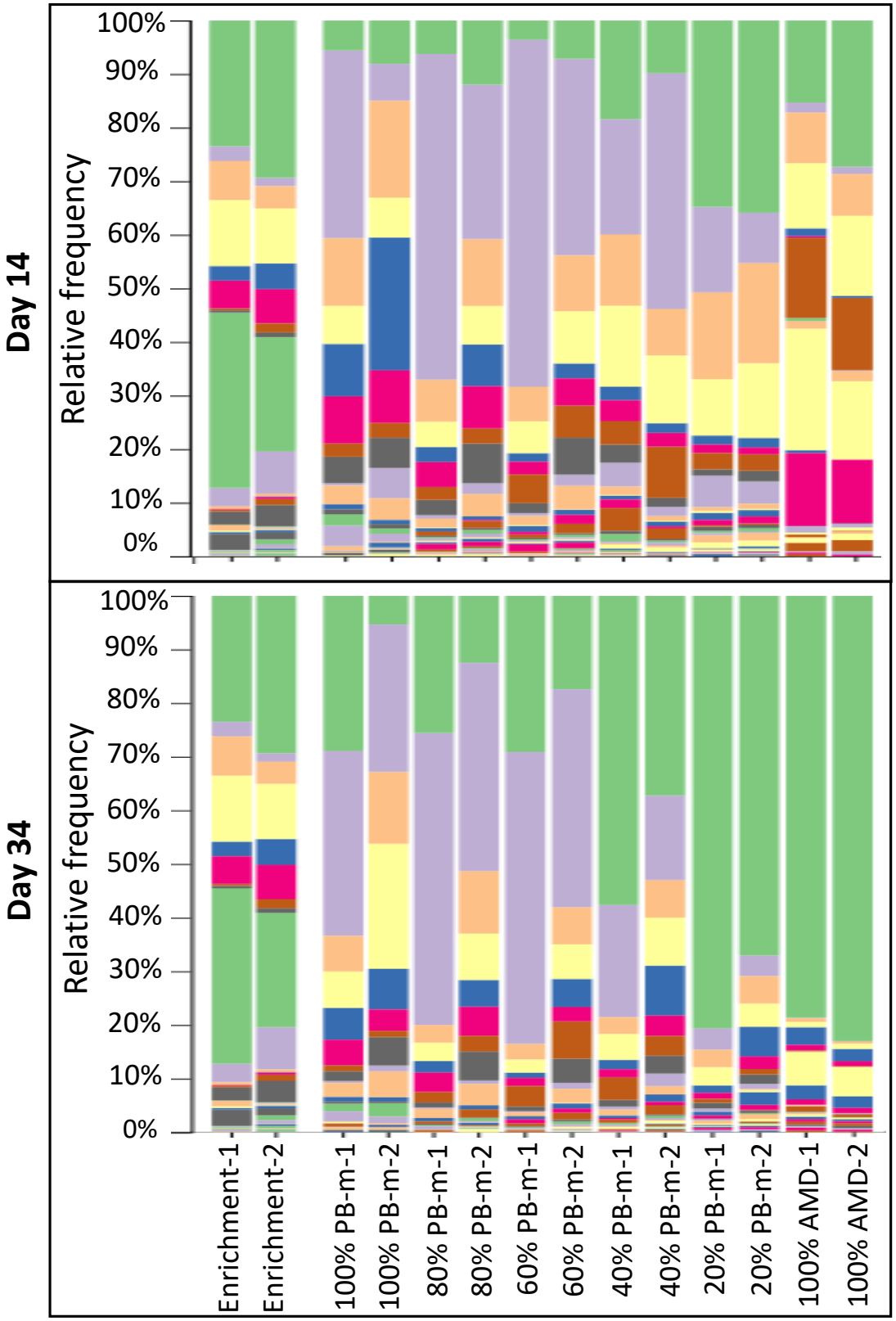
Day 14
Relative frequency
100%
90%
80%
70%
60%
50%
40%
30%
20%
10%
0%
Day 34
Relative frequency
100%
90%
80%
70%
60%
50%
40%
30%
20%
10%
0%
Enrichment-1
Enrichment-2
100% PB-m-1
100% PB-m-2
80% PB-m-1
80% PB-m-2
60% PB-m-1
60% PB-m-2
40% PB-m-1
40% PB-m-2
20% PB-m-1
20% PB-m-2
100% AMD-1
100% AMD-2

Figure 4.6. Relative abundances of the prokaryotic phylotypes at the genus level for the enrichment sample used as consortium (at Postgate B media, methanol as carbon source at pH 4.00) and inoculated samples containing different ratios of AMD to Postgate B media at pH 4.50 and 25 ± 3℃.

Different works have reported the presence of *Clostridium* members in sulfidogenic AMD remediation reactors together with *Desulfitobacteriaceae* members (Hong et al. 2007; Martins et al. 2011; Lefticariu et al. 2015; Vasquez et al. 2018; Rodrigues et al. 2019). Aoyagi et al. (2017) remarked the importance of *Clostridium* members in SRB based AMD remediation reactors due to their capabilities in breaking down complex organic substances into small molecules that can be used by *Desulfitobacteriaceae* members. Moreover, in some works sulfate reduction activity has been also attributed to *Clostridium* members in AMD treatment operations (Sallam and

Steinbuchel 2009; Bao et al. 2012, 2017; Zhao et al. 2016; Rodrigues et al. 2020; Wu et al. 2022). In the investigation by Rodrigues et al. (2020), sediments from mine impacted waters from Sangão River (Brazil) were directly used as inoculum in AMD remediation studies with chitin as the only organic supplement, and their meta-taxnomic studies of the prokaryotic populations revealed very low abundances of *Desulfitobacteriaceae* members (<0.28%) and relative high abundances of *Clostridium* members (27.04% to 12.75%) during AMD bioremediation operations, thus suggesting the *Clostridium* members were putatively the main sulfate reducers in their tested conditions.

Therefore, in the present study, the *Clostridium* members might have been acting as SRB in the tested samples with lower AMD content (where they prevailed with high abundancies) and/or they contributed mainly to maintain suitable conditions for SRB from the *Desulfitobacteriaceae* family, in the tests with higher PB-m supplements, by breaking down the complex compounds present in the yeast extract from the PB-m.

The dominance of bacteria from *Desulfitobacteriaceae* family belonging to *Desulfosporosinus* genus in the samples containing 100% AMD and 20% or 40% PB-m plus 80% or 60% AMD, respectively (Figure **4.6**), confirms the potential of this group of bacteria by their versatile behavior to extreme conditions, mainly as low pH and heavy metal toxicity, as well as their resistance to oxic conditions (Sánchez-Andrea et al. 2014a). Bacteria from *Desulfosporosinus* genus consisted of about 26% of the total prokaryotic population in the enriched inoculum (grown in Postgate B base with methanol as carbon source) and in the metal attenuation experiments, their relative abundances were relatively high even in the tests with lowest to highest AMD contents: 12.5% to 83% *Desulfosporosinus* spp. (80% PB-m plus 20% AMD to 100% AMD).

Desulfosporosinus-related sulfate reducers are known to be present in diverse SRB reactors treating AMD from laboratory to real scale (Habe et al. 2020). Various AMD bioremediation studies by SRB report high (26% to 60%) (Sato et al. 2019; Valdez-Nuñez et al. 2022) to quite low abundancy (<1%) (Pester et al. 2010; Rezadehbashi and Baldwin 2018; Rodrigues et al. 2019) of bacteria in *Desulfosporosinus* genus. Yet, even with their low relative abundances (*e.g.* 0.006%), *Desulfosporosinus* spp. have demonstrated to contribute in high rates to SR (Pester et al. 2010). Therefore, considering the relative high abundancies of this genus in the batch tests reported (above) in this work, their role in SR and consequent metal removal from AMD was probably

important. Indeed, other works point to this evidence. For example, *Desulfosporosinus* spp. were the most predominant SRB in several passive bioreactors treating AMD studied by Sato et al. (2019), regardless of reactor configurations, sizes, and operating conditions.

In the study by Dev et al. (2021) on AMD bioremediation at 4.5 with glycerol as electron donor, 34% of SR and ~99% metals removal was also observed with a progressive domination of *Desulfosporosinus* spp. in the community during the incubation. The microbial metabolic process suggested by the authors was the initial fermentation of glycerol to acetic acid mainly by *Desulfosporosinus* when in low pH, followed by acetic acid oxidation to H_2 and CO_2 mainly by *Desulfitobacterium* when the pH raised to neutral values, and finally H_2 consumption by *Desulfosporosinus* (Dev et al. 2021). On the other hand, it is known that the fate of the methanol in sulfidogenic reactors is related to the outcome of the competition among SRB, methanogens and homoacetogens, and that the use of methanol by anaerobic microorganisms, mainly by SRB, also results in acetate generation (Cao et al. 2012). Moreover, it has already been shown that the oxidation of generated acetate can be undertaken by other bacteria present in the community such as *Clostridium* spp. (Du et al. 2020). Thus, in our work there was probably production of acetate, and since *Desulfitobacterium* spp. were not detected in the studied cultures, the produced acetate was probably consumed by *Clostridium* spp. (Du et al. 2020) and/or other bacteria. Another possibility could be the absence of acetate oxidizing activity in the consortium, and for that reason, acetate accumulation resulted in acetic acid toxicity and incomplete SR. This is due to the fact that, according to its pKa (4.76), the dominant form of this compound at low pH values (especially at pH<4.76), is acetic acid rather than acetate, which has high inhibitory effect on aSRB (Reis et al. 1990; Sánchez-Andrea et al. 2014a).

4.4. **Conclusions**

A microbial consortium having an acidophilic sulfate reducing bacteria (aSRB) community with sulfate reduction activity at pH 4.00 with methanol as electron donor has been successfully enriched from the sediments of a confluence area between an AMD stream and a water stream receiving the municipal WWTP effluent of the São Domingos Mine village, at an inactive copper mine site.

The strategy of isolating aSRB colonies from the enrichment cultures in closed centrifuge tubes with solid medium was more efficient than using petri dishes in a jar with burning candles, and the DNA sequences analyzed to classify the isolates revealed that all SRB colonies were *Desulfosporosinus* spp. However, a fungus from *Trichoderma* genus was also present in the solid medium where the colonies grew, suggesting a possible interaction of symbiosis or commensalism favoring the growth of SRB.

The aSRB consortium enriched at pH 4.00 with methanol was then tested for metal attenuation from AMD collected at São Domingos mine with pH adjusted to pH 4.50 in batch tests using methanol (30 mM) as carbon source and different volumes of Postgate B medium base as supplements of basal salts and yeast extract. The lowest dose tested (20% v/v of Postgate B base – corresponding to 1.15 g/L of basal salts and 0.2 g/L of yeast extract) allowed the removal of more than 99% of metals after 28 days.

A meta-taxonomic study of the communities revealed that the most abundant prokaryotes in the AMD remediation tests were *Clostridium* members and *Desulfosporosinus* genus. The first were found more abundant in the tests with higher Postgate B base supplements, (≥60%), while *Desulfosporosinus,* on the other hand, was the dominant bacterial genus when lower doses of basal salts and yeast extract were used.

The studied consortium has potential for different applications, which may include the elimination/minimization of the AMD neutralization step prior to AMD bioremediation, make SRB bioreactors more resistant to acidification phenomena during operation when sugars-rich residues are used as carbon sources, and possibility of utilization in selective metal recovery systems.

4.5. References

Alazard D, Joseph M, Battaglia-Brunet F, et al (2010) Desulfosporosinus acidiphilus sp. nov.: a moderately acidophilic sulfate-reducing bacterium isolated from acid mining drainage sediments: New taxa: Firmicutes (Class Clostridia, Order Clostridiales, Family Peptococcaceae). Extremophiles 14:305–312. https://doi.org/10.1007/s00792-010-0309-4

Aoyagi T, Hamai T, Hori T, et al (2017) Hydraulic retention time and pH affect the performance and microbial communities of passive bioreactors for treatment of acid mine drainage. AMB Express 7:142. https://doi.org/10.1186/s13568-017-0440-z

Bao P, Hu Z-Y, Wang X-J, et al (2012) Dechlorination of p,p′-DDTs coupled with sulfate reduction by novel sulfate-reducing bacterium Clostridium sp. BXM. Environ Pollut 162:303–310. https://doi.org/10.1016/j.envpol.2011.11.037

Bao Y, Guo C, Wang H, et al (2017) Fe- and S-Metabolizing Microbial Communities Dominate an AMD-Contaminated River Ecosystem and Play Important Roles in Fe and S Cycling. Geomicrobiol J 34:695–705. https://doi.org/10.1080/01490451.2016.1243596

Bijmans MFM, de Vries E, Yang C-H, et al (2010) Sulfate reduction at pH 4.0 for treatment of process and wastewaters. Biotechnol Prog NA-NA. https://doi.org/10.1002/btpr.400

Brahmacharimayuma B, Prakash Mohanty M, Kumar Ghosh P (2019) Theoretical and Practical Aspects of Biological Sulfate Reduction: A Review. Glob NEST J. https://doi.org/10.30955/gnj.002577

Cabrera G, Perez R, Gomez J, et al (2006) Toxic effects of dissolved heavy metals on Desulfovibrio vulgaris and Desulfovibrio sp. strains. J Hazard Mater 135:40–46. https://doi.org/10.1016/j.jhazmat.2005.11.058

Cao J, Zhang G, Mao Z-S, et al (2012) Influence of electron donors on the growth and activity of sulfate-reducing bacteria. Int J Miner Process 106–109:58–64. https://doi.org/10.1016/j.minpro.2012.02.005

Carlier JD, Alexandre LM, Luís AT, Costa MC (2019) Potential of industrial by-products and wastes from the Iberian Peninsula as carbon sources for sulphate-reducing bacteria. Int J Environ Sci Technol 16:4719–4738. https://doi.org/10.1007/s13762-018-02197-z

Carlier JD, Ettamimi S, Cox CJ, et al (2020a) Prokaryotic diversity in stream sediments affected by acid mine drainage. Extremophiles 24:809–819. https://doi.org/10.1007/s00792-020-01196-8

Carlier JD, Luís AT, Alexandre LM, Costa MC (2020b) Feasibility of Co-Treating Olive Mill Wastewater and Acid Mine Drainage. Mine Water Environ 39:859–880. https://doi.org/10.1007/s10230-020-00719-1

Church CD, Wilkin RT, Alpers CN, et al (2007) Microbial sulfate reduction and metal attenuation in pH 4 acid mine water. Geochem Trans 8:10. https://doi.org/10.1186/1467-4866-8-10

Comeau AM, Douglas GM, Langille MGI (2017) Microbiome Helper: a Custom and Streamlined Workflow for Microbiome Research. mSystems 2:e00127-16. https://doi.org/10.1128/mSystems.00127-16

Dev S, Galey M, Chun CL, et al (2021) Enrichment of psychrophilic and acidophilic sulfate-reducing bacterial consortia – a solution toward acid mine drainage treatment in cold regions. Environ Sci Process Impacts 23:2007–2020. https://doi.org/10.1039/D1EM00256B

Diaby N, Dold B, Pfeifer H-R, et al (2007) Microbial communities in a porphyry copper tailings impoundment and their impact on the geochemical dynamics of the mine waste. Environ Microbiol 9:298–307. https://doi.org/10.1111/j.1462-2920.2006.01138.x

Du Y, Zou W, Zhang K, et al (2020) Advances and Applications of Clostridium Co-culture Systems in Biotechnology. Front Microbiol 11:560223. https://doi.org/10.3389/fmicb.2020.560223

Falagán C, Yusta I, Sánchez-España J, Johnson DB (2017) Biologically-induced precipitation of aluminium in synthetic acid mine water. Miner Eng 106:79–85. https://doi.org/10.1016/j.mineng.2016.09.028

Foucher S, Battaglia-Brunet F, Ignatiadis I, Morin D (2001) Treatment by sulfate-reducing bacteria of Chessy acid-mine drainage and metals recovery. Chem Eng Sci 56:1639–1645. https://doi.org/10.1016/S0009-2509(00)00392-4

Frederiksen W (2015) *Citrobacter*. In: Whitman WB, Rainey F, Kämpfer P, et al. (eds) Bergey's Manual of Systematics of Archaea and Bacteria, 1st edn. Wiley, pp 1–23

García-Moyano A, Austnes A, Lanzén A, et al (2015) Novel and Unexpected Microbial Diversity in Acid Mine Drainage in Svalbard (78° N), Revealed by Culture-Independent Approaches. Microorganisms 3:667–694. https://doi.org/10.3390/microorganisms3040667

Gardes M, Bruns TD (1993) ITS primers with enhanced specificity for basidiomycetes - application to the identification of mycorrhizae and rusts. Mol Ecol 2:113–118. https://doi.org/10.1111/j.1365-294X.1993.tb00005.x

González-Toril E, Aguilera A, Rodriguez N, et al (2010) Microbial ecology of Río Tinto, a natural extreme acidic environment of biohydrometallurgical interest. Hydrometallurgy 104:329–333. https://doi.org/10.1016/j.hydromet.2010.01.011

Habe H, Sato Y, Aoyagi T, et al (2020) Design, application, and microbiome of sulfate-reducing bioreactors for treatment of mining-influenced water. Appl Microbiol Biotechnol 104:6893–6903. https://doi.org/10.1007/s00253-020-10737-2

Hallberg KB (2010) New perspectives in acid mine drainage microbiology. Hydrometallurgy 104:448–453. https://doi.org/10.1016/j.hydromet.2009.12.013

Hallberg KB, Johnson DB (2005) Biological manganese removal from acid mine drainage in constructed wetlands and prototype bioreactors. Sci Total Environ 338:115–124. https://doi.org/10.1016/j.scitotenv.2004.09.011

Hong H, Pruden A, Reardon KF (2007) Comparison of CE-SSCP and DGGE for monitoring a complex microbial community remediating mine drainage. J Microbiol Methods 69:52–64. https://doi.org/10.1016/j.mimet.2006.11.016

Hwang SK, Jho EH (2018) Heavy metal and sulfate removal from sulfate-rich synthetic mine drainages using sulfate reducing bacteria. Sci Total Environ 635:1308–1316. https://doi.org/10.1016/j.scitotenv.2018.04.231

Ighalo JO, Kurniawan SB, Iwuozor KO, et al (2022) A review of treatment technologies for the mitigation of the toxic environmental effects of acid mine drainage (AMD). Process Saf Environ Prot 157:37–58. https://doi.org/10.1016/j.psep.2021.11.008

Jameson E, Rowe OF, Hallberg KB, Johnson DB (2010) Sulfidogenesis and selective precipitation of metals at low pH mediated by Acidithiobacillus spp. and acidophilic sulfate-reducing bacteria. Hydrometallurgy 104:488–493. https://doi.org/10.1016/j.hydromet.2010.03.029

Johnson DB, Sánchez-Andrea I (2019) Dissimilatory reduction of sulfate and zero-valent sulfur at low pH and its significance for bioremediation and metal recovery. In: Advances in Microbial Physiology. Elsevier, pp 205–231

Koschorreck M (2008) Microbial sulphate reduction at a low pH: Microbial sulphate reduction at low pH. FEMS Microbiol Ecol 64:329–342. https://doi.org/10.1111/j.1574-6941.2008.00482.x

Koschorreck M, Wendt-Potthoff K, Geller W (2003) Microbial Sulfate Reduction at Low pH in Sediments of an Acidic Lake in Argentina. Environ Sci Technol 37:1159–1162. https://doi.org/10.1021/es0259584

Labrenz M, Banfield JF (2004) Sulfate-Reducing Bacteria-Dominated Biofilms That Precipitate ZnS in a Subsurface Circumneutral-pH Mine Drainage System. Microb Ecol 47:. https://doi.org/10.1007/s00248-003-1025-8

Lane DJ (1991). In: 16S/23S rRNA Sequencing. , , ,. John Wiley and Sons, New York, pp 115–175

Lee Y-J, Romanek CS, Wiegel J (2009) Desulfosporosinus youngiae sp. nov., a spore-forming, sulfate-reducing bacterium isolated from a constructed wetland treating acid mine drainage. Int J Syst Evol Microbiol 59:2743–2746. https://doi.org/10.1099/ijs.0.007336-0

Lefticariu L, Walters ER, Pugh CW, Bender KS (2015) Sulfate reducing bioreactor dependence on organic substrates for remediation of coal-generated acid mine drainage: Field experiments. Appl Geochem 63:70–82. https://doi.org/10.1016/j.apgeochem.2015.08.002

Lewis AE (2010) Review of metal sulphide precipitation. Hydrometallurgy 104:222–234. https://doi.org/10.1016/j.hydromet.2010.06.010

Lindsay MBJ, Wakeman KD, Rowe OF, et al (2011) Microbiology and Geochemistry of Mine Tailings Amended with Organic Carbon for Passive Treatment of Pore Water. Geomicrobiol J 28:229–241. https://doi.org/10.1080/01490451.2010.493570

Liu H, Wang H (2016) Characterization of Fe (III)-reducing enrichment culture and isolation of Fe (III)-reducing bacterium Enterobacter sp. L6 from marine sediment. J Biosci Bioeng 122:92–96. https://doi.org/10.1016/j.jbiosc.2015.12.014

Mardanov AV, Panova IA, Beletsky AV, et al (2016) Genomic insights into a new acidophilic, copper-resistant *Desulfosporosinus* isolate from the oxidized tailings area of an abandoned gold mine. FEMS Microbiol Ecol 92:fiw111. https://doi.org/10.1093/femsec/fiw111

Martins M, Faleiro ML, Silva G, et al (2011) Dynamics of bacterial community in up-flow anaerobic packed bed system for acid mine drainage treatment using wine wastes as carbon source. Int Biodeterior Biodegrad 65:78–84. https://doi.org/10.1016/j.ibiod.2010.09.005

Meier J, Piva A, Fortin D (2012) Enrichment of sulfate-reducing bacteria and resulting mineral formation in media mimicking pore water metal ion concentrations and pH conditions of acidic pit lakes. FEMS Microbiol Ecol 79:69–84. https://doi.org/10.1111/j.1574-6941.2011.01199.x

Moreau JW, Zierenberg RA, Banfield JF (2010) Diversity of Dissimilatory Sulfite Reductase Genes (*dsrAB*) in a Salt Marsh Impacted by Long-Term Acid Mine Drainage. Appl Environ Microbiol 76:4819–4828. https://doi.org/10.1128/AEM.03006-09

Ňancucheo I, Bitencourt JAP, Sahoo PK, et al (2017) Recent Developments for Remediating Acidic Mine Waters Using Sulfidogenic Bacteria. BioMed Res Int 2017:1–17. https://doi.org/10.1155/2017/7256582

Ňancucheo I, Johnson DB (2012) Selective removal of transition metals from acidic mine waters by novel consortia of acidophilic sulfidogenic bacteria: Acidophilic sulfidogenic bioreactors. Microb Biotechnol 5:34–44. https://doi.org/10.1111/j.1751-7915.2011.00285.x

Ňancucheo I, Rowe OF, Hedrich S, Johnson DB (2016) Solid and liquid media for isolating and cultivating acidophilic and acid-tolerant sulfate-reducing bacteria. FEMS Microbiol Lett 363:fnw083. https://doi.org/10.1093/femsle/fnw083

Paliy O, Kenche H, Abernathy F, Michail S (2009) High-Throughput Quantitative Analysis of the Human Intestinal Microbiota with a Phylogenetic Microarray. Appl Environ Microbiol 75:3572–3579. https://doi.org/10.1128/AEM.02764-08

Pester M, Bittner N, Deevong P, et al (2010) A 'rare biosphere' microorganism contributes to sulfate reduction in a peatland. ISME J 4:1591–1602. https://doi.org/10.1038/ismej.2010.75

Phyo AK, Jia Y, Tan Q, et al (2020) Competitive Growth of Sulfate-Reducing Bacteria with Bioleaching Acidophiles for Bioremediation of Heap Bioleaching Residue. Int J Environ Res Public Health 17:2715. https://doi.org/10.3390/ijerph17082715

Pickering WF (1986) Metal ion speciation — soils and sediments (a review). Ore Geol Rev 1:83–146. https://doi.org/10.1016/0169-1368(86)90006-5

Plugge CM, Zhang W, Scholten JCM, Stams AJM (2011) Metabolic Flexibility of Sulfate-Reducing Bacteria. Front Microbiol 2:. https://doi.org/10.3389/fmicb.2011.00081

Postgate JR (1984) The Sulphate-Reducing Bacteria. Camb Univ Press

Qian Z, Tianwei H, Mackey HR, et al (2019) Recent advances in dissimilatory sulfate reduction: From metabolic study to application. Water Res 150:162–181. https://doi.org/10.1016/j.watres.2018.11.018

Reis MAM, Lemos PC, Almeida JS, Carrondo MJT (1990) Influence of produced acetic acid on growth of sulfate reducing bacteria. Biotechnol Lett 12:145–148. https://doi.org/10.1007/BF01022432

Rezadehbashi M, Baldwin S (2018) Core Sulphate-Reducing Microorganisms in Metal-Removing Semi-Passive Biochemical Reactors and the Co-Occurrence of Methanogens. Microorganisms 6:16. https://doi.org/10.3390/microorganisms6010016

Rodrigues C, Núñez-Gómez D, Follmann HVDM, et al (2020) Biostimulation of sulfate-reducing bacteria and metallic ions removal from coal mine-impacted water (MIW) using shrimp shell as treatment agent. J Hazard Mater 398:122893. https://doi.org/10.1016/j.jhazmat.2020.122893

Rodrigues C, Núñez-Gómez D, Silveira DD, et al (2019) Chitin as a substrate for the biostimulation of sulfate-reducing bacteria in the treatment of mine-impacted water (MIW). J Hazard Mater 375:330–338. https://doi.org/10.1016/j.jhazmat.2019.02.086

Sallam A, Steinbuchel A (2009) Clostridium sulfidigenes sp. nov., a mesophilic, proteolytic, thiosulfate- and sulfur-reducing bacterium isolated from pond sediment. Int J Syst Evol Microbiol 59:1661–1665. https://doi.org/10.1099/ijs.0.004986-0

Sánchez-Andrea I, Knittel K, Amann R, et al (2012) Quantification of Tinto River Sediment Microbial Communities: Importance of Sulfate-Reducing Bacteria and Their Role in Attenuating Acid Mine Drainage. Appl Environ Microbiol 78:4638–4645. https://doi.org/10.1128/AEM.00848-12

Sánchez-Andrea I, Rodríguez N, Amils R, Sanz JL (2011) Microbial Diversity in Anaerobic Sediments at Río Tinto, a Naturally Acidic Environment with a High Heavy Metal Content. Appl Environ Microbiol 77:6085–6093. https://doi.org/10.1128/AEM.00654-11

Sánchez-Andrea I, Sanz JL, Bijmans MFM, Stams AJM (2014a) Sulfate reduction at low pH to remediate acid mine drainage. J Hazard Mater 269:98–109. https://doi.org/10.1016/j.jhazmat.2013.12.032

Sánchez-Andrea I, Sanz JL, Stams AJM (2014b) Microbacter margulisiae gen. nov., sp. nov., a propionigenic bacterium isolated from sediments of an acid rock drainage pond. Int J Syst Evol Microbiol 64:3936–3942. https://doi.org/10.1099/ijs.0.066241-0

Sánchez-Andrea I, Stams AJM, Amils R, Sanz JL (2013) Enrichment and isolation of acidophilic sulfate-reducing bacteria from Tinto River sediments: Acidophilic SRB from Tinto River. Environ Microbiol Rep n/a-n/a. https://doi.org/10.1111/1758-2229.12066

Sánchez-Andrea I, Stams AJM, Hedrich S (2015) Desulfosporosinus acididurans sp. nov.: an acidophilic sulfate-reducing bacterium isolated from acidic sediments. Extremophiles 19:39–47. https://doi.org/10.1007/s00792-014-0701-6

Sánchez-Andrea I, van der Graaf CM, Hornung B, et al (2022) Acetate Degradation at Low pH by the Moderately Acidophilic Sulfate Reducer Acididesulfobacillus acetoxydans gen. nov. sp. nov. Front Microbiol 13:816605. https://doi.org/10.3389/fmicb.2022.816605

Santos AL, Johnson DB (2017) The effects of temperature and pH on the kinetics of an acidophilic sulfidogenic bioreactor and indigenous microbial communities. Hydrometallurgy 168:116–120. https://doi.org/10.1016/j.hydromet.2016.07.018

Sato Y, Hamai T, Hori T, et al (2019) Desulfosporosinus spp. were the most predominant sulfate-reducing bacteria in pilot- and laboratory-scale passive bioreactors for acid mine drainage treatment. Appl Microbiol Biotechnol 103:7783–7793. https://doi.org/de

Sen AM, Johnson B (1999) Acidophilic sulphate-reducing bacteria: candidates for bioremediation of acid mine drainage. In: Process Metallurgy. Elsevier, pp 709–718

Senko JM, Zhang G, McDonough JT, et al (2009) Metal Reduction at Low pH by a *Desulfosporosinus* species: Implications for the Biological Treatment of Acidic Mine Drainage. Geomicrobiol J 26:71–82. https://doi.org/10.1080/01490450802660193

Serrano J, Leiva E (2017) Removal of Arsenic Using Acid/Metal-Tolerant Sulfate Reducing Bacteria: A New Approach for Bioremediation of High-Arsenic Acid Mine Waters. Water 9:

Sheoran A, Sheoran V, Choudhary R (2010) Bioremediation of acid-rock drainage by sulphate-reducing prokaryotes: a review. Minerals Eng 23:1073–1100

Sogin ML (1990) Amplification of Ribosomal RNA Genes for Molecular Evolution Studies. In: Innis MA, Gelfand DH, Sninsky JJ, White TJ (eds) PCR protocols: a guide to methods and applications. San Diego, CA: Academic Press

Sun W, Sun X, Li B, et al (2020) Bacterial response to sharp geochemical gradients caused by acid mine drainage intrusion in a terrace: Relevance of C, N, and S cycling and metal resistance. Environ Int 138:105601. https://doi.org/10.1016/j.envint.2020.105601

Thomas GW (1996) Soil pH and Soil Acidity. In: Sparks DL, Page AL, Helmke PA, et al. (eds) SSSA Book Series. Soil Science Society of America, American Society of Agronomy, Madison, WI, USA, pp 475–490

Valdez-Nuñez LF, Ayala-Muñoz D, Sánchez-España J, Sánchez-Andrea I (2022) Microbial Communities in Peruvian Acid Mine Drainages: Low-Abundance Sulfate-Reducing Bacteria With High Metabolic Activity. Geomicrobiol J 39:867–883. https://doi.org/10.1080/01490451.2022.2087808

van Houten RT, Pol LWH, Lettinga G (1994) Biological sulphate reduction using gas-lift reactors fed with hydrogen and carbon dioxide as energy and carbon source. Biotechnol Bioeng 44:586–594. https://doi.org/10.1002/bit.260440505

Vasquez Y, Escobar MC, Saenz JS, et al (2018) Effect of hydraulic retention time on microbial community in biochemical passive reactors during treatment of acid mine drainage. Bioresour Technol 247:624–632. https://doi.org/10.1016/j.biortech.2017.09.144

Vilela R, Saia FT, Gregoracci GB, et al (2019) Hydrogen production in reactors: The influence of organic loading rate, inoculum and support material. Int J Hydrog Energy 44:27259–27271. https://doi.org/10.1016/j.ijhydene.2019.08.180

Vilela RS, Fuess LT, Saia FT, et al (2021) Biofuel production from sugarcane molasses in thermophilic anaerobic structured-bed reactors. Renew Sustain Energy Rev 144:110974. https://doi.org/10.1016/j.rser.2021.110974

Weisburg WG, Barns SM, Pelletier DA, Lane DJ (1991) 16S ribosomal DNA amplification for phylogenetic study. J Bacteriol 173:697–703. https://doi.org/10.1128/jb.173.2.697-703.1991

White TJ, Bruns T, Lee S, Taylor JW (1990) Amplification and direct sequencing of fungal ribosomal RNA genes for phylogenetics. In: Innis MA, Gelfand DH, Sninsky JJ, White TJ

(eds) PCR Protocols: A Guide to Methods and Applications. New York: Academic Press Inc

Willis G, Nancucheo I, Hedrich S, et al (2019) Enrichment and isolation of acid-tolerant sulfate-reducing microorganisms in the anoxic, acidic hot spring sediments from Copahue volcano, Argentina. FEMS Microbiol Ecol 95:fiz175. https://doi.org/10.1093/femsec/fiz175

Wu Z, Firmin KA, Cheng M, et al (2022) Biochar enhanced Cd and Pb immobilization by sulfate-reducing bacterium isolated from acid mine drainage environment. J Clean Prod 366:132823. https://doi.org/10.1016/j.jclepro.2022.132823

Yoo K, Sasaki K, Hiroyoshi N, et al (2004a) The Effect of Mn²⁺ Concentration on Mn Removal by a Sulfate Reducing Bacteria Bioreactor. Mater Trans 45:2429–2434. https://doi.org/10.2320/matertrans.45.2429

Yoo K, Sasaki K, Hiroyoshi N, Tsunekawa M (2004b) Fundamental Study on the Removal of Mn²⁺ in Acid Mine Drainage using Sulfate Reducing Bacteria. Mater Trans 45:2422–2428. https://doi.org/10.2320/matertrans.45.2422

Zhang L, Lin X, Wang J, et al (2016a) Effects of Lead and Mercury on Sulfate-Reducing Bacterial Activity in a Biological Process for Flue Gas Desulfurization Wastewater Treatment. Sci Rep 6:30455. https://doi.org/10.1038/srep30455

Zhang M, Wang H (2016) Preparation of immobilized sulfate reducing bacteria (SRB) granules for effective bioremediation of acid mine drainage and bacterial community analysis. Miner Eng 92:63–71. https://doi.org/10.1016/j.mineng.2016.02.008

Zhang M, Wang H, Han X (2016b) Preparation of metal-resistant immobilized sulfate reducing bacteria beads for acid mine drainage treatment. Chemosphere 154:215–223. https://doi.org/10.1016/j.chemosphere.2016.03.103

Zhang X, Tang S, Wang M, et al (2019) Acid mine drainage affects the diversity and metal resistance gene profile of sediment bacterial community along a river. Chemosphere 217:790–799. https://doi.org/10.1016/j.chemosphere.2018.10.210

Zhao D, Cao X, Huang R, et al (2017) Variation of bacterial communities in water and sediments during the decomposition of Microcystis biomass. PLOS ONE 12:e0176397. https://doi.org/10.1371/journal.pone.0176397

Zhao F, Zhou J-D, Ma F, et al (2016) Simultaneous inhibition of sulfate-reducing bacteria, removal of H2S and production of rhamnolipid by recombinant Pseudomonas stutzeri Rhl: Applications for microbial enhanced oil recovery. Bioresour Technol 207:24–30. https://doi.org/10.1016/j.biortech.2016.01.126

4.6. **Annexes**

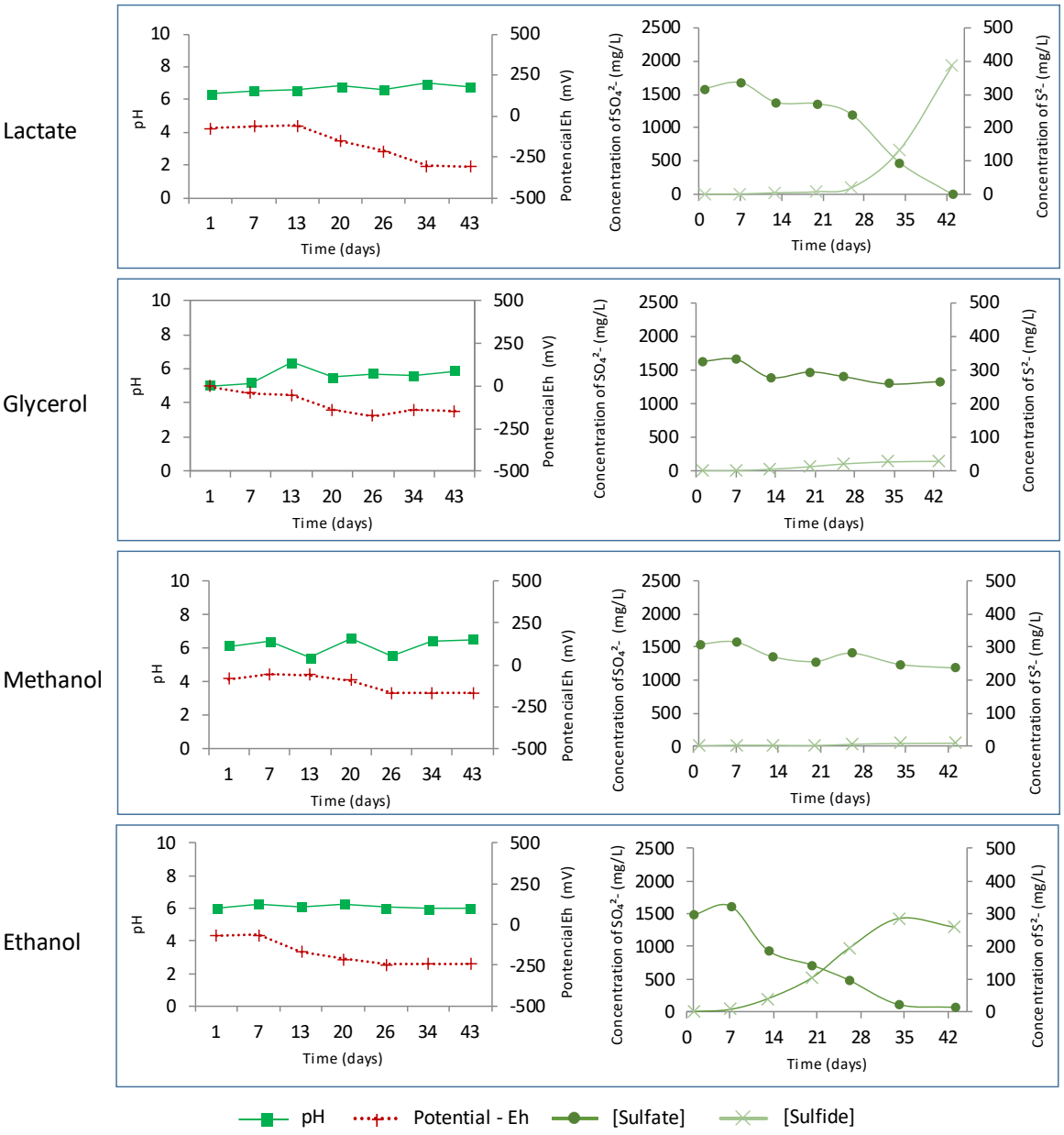

Figure S- 4.1. Time-course changes of pH, redox potential, sulfate reduction and sulfide generation in enrichment studies inoculated with a SRB consortium from wastewater treatment plant as positive control enriched, in Postgate B media in the presence of lactate and three carbon sources (methanol, ethanol and glycerol) at pH 6.00 (25 ± 3℃).

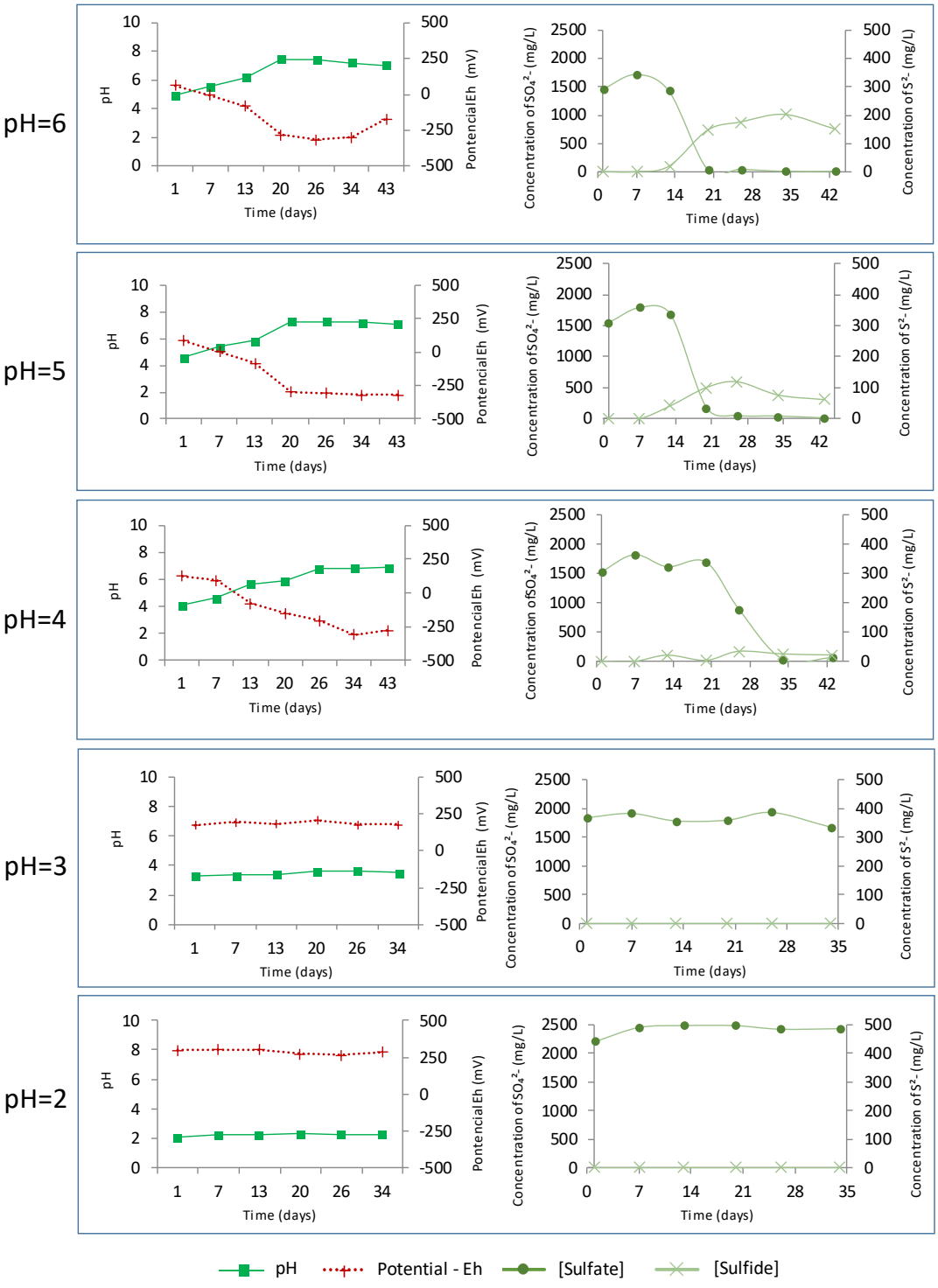

Figure S- 4.2. Time-course changes of pH, redox potential, sulfate reduction and sulfide generation in enrichment studies with sediments collected from Sao Domingos mine as inoculum, enriched in Postgate B media in the presence of **methanol** as carbon source at different pH values (pH 2.00, 3.00, 4.00, 5.00 and 6.00) (25 ± 3℃).

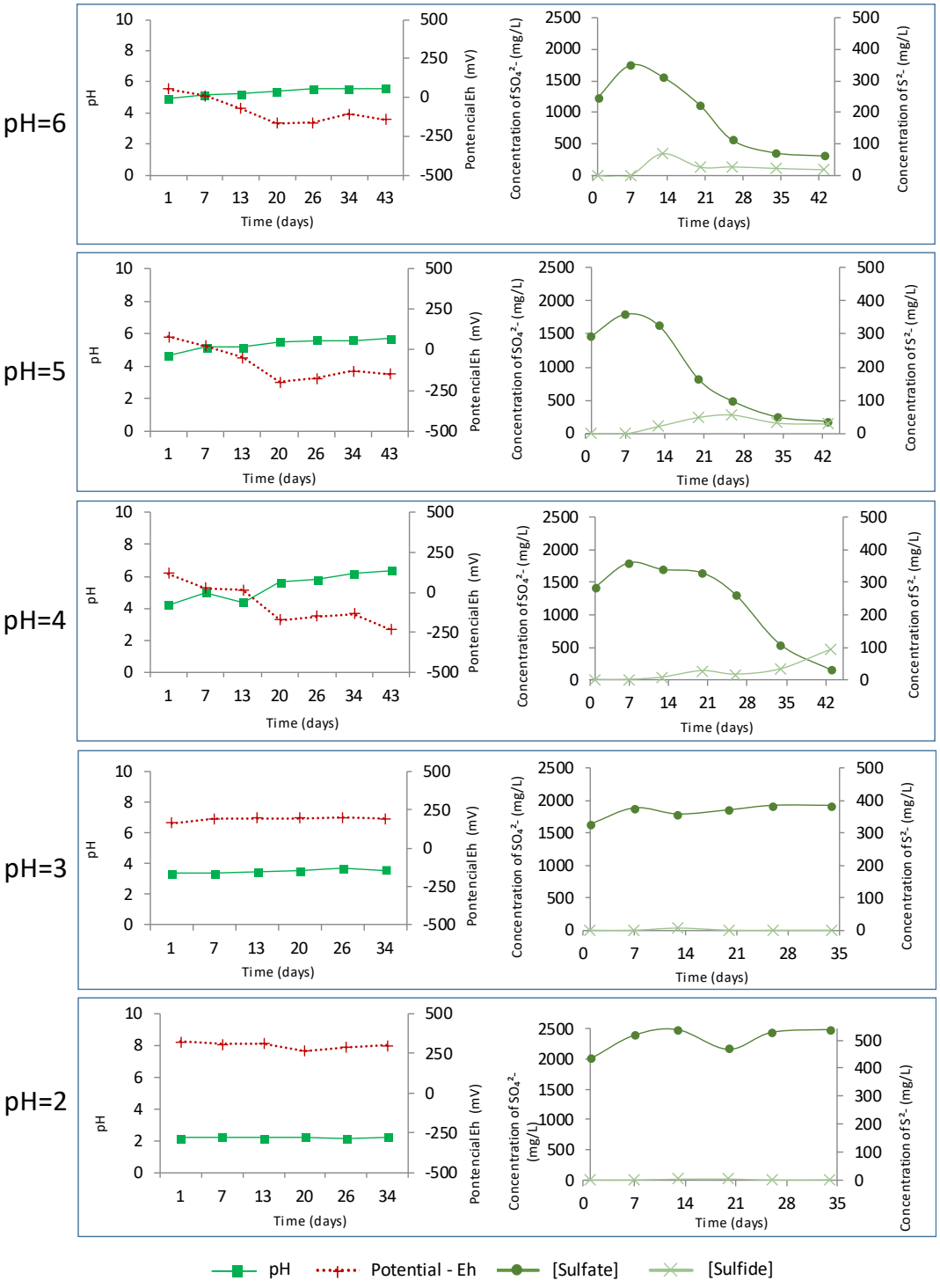

Figure S- 4.3. Time-course changes of pH, redox potential, sulfate reduction and sulfide generation in enrichment studies with sediments collected from Sao Domingos mine as inoculum, enriched in Postgate B media in the presence of **glycerol** as carbon source at different pH values (pH 2.00, 3.00, 4.00, 5.00 and 6.00) (25 ± 3℃).

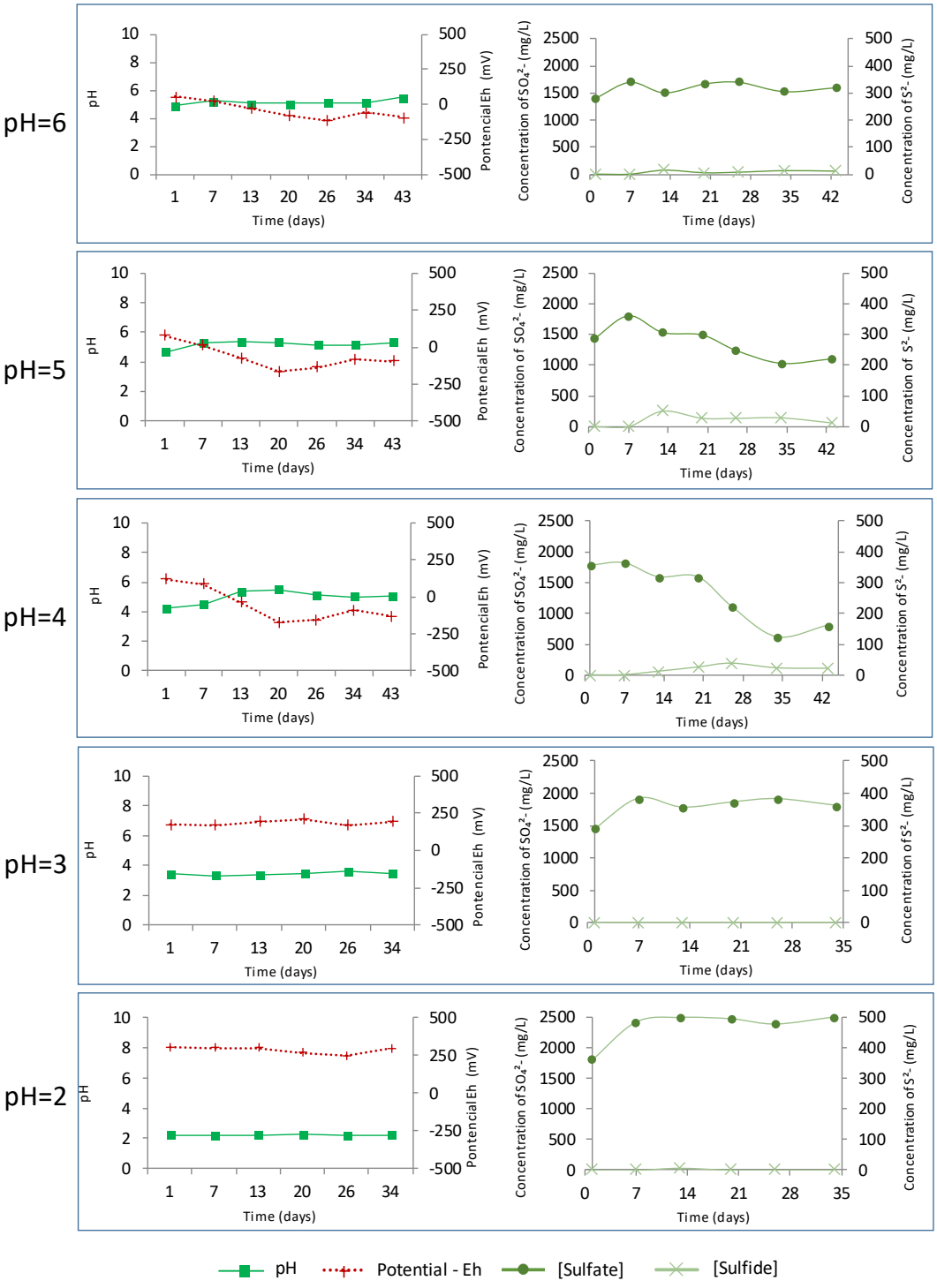

Figure S- 4.4. Time-course changes of pH, redox potential, sulfate reduction and sulfide generation in enrichment studies with sediments collected from Sao Domingos mine as inoculum, enriched in Postgate B media in the presence of **ethanol** as carbon source at different pH values (pH 2.00, 3.00, 4.00, 5.00 and 6.00) (25 ± 3 ℃).

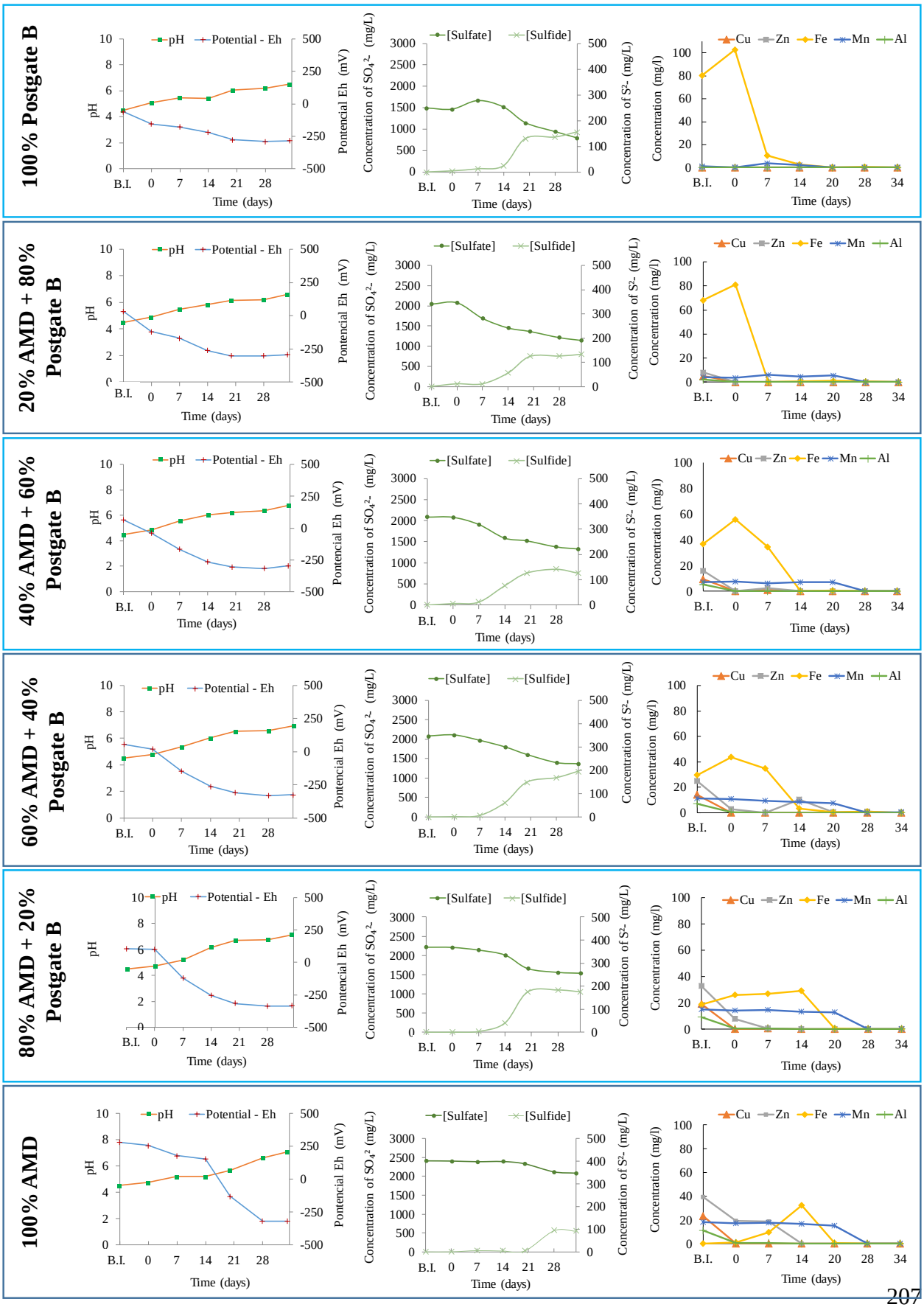
100% Postgate B
20% AMD + 80% Postgate B
40% AMD + 60% Postgate B
60% AMD + 40% Postgate B
80% AMD + 20% Postgate B
100% AMD
pH
Potential - Eh
Pontencial Eh (mV)
[Sulfate]
[Sulfide]
Concentration of SO4 2- (mg/L)
Concentration of S2- (mg/L)
Cu
Zn
Fe
Mn
Al
Concentration (mg/l)
B.I.
Time (days)

Figure S- 4.5. Time-course changes of pH, redox potential, sulfate reduction, sulfide generation and concentration of main metals in the studied AMD (Cu, Zn, Fe, Al and Mn) in metal attenuation batch experiments with the enriched consortium in methanol at pH 4.00 as enriched inoculum in different ratios of AMD to Postgate B media with methanol as carbon at pH 4.50 and 25 ± 3℃ (B.I.: before inoculation).

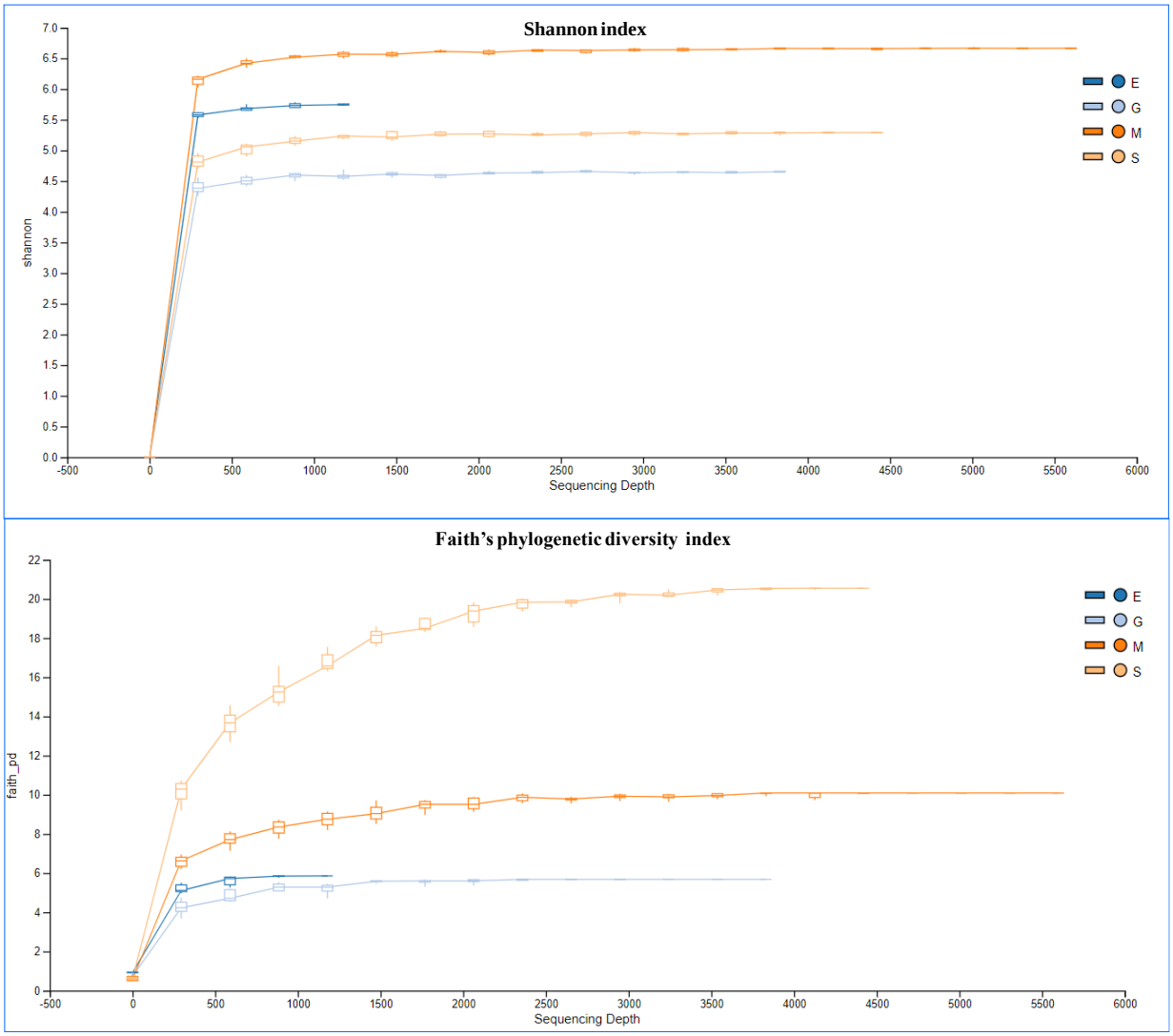

Figure S- 4.6. Rarefaction curves for the alpha-diversity indexes Shannon and Faith's phylogenetic diversity of the samples from enrichment studies (E – ethanol, G – glycerol and M – methanol enrichments; S – sludge inoculum).

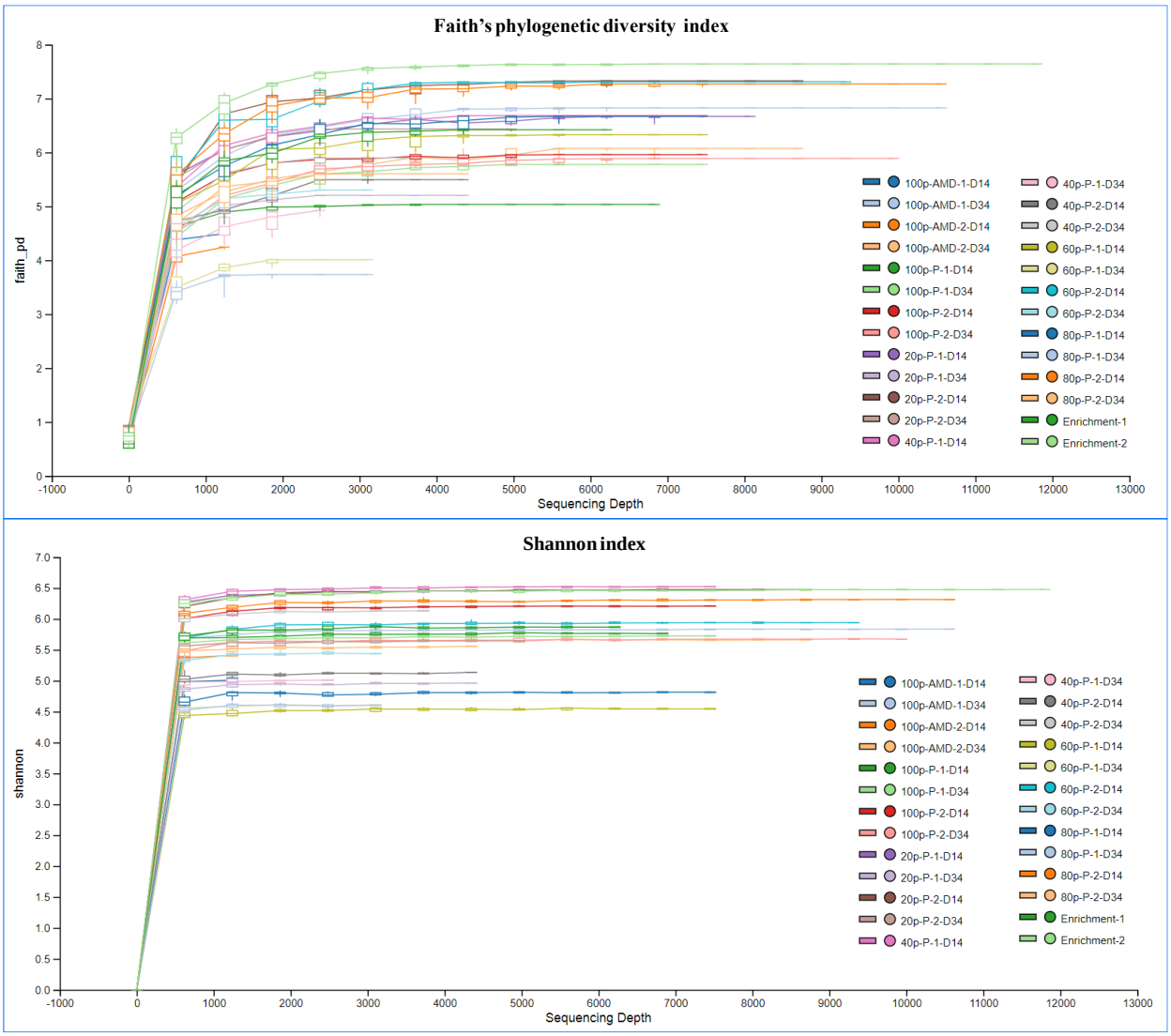

Figure S- 4.7. Rarefaction curves for the alpha-diversity indexes Shannon and Faith's phylogenetic diversity of the samples from AMD treatment studies. (PB-m: Postgate B media with methanol as carbon source).

Table S- 4.1. Number of reads obtained for each sample from AMD treatment experiments in enrichment consortium and in tests with different ratios of AMD and Postgate B media.

Sample-ID	**Input reads**	**Correct reads (primer and size)**	**Quality reads**	**Non-chimeric reads**	after filtering/ decontamination
Enrichment-1	17610	11636	7288	6833	6817
Enrichment-2	19894	14664	12138	11853	11800
			Day 14		
100% PB-m-1	16610	10917	7615	7384	7371
100% PB-m-2	11689	8757	7887	7853	7844
80% PB-m-1	20350	12438	8670	7933	7933
80% PB-m-2	17077	12626	10912	10818	10806
60% PB-m-1	21117	12837	9003	7916	7912
60% PB-m-2	15126	10997	9597	9478	9442
40% PB-m-1	12430	9025	7624	7565	7557
40% PB-m-2	15722	9217	4982	4489	4479
20% PB-m-1	18970	12369	8612	8290	8277
20% PB-m-2	13248	9813	8858	8796	8794
100% AMD-1	2459	1916	1788	1788	1764
100% AMD-2	2503	1931	1835	1835	1808
			Day 34		
100% PB-m-1	18596	12416	8786	8023	8023
100% PB-m-2	15180	11091	10175	9964	9940
80% PB-m-1	7228	4783	3211	3162	3162
80% PB-m-2	6846	5134	4488	4478	4476
60% PB-m-1	7840	4946	3387	3227	3227
60% PB-m-2	5509	4023	3424	3401	3401
40% PB-m-1	7946	5019	3137	3078	3078
40% PB-m-2	6319	4746	4158	4137	4137
20% PB-m-1	9026	5896	4422	4379	4379
20% PB-m-2	8498	6121	5414	5355	5351
100% AMD-1	19575	13144	11428	10790	10773
100% AMD-2	17583	11553	9504	8750	8737
total	334951	228015	178343	171575	171288

Table S- 4.2. Alpha-diversity indexes of Shannon and Faith's phylogenetic diversity using maximum sequencing depth of samples from AMD treatment studies. (PB-m: Postgate B media with methanol as carbon source).

	Day 0 (enriched inoculum)	Day 14	Day 34
Shannon index			
100% AMD	6.170 ± 0.30	5.21 ± 0.20	5.75 ± 0.09
20% PB-m		6.47 ± 0.01	5.30 ± 0.34
40% PB-m		5.83 ± 0.69	5.57 ± 0.56
60% PB-m		5.24 ± 0.70	5.02 ± 0.42
80% PB-m		5.56 ± 0.75	5.08 ± 0.48
100% PB-m		5.99 ± 0.22	5.70 ± 0.03
Faith's phylogenetic diversity index			
100% AMD	7.03 ± 0.61	4.37 ± 0.13	6.45 ± 0.38
20% PB-m		7.00 ± 0.33	5.82 ± 0.62
40% PB-m		6.09 ± 0.60	5.41 ± 0.49
60% PB-m		6.82 ± 0.49	4.65 ± 0.65
80% PB-m		6.97 ± 0.30	4.67 ± 0.94
100% PB-m		5.50 ± 0.46	5.83 ± 0.05

Table S- 4.3. Distance matrix based on the Bray-Curtis Dissimilarity metrics of the AMD treatment studies at day 14 (A – AMD, P – Postgate B with methanol and Enrich– Enrichment consortium).

	100% AMD-1	**100% AMD-2**	**100% PB-m-1**	**100% PB-m-2**	**20% PB-m-1**	**20% PB-m -2**	**40% PB-m -1**	**40% PB-m -2**	**60% PB-m -1**	**60% PB-m -2**	**80% PB-m -1**	**80% PB-m -2**	**Enrichment-1**	**Enrichment-2**
100% AMD-1	0													
100% AMD-2	0.407	0												
100% PB-m-1	0.895	0.895	0											
100% PB-m-2	0.881	0.889	0.436	0										
20% PB-m-1	0.782	0.744	0.682	0.7	0									
20% PB-m -2	0.763	0.706	0.666	0.67	0.278	0								
40% PB-m -1	0.78	0.751	0.463	0.595	0.489	0.428	0							
40% PB-m -2	0.825	0.801	0.422	0.694	0.58	0.588	0.428	0						
60% PB-m -1	0.873	0.884	0.443	0.721	0.709	0.709	0.532	0.38	0					
60% PB-m -2	0.834	0.815	0.35	0.577	0.647	0.621	0.373	0.368	0.367	0				
80% PB-m -1	0.896	0.901	0.425	0.696	0.738	0.729	0.549	0.417	0.217	0.384	0			
80% PB-m -2	0.859	0.867	0.302	0.476	0.627	0.604	0.417	0.474	0.49	0.323	0.441	0		
Enrichment-1	0.869	0.864	0.887	0.886	0.84	0.826	0.849	0.863	0.907	0.869	0.925	0.893	0	
Enrichment-2	0.858	0.839	0.847	0.835	0.841	0.804	0.793	0.832	0.881	0.827	0.891	0.854	0.376	0

Table S- 4.4. Distance matrix based on the Bray-Curtis Dissimilarity metrics of the AMD treatment studies at day 34 (A – AMD, P – Postgate B with methanol and Enrich– Enrichment consortium).

	100% AMD-1	**100% AMD-2**	**100% PB-m-1**	**100% PB-m-2**	**20% PB-m-1**	**20% PB-m -2**	**40% PB-m -1**	**40% PB-m -2**	**60% PB-m -1**	**60% PB-m -2**	**80% PB-m -1**	**80% PB-m -2**	**Enrichment-1**	**Enrichment-2**
100% AMD-1	0													
100% AMD-2	0.300	0												
100% PB-m-1	0.714	0.741	0											
100% PB-m-2	0.909	0.923	0.388	0										
20% PB-m-1	0.62	0.67	0.633	0.853	0									
20% PB-m -2	0.566	0.626	0.564	0.778	0.277	0								
40% PB-m -1	0.682	0.738	0.441	0.65	0.369	0.417	0							
40% PB-m -2	0.62	0.658	0.409	0.557	0.545	0.46	0.399	0						
60% PB-m -1	0.723	0.745	0.389	0.58	0.67	0.636	0.466	0.497	0					
60% PB-m -2	0.786	0.803	0.351	0.43	0.763	0.673	0.508	0.443	0.338	0				
80% PB-m -1	0.771	0.797	0.368	0.518	0.731	0.673	0.511	0.534	0.237	0.327	0			
80% PB-m -2	0.831	0.843	0.321	0.374	0.788	0.71	0.575	0.459	0.41	0.249	0.35	0		
Enrichment-1	0.842	0.849	0.88	0.86	0.916	0.868	0.933	0.866	0.962	0.896	0.936	0.886	0	
Enrichment-2	0.811	0.837	0.851	0.828	0.913	0.844	0.913	0.828	0.942	0.862	0.92	0.841	0.376	0

Table S- 4.5. Distance matrix based on the Weighted UniFrac metrics of the AMD treatment studies at day 14 (A – AMD, P – Postgate B with methanol and Enrich– Enrichment consortium).

	100% AMD-1	**100% AMD-2**	**100% PB-m-1**	**100% PB-m-2**	**20% PB-m-1**	**20% PB-m -2**	**40% PB-m -1**	**40% PB-m -2**	**60% PB-m -1**	**60% PB-m -2**	**80% PB-m -1**	**80% PB-m -2**	**Enrichment-1**	**Enrichment-2**
100% AMD-1	0													
100% AMD-2	0.0884	0												
100% PB-m-1	0.369	0.345	0											
100% PB-m-2	0.321	0.301	0.147	0										
20% PB-m-1	0.263	0.214	0.189	0.182	0									
20% PB-m -2	0.259	0.207	0.198	0.181	0.031	0								
40% PB-m -1	0.304	0.268	0.107	0.184	0.111	0.113	0							
40% PB-m -2	0.390	0.363	0.148	0.267	0.201	0.214	0.135	0						
60% PB-m -1	0.437	0.409	0.178	0.308	0.256	0.269	0.195	0.071	0					
60% PB-m -2	0.365	0.341	0.086	0.202	0.193	0.202	0.101	0.098	0.136	0				
80% PB-m -1	0.416	0.391	0.139	0.269	0.237	0.247	0.164	0.062	0.057	0.100	0			
80% PB-m -2	0.327	0.304	0.0770	0.132	0.156	0.163	0.095	0.179	0.214	0.100	0.172	0		
Enrichment-1	0.353	0.306	0.289	0.277	0.206	0.209	0.224	0.310	0.359	0.302	0.337	0.261	0	
Enrichment-2	0.338	0.289	0.296	0.250	0.193	0.195	0.241	0.338	0.384	0.316	0.348	0.255	0.106	0

Table S- 4.6. Distance matrix based on the Weighted UniFrac metrics of the AMD treatment studies at day 34 (A – AMD, P – Postgate B with methanol and Enrich– Enrichment consortium).

	100% AMD-1	100% AMD-2	100% PB-m-1	100% PB-m-2	20% PB-m-1	20% PB-m -2	40% PB-m -1	40% PB-m -2	60% PB-m -1	60% PB-m -2	80% PB-m -1	80% PB-m -2	Enrichment-1	Enrichment-2
100% AMD-1	0													
100% AMD-2	0.024	0												
100% PB-m-1	0.377	0.378	0											
100% PB-m-2	0.526	0.526	0.159	0										
20% PB-m-1	0.111	0.101	0.306	0.454	0									
20% PB-m -2	0.148	0.151	0.258	0.400	0.075	0								
40% PB-m -1	0.248	0.245	0.155	0.300	0.161	0.135	0							
40% PB-m -2	0.317	0.320	0.125	0.240	0.248	0.196	0.105	0						
60% PB-m -1	0.420	0.416	0.105	0.153	0.340	0.322	0.197	0.207	0					
60% PB-m -2	0.452	0.454	0.108	0.098	0.383	0.332	0.231	0.176	0.083	0				
80% PB-m -1	0.439	0.435	0.103	0.129	0.360	0.332	0.211	0.209	0.033	0.075	0			
80% PB-m -2	0.478	0.478	0.118	0.078	0.408	0.358	0.255	0.200	0.103	0.049	0.077	0		
Enrichment-1	0.396	0.392	0.219	0.313	0.321	0.288	0.237	0.226	0.246	0.263	0.248	0.275	0	
Enrichment-2	0.337	0.338	0.190	0.327	0.274	0.233	0.205	0.182	0.257	0.271	0.263	0.280	0.107	0

CHAPTER 5

Palladium bio-recovery from spent automotive catalytic converter leachates as nanoparticles using plant extracts

Palladium bio-recovery from automotive catalytic converter leachates as nanoparticles using *Rubus idaeus* leaf extracts

A modified version of this chapter would be published as:

Nobahar, Amir; Carlier, Jorge Dias; Costa, Maria Clara. "Palladium bio-recovery from automotive catalytic converter leachates as nanoparticles using Rubus idaeus leaf extracts". Clean Technologies and Environmental Policy (submitted, 2022).

Abstract

This study investigates the potential of hydroalcoholic extracts of *Cistus ladanifer* L., *Erica andevalensis* and *Rubus idaeus* L. as a green method for the recovery of platinum group metals (PGMs) from both synthetic unimetallic solutions and multimetallic solutions obtained from the leaching of two different spent automotive catalytic converters (ACC). Experiments with unimetallic solutions revealed that *E. andevalensis* and *R. idaeus* extracts could separate about 70% of Pd and less than 40% of other tested metals (Al, Ce, Fe and Pt) from the solutions. Then, application of the plant extracts to two different ACCs leachates showed that *E. andevalensis* and *R. idaeus* extracts can induce high precipitation (>60%) of Pd and Pt with co-precipitation of less than 20% of other metals. UV-Visible spectra analysis confirmed the bio-reduction of Pd^{2+} ions into Pd^{0} nanoparticles by *R. idaeus* extract and Fourier-transform infrared spectroscopy (FTIR) analysis revealed the contribution of functional groups of the phytochemicals present in the extract (such as phenols, flavonoids, and anthocyanins) in the Pd^{2+} bio-reduction and stabilization. Afterwards, scanning electron microscopy with energy dispersive X-ray spectroscopy (SEM-EDX) analysis of the precipitate obtained from one

leachate with *R. idaeus* extract demonstrated the presence of Pd particles along with organic compounds and particles containing other metals. Therefore, particles were subjected to a washing step with acetone for further purification. Finally, scanning transmission electron microscopy with energy dispersive X-ray spectroscopy (STEM-EDX) analysis showed the high purity of the final Pd particles and high-resolution STEM allowed to determine their size variation of 2.5 to 17 nm with an average Feret size of 6.1 nm, and confirmed their crystalline structure with an interplanar lattice distance of ~0.22 nm. This green approach offers various benefits including simplicity of Pd separation from the leachates as valuable nanoparticles that makes the process more feasible from economic and environmental standpoints. A process cost of ~20 $ / g of Pd particles recovered was estimated (excluding manpower).

Keywords: plant extract, metal, recovery, remediation, platinum group metals, nanoparticle

Graphical abstract

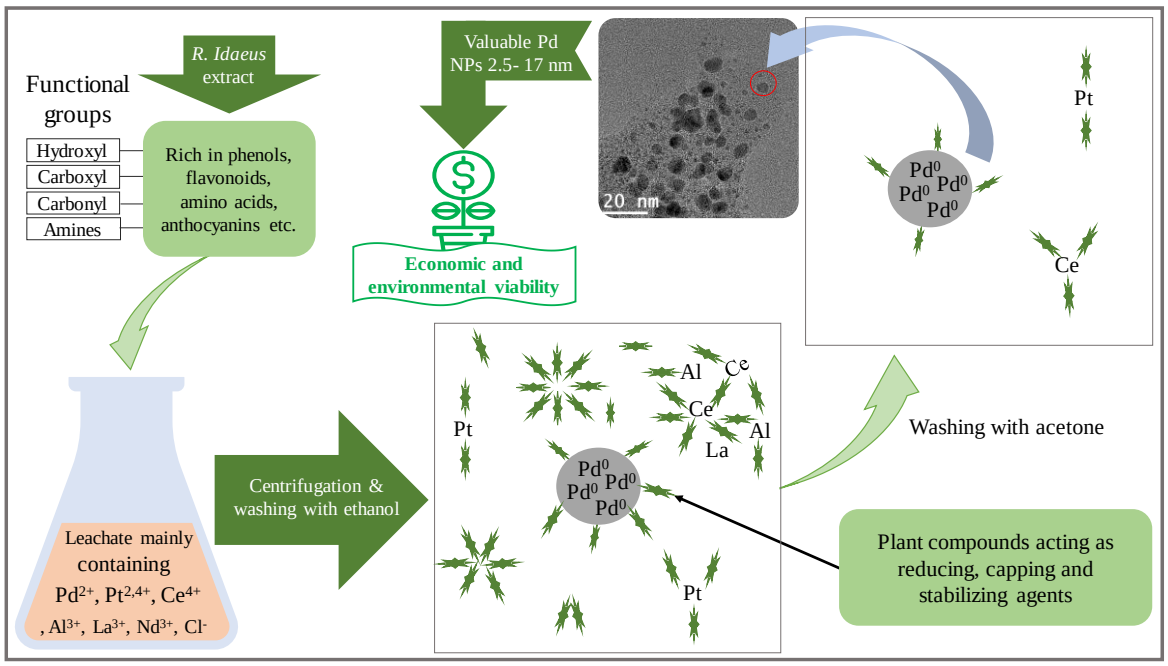

5.1. **Introduction**

In the last century, due to rapid industrialization, the application of platinum group metals (PGMs) emerged in various industrial sectors. The demand for PGMs is continuously increasing and more than 90% of their applications in the industries are in the catalysts' processing (Wongsawa et al. 2020). The rising demand for these metals is reported to be at a higher pace than the other base metals used primarily in catalysts (Wei et al. 2019).

Automotive catalytic converters (ACC) have been increasingly applied for the transformation of carbon monoxide and hydrocarbons into carbon dioxide and water since the mid-1970 (Benson et al. 2000). Every year, a considerable part of the global extraction of PGMs is applied in ACC production, comprising 30% of Pt, 80% of Pd and Rh (Supply Chain Deep Dive Assessment 2022). Thus, used ACCs that are replaced or from automotives that reach the end of their life become a secondary source of these metals. PGMs grades in the ores range from 3 to 8 g/t (Kyriakakis, 2005), while, the monoliths of ACCs contains PGMs in a range of 1-3 Kg/t (Karim and Ting 2021). Therefore, PGMs

recovery from spent ACCs reduces the energy consumption, waste disposals and environmental pollutants. For example, Fornalczyk and Saternus (2011) reported that in order to obtain 1 Kg of Pt, about 150 tons of natural ores need to be processed, which generates 400 tons of wastes, while the recycling of the same amount of Pt can be achieved by processing of 2 tons of ACCs. From 2008 to 2018, demand for PGMs has been raised about 10%, and they are mostly used in the catalytic converter industry (Platinum, 2008 2008; PGM Market Report 2018). In fact, it is expected that due to more strict environmental regulations, the demand trend for PGMs will continuously increase (Saguru et al. 2018). Considering this increasing secondary source of PGMs in ACCs, recycling these metals is critical from both financial and environmental standpoints. Recycling and long-term management of these wastes is a critical step to ensure the long-term viability of mining resources, thus mitigating the rising resource scarcity. However, due to the low concentration and high metal complexity in these wastes, their recycling still remains a challenge (Zhang and Xu 2018).

Currently for the metal recovery processes, hydrometallurgical methods are favored over pyrometallurgical methods and are developing every day since they are more environmentally and economically viable with possibility of performing in wide scale, diverse reagent options, using leachates from materials containing very low to very high grade of metals (Jeon et al. 2020; Kumari and Samadder 2022). PGM hydrometallurgical recovery from wastes starts with a metal leaching procedure (typically non-metal specific) and is followed by a metal separation phase from the generated leachates (Karim and Ting 2021). In the conventional and long-established acid leaching systems, highly aggressive and acidic leaching solutions are employed for the PGMs separation from ACCs such as HCl-based leachates, cyanide solution media and aqua regia (Yakoumis et al. 2021). However, the mainstream employs HCl-H_2O_2 systems, which is known to be greener than other leaching systems with PGMs recovery of about 95% (Jimenez de Aberasturi et al. 2011). The addition of oxidizing agent reduces the pollutant gases in this leaching system and more improvement have been introduced by balancing the ratio of

HCl to H_2O_2 and other oxidizing and chlorine sources including $AlCl_3$, NaCl, NaClO and $CuCl_2$ (Yakoumis et al. 2021). Regarding economic aspects, the interests of the concerned industries are monopolized by the efficient hydrometallurgical techniques (Trinh et al. 2020). In the leaching step, which is the most crucial stage in hydrometallurgy, mild leaching procedures are known to prevent liquid waste generation that will further lower waste management and operational costs; as instance, unlike aqua regia and cyanide, mild chloride-based leaching systems do not emit toxic by-products and gases (Yakoumis et al. 2021). Moreover, direct leaching also valuates whole leaching process without the necessity of prior pretreatment processes such as thermal reduction or pre-concentration, by directly feeding the mechanically processed ACCs into leaching media (Dong et al. 2015). Therefore, HCl-H_2O_2 based systems are among the most efficient PGM recovery from ACCs with sustainability prospects.

Furthermore, different physiochemical methods for PGMs separation from the leaching solutions are described in the literature, such as solvent extraction (Costa et al. 2013; Paiva et al. 2022), ion exchange (Lanaridi et al. 2022), molecular recognition technology (Izatt et al. 2015), molecular ion imprinted polymer (Limjuco and Burnea 2022) etc. However, some of those techniques may have drawbacks such as inadequate metal recovery (especially for low concentrations of metals), high energy requirements, as well as high chemical costs and environmental problems. This issue, leaves open space for the emergence of new advanced technologies aiming efficient PGMs recovery with less operational costs and reduction in energy consumption while being environmentally friendly (Granados-Fernández et al. 2021). As a result, metal bio-recovery strategies, that make use of biological materials and/or processes, have attracted growing attention in recent years.

Recovery of PGMs from ACCs through bio-hydrometallurgical methods have not been extensively studied yet, which shows the importance of further investigations into alternative sustainable and effective with a low carbon footprint in PGMs recovery processes (Karim and Ting 2021). Based on the authors' knowledge, by now, studied bio-

hydrometallurgical procedures are mainly focused on the PGMs bioleaching from ACCs benefiting from different organic acids or microorganisms. Bio-leaching processes employ organic acids such as oxalic or lactic acids (Wiecka et al. 2022) or microorganisms including bacteria, such as works performed by Ilyas et al. (2022) and Karim and Ting (2022), or fungus like the work performed by Bahaloo-Horeh and Mousavi (2022). In addition, different mechanisms including bio-reduction, bio-precipitation, chelation, extracellular sequestration and bio-sorption are known as the main mechanisms that microorganisms can interact with PGMs and separate them from the solutions (Zhang et al. 2020). However, studies on the potential role of the plants' secondary metabolites in separation and purification of the PGMs from the multimetallic solutions are scarce in the literature.

Plants synthesize a wide variety of bioactive compounds with a large range of functional abilities. Their secondary metabolites, including phenols, saponins, alkaloids, organic acids, proteins etc. possess polar functional groups such as phenolic, hydroxyl, carboxyl, amino and sulfo, that capacitates these compounds to interact with metals through different processes such as reduction (Ishak et al. 2019), chelate/complex formation and precipitation (Ma et al. 2016) etc. Thus, those compounds have application potential in various metal related industrial sectors such as metal recovery/removal from solutions, biosynthesis of nanoparticles, treatment of metal bearing wastewaters (Nobahar et al. 2021). In the case of PGMs, Ishak et al (2019) reviewed different studies about their interaction with plant compounds, pointing phenols, flavonoids, terpenoids, carbohydrates, proteins, amino acids and polysaccharides as the most important secondary metabolites having interaction potential with metals of this group. Application of plant-based compounds in metal recovery industrial activities is an attractive alternative from economic and environmental standpoints with the potential to replace conventional physiochemical methods (Nobahar et al. 2021). Despite the lack of investigations in PGMs recovery from multimetallic solutions benefiting plant metabolites, there are different works reporting the application of different secondary

plant metabolites with PGMs ions and their separation potential from unimetallic solutions as nanoparticles. As instance, Areca Nut Husk (Hegde et al. 2021), Tea polyphenols (Hu et al. 2022) and *Aspalathus linearis* (Ismail et al. 2017) natural plant extracts are reported to separate successfully Pd, Pt and Rh ions respectively, from unimetallic solutions as nanoparticles.

The present work investigates a novel process in PGMs' separation from unimetallic solutions and from multimetallic bearing leachates using three plant-based extracts and then studies the precipitates obtained from one leachate with a selected extract aiming to contribute for the development of eco-friendly and efficient green technologies as alternatives for the recovery of these metals from secondary sources.

5.2. **Materials and methods**

5.2.1. Experimental approach

The capacity of 70% (v/v) ethanolic plant extracts to precipitate metals was tested on different metal bearing aqueous solutions: (1) first on unimetallic solutions prepared from standards commercialized for metals analysis; (2) then on leachates from spent automobile catalytic converters. For that purpose, the plant extracts were mixed and homogenized at a 1/1 (v/v) ratio with the metal bearing solutions and mixtures prepared in the same way but using pure 70% ethanol (without plant compounds) were used as controls. The initial and the final concentrations of metals in the mixture were used to calculate percentages of removal from solution.

In addition, the putative effect of pH changes on metal removals was evaluated by comparing the initial pH measured in the metal bearing solutions, the pH values in the mixtures, and the estimated lowest pH at which metals precipitation is expected to occur according to theoretical simulations on the Medusa-Hydra software (Puigdomenech 2015) for increasing pH values (-1 to 14) in aqueous solutions using parameters that mimic the tested matrices.

Experiments were carried out in triplicates in 50 mL centrifuge tubes at room temperature (20 ± 3°C) and samples were collected for pH measurements and for metal analysis after 1 and 48 hours of reaction.

The significance of differences between means of different experimental treatments (test 1 h, test 48 h, control 1 h and control 48 h) were assessed by the single factor analysis of variance (ANOVA) considering a significance threshold level of 5%. Then, when ANOVA revealed significant differences among treatments, post-hoc tests were carried out with Tukey Kramer's tests (also for 5% significance level).

5.2.2. Plant extracts

Three types of plant leaves were collected for this study: leaves from *Cistus ladanifer* L. (crimson spot rockrose); from *Erica andevalensis* Cabezudo & Rivera (a shrub growing in the Iberian Peninsula next to acidic mine waters contaminated with sulfate and metals) and from *Rubus idaeus* L. (red raspberry). The choice of plants for this work considered criteria such as being available in the region, being reported as metal accumulators and/or being plants (or parts of them) considered industrial or agricultural waste. *C. ladanifer* has developed several tolerance mechanisms that allow its adaptability to contaminated environments. The immobilization of metallic elements in roots and accumulation in senescent leaves are examples of these adaptability mechanisms and make this plant a promising species for phyto-stabilization of mining areas (Abreu et al. 2011; Santos et al. 2012, 2014, 2016). *E. andevalensis* is an endemic species of the Iberian pyrite Belt (IPB) (Cabezudo and Rivera 1980) that grows under extreme conditions of pH values between 3 and 4 and high metal contents, being able to accumulate Mn (Rossini-Oliva et al. 2018). It colonizes mine tailings and the bank sediments of water bodies contaminated with acid mine drainage (AMD), such as the Tinto and Odiel rivers in Spain and the channels and dams at the São Domingos mine in Portugal (Abreu et al. 2008; Monaci et al. 2011). *R. idaeus* is an agricultural crop widely cultivated in Asia, Europe, and North America for

its fruits, being its leaves a residue highly rich in phenolic compounds (Pantelidis et al. 2007; Wang et al. 2019).

Young and mature leaves were collected and immediately dried to remove the moisture in an INCU-Line oven (VWR international) at 45°C until their weights stabilized. The dried leaves were then grinded into powder using an electric coffee grinder and the powder was mixed at a 10% (w/v) ratio with 70% (v/v) ethanol. Afterwards, the mixture was sonicated using an ultrasonic bath FB15054 (Fisher Scientific, USA) for 1 h and homogenized by orbital shaking at 150 rpm for 16 hours. Finally, the mixture was centrifuged at 2800 g for 5 min at room temperature and the supernatant was filtered using 310-150 mm qualitative filter paper (VWR international) in a vacuum system.

5.2.3. Unimetallic solutions

Five 100 mg/L unimetallic solutions were prepared by diluting in 0.02 M HCl the following metal standard solutions of 1000 mg/L to a 1/10 (v/v) ratio: $Pd(NO_3)_2$ in 0.5 M HNO_3, $Ce(NO_3)_3$ in 5% HNO_3, $Al(NO_3)_3$ in 0.5 M HNO_3 and $Fe(NO_3)_3$ in 0.5 M HNO_3 (from Merck Certipur, Germany), $PtCl_2$ in 5% HCl from (Sigma-Aldrich standard for AAS, EUA).

5.2.4. Leachates from spent Automobile Catalytic Converters (ACCs)

Leachates from two different spent ACCs were used: (1) a spent ACC from a Seat Ibiza 1995 with 23 years of use, henceforth I95 and (2) a spent ACC from a Honda Civic 1998, with 20 years of use, henceforth H98. The leachates were provided by Professor Ana Paula Paiva from Faculdade de Ciências - Universidade de Lisboa (FCUL) and were prepared after several leaching experiments reported by Paiva et al. (2022) as follows. Both I95 and H98 metallic components were removed with a metal saw to extract the honeycomb. Once the honeycombs were extracted, a grinding operation was performed

using a K, MF 10 Basic IKA Werke cutting mill at a speed of 3000 rpm with a 2.0 mm discharged grid. Afterwards, leaching was carried out using the following conditions: [HCl] = 11.6 M, oxidizer H_2O_2 = 1% (w/v), liquid/solid = 2 L/kg, temperature = 60 ºC, time = 3 h; stirring = 250 rpm. The HCl concentration of 11.6 M is due to the use of concentrated acid (37 wt% or 12 M), which is slightly diluted by the addition of 1% (w/v) oxidizer H_2O_2. Both leaching solutions were then diluted 1/6 (v/v) in demineralized water, reaching ~2 M HCl, to avoid the fast digestion of bio-compounds in the tests using plant extracts.

5.2.5. Analytical procedures

To measure the pH, a pH Meter GLP 21 (Crison, Spain) with a glass electrode (VWR, pH electrode SJ223) was used. For metal analysis on the mixtures of metal bearing solutions with plant extracts, 2 mL samples were centrifuged at 2800 g for 5 min at room temperature (Hettich, ROTOFIX 32A) and 1 mL of the supernatant was diluted in 4 mL of 5% HNO_3. However, this dilution led to the formation of precipitates. Thus, samples were then digested through addition of 2.5 ml of 65% HNO_3 (PanReac AppliChem, Germany, analytical grade) and 2.5 ml of 30% hydrogen peroxide (VWR Chemical, analytical grade) and heating at 70°C during 1 h. Sample dilutions were prepared in 5% nitric acid. Afterwards, a Microwave Plasma-Atomic Emission Spectroscopy (MP-AES 4200, Agilent Technologies, USA) was used to determine the metals concentrations using standard calibration curves. Calibration curves were prepared from the following standard solutions in 5% nitric acid: $Pd(NO_3)_2$ in 0.5 M HNO_3, $Ce(NO_3)_3$ in 5% HNO_3, $Al(NO_3)_3$ in 0.5 M HNO_3 and $Fe(NO_3)_3$ in 0.5 M HNO_3, Nd_2O_3 in 2-3% HNO_3, La_2O_3 in 2% HNO_3 (from Merck Certipur, Germany), $PtCl_2$ in 5% HCl (from Sigma-Aldrich standard for AAS, EUA), Rh in 10% HCl (from Acros organics, USA) in a dilution series of 0, 1, 5, 10, 20, 30, 40 and 50 mg/L for all elements. The correlation coefficients R^2 of all calibration curves were above 0.99.

The bio-reduction of Pd^{2+} ions and particle formation were studied by UV-visible spectral analysis using wavelengths between 300 to 700 nm with 1 nm intervals in a BioTek Synergy 4 microplate reader (BioTek InstrumentsInc., USA). The optical absorption spectra of the Pd^{2+} solution (100 mg/L) (Gaikwad and Rothenberg 2006), of a 5% (v/v) dilution of *R. idaeus* extract in 0.02 M HCl, and of a 5% (v/v) dilution of *R. idaeus* extract in 100 mg/L of Pd^{2+} solution (one hour after reaction) (Sheny et al. 2012; Siddiqi and Husen 2016) were investigated.

Fourier Transform Infrared Spectroscopy (FTIR) measurements of a Pd^{2+} solution, the *R. idaeus* extract and the mixture of Pd^{2+} solution and *R. idaeus* extract (Siddiqi and Husen 2016) were performed using a Nicolet iN10MX micro-FTIR (Thermo Scientific, USA) equipped with a MCT detector cooled with liquid nitrogen. Analyzes were conducted in reflection mode, by spreading a drop of the sample onto a reflectance holder. Spectra were collected in the infrared region (from 4000 to 675 cm^{-1}). Three measurements were performed for each sample to assure the robustness of the analysis.

The particles obtained from applying the *R. idaeus* extract to the H98 leachate were centrifuged and washed with 96% (v/v) ethanol for 1 h under orbital shaking and then centrifuged (2800 g for 60 min at room temperature) for liquid removal and finally dried under vacuum (two washing cycles were performed). Subsequently, Scanning Electron Microscopy-Energy Dispersive X-ray spectroscopy (SEM-EDX) analysis were carried out using a 324 S3700N SEM system (Hitachi, Japan) coupled to a XFlash 5010 SDD EDS Detector (Bruker, Germany). The samples were analyzed at low vacuum (40 Pa) with an accelerating voltage of 5 and 20 kV. Then, the particles obtained from the prior washing step with 96% ethanol were further washed for two cycles with pure acetone to remove excess of organic compounds as follows: mixed during 1 h under orbital shaking and then centrifuged (2800 g for 60 min at room temperature) for liquid removal and dried under vacuum. Thereafter, Scanning Transmission Electron Microscope (STEM) imaging was carried out on a Titan ChemiSTEM (Thermo Fisher Scientific, Waltham, USA) microscope operating with a field emission gun and aberration corrector on the

probe and four Energy Dispersive X-ray spectroscopy (EDX) detectors operating at 200 kV. Before the STEM analysis, particles were resuspended in ethanol and sonicated for 30 min to pulverize the samples. Then, 5 µl of each sample were dispersed on copper coated grids, and the grids were dried and stored in a desiccator until imaging.

5.3. Results and discussion

5.3.1. Metals removal from unimetallic solutions

The experiments with the unimetallic solutions revealed similar metal removal trends with the three plant extracts (Figures 1). Highest removals, significantly different from the controls, were achieved for Pd^{2+}, varying from 48% to 81%. At a lower extent, Pt^{2+} and Fe^{3+} were also significantly removed in the three experiments: Pt^{2+} removals were between 19% and 33% and Fe^{3+} removals were between 15 and 37%. On the other hand, the removals of Ce^{3+} and Al^{3+} were, in general, not significantly different from those achieved in the controls, and were just in the range from 3% to 28%.

It must be emphasized that the removals achieved in the unimetallic solutions of Pt^{2+}, Pd^{2+}, Al^{3+} and Ce^{3+} were not caused by alkalization, since the pH values in the mixtures were below the estimated pH at which these metals are expected to start precipitating according to simulations using the Medusa-Hydra software (Puigdomenech 2015) (Table S- 5.1). However, in the experiment with the unimetallic solution of Fe^{3+}, the pH values in the mixtures were above the theoretical estimates at which this ion would start forming solid complexes of $Fe(OH)_2.7Cl_{0.3}$; therefore, in this case, the removals could have been caused by pH changes. In addition, generally reaction time of 1 hour and 48 hours does not have high impact on the removal of metals from the unimetallic solutions (Figure 5.1), indicating the fast kinetics of the reactions between phytochemicals and studied metal ions.

Hence, the results indicate a tendency toward a higher interaction of plant compounds with Pd^{2+} than with the other tested metal ions, especially in the experiments with the

extracts of *R. idaeus* and *E. andevalensis* (Figure 5.1). This confirms the potential of some plant extracts for Pd^{2+} separation from solutions, which was already demonstrated using unimetallic solutions and several plant materials, as for example extracts of leaves from *Euphorbia granulate* (Nasrollahzadeh and Mohammad Sajadi 2016), from Soybean (Glycine max) (Kumar Petla et al. 2012), from *Origanum vulgare* (Seyedi et al. 2018), from *Eryngium caeruleum* (Saleh et al. 2021), or, for instance, extracts of peels from *Punica granatum* (Şahin Ün et al. 2020), and from orange (Wicaksono et al. 2020). In fact, this is a very interesting feature with potential applications for the recovery of this valuable metal from wastewaters and/or leachates of waste materials. Therefore, further experiments were performed using real solutions containing PGMs, aiming to assess the potential of the three plant extracts prepared in this work for the recovery of Pd from complex matrices.

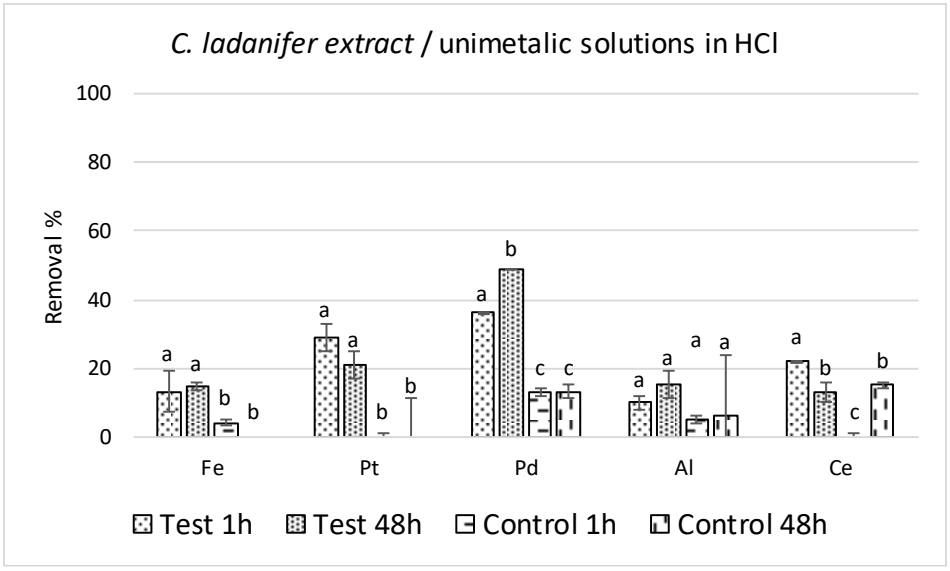
C. ladanifer extract / unimetalic solutions in HCl
Removal %
100
80
60
40
20
0
Fe
Pt
Pd
Al
Ce
Test 1h
Test 48h
Control 1h
Control 48h

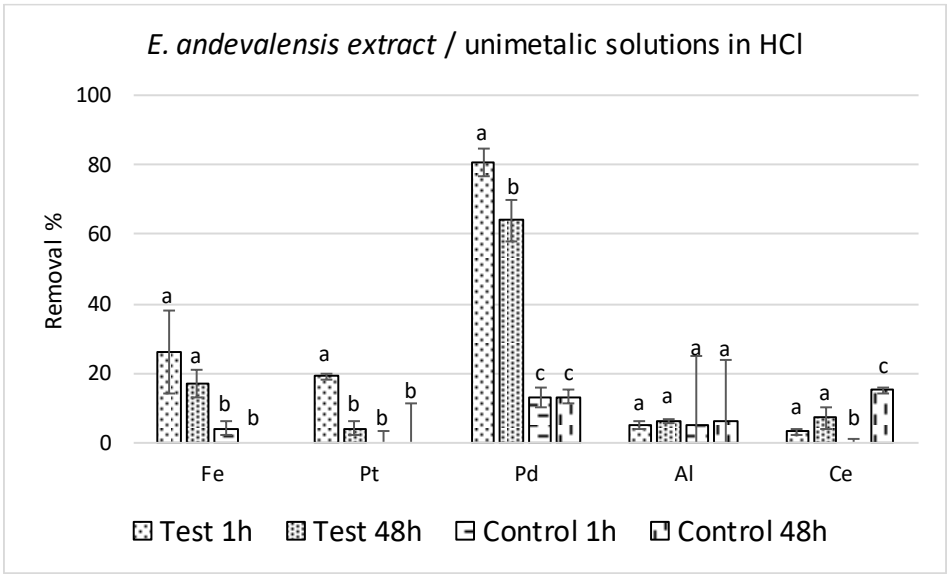
E. andevalensis extract / unimetalic solutions in HCl
Removal %
100
80
60
40
20
0
Fe
Pt
Pd
Al
Ce
Test 1h
Test 48h
Control 1h
Control 48h

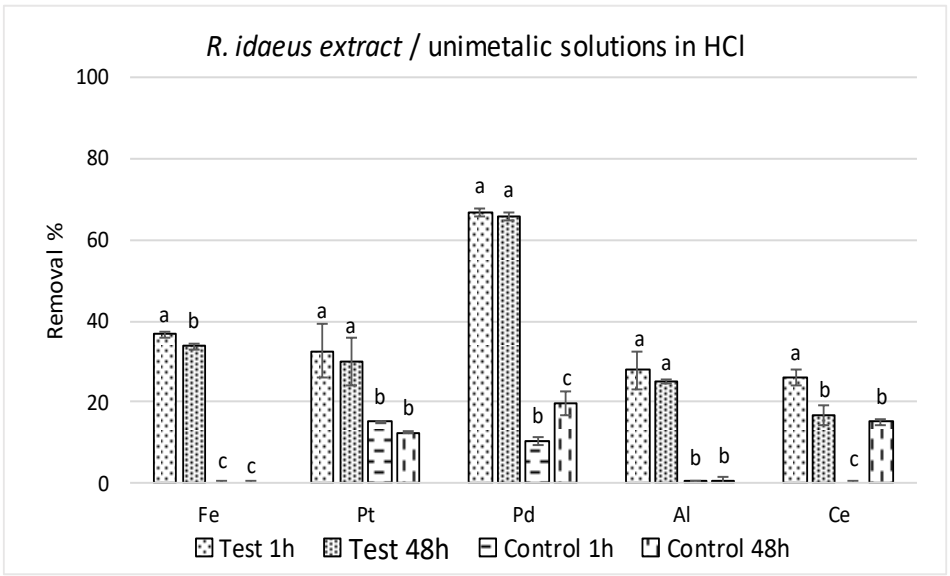
R. idaeus extract / unimetalic solutions in HCl
Removal %
100
80
60
40
20
0
Fe
Pt
Pd
Al
Ce
Test 1h
Test 48h
Control 1h
Control 48h

Figure 5.1. Metal removals achieved after 1 h and 48 h of mixing *C. ladanifer*, *E. andevalensis* and *R. idaeus* 70% ethanolic extracts at a 1/1 (v/v) ratio to the unimetallic solutions (~100 mg/L) at room temperature (25 ± 3 °C). Results for controls, consisting of the addition of just 70% ethanol (without plant extract), are included. Removals with the same letters do not significantly differ at 0.05 level (ANOVA and Tukey Kramer's tests).

5.3.2. PGMs recovery from ACC leachates

5.3.2.1. ACC leachates characterization

The metal bearing leachates from spent ACCs (I95 and H98) were diluted in a 1/6 ratio (v/v) in demineralized water before being used in the experiments with plant extracts, and were analyzed in terms of the main metals, pH and chloride anion (Cl^-) associated to the acidic matrices (Table 5.1). The leaching step provided satisfactory results for the PGMs usually present in these devices: Pt and Rh were leached from I95, while Pt and Pd were leached from H98. However, as expected, other metals which can be considered as contaminants in the recovery process were also leached (Table 5.1). Although the focus of this paper is not to study the efficiency of the leaching process, it is important to have realistic leaching liquors for target metal recovery studies.

Table 5.1. Characterization of 1/6 (v/v) diluted leachates from spent ACCs used for metal removal tests with plant extracts.

Parameter	I95 leachate (1/6)	H98 leachate (1/6)	Units
Pd	< LOD*	204 ± 2	mg/L
Pt	61.7 ± 0.7	45.2 ± 0.4	
Rh	5.99 ± 0.04	< LOD*	

Al	281 ± 3	487 ± 4	
Ce	671 ± 6	751 ± 3	
Fe	17.0 ± 0.1	27.8 ± 0.3	
La	< LOD*	145 ± 2	
Nd	< LOD*	134 ± 1	
Cl^-	2	2	M
pH	0.41	0.44	Sorensen scale

* LOD = limit of detection (LODs: Pd = 1.11, Rh = 0.08, La = 0.03, Nd = 0.05)

5.3.2.2. Metals removal from ACCs leachates

In the experiments using the ACC leachates the pH values in the tests and in the controls were all below the values at which precipitation of the tested metals starts to occur, according to the theoretical simulations (Table S- 5.2). This suggests that none of the observed removals were caused by pH changes. In fact, the results were encouraging regarding the use of plant extracts for the recovery of metals from the ACCs leachates. The removals of the tested PGMs were significantly higher in the tests with plant extracts than in the controls and were in general higher than the removals of contaminant metals (Figure 5.2 and Figure 5.3). This relative specificity for the target metals was particularly evident in the experiments with *E. andevalensis* and *R. idaeus* extracts added to the H98 leachate, in which precipitations of 60% to 90% of the initial Pd^{2+} (~200 mg/L) and 60% to 75% of the initial Pt^{2+} (~45 mg/L) was achieved. Also, the differences observed in elements removals between the two studied reaction times (1hr. and 48 hrs.) were relatively small in both leachates when using each of the three plant extracts, as previously reported for the unimetallic solutions.

Despite the encouraging results, there was an incomplete separation of Pd and Pt in these experiments, which can possibly be explained by the increasing difficulty of new metal nuclei formation due to the lowering chance of metal atoms encounters as their

concentrations decrease. Accordingly, the initial lower concentrations of PGMs in the I95 ACC leachate could be a possible explanation for the lower removals achieved with it. Thirumurugan et al. (2016) suggested operation processes at high temperatures and long reaction times for a complete recovery of Pd by plant extracts. However, since the aim of this study is to investigate the potential of plant extracts in PGMs recovery in an eco-friendly and economically viable process suitable for industrial scale operations, experiments at high temperatures were avoided.

The only metal contaminant with removal percentages significantly higher in the tests than in the controls was Fe. However, the removals were below ~40% and the initial concentration of iron was relatively low ([Fe] < 30 mg/L) in both diluted leachates I95 (1/6) and H98 (1/6), comparing with other contaminants (Table 5.1). Moreover, some removal of Ce was observed in the experiments, both in the tests and in the controls, and although the removal percentages were low (< 18%), they may correspond to high amounts of this metal due to its high initial concentrations (~671 and ~751 mg/l in diluted (1/6) leachates of I95 and H98). Despite this possible contamination of the PGMs recovered by this strategy, they could still be useful, depending on their applications. It is reported that the combination of oxide and metal nanocomposites into a hybrid composite gives rise to new collective properties, which are different to the properties of each individual component (Tan et al. 2014). For instance, Wang et al. reported that the addition of CeO_2 to Pd nanoparticles improves the catalytic activity (Wang et al. 2009). Moreover, Rajesh et al. (2019) and Tan et al. (2014) reported that the CeO_2 content highly increases the electrochemical reaction of Pd/CeO_2 and causes very efficient mass transport in ethanol and methanol oxidation reactions than Pd particles alone. Other examples of Pd/CeO_2 nanocomposites applications are: as efficient formic acid electrooxidation catalyst (Feng et al. 2012), and high-performance catalytic electrodes for fuel cell applications (Kannan et al. 2015).

E. andevalensis only exists in nature in small areas near lagoons contaminated with acid mine water in the Iberian Peninsula, so it is not interesting as a raw material for

hydrometallurgical processes. Despite this, it may be interesting to study the interactions of target metals with compounds present in the leaves of this shrub that grows in such extreme environments, because it may lead to the discovery of biomolecules with interesting properties that could inspire the production of new synthetic molecules. Moreover, if future studies reveal more potential effectiveness of the *E. andevalensis* extract for different industrial purposes with economical viabilities, new plantations of this plant as a new bio-economic enterprise can be hypothesized. On the contrary, *R. idaeus* leaves are available in large quantities due to the agro-industrial production of red raspberry fruits. For this reason, the further study on the PGM recovery mechanism and on the characterization of the obtained precipitates was focused on the extract from these leaves.

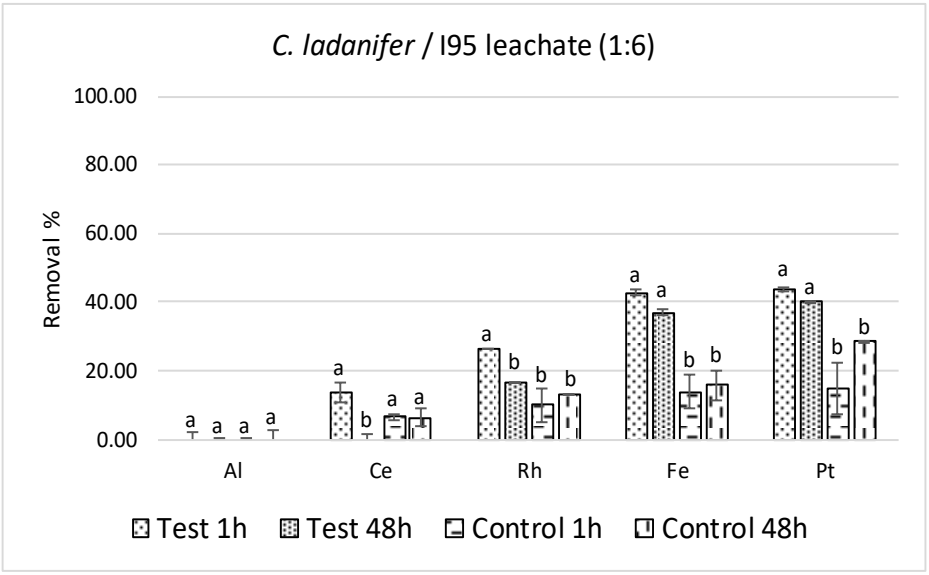
C. ladanifer / I95 leachate (1:6)
Removal %
100.00
80.00
60.00
40.00
20.00
0.00
Al
Ce
Rh
Fe
Pt
Test 1h
Test 48h
Control 1h
Control 48h

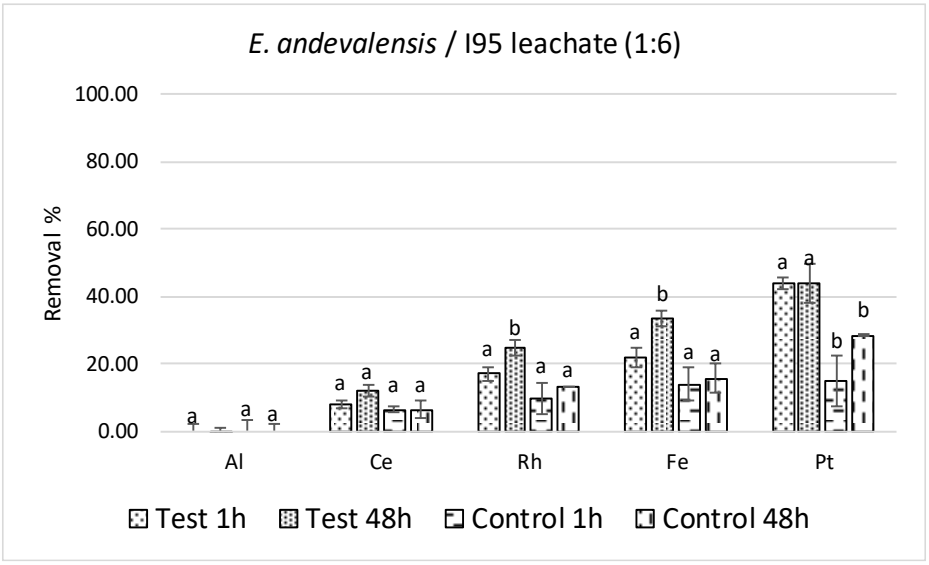
E. andevalensis / I95 leachate (1:6)
Removal %
100.00
80.00
60.00
40.00
20.00
0.00
Al
Ce
Rh
Fe
Pt
Test 1h
Test 48h
Control 1h
Control 48h

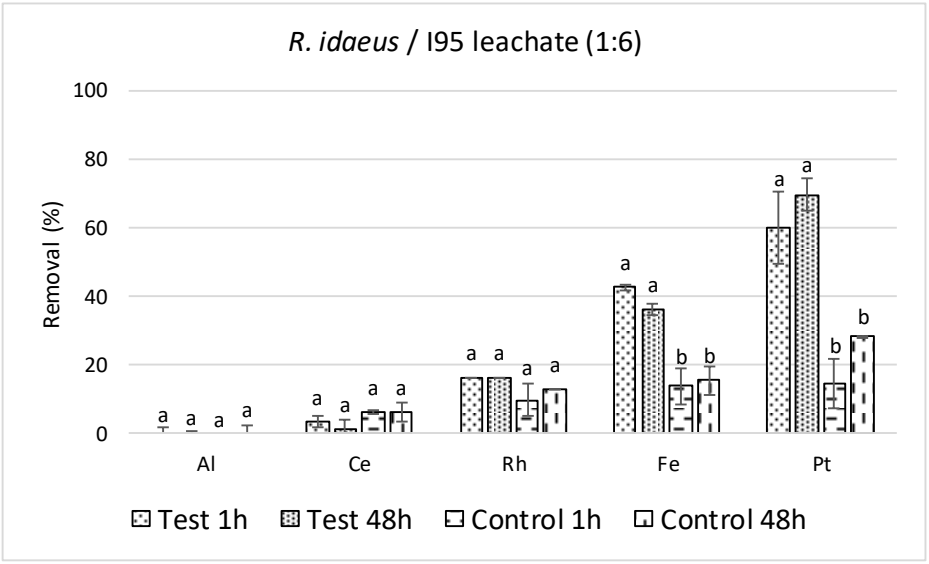
R. idaeus / I95 leachate (1:6)
Removal (%)
100
80
60
40
20
0
Al
Ce
Rh
Fe
Pt
Test 1h
Test 48h
Control 1h
Control 48h

Figure 5.2. Removal of main metals present in the diluted (1/6 (v/v)) I95 leachate solution, achieved after 1 h and 48 h addition of *C. ladanifer*, *E. andevalensis* and *R. idaeus* 70% ethanolic extracts at a 1/1 (v/v) ratio at room temperature (25 ± 3 °C). Results for controls, consisting of the addition of just 70% ethanol (without plant extract), are included. Removals with the same letters do not significantly differ at 0.05 level (ANOVA and Tukey Kramer's tests).

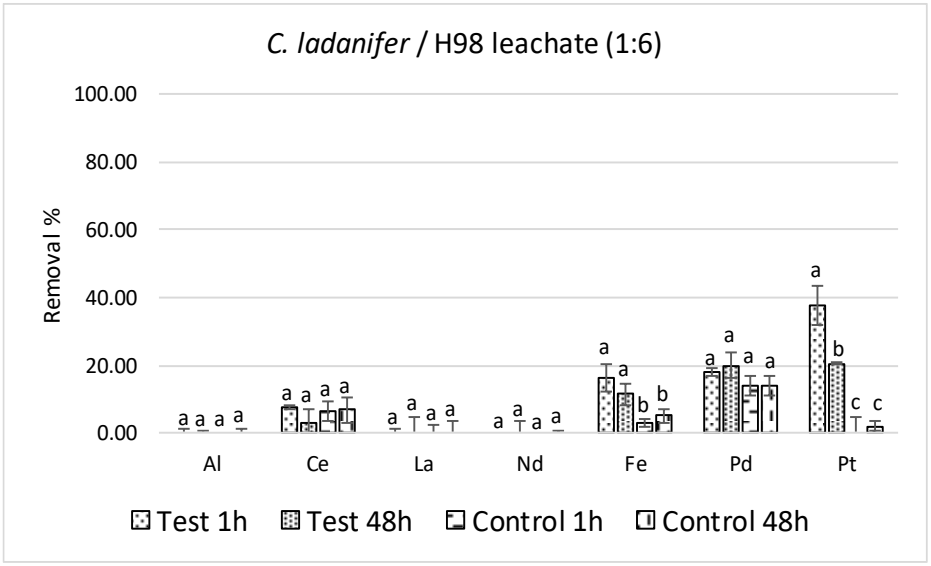
C. ladanifer / H98 leachate (1:6)
Removal %
100.00
80.00
60.00
40.00
20.00
0.00
Al
Ce
La
Nd
Fe
Pd
Pt
Test 1h
Test 48h
Control 1h
Control 48h

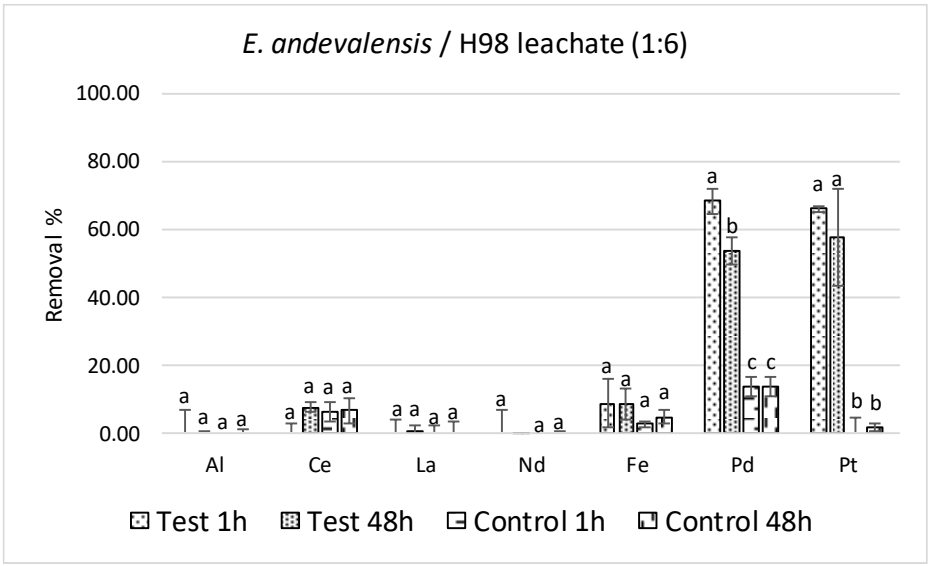
E. andevalensis / H98 leachate (1:6)
Removal %
100.00
80.00
60.00
40.00
20.00
0.00
Al
Ce
La
Nd
Fe
Pd
Pt
Test 1h
Test 48h
Control 1h
Control 48h

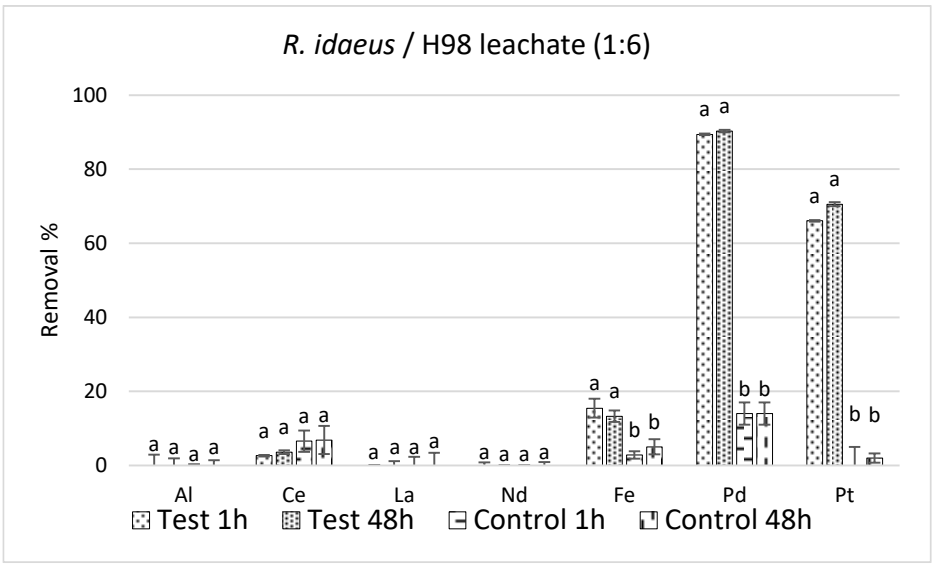
R. idaeus / H98 leachate (1:6)
Removal %
100
80
60
40
20
0
Al
Ce
La
Nd
Fe
Pd
Pt
Test 1h
Test 48h
Control 1h
Control 48h

Figure 5.3. Removal of main metals present in the diluted (1/6 (v/v)) H98 leachate solution, achieved after 1 h and 48 h addition of *C. ladanifer*, *E. andevalensis* and *R. idaeus* 70% ethanolic extracts at a 1/1 (v/v) ratio at room temperature (25 ± 3 °C). Results for controls, consisting of the addition of just 70% ethanol (without plant extract), are included. Removals with the same letters do not significantly differ at 0.05 level (ANOVA and Tukey Kramer's tests).

5.3.3. PGMs recovery mechanism

The high percentages of precipitation achieved in the unimetallic solutions containing Pd^{2+} and Pt^{2+} by addition of 70% ethanolic extracts of leaves from *R. idaeus*, and the particularly high and selective precipitations achieved for those metals in the HCl based leachate from the H98 spent ACC with these extracts, might have been caused by two different phenomena: the reduction of the soluble ions of these metals into their metallic/elemental state and aggregation in nanoparticles, caused by the known high reducing properties of plant extracts, and/or the specific binding of these ions to some plant compounds resulting in their precipitation. Pd^{2+} and Pt^{2+} ions have higher reduction potential compared to other metals, as it can be seen in metals' reduction potential tables published by Bratsch (1989) and Bard et al. (1985). Moreover, several works revealing the ability of different plants hydroalcoholic extracts to reduce and form Pd nanoparticles have been published (Khodadadi et al. 2017; Seyedi et al. 2018; Rostami-Vartooni et al. 2019).

5.3.3.1. UV–Visible Spectroscopy

The UV-visible spectra analysis is a helpful tool for the determination of the metal precursors' reduction (Zhang et al. 2007; Borodko et al. 2010). In this study, reduction of the Pd^{2+} ion was tracked by assessing the absorbance spectra in the optical range from 300 to 700 nm on the following samples: (i) a 100 mg/L Pd^{2+} solution in 0.02 M HCl, (ii)

the *R. idaeus* extract added in a 5% (v/v) ratio to a 0.02 M HCl solution, and (iii) the *R. idaeus* extract added in a 5% (v/v) ratio to the 100 mg/L Pd^{2+} solution in 0.02 M HCl (Figure 5.4).

The initial Pd^{2+} bearing solution has high absorbance at 300 nm, which decays as the wavelength raises to ~350 nm, and then one peak occurs at approximately 397 nm. With the plant extract the absorbance at 300 nm is even higher, probably due to the presence of plant compounds, but it also decays continuously as the wavelength raises and the peak at 397 nm does not exist. In the mixture with *R. idaeus* extract added to the Pd^{2+} solution, the previously observed peak at 397 nm in the Pd^{2+} solution disappears under a continuum absorption spectrum. Thus, this evolution of the absorption spectra could be due to a change of the Pd specimen and Pd nanoparticle formation, and/or change of plant compounds, and/or formation of complexes between Pd atoms and plant compounds. The peak at 397 nm has been attributed to the presence of Pd^{2+} ions and its disappearance under an increased continuum absorption spectra reported as an indication of Pd^{2+} ions reduction into Pd^{0} nanoparticles (Kumar Petla et al. 2012). The continuum absorption of UV-visible spectra in the solution containing Pd^{0} nanoparticles is due to the Surface Plasmon Resonance (SPR) of the Pd^{0} nanoparticles (Mulvaney 1996).

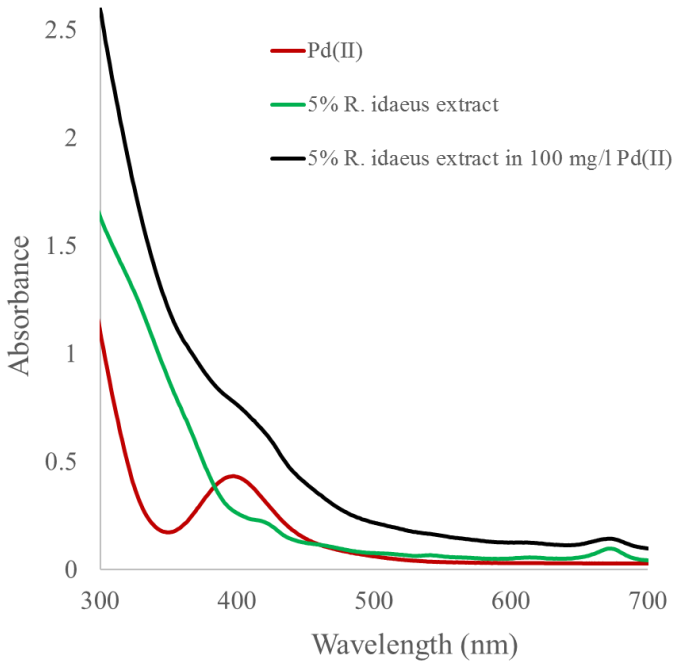

Figure 5.4. UV-Visible spectrum of (red) 100 mg/L Pd^{2+} solution in 0.02M HCl, (green) *R. idaeus* extract added in a 5% (v/v) ratio to a 0.02 M HCl solution (1 hour after mixing), and (black) *R. idaeus* extract added in a 5% (v/v) ratio to the 100 mg/L Pd^{2+} solution in 0.02 M HCl (1 hour after mixing at room temperature (25 ± 3 °C)).

5.3.3.2. Fourier Transform Infrared Spectroscopy

FTIR analysis was performed for the detection of biomolecules' functional groups present in the *R. idaeus* hydroalcoholic extract that were possibly associated to bio-reduction of Pd^{2+} ions and stabilization of the formed Pd^{0} nanoparticles. Figure 5.5 presents the FTIR spectra of *R. idaeus* extract before and after reaction with Pd^{2+} ions.

The spectra of the *R. idaeus* extract before the reaction revealed several peaks in different regions, suggesting the complex nature of the biomolecules present in the extract: the peaks appearing at 1059, 1098 and 2989 cm^{-1} correspond to the ethanol (Silverstein and Webster 1997), which is the solvent of the plant extract, while the peaks observed at 841,

890, 1462, 1691, 1920, 2138, 2505 and 3578 cm^{-1} correspond to plant compounds. After the mixture of *R. idaeus* extract with Pd^{2+} solution, some peaks corresponding to functional groups of plant compounds were shifted to a higher wavenumber. The curve of the *R. idaeus* extract showed a peak at 841 cm^{-1}, corresponding to the C-Cl stretching in the alkyl halides, that after the reaction with Pd^{2+} solution shifted to 848 cm^{-1}. The peak at 890 cm^{-1} changed to 891 cm^{-1} and is attributed to the C=C bending in alkenes. A weak band observed at 1462 cm^{-1} shifted to 1463 cm^{-1}, indicating the involvement of the C-H bending of the methylene group existing in the plant extract. Another peak at 1691 cm^{-1}, related to (NH)C=O and/or C=O stretching vibrations groups of conjugated aldehydes and carboxylic acids, changed to 1694 cm^{-1}, suggesting the participation of some phenolic acids or organic acids (Lu and Hsieh 2012) mainly as ellagic acids (Oszmiański et al. 2011) in the bio-reduction of Pd^{2+} ions. Moreover, three peaks at 1920, 2138 and 2505 cm^{-1}, that correspond to C-H bending of the aromatic compounds, N=C=N stretching of the carbodiimide group and S-H stretching in the thiol group respectively, were vanished after the reaction of plant extract with Pd^{2+} solution. The C-H bending of the aromatic compounds observed at 1920 cm^{-1} could be related to the presence of high concentrations of phenolic compounds in the *R. idaeus* extract including flavonoids, tannins and anthocyanins as reported by Veljković et al. (2018). Moreover, the band observed at 2138 cm^{-1} is related to N=C=N stretching of the carbodiimide group and might be an indication of the amino acids or proteins (Fiehn et al. 2000) and/or anthocyanin (Demirbas et al. 2019; Ekrikaya et al. 2021). The peak observed at 2505 cm^{-1} of S-H stretching in the thiol group could be related to the cysteine rich phytochemicals (Harada et al. 2002) and/or metallothioneins (Leszczyszyn et al. 2013), since both are known for their high metal interaction potential (Nobahar et al. 2021). The presence of high levels of cysteine in *R. idaeus* hydroalcoholic extract has been previously reported by (Komisarenko et al. 2021). The band observed at 3578 cm^{-1} can be related to the –OH vibrations of phenols, carboxylic acids or alcohols and/or -NH vibrations of proteins, peptides and amines.

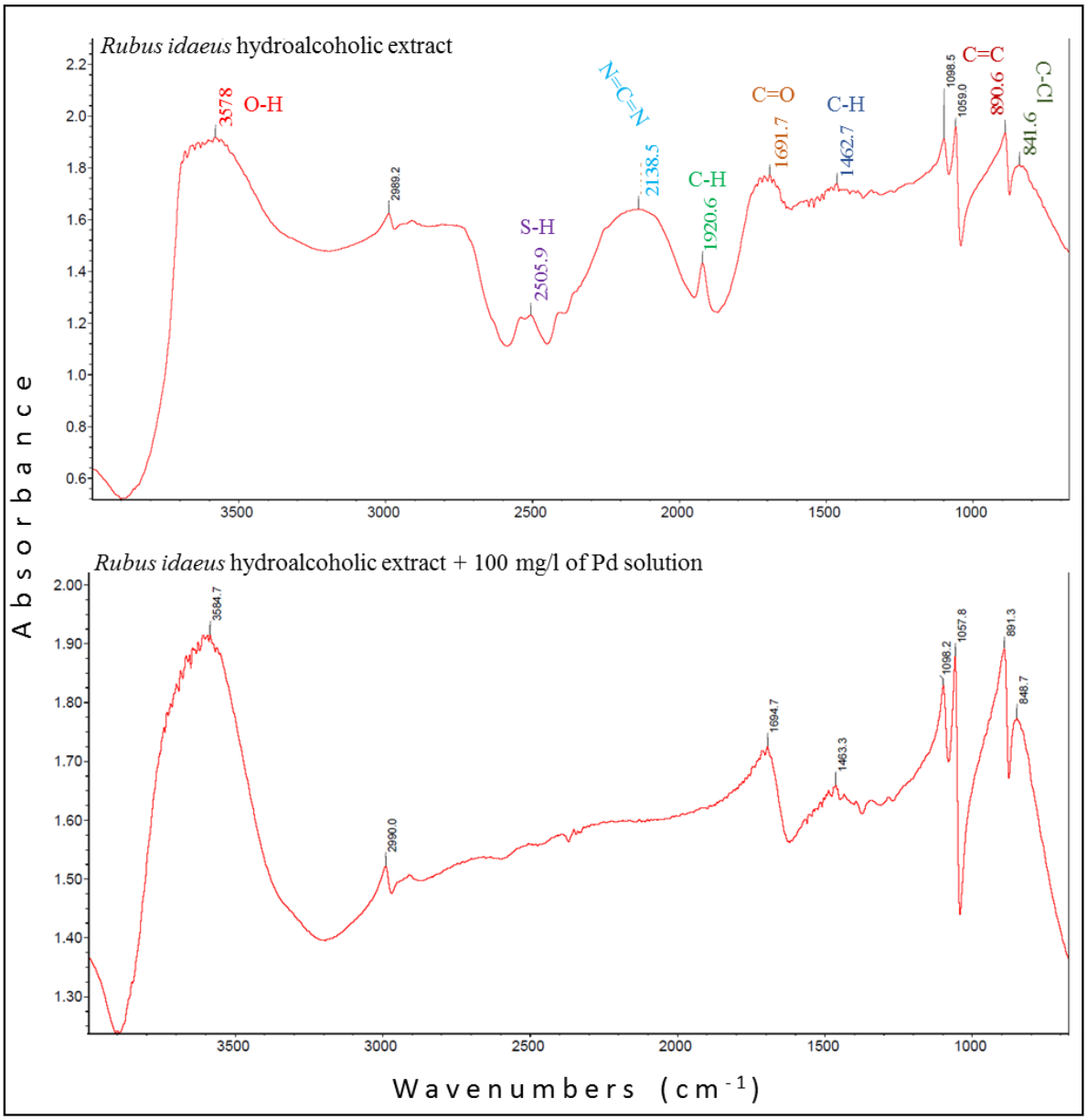

Figure 5.5. FTIR spectra of (above) *R. idaeus* hydroalcoholic extract diluted for analysis to a 15% (v/v) ratio in 0.02M HCl and (below) *R. idaeus* extract added in a 50% (v/v) ratio to a 100 mg/L Pd^{2+} solution in 0.02 M HCl and 1 hour after mixing diluted for analysis to a 7.5% (v/v) ratio in 0.02 M HCl at room temperature (25 ± 3 °C).

The presence of high contents of polyphenols (2.6% to 6.9% (w/w)) in the *R. idaeu*s dried leaves, principally as ellagic acids, is described in the literature (Oszmiański et al. 2011; Moreno-Medina et al. 2018). The second compound with high abundancy in *R. idaeus* leaves are known to be flavonoids, ranging from 0.46% to 1.05% of the dried leaves (w/w) (Gudej 2003). Based on a study by (Oszmiański et al. 2011), a major fraction of the phenolic content of *R. idaeus* leaves is reported as flavonoids, comprising about 11% of the leaf extract powder weight. In addition, some other phenolic compounds such as caffeic and chlorogenic acid (Durgo et al. 2012), p-coumaric, ferulic, protocatechuic, gentisic, caffeoyltartaric, feruloyl tartaric, p-coumaroyl-glucoside acids, p-hydroxybenzoic, vanillic acids (Brandely 2006), as well as terpenoids including mono- and sesquiterpenes, like terpinolene and triterpenes, squalene and cycloartenol, are reported in *R. idaeus* leaves (Kylli 2010; Committee on Herbal Medicinal Products (HMPC) 2012).

In a study similar to the one here reported, Nasrollahzadeh et al. (2015) used hydroalcoholic leaf extract of *Hippophae rhamnoides* Linn with an aqueous solution of $PdCl_2$ and reported the synthesis of stable Pd^0 nanoparticles, suggesting that OH functional groups, carbonyl groups, stretching aromatic rings and C-OH stretching vibrations present in the structure of phenols and flavonoids of the plant extract may have had the most important role in Pd^{2+} reduction and stabilization of the synthesized Pd^0 nanoparticles. Some other reports have also described different types of plant compounds in the groups of phenols (Behnia et al. 2019) and polyphenols (Ho Kim and Nakano 2005; Kim et al. 2007; Morisada et al. 2011; Khan et al. 2017) with high tendency to bind specifically to PGMs.

Moreover, there are some known interaction mechanisms of phenolic compounds with metals; for instance, the high potential of free radical scavenging through phenols' functional groups, as well as their electron or proton donation capacity, are substantial in their metal interaction capacities (Kaurinovic and Vastag 2019). Moreover, metal interaction properties of phenols are also explained by the presence of nucleophilic

aromatic rings in conjunction with some functional groups such as carbonyl, carboxyl and hydroxyl groups (Kulbat 2016; Liu et al. 2018).

5.3.4. Characterization of the particles

5.3.4.1. Particles washed with ethanol

The precipitates resulting from the highest PGMs recovery obtained by mixing the 70% ethanolic extract of *R. idaeus* with the H98 leachate were washed twice with 96% ethanol aiming the removal of organic residues. Thereafter, the elemental composition of the particles was examined using SEM-EDX mapping. This analysis revealed that apart from the O and C of the plant compounds, which are spread throughout the area, Pd appears to be alone in some particles and together with Cl and Na in other particles, while Ce seems to be always together with P and Al (Figure S- 5.1). These three types of particles were selected for point analysis to study in more detail their elemental composition (Figure S-5.2). At spot 1, apart from O and C, the main estimated normalized atomic percentages were 0.22% for Pd, 6.45% for Na and 7.77% for Cl, while at spot 2 they were 2.27% for Pd, 1.66% for Na and 1.51% for Cl. Thus, the co-occurrence of Pd with Cl and Na in the two spots might be due to the grouping of NaCl and Pd^0 particles in the same aggregate and not due to the presence of a compound formed by the three elements, since in spot 1 and 2, Cl and Na were found in approximately the same ratios, most possibly as NaCl, while Pd was in these two spots at different ratios with these elements. At spot 3, the point analysis revealed, apart from O and C, the following main atomic normalized abundances: 0.73% of Ce, 1.51% Na, 1.47% Al, 1.35% P, and a minor quantity of La (0.14%), an element which usually occurs together with Ce that was present in the H98 leachate. Probably some biomolecules from the plant leaves have bonded to these metal ions or their metal salts, making stable compounds. Indeed, it is known that many plant compounds can form stable complexes with metal ions or metal complexes generating precipitates (Nobahar et al. 2021). For example, it has been reported that plant extracts

can induce the formation of CeO_2 (Rajeshkumar and Naik 2018), Al_2O_3 (Ghotekar 2019) and La_2O_3 (Dabhane et al. 2020). However, according to Singh et al. (2020), the CeO_2 particle formation by plant extracts requires high temperatures, and, therefore, Ce particles are most probably not formed as CeO_2. Moreover, the co-occurrence of Ce, P and Al in large particles could indicate the presence of a mineral with the three elements, or a complex structure of different minerals aggregated with plant compounds. The presence of these elements in the same particles opens the possibility of Florencite-(La) ($(La,Ce)Al_3(PO_4)_2(OH)_6$) and/or Florencite-(Ce) ($CeAl_3(PO_4)_2(OH)_6$). Yet, there are other possible explanations. The observed phenomena could be complex/chelate formation of those elements with P rich phytochemicals, which then bind forming aggregates due to molecular interactions, or the presence of P could also indicate that Ce and Al appear as interspersed metal phosphate salts.

In these particles, C and O were found as the main constituents (60-70% C and 20-35% O of normalized atomic abundances) (Figure S- 5.2), indicating the presence of high contents of organic material in the particles. This could be explained by (i) the reactivity of some plant compounds with Pd ions, reducing them into Pd^0 nanoparticles and finally binding to the particles and acting as stabilizing agents (Ghosh et al. 2021), (ii) interaction of plant compounds with the other metal ions present in the leachate and (iii) insolubility of a part of the plant compounds in the acidic conditions of the leachate. However, the existence of plant material as main constituent of the particles may be unfavorable for future applications. Therefore, after the washing steps with 96% ethanol the particles were subjected to further two cycles of washing with pure acetone followed by centrifugation.

5.3.4.2. Particles washed with ethanol and acetone

The STEM-EDX mapping of the final particles (Figure 5.6) showed strong Pd signals coincident with the particles' positions, while the signals of the remaining elements detected (Cl, Na, Pt, Ce, P, Al and Fe) were weak and spread throughout all the area. This

shows that the washing steps with acetone efficiently solubilized a major part of the plant compounds, which led to the solubilization of contaminant particles, thus leaving the Pd^0 particles better purified.

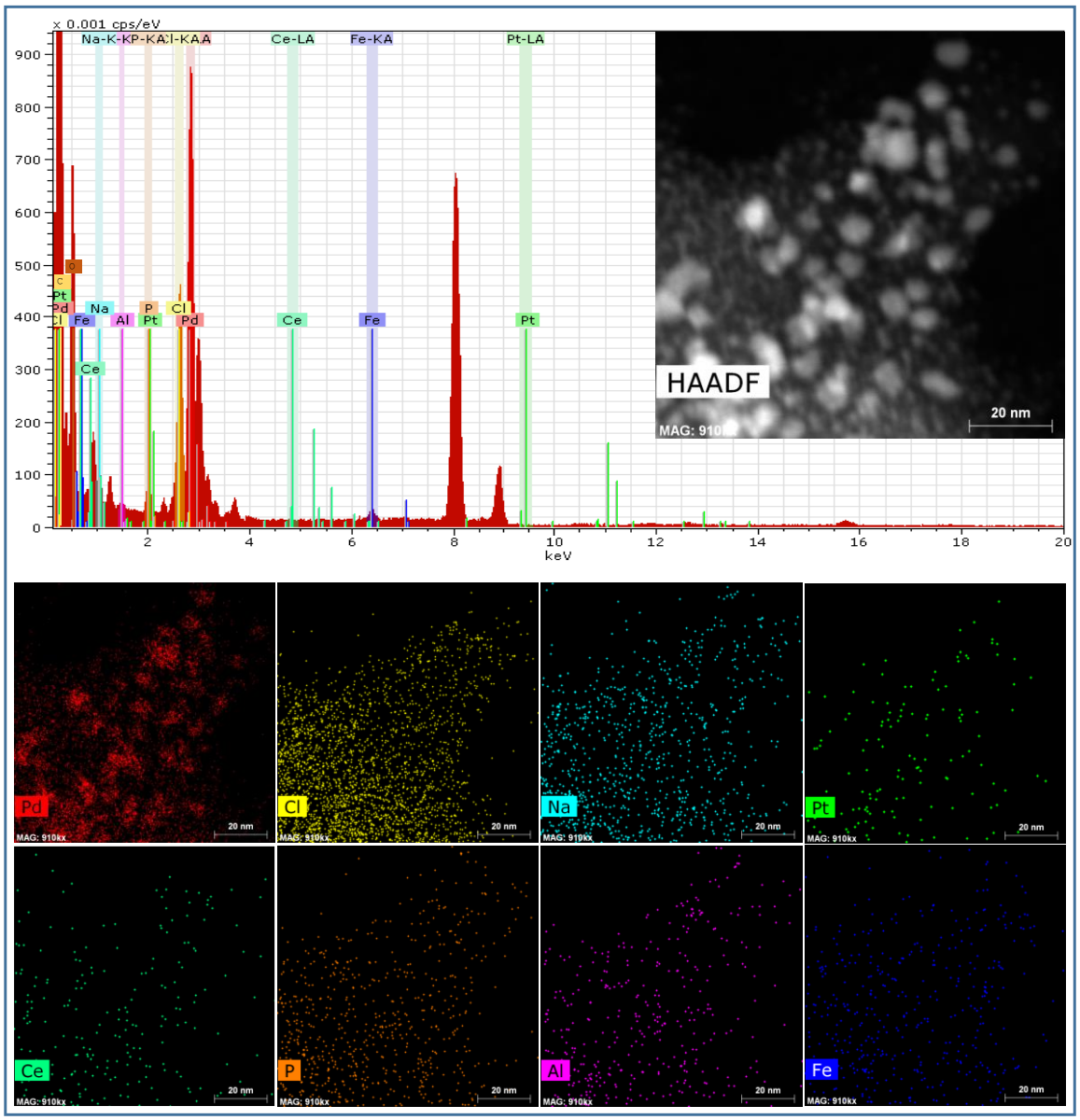

Figure 5.6. STEM image of Pd nanoparticles obtained by adding 70% ethanolic extract of *R. idaeus* to the H98 leachate and corresponding EDX elemental mapping of Pd, Cl, Na, Pt, Ce, P, Fe and Al. Precipitates washed twice with ethanol, then two times with

acetone and dry before analysis. Strong signal for Pd matching the particles; strong signal from Cl scattered in all the area with precipitates; and relatively weak signals for other elements in the spaces between particles.

The relative abundances of elemental composition determined by STEM-EDS spectra from the whole area of one image (Figure S- 5.3) confirmed the particles purity (Table 5.2). Approximately 30% of the normalized atomic abundances corresponds to Pd, while the other metals have normalized atomic abundances between 0.3% and 3.4. In addition, ~40% corresponds to O and ~15% to Cl, which may be from phytochemicals of the plant extract and/or the acidic matrix of the leachate. Si concentration was not analyzed during the leaching experiments (Paiva et al. 2022). However, the detection of this metal in the final precipitate indicates its leaching from the ACCs monoliths as suggested by Abo Atia et al. (2021), and subsequent precipitation by phytochemicals.

Table 5.2. Normalized weight and atomic abundances of different elements present in the final precipitate determined from quantitative spectra analysis by STEM-EDX on the whole area of Figure S- **5.3**.

Element	[norm. wt.%]	[norm. at.%]
O	13.0	40.3
Pd	64.9	30.3
Ce	1.5	0.5
Pt	1.1	0.3
Fe	1.3	1.2
Al	0.9	1.6
Na	1.6	3.4
Cl	10.6	14.8
P	1.4	2.2
Si	1.4	2.4
Ca	2.5	3.0
Sum	100	100

The STEM images revealed particles with sizes below 20 nm, thus confirming the recovery of Pd as nanoparticles. The synthesized Pd nanoparticles were then analyzed with high-resolution scanning transmission microscopy (HRSTEM) for further characterization on the atomic scale. HRSTEM analysis of the particles showed very tiny Pd nanoparticles well dispersed with no aggregate formation. HRSTEM images revealed that the morphology of the nano-sized particles is generally quasi-spherical (Figure 5.7-A, B and D). Sizes of a total of 265 particles were automatically measured in HRSTEM images by ParticleSizer v1.0.9 plugin (Wagner and Eglinger 2021) on the Fiji-ImageJ software (Schindelin et al. 2012), revealing particles varying from 2.5 to 17 nm, with a Feret size average of 6 ± 2 nm, and fitting a normal distribution (for a 1% probability (α=0.01) in a Kolmogorov-Smirnov test) (Figure 5.7-C). The presence of well stabilized and dispersed tiny nanoparticles could be due to the effectiveness of phytochemicals present in *R. idaeus* extract to act as capping and stabilizing agents. Finally, some HRSTEM images showed well defined adjacent lattice fringes on the particles (Figure 5.7-D) and the fast Fourier transform (FFT) pattern of a selected particle revealed diffraction spots indicating an interplanar lattice distance of ~0.22 nm (Figure 5.7-E), which is characteristic of (111) planes (Cheong et al. 2010; Sarıbıyık et al. 2020). In addition, the Selected Area Electron Diffraction (SAED) pattern of the same particle (Figure 5.7-F) confirmed the crystalline nature of the nanoparticles. Thus, this work confirms the potential application of *R. idaeus* extracts for valuable metals nanoparticles synthesis with high stability, as previously reported by Singh et al. (2020) for silver, and by (Demirbas et al. 2019).

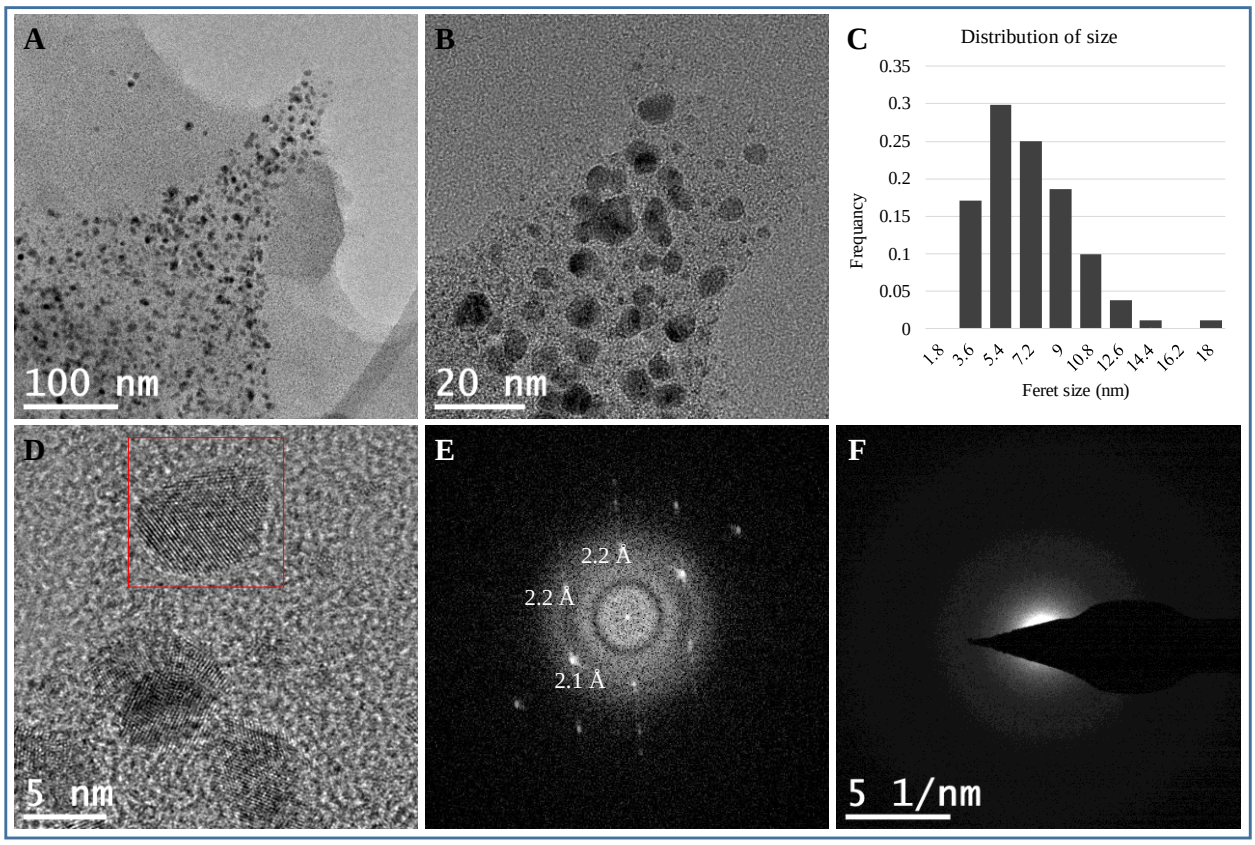

Figure 5.7. A, B) TEM images of the Pd nanoparticles obtained by adding 70% ethanolic extract of *R. idaeus* to the H98 leachate C) histogram representing the size distribution of Pd nanoparticles, D) magnified high resolution TEM with lattice fringes visible on the particles, E) Fast Fourier Transform (FFT) pattern of a single nanoparticle (red square in figure D) and F) selected-area electron diffraction (SAED) patterns of the same nanoparticle, with visible spectra profile rings. Precipitates washed twice with ethanol, then two times with acetone and were dried before analysis.

5.3.4.3. Economic & environmental perspectives

Concerning the economic and environmental aspects, it is crucial to understand the balance between material, energy flow and waste generation (Kliestik et al. 2020; Maroušek and Trakal 2022). Hydrometallurgical processes using HCl-based leaching

solvents with high PGMs recovery rates, such as the method employed to prepare the leachates used in this study, are considered Mild and Green systems economically favorable since no hazardous gas or by-products are generated and low temperature reactions are used (Karim and Ting 2021; Yakoumis et al. 2021). For example Hereaus, Germany, which is one of the PGM refining corporations from spent ACCs in the Europe, employs hydrometallurgical processes including HCl-H_2O_2 leaching process (Jha et al. 2013; Padamata et al. 2020).

Regarding the PGMs separation from the leaching solution, different methods that are described in the literature can be employed, such as reduction, chemical precipitation, solvent extraction etc. (Saguru et al. 2018). Some of these methods are described for their high recovery efficiency, however, there is always space for improvements in economic and environmental aspects (Karim and Ting 2021). For example, PGMs solvent extraction results obtained with model solutions are usually more promising than the application of the solvents to real leaches, and PGMs solvent extraction reports with real spent ACCs leachates are generally still missing in recent literature (Paiva et al. 2022). Moreover, solvent extraction makes use of organic extractants (e.g. Aliquat 336 and Cyanex 301) and solvents to dilute them (e.g. Kerosene) which have a cost, and after a certain time of use require waste management (Yakoumis et al. 2021). Both leachates used in this work, I95 and H98 leachates, have already been used for solvent extraction experiments by several commercial extractants and the results showed that the most promising were Cyanex® 471X and Cyphos® IL 101, with extraction efficiencies over 99%. However, in both cases there was a high (>99%) co-extraction of iron, which could not be totally removed from the extractant before Pd stripping, and the final stripping efficiencies of Pd were low (<50%) (Paiva et al. 2022). The method proposed in this study uses an ethanolic extract of *R. idaeus* leaves, which are agricultural wastes, for the separation of the Pd from the solution as nanoparticles. Thus, it eliminates the need to purchase extractants and their solvents. Plus, leaves obtained for free as a waste can be air dried before grinding for extract preparation. Table 5.3, summarizes the approximate

operational costs of the proposed method regarding the PGM leaching and recovery from spent ACCs.

Table 5.3. Approximate operational costs for PGMs recovery from ACCs as Pd nanoparticles (except manpower).

Reagents and operations	**Demand / Kg ACC honeycomb**	**Processing cost / Kg ACC honeycomb (€)**	**Source**
		Leaching step	
Honeycombs grinding	0.2 KW	0.05	(according to Power input needed on the used grinder - MF 10 basic Microfine
11.6 M HCl (37 %)	2 L	7.44	https://www.chemicals.co.uk/hydrochloric-acid
30 % H2O2	0.07 L	0.3	https://www.chemicals.co.uk/hydrogen-peroxide-tech
60℃ temperature for 3	2.4 KW	0.53	(according to Power input needed on the heater MR Hei-Tec from Heidolph)
		Extract preparation and precipitate washing	
R. idaeus leaves	1.2 Kg	Free (agricultural waste)	-
Leaves grinding (electricity)	0.28 KW	0.06	(according to Power input needed on the coffee grinder)
70% ethanol for plant extract	12 L	21	https://www.laballey.com/products/ethanol-190-proof-denatured-sda-3a-reagent?variant=36012350701723
96% ethanol for Pd particles washing	0.86 L	2.23	
Acetone for Pd particles washing	0.86 L	7.7	https://www.laballey.com/products/acetone-lab?variant=40856192024731
	Sum	39.31	

In order to evaluate the financial viability of process it is necessary to predict the process costs per weight of recovered product. The average Pd content in ACCs is considered as ~1580 mg per ACC and the average weight of honeycombs in each ACC is about 0.737 Kg (Yakoumis et al. 2018). The leaching step proposed in this study allows a recovery efficiency of ~99% (Paiva et al. 2022); thus, ~2.14 g of Pd can be leached per Kg of ACC combs. Afterwards, ~1.93 of Pd nanoparticles can be recovered from that leachate using an extract of *R. idaeus* leaves, according to the ~90% separation efficiency achieved in our work. Therefore, the estimated operation cost (Table 5.3) expressed per weight of recovered product is 20.36 € (or 19.87 $ on 23 Sept. 2022) / g of Pd particles. It must be said that this cost estimate is based on non-negotiated prices and relatively small quantities. It is likely possible to lower costs with more thorough market research and negotiations for bulk orders.

In this method, not only Pd is separated from the solution, but Pd nanoparticles are produced, which rises the financial viability of the process. For example currently, the price of metallic Pd in the stock market is about 2000 $ per ounce (~ 65 $ per gram) (https://www.goldpriceoz.com/palladium/palladium-price-per-gram/), while the price per gram of highly pure (>99.5%) Pd nanoparticles with sizes <1 μm is 191 $ (https://www.sigmaaldrich.com/PT/en/product/aldrich/326666) and <25 nm is 1942 $ (https://www.sigmaaldrich.com/PT/en/product/aldrich/686468). Even though the produced Pd nanoparticles in this study have much less purity, ~75% excluding oxygen (Table 5.2), they have still various application potentials due to their very small size (2.5-17 nm) and large surface area. Therefore, the price of the synthesized nanoparticles can be significantly higher than metallic Pd, enhancing the financial viability of the process. Indeed, there are a wide range of applications known for Pd nanoparticles that may require different levels of purity, as for example: photocatalytic activity of phenol red dye (Kora and Rastogi 2018), removal of pathogenic microbes from wastewaters (Mishra et al. 2019), catalytic reduction of 4-nitrophenol (Tuo et al. 2017), decomposition of methyl

orange (Ahmed et al. 2018) to bio-sensing, fuel cells, and other fields (Mubeen et al. 2007; Wang et al. 2012; Azharuddin et al. 2019).

To enhance the financial feasibility of the process, other PGMs (Pt and Rh), or even other metals with market value (Ce, La, Nd), that may be preset in the leachate can be recovered by a previous or subsequent application of other methods such as molecular recognition technology (Zheng et al. 2021) or ion exchange and chelating resins (Lee et al. 2020).

5.4. **Conclusions**

The current study reinforces the idea that plant extracts include a variety of compounds with different metal binding potentials and their interactions through different mechanisms results in metals precipitation. It was found that 70% ethanolic extracts from leaves of *R. idaeus* can induce high precipitation of Pd^{2+} and Pt^{2+} ions from aqueous solutions, thus suggesting potential use of polar extracts for the recovery of these metals from different metal bearing waters. More specifically, it was demonstrated that the addition of such extracts from *R. idaeus* leaves to spent ACC leachates can induce the production of a precipitate containing agglomerates of particles (of sizes up to 10 μm) having Pd and other elements such as Na, Cl, Ce, P and Al, along with plant material, which after washing with acetone results in a purified (~75%) precipitate with Pd^0 nanoparticles (6 ± 2 nm) and traces of those other elements present in the spaces between particles.

The method allows to recover ~90% of Pd from the spent ACCs leachates which is comparable with the lowest efficiencies generally achieved by solvent extraction (90 – 99%). Therefore, there is place for improvement aiming higher recovery efficiencies. Yet, the process is highly environmentally friendly, cost efficient (rough cost estimate = ~20 $ / g of Pd particles – excluding manpower) and relatively fast (~1h reaction). *R. idaeus* is an agricultural crop widely cultivated in Europe, Asia and North America for its fruits, and its leaves are the main waste of the fruits' harvesting, and therefore is available in

large quantities. The method developed in this study using ethanolic extracts of these wastes could be applied for Pd^0 nanoparticles synthesis from both unimetallic Pd^{2+} solutions and multimetallic leachates. In the first case, such green synthesis would produce pure Pd^0 nanoparticles without other metals as contaminants. In the second case, the produced Pd^0 nanoparticles would have a certain level of contamination with other metals', depending on the composition of the used leachate.

Regarding the Pd recovery mechanism, after taking all the studies of this work into account, it can be suggested that the involved mechanism in Pd recovery from the solution as nanoparticles was neither adsorption or precipitation, since in both cases, Pd nanoparticle formation is not possible and all Pd recovered from the solution with phytochemicals would have been washed out along with phytochemicals from the precipitates during washing steps with ethanol and acetone. Thus, the most probable mechanism involved in Pd recovery is reduction, since results in the UV-visible spectroscopy revealed signs of Pd^{2+} reduction and Pd nanoparticle formation. Moreover, FTIR analysis revealed changes after mixing the Pd^{2+} solution with plant extract in different functional groups (such as OH group) that are mainly related to phenols and polyphenols and flavonoids, which are known as compounds with high capacity to reduce PGM.

For the improvement of the technology aiming a highly sustainable circular economy more investigations are required, including: improvement of phytochemicals extraction by more available and cheaper extractants, mainly as water; combining other recycling methods to recover Pt and Rh, etc.; optimization of the metallic particles washing steps to minimize the amount of solvents used; identification of the main bio-active compounds interacting with Pd followed by their purification from the extract; applying the proposed process to other ACC leaching solutions such as those from bioleaching.

5.5. References

Abo Atia T, Wouters W, Monforte G, Spooren J (2021) Microwave chloride leaching of valuable elements from spent automotive catalysts: Understanding the role of hydrogen peroxide. Resour Conserv Recycl 166:105349. https://doi.org/10.1016/j.resconrec.2020.105349

Abreu MM, Santos E, Fernandes E, et al (2011) Accumulation and translocation of trace elements in Cistus ladanifer L. from IPB portuguese mining areas. Revista de Ciências Agrárias 45–56

Abreu MM, Tavares MT, Batista MJ (2008) Potential use of Erica andevalensis and Erica australis in phytoremediation of sulphide mine environments: São Domingos, Portugal. J Geochem Explor 96:210–222. https://doi.org/10.1016/j.gexplo.2007.04.007

Ahmed E, Kalathil S, Shi L, et al (2018) Synthesis of ultra-small platinum, palladium and gold nanoparticles by Shewanella loihica PV-4 electrochemically active biofilms and their enhanced catalytic activities. J Saudi Chem Soc 22:919–929. https://doi.org/10.1016/j.jscs.2018.02.002

Arsiya F, Sayadi MH, Sobhani S (2017) Green synthesis of palladium nanoparticles using Chlorella vulgaris. Mater Lett 186:113–115. https://doi.org/10.1016/j.matlet.2016.09.101

Atarod M, Nasrollahzadeh M, Mohammad Sajadi S (2016) Green synthesis of Pd/RGO/Fe3O4 nanocomposite using Withania coagulans leaf extract and its application as magnetically separable and reusable catalyst for the reduction of 4-nitrophenol. J Colloid Interface Sci 465:249–258. https://doi.org/10.1016/j.jcis.2015.11.060

Azharuddin M, Zhu GH, Das D, et al (2019) A repertoire of biomedical applications of noble metal nanoparticles. Chem Commun 55:6964–6996. https://doi.org/10.1039/C9CC01741K

Bahaloo-Horeh N, Mousavi SM (2022) A novel green strategy for biorecovery of valuable elements along with enrichment of rare earth elements from activated spent automotive catalysts using fungal metabolites. J Hazard Mater 430:128509. https://doi.org/10.1016/j.jhazmat.2022.128509

Bard AJ, Parsons R, Jordan J (1985) International Union Of Pure And Applied Chemistry. N Y M Dekker

Behnia A, Fard MA, Boyle PD, Puddephatt RJ (2019) Complexes Containing a Phenol-Platinum(II) Hydrogen Bond: Synthons for Supramolecular Self-Assembly and Precursors for Hydridoplatinum(IV) Complexes: Complexes Containing a Phenol-Platinum(II) Hydrogen Bond: Synthons for Supramolecular Self-Assembly and Precursors for Hydridoplatinum(IV) Complexes. Eur J Inorg Chem 2019:2899–2906. https://doi.org/10.1002/ejic.201900480

Benson M, Bennett CR, Harry JE, et al (2000) The recovery mechanism of platinum group metals from catalytic converters in spent automotive exhaust systems. Resour Conserv Recycl 31:1–7. https://doi.org/10.1016/S0921-3449(00)00062-8

Borodko Y, Lee HS, Joo SH, et al (2010) Spectroscopic Study of the Thermal Degradation of PVP-Capped Rh and Pt Nanoparticles in H_2 and O_2 Environments. J Phys Chem C 114:1117–1126. https://doi.org/10.1021/jp909008z

Brandely P (2006) Raspberry leaf. In British Herbal Compendium. A Handbook of Scientific Information on Widely Used Plant Drugs. British Herbal Medicine Association, Bournemouth, UK

Bratsch SG (1989) Standard Electrode Potentials and Temperature Coefficients in Water at 298.15 K. J Phys Chem Ref Data 18:1–21. https://doi.org/10.1063/1.555839

Cabezudo B, Rivera J (1980) Notas taxonómicas y corológicas sobre la Flora de Andalucía occidental. 2: Erica andevalensis Cabezudo y Rivera sp. nov. Lagascalia 9:223–226

Cheong S, Watt JD, Tilley RD (2010) Shape control of platinum and palladium nanoparticles for catalysis. Nanoscale 2:2045. https://doi.org/10.1039/c0nr00276c

Committee on Herbal Medicinal Products (HMPC) (2012) Assessment Report on Rubus idaeus L., Folium.

Costa MC, Assunção A, da Costa AMR, et al (2013) Liquid-Liquid Extraction of Platinum from Chloride Media by Dimethyl-Dicyclohexyltetradecylmalonamide. Solvent Extr Ion Exch 31:12–23. https://doi.org/10.1080/07366299.2012.700588

Dabhane H, Ghotekar S, Tambade P, Medhane V (2020) Plant mediated green synthesis of lanthanum oxide (La2O3) nanoparticles: A review. Asian J Nanosci Mater 3:. https://doi.org/10.26655/AJNANOMAT.2020.4.3

Demirbas A, Büyükbezirci K, Celik C, et al (2019) Synthesis of Long-Term Stable Gold Nanoparticles Benefiting from Red Raspberry (*Rubus idaeus*), Strawberry (*Fragaria ananassa*), and Blackberry (*Rubus fruticosus*) Extracts–Gold Ion Complexation and Investigation of Reaction Conditions. ACS Omega 4:18637–18644. https://doi.org/10.1021/acsomega.9b02469

Dong H, Zhao J, Chen J, et al (2015) Recovery of platinum group metals from spent catalysts: A review. Int J Miner Process 145:108–113. https://doi.org/10.1016/j.minpro.2015.06.009

Durães N, Bobos I, Ferreira da Silva E, Dekayir A (2015) Copper, zinc and lead biogeochemistry in aquatic and land plants from the Iberian Pyrite Belt (Portugal) and north of Morocco mining areas. Environ Sci Pollut Res 22:2087–2105. https://doi.org/10.1007/s11356-014-3394-6

Durgo K, Belščak-Cvitanović A, Stančić A, et al (2012) The Bioactive Potential of Red Raspberry (*Rubus idaeus* L.) Leaves in Exhibiting Cytotoxic and Cytoprotective Activity on Human Laryngeal Carcinoma and Colon Adenocarcinoma. J Med Food 15:258–268. https://doi.org/10.1089/jmf.2011.0087

Ekrikaya S, Yilmaz E, Celik C, et al (2021) Investigation of ellagic acid rich-berry extracts directed silver nanoparticles synthesis and their antimicrobial properties

with potential mechanisms towards Enterococcus faecalis and Candida albicans. J Biotechnol 341:155–162. https://doi.org/10.1016/j.jbiotec.2021.09.020
Feng L, Yang J, Hu Y, et al (2012) Electrocatalytic properties of PdCeOx/C anodic catalyst for formic acid electrooxidation. Int J Hydrog Energy 37:4812–4818. https://doi.org/10.1016/j.ijhydene.2011.12.114
Fiehn O, Kopka J, Trethewey RN, Willmitzer L (2000) Identification of Uncommon Plant Metabolites Based on Calculation of Elemental Compositions Using Gas Chromatography and Quadrupole Mass Spectrometry. Anal Chem 72:3573–3580. https://doi.org/10.1021/ac991142i
Fornalczyk A, Saternus M (2011) Catalytic converters as a source of platinum. Metalurgija 261–264
Gaikwad AV, Rothenberg G (2006) In-situ UV-visible study of Pd nanocluster formation in solution. Phys Chem Chem Phys 8:3669. https://doi.org/10.1039/b604665g
Ghosh A, Hegde RV, Gholap SS, et al (2021) Green Pathways for Palladium Nanoparticle Synthesis: Application and Future Perspectives. In: Hussain CM, Shukla SK, Mangla B (eds) Functionalized Nanomaterials for Catalytic Application, 1st edn. Wiley, pp 303–328
Ghotekar S (2019) Plant extract mediated biosynthesis of Al2O3 nanoparticles- a review on plant parts involved, characterization and applications. Nanochemistry Res 4:. https://doi.org/10.22036/ncr.2019.02.008
Granados-Fernández R, Montiel MA, Díaz-Abad S, et al (2021) Platinum Recovery Techniques for a Circular Economy. Catalysts 11:937. https://doi.org/10.3390/catal11080937
Gudej J (2003) Kaempferol and quercetin glycosides from Rubus idaeus L. leaves. Acta Poloniae Pharmaceutica 60:313–316
Harada E, Yamaguchi Y, Koizumi N, Hiroshi S (2002) Cadmium stress induces production of thiol compounds and transcripts for enzymes involved in sulfur assimilation pathways in Arabidopsis. J Plant Physiol 159:445–448. https://doi.org/10.1078/0176-1617-00733
Hegde RV, Ghosh A, Jadhav AH, et al (2021) Biogenic synthesis of Pd-nanoparticles using Areca Nut Husk Extract: a greener approach to access α-keto imides and stilbenes. New J Chem 45:16213–16222. https://doi.org/10.1039/D1NJ02858H
Ho Kim Y, Nakano Y (2005) Adsorption mechanism of palladium by redox within condensed-tannin gel. Water Res 39:1324–1330. https://doi.org/10.1016/j.watres.2004.12.036
Hu H, Wang F, Ding X, et al (2022) Green fabrication of Pt nanoparticles via tea-polyphenols for hydrogen peroxide detection. Colloids Surf Physicochem Eng Asp 637:128201. https://doi.org/10.1016/j.colsurfa.2021.128201
Ilyas S, Srivastava RR, Kim H (2022) Mobilization of platinum and palladium from exhausted catalytic converters using bio-cyanide and an ionic-liquid as mass transport carriers. Green Chem 24:5204–5218. https://doi.org/10.1039/D2GC00874B

Ishak NAI, Kamarudin SK, Timmiati SN (2019) Green synthesis of metal and metal oxide nanoparticles via plant extracts: an overview. Mater Res Express 6:112004. https://doi.org/10.1088/2053-1591/ab4458

Ismail E, Kenfouch M, Dhlamini M, et al (2017) Green Biosynthesis of Rhodium Nanoparticles Via Aspalathus Linearis Natural Extract. J Nanomater Mol Nanotechnol 06: https://doi.org/10.4172/2324-8777.1000212

Izatt RM, Izatt SR, Izatt NE, et al (2015) Industrial applications of molecular recognition technology to separations of platinum group metals and selective removal of metal impurities from process streams. Green Chem 17:2236–2245. https://doi.org/10.1039/C4GC02188F

Jeon S, Tabelin CB, Park I, et al (2020) Ammonium thiosulfate extraction of gold from printed circuit boards (PCBs) of end-of-life mobile phones and its recovery from pregnant leach solution by cementation. Hydrometallurgy 191:105214. https://doi.org/10.1016/j.hydromet.2019.105214

Jha MK, Lee J, Kim M, et al (2013) Hydrometallurgical recovery/recycling of platinum by the leaching of spent catalysts: A review. Hydrometallurgy 133:23–32. https://doi.org/10.1016/j.hydromet.2012.11.012

Jimenez de Aberasturi D, Pinedo R, Ruiz de Larramendi I, et al (2011) Recovery by hydrometallurgical extraction of the platinum-group metals from car catalytic converters. Miner Eng 24:505–513. https://doi.org/10.1016/j.mineng.2010.12.009

Kannan R, Jang H-R, Yoo E-S, et al (2015) Facile green synthesis of palladium quantum dots@carbon on mixed valence cerium oxide/graphene hybrid nanostructured bifunctional catalyst for electrocatalysis of alcohol and water. RSC Adv 5:35993–36000. https://doi.org/10.1039/C5RA04226G

Karim S, Ting Y-P (2021) Recycling pathways for platinum group metals from spent automotive catalyst: A review on conventional approaches and bio-processes. Resour Conserv Recycl 170:105588. https://doi.org/10.1016/j.resconrec.2021.105588

Karim S, Ting Y-P (2022) Bioleaching of platinum, palladium, and rhodium from spent automotive catalyst using bacterial cyanogenesis. Bioresour Technol Rep 18:101069. https://doi.org/10.1016/j.biteb.2022.101069

Kaurinovic B, Vastag D (2019) Flavonoids and Phenolic Acids as Potential Natural Antioxidants. In: Shalaby E (ed) Antioxidants. IntechOpen

Khan M, Albalawi GH, Shaik MR, et al (2017) Miswak mediated green synthesized palladium nanoparticles as effective catalysts for the Suzuki coupling reactions in aqueous media. J Saudi Chem Soc 21:450–457. https://doi.org/10.1016/j.jscs.2016.03.008

Khodadadi B, Bordbar M, Nasrollahzadeh M (2017) Green synthesis of Pd nanoparticles at Apricot kernel shell substrate using Salvia hydrangea extract: Catalytic activity for reduction of organic dyes. J Colloid Interface Sci 490:1–10. https://doi.org/10.1016/j.jcis.2016.11.032

Kim Y-H, Ogata T, Nakano Y (2007) Kinetic analysis of palladium(II) adsorption process on condensed-tannin gel based on redox reaction models. Water Res 41:3043–3050. https://doi.org/10.1016/j.watres.2007.02.016

Kliestik T, Nica E, Musa H, et al (2020) Networked, Smart, and Responsive Devices in Industry 4.0 Manufacturing Systems. Economics, Management, and Financial Markets 15:

Komisarenko MA, Polischuk IM, Upyr TV, Saidov NB (2021) Study of Amino acid composition and immunomodulatory activity of Rubus idaeus alcoholic extract. Res J Pharm Technol 14:1329–1332. https://doi.org/10.5958/0974-360X.2021.00236.5

Kora AJ, Rastogi L (2018) Green synthesis of palladium nanoparticles using gum ghatti (Anogeissus latifolia) and its application as an antioxidant and catalyst. Arab J Chem 11:1097–1106. https://doi.org/10.1016/j.arabjc.2015.06.024

Kulbat K (2016) The role of phenolic compounds in plant resistance. 80:97–108

Kumar Petla R, Vivekanandhan S, Misra M, et al (2012) Soybean (Glycine Max) Leaf Extract Based Green Synthesis of Palladium Nanoparticles. J Biomater Nanobiotechnology 03:14–19. https://doi.org/10.4236/jbnb.2012.31003

Kumari R, Samadder SR (2022) A critical review of the pre-processing and metals recovery methods from e-wastes. J Environ Manage 320:115887. https://doi.org/10.1016/j.jenvman.2022.115887

Kylli P (2010) Berry phenolics : isolation, analysis, identification, and antioxidant properties. Doctoral dissertation, Helsingin yliopisto

Lanaridi O, Schnürch M, Limbeck A, Schröder K (2022) Liquid- and Solid-based Separations Employing Ionic Liquids for the Recovery of Platinum Group Metals Typically Encountered in Catalytic Converters: A Review. ChemSusChem 15:. https://doi.org/10.1002/cssc.202102262

Lebaschi S, Hekmati M, Veisi H (2017) Green synthesis of palladium nanoparticles mediated by black tea leaves (Camellia sinensis) extract: Catalytic activity in the reduction of 4-nitrophenol and Suzuki-Miyaura coupling reaction under ligand-free conditions. J Colloid Interface Sci 485:223–231. https://doi.org/10.1016/j.jcis.2016.09.027

Lee J, Kurniawan, Hong H-J, et al (2020) Separation of platinum, palladium and rhodium from aqueous solutions using ion exchange resin: A review. Sep Purif Technol 246:116896. https://doi.org/10.1016/j.seppur.2020.116896

Leszczyszyn OI, Imam HT, Blindauer CA (2013) Diversity and distribution of plant metallothioneins: a review of structure, properties and functions. Metallomics 5:1146. https://doi.org/10.1039/c3mt00072a

Limjuco LA, Burnea FK (2022) Evaluation of dithiadiamide-based molecular ion imprinted polymer (MIIP) for selective recovery of platinum from acid-digested spent automobile catalytic converter (ACC) solution. MRS Commun 12:175–182. https://doi.org/10.1557/s43579-022-00158-9

Liu Y-S, Chang Y-C, Chen H-H (2018) Silver nanoparticle biosynthesis by using phenolic acids in rice husk extract as reducing agents and dispersants. J Food Drug Anal 26:649–656. https://doi.org/10.1016/j.jfda.2017.07.005

Lu P, Hsieh Y-L (2012) Cellulose isolation and core–shell nanostructures of cellulose nanocrystals from chardonnay grape skins. Carbohydr Polym 87:2546–2553. https://doi.org/10.1016/j.carbpol.2011.11.023

Ma Y, Oliveira RS, Freitas H, Zhang C (2016) Biochemical and Molecular Mechanisms of Plant-Microbe-Metal Interactions: Relevance for Phytoremediation. Front Plant Sci 7:. https://doi.org/10.3389/fpls.2016.00918

Maroušek J, Trakal L (2022) Techno-economic analysis reveals the untapped potential of wood biochar. Chemosphere 291:133000. https://doi.org/10.1016/j.chemosphere.2021.133000

Mishra V, Arya A, Chundawat TS (2019) High Catalytic Activity of Pd Nanoparticles Synthesized from Green Alga Chlorella vulgaris in Buchwald-hartwig Synthesis of N-Aryl Piperazines. Curr Organocatalysis 7:23–33. https://doi.org/10.2174/2213337206666190515091945

Monaci F, Leidi EO, Mingorance MD, et al (2011) Selective uptake of major and trace elements in Erica andevalensis, an endemic species to extreme habitats in the Iberian Pyrite Belt. J Environ Sci 23:444–452. https://doi.org/10.1016/S1001-0742(10)60429-9

Moreno-Medina BL, Casierra-Posada F, Cutler J (2018) Phytochemical Composition and Potential Use of Rubus Species. Gesunde Pflanz 70:65–74. https://doi.org/10.1007/s10343-018-0416-1

Morisada S, Kim Y-H, Ogata T, et al (2011) Improved Adsorption Behaviors of Amine-Modified Tannin Gel for Palladium and Platinum Ions in Acidic Chloride Solutions. Ind Eng Chem Res 50:1875–1880. https://doi.org/10.1021/ie102193a

Mubeen S, Zhang T, Yoo B, et al (2007) Palladium Nanoparticles Decorated Single-Walled Carbon Nanotube Hydrogen Sensor. J Phys Chem C 111:6321–6327. https://doi.org/10.1021/jp067716m

Mulvaney P (1996) Surface Plasmon Spectroscopy of Nanosized Metal Particles. Langmuir 12:788–800. https://doi.org/10.1021/la9502711

Nasrollahzadeh M, Mohammad Sajadi S (2016) Pd nanoparticles synthesized in situ with the use of Euphorbia granulate leaf extract: Catalytic properties of the resulting particles. J Colloid Interface Sci 462:243–251. https://doi.org/10.1016/j.jcis.2015.09.065

Nasrollahzadeh M, Mohammad Sajadi S, Rostami-Vartooni A, et al (2016) Green synthesis of the Pd nanoparticles supported on reduced graphene oxide using barberry fruit extract and its application as a recyclable and heterogeneous catalyst for the reduction of nitroarenes. J Colloid Interface Sci 466:360–368. https://doi.org/10.1016/j.jcis.2015.12.036

Nasrollahzadeh M, Sajadi SM, Maham M (2015) Green synthesis of palladium nanoparticles using Hippophae rhamnoides Linn leaf extract and their catalytic

activity for the Suzuki–Miyaura coupling in water. J Mol Catal Chem 396:297–303. https://doi.org/10.1016/j.molcata.2014.10.019
Nobahar A, Carlier JD, Miguel MG, Costa MC (2021) A review of plant metabolites with metal interaction capacity: a green approach for industrial applications. BioMetals. https://doi.org/10.1007/s10534-021-00315-y
Oszmiański J, Wojdyło A, Gorzelany J, Kapusta I (2011) Identification and Characterization of Low Molecular Weight Polyphenols in Berry Leaf Extracts by HPLC-DAD and LC-ESI/MS. J Agric Food Chem 59:12830–12835. https://doi.org/10.1021/jf203052j
Padamata SK, Yasinskiy AS, Polyakov PV, et al (2020) Recovery of Noble Metals from Spent Catalysts: A Review. Metall Mater Trans B 51:2413–2435. https://doi.org/10.1007/s11663-020-01913-w
Paiva AP, Piedras FV, Rodrigues PG, Nogueira CA (2022) Hydrometallurgical recovery of platinum-group metals from spent auto-catalysts – Focus on leaching and solvent extraction. Sep Purif Technol 286:120474. https://doi.org/10.1016/j.seppur.2022.120474
Pantelidis G, Vasilakakis M, Manganaris G, Diamantidis G (2007) Antioxidant capacity, phenol, anthocyanin and ascorbic acid contents in raspberries, blackberries, red currants, gooseberries and Cornelian cherries. Food Chem 102:777–783. https://doi.org/10.1016/j.foodchem.2006.06.021
PGM Market Report (2018) Summary of platinum supply and demand in 2017, 2018. URL. Johns Matthey
Platinum, 2008 (2008) Platinum 2008, [WWW Document]
Puigdomenech I (2015) Hydra/medusa chemical equilibrium database and plotting software (database update: 01–01–2015; Hydra: 32 bit version 18 Aug. 2009; Medusa: 32 bit version 16 Dec. 2010). KTH R Inst Technol Stock
Quental L, Bourguignon A, Sousa AJ, et al (2002) MINEO Southern Europe environment test site. Contamination impact mapping and modelling-Final Report. Assessing and Monitoring the Environmental Impact of Mining Activities in Europe Using Advanced Earth Observation Techniques 5yth FP-IST. (MINEO) 1999--10337
Rajesh D, Mahendiran C, Suresh C, et al (2019) Hydrothermal synthesis of three dimensional reduced graphene oxide-multiwalled carbon nanotube hybrids anchored with palladium-cerium oxide nanoparticles for alcohol oxidation reaction. Int J Hydrog Energy 44:4962–4973. https://doi.org/10.1016/j.ijhydene.2019.01.025
Rajeshkumar S, Naik P (2018) Synthesis and biomedical applications of Cerium oxide nanoparticles – A Review. Biotechnol Rep 17:1–5. https://doi.org/10.1016/j.btre.2017.11.008
Rossini-Oliva S, Abreu MM, Leidi EO (2018) A review of hazardous elements tolerance in a metallophyte model species: Erica andevalensis. Geoderma 319:43–51. https://doi.org/10.1016/j.geoderma.2017.12.035

Rostami-Vartooni A, Rostami L, Bagherzadeh M (2019) Green synthesis of Fe3O4/bentonite-supported Ag and Pd nanoparticles and investigation of their catalytic activities for the reduction of azo dyes. J Mater Sci Mater Electron 30:21377–21387. https://doi.org/10.1007/s10854-019-02514-3

Saguru C, Ndlovu S, Moropeng D (2018) A review of recent studies into hydrometallurgical methods for recovering PGMs from used catalytic converters. Hydrometallurgy 182:44–56. https://doi.org/10.1016/j.hydromet.2018.10.012

Şahin Ün Ş, Ünlü A, Ün İ, Ok S (2020) Green synthesis, characterization and catalytic activity evaluation of palladium nanoparticles facilitated by *Punica granatum* peel extract. Inorg Nano-Met Chem 1–9. https://doi.org/10.1080/24701556.2020.1832118

Saleh EAM, Khan AU, Tahir K, et al (2021) Phytoassisted synthesis and characterization of palladium nanoparticles (PdNPs); with enhanced antibacterial, antioxidant and hemolytic activities. Photodiagnosis Photodyn Ther 36:102542. https://doi.org/10.1016/j.pdpdt.2021.102542

Santos ES, Abreu MM, Batista MJ, et al (2014) Inter-population variation on the accumulation and translocation of potentially harmful chemical elements in Cistus ladanifer L. from Brancanes, Caveira, Chança, Lousal, Neves Corvo and São Domingos mines in the Portuguese Iberian Pyrite Belt. J Soils Sediments 14:758–772. https://doi.org/10.1007/s11368-014-0852-1

Santos ES, Abreu MM, Magalhães MCF (2016) Cistus ladanifer phytostabilizing soils contaminated with non-essential chemical elements. Ecol Eng 94:107–116. https://doi.org/10.1016/j.ecoleng.2016.05.072

Santos ES, Abreu MM, Nabais C, Magalhães MCF (2012) Trace element distribution in soils developed on gossan mine wastes and Cistus ladanifer L. tolerance and bioaccumulation. J Geochem Explor 123:45–51. https://doi.org/10.1016/j.gexplo.2012.05.006

Sarıbıyık OY, Weilach C, Serin S, Rupprechter G (2020) The Effect of Shape-Controlled Pt and Pd Nanoparticles on Selective Catalytic Hydrodechlorination of Trichloroethylene. Catalysts 10:1314. https://doi.org/10.3390/catal10111314

Schindelin J, Arganda-Carreras I, Frise E, et al (2012) Fiji: an open-source platform for biological-image analysis. Nat Methods 9:676–682. https://doi.org/10.1038/nmeth.2019

Seyedi N, Saidi K, Sheibani H (2018) Green Synthesis of Pd Nanoparticles Supported on Magnetic Graphene Oxide by Origanum vulgare Leaf Plant Extract: Catalytic Activity in the Reduction of Organic Dyes and Suzuki–Miyaura Cross-Coupling Reaction. Catal Lett 148:277–288. https://doi.org/10.1007/s10562-017-2220-4

Sharmila G, Farzana Fathima M, Haries S, et al (2017) Green synthesis, characterization and antibacterial efficacy of palladium nanoparticles synthesized using Filicium decipiens leaf extract. J Mol Struct 1138:35–40. https://doi.org/10.1016/j.molstruc.2017.02.097

Sheny DS, Philip D, Mathew J (2012) Rapid green synthesis of palladium nanoparticles using the dried leaf of Anacardium occidentale. Spectrochim Acta A Mol Biomol Spectrosc 91:35–38. https://doi.org/10.1016/j.saa.2012.01.063

Siddiqi KS, Husen A (2016) Green Synthesis, Characterization and Uses of Palladium/Platinum Nanoparticles. Nanoscale Res Lett 11:482. https://doi.org/10.1186/s11671-016-1695-z

Silverstein RM, Webster FX (1997) Spectrometric Identification of Organic Compounds. John Wiley Sons Inc

Singh KR, Nayak V, Sarkar T, Singh RP (2020) Cerium oxide nanoparticles: properties, biosynthesis and biomedical application. RSC Adv 10:27194–27214. https://doi.org/10.1039/D0RA04736H

Supply Chain Deep Dive Assessment (2022) Platinum Group Metal Catalysts

Tan Q, Du C, Sun Y, et al (2014) Pd-around-CeO_{2-x} hybrid nanostructure catalyst: three-phase-transfer synthesis, electrocatalytic properties and dual promoting mechanism. J Mater Chem A 2:1429–1435. https://doi.org/10.1039/C3TA13843G

Trinh HB, Lee J, Suh Y, Lee J (2020) A review on the recycling processes of spent auto-catalysts: Towards the development of sustainable metallurgy. Waste Manag 114:148–165. https://doi.org/10.1016/j.wasman.2020.06.030

Tuo Y, Liu G, Dong B, et al (2017) Microbial synthesis of bimetallic PdPt nanoparticles for catalytic reduction of 4-nitrophenol. Environ Sci Pollut Res 24:5249–5258. https://doi.org/10.1007/s11356-016-8276-7

Veisi H, Faraji AR, Hemmati S, Gil A (2015a) Green synthesis of palladium nanoparticles using *Pistacia atlantica kurdica* gum and their catalytic performance in Mizoroki-Heck and Suzuki-Miyaura coupling reactions in aqueous solutions: Biosynthesis of palladium nanoparticles using *P . a . kurdica* gum. Appl Organomet Chem 29:517–523. https://doi.org/10.1002/aoc.3325

Veisi H, Ghorbani-Vaghei R, Hemmati S, et al (2015b) Green and effective route for the synthesis of monodispersed palladium nanoparticles using herbal tea extract (Stachys lavandulifolia) as reductant, stabilizer and capping agent, and their application as homogeneous and reusable catalyst in Suzuki couplin: Biosynthesis of monodispersed palladium nanoparticles. Appl Organomet Chem 29:26–32. https://doi.org/10.1002/aoc.3243

Veljkovic B, Djordjevic N, Dolicanin Z, et al (2018) Antioxidant and Anticancer Properties of Leaf and Fruit Extracts of the Wild Raspberry (Rubus idaeus L.). Not Bot Horti Agrobot Cluj-Napoca 47:359–367. https://doi.org/10.15835/nbha47111274

Wagner T, Eglinger J (2021) particlesizer: v1.0.9. ImageJ plugin to derive number based size distributions based on recorded TEM images

Wang L, Lin X, Zhang J, et al (2019) Extraction methods for the releasing of bound phenolics from Rubus idaeus L. leaves and seeds. Ind Crops Prod 135:1–9. https://doi.org/10.1016/j.indcrop.2019.04.003

Wang Q, Cui X, Chen J, et al (2012) Well-dispersed palladium nanoparticles on graphene oxide as a non-enzymatic glucose sensor. RSC Adv 2:6245. https://doi.org/10.1039/c2ra20425h

Wang Y, Wang S, Wang X (2009) CeO[sub 2] Promoted Electro-Oxidation of Formic Acid on Pd⁄C Nano-Electrocatalysts. Electrochem Solid-State Lett 12:B73. https://doi.org/10.1149/1.3086263

Wei X, Liu C, Cao H, et al (2019) Understanding the features of PGMs in spent ternary automobile catalysts for development of cleaner recovery technology. J Clean Prod 239:118031. https://doi.org/10.1016/j.jclepro.2019.118031

Wicaksono WP, Kadja GTM, Amalia D, et al (2020) A green synthesis of gold–palladium core–shell nanoparticles using orange peel extract through two-step reduction method and its formaldehyde colorimetric sensing performance. Nano-Struct Nano-Objects 24:100535. https://doi.org/10.1016/j.nanoso.2020.100535

Wiecka Z, Rzelewska-Piekut M, Regel-Rosocka M (2022) Recovery of platinum group metals from spent automotive converters by leaching with organic and inorganic acids and extraction with quaternary phosphonium salts. Sep Purif Technol 280:119933. https://doi.org/10.1016/j.seppur.2021.119933

Wongsawa T, Traiwongsa N, Pancharoen U, Nootong K (2020) A review of the recovery of precious metals using ionic liquid extractants in hydrometallurgical processes. Hydrometallurgy 198:105488. https://doi.org/10.1016/j.hydromet.2020.105488

Yakoumis I, Moschovi AM, Giannopoulou I, Panias D (2018) Real life experimental determination of platinum group metals content in automotive catalytic converters. IOP Conf Ser Mater Sci Eng 329:012009. https://doi.org/10.1088/1757-899X/329/1/012009

Yakoumis I, Panou M, Moschovi AM, Panias D (2021) Recovery of platinum group metals from spent automotive catalysts: A review. Clean Eng Technol 3:100112. https://doi.org/10.1016/j.clet.2021.100112

Zhang D, Ma X, Gu Y, et al (2020) Green Synthesis of Metallic Nanoparticles and Their Potential Applications to Treat Cancer. Front Chem 8:799. https://doi.org/10.3389/fchem.2020.00799

Zhang L, Xu Z (2018) A critical review of material flow, recycling technologies, challenges and future strategy for scattered metals from minerals to wastes. J Clean Prod 202:1001–1025. https://doi.org/10.1016/j.jclepro.2018.08.073

Zhang Y, Grass ME, Habas SE, et al (2007) One-step Polyol Synthesis and Langmuir−Blodgett Monolayer Formation of Size-tunable Monodisperse Rhodium Nanocrystals with Catalytically Active (111) Surface Structures. J Phys Chem C 111:12243–12253. https://doi.org/10.1021/jp073350h

Zheng H, Ding Y, Wen Q, et al (2021) Separation and purification of platinum group metals from aqueous solution: Recent developments and industrial applications. Resour Conserv Recycl 167:105417. https://doi.org/10.1016/j.resconrec.2021.105417

5.6. **Annexes**

Table S- 5.1. pH values in the unimetallic solutions prepared with 0,01M HCl, in the tested mixtures of unimetallic solutions plus 1/1 (v/v) the 70% ethanol plant extracts, in the controls of unimetallic solutions plus 1/1 (v/v) 70% ethanol and the theoretical values (Theor. Val.) at which metals start precipitating according to simulations with Medusa-Hydra software (Puigdomenech, 2015) using conditions that mimic the tested matrices.

	Pt^{4+}	**Pd^{2+}**	**Ce^{3+}**	**Al^{3+}**	**Fe^{3+}**
Metallic solution	0.49	0.84	0.76	0.95	0.97
***C. ladanifer* test**	1.18 ± 0.01	1.63 ± 0.02	1.45 ±0.02	1.73 ±0.01	1.73 ± 0.01
***E. andevalensis* test**	1.11 ± 0.02	1.56 ± 0.02	1.53 ±0.04	1.64 ± 0.00	1.65 ± 0.01
***R. idaeus* test**	0.93 ±0.03	1.46 ± 0.04	1.60 ±0.03	1.64 ± 0.01	1.53 ± 0.04
Control	0.95 ± 0.04	1.33 ± 0.01	1.27 ±0.03	1.53 ± 0.12	1.47 ± 0.02
Theor. Val. for precipitation	3.83	3.11	7.80	3.85	0.48

Table S- 5.2. pH values in the diluted (1/6 (v/v)) leachate solutions, in the tested mixtures of these solutions plus 1/1 (v/v) 70% ethanol plant extracts, in the controls of real solutions plus 1/1 (v/v) 70% ethanol and the theoretical values (Theor. Val.) at which the main metals start precipitating according to estimates with Medusa-Hydra software (Puigdomenech, 2015) using conditions that mimic the tested matrices.

	I95 leachate (1/6)	**H98 leachate (1/6)**
Initial solution	0.41	0.44
***C. ladanifer* test**	0.81 ±0.02	0.84 ± 0.02
***E. andevalensis* test**	0.75 ±0.01	0.82 ± 0.04
***R. idaeus* test**	0.92 ±0.044	1.00 ± 0.06
Control	0.92 ± 0.04	1.00 ± 0.06
Theor. Val. for precipitation	7.92 (Pd^{2+}) 6.26 (Pt^{4+}) 7.42 (Rh^{3+}) 3.35 (Al^{3+}) 7.89 (Ce^{3+}) 1.19 (Fe^{3+}) 8.14 (La^{3+}) 7.44 (Nd^{3+})	

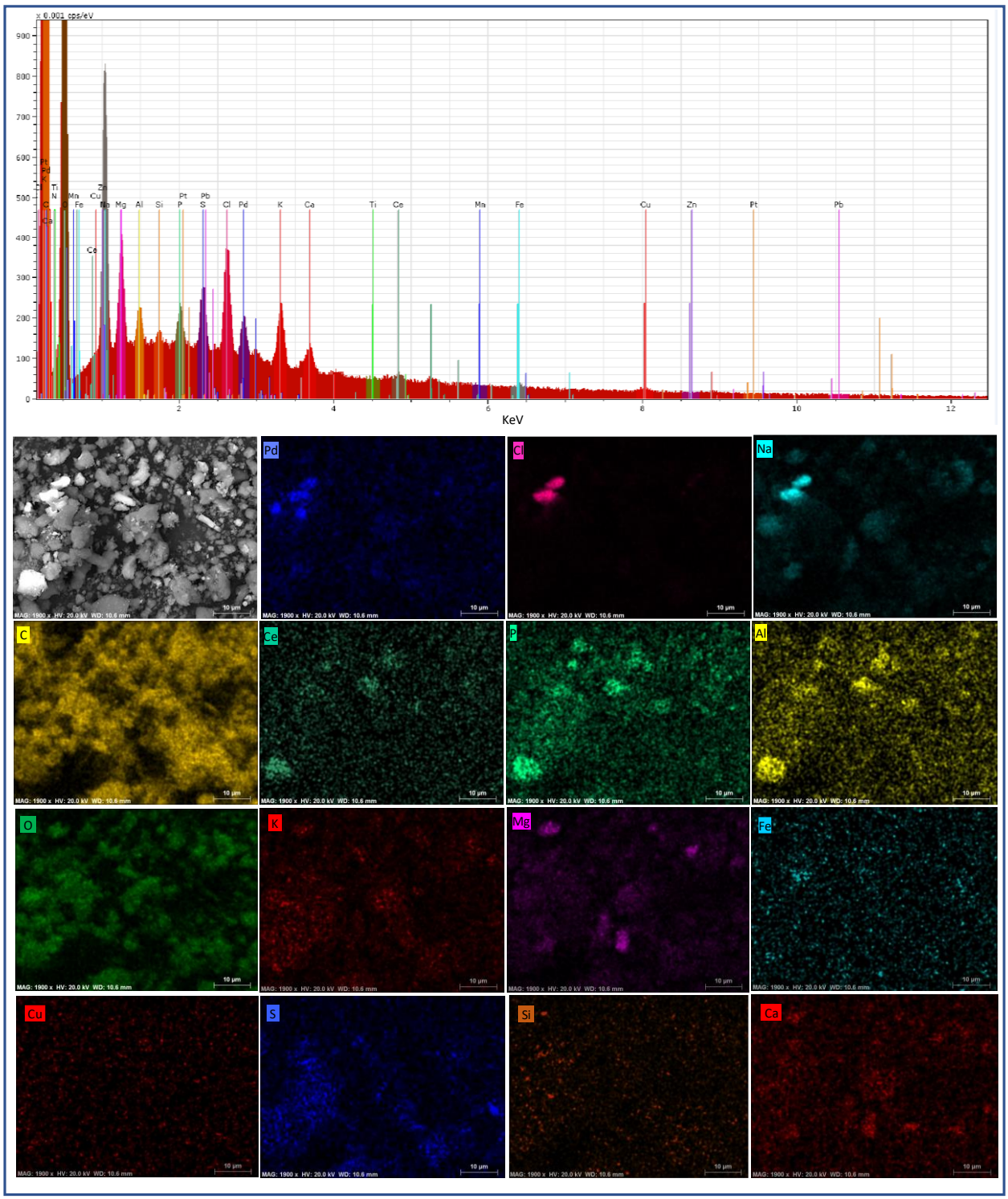
x 0.001 cps/eV
KeV
Pd
Cl
Na
C
Ce
P
Al
O
K
Mg
Fe
Cu
S
Si
Ca

Figure S- 5.1. SEM-EDX mapping of precipitates obtained from mixing 70% ethanolic extract of *Rubus idaeus* leaves with the H98 leachate at a 1/1 (v/v) ratio. Precipitates washed two times with ethanol and dry before analysis.

Spot 1

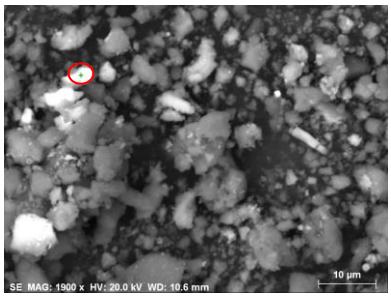

Element	[wt.%]	[norm. wt.%]	[norm. at.%]
Carbon	**66.29**	**50.88**	**66.08**
Oxygen	**25.37**	**19.48**	**18.99**
Chlorine	**23.00**	**17.65**	**7.77**
Sodium	**12.39**	**9.51**	**6.45**
Palladium	**1.92**	**1.47**	**0.22**
Calcium	0.53	0.41	0.16
Magnesium	0.37	0.28	0.18
Sulfur	0.35	0.27	0.13
Phosphorus	0.08	0.06	0.03
Sum	130.29	100.00	100.00

Spot 2

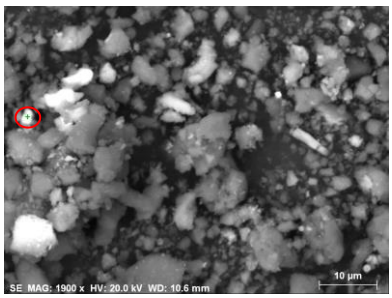

Element	[wt.%]	[norm. wt.%]	[norm. at.%]
Carbon	**40.86**	**51.37**	**67.84**
Oxygen	**20.90**	**26.27**	**26.04**
Palladium	**12.11**	**15.23**	**2.27**
Chlorine	**2.68**	**3.37**	**1.51**
Sodium	**1.91**	**2.40**	**1.66**
Calcium	0.58	0.73	0.29
Magnesium	0.38	0.47	0.31
Phosphorus	0.06	0.08	0.04
Sulfur	0.06	0.07	0.03
Aluminium	0.01	0.01	0.01
Sum	79.55	100.00	100.00

Spot 3

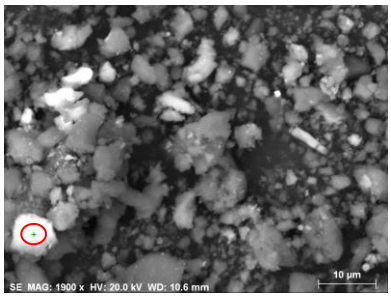

Element	[wt.%]	[norm. wt.%]	[norm. at.%]
Carbon	**39.65**	**43.95**	**57.55**
Oxygen	**32.27**	**35.77**	**35.16**
Cerium	**5.88**	**6.52**	**0.73**
Phosphorus	**2.40**	**2.66**	**1.35**
Aluminium	**2.28**	**2.53**	**1.47**
Sodium	**1.99**	**2.21**	**1.51**
Lanthanum	**1.11**	**1.23**	**0.14**
Potassium	0.96	1.06	0.43
Chlorine	0.77	0.86	0.38
Magnesium	0.77	0.85	0.55
Copper	0.69	0.76	0.19
Palladium	0.61	0.67	0.10
Sulfur	0.56	0.62	0.30
Calcium	0.21	0.23	0.09
Silicon	0.08	0.09	0.05
	90.22	100.00	100.00

Figure S- 5.2. SEM-EDX point analysis of three white particles present in precipitates obtained from mixing 70% ethanolic extract of *Rubus idaeus* leaves with the H98 leachate. Precipitates washed two times with ethanol and dry before analysis. [wt.%] = weight percentage, [norm. wt.%] = normalized weight percentage, [norm. at.%] = normalized atomic percentage.

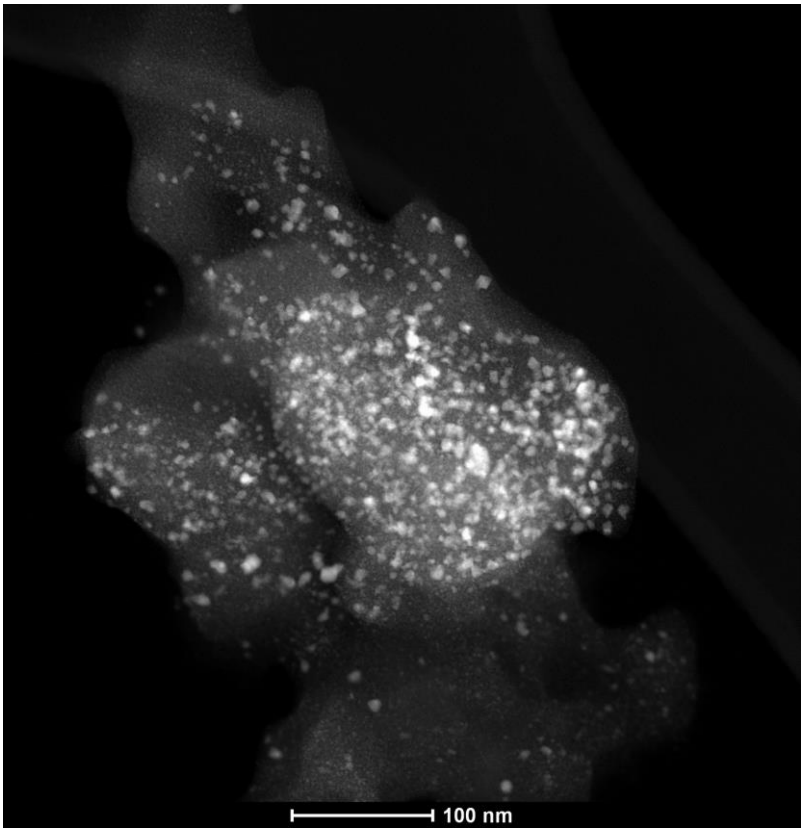

Figure S- 5.3. STEM image of precipitates with Pd nanoparticles that was used for quantitative spectra analysis by EDX on the whole area. Precipitates washed two times with ethanol, then two times with acetone and dry before analysis.

CHAPTER 6

Printed circuit boards leaching followed by synthesis of gold nanoparticle clusters using plant extracts

Printed circuit boards leaching followed by synthesis of gold nanoparticle clusters using plant extracts

A modified version of this chapter would be published as:

Nobahar, Amir; Lourenço, João Paulo; Costa, Maria Clara; Carlier, Jorge Dias. "Printed circuit boards leaching followed by synthesis of gold nanoparticle clusters using plant extracts". Journal of chemical technology and biotechnology (submitted, 2022).

Abstract

This work investigates the potential of 70% ethanolic leaf extracts of *Rubus idaeus* L., *Cistus ladanifer* L. and *Erica andevalensis* in the metal separation from synthetic unimetallic solutions of different metals and a leachate obtained from the leaching of PCBs. Results from the experiments with unimetallic solutions revealed *R. idaeus* and *E. andevalensis* extracts induced separation of more than 95% of the initial Au(III), while *C. ladanifer* separated ~78% of this metal. Thereafter, application of three plant extracts to real Au bearing leachate obtained from PCBs leaching, revealed about 96%, 95% and 90% Au recovery with *R. idaeus*, *C. ladanifer* and *E. andevalensis* extracts, respectively with 15%-60% co-removal of Pb and less than 15% of other metals. The reduction of Au(III) ions into Au(0) nanoparticles by *R. idaeus* extract was confirmed by molecular UV-Visible, and FT-IR analysis showed the involvement of plant secondary metabolites in Au bio-reduction and bio-stabilization. Particles obtained from the application of *R. idaeus* extract to the leachate were initially analyzed with XRD and results confirmed the presence of Au(0) with contamination of $PbSO_4$, which was completely removed by washing with 1 M HCl. Thereafter, results from STEM-EDS analysis showed the presence of Au particles conjugated with organic material and other metals. Consequently, particles were subjected to another washing step with acetone. Afterwards, STEM-EDS showed pure Au microparticle clusters (~0.8 μm) with flower-shaped or

apparently cubic morphologies, and HRSTEM showed the tiny nanoparticles (~20 nm), which form the clusters.

Keywords

gold recovery; printed circuit board; gold nanoparticles; plant extract; plant secondary metabolites

Graphical abstract

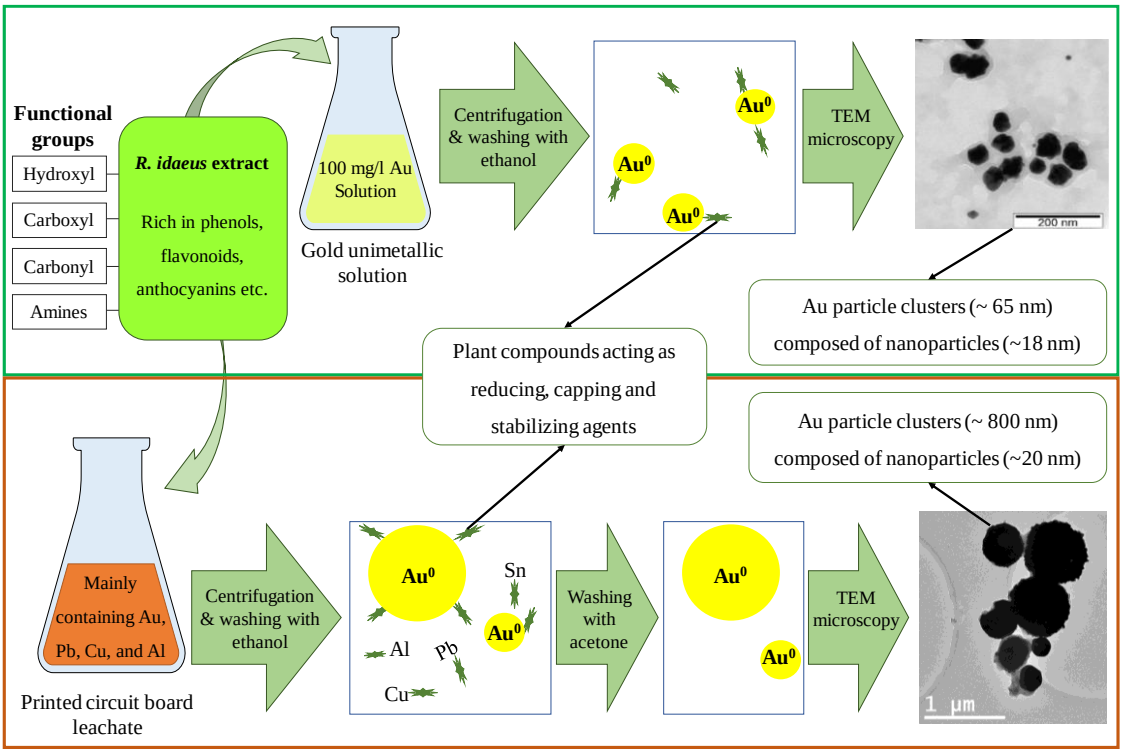

6.1. Introduction

In the last decades, due to the rapid industrialization, application of precious metals has been emerged in various industrial sectors. Nowadays, global demand for precious metals, such as Au, in the industry is continuously increasing and it is reported that more than 90% of this metal's industrial utilization is in the electronic devices (Wongsawa et

al. 2020). This high demand has been growing faster than the demand for base metals that are also used in the electronic devices industry (Kim 2013; Chen et al. 2021).

Waste electrical and electronic equipment in urban mining are considered as a secondary source of metals due to their higher metal content than those in primary ores (Kumar et al. 2018). Estimations demonstrate that in 2019, electronic wastes produced by consumer products alone were about 54 million metric tons (Mt), which is predicted to surpass 74 Mt by 2030 (Forti et al. 2020). Printed Circuit Boards (PCBs) are the essential constituent of every electronic devices. Metal recovery from waste PCBs has been attracted more attention since they normally contain 40% of wide range of metals including precious metals (e.g., Au, Ag, Pt, Pd), rare metals (e.g. Be, In), base metals (e.g. Cu, Al, Ni, Sn, Zn, Fe), and toxic heavy metals (e.g. Pb, Cd, Sb) (Luda 2011; Le et al. 2013; Mir and Dhawan 2022).

Considering this increasing secondary source of Au in PCBs, the need for recycling these metals is highly important for economic and environmental reasons. Recycling and sustainable management of these wastes are important steps toward development of mining resources sustainability and to mitigate the growing shortage of resources (Sverdrup and Ragnarsdottir 2016). However, the recycling methods for Au from secondary sources is still a challenge due to the low content of Au and high metal complexity of these wastes (Bourgeois et al. 2020; Gonzalez Baez et al. 2022).

Nowadays, hydrometallurgical methods are preferred over pyrometallurgical methods for the metals recovery from PCBs as they consume less energy and are less environmentally harmful. Metal recycling from these wastes through hydrometallurgical methods are normally performed by a leaching process (usually non-metal specific), followed by a metal recovery step from the obtained leachates. By now, different hydrometallurgical leaching methods are established and are expanding rapidly as they are economically and environmentally viable since they have a wide range of reagent options, they perform well in different scales (from small scales to larger ones), are applicable on very low to

high-grade metals in raw materials, and have low recycling cost and energy consumption (Janyasuthiwong et al. 2016; Jeon et al. 2020; Magoda and Mekuto 2022).

Various methods have been described for the separation and recovery of Au from leaching solutions such as chemical precipitation, solvent extraction, electrowinning, cementation, selective adsorption and coagulation (Islam et al. 2020; Magoda and Mekuto 2022). However, application of these methods are not usually economically viable due to their insufficient recovery rates (especially when applied to low concentration of Au), intensive electricity and energy consumption, high costs of chemicals assisting to other environment related issues (Li et al. 2018; Islam et al. 2021). Thereby, in the recent years, potential biological methods for metals' bio-recovery are gaining more attention over other methods (Islam et al. 2021). In this context, beneficiation of plant-based compounds as a potent alternative to other methods deserves more investigations.

Plants synthesize numerous compounds with many functional abilities, including those with metal interaction capabilities such as phenols, alkaloids, saponins, polysaccharides, proteins and organic acids (Nobahar et al. 2021). These compounds, based on their nature, contain polar functional groups, such as carboxyl, phenolic, hydroxyl, sulfo and amino groups, that are capable to interact with metal ions through different mechanisms like complex/chelate formation (Mejáre and Bülow 2001; Clemens 2001; Ma et al. 2016), reduction (Sharma et al. 1998; Ma et al. 2016; Ishak et al. 2019), precipitation (Pietrobelli et al. 2009; Ma et al. 2016). These secondary metabolites with suitable metal interaction characteristics can be promising substitutes of other compounds that are currently employed for Au recovery, since they are renewable resources, cheap and environmentally friendly. They have potential application in different metal related industrial applications and have already been explored for example in Au separation and recovery, and in Au nanoparticle synthesis and stabilization (Kumar and Yadav 2009; Sengani et al. 2017; Khan et al. 2019).

To our knowledge, the potential of plant extracts for the separation and recovery of Au from complex Au bearing solutions and leachates was not yet evaluated. Therefore, after

tests with unimetallic solutions to confirm the potential application of three plant extracts (*Rubus idaeus* L., *Cistus ladanifer* L. and *Erica andevalensis*) applied for first time for this purpose, additional experiments were performed with real PCBs leaching solutions. Finally, the best plant extract was selected for further optimization and characterization of the Au recovered particles.

6.2. **Materials and methods**

6.2.1. Unimetallic solutions

The unimetallic solutions were prepared by diluting 1/10 (v/v) the following 1000 mg/L metal standard solutions in 0.02 M HCl: $HAuCl_4$ in 2 M HCl (Merck Certipur, Germany), $Fe(NO_3)_3$ in 0.5 M HNO_3, $Al(NO_3)_3$ in 0.5 M HNO_3, $Cu(NO_3)_2$ in 0.5 M HNO_3, $Zn(NO_3)_2$ in 0.5 M HNO_3 and $Pb(NO_3)_2$ in 0.5 M HNO_3.

6.2.2. Au leaching from PCBs

Mechanical fragmentation

Initially, some electronic components (ECs), such as processor units, memory slots, power supplies, etc., were manually separated from the PCBs and then, the PCBs were broken in pieces of about 5 cm^2.

Leaching process

In this step, PCBs pieces together with the separated ECs (hereafter called just as PCBs) were used for Au recovery in two subsequent leaching steps:

Initially, a chemical pre-treatment for the separation of Cu, Zn, Fe, Al and Ni was accomplished using a mixture of 2 M sulfuric acid and 0.2 M of hydrogen peroxide. Small increments of PCBs were added to the leaching solution until a final 1 to 6 ratio (w/v), in

order to prevent the excessive heating and extreme froth formation as a result of the reaction, and the leaching occurred for 3 hours. Then, the aqueous solution was separated from large solids by decantation and from small solids by filtration with filter paper. In order to improve Cu and other metals' separation, this step was repeated two more times as suggested by (Birloaga et al. 2014).

Subsequently, a second leaching step was performed overnight to leach Au, Ag and platinum group metals from the solids obtained in the previous step, using aqua regia in a 1/20 ratio (w/v) (Park and Fray 2009).

The reaction of Au leaching by aqua regia is described below (Cui and Zhang 2008):

$$2HNO_3 + 6HCl \rightarrow 2NO + 4H_2O + 3Cl_2 \quad (1)$$

$$2Au + 11HCl + 3HNO_3 \rightarrow 2HAuCl_4 + 3NOCl + 6H_2O \quad (2)$$

$$Au + 4HCl + HNO_3 \rightarrow HAuCl_4 + 2H_2O + NO \quad (3)$$

Finally, the solution was diluted 1/3 (v/v) in distilled water and the obtained diluted leachate was characterized for the concentrations of Au, Ag, Pd, Pt, Cu, Pb, Zn, Fe, Al and Ni.

6.2.3. Separation of Pb from the Au bearing solution

Considering the low solubility of $PbSO_4$ ($Ksp = 6.7 \times 10^{-7}$) (Skoog et al. 2000), Pb can be recovered from the diluted aqua regia leachate as $PbSO_4$ (Neto 2018). Therefore, based on the chemical reaction ratio of Pb and SO_4 and the concentration of Pb in the solution, two times of the amount of sulfate required to remove the Pb content from the leachate was added as sodium sulfate solution to the leachate in 1/1 ratio (v/v). Then, 72 hours after sodium sulfate addition to the leachate, the formed white precipitates ($PbSO_4$) were separated through centrifugation at 2500 g for 10 minutes at room temperature.

6.2.4. Plant extract preparation

Three types of plant leaves were collected for this study: leaves from *Cistus ladanifer* L. (crimson spot rockrose); from *Erica andevalensis* Cabezudo & Rivera (a shrub growing in the Iberian Peninsula next to acidic mine waters contaminated with sulfate and metals) and from *Rubus idaeus* L. (red raspberry). The choice of plants for this work considered criteria such as being available in the region, being reported as metal accumulators and/or being plants (or parts of them) considered industrial or agricultural waste. *C. ladanifer* has developed several tolerance mechanisms that allow its adaptability to contaminated environments. The immobilization of metallic elements in roots and accumulation in senescent leaves are examples of these adaptability mechanisms and make this plant a promising species for phyto-stabilization of mining areas (Abreu et al. 2011; Santos et al. 2012, 2014, 2016). *E. andevalensis* is an endemic species of the Iberian pyrite Belt (IPB) (Cabezudo and Rivera 1980) that grows under extreme conditions of pH values between 3 and 4 and high metal contents, being able to accumulate Mn (Rossini-Oliva et al. 2018). It colonizes mine tailings and the bank sediments of water bodies contaminated with acid mine drainage (AMD), such as the Tinto and Odiel rivers in Spain and the channels and dams at the São Domingos mine in Portugal (Abreu et al. 2008; Monaci et al. 2011). *R. idaeus* is an agricultural crop widely cultivated in Asia, Europe, and North America for its fruits, being its leaves a residue highly rich in phenolic compounds (Pantelidis et al. 2007; Wang et al. 2019).

Young and mature leaves were collected and immediately dried to remove the moisture in an INCU-Line oven (VWR international) at 45°C until their weights stabilized. The dried leaves were then grinded into powder using an electric coffee grinder and the powder was mixed at a 10% (w/v) ratio with 70% (v/v) ethanol. Afterwards, the mixture was sonicated using an ultrasonic bath FB15054 (Fisher Scientific, USA) for 1 h and homogenized by orbital shaking at 150 rpm for 16 hours. Finally, the mixture was centrifuged at 2800 g for 5 min at room temperature and the supernatant was filtered using 310-150 mm qualitative filter paper (VWR international) in a vacuum system.

6.2.5. Au recovery using plant extracts

The capacity of 70% (v/v) ethanolic plant extracts for metals separation was tested on different metal bearing aqueous solutions: (1) three plant extracts were independently mixed and homogenized at 1/1 (v/v) with artificial unimetallic solutions prepared from standards commercialized for metals analysis; (2) three plant extracts were independently mixed and homogenized at 1/1 (v/v) with the diluted (1/6) PCBs leachate; (3) a selected plant extract (*R. idaeus*) was mixed in 1/1, 1/5 and 1/10 (v/v) ratios with the diluted (1/6) PCBs leachate; (4) the same selected plant extract was then mixed in a selected ratio (1/10 (v/v)) with the diluted (1/6) leachate at different pH values (0.3, 0.6 and 0.9). Simultaneously, mixtures prepared the same way but using pure 70% ethanol (without plant compounds) were used as negative controls. Experiments were carried out in triplicates in 50 mL centrifuge tubes at room temperature (20 ± 3°C), and after 1 and 48 hours of reaction aqueous samples were collected for metal analysis after centrifugation for 30 min at 2500 g to separate solids. Metal concentrations of the initial and final solutions in the mixtures were used for calculations of metal removal percentages. The significance of differences between means of different experimental treatments (test 1 h, test 48 h, control 1 h and control 48 h) was assessed by the single factor analysis of variance (ANOVA) considering a significance threshold level of 5%. Then, when ANOVA revealed significant differences among treatments, post-hoc tests were carried out with Tukey Kramer's tests (also for 5% significance level). The particles recovered from the PCB leachate using selected plant extract and conditions were characterized by XRD.

6.2.6. Pb washing from the Au precipitates

To eliminate any Pb content and other impurities from the particles obtained after the addition of plant extract to the PCBs leachates, a washing step was tested using different

solutions: 1 M hydrochloric acid, 1 M nitric acid, 1 M sodium hydroxide and 1 M ammonium acetate. A ratio of 1/1000 (w/v) of the particles to the washing solution was applied, the mixture shaken for 15 minutes by orbital shaker at room temperature, the supernatant separated through centrifugation for 30 min at 2500 g and the pellet dried in oven at 40℃ overnight. Then, the concentration of Pb was analyzed on the four tested solutions to evaluate the Pb leaching efficiency. Finally, the washing step was repeated, but with deionized water to eliminate traces of the washing agent and then with 96% (v/v) ethanol. Finally, the particles recovered from the best Pb washing solution (1 M hydrochloric acid) were dried and characterized by XRD and electronic microscopy.

Organic materials *washing* from the Au precipitates

After confirming the removal of Pb and having a more detailed characterization of the particles, they were further washed in two steps with pure acetone and the supernatant separated by centrifugation, aiming to eliminate organic compounds and metal contaminants. The final particles were also characterized by electronic microscopy.

Analytical methods

A bench centrifuge (Hettich, ROTOFIX 32A) was used to separate solid and liquid phases at specific conditions described above for each step.

For metal analysis, 1 mL of sample was diluted in 6.5 mL of 30% HNO_3 and 2.5 mL of 30% hydrogen peroxide (in 50 mL centrifuge tubes with loose caps) and heated in a water bath at 70°C during 1 h to digest organic compounds (if present). The concentrations of Au, Cu, Pb, Zn and Al were determined by microwave plasma atomic emission spectrometry with a 4200 MP-AES (Agilent Technologies, USA).

Calibration curves were built using standards prepared from the following stock solutions: $HAuCl_4$ in 2 M HCl, $AgNO_3$ in 0.5 M HNO_3, $Cu(NO_3)_2$ in 0.5 M HNO_3,

$Pb(NO_3)_2$ in 0.5 M HNO_3, $Zn(NO_3)_2$ in 0.5 M HNO_3, $Fe(NO_3)_3$ in 0.5 M HNO_3, $Al(NO_3)_3$ in 0.5 M HNO_3 and $Ni(NO_3)_2$ in 0.5 M HNO_3, $Pd(NO_3)_2$ in 0.5 M HNO_3 and $PtCl_2$ in 5% HCl from (Sigma-Aldrich standard for AAS, EUA).

The bio-reduction of Au ions and particles formation was monitored by molecular UV-visible spectroscopy. The optical absorption of the particles was investigated using the BioTek Synergy 4 microplate reader (BioTek InstrumentsInc., USA) using wavelengths between 200 to 700 nm at intervals of 1 nm.

Fourier Transform InfraRed (FTIR) Spectroscopy measurements of Au solution, *R. idaeus* extract and the mixture of Au solution and *R. idaeus* extract were performed using a Nicolet iN10MX micro-FTIR (Thermo Scientific, USA) equipped with a MCT detector cooled with liquid nitrogen. Analyzes were conducted in reflection mode, by spreading a drop of the sample onto a reflectance holder. Spectra were collected in the infrared region (from 4000 to 675 cm^{-1}). Three measurements were performed for each sample to assure the robustness of the analysis.

The crystallographic structures of obtained particles were analyzed by X-ray diffraction (XRD) using a PANalytical XPERT-PRO powder diffractometer operating at 45 kV and 35 mA with Cu Kα radiation filtered by Ni. The XRD patterns were recorded using an X'Celerator detector with a step size (2θ) of 0.03º and a time per step of 250 s. Peak analysis and the identification of crystalline phases were based on comparison using High-Score Plus software with the ICDD PDF-2 database.

The morphology and elemental composition of particles was analyzed either by Transmission Electron Microscopy (TEM) and/or by Scanning Transmission Electron Microscopy (STEM) imaging, in both cases coupled with Energy Dispersive X-ray Spectroscopy (EDS) analysis. Before TEM and STEM analysis, the particles were resuspended in ethanol and sonicated for 30 minutes for sample pulverization. Then, 5 µl of sample was dispersed on carbon coated grids of Cu for TEM and of molybdenum for STEM, and the grids were dried and stored in a desiccator until imaging. TEM was carried

out on a H8100 microscope (Hitachi, Tokyo, Japan) with a LaB6 filament, coupled with an EDS NORAN System (Thermo Scientific, Waltham, USA). STEM was carried out on the Titan ChemiSTEM (Thermo Fisher Scientific, Waltham, United States) microscope operating with a field emission gun and aberration corrector on the probe and four energy dispersive X-ray spectroscopy (EDS) detectors operating at 200 kV.

6.3. **Results and discussion**

6.3.1. Evaluation of Au recovery from unimetallic solutions using plant extracts

Experiments with unimetallic solutions diluted in HCl (final concentration ~100 mg/l) were performed to analyze the interaction potential of 70% hydroalcoholic extracts of *R. idaeus, C. ladanifer* and *E. andevalensis* with some of the metals known to be present in PCB leachates: Zn, Fe, Cu, Al, Pb and Au (Neto 2018). In these experiments, metal removal in the tests were significantly different from the negative controls and all the three plant extracts revealed a high Au removal from solution compared to the other metals (Figure 6.1). As depicted in Figure 6.1after 48 hours of reaction *R. idaeus* and *E. andevalensis* extracts effectively removed 99 ± 1% and 98 ± 4% of the initial Au, respectively, while 78 ± 17% of the Au was removed by the *C. ladanifer* extract. Beside Au, other metals with relatively high removals from the unimetallic solutions were Pb (10-40%), Fe (10-40%), Al (5-30%), Cu (2-20%) and Zn (1-10%) (Figure 6.1). The interesting tendency of these plant extracts to cause Au separation from the tested solutions, especially in the tests with *R. idaeus* and *E. andevalensis* extracts, confirms the interaction of their plants' compounds with Au. Probably such interaction was favored by the high reduction potential of Au(III) (E^{o}= 1.50 V), as reported in the reduction potential table of metals published by Bard et al. (1985) and Milazzo et al. (1978), and the high reduction (antioxidant) potential of plant compounds present in the extracts. In fact, other studies have previously demonstrated the potential of phytochemicals present in plant extracts to induce the formation of Au nanoparticles in aqueous solutions, as for example:

extracts of *Sageretia thea* (Shah et al. 2022), *Spinacia oleracea* L. (Zhu et al. 2022), *Solidago canadensis* (Botha et al. 2019), *Persea americana* (Yang et al. 2021).

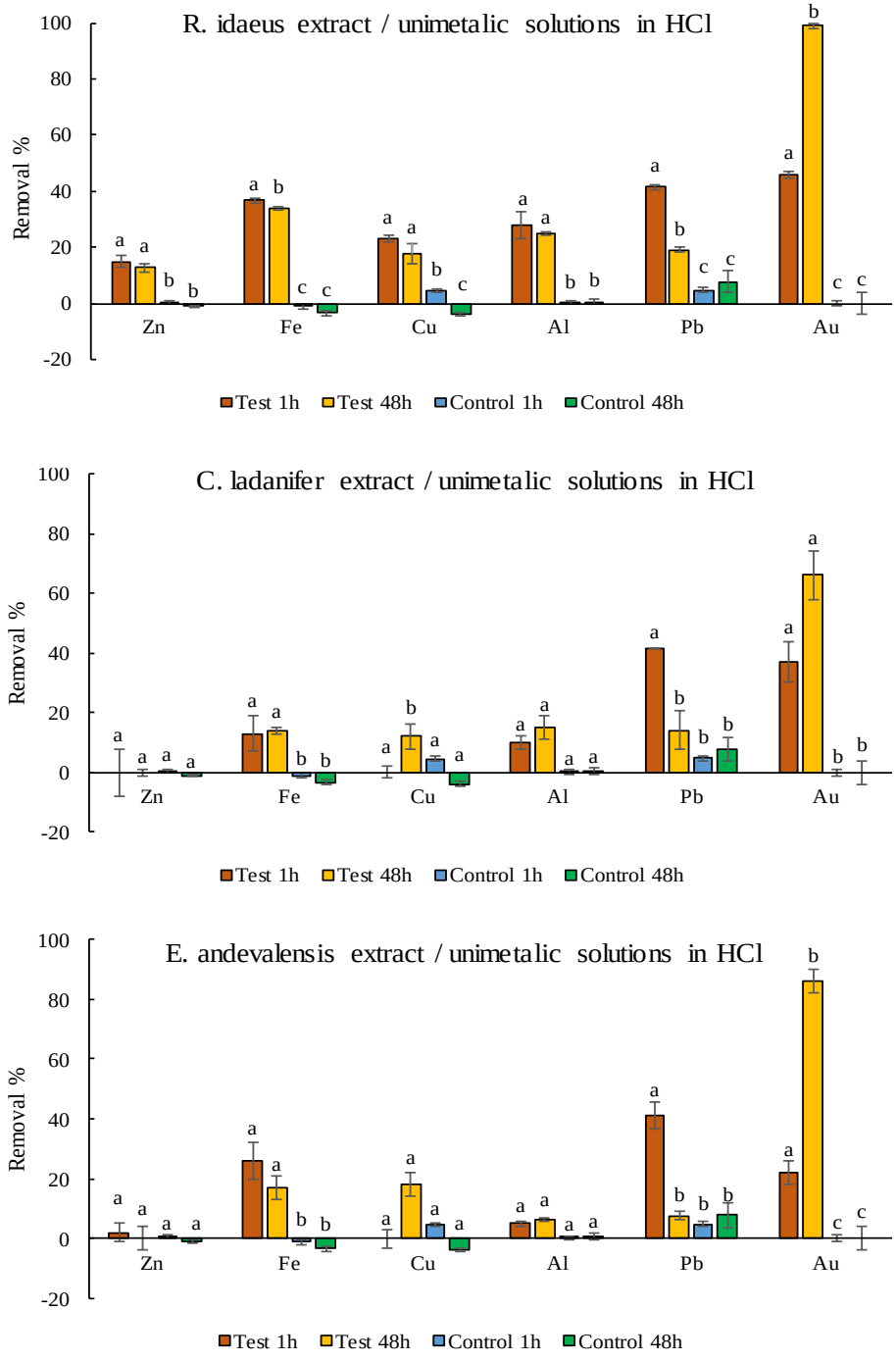

Figure 6.1. Metal removals achieved after 1 h and 48 h of mixing *R. idaeus, C. ladanifer*, *E. andevalensis* 70% hydroalcoholic extract, at a 1/1 (v/v) ratio to the unimetallic solutions (~100 mg/L) at room temperature (25 ± 3 °C). Results for controls, consisting of the addition of just 70% ethanol (without plant extract), are included. Removals with the same letters do not significantly differ at 0.05 level (ANOVA and Tukey Kramer's tests).

6.3.1.1. Characterization of particles obtained from the Au(III) unimetallic solution

The particles obtained from the reaction of Au(III) unimetallic solution with *R. idaeus* extract were selected for further analysis due to high Au removal efficiency by this plant extract and also vast availability of *R. idaeus* leaves as an agricultural waste. These particles were analyzed by XRD, EDS and TEM for the investigation of their elemental composition, size and morphology. The XRD pattern recorded with the particles illustrated the crystalline nature of the Au particles with strong peaks correlated to Au (Figure S- 6.1). Moreover, the EDS spectra of the particles confirmed the presence of Au as the sole element present in the precipitates (Figure S- 6.2). The peak observed for Cu corresponds to the used Cu based grid. The TEM analysis of the particles showed that the Au nanoparticles were monodispersed and had quasi-spherical and irregular shapes with a ferret particle size ranging from 31 to 85 nm with an average size of 57 nm. The selected-area electron diffraction (SAED) patterns of the nanoparticles added further evidence that Au nanoparticles are highly crystalline (Figure S- 6.3). Demirbas et al. (2019), in a similar study with synthetic Au(III) solutions but with addition of 5% (w/w) *R. idaeus* fruit extract (not leaves extract) showed formation of spherical Au nanoparticles with an average size of 18±3 nm.

All these evidence encouraged the attempt to use the leaf extracts in a real multimetallic solution containing Au, namely a PCBs leachate.

6.3.2. Au leaching from PCBs

After the mechanical fragmentation described in materials and methods, the PCBs were initially subjected to three cycles of leaching with 2 M H_2SO_4 and 0.2 M H_2O_2 aiming to leach the base metals and leave the Au parts more exposed to the leaching of this metal in the next step. This process provided satisfactory results by successful leaching mainly of the base metals (Cu, Ni, Zn and Fe) (Table 6.1) and separating the PCBs' parts as well as realizing small Au films, which were visible at the bottom of the leaching container. Moreover, during the leaching of base metals, a white precipitate was formed and settled in the bottom of the container together with PCBs' parts and Au particles. According to previous reports on PCBs leaching works this white precipitate is composed of $PbSO_4$ particles, which has low solubility in sulfuric acid solutions (Neto 2018). Therefore, this indicates that Pb was also leached from the PCBs.

Table 6.1. Characterization of the leachate solution achieved by applying 2 M H_2SO_4 and 0.2 M H_2O_2 to PCBs (mixture of leachates from the three successive cycles of leaching (3 h for each leaching cycle)).

Metal	Concentration in leachate (mg/L)
Au	15.4 ± 0.1
Ag	not detected
Pd	0.30 ± 0.04
Pt	not detected
Cu	1715 ± 7
Pb	8.5 ± 0.1
Zn	405.1 ± 3.3
Fe	143.2 ± 1.6
Al	10.0 ± 0.1
Ni	634 ± 4

After the leaching steps with sulfuric acid, the electronic components, except the supporting bases which were now free of metal parts, as well as the remaining solids (including the white precipitates which were mixed with Au particles) were treated with aqua regia in a 1/20 ratio (w/v) for 24 hours. Thereafter, the obtained solution was diluted in a 1/3 ratio with deionized water to avoid the digestion of bio-compounds in the subsequent Au recovery tests using plant extracts. As presented in Table 6.2, the diluted leaching solution contains valuable metals (232 mg/L of Au, 26 mg/L of Ag, 11 mg/L of Pd), as well as a high concentration of Pb (15 g/L) and still some contamination with the base metals Cu, Ni, Zn and Fe. Such high concentration of Pb originates from the $PbSO_4$ precipitates that were formed in the initial leaching step and which were scattered among the small fractions of PCBs in the bottom of the container and then were leached with aqua regia. Nevertheless, it is evident that the major part of the base metals leached from PCBs was leached in the initial leaching step with 2 M H_2SO_4 and 0.2 M H_2O_2 (~98% of Cu, ~97% of Ni, ~99% of Zn, 99% of Fe, and ~50% of Al), which is in agreement with previous reports (Birloaga et al. 2014).

6.3.2.1. Separation of Pb from the Au bearing PCBs leachate

Due to the very high Pb concentration in the aqua regia leachate, it was necessary to separate and recover this metal from the solution prior to Au recovery processes. With that aim, the leaching solution was submitted to a precipitation step with 0.15 M Na_2SO_4 (in 1/1 (v/v) ratio) and ~96% of Pb was removed from the solution (Table 6.2). XRD analysis of particles obtained through this precipitation step revealed that Pb was recovered as $PbSO_4$ and $PbCl_2$ crystals (Figure S- 6.4), which can be considered a by-product of the Au recovery process here reported.

Table 6.2. Characterization of the diluted aqua regia leachate, before and after Pb removal/recovery by addition of 0.15 M sodium sulfate solution at 1/1 (v/v) ratio.

Metal	Concentration (mg/L)	
	1/3 diluted ***aqua regia*** **leachate**	**1/6 diluted *aqua regia* leachate after adding sodium sulfate**
Au	232.2 ± 6.1	120.1 ± 1.7
Ag	26.2 ± 0.6	18.7 ± 0.2
Pd	10.8 ± 0.2	5.9 ± 0.1
Pt	-	-
Cu	151.3 ± 0.8	74.4 ± 0.3
Pb	15030 ± 136	636 ± 14
Zn	4.1 ± 0.1	1.8 ± 0.1
Fe	9.1 ± 0.1	7.3 ± 0.1
Al	57.0 ± 0.2	30.2 ± 0.1
Ni	10.2 ± 0.4	5.3 ± 0.3

6.3.3. Au recovery from the final PCBs leachate using plant extracts

In the experiments performed by adding each of the three plant extracts to the final 1/6 diluted Au bearing leachate at 1/1 (v/v) ratios, the target metal Au as well as Pb, Cu and Al as main contaminant metals were analyzed (Table 6.2; Figure 6.2). It was observed that the application of *R. idaeus, C. ladanifer* and *E. andevalensis* extracts is highly effective in recovering Au from the leachate with an efficiency of 96%, 95% and 90%, respectively. However, there was co-precipitation of Pb ranging between 15% to 60% of its initial concentration in all tested samples and respective controls, and since the concentration of this metal in the diluted (1/6) Au bearing leachate was very high (~630 mg/L), this corresponds to a high contamination of the obtained Au particles.

R. idaeus extract/diluted leachate

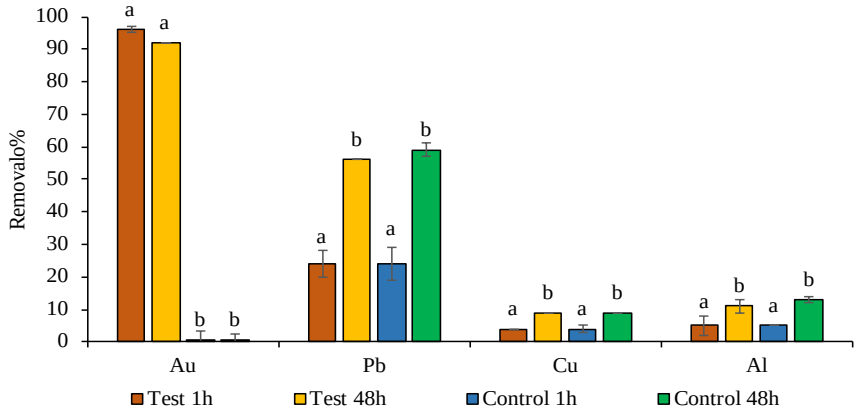

C. ladanifer extract/diluted leachate

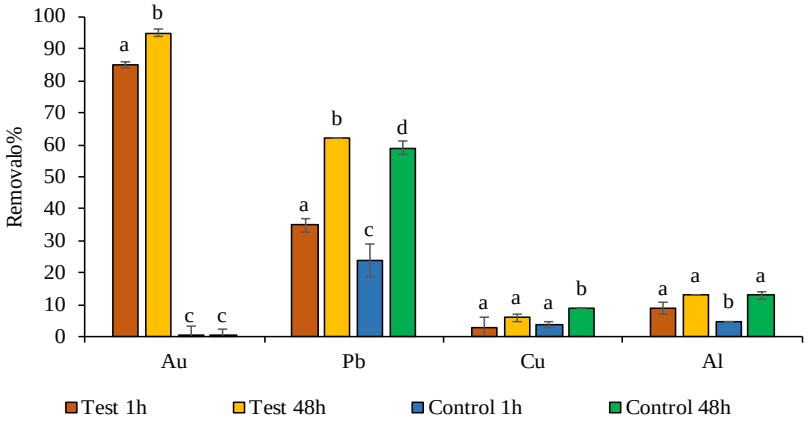

E. andevalensis extract/diluted leachate

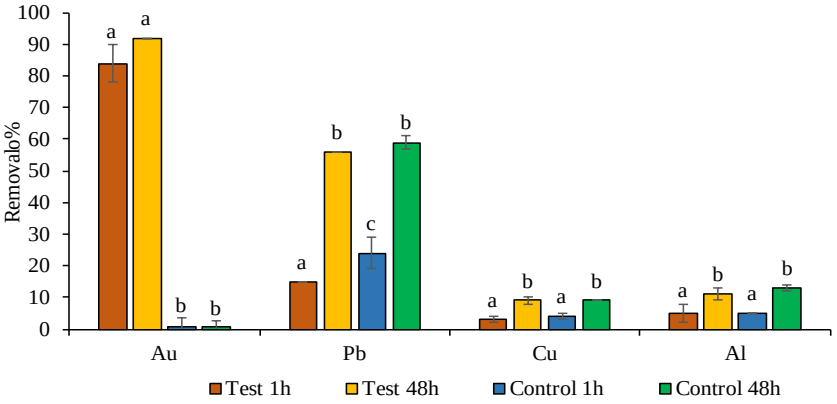

Figure 6.2. Removal of main metals present in the diluted (1/6 (v/v)) Au bearing leachate, achieved after 1 h and 48 h addition of *C. ladanifer*, *E. andevalensis* and *R. idaeus* 70% ethanolic extracts at a 1/1 (v/v) ratio at room temperature (25 ± 3 °C). Results for controls, consisting of the addition of just 70% ethanol (without plant extract), are included. Removals with the same letters do not significantly differ at 0.05 level (ANOVA and Tukey Kramer's tests).

Based on the results obtained from experiments with unimetallic solutions and leachates in 1/1 ratio, *R. idaeus* was found with the highest Au recovery potential from the leachate. Moreover, *R. idaeus* leaves are available in large quantities as wastes from agro-industrial production of red raspberry fruits and therefore, further studies were focused on the optimization of using the *R. idaeus* extract to recover Au from the leachate, on the Au recovery mechanism and on the characterization of the obtained brownish particles.

In this regard, 1/5 and 1/10 (v/v) ratios of *R. idaeus* extract to Au bearing leachate were tested to analyze Au recovery efficiencies and Pb contamination rates (Figure 6.3). Similar removals of Au and Pb from solution were observed in the tests with 1/1 and 1/5 ratios of *R. idaeus* to Au bearing leachate for both 1 and 48 hours of reaction times. In the experiment with the 1/10 ratio of plant extract to Au bearing leachate, a lower removal of Au and Pb was observed after 1 hour (~11% of Au and 21% Pb), but 48 hours after, the removal of Au from the leachate reached 95%. Yet, as it can be seen in Figure 6.3, different ratios of plant extract to leachate are not a successful strategy to prevent Pb contamination. With all this, the optimum ratio of plant extract to leachate was selected as 1/10 (v/v).

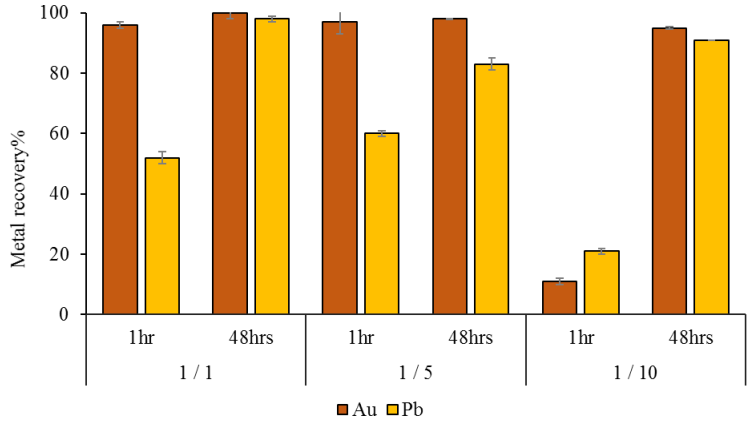

Figure 6.3. Au and Pb precipitation by applying *Rubus idaeus* extract to Au bearing leachate at different ratios (1/1, 1/5 and 1/10 (v/v)) at room temperature (25 ± 3 °C). Results are averages of two replicates and error bars are absolute mean deviations.

Another attempt was performed to test the possibility of Au recovery from the leachate without Pb contamination by an initial pH adjustment of the leachate to 0.3, 0.6 and 0.9, followed by *R. idaeus* extract addition in 1/10 ratio (v/v) (Figure S- 6.5). However, the results revealed similar Au and Pb removals in all tested pH values. Then, precipitates obtained without pH adjustment were analyzed by XRD and the results indicated the presence of Au and $PbSO_4$ crystalline structures (Figure S- 6.6).

6.3.3.1. Pb washing from the Au bearing precipitates from PCBs leachate

Precipitates obtained from applying *R. idaeus* extract to Au bearing leachate at 1/10 ratio were selected for purification. Attempts of $PbSO_4$ separation from the Au particles were performed by washing the precipitates in a ratio of 1/1000 (w/v) with hydrochloric acid, nitric acid, sodium hydroxide and ammonium acetate. Results from these experiments revealed that all the four tested solutions were able to dissolve and separate $PbSO_4$ from the precipitates, but three of them have a higher and similar efficiency (hydrochloric acid,

nitric acid and sodium hydroxide), thus suggesting total $PbSO_4$ leaching, while the other (ammonium acetate) results in a lower efficiency (Table 6.3). The XRD analysis of the brownish precipitates obtained after the washing step with 1 M hydrochloric acid and subsequent washings with water and 96% ethanol revealed the presence of Au as the only crystalline phase (Figure 6.4).

Table 6.3. Pb washing from precipitates obtained by applying *Rubus idaeus* extract to Au bearing leachate.

Washing solution	**Pb leached from precipitates (mg Pb / g precipitate)**
1 M hydrochloric acid	137
1 M nitric acid	136
1 M sodium hydroxide	128
1 M ammonium acetate	42

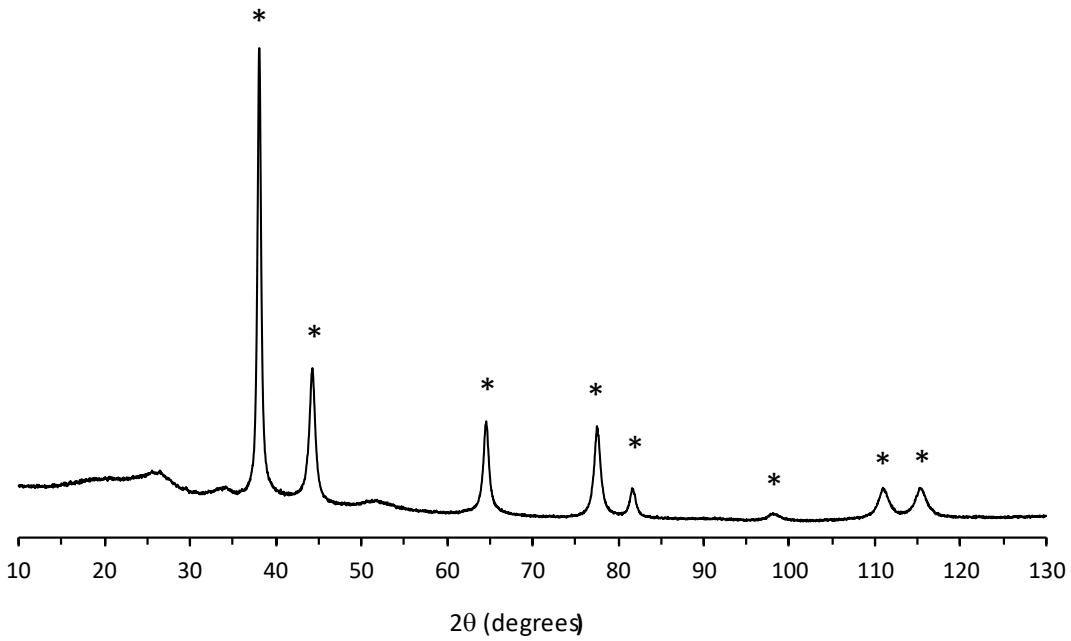

Figure 6.4. XRD analysis of precipitates obtained by adding *Rubus idaeus* extract to Au bearing leachate at a 1/10 (v/v) ratio, after $PbSO_4$ washing with 1 M hydrochloric acid. (*) denotes the peak position of Au crystalline phase according to the card #01-071-4073.

The STEM imaging of these precipitates revealed well defined bright white (indicative of heavy elements) flower-shaped porous particles of ~75 nm to ~360 nm scattered in a less shiny whitish (indicative of lighter elements) mass with no defined shape (Figure 6.5). Then, the STEM-EDS mapping of these precipitates (Figure 6.5) showed strong Au and S signals along with very weak signals of Cu, Si and Fe, which are coincident with the white bright flower-shaped particles, as well as O, Sn and Cl signals throughout all precipitate mass. The relative abundances of different elements evaluated by STEM-EDS from the whole area of two images of these precipitates (Figure S- 6.7) are presented in Table 6.4.

The flower-shaped particles revealed by STEM have the same appearance of Au nanoparticles obtained with different plant extracts and Au solutions by other authors (Firdhouse and Lalitha 2016), and the EDS signal revealed Au as the most abundant element (27.2 norm. at.%) after O, which are strong evidences that the production of Au particles using the *R. idaeus* extract was successful. Nevertheless, the high signal obtained for O (40.1 norm. at.%) and the fact that it maps together with Cl in the less shiny whitish mass indicates a high amount of plant material around the particles since these elements are present in plant compounds (Engvild 1986). Moreover, the relatively high signal of Sn (12.7 norm. at.%) following O and Cl in the mass surrounding the particles indicates the possibility of complex formation of this metal with organic compounds. The other elements with relatively high signals are Cu (7.9 norm. at.%) and S (5.6 norm. at.%), which seem to follow the Au particles. The presence of Cu might be due to incomplete removal of this metal in the leaching step performed to remove base metals, but these analyzes are not enough to theorize about its co-occurrence with Au particles. The

presence of S must be viewed with suspicion because this element has a peak very close to peaks of Pb and Au and, thus, the accuracy of its signal can be low.

The HRTEM analysis of these precipitates showed large clusters (~100 to 400 nm) of tiny Au nanoparticles (~20 nm) covered with high contents of plant material, and then the FFT analysis confirmed the crystalline nature of the Au particles (Figure S- 6.8).

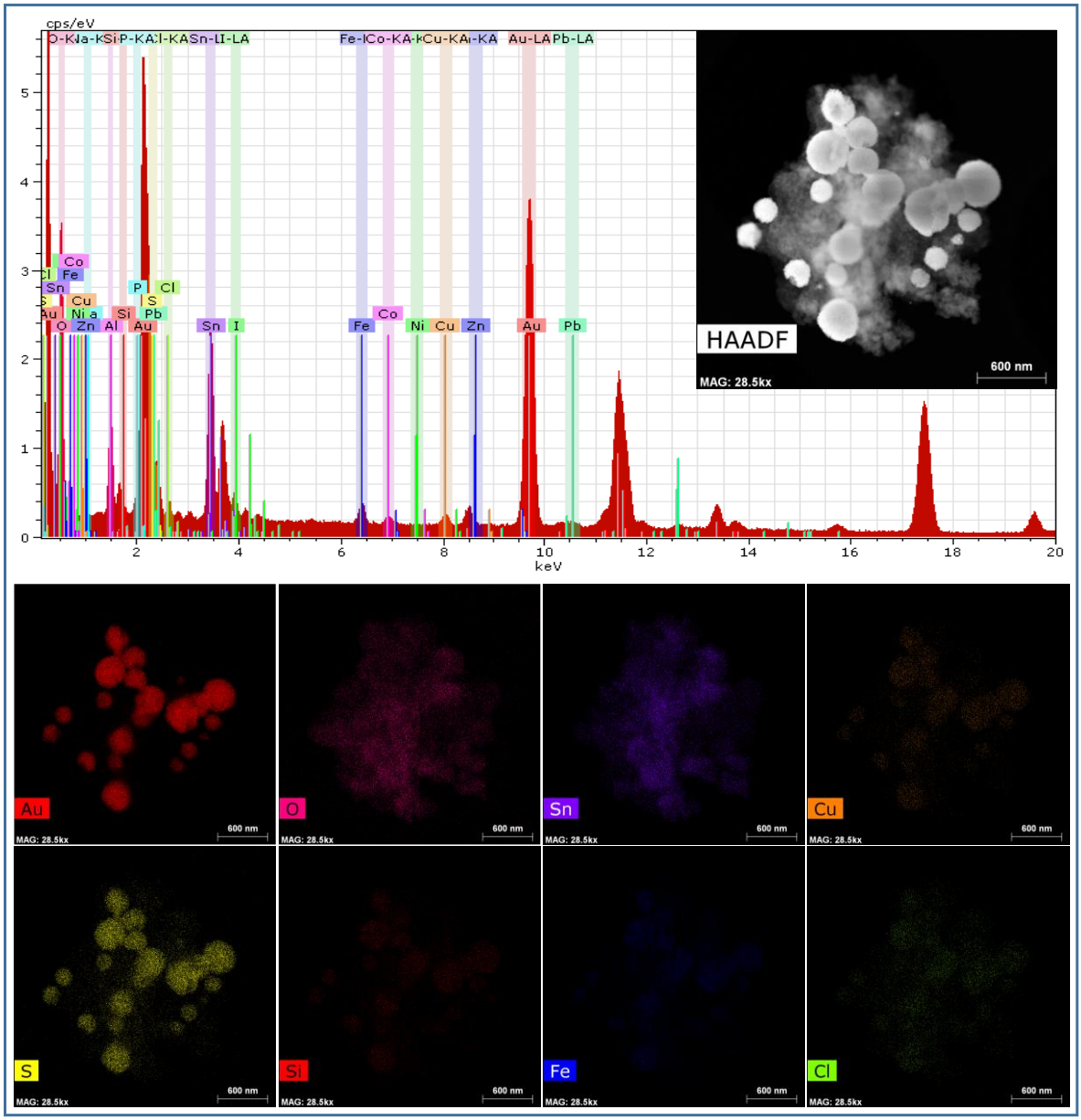

Figure 6.5. STEM image of Pd nanoparticles obtained by adding 70% ethanolic extract of *R. idaeus* to the Au bearing leachate (washed with ethanol) and corresponding EDS elemental mapping of Au, O, Sn, Pb, Ni, Al, Cu and Fe.

Table 6.4. Average values of normalized weight and atomic abundances of different elements obtained from two STEM-EDS images of Au particles washed with ethanol.

Element	[norm. wt.%]	[norm. at.%]
O	8.1	40.1
Al	0.1	0.4
S	2.1	5.6
Fe	0.8	1.3
Cu	5.8	7.9
Pb	2.0	0.8
Au	62.0	27.2
Zn	0.5	0.7
Ni	0.3	0.5
Sn	17.2	12.7
Si	0.6	1.7
Cl	0.5	1.1
Sum	100.0	100.0

6.3.3.2. Organics washing from the Au bearing precipitates from PCBs leachate

Based on the STEM-EDS results indicating the contamination of particles with excessive plant material and a few metals putatively complexed with it, another two washing steps with acetone were performed for the elimination of organic compounds. Thereafter, the obtained particles were also analyzed by STEM microscopy and the images revealed two types of particles: flower-shaped particles like those observed prior to acetone washing side by side with compact geometrical particles resembling cubic shapes (Figure 6.6), without evidence of other materials surrounding them. These results show that acetone

eliminated the organic material around the Au particles and suggest that organic compounds play an important role in the final shape of the Au particles. Synthesis of compact geometrical Au nanoparticles by mixing plant extract with an Au pure solution was reported before for example by Anbu et al. (2020), and though these authors described other shapes (such as spherical, triangular and octahedral), the cubic forms are also visible in their TEM images.

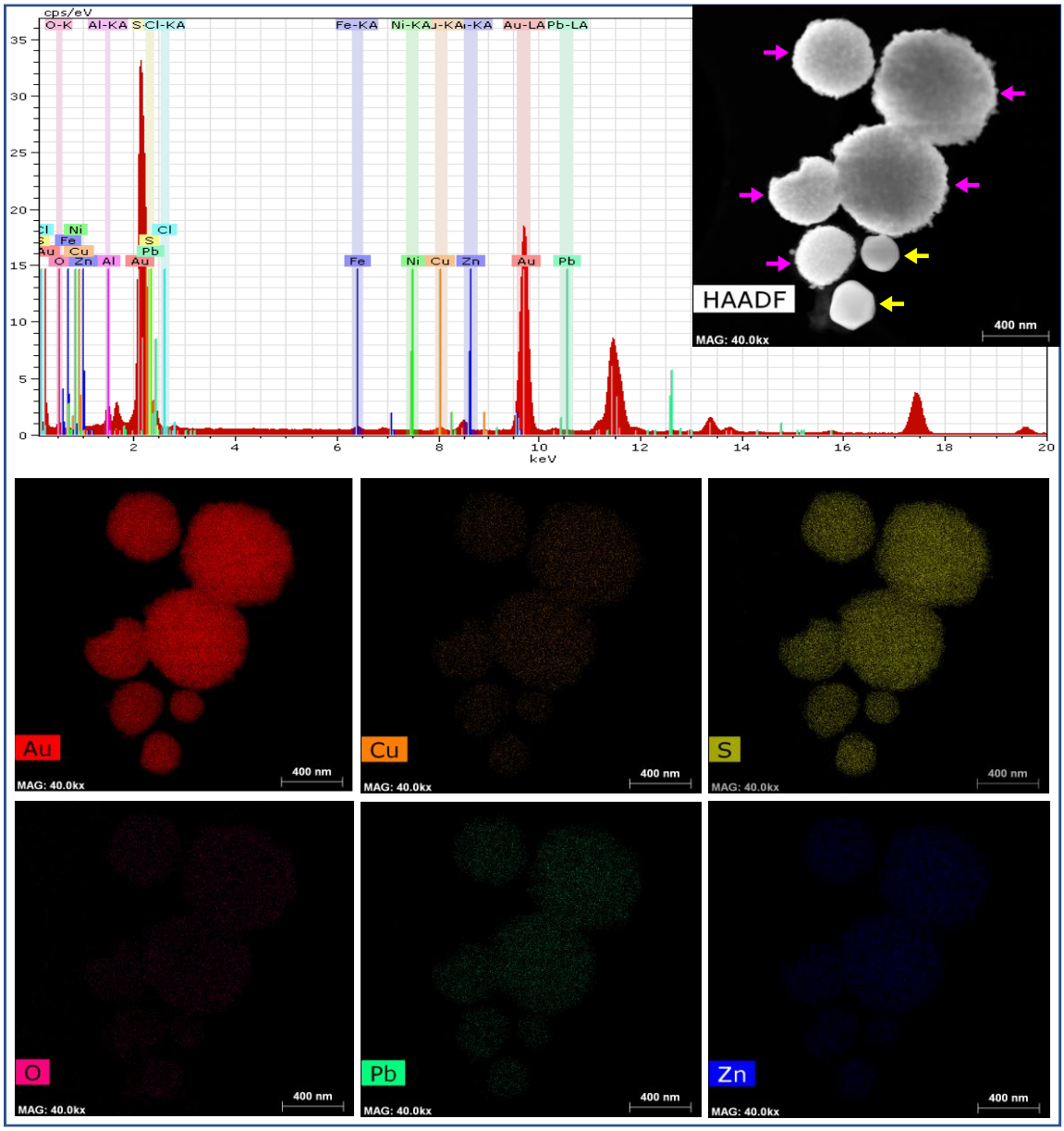

Figure 6.6. STEM image of Pd nanoparticles obtained by adding 70% ethanolic extract of *R. idaeus* to the Au bearing leachate (washed with pure acetone) and corresponding EDS elemental mapping of Au, O, Pb, Zn, Ni, Al, Cu and Fe. Pink arrows: flower-shaped particles. Yellow arrows: compact geometrical particles resembling cubic shapes.

Results of the STEM-EDS analysis revealed strong signals correlating with Au and S and relatively weaker signals for O and the contaminant metals Pb, Cu and Zn. On the contrary, the signals of Sn and Cl, which before acetone washing were detected in all the precipitate mass together with O, were much weaker now after organics removal (Figure 6.6). In fact, all signals detected now are present on the Au particles, confirming the efficacy of acetone washing.

The relative abundances of elemental composition of the particles determined by STEM-EDS from the whole area of four different images (Figure S- 6.9) are presented in Table 6.5. These results showed a much higher abundance for Au (63.5 norm. at.%), comparing to the value observed (27.2 norm. at.%) before acetone washings. This is mainly due to the sharp decrease of elements O and Sn since the reported abundances are relative to the sum of detected elements. Normalized atomic abundance of O was reduced from 40.1% to 3.7%, and of Sn from 12.7 to 0.1%. This almost disappearance of Sn after successful organic residues washing and the simultaneous decrease in O abundances, confirms that Sn was previously complexed with plant material that was removed with acetone. The sharped removal of O and Sn also caused a raise in the relative abundance of other elements that were not washed with acetone. Cu and S, the main contaminants after Sn, were found in almost the same ratio, but in relatively higher abundances (14.8 norm. at.% and 13.5 norm. at.%, respectively). The ratio of these elements is in fact close to 1, the stoichiometric value of CuS, which might indicate the presence of this compound in the free spaces in between smaller Au nanoparticles forming larger structures of Au nanoparticle clusters. Regarding the other minor contaminants, there was a decrease of Al and Si abundances after the acetone washing, and a raise of Pb and Ni. Thus, the first

two were probably complexed with phytochemicals while the last two were somehow bound to the Au particles. Probably Pb and Ni were, as $PbSO_4$ and as NiO, also placed in the porous structures of the flower-shaped larger Au nanoparticle clusters when they were formed by aggregation of tiny Au nanoparticles, and then remained trapped in those particles during the washing steps to which they were subjected.

Table 6.5. Average values of normalized weight and atomic abundances of different elements obtained from four STEM-EDS images of Au particles washed with pure acetone.

Element	[norm. wt.%]	[norm. at.%]
O	0.4	3.7
Al	0.0	0.1
S	3.0	13.5
Cu	6.5	14.8
Pb	2.5	1.7
Au	86.5	63.5
Zn	0.5	1.2
Ni	0.3	0.7
Sn	0.1	0.1
Si	0.1	0.8
Sum	100	100

The final Au particles were further analyzed with high-resolution scanning transmission microscopy (HRSTEM) for further characterization on the atomic scale. The HRSTEM images confirmed the presence of tiny cubic Au nanoparticles (~20 nm) and large Au particle clusters (~0.2 to 0.8 μm) with flower-shaped and cubic morphologies that seem to be formed by aggregates of the tiny particles (Figure 6.7-A, B). Moreover, the HRSTEM images showed clear lattice fringes on the tiny particles and the fast Fourier transform (FFT) pattern of the respective area revealed interplanar lattice distance values

of two types: ~2 Å and ~1.2 Å (Figure 6.7-D 9-E). In addition, the selected area electron diffraction (SAED) pattern confirmed the polycrystalline nature of the Au particles (Figure 6.7-F).

Finally, through High-angle annular dark-field scanning transmission electron microscopy (HAADF-STEM) imaging on one flower-shaped particle (Figure S- 6.10), the aggregation of tiny Au nanoparticles forming a porous nanoparticle cluster seems even more evident.

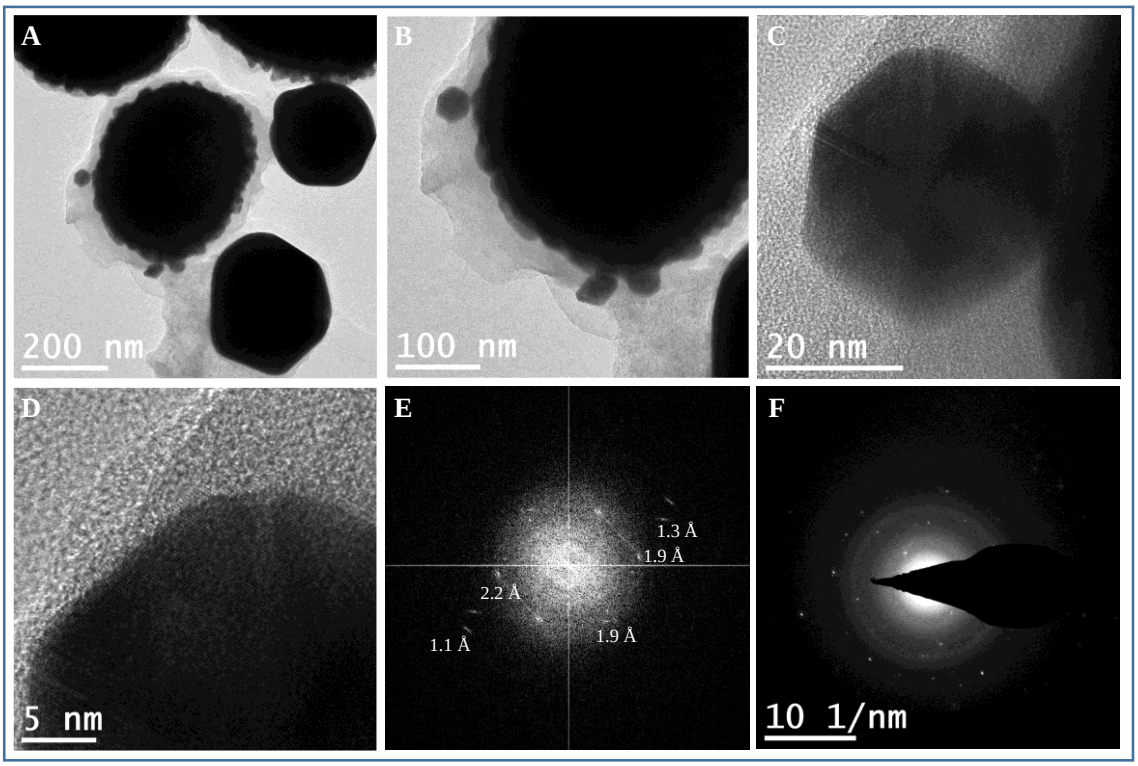

Figure 6.7. A, B) HRTEM images of the Au nanoparticles aggregates obtained by adding 70% ethanolic extract of *R. idaeus* to the Au bearing leachate C, D) magnified high resolution STEM, E) Fast Fourier Transform (FFT) pattern of a single tiny nanoparticle (all area of figure D) and F) selected-area electron diffraction (SAED) patterns of the same nanoparticle.

The use of *R. idaeus* extracts was previously tested with unimetallic solutions for Ag nanoparticles synthesis by leaf extracts (Stevanović et al. 2019) and for Au and Ag nanoparticles synthesis by fruit extracts (Demirbas et al. 2017, 2019; Ekrikaya et al. 2021). However, this work confirms for the first time the possibility of using *R. idaeus* leaf extracts for Au nanoparticles synthesis from Au unimetallic solutions, as well as from complex Au bearing leachates. This is important, not only because according to Kumar & Yadav (2009), Au nanoparticle synthesis by plant extracts in general can have advantages aiming the development of environmental friendly processes, but also because the *R. idaeus* leaves are a by-product of raspberry production available in large amounts, which is suitable for large-scale processes to satisfy the demand for this substance. Au nanoparticles can be used in different areas such as analytical methods like colorimetric methods for the identification and determination of heavy metal ions in aqueous solutions (Hyder et al. 2022), catalysts in CO oxidation (Al Soubaihi et al. 2018), water gas shift reactions (Pal et al. 2018), development of biosensors (Dimcheva 2020), medicine applications (Madkour 2018), biolistic delivery of nucleic acids in biotechnology applications (Svarovsky et al. 2008), coating for improved electrode surface area (Li et al., 2007) etc.

6.3.4. Au recovery mechanism with R. idaeus leaves' extract

6.3.4.1. UV–Visible Spectroscopy

The bio-reduction of Au(III) ions during the reaction with the phytochemicals present in the 70% hydroalcoholic extract of *R. idaeus* was monitored by molecular UV-visible spectroscopy. Figure 6.8 presents the UV-visible absorption spectra of the 100 mg/L Au(III) unimetallic solution, *R. idaeus* extract diluted in 0.02 M HCl (10% plant extract (v/v)) and also different ratios of *R. idaeus* extract in 100 mg/L Au(III) (4, 6, 8 and 10% plant extract (v/v)) after one hour reaction time. The change of the solution color from

yellow to red and the appearance of an absorption peak at λ = 520 nm in the UV-Vis spectrum are indications of Au(III) ions reduction into Au(0), which is due to the Surface Plasmon Resonance (SPR) of synthesized Au(0) nanoparticles (Lee et al. 2020). Thus, the SPR band of Au(0) nanoparticle samples prepared with lower amounts of *R. idaeus* extract (4% and 6%) illustrated by a broad lower peak is due to the partial reduction of Au(III) ions, while upon the increase of extract the SPR absorbance peak was steadily raised and reached the highest size when 10% (v/v) of extract was used (Figure 6.8).

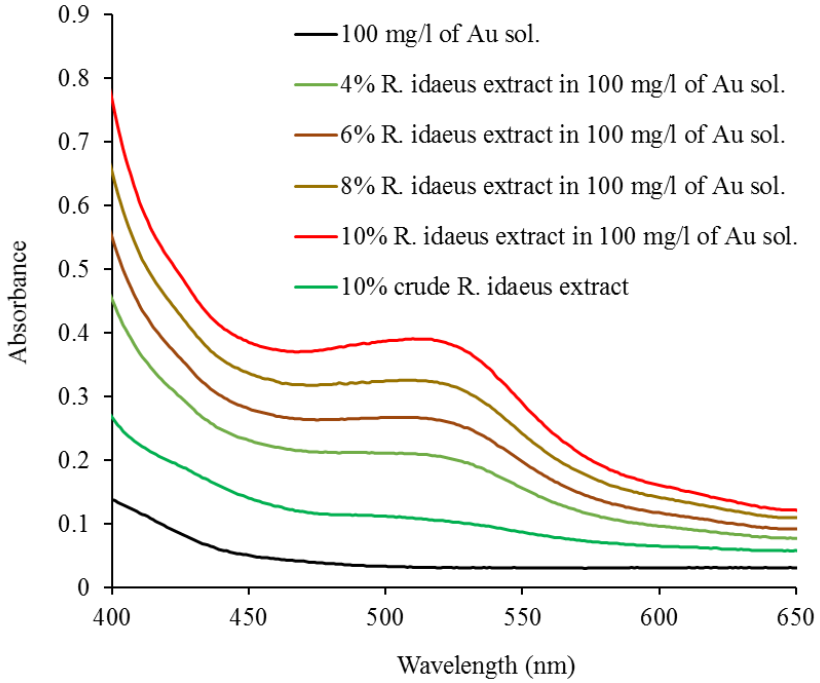

Figure 6.8. Molecular UV-Visible spectrum of Au(III) (100 mg/L) solution, 70% hydroalcoholic extract of *R. idaeus* diluted in 0.02 M HCl (1 to 10 ratio (v/v)) and mixtures of plant extract in 100 mg/L of Au solution (2, 4, 6, 8 and 10% (v/v) of plant extract in Au solution).

6.3.4.2. Fourier Transform Infrared Spectroscopy (FT-IR)

FT-IR spectroscopy was performed to monitor the involvement of functional groups of secondary metabolites present in the *R. idaeus* hydroalcoholic extract and their possible role in the formation and stabilization of Au particles. FT-IR spectra of crude *R. idaeus* extract as well as the mixture of the *R. idaeus* extract with 100 mg/L Au(III) solution (1/1 ratio (v/v) and 1 hour of reaction time) are shown in Figure 6.9. FT-IR spectra of *R. idaeus* extract reveals several peaks at different wavenumbers due to the used solvent and the presence of a variety of secondary metabolites in the extract: peaks occurring at 1058, 1097 and 2989 cm^{-1} are related to ethanol (Silverstein and Webster 1997), the solvent used to prepare the plant extract, while peaks observed at 842, 890, 1463, 1692, 1921, 2139, 2506 and 3579 are therefore correlated to plant phytochemicals. One hour after mixing the plant extract with the Au solution all the peaks related to phytochemicals, except the one at 890 cm^{-1} corresponding to the C=C bending of alkenes, disappeared or moved to different wavenumbers, suggesting the involvement of different chemical groups of the plant compounds in the bio-reduction and/or stabilization process producing the Au particles.

The peak observed at 842 cm^{-1}, related to the C-Cl stretching in the alkyl halides, after the reaction of extract's compounds with Au(III) solution shifted to 851 cm^{-1}. The peak at 1463 cm^{-1}, associated to the C-H bending of the methylene group, shifted to 1467 cm^{-1}. The band at 1692 cm^{-1}, which shifted to 1696 cm^{-1}, is related to stretching vibrations of (NH)C=O and/or C=O groups of conjugated aldehydes and carboxylic acids, and has been associated to phenolic acids or organic acids (Lu and Hsieh 2012), such as ellagic acids (Oszmiański et al. 2011). The peak that shifted from 1921 cm^{-1} to 1922 cm^{-1}, corresponds to the C-H bending of the aromatic compounds and is probably related to phenolics such as tannins, flavonoids and anthocyanins (Veljkovic et al. 2018). The peak first observed at 2139 cm^{-1} and then totally vanished, is related to N=C=N stretching of the carbodiimide group and probably indicates the presence of amino acids or proteins (Fiehn et al. 2000) and/or anthocyanin (Demirbas et al. 2019; Ekrikaya et al. 2021). The weak peak at 2506

cm^{-1} that shifted to 2505 cm^{-1} is related to the S-H stretching in the thiol group, which might be due to the presence of metallothioneins (Leszczyszyn et al. 2013) and/or cysteine rich metabolites (Harada et al. 2002), as both are known for their high metal interaction potential (Nobahar et al. 2021), and high concentrations of cysteine have been reported in the leaf extract of *R. idaeus* by Komisarenko et al. (2021). Finally, the band first occurring at 3579 cm^{-1} which shifted to 3585 cm^{-1} is probably related to the –OH vibrations of carboxylic acids, phenols or alcohols and/or -NH vibrations of amines, proteins and peptides.

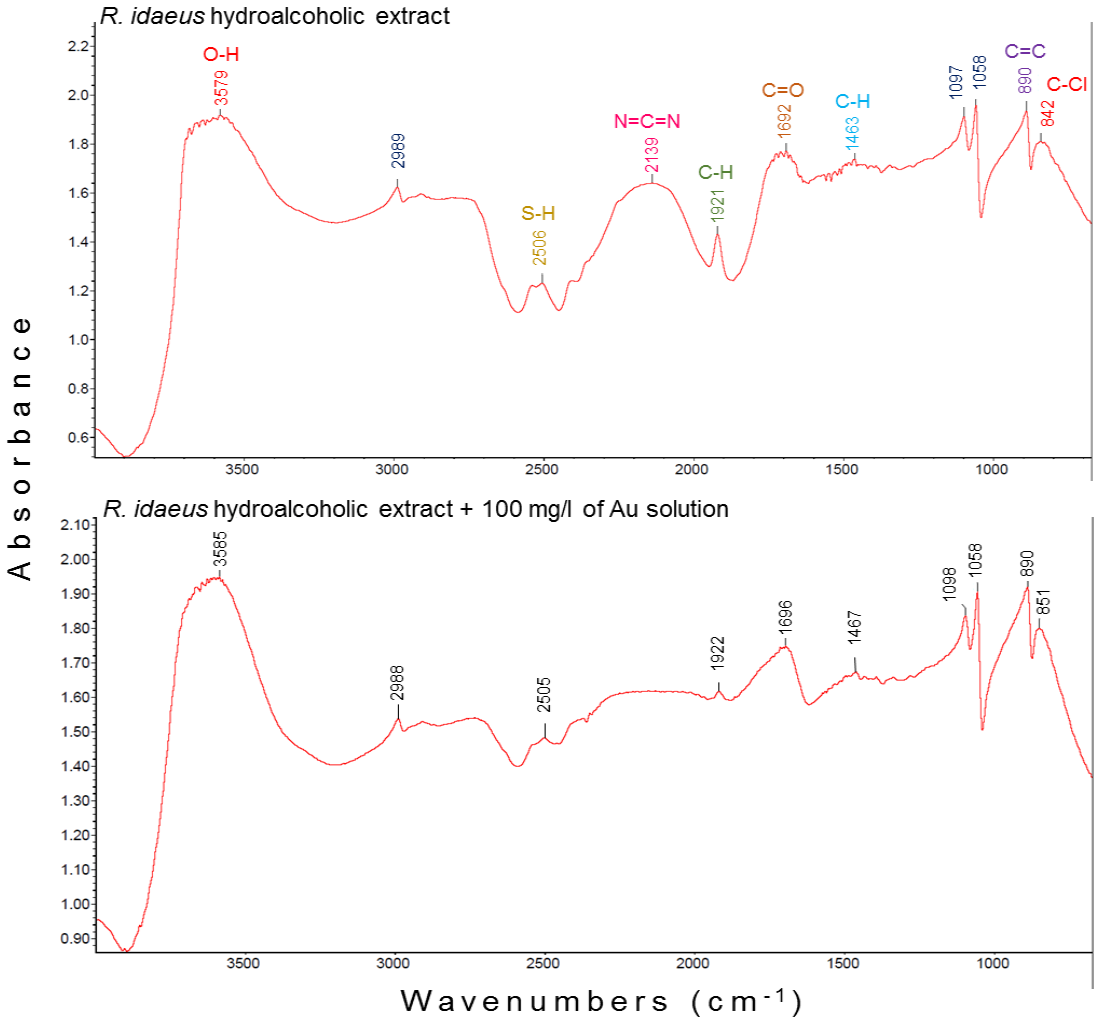

Figure 6.9. FTIR spectra of (above) *R. idaeus* hydroalcoholic extract diluted for analysis to a 15% (v/v) ratio in 0.02 M HCl and (below) *R. idaeus* extract added in a 50% (v/v) ratio to a 100 mg/L Au(III) solution in 0.02 M HCl and 1 hour after mixing diluted for analysis to a 7.5% (v/v) ratio in 0.02 M HCl.

Studies by Moreno-Medina et al (2018) and Oszmiański et al (2011) show the presence of phenols in high quantities (2.6% to 6.9% (w/w)), mainly as ellagic acids in the leaves of *R. idaeus*. Moreover, flavonoids are reported in high contents in the leaves of this plant; for instance, Gudej (2003) reports a flavonoid content range between 0.46% to 1.05% of the dried leaves (w/w), while, Durgo et al. (2012) reports the flavonoid of the leaves as the main constituent of the phenolic content, comprising about 11% of the leaf extract powder weight. Other types of phenolic compounds present in the leaves of *R. idaeus* are reported as vanillic acids, ferulic, caffeoyl tartaric, protocatechuic, gentisic, feruloyl tartaric, p-coumaric, p-coumaroyl-glucoside acids, p-hydroxybenzoic (Brandely 2006), caffeic and chlorogenic acid (Durgo et al. 2012), as well as terpenoids including mono- and sesquiterpenes, like terpinolene and triterpenes, squalene and cycloartenol (Kylli 2010; Committee on Herbal Medicinal Products (HMPC) 2012).

It is known that plant compounds in the groups of phenols and polyphenols have high interaction capabilities with metals in general, but specifically high with Au (Sengani et al. 2017; Santhoshkumar et al. 2017). The interaction mechanism of phenols with metals is not totally clear yet; however, it is known that the high capacity of free radical scavenging by the functional groups of phenols and also their high electron/proton donation potential are the main mechanism of interaction of these biomolecules with metals (Kaurinovic and Vastag 2019). In addition, another proposed mechanism is suggested by the presence of nucleophilic aromatic rings in conjunction with some functional groups such as carbonyl, carboxyl and hydroxyl groups in the phenolic compounds (Kulbat 2016; Liu et al. 2018).

In a similar study, Stevanović et al. (2019) used aqueous extracts of *R. idaeus* leaves for the synthesis of Ag nanoparticles and reported the polyphenolics, flavonoids, triterpenoids, proteins and organic acids as the possible reducing and stabilizing agents of Ag nanoparticles (Stevanović et al. 2019).

Moreover, another similar study by Demirbas et al. (2019), but using extracts of *R. idaeus* fruits (instead of leaves) for Au(III) reduction and Au nanoparticles synthesis, went further and indicated the specific catecholamine group of anthocyanin as the preferential site of coordination reaction with Au(III) and thus, the formation of anthocyanin-Au(III) complexes. Based on their conclusions, this reaction may initiate Au nucleation for seed formation and then, the oxidation of catecholamine groups results in electrons release, which boosts Au(III) reductin (Demirbas et al. 2019). Taking this into account and the fact that in the *R. idaeus* leaves there are contents of anthocyanines as high or higher than in the fruits (Veljkovic et al. 2019), it can be suggested that these compounds should also play an important role in the formation of Au particles when leaf extracts are used.

6.4. **Conclusions**

This work shows the high interaction potential of phytochemicals present in the leaves of three different plants (*R. idaeus*, *C. ladanifer* and *E. andevalensis*) with Au(III) ions when in simple unimetallic solutions, resulting in the separation of Au from the liquid phase. The work also shows that extracts from leaves of these three plants can be added to leachates obtained from PCBs, resulting in the separation of Au from the solution along with Pb as a major contaminant.

Moreover, specifically for the *R. idaeus* leaves extract, it was shown that pure Au nanoparticles can be obtained from Au unimetallic solutions, while Au nanoparticles obtained from PCBs leachates are contaminated with $PbSO_4$, which can be further separated from the Au particles by HCl washing. Plus, it was also shown that acetone efficiently removes the complexed organic-metals contaminants allowing to obtain highly

pure Au tiny nanoparticles (~18 nm) aggregated in larger Au microparticle clusters (~ 0.8 μm).

R. idaeus leaves are the main waste of red raspberry fruit industry, which is widely cultivated in Europe, Asia, and America. Therefore, this study reinforces the idea of beneficiation of those wastes in extract preparation and application for Au separation and recovery from secondary sources.

6.5. References

Abreu MM, Santos E, Fernandes E, et al (2011) Accumulation and translocation of trace elements in Cistus ladanifer L. from IPB portuguese mining areas. Revista de Ciências Agrárias 45–56

Abreu MM, Tavares MT, Batista MJ (2008) Potential use of Erica andevalensis and Erica australis in phytoremediation of sulphide mine environments: São Domingos, Portugal. Journal of Geochemical Exploration 96:210–222. https://doi.org/10.1016/j.gexplo.2007.04.007

Al Soubaihi R, Saoud K, Dutta J (2018) Critical Review of Low-Temperature CO Oxidation and Hysteresis Phenomenon on Heterogeneous Catalysts. Catalysts 8:660. https://doi.org/10.3390/catal8120660

Anbu P, Gopinath SC, Jayanthi S (2020) Synthesis of gold nanoparticles using *Platycodon grandiflorum* extract and its antipathogenic activity under optimal conditions. Nanomaterials and Nanotechnology 10:184798042096169. https://doi.org/10.1177/1847980420961697

Bard AJ, Parsons R, Jordan J (1985) International Union Of Pure And Applied Chemistry. Standard potentials in aqueous solution

Birloaga I, Coman V, Kopacek B, Vegliò F (2014) An advanced study on the hydrometallurgical processing of waste computer printed circuit boards to extract their valuable content of metals. Waste Management 34:2581–2586. https://doi.org/10.1016/j.wasman.2014.08.028

Botha TL, Elemike EE, Horn S, et al (2019) Cytotoxicity of Ag, Au and Ag-Au bimetallic nanoparticles prepared using golden rod (Solidago canadensis) plant extract. Sci Rep 9:4169. https://doi.org/10.1038/s41598-019-40816-y

Bourgeois D, Lacanau V, Mastretta R, et al (2020) A simple process for the recovery of palladium from wastes of printed circuit boards. Hydrometallurgy 191:105241. https://doi.org/10.1016/j.hydromet.2019.105241

Brandely P (2006) Raspberry leaf. In British Herbal Compendium. A Handbook of Scientific Information on Widely Used Plant Drugs. British Herbal Medicine Association, Bournemouth, UK

Cabezudo B, Rivera J (1980) Notas taxonómicas y corológicas sobre la Flora de Andalucía occidental. 2: Erica andevalensis Cabezudo y Rivera sp. nov. Lagascalia 9:223–226

Chen Y, Qiao Q, Cao J, et al (2021) Precious metal recovery. Joule 5:3097–3115. https://doi.org/10.1016/j.joule.2021.11.002

Clemens S (2001) Molecular mechanisms of plant metal tolerance and homeostasis. Planta 212:475–486. https://doi.org/10.1007/s004250000458

Committee on Herbal Medicinal Products (HMPC) (2012) Assessment Report on Rubus idaeus L., Folium.

Cui J, Zhang L (2008) Metallurgical recovery of metals from electronic waste: A review. Journal of Hazardous Materials 158:228–256. https://doi.org/10.1016/j.jhazmat.2008.02.001

Demirbas A, Büyükbezirci K, Celik C, et al (2019) Synthesis of Long-Term Stable Gold Nanoparticles Benefiting from Red Raspberry (*Rubus idaeus*), Strawberry (*Fragaria ananassa*), and Blackberry (*Rubus fruticosus*) Extracts–Gold Ion Complexation and Investigation of Reaction Conditions. ACS Omega 4:18637–18644. https://doi.org/10.1021/acsomega.9b02469

Demirbas A, Yilmaz V, Ildiz N, et al (2017) Anthocyanins-rich berry extracts directed formation of Ag NPs with the investigation of their antioxidant and antimicrobial activities. Journal of Molecular Liquids 248:1044–1049. https://doi.org/10.1016/j.molliq.2017.10.130

Dimcheva N (2020) Nanostructures of noble metals as functional materials in biosensors. Current Opinion in Electrochemistry 19:35–41. https://doi.org/10.1016/j.coelec.2019.09.008

Durães N, Bobos I, Ferreira da Silva E, Dekayir A (2015) Copper, zinc and lead biogeochemistry in aquatic and land plants from the Iberian Pyrite Belt (Portugal) and north of Morocco mining areas. Environ Sci Pollut Res 22:2087–2105. https://doi.org/10.1007/s11356-014-3394-6

Durgo K, Belščak-Cvitanović A, Stančić A, et al (2012) The Bioactive Potential of Red Raspberry (*Rubus idaeus* L.) Leaves in Exhibiting Cytotoxic and Cytoprotective Activity on Human Laryngeal Carcinoma and Colon Adenocarcinoma. Journal of Medicinal Food 15:258–268. https://doi.org/10.1089/jmf.2011.0087

Ekrikaya S, Yilmaz E, Celik C, et al (2021) Investigation of ellagic acid rich-berry extracts directed silver nanoparticles synthesis and their antimicrobial properties with potential mechanisms towards Enterococcus faecalis and Candida albicans. Journal of Biotechnology 341:155–162. https://doi.org/10.1016/j.jbiotec.2021.09.020

Engvild KC (1986) Chlorine-containing natural compounds in higher plants. Phytochemistry 25:781–791. https://doi.org/10.1016/0031-9422(86)80002-4

Fiehn O, Kopka J, Trethewey RN, Willmitzer L (2000) Identification of Uncommon Plant Metabolites Based on Calculation of Elemental Compositions Using Gas

Chromatography and Quadrupole Mass Spectrometry. Anal Chem 72:3573–3580. https://doi.org/10.1021/ac991142i

Firdhouse MJ, Lalitha P (2016) Flower-shaped gold nanoparticles synthesized using Kedrostis foetidissima and their antiproliferative activity against bone cancer cell lines. Int J Ind Chem 7:347–358. https://doi.org/10.1007/s40090-016-0098-4

Forti V, Balde C, Kuehr R, Bel G (2020) The Global E-waste Monitor 2020: Quantities, flows and the circular economy potential. United Nations University/United Nations Institute for Training and Research, International Telecommunication Union, and International Solid Waste Association, Bonn, Geneva and Rotterdam

Gonzalez Baez A, Pantoja Muñoz L, Garelick H, Purchase D (2022) Characterization of industrially pre-treated waste printed circuit boards for the potential recovery of rare earth elements. Environmental Technology & Innovation 27:102481. https://doi.org/10.1016/j.eti.2022.102481

Gudej J (2003) Kaempferol and quercetin glycosides from Rubus idaeus L. leaves. Acta Poloniae Pharmaceutica 60:313–316

Harada E, Yamaguchi Y, Koizumi N, Hiroshi S (2002) Cadmium stress induces production of thiol compounds and transcripts for enzymes involved in sulfur assimilation pathways in Arabidopsis. Journal of Plant Physiology 159:445–448. https://doi.org/10.1078/0176-1617-00733

Hyder A, Buledi JA, Nawaz M, et al (2022) Identification of heavy metal ions from aqueous environment through gold, Silver and Copper Nanoparticles: An excellent colorimetric approach. Environmental Research 205:112475. https://doi.org/10.1016/j.envres.2021.112475

Ishak NAI, Kamarudin SK, Timmiati SN (2019) Green synthesis of metal and metal oxide nanoparticles via plant extracts: an overview. Mater Res Express 6:112004. https://doi.org/10.1088/2053-1591/ab4458

Islam A, Ahmed T, Awual MdR, et al (2020) Advances in sustainable approaches to recover metals from e-waste-A review. Journal of Cleaner Production 244:118815. https://doi.org/10.1016/j.jclepro.2019.118815

Islam A, Swaraz AM, Teo SH, et al (2021) Advances in physiochemical and biotechnological approaches for sustainable metal recovery from e-waste: A critical review. Journal of Cleaner Production 323:129015. https://doi.org/10.1016/j.jclepro.2021.129015

Janyasuthiwong S, Ugas R, Rene ER, et al (2016) Effect of operational parameters on the leaching efficiency and recovery of heavy metals from computer printed circuit boards: Recovery of heavy metals from computer printed circuit boards. J Chem Technol Biotechnol 91:2038–2046. https://doi.org/10.1002/jctb.4798

Jeon S, Tabelin CB, Park I, et al (2020) Ammonium thiosulfate extraction of gold from printed circuit boards (PCBs) of end-of-life mobile phones and its recovery from pregnant leach solution by cementation. Hydrometallurgy 191:105214. https://doi.org/10.1016/j.hydromet.2019.105214

Kaurinovic B, Vastag D (2019) Flavonoids and Phenolic Acids as Potential Natural Antioxidants. In: Shalaby E (ed) Antioxidants. IntechOpen

Khan T, Ullah N, Khan MA, et al (2019) Plant-based gold nanoparticles; a comprehensive review of the decade-long research on synthesis, mechanistic aspects and diverse applications. Advances in Colloid and Interface Science 272:102017. https://doi.org/10.1016/j.cis.2019.102017

Kim JG (2013) Material flow and industrial demand for palladium in Korea. Resources, Conservation and Recycling 77:22–28. https://doi.org/10.1016/j.resconrec.2013.04.009

Komisarenko MA, Polischuk IM, Upyr TV, Saidov NB (2021) Study of Amino acid composition and immunomodulatory activity of Rubus idaeus alcoholic extract. RESEARCH JOURNAL OF PHARMACY AND TECHNOLOGY 14:1329–1332. https://doi.org/10.5958/0974-360X.2021.00236.5

Kulbat K (2016) The role of phenolic compounds in plant resistance. 80:97–108

Kumar A, Saini HS, Kumar S (2018) Bioleaching of Gold and Silver from Waste Printed Circuit Boards by Pseudomonas balearica SAE1 Isolated from an e-Waste Recycling Facility. Curr Microbiol 75:194–201. https://doi.org/10.1007/s00284-017-1365-0

Kumar V, Yadav SK (2009) Plant-mediated synthesis of silver and gold nanoparticles and their applications. J Chem Technol Biotechnol 84:151–157. https://doi.org/10.1002/jctb.2023

Kylli P (2010) Berry phenolics : isolation, analysis, identification, and antioxidant properties. Doctoral dissertation, Helsingin yliopisto

Le H-L, Yamasue E, Okumura H, Ishihara KN (2013) MEMRECS—A Sustainable View for Metal Recycling from Waste Printed Circuit Boards. JEP 04:803–810. https://doi.org/10.4236/jep.2013.48094

Lee KX, Shameli K, Yew YP, et al (2020) Recent Developments in the Facile Bio-Synthesis of Gold Nanoparticles (AuNPs) and Their Biomedical Applications. IJN Volume 15:275–300. https://doi.org/10.2147/IJN.S233789

Leszczyszyn OI, Imam HT, Blindauer CA (2013) Diversity and distribution of plant metallothioneins: a review of structure, properties and functions. Metallomics 5:1146. https://doi.org/10.1039/c3mt00072a

Li H, Eksteen J, Oraby E (2018) Hydrometallurgical recovery of metals from waste printed circuit boards (WPCBs): Current status and perspectives – A review. Resources, Conservation and Recycling 139:122–139. https://doi.org/10.1016/j.resconrec.2018.08.007

Li Z, Ravaine V, Ravaine S, et al (2007) Raspberry-like Gold Microspheres: Preparation and Electrochemical Characterization. Adv Funct Mater 17:618–622. https://doi.org/10.1002/adfm.200600667

Liu Y-S, Chang Y-C, Chen H-H (2018) Silver nanoparticle biosynthesis by using phenolic acids in rice husk extract as reducing agents and dispersants. Journal of Food and Drug Analysis 26:649–656. https://doi.org/10.1016/j.jfda.2017.07.005

Lu P, Hsieh Y-L (2012) Cellulose isolation and core–shell nanostructures of cellulose nanocrystals from chardonnay grape skins. Carbohydrate Polymers 87:2546–2553. https://doi.org/10.1016/j.carbpol.2011.11.023

Luda MP (2011) Recycling of Printed Circuit Boards. Integrated Waste Management

Ma Y, Oliveira RS, Freitas H, Zhang C (2016) Biochemical and Molecular Mechanisms of Plant-Microbe-Metal Interactions: Relevance for Phytoremediation. Front Plant Sci 7:. https://doi.org/10.3389/fpls.2016.00918

Madkour LH (2018) Applications of gold nanoparticles in medicine and therapy. PPIJ 6:. https://doi.org/10.15406/ppij.2018.06.00172

Magoda K, Mekuto L (2022) Biohydrometallurgical Recovery of Metals from Waste Electronic Equipment: Current Status and Proposed Process. Recycling 7:67. https://doi.org/10.3390/recycling7050067

Mejáre M, Bülow L (2001) Metal-binding proteins and peptides in bioremediation and phytoremediation of heavy metals. Trends in Biotechnology 19:67–73. https://doi.org/10.1016/S0167-7799(00)01534-1

Milazzo G, Caroli S, Sharma VK (1978) Tables of Standard Electrode Potentials. Wiley: London

Mir S, Dhawan N (2022) A comprehensive review on the recycling of discarded printed circuit boards for resource recovery. Resources, Conservation and Recycling 178:106027. https://doi.org/10.1016/j.resconrec.2021.106027

Monaci F, Leidi EO, Mingorance MD, et al (2011) Selective uptake of major and trace elements in Erica andevalensis, an endemic species to extreme habitats in the Iberian Pyrite Belt. Journal of Environmental Sciences 23:444–452. https://doi.org/10.1016/S1001-0742(10)60429-9

Moreno-Medina BL, Casierra-Posada F, Cutler J (2018) Phytochemical Composition and Potential Use of Rubus Species. Gesunde Pflanzen 70:65–74. https://doi.org/10.1007/s10343-018-0416-1

Neto IFF (2018) A simple and sustainable approach to recover metals from spent printed circuit boards. University of Porto

Nobahar A, Carlier JD, Miguel MG, Costa MC (2021) A review of plant metabolites with metal interaction capacity: a green approach for industrial applications. Biometals. https://doi.org/10.1007/s10534-021-00315-y

Oszmiański J, Wojdyło A, Gorzelany J, Kapusta I (2011) Identification and Characterization of Low Molecular Weight Polyphenols in Berry Leaf Extracts by HPLC-DAD and LC-ESI/MS. J Agric Food Chem 59:12830–12835. https://doi.org/10.1021/jf203052j

Pal DB, Chand R, Upadhyay SN, Mishra PK (2018) Performance of water gas shift reaction catalysts: A review. Renewable and Sustainable Energy Reviews 93:549–565. https://doi.org/10.1016/j.rser.2018.05.003

Pantelidis G, Vasilakakis M, Manganaris G, Diamantidis G (2007) Antioxidant capacity, phenol, anthocyanin and ascorbic acid contents in raspberries, blackberries, red

currants, gooseberries and Cornelian cherries. Food Chemistry 102:777–783. https://doi.org/10.1016/j.foodchem.2006.06.021
Park YJ, Fray DJ (2009) Recovery of high purity precious metals from printed circuit boards. Journal of Hazardous Materials 164:1152–1158. https://doi.org/10.1016/j.jhazmat.2008.09.043
Pietrobelli JMT de A, Módenes AN, Fagundes-Klen MR, Espinoza-Quiñones FR (2009) Cadmium, Copper and Zinc Biosorption Study by Non-Living Egeria densa Biomass. Water Air Soil Pollut 202:385–392. https://doi.org/10.1007/s11270-009-9987-x
Quental L, Bourguignon A, Sousa AJ, et al (2002) MINEO Southern Europe environment test site. Contamination impact mapping and modelling-Final Report. Assessing and Monitoring the Environmental Impact of Mining Activities in Europe Using Advanced Earth Observation Techniques 5yth FP-IST. (MINEO) 1999--10337
Rossini-Oliva S, Abreu MM, Leidi EO (2018) A review of hazardous elements tolerance in a metallophyte model species: Erica andevalensis. Geoderma 319:43–51. https://doi.org/10.1016/j.geoderma.2017.12.035
Santhoshkumar J, Rajeshkumar S, Venkat Kumar S (2017) Phyto-assisted synthesis, characterization and applications of gold nanoparticles – A review. Biochemistry and Biophysics Reports 11:46–57. https://doi.org/10.1016/j.bbrep.2017.06.004
Santos ES, Abreu MM, Batista MJ, et al (2014) Inter-population variation on the accumulation and translocation of potentially harmful chemical elements in Cistus ladanifer L. from Brancanes, Caveira, Chança, Lousal, Neves Corvo and São Domingos mines in the Portuguese Iberian Pyrite Belt. J Soils Sediments 14:758–772. https://doi.org/10.1007/s11368-014-0852-1
Santos ES, Abreu MM, Magalhães MCF (2016) Cistus ladanifer phytostabilizing soils contaminated with non-essential chemical elements. Ecological Engineering 94:107–116. https://doi.org/10.1016/j.ecoleng.2016.05.072
Santos ES, Abreu MM, Nabais C, Magalhães MCF (2012) Trace element distribution in soils developed on gossan mine wastes and Cistus ladanifer L. tolerance and bioaccumulation. Journal of Geochemical Exploration 123:45–51. https://doi.org/10.1016/j.gexplo.2012.05.006
Sengani M, Grumezescu AM, Rajeswari VD (2017) Recent trends and methodologies in gold nanoparticle synthesis – A prospective review on drug delivery aspect. OpenNano 2:37–46. https://doi.org/10.1016/j.onano.2017.07.001
Shah S, Shah SA, Faisal S, et al (2022) Engineering novel gold nanoparticles using Sageretia thea leaf extract and evaluation of their biological activities. J Nanostruct Chem 12:129–140. https://doi.org/10.1007/s40097-021-00407-8
Sharma SS, Schat H, Vooijs R (1998) In vitro alleviation of heavy metal-induced enzyme inhibition by proline. Phytochemistry 49:1531–1535. https://doi.org/10.1016/S0031-9422(98)00282-9
Silverstein RM, Webster FX (1997) Spectrometric Identification of Organic Compounds. John Wiley and Sons, Inc

Skoog DA, West DM, Holler FJ, Crouch SR (2000) Analytical Chemistry - An Introduction.

Stevanović M, Zvezdanović J, Stanojević L, et al (2019) Synthesis, characterization and antioxidant activity of silver nanoparticles stabilized by aqueous extracts of wild blackberry (Rubus spp.) and raspberry (Rubus idaeus L.) leaves. Adv Techol 8:47–58. https://doi.org/10.5937/SavTeh1901047S

Svarovsky S, Borovkov A, Sykes K (2008) Cationic gold microparticles for biolistic delivery of nucleic acids. BioTechniques 45:535–540. https://doi.org/10.2144/000112991

Sverdrup HU, Ragnarsdottir KV (2016) A system dynamics model for platinum group metal supply, market price, depletion of extractable amounts, ore grade, recycling and stocks-in-use. Resources, Conservation and Recycling 114:130–152. https://doi.org/10.1016/j.resconrec.2016.07.011

Veljkovic B, Djordjevic N, Dolicanin Z, et al (2018) Antioxidant and Anticancer Properties of Leaf and Fruit Extracts of the Wild Raspberry (Rubus idaeus L.). Not Bot Horti Agrobo 47:359–367. https://doi.org/10.15835/nbha47111274

Wang L, Lin X, Zhang J, et al (2019) Extraction methods for the releasing of bound phenolics from Rubus idaeus L. leaves and seeds. Industrial Crops and Products 135:1–9. https://doi.org/10.1016/j.indcrop.2019.04.003

Wongsawa T, Traiwongsa N, Pancharoen U, Nootong K (2020) A review of the recovery of precious metals using ionic liquid extractants in hydrometallurgical processes. Hydrometallurgy 198:105488. https://doi.org/10.1016/j.hydromet.2020.105488

Yang D, Fan R, Luo F, et al (2021) Facile and green fabrication of efficient Au nanoparticles catalysts using plant extract via a mesoporous silica-assisted strategy. Colloids and Surfaces A: Physicochemical and Engineering Aspects 621:126580. https://doi.org/10.1016/j.colsurfa.2021.126580

Zhu B, Xie N, Yue L, et al (2022) Formulation and characterization of a novel anti-human endometrial cancer supplement by gold nanoparticles green-synthesized using Spinacia oleracea L. Leaf aqueous extract. Arabian Journal of Chemistry 15:103576. https://doi.org/10.1016/j.arabjc.2021.103576

6.6. **Annexes**

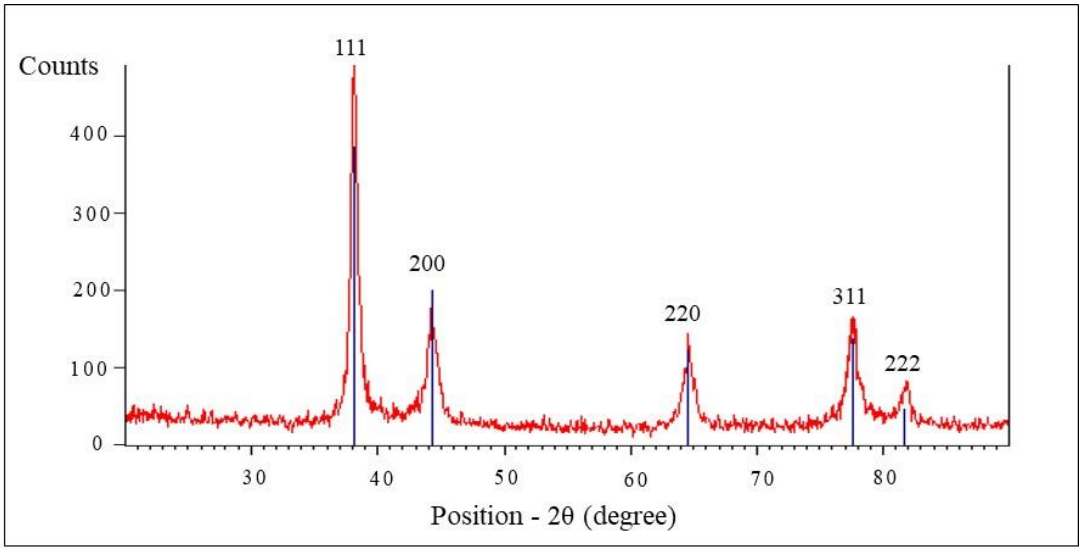

Figure S- 6.1. XRD analysis of gold particles obtained by adding *Rubus idaeus* extract to Au(III)unimetallic solution (100 mg/L metal standard solution) in 0.02 M HCl, at a 1/10 (v/v) ratio. The peak positions of Au crystalline phase are based on the card #01-071-4073.

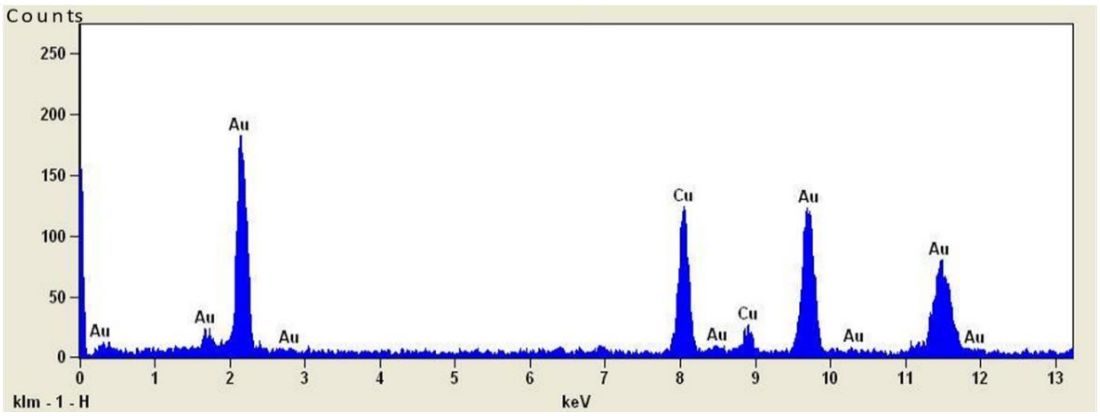

Figure S- 6.2. EDS spectroscopy of gold particles obtained by adding *Rubus idaeus* extract to Au(III) unimetallic solution (100 mg/L metal standard solution) in 0.02 M HCl, at a 1/10 (v/v) ratio.

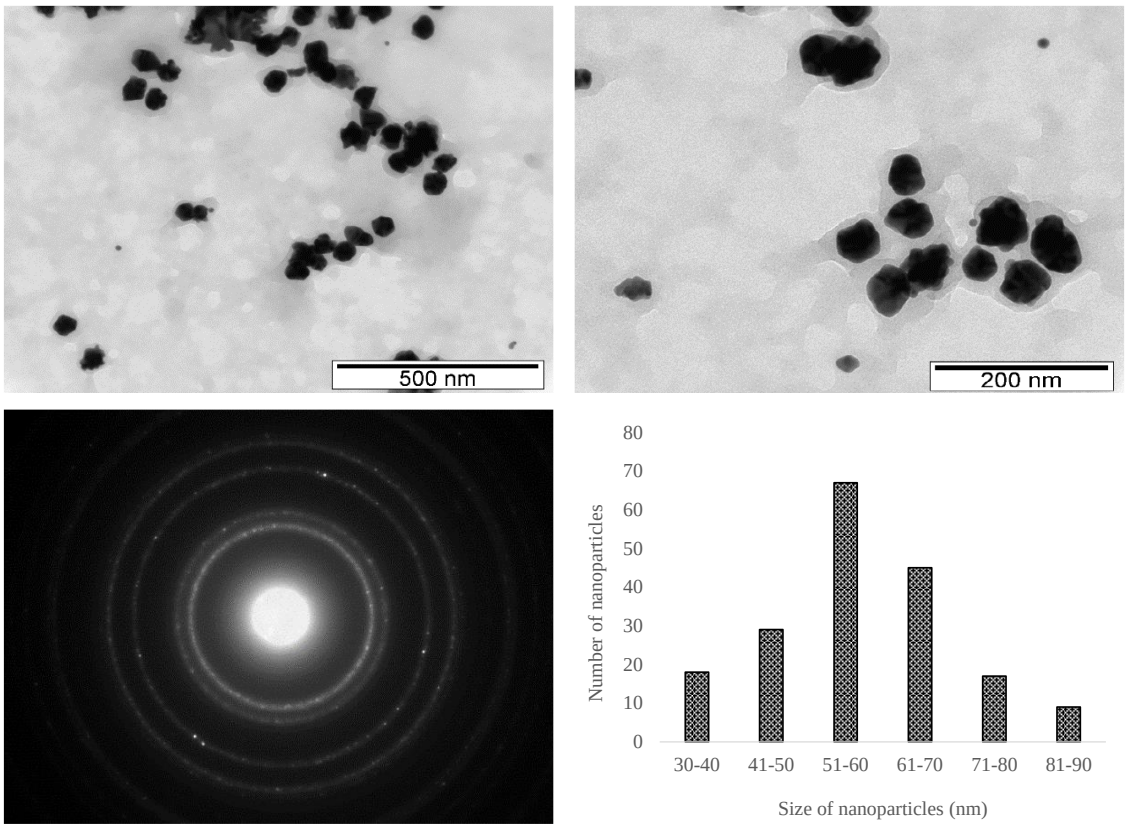

Figure S- 6.3. A, B) TEM images of the Au nanoparticles obtained by adding 70% ethanolic extract of *R. idaeus* to the Au(III) unimetallic solution, C) selected-area electron diffraction (SAED) patterns of the nanoparticle and D) Size distribution histogram of the particles.

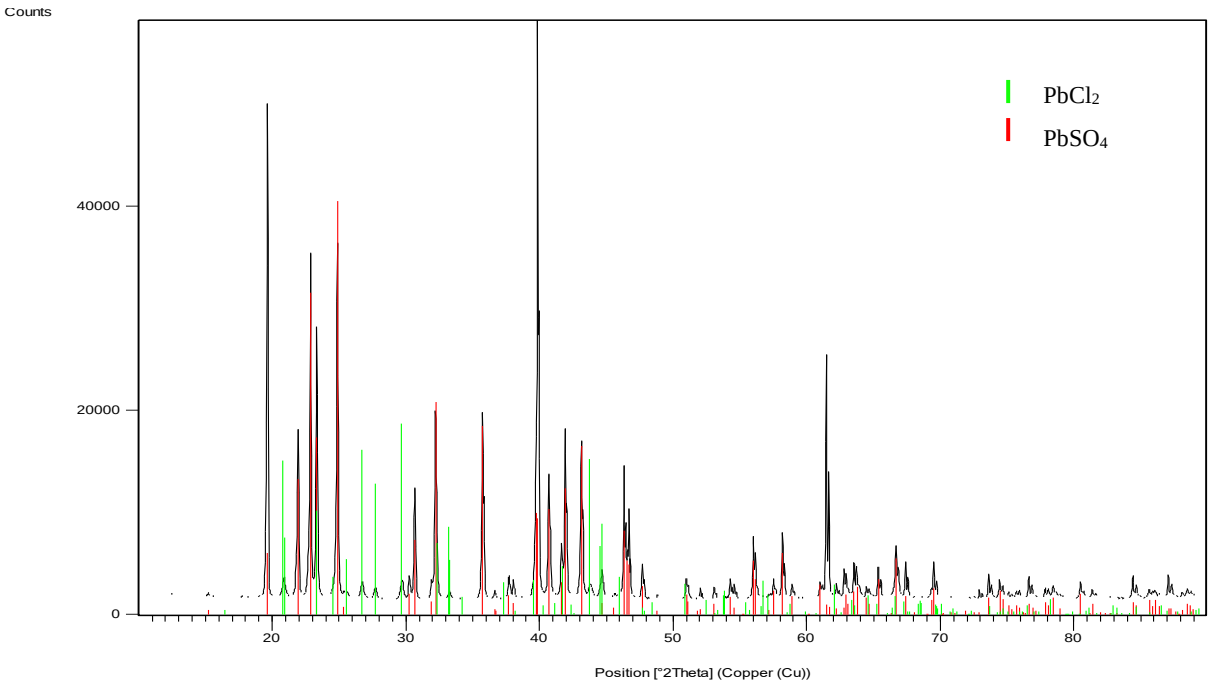

Figure S- 6.4. XRD analysis of precipitates obtained by adding 0.15 M Na_2SO_4 to the leachate (in 1/1 (v/v) ratio) aiming Pb separation. The peak positions of $PbCl_2$ and $PbSO_4$ crystalline phases are based on the cards #01-084-1177 and #01-082-1854, respectively.

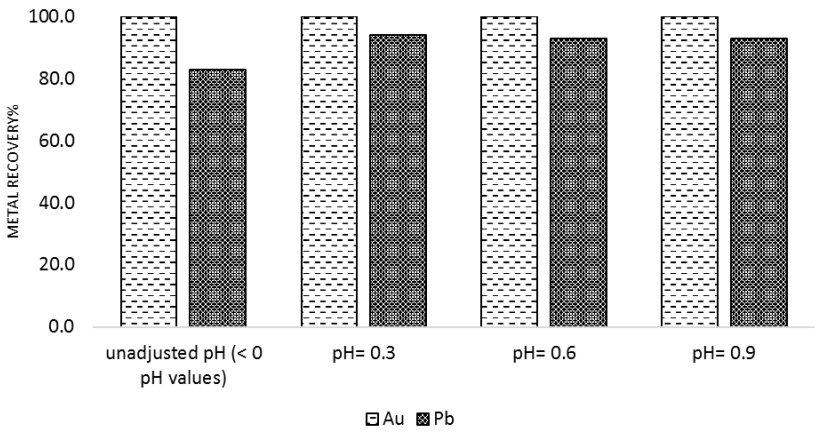

Figure S- 6.5. Au and Pb precipitation by applying *Rubus idaeus* extract to Au bearing leachate with different pH values after 48 hours.

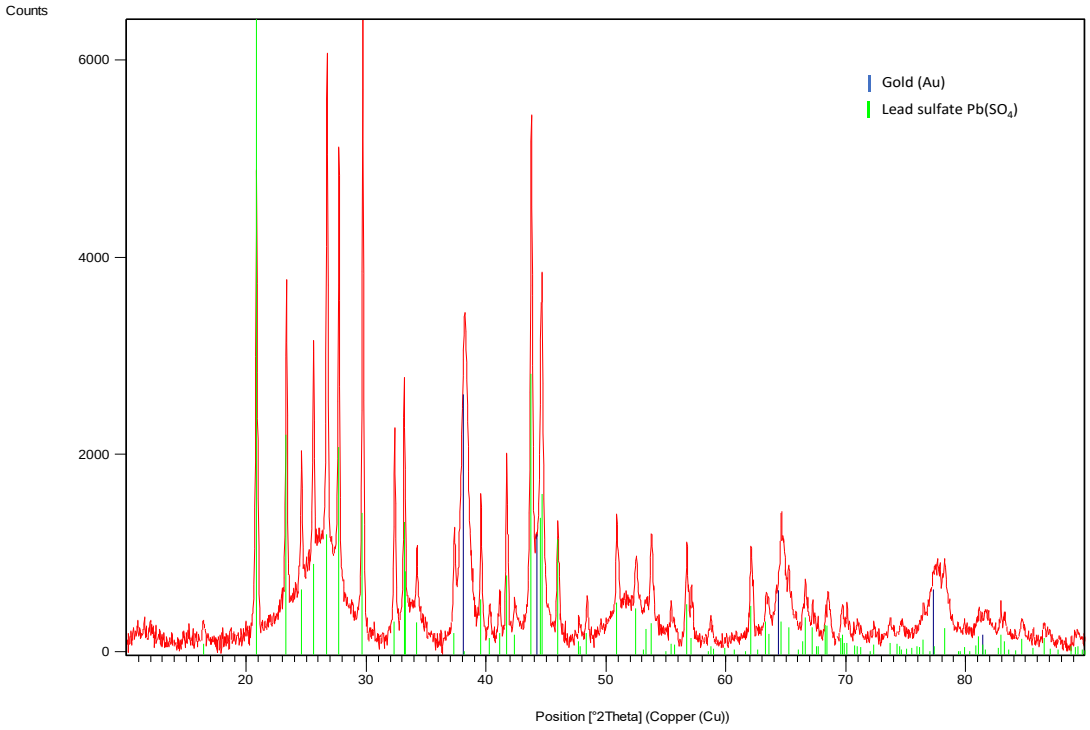

Figure S- 6.6. XRD analysis of precipitates obtained by adding *Rubus idaeus* extract to Au bearing leachate at a 1/10 (v/v) ratio. The peak positions of Au crystalline phase are based on the card #01-071-4073.

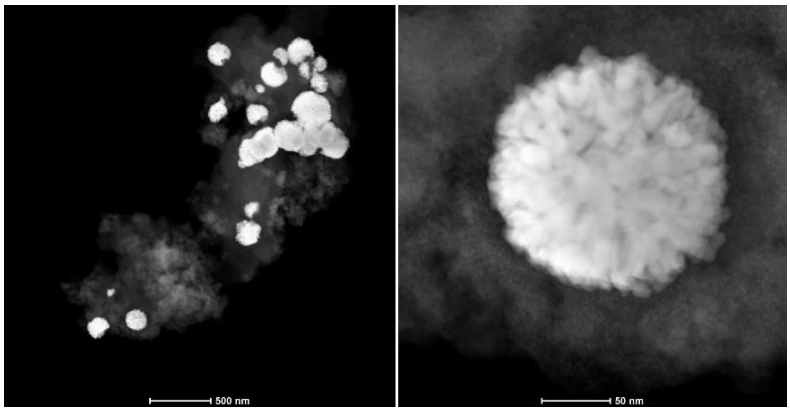

Figure S- 6.7. The area of two images of the particles synthesized by applying *R. idaeus* extract to leachate in 1/10 ratio (v/v) washed with 96% ethanol that were used for relative abundances measurements.

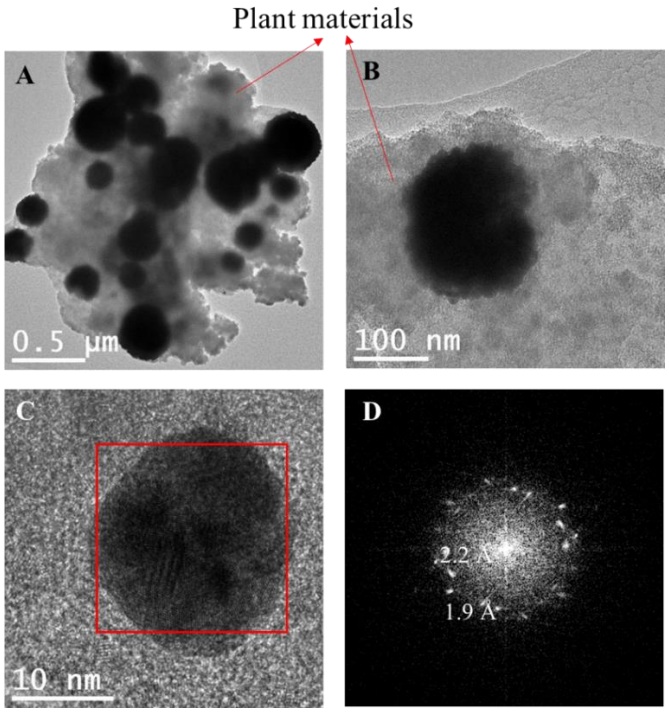

Figure S- 6.8. A) HRTEM images of the Au nanoparticles obtained by adding 70% ethanolic extract of *R idaeus* to the Au bearing leachate and washed with ethanol B,C) magnified high resolution STEM, D) Fast Fourier Transform (FFT) pattern of a single nanoparticle (red square in figure C).

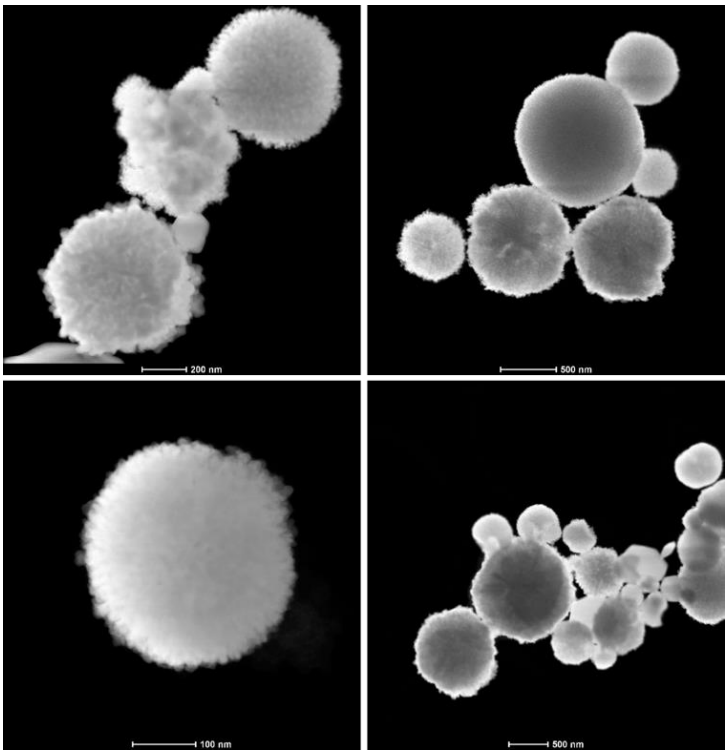

Figure S- 6.9. The area of four images of the particles synthesized by applying *R. idaeus* extract to leachate in 1/10 ratio (v/v) washed with pure acetone that were used for relative abundances measurements.

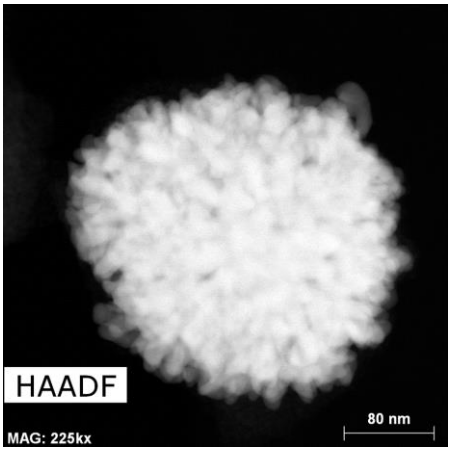

Figure S- 6.10. HAADF-STEM of a single Au particle.

CHAPTER 7

General conclusions and Future perspectives

7.1. General conclusions

Copper recovery from extreme acid mine drainage

- SX process with 30% (v/v) Acorga M5640 in kerosene-like solvents with 2.5% octanol can extract over 95% of the Cu present in highly acidic, metal-rich AMD;
- Application of 2M sulfuric acid can strip more than 99% of the loaded Cu from organic phase, allowing to rise the concentration of Cu in the stripping solution to ~46 g/L through successive striping steps with the potential of elemental Cu recovery using traditional electrowinning process;
- Combination of SX systems with biological processes by biogenic sulfide addition at S:Cu ratios of approximately 2:1 can be performed to recover the extracted Cu as covellite nanoparticles. The covellite produced can be used in a variety of renewable energy, biomedical, and other applications.

Zinc recovery from extreme copper-free acid mine drainage

- The ionic liquid called AliCy, can effectively extract ~90% of Fe^{3+} from extreme AMD waters with pH 1.0 to 1.5 and the alkalinization of the obtained raffinate to pH 3.25 to 3.5 allows the removal of remaining Fe^{3+} from the solution with low losses of Zn;
- ZnS nanoparticles can be produced from extreme copper-free AMD after Cu SX and Fe^{3+} separation by AliCy's SX followed by alkalinization to pH 3.25 to 3.5 and then biogenic sulfide addition.
- A first outline of possible processes to recover metals of interest from acidic solutions with Fe^{3+} contamination can be proposed: (i) Fe^{3+} separation by SX using AliCy, (ii) pH alkalinization to remove remaining Fe^{3+}, (iii) recovery of target metals.

Application of enriched acidophilic sulfate-reducing bacteria from São Domingos mine in metal attenuation from AMD

- A microbial consortium having an acidophilic sulfate reducing bacteria (aSRB) community with sulfate reduction activity at pH 4.00 with methanol as electron donor has been successfully enriched from the sediments of a confluence area between an AMD stream and a water stream receiving a municipal WWTP effluent at an inactive copper mine site;
- The strategy of isolating aSRB colonies from the enriched cultures in closed centrifuge tubes with solid medium was efficient and the obtained SRB isolates were *Desulfosporosinus* spp. However, a fungus from *Trichoderma* genus was also present in the solid medium where the colonies grew, suggesting a possible interaction of symbiosis or commensalism favoring the growth of SRB;
- The aSRB enriched consortium was then tested for metal attenuation from AMD with pH adjusted to pH 4.50 in batch tests and the lowest tested dose of nutrients supplement (20% v/v of Postgate B base – corresponding to 1.15 g/L of basal salts and 0.2 g/L of yeast extract) with 30 mM methanol allowed the removal of more than 99% of metals after 28 days;
- A meta-taxonomic study of the communities revealed that the most abundant prokaryotes in the AMD remediation tests were *Clostridium* members and *Desulfosporosinus* genus. The first were found more abundant in the tests with higher Postgate B base supplements, (≥60%), while *Desulfosporosinus* was the dominant bacterial genus when lower doses of basal salts and yeast extract were used.

Palladium bio-recovery from spent automotive catalytic converter leachates

- 70% ethanolic extracts from leaves of *R. idaeus* can induce high precipitation of Pd^{2+} and Pt^{2+} ions from unimetallic aqueous solutions, thus suggesting potential use of polar extracts for the recovery of these metals from different metal bearing waters;
- Application of *R. idaeus* leaves' extract to spent ACC leachates can induce the production of a precipitate containing agglomerates of particles (of sizes up to 10

μm) having Pd and other elements such as Na, Cl, Ce, P and Al, along with plant material, and washing the obtained agglomerates with acetone results in a purified (~75%) precipitate with Pd^0 nanoparticles (6 ± 2 nm) with some traces of other elements;

- The process was found to have a rough cost estimate of ~20 $ per g of synthesized Pd particles – excluding manpower;
- During this Pd recovery process, UV-visible spectroscopy revealed signs of Pd^{2+} reduction to Pd^0 and nanoparticles formation. Moreover, FTIR analysis revealed changes after mixing the Pd^{2+} solution with plant extract in different functional groups (such as OH group) that are mainly related to phenols and polyphenols and flavonoids, which are known as compounds with high capacity to reduce PGM.

Printed circuit boards leaching followed by synthesis of gold nanoparticle clusters using plant extracts

- Phytochemicals present in 70% ethanolic extracts from leaves of *R. idaeus*, *C. ladanifer* and *E. andevalensis* showed high interaction potential with Au^{3+} ions in simple unimetallic solutions, resulting in the separation of Au from the liquid phase;
- Application of *R. idaeus* leaves extract to printed circuit boards' leachates results in Au nanoparticles contaminated with $PbSO_4$, which can be further separated from the Au particles by HCl washing. Then, further washing with ethanol and acetone efficiently removes complexed organic-metals contaminants allowing to obtain highly pure Au tiny nanoparticles (~18 nm) aggregated in larger Au microparticle clusters (~ 0.8 μm).

7.2. **Future perspectives**

The present study was performed aiming to benefit the potential of SX and also biological methods for the metal recovery/removal from metal bearing wastewaters and leachates. From the obtained results with the performed studies, it is expected that they can help to find innovative, efficient, and cost-effective strategies in metal recovery/removal from metal bearing wastewaters and leachates. Thus, based on the obtained results of this thesis, the following recommendations are suggested for future study to onward increase the current knowledge on this subject:

Regarding metal recovery from extreme AMD using SX and aSRB based processes:

- Beneficiation of extraction potential of Acorga M5640 for Cu recovery from highly concentrated AMD in combination with sulfidogenic reactors in pilot scale, to determine the feasibility of the method in industrial scale;
- After the Cu recovery process, Fe^{3+} removal from Cu-free AMD through SX by AliCy followed by alkalinization, and finally Zn recovery using biogenic sulfide in pilot scale, to determine the feasibility of the method in industrial scale;
- Application of AliCy for Fe^{3+} separation from other types of metal bearing acidic waters, where Fe^{3+} is considered as nuisance in the recovery of target metal, such as PGMs recovery from automobile catalyst leach liquors, Mn recovery from ferruginous Mn ores, recovery of indium of Fe rich solutions etc. to prevent Fe contaminations in the recovery of valuable metals and to uncover the application potential of this IL in different industrial sectors;
- Optimize the AMD inlet flow rate to aSRB bioreactors to maintain pH > 4.0, thus eliminating the pH adjustment step prior to AMD bioremediation;
- Investigation for economically viable sources of nutrients supplements (such as basal salts and methanol containing wastes) able to maintain efficient sulfate reduction by the aSRB enriched consortium;

- Make SRB bioreactors more resistant to acidification phenomena during operation when sugars-rich residues are used as carbon sources;
- Possibility of utilization in biogenic sulfide production for selective metal recovery systems operating at low pH;
- Optimize liquid culture conditions to grow aSRB isolates from the selected consortium for further characterization studies (e.g. genomic and transcriptomic studies to characterize metabolic pathways) and deposit of characterized strains in bacterial collections;
- According to the results described in this thesis and their framing in the known state of the art as well as benefiting from future studies such as those suggested in this chapter, one can think of a system with several integrated processes to recover Cu and Zn from extreme AMD generating an effluent with low concentrations of contaminants. In figure Figure **7.1** a diagram of such putative system is presented.

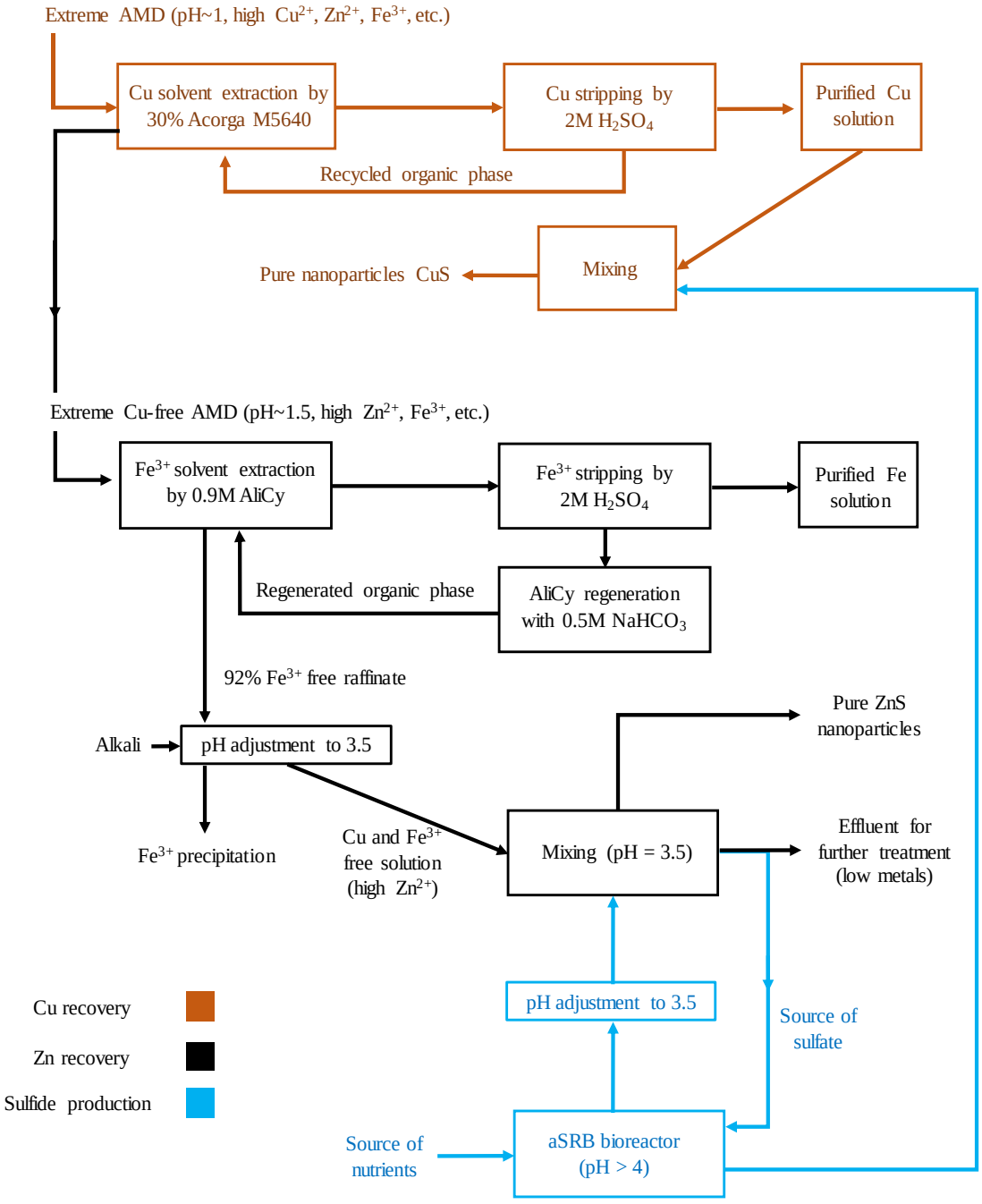

Figure 7.1. Possible integration of Cu and Zn recovery with AMD treatment processes, combining SX and sulfidogenic reactor operating at low pH.

Regarding metals recovery by phytochemicals:

- Applying the proposed process to other leaching solutions such as those from bioleaching;
- Optimization of the metallic particles washing steps to minimize the amount of solvents used;
- Improvement of economic viability of phytochemicals extraction by more available and cheaper extractants such as water, maintaining the metals recovery potential;
- Identification and/or purification of the main bio-active compounds from the extracts interacting with Pd and/or Au ions, to increase the available information for the development of functional synthetic compounds;
- *R. idaeus* leaves are the main waste of red raspberry fruit industry, which is widely cultivated in Europe, Asia, and America. On the other hand, the amount of spent ACCs as well as wastes with PCBs currently available is enormous and does not tend to decrease in the short term. Therefore, the achievements described in this thesis allow to foretell stations where both these types of secondary sources are used in systems integrating modules to produce *R. idaeus* wastes extracts and modules for the dismantling and leaching of spent ACCs and/or PCBs, both feeding materials to modules where the *green* Pd and/or *green* Au recovery processes are applied. In figure Figure **7.2**, a diagram representing a possible station of such type is presented.

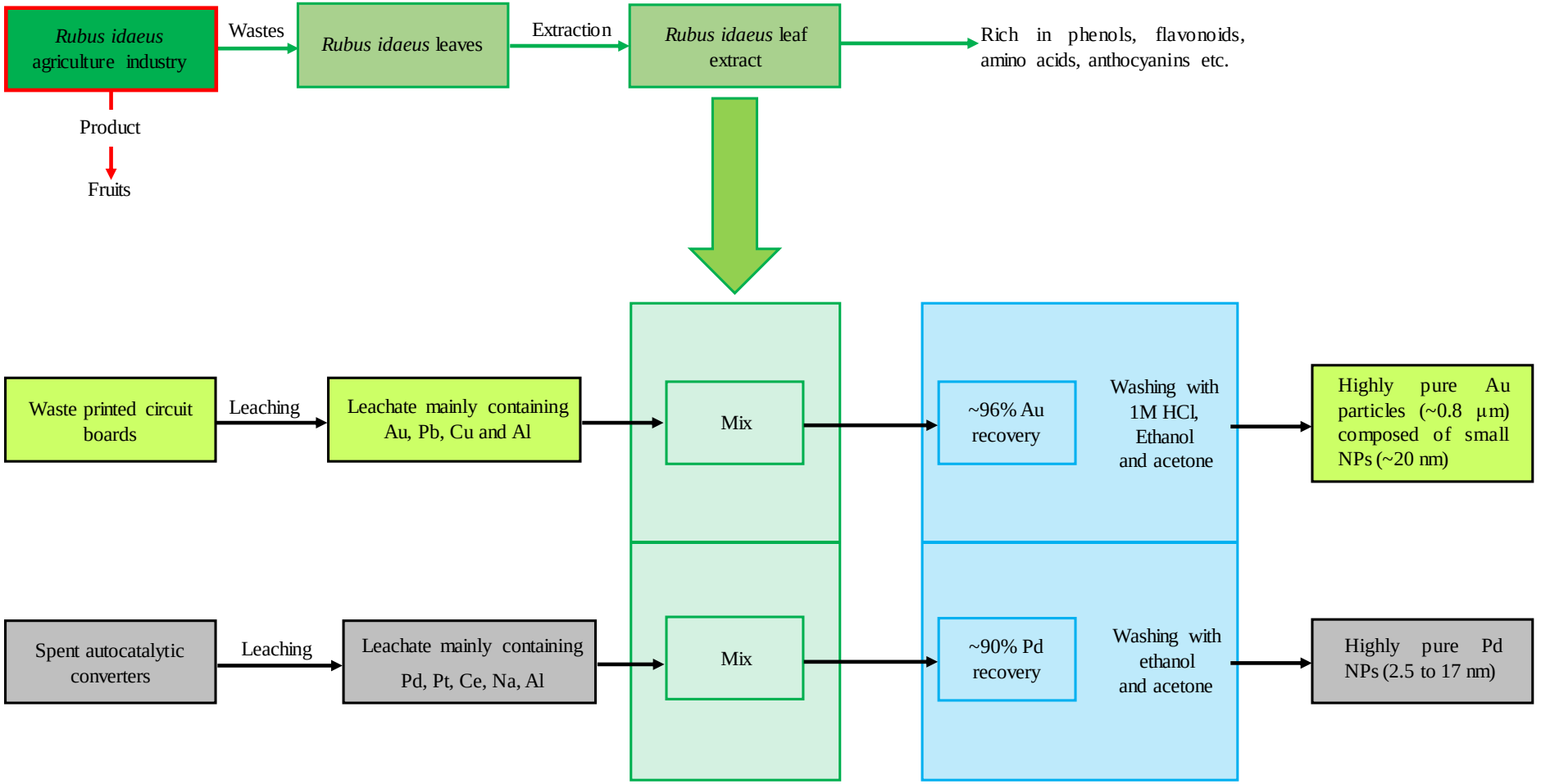

Figure 7.2. Suggested process for the green Pd and Au recovery from the spent ACCs and/or PCBs leachates using *R. idaeus* leaf extract.